

LEABHARLANN CHOLÁISTE NA TRÍONÓIDE, BAILE ÁTHA CLIATH | TRINITY COLLEGE LIBRARY DUBLIN
Ollscoil Átha Cliath | The University of Dublin

Terms and Conditions of Use of Digitised Theses from Trinity College Library Dublin

Copyright statement

All material supplied by Trinity College Library is protected by copyright (under the Copyright and Related Rights Act, 2000 as amended) and other relevant Intellectual Property Rights. By accessing and using a Digitised Thesis from Trinity College Library you acknowledge that all Intellectual Property Rights in any Works supplied are the sole and exclusive property of the copyright and/or other IPR holder. Specific copyright holders may not be explicitly identified. Use of materials from other sources within a thesis should not be construed as a claim over them.

A non-exclusive, non-transferable licence is hereby granted to those using or reproducing, in whole or in part, the material for valid purposes, providing the copyright owners are acknowledged using the normal conventions. Where specific permission to use material is required, this is identified and such permission must be sought from the copyright holder or agency cited.

Liability statement

By using a Digitised Thesis, I accept that Trinity College Dublin bears no legal responsibility for the accuracy, legality or comprehensiveness of materials contained within the thesis, and that Trinity College Dublin accepts no liability for indirect, consequential, or incidental, damages or losses arising from use of the thesis for whatever reason. Information located in a thesis may be subject to specific use constraints, details of which may not be explicitly described. It is the responsibility of potential and actual users to be aware of such constraints and to abide by them. By making use of material from a digitised thesis, you accept these copyright and disclaimer provisions. Where it is brought to the attention of Trinity College Library that there may be a breach of copyright or other restraint, it is the policy to withdraw or take down access to a thesis while the issue is being resolved.

Access Agreement

By using a Digitised Thesis from Trinity College Library you are bound by the following Terms & Conditions. Please read them carefully.

I have read and I understand the following statement: All material supplied via a Digitised Thesis from Trinity College Library is protected by copyright and other intellectual property rights, and duplication or sale of all or part of any of a thesis is not permitted, except that material may be duplicated by you for your research use or for educational purposes in electronic or print form providing the copyright owners are acknowledged using the normal conventions. You must obtain permission for any other use. Electronic or print copies may not be offered, whether for sale or otherwise to anyone. This copy has been supplied on the understanding that it is copyright material and that no quotation from the thesis may be published without proper acknowledgement.

Design and Synthesis of Tubulin-Binding Agents, and their Incorporation into Novel Dual-Acting Hybrid Molecules Targeting the Tumour Vasculature

Adrian Coogan

A thesis presented to the University of Dublin for the degree of Doctor of Philosophy

Based on the research carried out under the supervision and direction of **Dr. John Walsh**

School of Pharmacy and Pharmaceutical Sciences

University of Dublin

Trinity College

May 2013

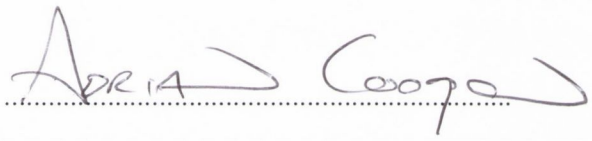
TRINITY COLLEGE
- 4 MAR 2014
LIBRARY DUBLIN

Thesis 10203

Declaration

I declare that this thesis has not been submitted as an exercise for a degree at this or any other university and it is entirely my own work, except where duly acknowledged.

I agree to deposit this thesis in the University's open access institutional repository or allow the library to do so on my behalf, subject to Irish Copyright Legislation and Trinity College Library conditions of use and acknowledgement.



Adrian Coogan

Abstract

This thesis involves the design and synthesis of tubulin binding agents, which aside from their anti-proliferative impact, seek to induce anti-vascular and anti-angiogenic responses on the unique vasculature derived by a growing tumour mass. Once synthesised, studies were conducted on the incorporation of the most active tubulin binding agents into a novel series of hybrid drugs or designed multiple ligands, which serve to complement their therapeutic effect.

The thesis is introduced by a comprehensive overview of the process of angiogenesis, the tumour vasculature network, and the myriad of differences between tumour blood vessels and those of normal vascular systems. Also discussed are the two main interrelated strategies for disrupting the microvasculature of tumours; the anti-angiogenic and anti-vascular approaches, with examples provided for each. The benefit of combination and hybrid therapies is outlined, with particular regard to each side of the concepts we intended to implement; dual targeting of both the tubulin subunits which can eventually cause occlusion of a tumour blood vessel, and the multifunctional enzymatic receptor Aminopeptidase N (APN), expressed solely on tumour vasculature undergoing angiogenesis but not on normal, quiescent vasculature. The introductory chapter ends by outlining the aims of the thesis.

Chapter 2 focuses on the procurement of promising tricyclic benzoxepinone compounds, previously shown to be competitive tubulin binding agents. As this synthesis is optimised, novel derivatives are prepared, and comprehensive biological testing carried out on the most promising compound. A phosphate prodrug of the same compound is also prepared.

Chapter 3 starts by discussing the bromination of the main benzoxepinones from Chapter 2, and the novel ring contraction reaction discovered that converts these to an even more active 4-aryl coumarin series. The novel reaction itself is studied and a mechanism proposed, before the effects of various other nucleophiles are investigated on the bromide intermediate. Two of these in particular give rise to quite unexpected rearrangements and again these transformations are discussed. A new, more efficient synthetic methodology for the procurement of 4-aryl coumarins

is implemented, and using this, a range of these chromenone structures are prepared and evaluated.

Chapter 4 centres on the integration of the most active tubulin binding, anti-vascular compounds described in Chapters 2 and 3 into multi-valent drug systems. These include a variety of hybrid drugs based on the existing APN inhibitor bestatin, and also designed multiple ligands which possess a hydroxamic acid functionality, known to have excellent affinity for the zinc containing APN binding site. Following their synthesis they were then evaluated for their APN inhibition activity. Furthermore, one hybrid lead compound was evaluated in a rigorous evaluation regimen not only for *ex vivo* anti-vascular and anti-angiogenic activity, but also for *in vivo* activity in a PC-3 tumour xenograft model, where it was successfully shown by another PhD student to inhibit tumour growth.

Chapter 5 outlines the experimental procedures used in the syntheses of agents from Chapters 2, 3 and 4, and recorded their structural data.

Acknowledgements

First of all, I would like to thank my supervisor, Dr. John Walsh for his help, patience and dedication through our endeavours over the past years. I wish him all the best in his continued efforts in taking this project forward to the next level.

I would also like to state my gratitude to the IRCSET Embark Initiative for their generous funding of the first three years, Enterprise Ireland for financially supporting the project as a whole, and Dr. Andrew Harkin for his assistance in securing additional financial help in fourth year. Also to Mary Caffrey and the Hamilton library staff for the opportunity of employment over the past two years, allowing me to sustain my studies without major disruption.

I would like to thank Drs John O'Brien and Manuel Reuther for their insight and for sharing their expertise regarding the hundreds, if not thousands of NMR spectra run over the course of the project. I really learnt a lot and much appreciated the valiant undertaking of even the most challenging of samples. Similarly, I would like to express my thanks to Dr. Paul O'Byrne and especially Brian Talbot, initially for running Mass Spec and LC-MS samples, and later for passing their skills over to me. Furthermore, I also wish to thank Joe Reilly and all the technical staff in the School of Pharmacy for their cooperation and assistance in times of need.

To my lab colleagues on the cancer project; Brian Moran, Gary Stack and Elaine Breen, thanks not only for putting up with me, but for your help and cooperation, through good days and bad, and to Katerina Prokopiou for the skilled evaluation of my compounds. To these and also to those on the other projects; Tao Zhang, Deirdre Finn, Orla Woods and Paul O'Byrne, thank you for your wisdom and counsel regarding lab matters, and for the invaluable friendship and support besides. Long may it continue. A special mention too to my fellow postgraduates in the School of Pharmacy, for the comic relief but also for believing in me, probably more than I did myself, in particular the PharmChemmers; Patrick, Yvonne, Michael, Juan, Billy, Tadhg, Andy, Conor, Jason amongst the countless others, but also those in other fields; Stefano, Vincent, Cathal, Keith, Tall Claire, Small Clare, Susan, Joanna, Christine, Jenny and of course Stephany. Not sure I would have survived if it were not for you guys!

To my close friends, Brian, David, Sean and Shane, thank you for your faith and always uplifting my spirits. Thanks also to Frances, for her patience, encouragement and sympathetic ear, and to the lads; John K, John C, Damien, Dave and Paddy for all the welcome distractions throughout the years. Most of all I would like to thank my parents, Brian and Maura, to whom I am eternally grateful for their steadfast confidence and unequivocal support, from beginning to end.

Abbreviations

ABP	Activity Based Probes
ACN	Acetonitrile
AHPA	3-Amino-2-Hydroxy-4-Phenylbutanoyl Acetate
APA	Aminopeptidase A
APN	Aminopeptidase N
ATP	Adenosine-5'-triphosphate
bFGF	Basic Fibroblast Growth Factor
Boc	*tert*-butoxycarbonyl
BTMS	Bromotrimethylsilane
CA-4	Combretastatin A-4
CA-4-P	Combretastatin A-4 Phosphate
CHO	Chinese Hamster Ovary
CNGRC	Cysteine-Asparagine-Glycine-Arginine-Cysteine
CNS	Central Nervous System
DABCO	1,4-diazabicyclo[2.2.2]octane
DAPI	4',6-Diamidino-2-phenylindol
DCC	Dicyclohexylcarbodiimide
DCM	Dichloromethane
DCU	Dicyclohexylurea
DEPT	Distortionless Enhancement by Polarization Transfer
DIPEA	Diisopropylethyl amine
DMAP	4-Dimethylaminopyridine
DMF	Dimethylformamide
DML	Designed Multiple Ligand
DMSO	Dimethyl Sulfoxide
DMXAA	5,6-Dimethylxanthenone-4-Acetic Acid

Dppf	1,1'-Bis(diphenylphosphino)ferrocene
ECM	Extracellular Matrix
EDC	Ethyl Dimethylaminopropyl Carbodiimide
EtOH	Ethanol
FAA	Flavone Acetic Acid
FDA	Food and Drug Administration
5-FdUrd	5-Fluoro-2-Deoxyuridine
FGF	Fibroblast Growth Factor
Fmoc	Fluorenylmethyloxycarbonyl Chloride
FTIR	Fourier Transform Infrared Spectroscopy
GI	Gastrointestinal
GMP	Glomeruloid Microvascular Proliferation
GTP	Guanosine-5'-triphosphate
H&E	Haematoxylin and Eosin
HEPES	4-(2-Hydroxyethyl)piperazine-1-ethanesulfonic acid
HIF	Hypoxia Inducible Factor
HMBC	Heteronuclear Multiple-bond Correlation spectroscopy
HSPG	Heparan Sulphate Proteoglycans
HSQC	Heteronuclear Single-Quantum Correlation spectroscopy
HUVEC	Human Umbilical Vein Endothelial Cells
i.p.	Intraperitoneal
IR	Infrared
LDA	Lithium Diisopropylamide
Leu	Leucine
MARK	Mitogen-Activated Protein Kinase
*m*CPBA	*meta*-Chloroperoxybenzoic Acid
MeOH	Methanol

MLC	Myosin Light Chain
MMP	Matrix Metalloproteinase
mRNA	Messenger RNA
MS	Mass Spectroscopy
mTor	Mammalian target of rapamycin
MTT	(3-(4,5-Dimethylthiazol-2-yl)-2,5-diphenyltetrazolium bromide
MV	Mother Vessel
*n*BuLi	*n*-Butyllithium
NMR	Nuclear Magnetic Resonance
NP	Neuropilin
NSAID	Non-steroidal Anti-Inflammatory Drug
PCC	Pyridinium Chlorochromate
PC-3	Human Prostate Cancer cell line
PDC	Pyridinium Dichromate
PDGFB	Platelet-Derived Growth Factor B
PDGFB-β	Platelet-Derived Growth Factor β Receptor
Pet	Petroleum
PFP	Pentafluorophenyl
pH	Minus log of Hydronium Ion Concentration
Phe	Phenylalanine
PI	Propidium Iodide
PlGF	Placenta Derived Growth Factor
ppm	Parts per million
Pro	Proline
PTT	Phenyltrimethylammonium tribromide
PyBroP	Bromo-*tris*-pyrrolidino phosphoniumhexafluorophosphate
QALY	Quality Adjusted Life Year

QSAR	Quantitative Structure-Activity Relationship
Rf	Retardation Factor
RNA	Ribonucleic Acid
ROESY	Rotating-frame Overhauser Effect Spectroscopy
RT	Room Temperature
RTV	Relative Tumour Volume
SAPK	Stress Activated Protein Kinase
SARS	Severe Acute Respiratory Syndrome
SC	Stalk Cells
s.c.	Subcutaneous
SMA	Smooth Muscle Actin
TBA	Tubulin Binding Agent
TBAF	Tetrabutylammonium Fluoride
TBDMSiCl	*tert*-butyldimethylsilyl Chloride
TBDMSi	*tert*-butyldimethylsilyl protecting group
TBDPSi	*tert*-butyldiphenylsilyl protecting group
TC	Tip Cell
TFA	Trifluoroacetic Acid
THF	Tetrahydrofuran
TKI	Tyrosine Kinase Inhibitors
TLC	Thin Layer Chromatography
TNF	Tumour Necrosis Factor
TOCSY	Total Correlation Spectroscopy
UV	Ultraviolet
Val	Valine
VDA	Vascular Disrupting Agent
VEGF	Vascular Endothelial Growth Factor

VEGF-R	Vascular Endothelial Growth Factor Receptor
VHI	Voluntary Health Insurance
VM	Vascular Malformations
wfi	Water for injection

Table of Contents

Chapter 1.0 – Introduction 2

1.1 Angiogenesis 3

1.2 Angiogenesis of tumours and their consequent vascular network 6

1.2.1 Structural abnormalities of tumour blood vessels 8

1.2.2 Classes of tumour blood vessels 15

1.3 Targeting Angiogenesis and Tumour Vasculature 16

1.3.1 Anti-angiogenic therapy 19

1.3.2 Anti-Vascular Therapy 25

1.3.2.1 Tubulin and Microtubule based VDAs 26

1.3.2.2 Mode of action of Tubulin Based VDAs 29

1.3.2.3 Combretastatins in the clinic 32

1.3.2.4 Other VDAs 35

1.4 Combination therapy and Hybrid Drugs 36

1.5 Aminopeptidase N 38

1.5.1 Inhibitors of APN 41

1.6 Aims of project 44

Chapter 2 – Synthesis of benzoxepinone series 46

2.0 Background 47

2.1 Synthetic strategy 1 49

2.1.1 Early synthetic steps 49

2.1.2 Problematic reduction of ketone functionality 53

2.1.3 Formation of cyclised intermediate 2.10 54

2.1.4 C-ring synthesis 55

2.2 Synthetic strategy 2 56

2.2.1 Deprotection and coupling step 57

2.2.2 Structural elucidation of 2.17 60

2.3 Analogues of 2.17 – Synthetic strategy 3 63

2.3.1 Para-methoxy C ring analogues 63

2.3.2 Aniline C ring analogue 64

2.3.2.1 Synthesis of new C ring precursor for aniline based TBA 65

2.3.3 Aniline C-ring analogue 67

2.3.4 Aniline C-ring coupling 68

2.3.5 Aniline C-ring analogue – final steps 69

2.3.6 Aniline C-ring – structural elucidation 70

2.4 Phosphate Prodrug 73

2.5 Biological Evaluation of benzoxepinone compounds 74

2.6 Conclusions from Chapter 2 79

Chapter 3 – Novel Ring contraction and Synthesis of 4-aryl Coumarin Series of TBAs 80

3.0 Background 81

3.1 Optimisation of bromination reaction 83

3.2 NMR studies of nucleophilic substitution rearrangements 86

3.2.1 Substrate Overview 86

3.2.2 Azide substitution and ring contraction of 3.01 88

3.2.3 Ring contraction of aniline and paramethoxy benzoxepinones 93

3.2.4 Proposed mechanism for novel ring contraction 94

3.2.5 Effect of different nucleophiles on bromoketone functionality 96

3.2.6 Proposed mechanisms for MeOH and NH_3 induced rearrangements..... 102

3.3.1 Shorter synthetic route to 4-aryl coumarin compounds 104

3.3.2 Coupling of chromenone precoursor 3.19 to various C-ring 107

3.4 Functionalisation and creation of bi-faceted tubulin binding ligand 111

3.5 Phosphate salt prodrug of phenol 3.03 114

3.6 Biological evaluation of 4-aryl coumarin series of TBAs..... 115

3.7 Conclusions 119

Chapter 4 – Synthesis of a series of Novel Hybrid Molecules

and Designed Multiple Ligands 120

4.0 Background 121

4.1 Peptide based hybrid drugs 122

4.1.1 Phenolic ester hybrid based on benzoxepinone 2.17..... 123

4.1.2 Structural Elucidation of hybrid 4.06..... 128

4.1.3 Phenolic ester hybrid based on 4-aryl coumarin 3.03..... 132

4.2.1 Anilide hybrid based on 4-aryl coumarin 3.06 133

4.3.1 Tripeptide based hybrids 136

4.3.2 Synthesis of tripeptide based hybrids 137

4.4.1 The Designed Multiple Ligand approach 142

4.4.2 Synthesis of hydroxamic acid DMLs 144

4.4.3 Structural Elucidation of hydroxamic acid 4.36 147

4.4.4 Aniline derivative of 4.26..... 150

4.5.1 Controlled release of DML 4.30 152

4.5.2 Synthesis of controlled release DML 4.35 153

4.6 Attempts to incorporate a hydroxamic acid on 4-aryl coumarin..... 155

4.7 APN inhibition assay..... 158

4.8 Biological evaluation of hybrid compound 4.06 160

4.9 Conclusions..... 164

Chapter 5 – Experimental 166

5.1 General Methods 167

5.2 Experimental for Chapter 2 169

5.3 Experimental for Chapter 3 192

5.4 Experimental for Chapter 4 217

5.5 APN enzyme assay 251

Chapter 6 – References..... 253

Table of Figures

Figure 1.1 Cancer Incidence Worldwide 2

Figure 1.2 Mechanism of normal angiogenesis 5

Figure 1.3 Normal vascular network 7

Figure 1.4 Comparison of vascular networks 8

Figure 1.5 Characteristics of the endothelium 10

Figure 1.6 Schematic of Pericytes 12

Figure 1.7 Pericyte arrangement 13

Figure 1.8 Tumour blood vessels after VEGF treatment 14

Figure 1.9 Mother Vessels and GMPs 16

Figure 1.10 Different classes of tumour blood vessel 17

Figure 1.11 Overview of VEGFs 20

Figure 1.12 Tumour vascular normalisation 25

Figure 1.13 Characteristics of anti-vascular and anti-angiogenic therapies 26

Figure 1.14 Basic components of microtubules 27

Figure 1.15 TBA binding sites 29

Figure 1.16 Colchicine and Combretastatin A4 Phosphate 30

Figure 1.17 Signalling pathways of CA-4-P 31

Figure 1.18 Rapid Vascular Shutdown 32

Figure 1.19 Viable Rim 35

Figure 1.20 Combination therapy of bevacizumab and CA-4-P 37

Figure 1.21 APN processes 38

Figure 1.22 Bestatin at APN active site 42

Figure 1.23 Lead compounds RS5.04 and GJH140 44

Figure 2.1 Component of QSAR for tubulin inhibitors 47

Figure 2.2 ^{1}H spectrum of 2.17 60

Figure 2.3 Full ^{13}C spectrum and DEPT135° of phenol 2.17 61

Figure 2.4 HSQC and HMBC correlation spectra spectra 2.17 62

Figure 2.5 ^{1}H spectrum of aniline 2.28 71

Figure 2.6 ^{13}C spectrum for 2.28 72

Figure 2.7 Cell cycle histograms 76

Figure 2.8 Microtubule disruption following immunofluorescent staining 76

Figure 2.9 Change in endothelial cell morphology 77

Figure 2.10 Rat Aortic ring assay – anti-vascular model 78

Figure 2.11 Rat Aortic ring assay – anti-angiogenesis model 78

Figure 3.1 ^{1}H NMR of 3.01 87

Figure 3.2 ^{13}C NMR of 3.01 87

Figure 3.3 Superimposed ^{1}H spectra during ring contraction 89

Figure 3.4 ^{13}C Spectrum of ring contraction over time 90

Figure 3.5 Closer look at carbonyl during ring contraction 91

Figure 3.6 Loss of C-Br on NMR 91

Figure 3.7 ^{1}H spectrum of 3.09 97

Figure 3.8 Comparison of the downfield region in ^{1}H NMR 3.01 and 3.09 97

Figure 3.9 Complete ^{13}C spectrum for 3.09 98

Figure 3.10 HSQC and HMBC spectra of 3.09 98

Figure 3.11 ^{1}H spectrum of 3.12 100

Figure 3.12 HCQ and HMB spectra of 3.12 101

Figure 3.13 Distruption of microtubule cytoskeleton 117

Figure 3.14 Anti-vascular effect of 4-aryl coumarins 118

Figure 3.15 Anti-angiogenic effect of 4-aryl coumarins 118

Figure 4.1 Complete ^{1}H spectrum of 4.06 129

Figure 4.2 Complete 13C spectrum of 4.06 129

Figure 4.3 NH COSY and HMBC spectra of 4.06 130

Figure 4.4 HMBC and HSQC of 4.06 131

Figure 4.5 APN binding 136

Figure 4.6 Representation of pharmacophore position on DMLs 143

Figure 4.7 Hydroxamic acid based APN inhibitor Tosedostat 144

Figure 4.8 Syn and anti stereoisomers of oxime 4.26 147

Figure 4.9 ^{1}H spectrum of 4.26 148

Figure 4.10 ^{13}C spectrum of 4.26 149

Figure 4.11 HSQC spectrum of 4.26 150

Figure 4.12 Chromatogram of LC-MS separation of 4.40 and 4.39 158

Figure 4.13 Difference in tumour growth and % body weight 162

Figure 4.14 Tumour necrosis 163

Figure 4.15 Comparison of functional vasculature 164

Table of Schemes

Scheme 2.1 Retrosynthetic rational and proposed synthetic target 49

Scheme 2.2 Baeyer-Villiger oxidation and hydrolysis 50

Scheme 2.3 Improved synthesis of 2.02 51

Scheme 2.4 Alkylation and basic hydrolysis of 2.02 52

Scheme 2.5 Meldrum's acid coupling of 2.04 52

Scheme 2.6 Methanolysis of 2.05 53

Scheme 2.7 Reduction methods of keto-ester 2.06 53

Scheme 2.8 Silyl protection of 2.07 and basic hydrolysis of 2.08 55

Scheme 2.9 Friedel-crafts acylation and cyclization of 2.09 55

Scheme 2.10 Baeyer-Villiger oxidation and hydrolysis 56

Scheme 2.11 Silyl protection of C-ring phenol 2.12 56

Scheme 2.12 Deprotection of 2.10 57

Scheme 2.13 Organolithium coupling with acidic work up 2.15 58

Scheme 2.14 Oxidation of alcohol 2.15 to ketone 2.16 59

Scheme 2.15 Deprotection methods for dimethylsilyl ethers 60

Scheme 2.16 Synthesis of alcohol 2.18 to ketone 2.19 64

Scheme 2.17 Aniline synthesis 2.21 65

Scheme 2.18 Boc protection of aniline 2.21 66

Scheme 2.19 Miyaura borylation of boronic ester 2.23 67

Scheme 2.20 One pot synthesis of triflate 68

Scheme 2.21 Suzuki coupling 69

Scheme 2.22 Catalytic cycle for Suzuki coupling 69

Scheme 2.23 Deprotection and Oxidation of 2.25 70

Scheme 2.24 Deprotection of Boc group 2.27 70

Scheme 2.25 Formation of phosphate ester 73

Scheme 2.26 Formation of phosphate salt 74

Scheme 3.1 Hudson attempted synthesis of amino-ketones 82

Scheme 3.2 Azide ring contraction 83

Scheme 3.3 First Hudson method for selective bromination 84

Scheme 3.4 Optimised PTAB bromination 85

Scheme 3.5 Azide induced ring contraction and deprotection 92

Scheme 3.6 Bromination and ring contraction 93

Scheme 3.7 Deprotection of Boc group 93

Scheme 3.8 Bromination and ring contraction on 2.19 94

Scheme 3.9 Proposed mechanism of azide mediated ring contraction 95

Scheme 3.9a Methanol induced rearrangement of 3.01 96

Scheme 3.10 Methanol rearrangement for 3.07 to give 3.11 99

Scheme 3.11 Ammonia rearrangement reaction on 3.01 giving 3.13 100

Scheme 3.12 Sulphur based nucleophiles 102

Scheme 3.13 Proposed mechanism for methanol to 7-membered lactones 103

Scheme 3.14 Proposed mechanism for ammonia to 7-membered lactones 103

Scheme 3.15 Alternate proposals for epoxide ring opening 104

Scheme 3.16 Synthesis of 2.02 and subsequent hydrolysis or Dakin oxidation ... 105

Scheme 3.17 Acetylation of phenol 2.02 and Fries rearrangement to 3.17 105

Scheme 3.18 4-Hydroxycoumarin 3.18 formation 106

Scheme 3.19 Triflation of 4-hyrdoxycoumarin 3.18 107

Scheme 3.20 Conversion of aryl bromide 2.13 to boronic acid 3.20 108

Scheme 3.21 Coupling of 3.09 with 3.20 and TBAF deprotonation 108

Scheme 3.22 Coupling of 2.23 with 3.19 109

Scheme 3.23 Coupling of aryl boronic acids 109

Scheme 3.24 Boron based hydration of triobromoanisole 110

Scheme 3.25 Diol protection and conversion to boronic acid 111

Scheme 3.26 Coupling of 3.25 to 3.19 111

Scheme 3.27 Bromination of 3.02 to 3.28 113

Scheme 3.28 Coupling of 3.28 with trimethoxyphenyl boronic acid 114

Scheme 3.29 Deprotonation of silyl ether 3.29 to give free phenol 3.30 114

Scheme 3.30 Synthesis of phosphate salt prodrug 3.32 of phenol 3.03 115

Scheme 4.1 Direct coupling of phenol 2.17 123

Scheme 4.2 Coupling with 2,6 dichlorobenzoyl chloride 124

Scheme 4.3 EDC coupling 125

Scheme 4.4 TFA deprotection 125

Scheme 4.5 Boc-protection of AHPA 126

Scheme 4.6 Coupling of PFP ester 127

Scheme 4.7 Final deprotection to give 4.06 127

Scheme 4.8 Synthesis of 4-aryl coumarin derivative 4.10 132

Scheme 4.9 PyBroP coupling of aniline 3.06 133

Scheme 4.10 Trifluoroacetamide formation 134

Scheme 4.11 Synthesis of aniline hybrid 4.15 135

Scheme 4.12 Boc-protection of bestatin 138

Scheme 4.13 Coupling of N-Boc bestatin 138

Scheme 4.14 Deprotection to give tripeptide 4.18 139

Scheme 4.15 Synthesis of alanine tripeptide hybrid 140

Scheme 4.16 Deprotection of Boc protected alanine 141

Scheme 4.17 Coupling of alanine prodrug 141

Scheme 4.18 Final step for alanine aniline tripeptide hybrid 142

Scheme 4.19 Oxime formation of ketone 2.17 145

Scheme 4.20 PFP ester formation of 4.24 146

Scheme 4.21 Formation of phenolic hydroxamic acid DML 146

Scheme 4.22 Unsuccessful attempt at PFP ester synthesis 151

Scheme 4.23 Oxime and PFP ester synthesis of 2.27 151

Scheme 4.24 Final steps in the synthesis of aniline hydroxamic acid 4.30 152

Scheme 4.25 N-Boc leucine coupling on to 2.28 153

Scheme 4.26 Hydroxamic acid 4.34 synthesis on N-Boc Leucine 154

Scheme 4.27 Deprotection of 4.34 to give 4.35 155

Scheme 4.28 Carboxylic acid formation 156

Scheme 4.29 Formation of lactam 4.40 157

Scheme 4.30 APN cleavage on L-leucine-p-nitroaniline 159

Table of Tables

Table 1.1 Endogenous Regulators of Angiogenesis 4

Table 1.2 Enzymatic behaviour of APN 39

Table 2.1 IC_{50} values of benzoxepinone lead compounds from MTT assay 75

Table 3.1 IC_{50} values of 4-aryl coumarin from MTT assay 116

Table 4.1 IC_{50} values of APN enzymatic inhibition assay 159

Chapter 1 - Introduction

1.0 Introduction

Despite consistent advances in therapy and diagnosis, the threat of cancer remains a major concern to human health across the globe. According to statistics published by the GLOBOCAN project in June 2010[7], an estimated 12.7 million *new* cases of cancer were diagnosed worldwide in 2008 (Figure 1.1), with 7.6 million cancer related fatalities; representing 12% of all deaths recorded[8]. The incidence is even more pertinent in the developed world with cancer accounting for 23% of deaths in North America, 27% in the United Kingdom and 28% in the Republic of Ireland[9].

Cancer is the British public's biggest fear, ahead of crime, debt, unemployment and other diseases such as Alzheimer's or even having a heart attack[10]. One in three Irish people will develop the disease in their lifetime, with around 20,000 new cases recorded each year[11]. The knock-on effects of this are quite staggering. In an era of economic scrutiny, the Irish government is currently spending hundreds of millions on cancer care, while the Irish health insurer VHI recently paid out some €185 million on essential cancer treatment; 16% of all claims[12]. Our American counterparts were similarly affected; with a reported $102.8 billion estimated spend in 2010 on care alone[13] and a further $4.97 billion spent by the NCI on cancer research in the 2009 fiscal year[14]. With an approximated cost of $161 billion to the American

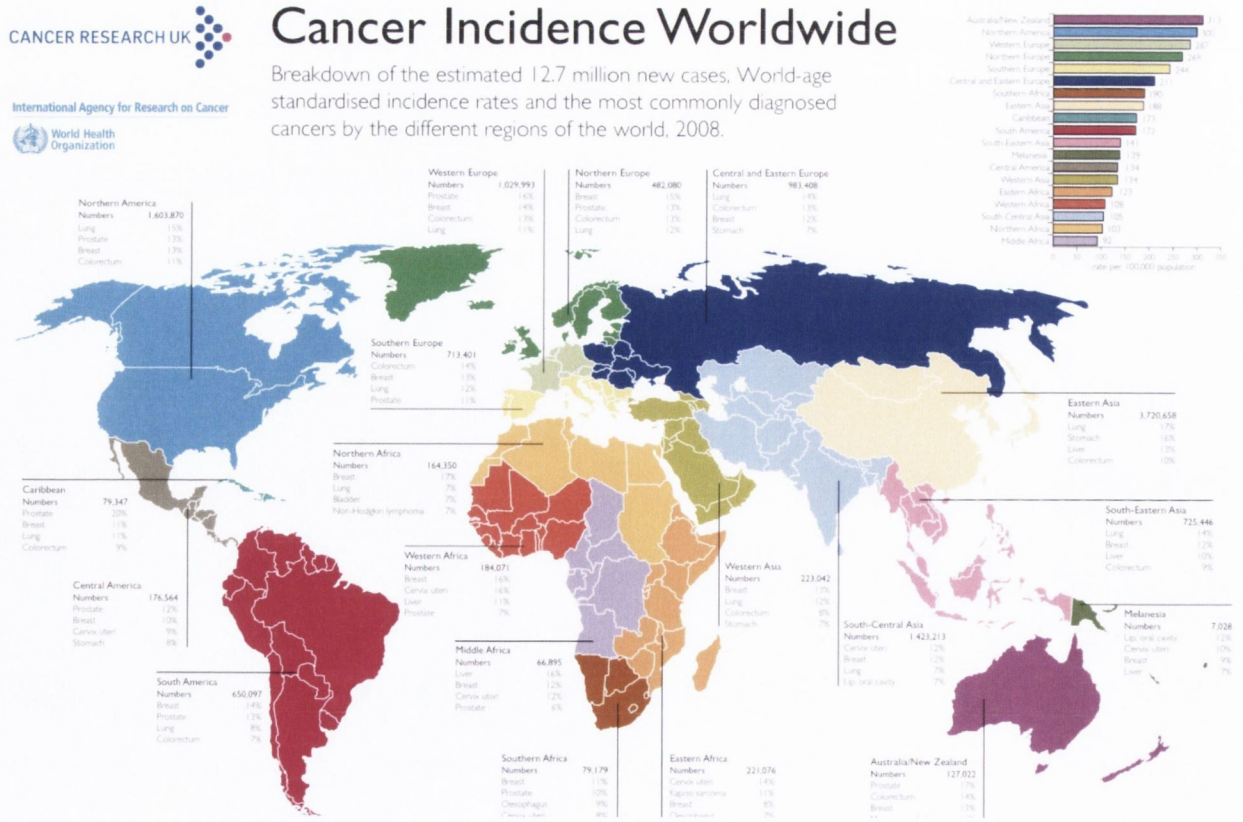


Figure 1.1. Cancer Incidence Worldwide[1]

economy due to morbidity and premature mortality, the total US economic burden is close to $270 billion annually[13].

Cancer refers to a group of diseases characterised by uncontrolled growth and spread of abnormal cells, which are otherwise tightly controlled processes. An aggregation of cancerous cells is termed a tumour, and can be either benign or malignant. Benign tumours, although cause for concern in their own right, limit themselves to an organ and do not spread[15]. It may be possible to remove the tumour surgically and thus the cancer is eradicated. Malignant tumours on the other hand do spread, from the site of origin through different organs making treatment much more difficult. This can occur by the direct extension of the tumour to nearby organs, or by *metastasis*, where small fragments of cancerous cells fall into the bloodstream or lymph canals[15]. The latter cases can cause migration of cancerous material to distal sites throughout the body, forming the basis for new tumour sites far from the primary tumour.

There are well over 200 different types of cancer recorded, but over fifty percent of all diagnoses are caused by just four – breast, lung, colorectal and prostate[16]. Although reported mortality rates have fallen in the UK by 20% over the last 30 years and life expectancy continues to be prolonged, the overall survival rate remains quite poor (50% over five year period 2001-2006)[17]. Two major reasons why chemotherapy can fail are the dissemination of the tumour at diagnosis and multidrug resistance. Multidrug resistance is perhaps the more important of the two and occurs during treatment when the drug of choice eliminates only cells vulnerable to the drug, leaving behind more resistant cells. These resistant cells then multiply into a new population which is much more impervious to chemotherapy[18]. Finding new classes of drugs that will circumvent this defence mechanism would have very significant therapeutic potential.

1.1 Angiogenesis

There are a myriad of possible targets through each stage of cancer development which are feasible points for treatment. Our focus is centred on the unique vasculature that accrues around solid tumours, which together account for 85% of cancer fatalities[19]. In the early stages of development, when tumour demand for oxygen, nutrients (e.g. glucose) and a means to

remove waste products surpass those locally available via diffusion[20] (generally occurring before the tumour reaches a diameter of 1-2 mm [21]; roughly 10^5 cells) a hypoxic microenvironment arises leading to the activation of *angiogenesis*. This is largely mediated through the expression of hypoxia-inducible factors[22] (HIFs), basic fibroblast growth factors (bFGFs) and vascular endothelial growth factors[23] (VEGFs, also known as vascular permeability factors) among others (Table 1.1). Angiogenesis is the term that describes the creation of new blood vessels from the endothelium of *pre-existing* vasculature. In normal vascular systems, this is a meticulously regulated process; complex in that it requires communication between different cell types, the extracellular matrix and a diverse cocktail of growth factors and other cytokines. The fastidious nature of the angiogenic process is essential to ensure that the quiescent endothelial monolayer divides and expands only to the necessary extent imposed by the growing tissue demands. Pertaining to cancerous cells, in addition to subsidising a growing tumour mass, angiogenesis provides an early opportunity for metastasis; facilitating the dissemination of tumour cells into the blood supply, and as such represents a promising therapeutic target.

Table 1.1. Endogenous Regulators of angiogenesis[24]

Endogenous Regulators of Angiogenesis	
Stimulatory Angiogenic Factors *(Pro)*	**Inhibitory Angiogenic Factors *(Anti)***
Acidic fibroblast growth factor	Angiostatin
Angiogenin	Anti-thrombin III fragment
Basic fibroblast growth factor (bFGF)	Endostatin
Fibroblast growth factor -3, -4	Fragment of platelet factor-4
Hepatocyte growth factor	Inferon α, β
Interleukin-8 (IL-8)	Interferon-inducible protein -10
Placental growth factor (PlGF)	Maspin
Platelet derived growth factor (PDGF)	METH-1, 2
Pleiotropin	Prolactin fragment
Proliferin	Thrombospondin-1, 2
Transforming growth factor α, β	Tumstatin
Tumour necrosis factor α (TNFα)	Vascular endothelial growth inhibitor
Vascular endothelial growth factor (VEGF)	Vasostatin

Hypoxia and ischemia are typical driving forces towards angiogenesis, causing controlled release of the aforementioned VEGFs, which start the process by signalling so called endothelial 'tip cells' (TCs) to begin forming abluminal sprouts[25]. The sprouting of TCs is aided by a loosening of

nearby endothelial cells at their junctions with one another (mediated by the cytokine cadherin[26]), the activation of proteases to degrade the surrounding extracellular matrix and detachment of supportive pericytes[25]. As the sprout begins to migrate and develop into the extracellular space, 'stalk cells' (SCs) are evolved to consolidate the connections between the new branches and the parent vessel, and within SCs the vascular lumen begins to develop[27]. Eventually, with assistance from guiding pro-angiogenic factors, TCs converge with other sprouts and begin the process of fusing together in a process termed anastomosis, generating rigid endothelial cell junctions and a continuous patent lumen[25]. To complete the maturation of these new blood vessels, they are then reinforced by the VEGF-mediated chemotactic acquisition of pericytes (in the case of microvasculature; smooth muscle cells are instead recruited for larger vessels) on the abluminal surface of the endothelium, and deposition and remodelling of the extracellular matrix. Cell-cell contacts are tightened and quiescence is restored. Figure 1.2 below captures the overall process succinctly.

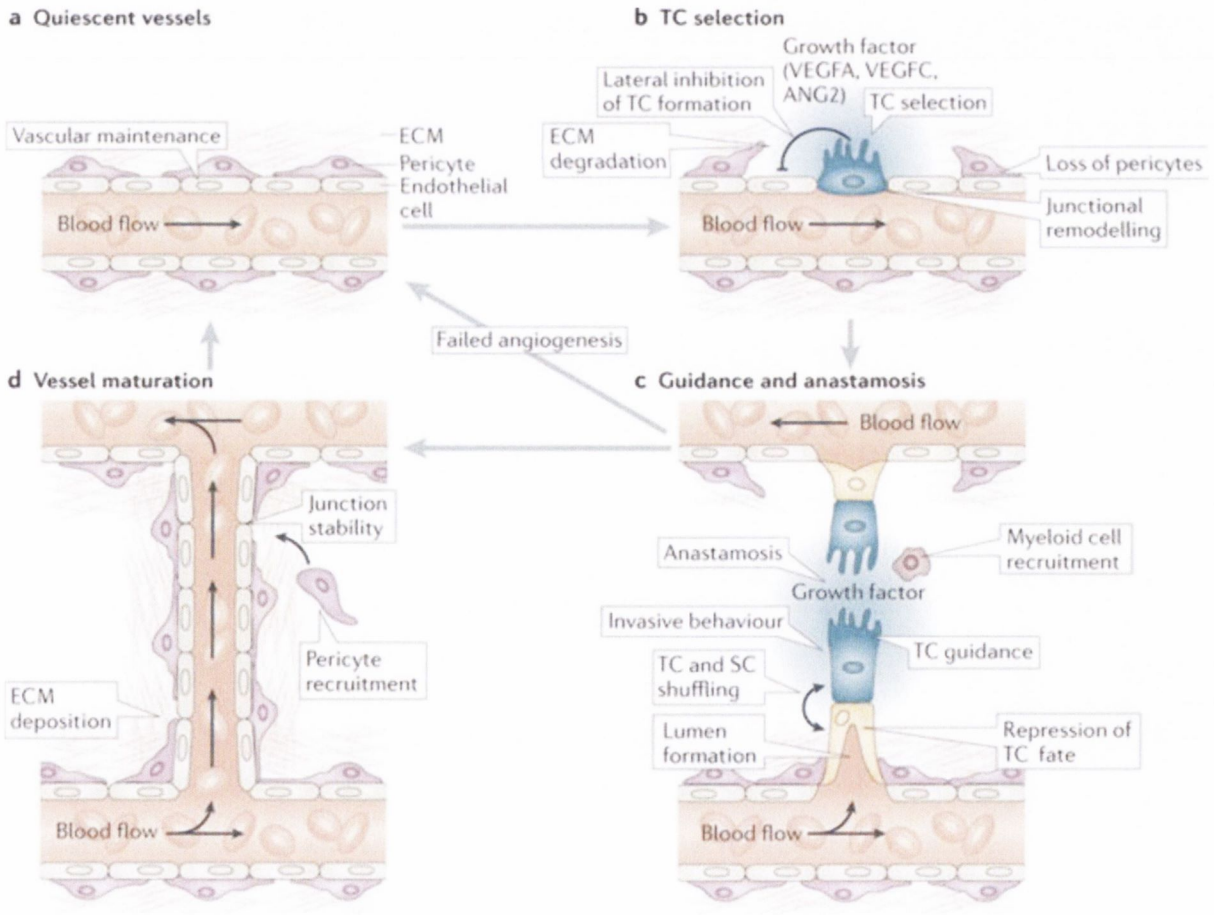


Figure 1.2. Mechanism of normal angiogenesis[25]

Although angiogenesis is prominent in wound healing processes and the ovarian cycle, normal adult vasculature is largely quiescent, kept in a state of dynamic equilibrium by pro and anti-angiogenic factors (Table 1.1), with a mere 0.01% of endothelial cells undergoing cell division at any instance[28]. Average turnover of adult capillary epithelial cells is in the region of 1000 days; in contrast to elsewhere in the body where it can take just 2-3 days to turnover highly regenerative cells like those of the gut epithelium[29].

1.2 Angiogenesis of tumours and their consequent vascular network

Tumour initiated angiogenesis however, is an altogether more rapid, cursory process; a consequence of an unbalanced secretion of cytokines, in particular the VEGFs[23, 30] and as a result several structural, morphological and behavioural differences in the subsequent vascular network exist. Firstly, whereas normal vasculature is neatly arranged in a hierarchy of evenly-spaced, well-differentiated tubular network of arteries, arterioles, capillaries, venules and veins, tumour vasculature is unevenly distributed, serpentine and chaotic[31] (Figures 1.3 and 1.4). As opposed to the dichotomous branching found in healthy vasculature, tumour blood vessels often go on to form trifurcations of irregular diameter[5, 32] and superfluous loops. Narrow vessels (20-40 μm diameter) frequently branch out from larger vessels (200 μm) leading to a skimming of plasma, and hence heterogeneous local haematocrit values in tumour blood flow are common[32]. Efferent venous convolutions are regularly found close to afferent vessels, and often the two may not even be fully discernable. Rarely are all accessible capillaries perfused continuously, what blood flow is present tends to be sluggish, and over the course of a matter of minutes the blood can follow different paths or even reverse direction through the same vessel[33].

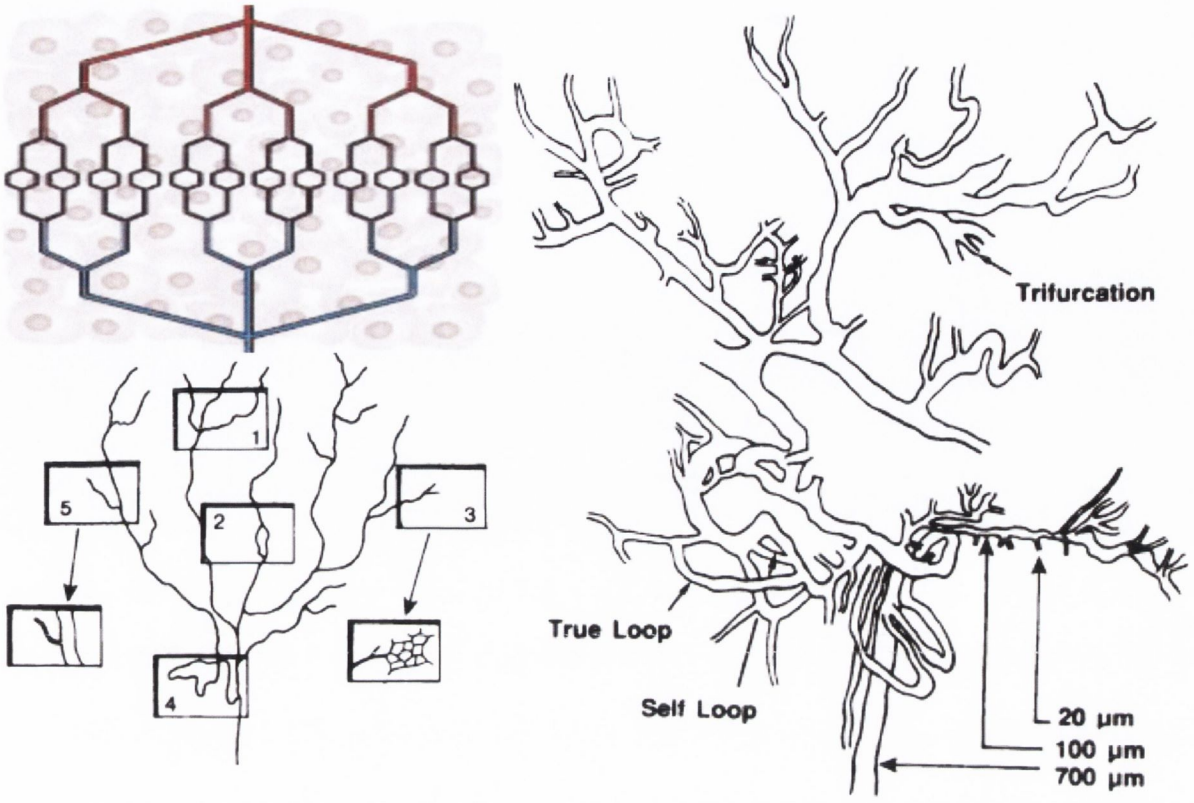


Figure 1.3. Normal vascular network[34] (top left). Basic outline of tumour network abnormalities[32] (bottom left and right) (1) trifurications, (2) self-loops, (3) polygonal capillary mesh, (4) venules proximal to feeding capillaries, (5) narrow branches from larger vessels[32]

The reasons behind these abnormalities come chiefly from the impairment of cellular signalling. Under normal angiogenic conditions, the host tissue influences the patterning of growing vessels by providing local chemotactic cues which control the branching, morphogenesis and co-patterning of the new blood vessels with nerves and arterio-venous shunts. Such an intricate elaboration of vessel pattern is not recapitulated from a neoplasmic mass; a malfunctioning heterogenous tumour could only ever provide disorganised cues and, macroscopically speaking, vascular networks differ between tumour to tumour. In addition to this, genetic mutations associated within cancerous cell malignancy surely trigger a gross imbalance in the level of tumour derived pro and anti-angiogenic factors. As a repercussion of this, tumour vascular density varies throughout different tumour regions, tending to be greatest in areas of active growth and proliferation[35]. Conversely, vasculature can be very limited or even absent in areas of necrosis. Indeed, the vascularity of a tumour can be used to gauge the aggressiveness of particular cancer growth[35-36].

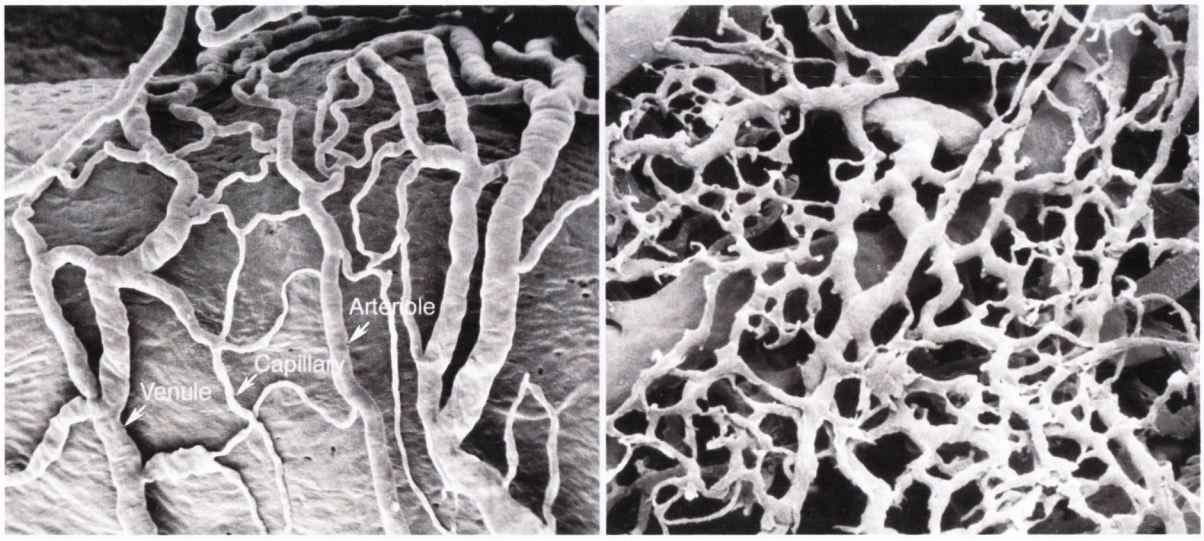


Figure 1.4. Comparison of vascular networks, normally (left) and in tumours (right) using microscopic imaging[5]

1.2.1 Structural abnormalities of tumour blood vessels

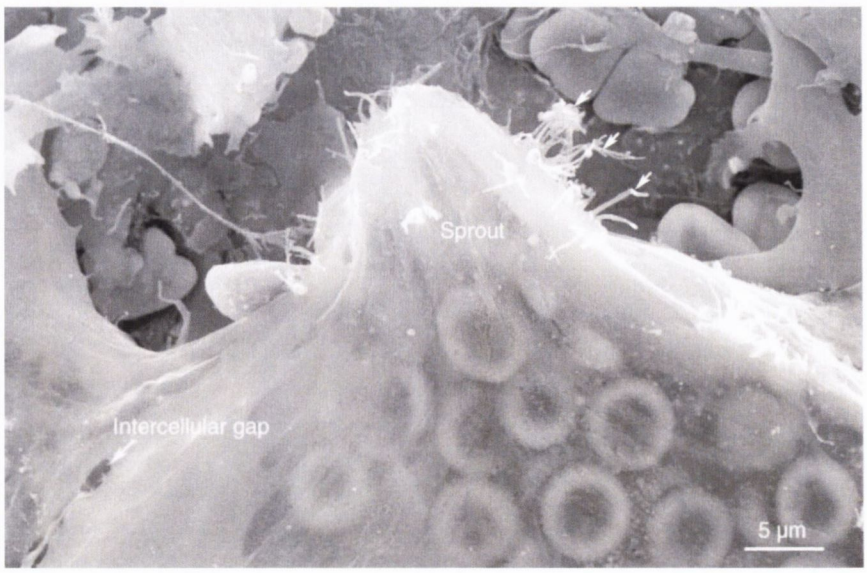
The same basic components that normally constitute healthy vasculature – the endothelium, pericytes and basement membrane – remain present in tumour vasculature, although crucial morphological aberrances exist extensively in each. Together, the results of these are poorly formed individual vessels which are attenuated, defective, fragile and leaky.

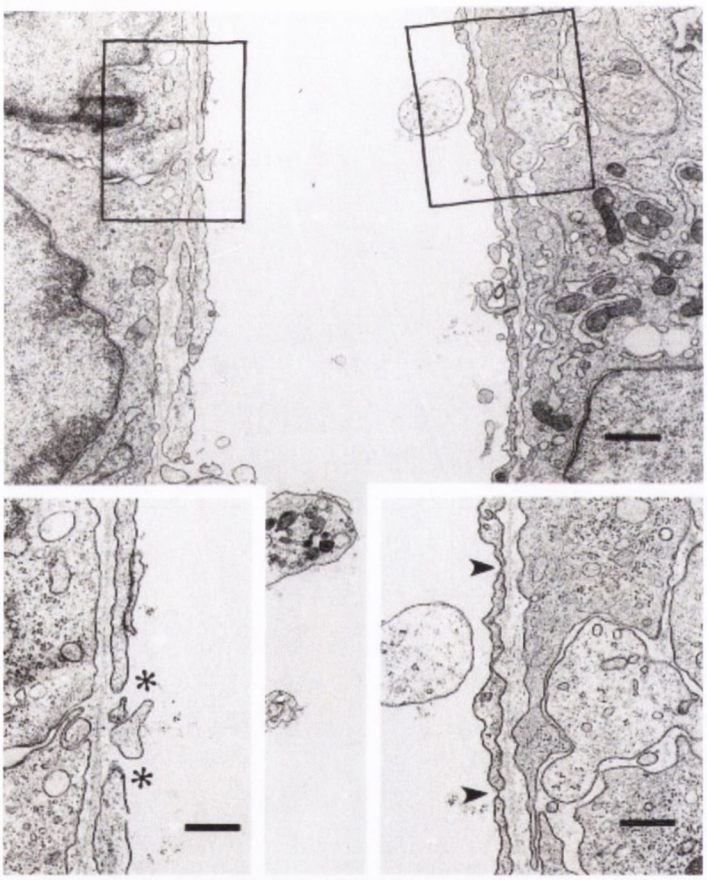
As the most prominent pro-angiogenic factor VEGF acts primarily on endothelial cells, it therefore comes as no surprise that the endothelium of nascent tumour blood vessels exhibit patent structural deviations from those of healthy vessels. Absent is the sturdy monolayer of tight endothelial cell junctions; instead a discontinuous cellular sheet with dispersed regions of either cell overlap or intercellular gaps is observed. The usually genetically stable endothelial cells, exposed to an uncontrolled source of VEGF, undergo altered gene expression and engage a proliferative phenotype, to such an extent that they eventually necessitate continued supply of VEGF in order to survive[37]. The cells also over-express a number of surface receptors, such as integrins and VEGF-receptors[38], although as of yet no receptor truly *unique* to the cancerous phenotype has been identified. Cells may often be individually thicker than usual, with more mitochondria, polysomes and a rough endoplasmic recticulum[6]; all indicative of proliferation. Extraneous luminal projections that bridge the vessel interior are common[4] (Figure 1.5 iii), like

remnants of failed or incomplete intususception[39]. Clusters of fused caveolae - flask shaped invaginations on the cell surface used as trafficking vesicles and signal transducers - widely expressed in the normal endothelium become progressively infrequent. It is hypothesised that these diminish during neovascularisation, as the two previously mentioned primary functions of caveolae are less pivotal during a period of hyperproliferation and cell migration, when vessels need fluidity and permeability[40].

The most important consequence of prolonged exposure to VEGF is undoubtedly this gross change in vessel permeability. Extravasation of plasma proteins and blood macromolecules encourages endothelial cell spouts and filopodia to migrate in the newly formed matrix. In addition to the intercellular gaps mentioned earlier (which can be some 60-300 nm in diameter), VEGF massively induces fenestrations across the lumen of the vasculature. Fenestrae are small pores in endothelial cells that allow for rapid exchange of molecules between sinusoid blood vessels and surrounding tissue, which normally may enlarge and contract at the action of various stimuli such as noradrenaline. A study from Roberts *et al.* showed that in four selected tumours they implanted (EMT\murine mammary tumour, MIS\murine rhadbomyosarcoma, U87\human glioblastoma and VEGF transfected CHO cell tumour), the neovessels formed had a remarkable increase in fenestrations (41%, 35%, 37% and 56% respectively) from the surrounding host skin and muscle vasculature (2% and 0% respectively)[41]. They also showed that these fenestrae have considerably less anionic charge (from glycocalyx on their luminal surface, which governs permaselectivity), that VEGF alone can induce fenestration, and that increased fenestration is found on the periphery of the vascular conduit while at the core of the vasculature intercellular gaps are more prevalent. It is strongly implied that these gaps could originate from fenestrae themselves. Later the same group

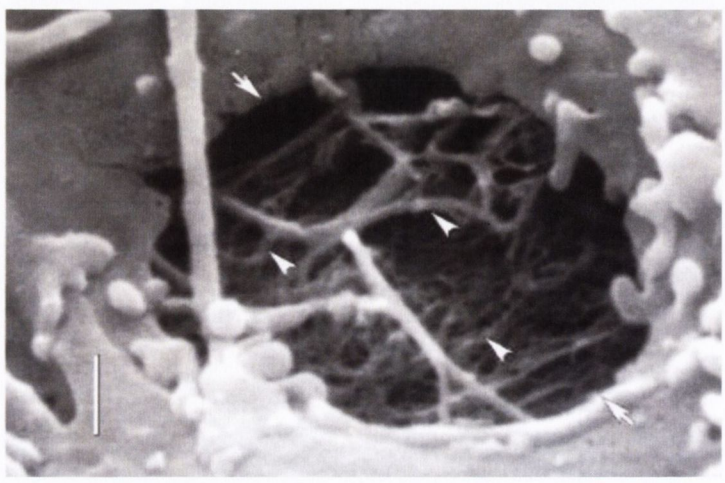
Figure 1.5. Characteristics of the endothelium in tumour vasculature illustrated by electron microscopy. Clockwise from top: (i) Abluminal sprout formation (arrows: filopodia); endothelium so thin individual blood cells are clearly identifiable[3]. (ii) Smooth, tight monolayer of a normal vessel[3] in contrast with (iii) unsystematic luminal surface of tumour vessel, showing extensive cell overlap (arrows: projections)[4]. (iv) Magnification of gap in endothelium showing underlying basement membrane filaments (arrowheads, scale bar: 0.5 μm)[5]. (v) Endothelial monolayer gaps (*) in comparison to fenestrations (arrowheads)[6].











demonstrated via a comparative study that identical tumours implanted intracerebrally bore neovessles with considerably less fenestrations and gaps than those implanted subcutaneously[6], illustrating that perhaps the VEGFs are not the only source of influence on tumour morphology; the surrounding environment must still maintain some jurisdiction.

The endothelium has an intimate association with Mural Cells (pericytes and smooth muscle cells), which play key roles in the stabilisation, maturation and remodelling of neovasculature, with ancillary contributions in the regulation of blood flow. They strictly regulate the numbers of endothelial cells in two apparently contradictory ways; mural cells promote endothelial cell survival[37] after VEGF withdrawal (indeed there is speculation that they secrete an almost private source of VEGF[42]) but on the other hand it has been shown that a lack of mural cells actually induces hyperplasia[43]. Pericytes in particular are enigmatic at the best of times; they are acquired through mesenchymal cells during vascular stabilisation, although this is not fully understood, their phenotype plasticity is hypersensitive to changes in environment, and although they express molecular marker proteins, none of these are unique nor consistent throughout, rendering pericytes difficult to track or characterise[44]. In tumours, pericytes become even more confusing; their affiliation to endothelial cells becomes much looser[45] and chaotically organised[46] (Figures 1.6 and 1.7), further diminishing the structural integrity of the vessels. It is widely reported that pericytes are lacking on much of the tumour vasculature[37, 47], although this has been challenged[48] with marker protein issues the probable cause for this discrepancy. Either way it is interesting to note that mice can survive with up to a 90% reduction in pericyte coverage[49], therefore only a low percentage threshold is really essential for adequate basal vasomotor function.

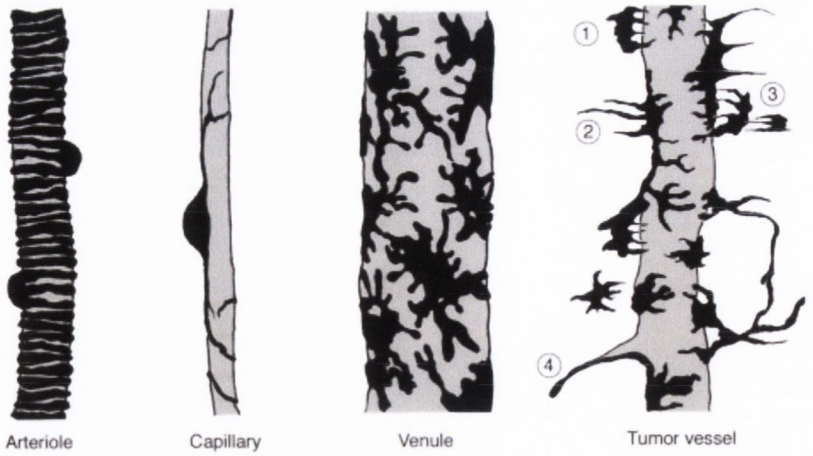


Figure 1.6. Schematic diagram of close pericyte (black) association with endothelium on normal vasculature (first three) compared with tumour vasculature (far right), which has (1) loose association, (2) outward projections, (3) pericyte overlap & (4) pericyte association on endothelial sprouts[48a]

As the adventitial mural cell layer expands over the endothelium longitudinally, the quality of pericyte-endothelial cell attachment is evidently governed predominantly by platelet-derived growth factor B (PDGFB) and its receptor (PDGFB-β)[50]. It seems to be not only the presence of this duo that is of significance, but also the manner in which they are presented to each other. The hypothesis is that an extracellular gradient of PDGFB guides would-be pericytes close to the endothelial cells, and that a 'retention motif' on the PDGFB binds to glycoproteins on the cell surface to help localise PDGFB near the endothelial cell surface. In tumours, it is possible that aberrant isoforms of PDGFB, its retention motif or its receptor are secreted or expressed, explaining both the unreliable mural cell investiture and the looseness of the connections present. Studies with transgenic mice that express altered PDGFB (minus the retention motif) support this theory[45]; the likelihood being that the growth factor is allowed to simply diffuse around the extracellular matrix.

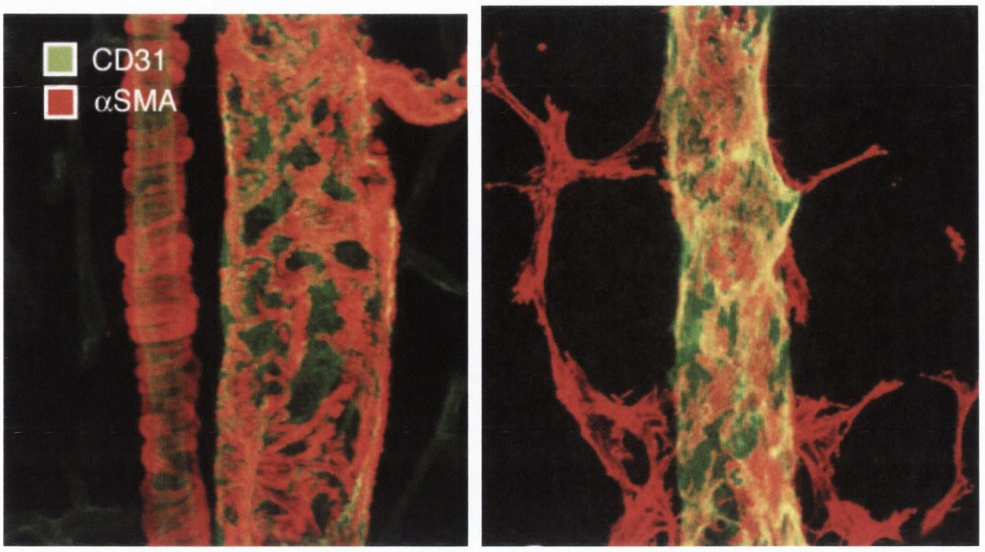


Figure 1.7. Pericyte arrangement on healthy vasculature (left, arteriole & venule) compared with ambiguous tumour blood vessel (right). CD31 containing endothelium stained green, smooth muscle actin containing pericytes stained red[48a].

Enveloping the pericyte-endothelial cell bundles is the dynamic basement membrane, an amorphous proteinaceous complex 50-100 nm thick. Distinct from the extracellular matrix in that it is always associated with cells, the basement membrane (also known as the basal lamina) regulates cell behaviour, segregates and compartmentalises tissues, and provides structural reinforcement[51]. In blood vessels it is present as a supramolecular crosslinked glycoprotein sheet that helps separate the stroma from the epithelium. The role of basement membrane in normal vasculature is an important one; defective basement membrane is heavily linked to diseases such as Alport Syndrome[52], Knoblach syndrome[53] and Goodpasture syndrome[54]. Up to 50 different proteins make up basement membrane, and the composition is unique to each tissue. 50% of this consists of the various isoforms of Type IV Collegen[54] (at least 7) and laminin (12 isoforms), with the latter serving as a focal point for the former to form a scaffold around[55]. As all of the necessary information for basement membrane formation is present inside the components themselves; it is considered that the basement membrane performs 'self assembly', directed by anchors such as integrins and dystroglycans on associated cell surfaces[55].

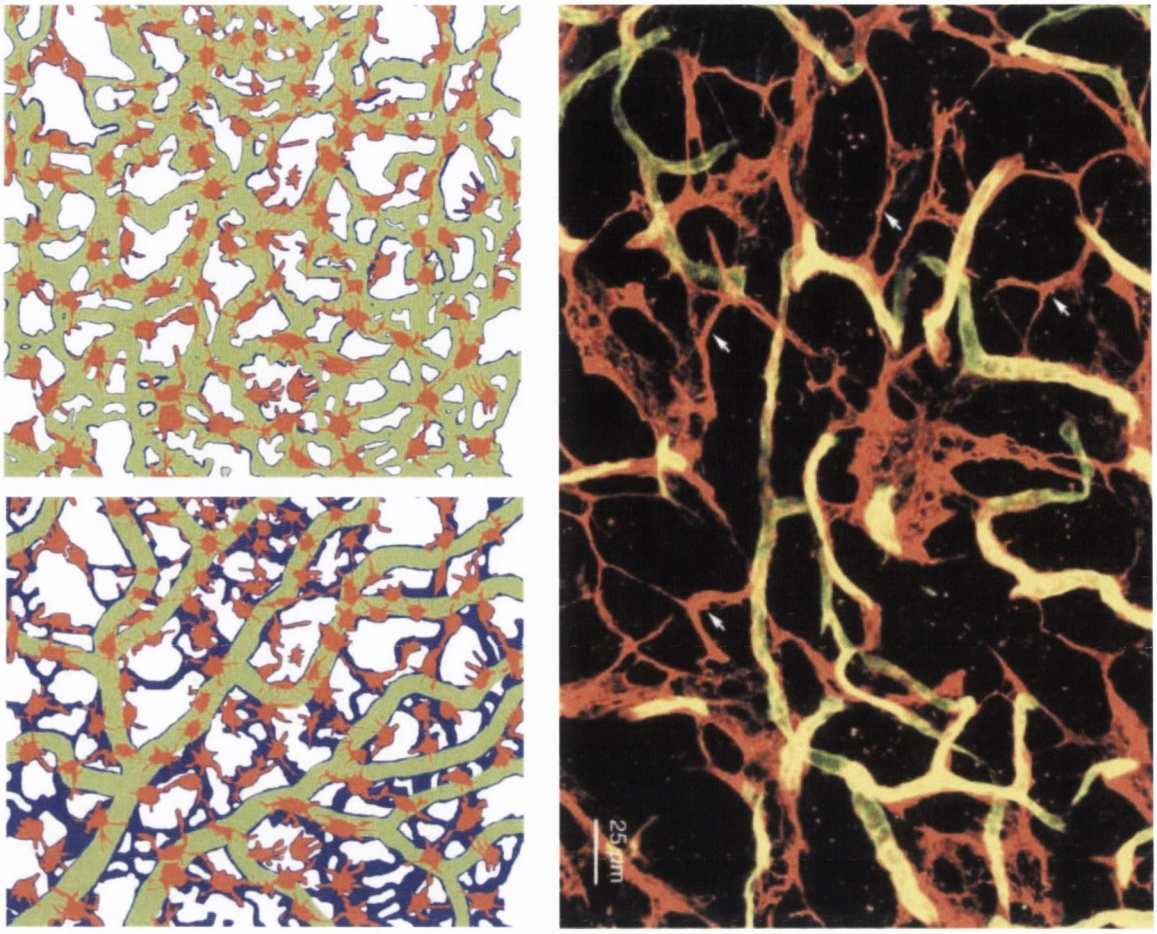


Figure 1.8. Tumour blood vessels; before (top left), and after (bottom left and right) anti-VEGF treatment. After endothelium (left: green, right: yellow) regression, empty basement membrane 'sleeves' (left: blue, right: red, also arrows) persevere.

In tumours, endothelial cells and pericytes generate a defective basement membrane[3]. As was the case with pericytes it was reported to be absent or lacking[56], but again these claims have been refuted[57]. Abnormalities are definitely present however, with basement membrane on tumour vasculature, having a very loose association with endothelial cells, forming multiple redundant layers of uneven thickness, often with broad protrusions into the stroma (5-61 μm) and focal holes throughout[57a]. Tumour-derived basement membrane possesses much less crosslinkages, rendering it more susceptible to proteolysis and higher turnover[55]. With regard to angiogenesis, degradation of the basement membrane promotes endothelial cell proliferation and sprouting through its resulting provisional matrix, and during degradation many important positive or negative regulatory angiogenic factors are released from the collegen and laminin in the membrane itself. Endostatin, tumstatin, arrestin and canstatin are examples of endogenous inhibitors of angiogenesis that come from fragments of collagen broken down by matrix

metalloproteinases[55]. Perhaps of most importance from an angiogenic point of view is that after VEGF inhibition and subsequent vessel regression in tumours, basement membrane largely remains intact, in the form of empty 'sleeves'[3, 58]. These persistent sleeves (Figure 1.8) form the framework around which blood vessels could quickly repopulate after VEGF inhibition ceases.

1.2.2 Classes of tumour blood vessels

Despite the seemingly anarchic and erratic organisation of tumour vasculature relative to their normal endogenous equivalents, blood vessels associated with cancer can nevertheless be broken down and categorised in to no less than six distinct groups[31, 59] (a-f). The first kind (a) 'Mother Vessels' (MVs), are the earliest to form in response to VEGF (after around 18 hours, peaking after 5 days) and from these classes (b-d) of tumour blood vessels evolve by angiogenesis, themselves regarded as 'daughter vessels'[60]. Mother vessels (Figure 1.9) are highly permeable sinusoids which develop from pre-existing adult venules and capillaries but are maintained only as long as high concentrations of exogenous VEGF are present. Nascent Mother Vessels have lumens 3-5 times larger than the host vessel they were derived from[60]. As vessel expansion is restricted to at most 30% increase in area[61] due to constrictive collagenous extracellular matrix, non-elastic basement membrane and rigid pericyte support; it is clear degradative processes must be taking place. VEGF sparks extravasation of plasma proteins which alleviate the collagenous ECM, as well as activation of the proteinase cathepsin, which digests collagen IV and laminin in the basement membrane[62]. These processes, along with a shedding of pericytes confer the necessary flexibility for endothelial cells to stretch out, enabling vessel expansion by centripetal vascular pressure. MVs in particular exhibit very stereotypical features of tumour vasculature we have previously described; thin walls, lazy blood flow, lack of pericytes and impaired basement membrane scaffolding etc. Nuclei of endothelial cells have a tendency to protrude into the lumen, hence the interior is warped and blood flow is compromised and turbulent[63]. These characteristics make MVs very vulnerable to thrombosis and collapse; hence tend to be transitory structures that mature into more stable daughter vessels.



Figure 1.9 Left - Larger mother vessels growing from smaller venules. Right – tangles of GMPs (arrows) which originated from surrounding mother vessels[23].

Another type, (b), glomeruloid microvascular proliferations (GMPs, so called as they resemble renal glomeruli macroscopically) are disorganised tangles of tiny vessels immersed in a complex mixture of irregular ordered pericytes and extensive basement membrane that form from MVs[30, 60]. They often originate as focal accumulations of large endothelial cells on the wall of MVs, before repopulating into the lumen and/or outwards into the extracellular matrix where they then recruit pericytes. This clustered proliferation forces GMPs to have narrow tubular cavities which like MVs are hyperpermeable and equally require a constant VEGF supply for maintenance. Capillaries (c) are not quite hyperpermeable, though smaller and functionally similar to normal host capillaries. They form as endothelial cell projections (or 'processes') transverse the lumen of MVs forming bridges which divide and compartmentalise the interior into smaller channels[23, 64]. Over time, these fused channels separate via intussusception into fully fledged individual capillary vessels (see Figure 10). This process is not fully understood, and although first observed in tumour vasculature is known to occur in healthy wound healing[65] and exercised skeletal muscle tissue[66]. Often GMPs will also spawn from MVs in this fashion, and furthermore GMPs can themselves likewise devolve into capillaries over time[62].

While MVs ultimately shrink in diameter as they mature into GMPs and capillaries, they can also retain their incongruous size in the formation of vascular malformations. Vascular malformations (d, VMs), acquire a thin asymmetrical smooth muscle cell coat, which affords the necessary backbone for vessels of this unusually large size to sustain themselves indefinitely in ectopic position. Unlike the classes already discussed, once formed VMs are *not* permeable to plasma proteins[31] and do not require an ongoing exogenous supply of VEGF to survive[60], thus

may persist for months at a time. However, it is likely although not proven, that a paracrine supply of VEGF may be administered via closely associated mural cells.

Feeder arteries (e) and draining veins (f) form not via angiogenesis, but by a distinct parallel process termed 'arterio-venogenesis'[62]. Little is known mechanistically about this method of vessel formation (Figure 1.10), just that existing arteries and veins are co-opted, pruned and remodelled extensively. The resulting bodies of feeder arteries and draining veins are greatly enlarged (larger than MV and VMs), tortuous blood vessels that furnish and drain the microvascular conduit respectively. As they expand radially, it is salient to note that unlike MVs and VMs, which stretch endothelial cells as they grow, feeder arteries and draining veins proliferate fresh endothelial cells and attach mural cells accordingly[59]. Though generally fewer in number than the other classes of vessel mentioned, they are important as they are based upstream and downstream, thus service the tumour, its zones of angiogenesis and the rest of the core vascular network. These blood vessels, along with capillaries and VMs, similarly do not require a continuous high source of exogenous VEGF and persist indefinitely, a significance that will be addressed later.

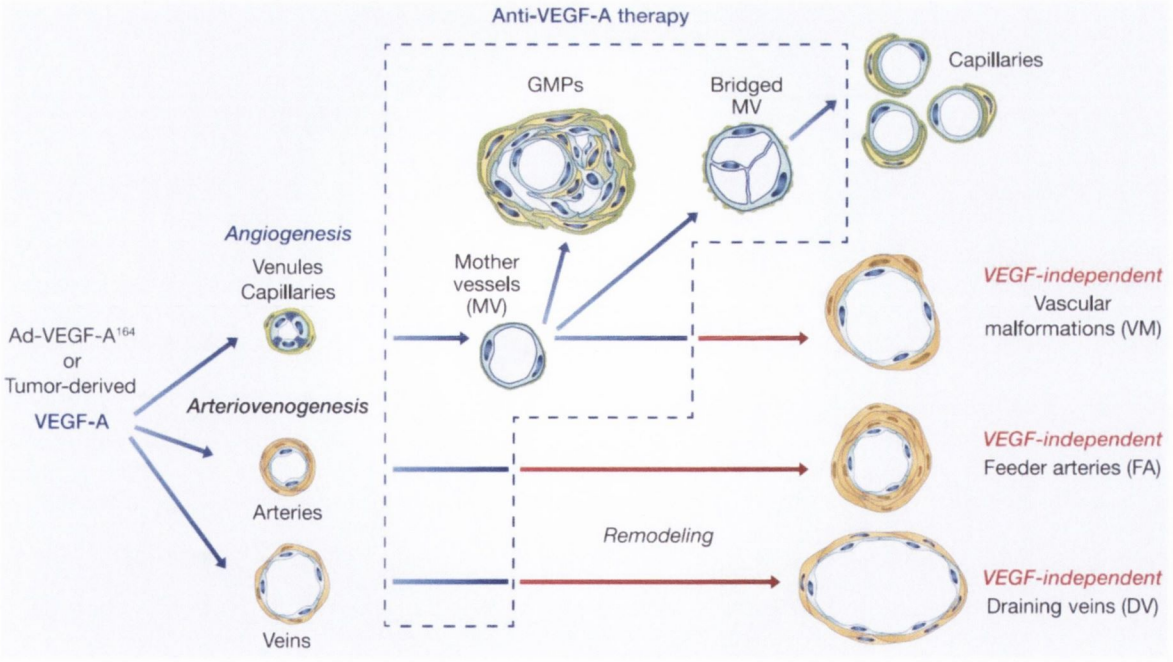


Figure 1.10 Representation of different classes of tumour blood vessels in response to VEGF by angiogenesis or arteriovenogenesis [59]. (Endothelial cells - blue (nuclei – navy), membrane – green, pericytes – yellow, smooth muscle cells – orange)

1.3 Targeting Angiogenesis and Tumour Vasculature

There are many reasons why the tumour vasculature and the process of angiogenesis make excellent targets for new therapies. Firstly, the unrefined, almost flimsy nature of tumour vasculature we have just discussed means they are more susceptible to damage by chemotherapeutic agents, and due to the multitude of differences between themselves and normal adult vasculature a degree of specificity should be achievable, thus avoiding a broad spectrum of adverse effects. Theoretically, the histological nature of the cancer itself would be largely irrelevant; all solid-state tumours which initiate angiogenesis and depend on it for survival should be equally prone to its antagonistic treatment. Only during certain physiological conditions, such as healing and the reproductive cycle, does angiogenesis naturally take place, so to focus on the process itself should not have any detrimental consequence to the rest of the body. Another promising fact is that endothelial cells of blood vessels themselves have long lifetimes and are quite genetically stable, therefore it is less likely that drug resistance via genetic mutation will develop over time[67]; a primary reason why so often novel drug schemes have ended in failure. Accrued vasculature brought about by the angiogenic phenotype is in constant direct contact with the blood supply, promising intrinsic accessibility in terms of drugs being readily able to reach their destination with minimal physiological interference. Finally, as a relatively small number of endothelial cells govern a vascular system which caters for an exponentially larger number of recipient cells, targeting only these select few could in turn cascade into emphatic necrosis of all proximate tumour cells (100-150 μm[68]).

The hypothesis for targeting the dependency that tumours have for vasculature systems was first put forward by Folkman circa 1971[21]. Over four decades have since passed, with over 17,000 papers published (as of 2008[34]), yet there is a feeling that we are still only at the embryonic stages of anti-angiogenic research; too few of these have been widely implemented clinically. There are two distinct yet reciprocal sides to the antiangiogenic coin, which although interrelated should be considered independently, each on its own merits[69]. Strictly speaking, the *anti-angiogenic* perspective is concerned solely with the 'modus operandi' whereby vascularisation is established; the how and the why. On the flipside, the *anti-vascular* perspective involves the selective destruction of the newly formed tumour vessel network, after the fact, and aims to preclude any nascent sprouts from becoming established. More often a drug in this field will exhibit elements of both, although to vastly differing degrees.

1.3.1 Anti-Angiogenic Therapy

Anti-angiogenic therapies have been the more extensively investigated, with some success. The bulk of the research in this field so far has been addressing VEGF, its receptors or its consequent signalling pathways. Much has been detailed about VEGF since its isolation in 1989[70]: it exists as one of seven glycoprotein isomers, VEGF-A, VEGF-B, VEGF-C, VEGF-D, VEGF-E and PlGF (placental growth factor) 1 & 2, all differing in their binding affinities for heparin, which affects their bioavailability[71]. As the name implies, their primary focus lies with endothelial cells and their growth, over multiple stages, but other roles for VEGFs have been confirmed; trophic for cardiac muscle fibres[72], lung epithelial cells[73] and neurons[74]. VEGFs bind to VEGF-receptors, of which there are three, VEGFR-1, VEGFR-2 and VEGFR-3, and the binding affinity of each ligand differs for each receptor (Figure 1.11). Co-receptors such as neuropilins (NP1 & NP2), and heparan sulphate proteoglycans (HSPGs) activate these receptors and increase binding affinity even more[75]. While VEGFR-1 (both pro and antiangiogenesis; VEGF-A, B, PlGF[76]) and VEGFR-3 (lymphangiogenesis; via VEGF-C, D[27]) both have relevant angiogenic character in their own right, it is VEGFR-2 which plays the most influential role in gross tumour angiogenesis. Although VEGF-A actually binds to VEGFR-1 with 10 fold higher binding affinity, it is when affixed to VEGFR-2 that it exerts much more powerful signalling capability toward a proliferative and migratory endothelial response[77]. Unsurprisingly, the VEGF-A\VEGFR-2 axis has ergo become the focal point for purely anti-angiogenic therapy.

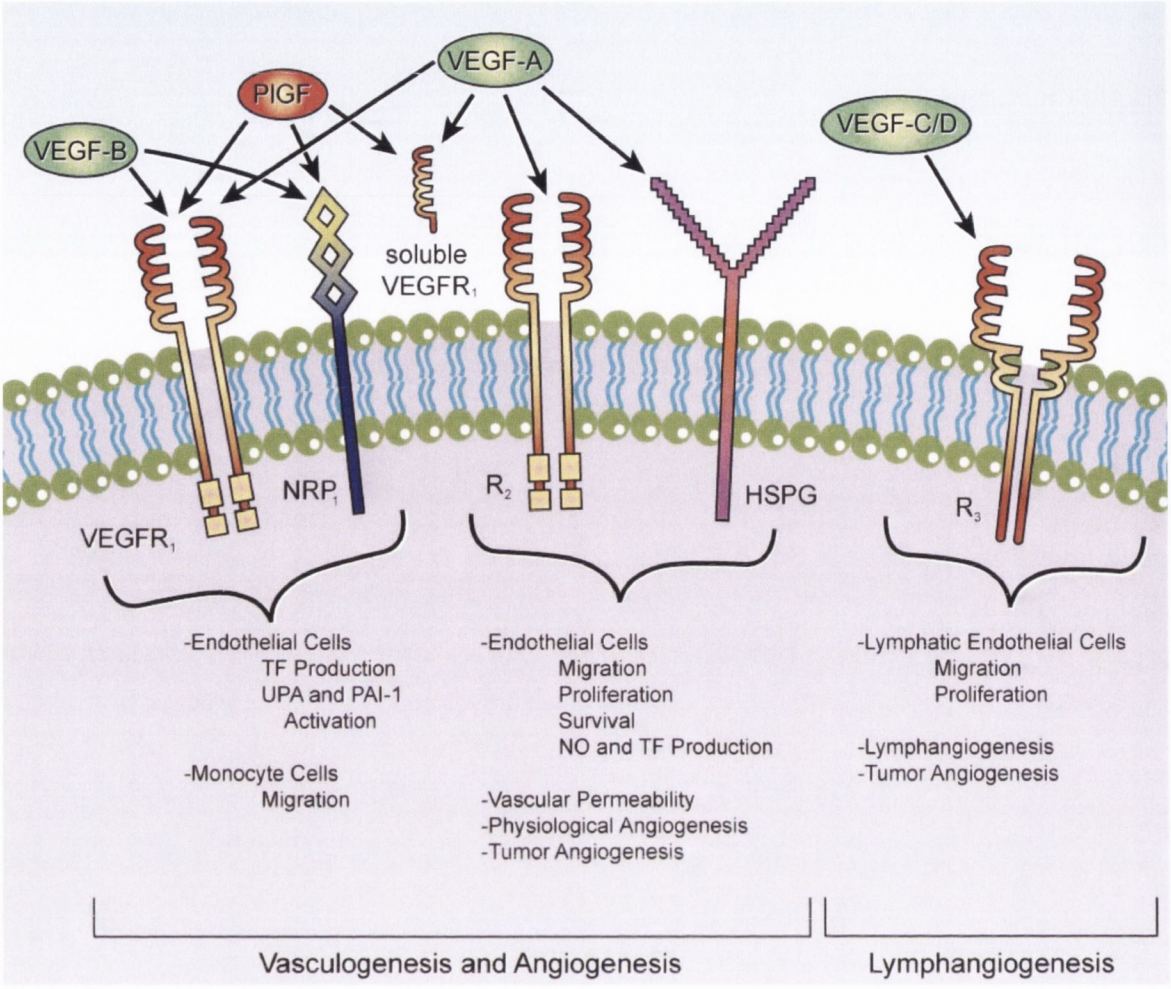


Figure 1.11. Overview of the VEGFs and their receptors[78]

One such VEGF-A\VEGFR-2 based agent is Bevacizumab (Avastin); once considered the big success story of anti-angiogenic treatment. Bevacizumab is a humanised monoclonal antibody which sequesters circulating VEGF-A, preventing VEGFR-2 binding, and in February 2004 became the first approved anti-angiogenic to be FDA approved for metastatic colorectal cancer; and later metastatic renal, lung and glioblastoma multiforme cancers. The drug itself is reasonably well tolerated toxicologically; hypertension, proteinuria, bleeding and occasional gastrointestinal perfusions amongst the side effects[79], although just how serious these are considered to be is subjective, with opinion differing throughout the literature. A testimony to its accomplishment is that it was the most claimed anti-cancer drug from VHI for the year 2008[12], at a cumulative cost of almost €5.5 million. However, the initial verve upon its release has since been quelled somewhat in recent years as various limitations became apparent. Firstly, bevacizumab has never shown any significant activity as a single agent; all observable benefits came as a result of

use in combination with already established chemotherapeutics (i.e. Taxol, 5-fluorouracil etc)[80]. Next, the progression free survival is transient and the overall survival is only ever a few months for each cancer type[80]. Bevacizumab is also expensive, with treatment costing at least £21,000 per patient. Bevacizumab had once been given FDA approval for breast cancer, but this was soon revoked in November 2011, after four separate clinical trials demonstrated results too modest to compensate for the health risk involved. It has been approximated in the States that the cost per year of progression free survival in metastatic breast cancer was $204,000 with an incremental cost effectiveness ratio of $745,000 per quality adjusted life year (QALY), well above the willingness to pay threshold of $150,000 per QALY[80-81]. It nevertheless remains available for 'compassionate use' under oncologists' discretion. Another monoclonal antibody which binds VEGF is Ranibizumab (Leucentis), which is derived from the same parent antibody as bevacizumab, although so far is only used to treat ophthalmic diseases such as wet macular degeneration rather than for anti-cancer purposes.

A similar type of drug is Aflibercept (VEGF-trap, Ziv-aflibercept, Zaltrap). Aflibercept consists of fused sections of the binding domains of VEGFR-1, VEGFR-2 and human IgG1 to form a soluble receptor replica that selectively binds itself 1:1 with VEGF-A, VEGF-B or PlGF, preventing them from docking to their endogenous receptors, including VEGFR-2[59, 82]. The binding affinity of VEGF-A to aflibercept is 9 and 181 fold higher than endogenous receptors VEGFR-1 and VEGFR-2 respectively[83]. It too has been FDA approved for use in combination (5-fluorouracil, leucovorin & irinotecan) since 2012 for metastatic colorectal cancer and future performance will be monitored with keen interest.

Aside from VEGF sequestration, an alternative anti-angiogenic strategy is direct inhibition of the VEGF receptors. Sorafenib (Nexavar) is one of several small molecule Tyrosine Kinase Inhibitors (TKIs) to fare well in phase III trials, and has even attained FDA approval. Sorafenib and other TKIs of this ilk are selective but not specific; multi-targeted to several different tyrosine kinases, thus interrupting several different pro-angiogenic signalling pathways, although these do include the crucial VEGFR-2 and VEGFR-3 receptors[84]. While some of the other kinase receptors susceptible to inhibition can have a synergistic antiangiogenic effect, there is also the corresponding risk of new, unexpected side effects. Small molecule TKIs tend to penetrate the vascular barrier more effectively than larger antibodies, to bind competitively to the ATP binding

pockets of the receptors. These are often not considered true anti-angiogenics as they have demonstrated some action on tumour cells directly in preclinical trials, in addition to their role on the vasculature. Sorafenib was shown to prolong lifetimes for 2.8 months compared to placebo[85] as a single agent and is also used in combination therapy for renal cell carcinoma and hepatocellular carcinoma. Sunitinib (Sutent), another TKI, targets all three VEGFRs amongst others. It has been approved for renal cell carcinoma and patients with gastrointestinal stromal tumours which are resistant or intolerant of the TKI imatinib (Gleevec, non-angiogenic); offering up to 6 months progression free survival as a single agent for both cancer types over the controls in clinical trials[84]. Pazopanib (Votrient) a TKI of VEGFR-1-3, which is FDA approved for renal cell carcinoma and soft tissue carcinoma, offered 5 months progression free survival[86]. Cediranib (Recentin) is a TKI currently in development for glioblastoma multiforme, although earlier investigations for use against non-small cell lung cancer failed[84]. Vandetanib (Caprelsa), which targets VEGFR-2, had similar unsuccessful clinical trials regarding non-small cell lung cancer, but was ultimately FDA approved for patients with unresectable advanced metastatic medullary thyroid cancer. Axitinib (Inlyta), active on VEGFR-1-3[87], was initially tried with pancreatic cancer with no observable benefit, but has since been used in treatment of metastatic renal cell carcinoma, with even better results than sorafenib[88], and hence was granted FDA approval in 2012. Other VEGFR based TKIs include motesanib[89], linifanib[90], vatalanib[91] and brivanib[92] although no significant breakthroughs have been determined yet.

Besides VEGF binding and tyrosine kinase inhibition, other methods of inducing an anti-angiogenic response exist. Some mTor inhibitors (mammalian target of rapamycin) like temsirolimus (Torisel) and everolimus (Afinitor) indirectly interfere with VEGF synthesis through hypoxia inducible factor (HIF) signalling depression and were FDA approved for renal cancers[93]. The controversial drug thalidomide (Thalomid) and its analogues have shown potent anti-angiogenic activity[94], but the exact mechanism remains contested. Angiozyme, a ribozyme, is used to cleave the mRNA associated with the assembly of VEGFR-1-2[95]. Natural peptide inhibitors (eg endostatin, angiostatin) and matrix metalloproteinase inhibitors are also being assessed[96].

Regardless of the progress made, it is becoming more and more apparent that the anti-angiogenic approach has been somewhat underwhelming; the great anticipated therapeutic

gains discussed previously have simply not materialised. To start with, performance of each antiangiogenic agent did vary with different tumour types, opposing the assumption that tumour origin would be irrelevant. Secondly, while many agents fared very well in earlier trials on mice these did not translate very well to human patients. Explanations for this have been postulated: cancer patient are older and sicker with tumours that took months to develop, while mice tend to be young and healthy with tumours induced within days or weeks. Furthermore, mice cannot communicate their complaints regarding the more subtle side-effects or perhaps just are not as prone to major adverse reactions. Next, while some agents did successfully suspend tumour growth for a period of time, very few cases demonstrated worthy tumour regression. Alluding to earlier in the chapter, this can be attributed to the fact that only certain subsets of the tumour vasculature, MVs and GMPs, are fully dependent on constant VEGF supply; others are more mature and robust, VEGF independent or indulged by a juxtacrine reserve.

Even still, bigger problems compromise anti-angiogenic therapy. A body of research is suggesting that diminishing the impact on VEGF signalling in any way eventually causes up-regulation of compensatory pro-angiogenic growth factors (PlGFs, FGFs, ephrins etc)[77a, 97]. Concurrently, other collaborative mechanisms take place to boost this type of 'evasive resistance' (distinct from genetic mutation based resistance)[98]. Hypoxia triggers the recruitment of bone marrow derived cells (BMDCs) which contain vascular progenitors which obviate the need for VEGF to continue angiogenesis. Pericyte coverage can also increase to reinforce vessel stability and keep endothelial cells alive, while invasion and co-option of existing vessels in vasculature-rich areas (i.e. liver, lung & brain) further detracts VEGF necessity. As the antiangiogenic agents remain active on their receptors and pathways, this type of resistance negates their overall benefit to an immeasurable degree. For this reason, the discovery of compelling 'biomarkers' of angiogenesis, or the inhibition thereof, remains one of the most important objectives in anti-cancer research; to enable determination of both tumour and vasculature progression, with scope for validation and evaluation of its subsequent therapeutics[99].

An interesting observation from anti-VEGF therapies was that of 'normalisation'. Although tumour vasculature is characterised by much higher vessel density, this does not correspond to ample, uniform blood flow to all tumour regions due to vessel permeability and desultory network macro-organisation. The phenomenon of normalisation involves the pruning and

remodelling of these erroneous tumour vessels, rendering them less permeable, tortuous and dilated; instead more coordinated, stable and with better support[100]. During this 'normalisation window' (Figure 1.12), redundant or unperfused vessels regress and angiogenesis is arrested, bereft of VEGF. This greatly improves blood flow throughout the prevailing vascular conduit[101]. This presents an apparent paradox; is anti-VEGF therapy now provascular rather than antivascular? The rationale is that these concepts are contextually interchangeable; improving the efficiency of blood flow increases oxygen supply, which in turn satiates the hypoxia which is considered the main driving force behind angiogenesis and tumour progression. Oxygenated cells are much less resistant to radiotherapy than hypoxic cells, which can need a dose three times stronger to eradicate a population of analogous size[102]. In addition, improving perfusion also means more competent delivery of a cytotoxic agent, while increased oxygen supply affords a higher concentration of reactive oxygen species that can be generated via radiotherapy. As anti-angiogenics have really only shown their most potent activity in combination treatment this is a pertinent consideration. Furthermore, the more integrity maintained by tumour blood vessels the less likely cancerous cells will shed into the systemic circulation. With these points in mind, normalisation presents an opportune behavioural vulnerability which can be exploited for clinical benefit when appropriate. Other groups have gone even further with the vascular modulation theme, beyond simple feed/starve tactics, and formulated 'redistributive' strategies, inducing regional hemodynamic changes in the microvasculature, whereby blood flow is 'gerrymandered' through differing vascular zones without affecting overall net tumour blood supply[103]. Agents like this (eg RRx-001), donate smooth muscle actin (SMA) mediator nitric oxide molecules in a concentration and time dependent manner to selectively close mature, pericyte rich tumour vessels, and open nascent, pericyte deficient vessels to influence change in blood perfusion, and hence distribution of hypoxia.

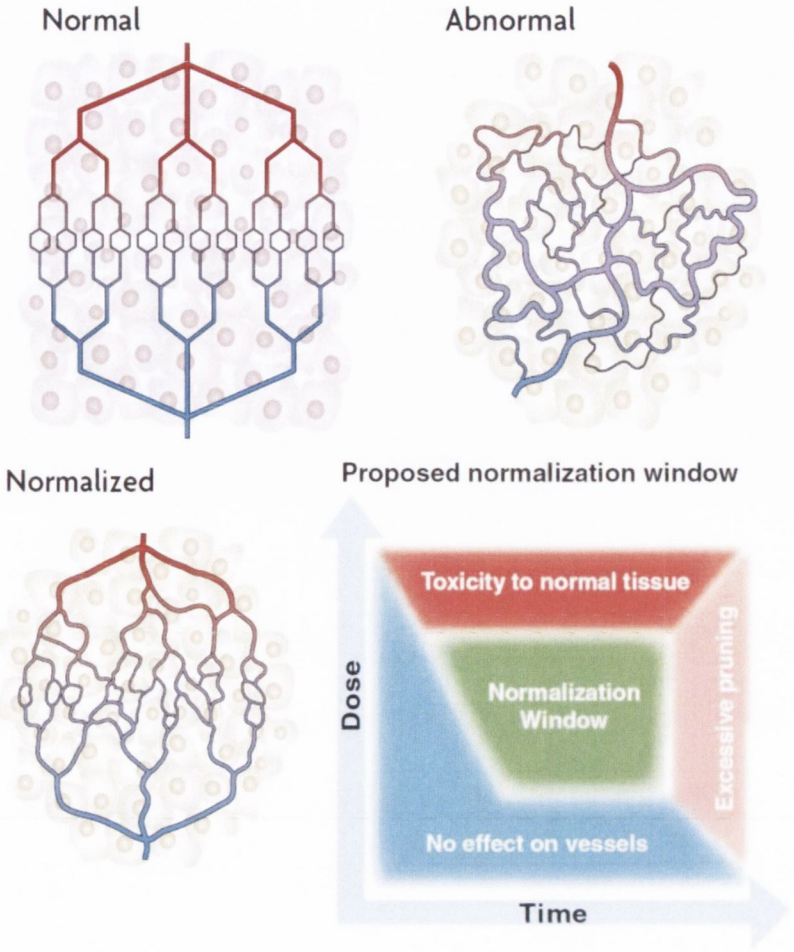


Figure 1.12. Tumour vasculature 'normalisation'[34] and the 'normalisation window'[100]

1.3.2 Anti-Vascular Therapy

Normal blood vessels and the CNS also require VEGF in some capacity for essential maintenance and without a certain level they can be severely compromised (Figure 1.13)[104]. In addition to this anti-VEGF approaches only target those classes of vessels vulnerable to environments of lower VEGF concentration; MVs and GMPs are likely to be affected but the other four kinds are not susceptible and can therefore survive indefinitely, hence they are as such impervious to this treatment. Tumours tend to be detectable quite late during the course of their development, so by the time a potential patient is ready for anti-VEGF chemotherapy, early stage blood vessels like MVs and GMPs account for only a modest percentage of total tumour vasculature. Feeding arteries and draining veins in particular would be far more effective targets as ultimately they communicate with all the smaller angiogenic vessels enclosed within the actual tumour mass.

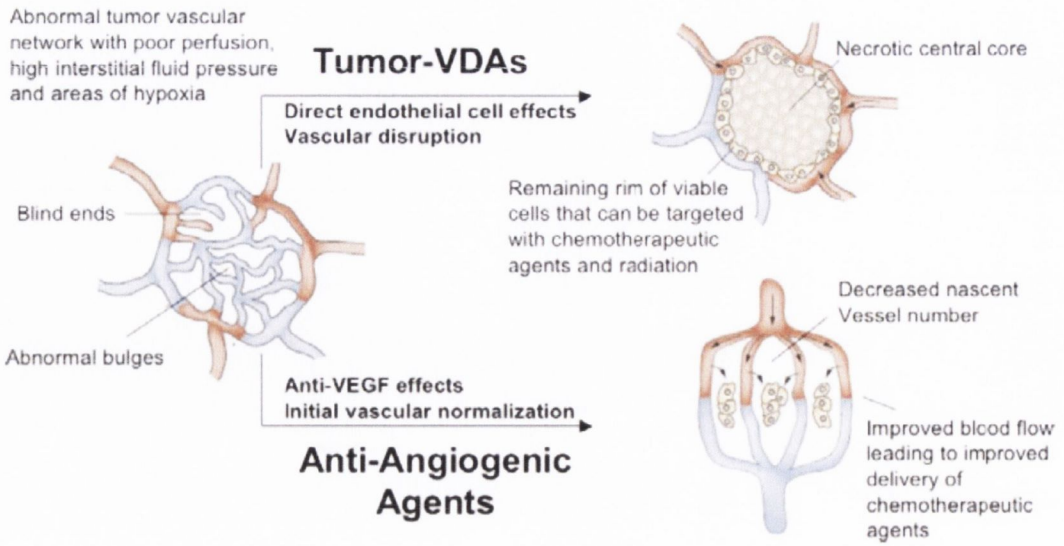


Figure 1.13. Divergent characteristics of anti-vascular and anti-angiogenic therapy[105]

Our approach is somewhat different from that of bevacizumab and the other anti-angiogenics, focusing instead on the existing tumour blood vessels: the anti-vascular approach. This facet of angiogenic therapy aims to selectively cripple the unique acquired vascular network, usually by some form of embolisation. This leads to direct apoptosis of nearby cancer cells through deprivation, and with cancerous tissue arranging itself into tightly packed cords (up to 610 cell layers per vessel[102a] compared with 1-2 layers normally) the response can be pronounced with thousands of cells affected from the closure of a single vessel. The contrast between agents that act in this way, termed vascular disrupting agents (VDAs), and the anti-angiogenics is quite stark. VDAs are administered acutely, with necrosis observed almost immediately, whereas protracted exposure typifies anti-angiogenic therapy, generally with a more cytostatic effect. VDAs favour necrosis in the central areas of larger tumour masses[106]; anti-angiogenics have greater repercussion around the periphery, where fledgling vessels are more often found.

1.3.2.1 Tubulin and Microtubule based VDAs

Despite the encouraging properties of VDAs, they have been investigated to a much lesser degree than their anti-angiogenic relatives. The majority of the work that has been done in this area has focused on the globular protein tubulin. Tubulin is present as either one of two different subunits, α and β (Figure 1.14), although in truth these are actually quite similar to

each other. α and β combine non-covalently to form tubulin heterodimers, which themselves bind one molecule of GTP to each subunit, which in turn allows them to bind with other tubulin αβ heterodimers at opposite ends[107]. Helical arrangement of alternating tubulin subunits through fusion of heterodimers form hollow, cylindrical structures called microtubules, typically 13 protofilaments in circumference, 25-30 nm in diameter and can be up to 25 microns in length[108]. Continuous association and dissociation of tubulin heterodimers along the protofilaments mean microtubules are highly dynamic, although the rate of polymerisation is ultimately dependent on the particular phase of the cell cycle[109].

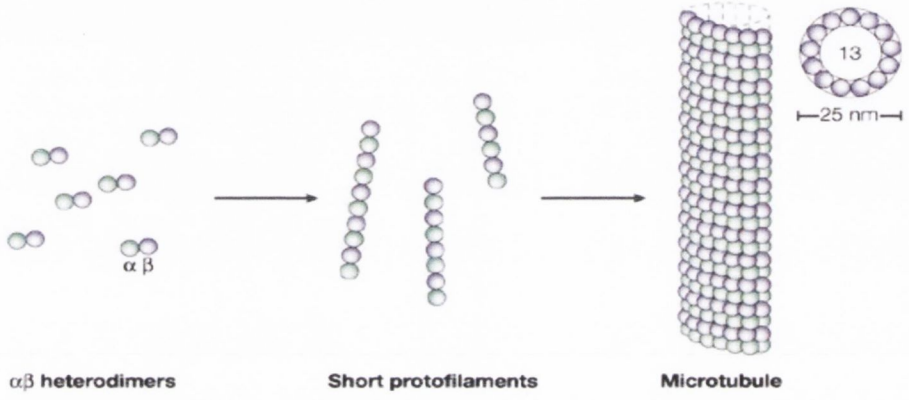


Figure 1.14. Basic structural components and form of a microtubule[110]

The functions of microtubules are diverse. As long, rigid and polar structures they are key players in the cytoskeleton, involved in the maintenance of cell shape and integrity. They are heavily involved in mitosis and cell division, forming an oval shaped mitotic spindle in which they also help move and segregate daughter chromatids. Microtubules can self arrange into axenomes, consisting of a ring of nine pairs surrounding two singlets, which form the basis of cilia and flagella on cells which require them for motility. The motor protein dynein binds to these axenomes, causing the appendages to bend, and upon its release causes a whipping motion back to a straightened form; a movement that when synchronised across the cell membrane causes cellular propulsion[110-111]. Another function of microtubules is that they form the platform for the motor protein kinesin to direct cellular transport[111]. Powered by ATP, kinesin travels along the microtubule track carrying cellular components (such as organelles and vesicles) from the centre of the cell to the outer realms and to membrane bound proteins. Differentiation of the various

roles just discussed transpires via binding of auxiliary proteins or reversible post-translational modifications[110].

For these functions, the flexibility conferred on microtubules by their dynamic ability to polymerise and depolymerise swiftly is vital. Tubulin binding agents (TBA) have long exploited this requisition, in particular with regard to the cell cycle and division, which are hypersensitive to subtle alterations in spindle microtubule dynamics. TBAs which bind to microtubules and thus meddle with mitosis cause delays in the metaphase-anaphase transition, and cells affected are subsequently 'rejected' and directed towards apoptosis[112]. Cancer cells are more vulnerable than normal cells to this fate via TBA action. TBAs are often natural products or derivatives thereof, from plants, marine sponges and bacteria, and can be classed either as microtubule stabilising/destabilising agents or by which of the three main binding sites (taxane site, vinca domain, colchicine site) the drug acts upon. Multiple binding sites on the same macromolecule mean synergistic antiproliferative effects are observed when a combination of two or more different TBAs are administered[113]. Drugs that bind to the taxane site are microtubule-stabilising in that they bind to the interior of the microtubule and permanently inhibit depolymerisation, even under inductive conditions, and so the microtubule becomes stuck in aggregations of cumbersome form leading to cell cycle arrest (Figure 1.15). Examples of these include the blockbuster anti-cancer drug paclitaxel (Taxol) and docetaxel (Taxotere), which have broad spectrum activity[114] and the promising epothilone series[115]. Vinca alkaloids are microtubule destabilizing agents, which rapidly bind to the vinca domain on the microtubule-bound tubulin, this time preventing polymerisation into larger microtubules. Vinblastine and vincristine are among this class of compounds which have been used on various solid cancer forms and leukaemia since the 1970's[113]. Drugs which target the colchicine binding site are similarly microtubule-destabilising agents; binding first to soluble tubulin to form a complex, which when incorporated prevents further polymerisation and growth of the microtubule. The colchicine binding site obviously binds the naturally occurring substrate colchicine, although its use as an anti-cancer agent is limited by its high toxicity. Despite this, of the three available, it is the colchicine binding site which offers the most compelling prospect for VDAs and an anti-angiogenic effect.

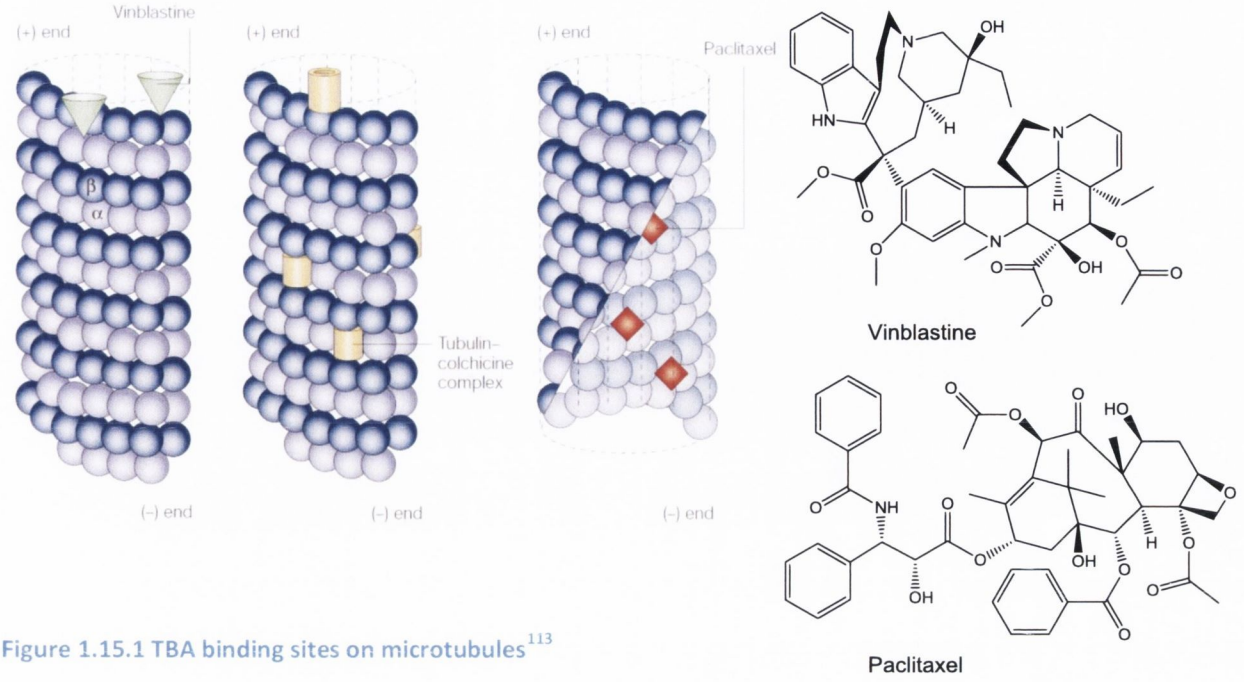


Figure 1.15.1 TBA binding sites on microtubules[113]

1.3.2.2 Mode of Action of Tubulin-Based VDAs

Structurally reminiscent to colchicine, the combretastatins are considered the paradigm of tubulin based VDAs (Figure 1.16). As with many of the TBAs, their origin is from nature, with 17 combretastatins isolated from a single source; *Combretum caffrum* - the South African Bush Willow[116]. Combretastatins exhibit potent cytotoxic and antiproliferative effects *in vitro*, on both tumour and endothelial cells, causing cell cycle arrest (G_2/M phase), although the extent is ultimately dependent on the duration of exposure, cell type and proliferative status[117]. Unfortunately, direct cytotoxic and anti-mitotic effects *in vivo* are compromised by the presence of plasma proteins which hamper bioavailability[118]. Compared with colchicine, combretastatins have much milder toxicity, most likely due to shorter plasma half-lives which mean less exposure to healthy tissue. Furthermore, combretastatins can be reasoned as 'mild' because they bind reversibly to the colchicine binding site, whereas when colchicine itself binds, its molecular interaction with tubulin is broken down over 100 times more slowly[119], and hence is considered a 'pseudo-irreversible' inhibitor[120].

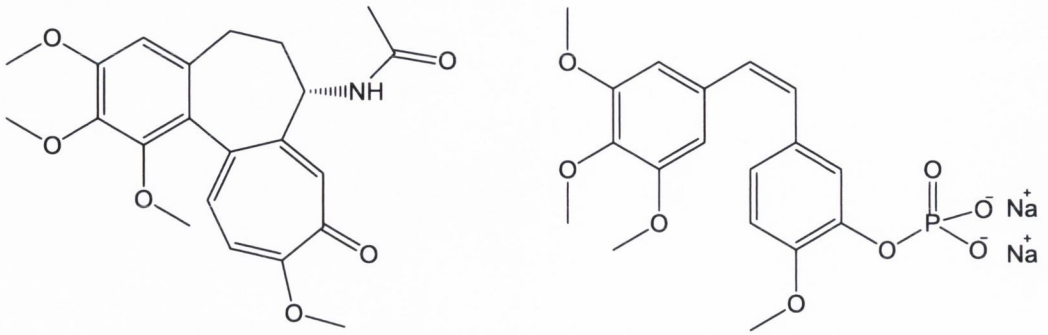


Figure 1.16. Inhibitors of the tubulin colchicine binding site: Colchicine and Combretastatin A4 Phosphate salt

Combretastatins and the other TBA-based VDAs exert their anti-vascular effects via cytoskeletal morphological changes to endothelial cells[121]. This process is complex and multi-faceted (Figure 1.17). Combretastatin based inhibition of microtubule polymerisation kick-starts the process by activating the Ras homology (Rho) family of GTPases, intricately involved in intracellular actin dynamics[122]. Actin is a globular protein which polymerises into thin two-stranded helices termed microfilaments, which like their thicker and more rigid microtubule cousins play central roles in the cytoskeleton. How exactly microtubule destabilisation triggers Rho-GTPases remains unclear, although it is thought to involve guanine exchange factors (GEFs), which are common factors to both[123]. Initiated Rho-GTPases act in two separate ways: firstly they activate Rho-Kinase enzymes which unusually phosphorylate the myosin light chain (MLC), and secondly, they provoke actin-myosin interaction. Myosin light chain is a subunit of myosin, a combination of proteins, which using ATP as fuel, acts like a motor in terms of generating force and aiding movement of actin fibres. Modulated by Rho, actin and myosin filaments become assembled into contractile structures known as stress fibres, and the phosphorylation of the MLC instigates cell contraction[124].

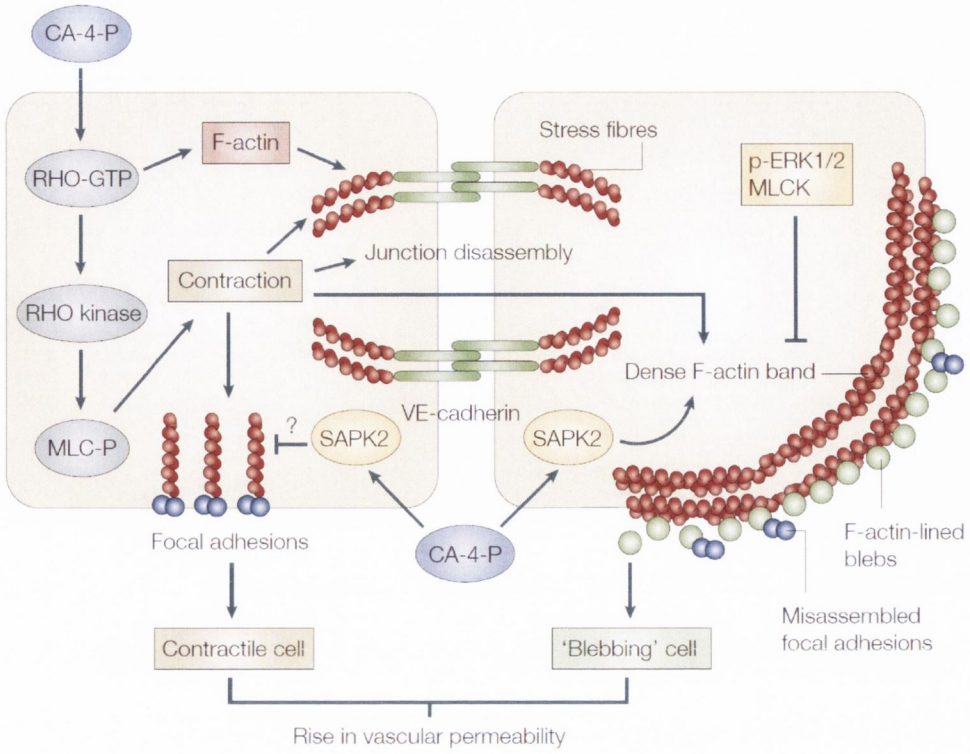


Figure 1.17. Signalling pathways involved in combretastatin (CA-4-P) mediated anti-vascular activity[121a]

Parallel to these processes, combretastatins also invoke 'blebbing' in a certain subset of the endothelial cell population. Again, Rho enzymes modulate this process, causing polymerisation of F-actin. Mediated by stress activated protein kinase 2 (SAPK2)[125], F-actin accumulates as a dense spherical band near the surface of the cells causing protrusions called blebs. It has been suggested that these blebs are derived via missasembly of stress fibres[122]. Blebbed cells are rounded up with characteristic bulges throughout the cell surface, and are indicative of an early cytotoxic and necrotic, rather than mitotic\apoptotic, cell death pathway[122, 125-126].

Rounding up of endothelial cells by blebbing and three-dimensional endothelial cell contraction disrupts the integrity of the endothelium monolayer. Combretastatins also cause cadherin-based cell-cell junctions to become dissociated[127] and cells pull away from each other or detach from the endothelium, leaving behind gaps and exposure to the basement membrane. Ultimately, vascular permeability is increased in already leaky blood vessels, resulting in loss of plasma proteins and macromolecules to the interstitium. This extravasation is accompanied by a loss of fluid volume by osmosis and hence interior oncotic pressure falls in turn causing a reciprocatory

rise interstitial fluid pressure. This change in pressure differential has a vasoconstrictive effect and the lumen of the vessel is drastically narrowed[128] (Figure 1.18). The rounding up of blebbed cells further closes down and stifles rheology in the vessel interior. The loss of fluid from blood to tissue leads to higher haematocrit levels and blood becomes much more viscous and resistant to flow, to the point where red blood cells eventually stack together to form 'rouleaux', reducing circulatory efficiency even more. Eventually, blood flow stagnates completely and the local blood supply is completely shut down by occlusion. A sudden loss of blood supply is catastrophic for a tumour already nutrient starved, hypoxic, acidic (from lactate production due to anaerobic glycolysis) and suffering from oxidative stress[129]. Widespread haemorrhagic necrosis of the tumour then takes place[130].

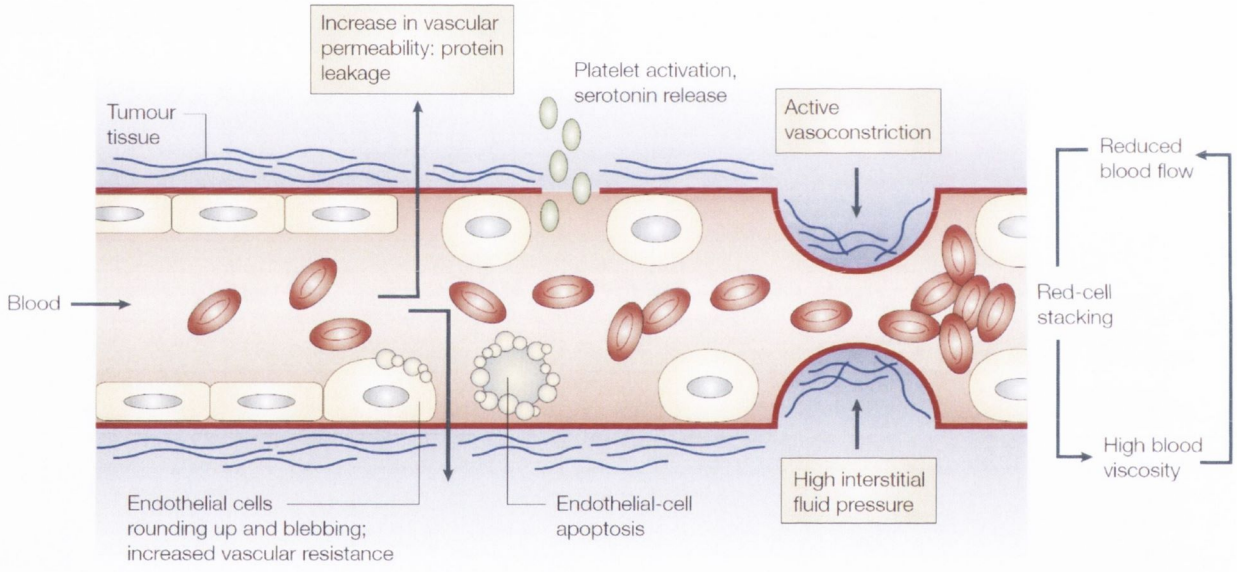


Figure 1.18. Rapid tumour vascular shutdown after treatment with CA-4-P[121a]

1.3.2.3 Combretastatins in the clinic

Combretastatins are a family of structurally related stilbenes, with both aryl groups at 50-60° to each other, and differing combinations of aromatic substitutions; typically methoxy or phenol groups. Of the naturally isolated combretastatins, combretastatin A-4 (CA-4) is the most active, although its activity is tempered by its poor solubility. Instead, CA-4 is presented in prodrug form, as combretastatin A-4 phosphate (CA-4-P, fosbretabulin, Zybrestat) a phenolic disodium phosphate salt, which is cleaved in vivo by endogenous non-specific phosphatases to release CA-

4. CA-4-P itself does not bind to tubulin[131]. The stereoisomerism of the double bond is of crucial importance; the *cis* isomer alone is active, whereas the *trans* isomer does not interact with tubulin. Conversion of the active *cis* to inactive *trans* can occur metabolically. Recent attempts at locking the configuration have involved incorporating the double bond into a heterocyclic ring, such as imidazole or oxazole[132]. A variety of combretastatin analogues have been synthesised and some are under evaluation in clinical trials: the even more potent combretastatin A-1 (CA-1) and its phosphate prodrug (Oxi4053)[133] and the serine based ombrabulin[134] are two of the more advanced CA-4-P derivatives. As of yet, no combretastatin-based VDA has been FDA approved, although CA-4-P has been made available for compassionate use in anaplastic thyroid cancer[103b] and ombrabulin was granted orphan drug status for rare cancers such as advanced-stage soft tissue sarcoma.

The effect on tumour blood flow by combretastatins can be observed within minutes of i.p. administration, correlating to a similar timeframe as changes in the actin cytoskeleton and cell shape. A 30 mg\kg dose of CA-4-P caused an almost complete cessation of intratumoural blood flow within 10-20 minutes, albeit reversible after 24 hours[135]. A higher 100 mg\kg dosage elicited a similar response (90-99%), this time with no recovery, and even this was just 10% the maximum tolerated dose. Small venules were the most effected type of vessel, in comparison to MVs and GMPs targeted in anti-angiogenic treatment. Extensive concomitant necrosis in both cases was observed. In addition to this promising activity, encouraging selectivity of CA-4-P for tumour vasculature over normal vasculature was demonstrated[136]; in the P22 carcinomas used above, a 100-fold reduction in blood flow in tumour vessels corresponded with, at most, a 7-fold reduction in flow, and even at that the effect was transient[130, 137]. There have been various reasons proposed to account for this innate selectivity. The most obvious are that blood flow in tumours is already sluggish by its nature, especially those with long lengths between branches, so only minor reductions in vessel diameter are enough to nudge them toward embolisation, and that healthy, mature vasculature with solid pericyte investiture is more enduring to endothelium injury. Further to these, differences in the rate of endothelial cell proliferation, post-translational modifications of tubulin, nitric oxide and oxygen participation, as well as interactions between microtubules and the actin skeleton have been suggested[135-136], although it is likely all factors could play some part. On an interesting aside, combretastatins have also shown activity on leukemic cells, despite their primary concern with solid state tumours. CA-4-P was shown induce leukemic cell arrest, death and inhibit proliferation by disrupting the

cytoskeletal stability required to maintain mitochondrial function[138]. These circumstances are especially encouraging with regard to the adherence of leukemic cells in treatment-resistant stromal niches.

Aided by rapid clearance, side effects of combretastatin based drugs are relatively mild in comparison to established chemotherapeutics. Hypertension and cardiac ischemia are the most prominent circulatory-based side effects, while tumour pain accounted for the most common side effect otherwise, and not considered dose-limiting due to its manageability with analgesics. Even though both the activity and toxicological profile is promising for CA-4-P and this class of drugs, there are limitations. This form of anti-vascular treatment works best on small, poorly developed small-calibre vessels like those found in the core areas of the tumour. The effect on larger vessels is more modest, leading incomplete circulatory shut down in some areas of the tumour mass[137]. Another form of resistance comes from the mobilisation and recruitment of circulating endothelial and bone-marrow derived progenitor cells, which home to ischemic sites like those induced by VDAs[139]. These differentiate and integrate into the damaged vasculature to restore or reinforce them. However, the most detrimental form of resistance to VDAs is the persistence of the 'viable rim' of tumour cells on the periphery of the tumour mass, even at VDA levels approaching their maximum tolerated dose[140] (Figure 1.19). These cells maintain excellent nutrition from normal vasculature as well as any remaining tumour vasculature, which tends to be quite dense on fringes in any case. Tumour vessels in the periphery are also less susceptible to VDAs due to innately lower interstitial pressures than vessels in the core[141]. Tumour cells in this region are highly proliferative and upon drug withdrawal quickly repopulate. For these reasons VDAs as single agents look likely to fail, as many clinical trials have already done, with no significant survival advantages demonstrated yet. As with anti-angiogenics, this area also suffers from a lack of predictive biomarkers that would aid the identification and selection of the most suited candidates for VDA-based chemotherapy[142].

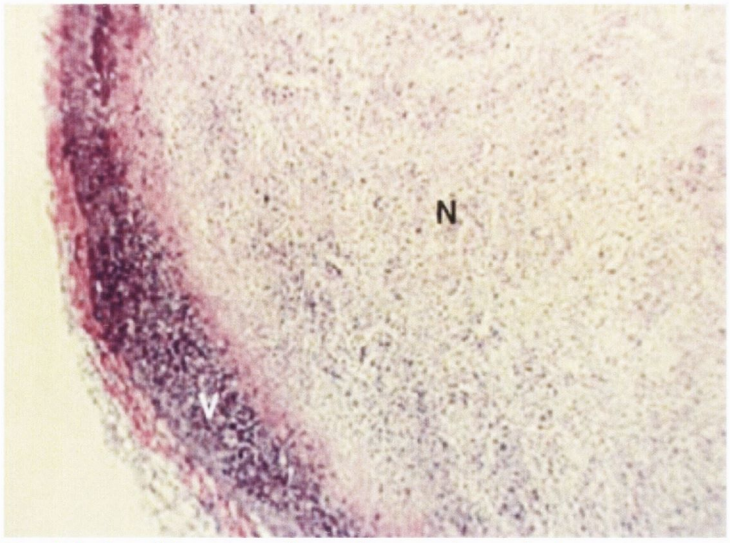


Figure 1.19. Viable Rim (V) of proliferative cells on the periphery of a tumour, contrasting with extensive central necrosis (N) after VDA treatment in mouse mammary carcinoma[2]

1.3.2.4 Other VDAs

Other non-combretastatin-based TBA-acting VDAs include the vinca alkaloids, vinblastine and vincristine, which exhibit some degree of anti-vascular activity to supplement their anti-mitotic activity. Auristatin PE (Soblidotin, TZT-1027) is a derivative of the pentapeptide dolastatin 10, and similarly acts at the vinca domain[143] and shows activity even as a single agent. Colchicine-based analogues such as ZD6162 were investigated but despite good early performance with stasis of blood flow at small doses and with good specificity for tumour vessels[144], these were later shelved due to unacceptable cardiotoxicity[145].

A second major group of VDAs, the flavonoid-based VDAs, are attracting significant interest, though their mode of action is tubulin independent[146]. Flavone acetic acid (FAA), originally intended as a NSAID[147], was the first of these compounds to demonstrate anti-vascular activity in mice but not humans and was since modified to 5,6-dimethylxanthenone-4-acetic acid (DMXAA, Vadimezan, ASA404), which has reached phase III clinical trial evaluation. In the case of non-small cell lung carcinoma, DMXAA was shown to improve overall survival from 5.5 months to 14 months in combination therapy[120]. This class of compounds display both direct and indirect anti-vascular effects. In terms of the direct response, endothelial cells on the tumour vasculature are rendered apoptopic within 30 minutes after administration of DMXAA[148]. How exactly this

happens is still unclear, which is hampering development of better analogues, although neutrophils have been implicated as mediators[149]. The resulting rupture of the vessel wall, with extravasation of macromolecules is similar to the action of the combretastatins, but the flavonoids are unique in that they trigger accumulation of platelets inside the vessel, who in turn prompt release of serotonin (or its metabolite), a vasoconstrictor. Indirectly, DMXAA induces secretion of toxic cytokines such as tumour necrosis factor α (TNFα). Besides their toxicity to cancerous cells, cytokines like TNFα apparently amplify the influx of neutrophils and thus help maintain the anti-vascular response in a supplementary way[149].

1.4 Combination therapy and Hybrid Drugs

Through the long history of cancer research, the 'perfect', all-encompassing therapeutic resolution is yet to blossom. On both flanks of the anti-angiogenic approach, the shortcomings we have discussed in each highlight the need for some form of combination therapy. Carefully selecting a congruent partner could drastically enhance the efficacy relative to a single-pronged venture. Theoretically, agents with independent molecular targets and differing mechanisms of action could synergistically boost the overall anti-cancer effect, while also compensating for those issues which typically undermine a given monotherapy; resistance, toxicity, limitations on activity etc. Conversely, a degree of prudence must still be retained lest adverse effects be potentiated. It must have been almost intuitive that the two outstanding antiangiogenic candidates on each side, bevacizumab and CA-4-P, be tested in tandem given their complimentary traits. Together they were well tolerated, with improved anti-tumour activity (Figure 1.20), as bevacizumab mitigates revascularisation from the viable rim following CA-4-P mediated destruction of the core vascular conduit[150]. Similarly, each party has also undergone combination with some of the most established cytotoxic agents available with many encouraging results[131, 151]. In particular, VDAs are compelling as partners due to their unique inclination to increase vascular permeability; blood-borne cytotoxic drugs of high-molecular weight often have difficulty reaching tumour cells as they can't usually pass through tight endothelial barriers. Moreover, VDAs could potentially play an instrumental role with regard to so called 'bioreductive drugs'; prodrugs protected from catabolic enzymes by O_2 which only become active under hypoxic conditions like those in the tumour, induced via VDA-mediated ischemia[152]. Given the comprehensive data and sheer variety of combinations in these studies, they will not be discussed here, suffice to say that combination therapy, for both anti-

angiogenics and VDAs, has shown almost across-the-board improvement in efficacy, although unfortunately not yet to a fully curative extent.

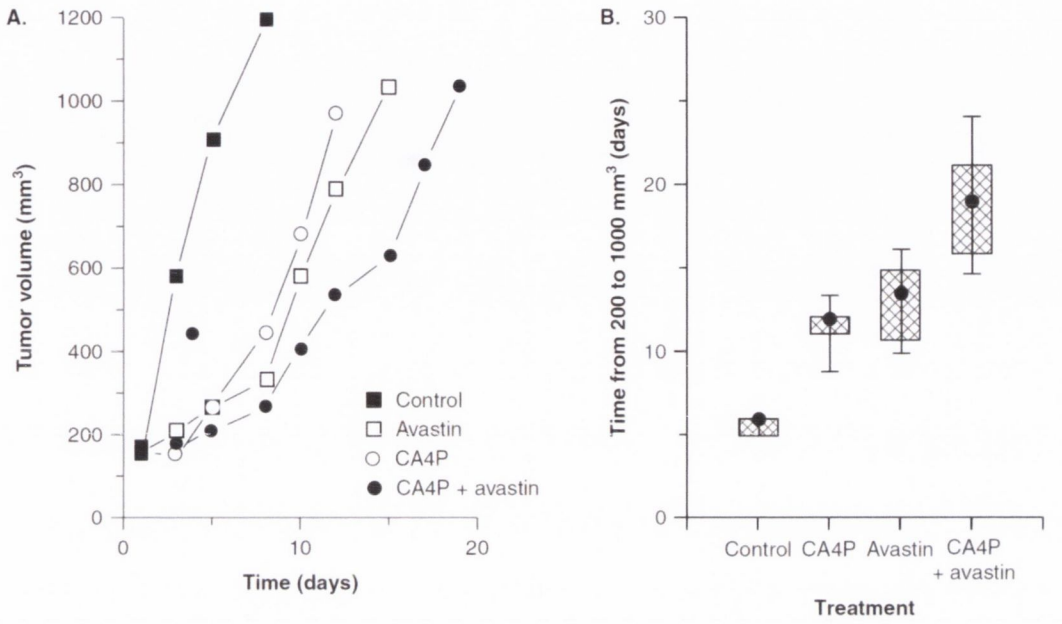


Figure 1.20 Example of the benefit of combination therapy. CA-4-P & bevacizumab (Avastin) show improved activity in renal cell carcinoma together than either on their own; both in terms of growth (A) and in rate (B, median 75th and 95th percentile)[131, 150b]

Taking the concept of combination therapy a step further, it may be more advantageous to unite two complementary pharmacophores together in a single bivalent molecule. Again, synergism between two agents is the idea, though in this case it becomes especially pertinent to see if they can invoke an even more powerful response when joined together than the two separately in combination. Strategy in these types of 'hybrid' molecules is important; should covalent link between the two moieties stay linked or cleavable in vivo, should pharmacophores be exposed in the hybrid or masked until release similar to prodrugs, should bound pharmacophores reside close to one another or spaced out by a drug scaffold? The role of molecular 'sidekick' too is variable; possibly serving to offer solubility support, enrich cellular uptake, enhance drug delivery or act as a site specific homing device, interfere with resistance mechanisms or simply deliver another therapeutic payload. Better yet it would be a component that could fulfil several of these duties simultaneously.

Hypothetical disadvantages are due consideration. First off, creation of a hybrid invariably adds bulk to a molecule. Masking important functional groups introduces the possibilty of reduced activity, not to mention the likelihood of new complicating drug-drug interactions. Issues with release, the optimal delay involved and the nature of its trigger can all serve to undermine otherwise complementary partners. Finally, merging drugs as a single entity means they are confined as a fixed ratio, therefore the active concentration of each element would have to be compatible. That said, hybrid drug approaches have become a reality, particularly with TBAs[153]. Our goal is likewise to graft an active tubulin-based VDA on to a promising hybrid drug candidate, having already identified an auspicious target for the second pharmacophore component – Aminopeptidase N.

1.5 Aminopeptidase N

Aminopeptidase N (APN), also known as cluster differentiation antigen 13 (CD13), is a type II, zinc dependent membrane-bound protease, and in non-covalent dimer form is extensively distributed throughout a broad range of tissue types[154], especially common on monocytes and at the brush-border membranes of kidney proximal tubes, intestine and placenta[155]. APN can also be found solubilised in plasma[156]. Although its primary function is still somewhat obscure, as an ectopeptidase APN is known to catalyse preferentially the removal of neutral amino acid residues from the NH_2 terminal of small peptides, unless proline is in the penultimate position[157], with leucine and alanine among the most favoured substrates[157b].

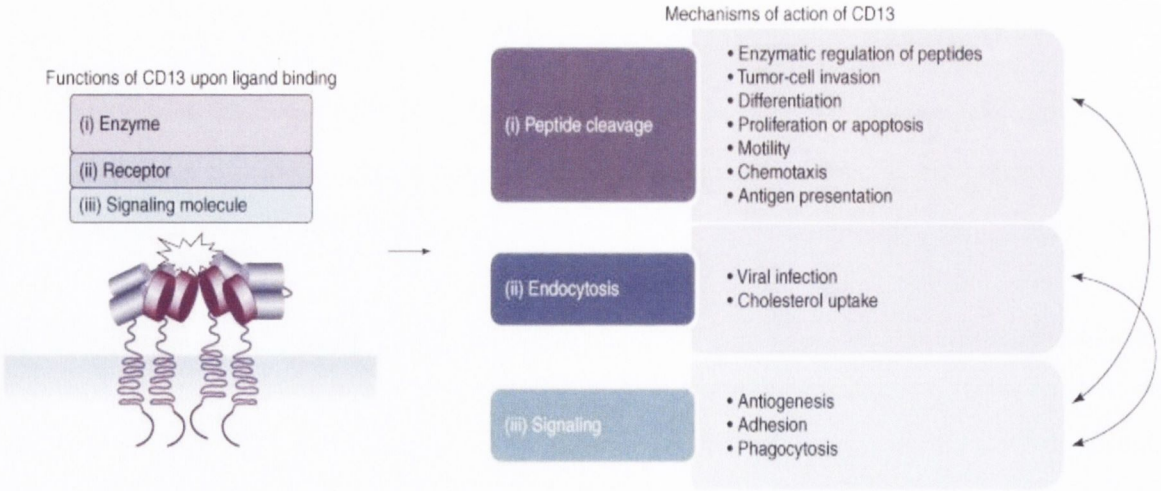


Figure 1.21. Summary of some of the main APN processes (adapted from Mina-Osario et al[157b])

Functionally, APN is very diverse, to the point where the phrase 'moonlighting protein' is now frequently used to describe it[157b]. In an attempt to capture the essence of these processes succinctly, it is best to present these functions either in terms of APNs role as an enzyme, a receptor or as a signal transducer, although considerable overlap is unavoidable (Figure 1.21). As an enzyme, APN peptidase activity is exerted on a myriad of endogenous regulatory peptides, including hormones, neuropeptides, vasoactive peptides and chemotactic peptides, as summarised in Table 1.2 below. For example, APN influences chemotaxis via the degradation of chemokines[158]. Similarly, enzymatic activity is also implicated in cell differentiation and motility, while in terms of cancer, proteolytic break down of components of the extracellular matrix via APN encourages tumour cell invasion, metastasis and angiogenesis, in addition to metabolising peptides into pro-angiogenic molecules[159]. Furthermore, there are suggestions that enzymatic participation governs proliferation and even apoptosis[157b, 160]. The ability of APN to degrade small proteins extends to antigens and hence the immune response, where the enzymes fine-tune antigen presentation[161].

Table 1.2. Enzymatic behaviour of APN on regulatory endogenous peptides (adapted from Mina-Osario *et al*[157b])

Natural Substrates	General Comments
Enkephalins	CD13 participates in the metabolism of enkephalins. CD13 hydrolyses the N-terminal Tyr-Gly bond of Leu-enkephalin & Met-enkephalin, accounting for the short half-life of these in vivo. Although resistant to hydrolysis, the neuropeptide substance P inhibits enkephalin cleavage by
Angiotensins	CD13 hydrolyzes the N-terminal Arg of angiotensin III to generate angiotensin IV. In rats, infusion of CD13 into the third ventricle causes lowering of blood pressure. CD13 inhibitors block this drop in blood pressure & increase vasopressin release as a result of the increased half-life of angiotensin III. Dietary salt regulates the expression of CD13 in the kidneys, and CD13 is more highly expressed in the kidneys of Dahl salt-resistant rats. CD13 reduces basolateral Na+/K+ ATPase levels via angiotensin IV receptor signaling.
Tuftsin	The first peptidic bond of this immunoregulatory tetrapeptide is hydrolyzed by CD13, generating an antagonist that competes for receptor binding and thus regulating tuftsin functions.
Kinins	Both kallidin (lysyl-bradykinin) & its derivative Lys-des-Arg9-bradykinin are CD13 substrates. The latter generates bradykinin upon hydrolysis. Bradykinin is resistant to hydrolysis by CD13, not a natural inhibitor. The bradykinin inhibitor Icatibant is a CD13 inhibitor, and there is the danger of possible crosstalk in systems where bradykinin-receptor targeting can result in CD13
Hemorphins	Because these peptides, derived from the β-chain of hemoglobin, share their N-terminal sequence with angiotensin IV, they compete with it for the catalytic site of CD13, resulting in an inhibitory effect of CD13 activity on angiotensin IV.
Cytokines or chemokines	In vitro, CD13 hydrolyses synthetic oligopeptides corresponding to the N-terminus of IL-α, IL-β & IL-2, although natural IL-2 & G-CSF are resistant to hydrolysis. Because hCD13 is believed to cleave small peptides only, activity on chemokines would require auxiliary enzymes, as with CXCL11, where initial removal of the NH2-terminal dipeptide by CD26 allows for further
Extracellular matrix proteins	Their high molecular weight makes it unlikely that CD13 alone is capable of degrading them. Nevertheless, at least 2 proteins have been proposed cleavable by CD13: entactin and type IV collagen 76 & 106. Due to the potential relevance of this type of cleavage in tumor cell invasion, this assumption needs to be confirmed.
Other substrates	In vitro, CD13 participates in the metabolism of glutathione, somatostatin, thymopentin, neurokinin A, splenopentin, nociceptin (orphanin) FQ and peptides derived from the thrombin receptor 107 & 108.

As a receptor, APN is known to bind several viruses[162], potentially including SARS[163]. Some of the receptor based actions of APN involve its internalisation by endocytosis[164], thus reducing its surface density and consequently diminishing enzymatic activity. In addition to viruses, APN has also been associated with the endocytosis of cholesterol[157b, 165]. Despite possessing a rather short cytoplasmic domain with no known signalling motif, APN is prominent in cellular signalling pathways, albeit through an unidentified auxiliary protein. Most pathways remain elusive although studies with APN inhibitors confirm such actions which are enzymatic and receptor independent. In fact, it seems APN often governs signals elicited from other receptors, and as such are more accurately thought of as 'signal regulators'[166]. For instance, APN potentiates the ingestion of large particles, termed phagocytosis, rearranging to the target zones and internalising into the newly formed phagosomes, all while acting as a signal regulator of the phagocytosis-mediating receptor FcγR[167] via crosslinking. Angiogenic cytokines and growth factors are similarly modulated by APN[159], and APN-signalling is influential in endothelial cell migration and the formation of the tubes in new capillaries[168]. Ligation of APN also causes cells to adjust expression and affinity for adhesion molecules, denoting APN control over homotypic aggregation and adhesion[169]; processes which are associated with the extension of new vessels in angiogenesis[170] as well as the attachment and transmigration of circulating metastases with regard to endothelial cells[171]. The pro-adhesive cascade starts by crosslinking or ligand-instigated conformational alterations, exposing a cryptic epitope on APN which regulates binding or dissociation of another pro-adhesive ligand necessary to induce aggregation or adhesion[172]. Other APN signal transducing functions include mitogen-activated protein kinase (MARK) phosphorylation, Ca^{2+} flux, cytokine secretion, integrin activation and cytoskeletal rearrangement[173].

As we have just discussed, APN is heavily implicated in angiogenesis, though various distinct means. Studies in APN-null mice have even shown that APN is absolutely necessary for pathological angiogenesis, but physiological angiogenesis proceeds unabated[174]. Endothelial cells cultured alongside a series of known APN antagonists fail to construct a functional capillary network[168a]. Moreover, APN has been shown to be expressed exclusively on endothelial cells undergoing angiogenesis like in tumour vascular networks, but not on quiescent endothelial cells[175]. The explanation is thus: APN expression is known to be induced under hypoxic

conditions, and is potently upregulated by several different hypoxia-induced pro-angiogenic cytokines, including VEGF and bFGFs[168a]. Immunoperoxidase staining has revealed that APN can be expressed on certain types of tumour cells themselves; in human breast[175], prostate[176] and thyroid carcinomas[177]. Tumours of the colon which express APN correlated with a lower 3-year survival rate (80.8%) than APN negative tumours (95.6%)[168b]. On endothelial cells, cytokine induced APN involves Ras\MAPK-mediated transcription of mRNA[178]. This specific APN-expression connotation is used to signify APN as a valuable prognostic indicator[168b] and a useful biomarker for angiogenic vessels. Crucially, this gives us a viable target to which to home; in theory using a substrate that could home to only nascent vasculature that is associated with tumour growth, and neglects healthy normal tissue, would confer specificity. Additionally, many compounds that home directly to APN are themselves considered dual-acting; having adjuvant inhibitory properties that regulate alterations in the angiogenic response.

1.5.1 Inhibitors of APN

Several natural and synthetic inhibitors of APN have been identified. Bradykinin and substance P are among the natural inhibitors found in the body, while a range of potent inhibitors determined have been harvested from bacterial sources, in particular the genera of *Streptomyces*[155]. Many of these slow but tight binding peptides possess an AHPA (3-amino-2-hydroxy-4-phenylbutanoyl acetate) moiety, of which the (2*S*,3*R*) stereochemistry is of unequivocal importance for their activity. Indeed, their diastereomers with inverse stereochemical configuration actually serve faithfully as negative controls (eg epibestatin[179]). AHPA-valine, phebestin (AHPA-val-phe), probestin[180] (AHPA-val-pro-pro) and amastatin are just a few of the growing library of these APN inhibitors, although to date, the dipeptide bestatin (Ubenimex, AHPA-leu) that has been the furthest advanced, even granted license in Japan for combination based therapy against remissive acute myeloid leukaemia. Bestatin (Figure 1.22) is a transition-state analogue, a drug that resembles the transition state of a substrate of an enzyme-catalysed reaction; though unable to be transformed itself, it obstructs the active site. Typically, compounds of this type co-ordinate the catalytic zinc ion from the active site of APN, between the carbonyl and hydroxyl group on the AHPA moiety[181]; the key to their competitive inhibitory activity. Interestingly, analogous divalent metal cations that usurp the zinc role in the APN site also show inhibitory activity, i.e. Co^{2+}, Mn^{2+}, Ca^{2+}, Ni^{2+} [182].

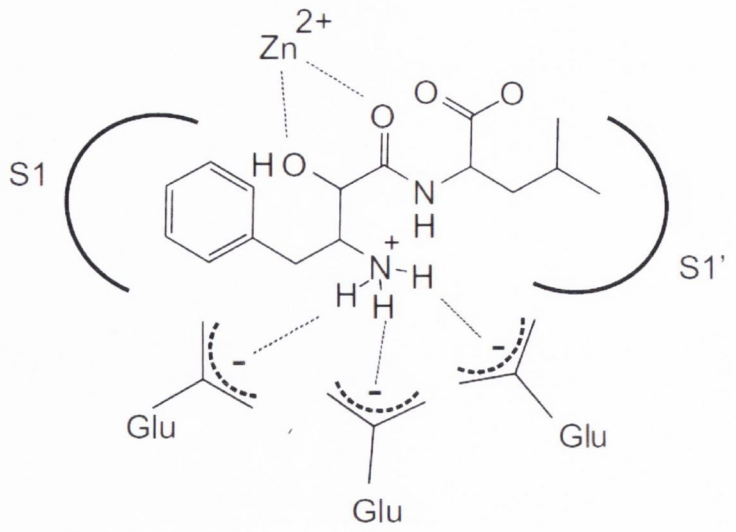


Figure 1.22. Bestatin at the active site of APN[183] where S1 and S1' are hydrophobic pockets

Bestatin has shown broad spectrum activity against metalloproteinases, and is not specific to APN; in fact it exhibits better binding affinity and inhibitory activity against aminopeptidases that associate with two metal ions rather than one. Equivalently, the responses evoked by the drug are not exactly specific either; bestatin modulates inflammatory[184] and apoptopic[160] pathways, and in blocking the metabolism of enkephalin it modulates nociception, leading to hypoalgesia[185]. With regard to cancer, bestatin inhibits tumour invasion by preventing degradation of Type IV collagen in the basement membrane and extracellular matrix[186]. Bestatin also displayed suppression of angiogenesis[175]. Moreover, bestatin was shown to act as a radiosensitizer *in vitro* and *in vivo*[187]. Several bestatin analogues have been synthesised, the more potent dimethylaminoethyl ester LYP[188], para-hydroxybestatin[189], bestatin thioamide[190], 2-thiolbestatin[191] etc and work into bestatin-based activity-based probes (ABPs) to characterise the activity of metallo-aminopeptidases is ongoing[183]. Toxicity of bestatin is low, with adverse effects of the liver, GI tract and skin culminating to just 1.6%, demonstrating the value of bestatin as a therapeutic prospect. Orally bioavailable, bestatin is rapidly absorbed into the circulation, and on the other hand clearance is similarly swift, by any of the usual elimination routes.

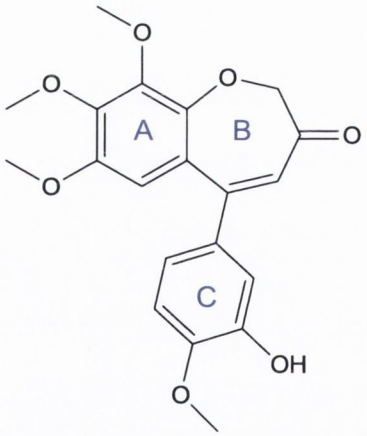
The most successful APN substrate to date has been that of the cyclic CNGRC (cysteine-asparagine-glycine-arginine-cysteine) peptide motif[192], bound with a disulphide link between

both cysteines, which has been tried with cytotoxic agents, viral particles, DNA complexes, cytokines and antiangiogenic compounds. It has been shown that molecules of this type bind exclusively to APN in tumour vasculature, but not in other APN-rich tissues such as the epithelia of the kidney[193]. The first anticancer-CNGRC hybrid compound evaluated was that of doxorubicin[194]. Studies found that this caused significant rises in efficacy with concurrent diminution of toxicity against human xenografts in mice in comparison to doxorubicin alone. 5-fluoro-2-deoxyuridine (5-FdUrd), a blocker of thymidylate synthase and thus inhibits DNA synthesis, was also hybridised with CNGRC to conceal its nonspecific toxicity until tumour delivery is completed, where the compound is released via hydrolysis under physiological conditions[195], with results that it echoed that of doxorubicin. Tumour necrosis factor alpha (TNFα), was also tested as a CNGRC conjugate, as it is usually associated with poor delivery to its destination and systemic toxicity which undermines its clinical potential. By coupling with CNGRC it has been possible to deliver picogram doses of TNFα directly to the tumour site[196] which helped avoid toxicity issues, whilst at the same time exhibiting greater inhibition of tumour growth than TNFα alone[197]. In addition, these ultra-low doses have shown synergistic effects with various other anticancer drugs such as paclitaxel, cisplatin, doxorubicin and melphalan by altering drug-penetration barriers[197-198]. This is not the only cytokine which has shown enhanced activity with the CNGRC fragment; endostatin, tumstatin[199] and IFNγ have all been conjugated, with tiny concentrations of the latter overcoming strategic counterregulatory mechanisms[200] that previously led to modest efficacy.

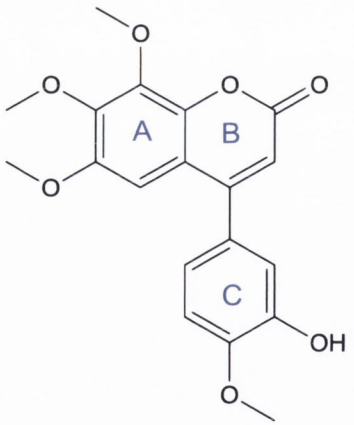
The cyclised form of the CNGRC has proven to be ten times more active than its linear analogue[201], with cyclisation giving rise to the preferential bend geometery between glycine and arginine. It is therefore important to maintain this shape and keep the disulphide bond between both flanking cysteine groups which is critical to stabilizing the bent conformation needed, rather than forming a peptide bond between the two. Addition of a proline residue into the backbone (CPNGRC) appears to stabilise the conformation even further, met with a 30-fold increase in binding affinity and inhibition of proteolytic APN activity[202]. In hybrid systems where the presence of cysteine could be problematic, or where the disulphide bridge is likely to be compromised, the cyclic peptide KNGRE can also mimic the bent conformation favoured for APN binding, with binding affinity 3.6 times higher than linear NGR for liposome delivery to APN positive cancer cells[203], illustrating the range of options available for NGR based APN targeting.

1.6 Aims of the Project

The research outlined in this doctoral thesis involves first the continuation on the promising work carried out by previous PhD students; namely Shah[204], McCormack[205], Hudson[206] and White[207]. Collectively, this group synthesised a novel series of TBAs, generally consisting of a tricyclic backbone, denoted the A, B and C rings, two of which (the A and C-rings) were methoxy-substituted aryl rings that contributed to a loose structural resemblance to both colchicine and combretastatin A-4. Together, these TBAs successfully demonstrated tubulin inhibition to varying degrees, but their full potential remained largely unexplored. A synopsis of the quantitative structure-activity relationship (QSAR) is presented at the start of Chapter 2. Of the TBAs synthesised to date, two compounds were of particular interest due to their encouraging potency; a 7 membered benzoxepinone first synthesised by Shah[204], and a 4-aryl coumarin synthesised by Hudson[206] via a unique ring contraction of the Shah lead compound (discussed in Chapter 3), both of which possessed a free phenol on their C-ring (Figure 1.23). These two lead compounds were centric to the premise of this thesis, the aims of which are presented below:



Shah compound ***RS5.04***



Hudson compound ***GJH140***

Figure 1.23. Lead Compounds from our group so far

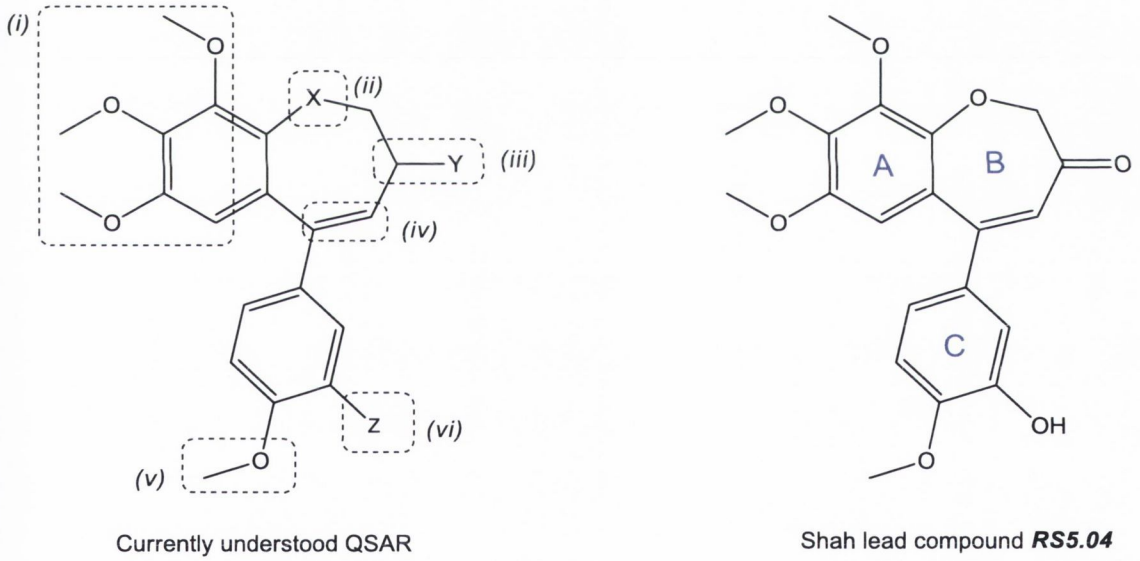
- To improve the efficiency of the synthetic routes of both lead compounds ***RS5.04*** and ***GJH140***, and in the case of the 4-aryl coumarins, reform their synthesis by implementing a new synthetic strategy

- To design and synthesise analogues of both of these compounds, with particular attention to variety on their C-ring substituents, and submit these for more extensive biological evaluation; *in vitro, ex vivo and in vivo,* with focus on their performance as anti-mitotics and VDAs.
- To investigate the nature and applicability of the novel ring contraction reaction entailed in the 4-aryl coumarin synthesis.
- To synthesise phosphate prodrugs of both these compounds, in the same manner that had been done for combretastatin A-4.
- To construct a prototype hybrid drug, based on the most efficacious tubulin binding VDAs, combining these with an inhibitor of our second target, APN, namely bestatin.
- To vary the nature of the hybrid drug, to allow flexibility in terms of dissociation rate *in vivo* and binding affinity to APN.
- To design and construct a series of dual-acting designed multiple ligand molecules, with tubulin binding and APN binding components.
- To assess the impact of the hybrid drugs, if any, on the enzymatic activity of APN itself

Chapter 2 – Synthesis of Benzoxepinone Series of TBAs

2.0 Background

A library of novel tubulin inhibitors has been previously designed and synthesised by the former PhD students of this lab group, namely R. Shah[204], E. McCormack[205], G. Hudson[206] and M. White[207]. Generally, these compounds follow the general scheme that includes three ring systems: a trimethoxy substituted aromatic A-ring, a 7-membered aliphatic B-ring and a singularly methoxy substituted aromatic C-ring. Although investigation has by no means been exhaustive, an evident Quantitative Structure-Activity Relationship (QSAR) regarding some of the basic fragments of these molecules and their affinity for tubulin binding has been proposed (Figure 2.1), based on their performance *in vitro*[208].



Currently understood QSAR

Shah lead compound ***RS5.04***

Figure 2.1 Components (i – vi) of QSAR for tubulin inhibitors synthesised in this laboratory (left), and initial target molecule (right)

Firstly, in the general scheme, the two substituted aromatic rings should be bound close to each other to form the rigid, hydrophobic architecture reminiscent of both colchicine and combretastatin A-4 to permit tubulin binding. Like CA-4, it is believed the aromatic rings must be noncoplanar for optimal fit; twisted relative to each other in three dimensional space (torsion angle 53 ° for CA-4[209]). On the A-ring, ample electron density is critical[210] and it has been

demonstrated that the 2,3,4 methoxy substitution arrangement *(i)* is essential for activity; by comparison this was drastically reduced in the case of molecules with the 3,4,5 substitution pattern. With regard to the B-ring, in the case *(ii)* whereby X was an oxygen atom, activity was marginally improved over that where X consisted of a methylene group. That said, the latter aliphatic B-ring systems are promising enough to warrant further investigation, and these compounds form the basis for the doctoral theses of Breen[211], Moran and Stack. It is not fully understood whether the oxygen atom benefits the system by its influence on the conformation of the B-ring, or simply by increasing electron density on the A-ring. When Y = O *(iii)*, the presence of a carbonyl on the B-ring boosts activity to a greater extent than the corresponding alcohol group, although the most favoured position has yet to be fully deduced and was undertaken for the thesis of B. Moran. It could well be that functionalization at this position not only plays a role in binding to tubulin, but also stabilises the B-ring conformation to one more amenable to fit in the colchicine binding site. When Y is conjugated to a small peptide, the activity is maintained up to the second amino acid residue, beyond that and activity decreases. The alkene group *(iv)* is imperative for tubulin binding, presumably restricting the active conformational shape of the tricyclic molecule. Interestingly, in the event of elimination of Y, whereby a diene compound is formed in its place, activity diminishes 9-fold. Bereft of any functional groups, the activity of an aliphatic B-ring drops substantially.

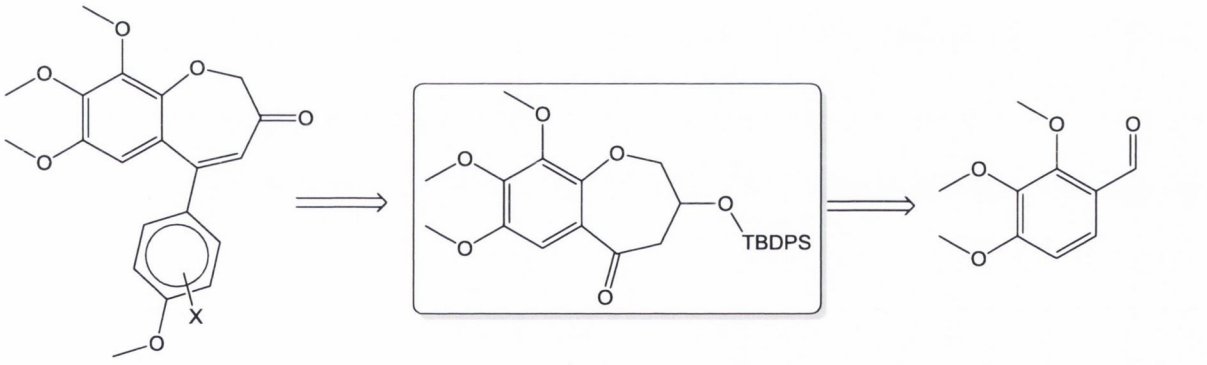
On the C-ring, the methoxy group on the *para* position *(v)* is crucial for activity. It is believed that the importance of this methoxy group for tubulin binding is due to its alignment with the cysteine 239 residue on β-tubulin[212]. Small, electron rich functional groups on the *meta* position (*ortho* to the methoxy group), are not only tolerated but seemingly enhance tubulin binding, providing an outlet for hydrogen bonding to the carbonyl oxygen of the threonine α177 residue[212b, 213].

Based on the QSAR postulations, and reaffirmed by the encouraging tubulin binding results of the Shah compound ***RS5.04***, we decided to undertake the synthesis of 7 membered benzoxepinone compounds. The initial objective upon commencing this project was the procurement of this lead compound in sufficient quantities for comprehensive biological evaluation. From the same benzoxepinone skeleton, we aimed to synthesise and evaluate

derivatives of this system to broaden the scope of future QSARs and with an eye on future design and synthesis of bivalent, hybrid molecules.

2.1 Synthetic strategy 1

Early synthetic strategy closely followed those established by former colleagues Shah[204], Hudson[206] and White[207]. The initial focus was to procure gram-scale quantities of a common synthetic intermediate, from which we could begin to introduce diversity on to the molecule via the C-ring. The protected cyclic ketone ***2.10*** was chosen as a suitable checkpoint as this would allow scope to attempt different coupling approaches with regard to coalescence of the AB and C-ring moieties. To guarantee the necessary 2,3,4 trimethoxy configuration on the A-ring, we would need to start with the commercially available starting material of the same spatial arrangement, i.e. 2,3,4 trimethoxybenzaldehyde, and from that we would introduce the requisite phenolic B-ring oxygen. Stepwise elongation from this oxygen would eventually lead to the functionalization necessary for cyclisation to occur.

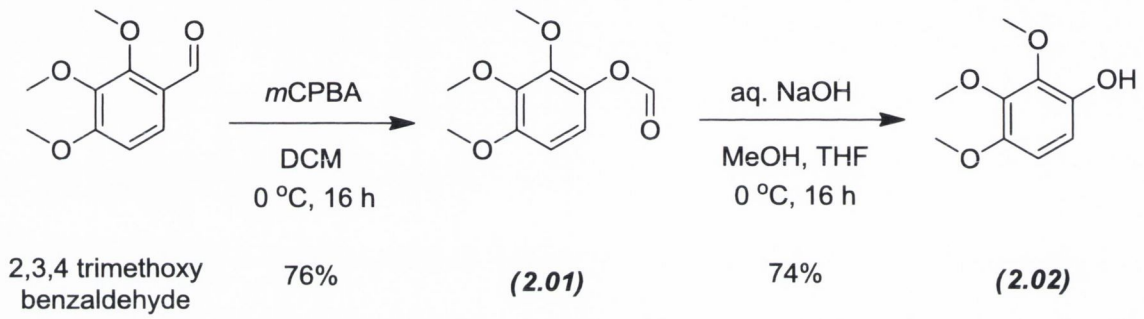


Scheme 2.1. Retrosynthetic rationale and proposed synthetic target

2.1.1 Early Synthetic Steps

The first step towards ***2.10*** was Baeyer-Villiger oxidation[214] of 2,3,4-trimethoxybenzaldehyde with *meta*-chloroperoxybenzoic acid (*m*CPBA) to give the formate ester ***2.01.*** This allowed us introduce oxygen to the would-be heterocyclic B-ring, distinguishing this family of compounds

from the aliphatic cycles synthesised by G. Stack, B. Moran (both unpublished) and E. Breen[211]. This transformation was facile (Scheme 2.2), although complete removal of the *m*CPBA was less so. Often, aldehydes under the conditions for Baeyer-Villiger rearrangements can over-oxidise to give rise to carboxylic acids, although in this case the electron donating substituents on the aromatic ring enhance its migratory capacity, which is governed by its ability to stabilise the transient positive charge. For this reason, the rearrangement was favoured over the oxidation of the aldehyde.



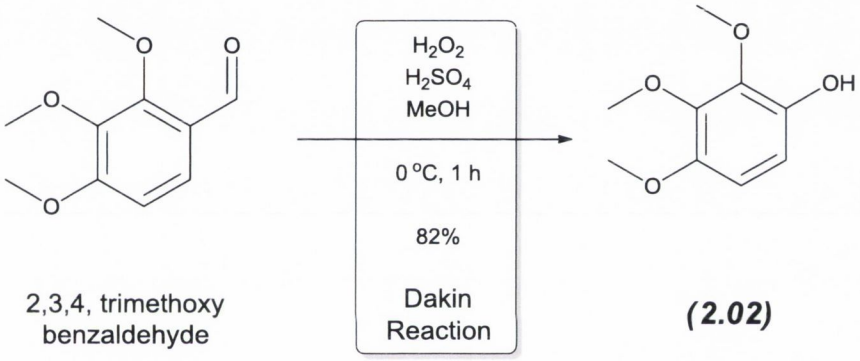
2,3,4 trimethoxy benzaldehyde | 76% | ***(2.01)*** | 74% | ***(2.02)***

Scheme 2.2. Baeyer-Villiger Oxidation and subsequent hydrolysis

The formate ester was next hydrolysed under basic conditions to afford the phenol, ***2.02*** (Scheme 2.2). An acid-base work up here rendered the compound reasonably pure, although flash column chromatography was nevertheless employed to fully remove any lingering *m*CPBA carried over from the previous step.

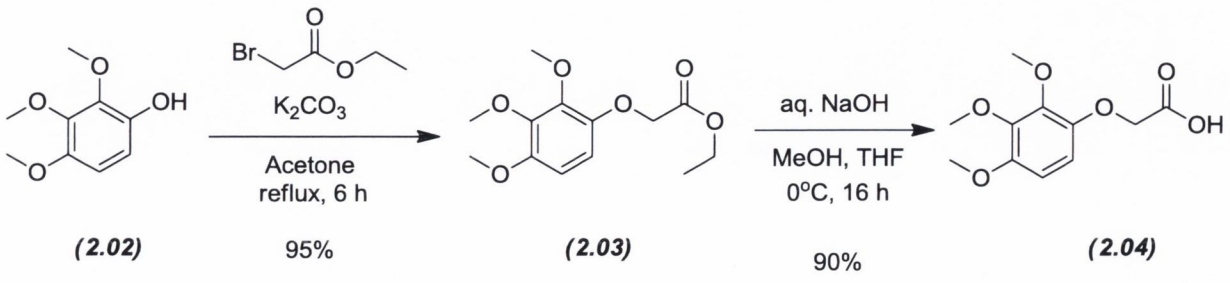
Over time, we became increasingly conscious of the inefficiency of the long synthetic route to both the target intermediate and final lead compounds. In order to minimise the number of steps involved in the synthesis of the benzoxepinones we looked at more effective ways to generate phenol ***2.02***. Conversion of the aryl aldehyde to the phenol in a single step would not only reduce the synthetic route but also circumvent the troublesome removal of large quantities of *m*CPBA; pertinent when repeating these steps on a large scale (approx 100 g). These two steps were suitably replaced with a variant of the Dakin oxidation[215], which uses hydrogen peroxide and concentrated sulphuric acid in methanol to successfully produce the phenol in one pot[216]. Acid protonation of the carbonyl invites peroxide attack at the carbon forming an

unstable intermediate that prompts aryl migration onto oxygen with the loss of water. The carbonyl remains protonated and is then attacked by methanol, forming another intermediate which collapses to give the free phenol ***2.02*** and methyl formate. This reaction is suitable only for electron rich aryl groups, and in this particular case the electron donating methoxy groups *ortho* and *para* to the aldehyde greatly contribute to the favourable migratory aptitude of the aromatic ring. Aldehydes are also much preferred over ketones. The reaction displayed a noticeable, delayed exothermic response so due care was taken with large scale attempts As a result of the success of this reaction, phenol ***2.02*** was accessible within 1 hour, even on large scale (>50 g) following simple base\acid work up in over 80% yield. This was in contrast to the preceding Baeyer-Villiger oxidation and base hydrolysis steps which required a reaction time of two days and the difficult removal of substantial quantities of *m*CPBA/*m*CBA.



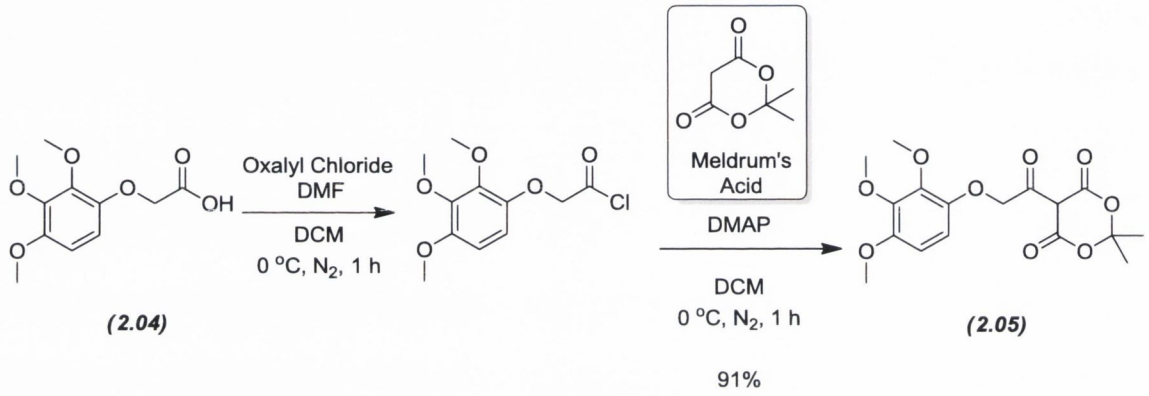
Scheme 2.3. Improved synthesis of 2.02 by employing the Dakin reaction

Alkylation of the phenol **2.02** was achieved with ethylbromoacetate with potassium carbonate as base by refluxing the mixture in acetone under basic conditions[217]. Once isolated, the ethyl ester ***2.03*** was hydrolysed under basic conditions to afford the carboxylic acid ***2.04*** (Scheme 2.4).



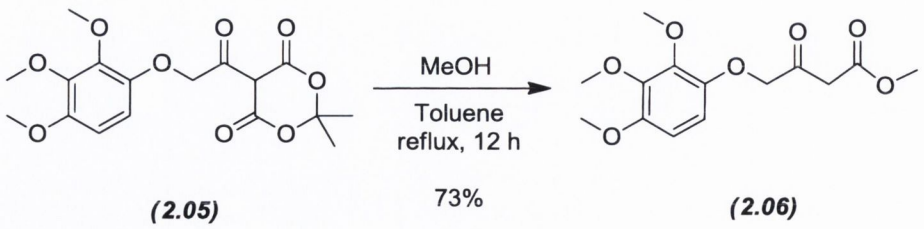
Scheme 2.4. Alkylation and basic hydrolysis of 2.02 to give acid 2.04

The next step involved coupling of the acid ***2.04*** with Meldrum's acid, by forming an acyl chloride *in situ*. The acyl chloride is formed using oxalyl chloride and DMF as a catalyst; these two react together to form a reactive iminium intermediate that the nucleophilic carboxylic acid then attacks. The resulting electrophilic cationic intermediate is highly labile, and the chlorine ion is nucleophilic enough to displace it, with simultaneous loss of gaseous CO and CO_2. The chloride itself is labile and is subsequently displaced by Meldrum's acid (Scheme 2.5).



Scheme 2.5. Meldrum's acid coupling of 2.04 via *in situ* acyl chloride formation

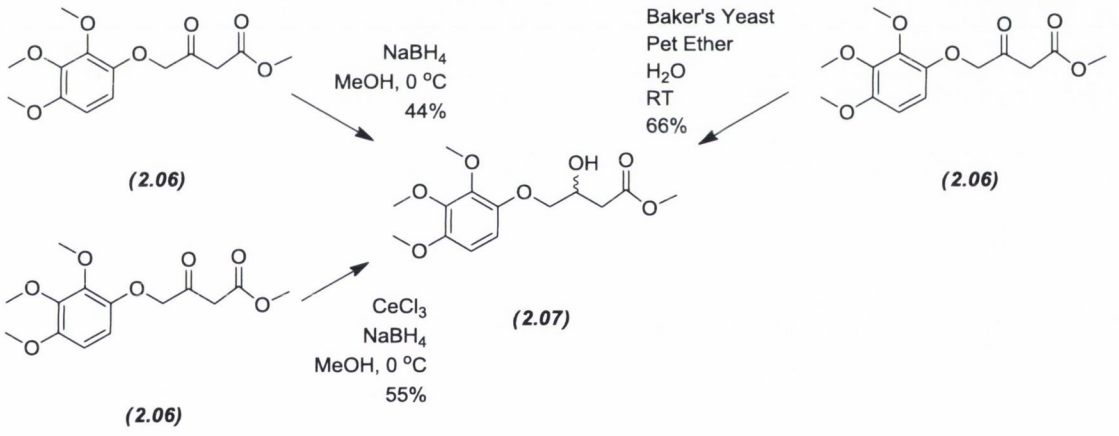
Though stable under ambient conditions, the Meldrum's coupled product is thermally unstable[218]. We exploited this to advantageous effect by refluxing the product ***2.05*** with methanol[219], prompting pericyclic solvolysis to generate the β-keto ester ***2.06*** (Scheme 2.6) with the loss of a molecule of acetone and CO_2.



Scheme 2.6 Methanolysis of 2.05

2.1.2 Problematic Reduction of ketone functionality

The synthesis towards the β-keto ester ***2.06*** has been carried out on multigram scales to date. Most transformations involved are quite facile and yields are relatively good. Although the Meldrum's acid coupling step needs a degree of care with regard to anhydrous conditions, the reaction itself was very reproducible on larger scales. Unfortunately the same cannot be said for the next step, reduction of the ketone ***2.06***. Reduction of the ketone functionality to the corresponding alcohol ***2.07*** initially proved to be quite inconsistent and low yielding, (Scheme 2.7). The transformation is somewhat hampered by the fact that our initial choice of reducing agent, sodium borohydride, also partially reduces the ester functionality. The challenge was to optimise the conditions to allow for complete reduction of the keto-functionality without adversely affecting the ester group. Regardless of the reaction conditions used, it was generally difficult to attain a yield much higher than 50%, with this reducing agent. Whilst not identified we also speculate that the transformation may be further complicated by elimination of the alcohol thus formed to generate the more favourable conjugated enoate derivative.



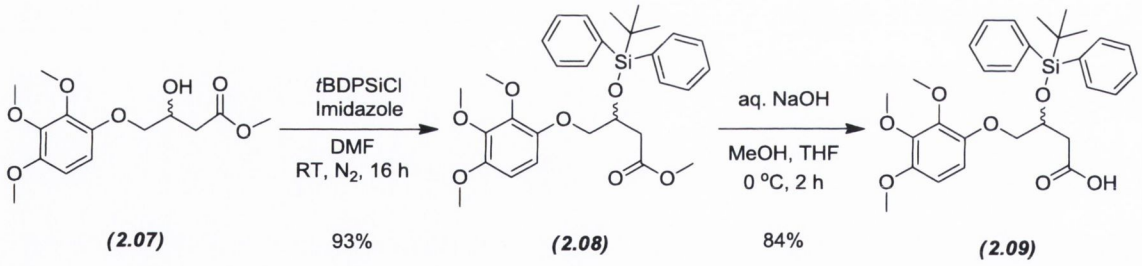
Scheme 2.7. Various methods tried in the reduction of keto-ester 2.06

The approach of pre-activating the solvent, methanol, with cerium (III) chloride (Luche Reduction)[220] led to slightly improved yields (55%). This was still considered insufficient and in light of this, our attention was focused on alternative reducing agents. It has been shown[221] that Baker's Yeast from *Saccharomyces cerevisiae* contains an enzyme which selectively reduces the carbonyl of β-keto esters to their corresponding alcohol derivatives. When we used this method, a yield of approximately 66% was recorded representing a substantial improvement. Practically, there are inconveniences regarding this method. First, a large quantity of yeast must be used per

gram of compound; approximately 10 g of yeast per gram of keto-ester. Secondly, after twenty-four hours the yeast becomes deactivated, , requiring an additional 10 g of yeast per gram of compound to drive the reaction. With large quantities of yeast it can be difficult to physically remove all of the product material from such a large mass of quite sticky material. Despite these drawbacks, it remains a consistently good method for the reduction of ***2.06***.

2.1.3 Formation of cyclised intermediate 2.10

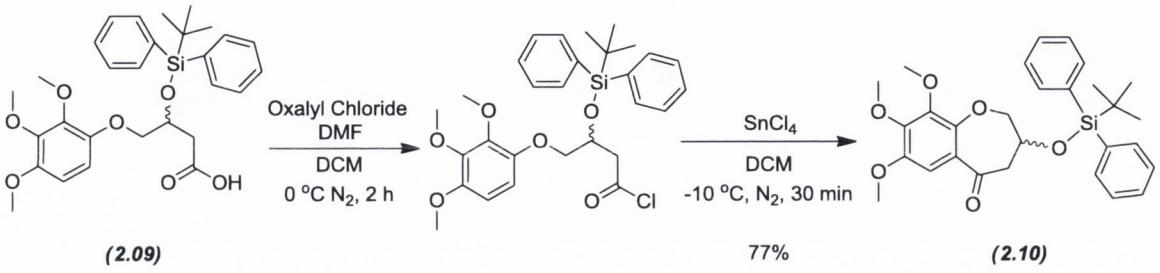
Once reduced, the alcohol ***2.07*** was then protected as a *tert*-butyldiphenylsilyl ether ***2.08*** in dry DMF. The ester group of ***2.08*** was subsequently hydrolysed under basic conditions (Scheme 2.8). Care was required in this transformation as a number of degradation by-products began to form if the reaction time was prolonged beyond 2-3 hours. Interestingly, this behaviour was only observed with these phenoxy compounds; the corresponding aliphatic analogues prepared by G. Stack, B. Moran and E.C. Breen[211] (with carbons in place of the phenoxy oxygen) were stable under the same conditions overnight or even several days. It was also noted in this case that if the reaction mixture was not a thoroughly homogenous solution, yield was drastically affected (as low as 35% in some cases).



Scheme 2.8. Silyl protection of hydroxy ester 2.07 and subsequent basic hydrolysis of methyl ester 2.08

Once pure, the carboxylic ester ***2.09*** was cyclised under Friedel-Crafts acylation conditions to give the benzocycloheptanone derivative ***2.10*** (Scheme 2.9). This cyclisation step can be a temperamental step, and requires an absolute dry environment and precision throughout. During the early stages of the project, these were carried out exclusively on a small scale; maximum 0.50 g of the carboxylic acid was used on each occasion that the reaction was carried out. Five molar equivalents of oxalyl chloride was used to ensure complete formation of the acyl

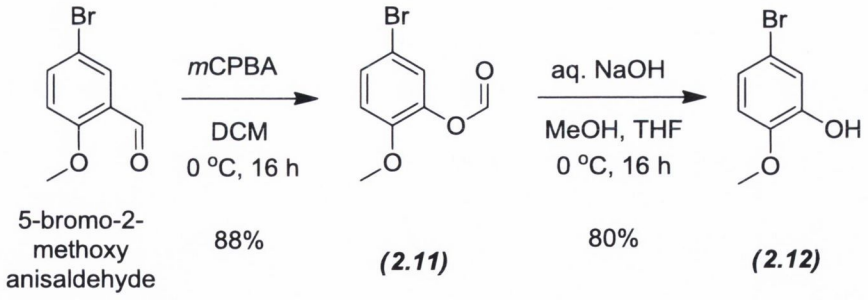
chloride intermediate, before tin chloride mediated the cyclisation reaction. It was imperative that the product was purified immediately after the reaction was completed in order to avoid deprotection and break down of the alcohol.



Scheme 2.9. Friedel-Crafts acylation and cyclization of 2.09

2.1.4 C-ring synthesis

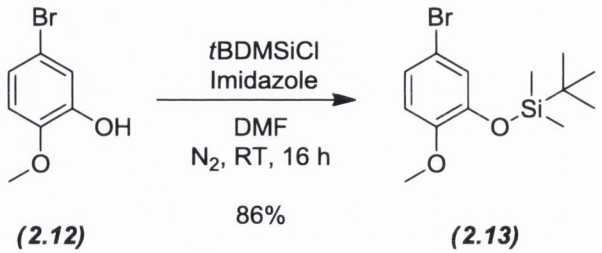
Having secured the appropriate presentation of the AB-ring, our attention was now focused on the procurement of a series of C-ring intermediates for attachment onto ***2.10***. Common to all C-ring intermediates is the presence of a *para*-methoxy group as this is deemed essential for binding to tubulin. The bromine moiety can be used as the point for direct coupling to ketone compounds like ***2.10***, but otherwise can be easily interchanged to afford alternative coupling substrates, such as the corresponding boronic acid derivatives for example.



Scheme 2.10. Baeyer-Villiger oxidation and basic hydrolysis of an ester

The first intermediate synthesised was ***2.13*** which was prepared from commercially available 5-bromo-2-methoxy-anisaldehyde. Again, as for the synthesis of ***2.01***, the aldehyde underwent Bayer-Villager oxidation to the formate ester ***2.11,*** which was then hydrolysed to the phenol

2.12 (Scheme 2.10). Attempts to incorporate the Dakin transformation to furnish the phenol ***2.12*** ended in failure, with interference by the bromine substituent the most probable cause. Protection of ***2.12*** afforded the silyl ether ***2.13*** (Scheme 2.11).



(2.12) ***(2.13)***

Scheme 2.11. *tert*-Butyl dimethyl silyl protection of the C-ring phenol 2.12.

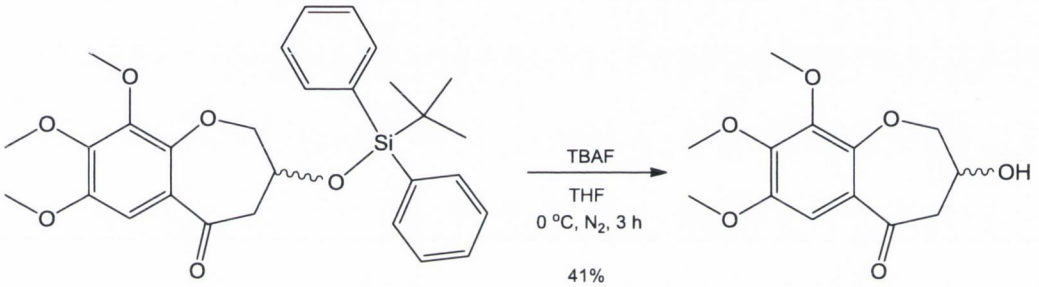
2.2 Synthetic Strategy 2

Having synthesised ketone ***2.10***, we were finally in possession of a versatile precursor to which we could build a range of potential benzoxepinone-based tubulin inhibitors. On to this molecular scaffold, we aimed to couple different C-rings like ***2.13*** synthesised above, although depending on the functional groups involved different coupling methods would need to be employed. In the case of coupling ***2.10*** to ***2.13***, organolithium coupling represented the most direct option available.

In terms of the overall synthesis, coupling of ***2.10*** to ***2.13*** paved the way to ***2.17*** (aka ***RS5.04***), first synthesised by Shah[204] and considered the archetypical benzoxepinone based TBA from our lab. Although it may seem intuitive to couple both protected compounds together, then remove both silyl groups together, practically this was not possible as the requisite oxidation of the alcohol afterward to give the target ketone proved difficult in the presence of the phenol. We also suspected that added bulk of the TBDPS protecting group on the AB-ring could potentially retard the coupling interactions. As we were sceptical of finding a reliable method of orthogonally removing a diphenyl silyl group without disturbing the more sensitive dimethyl silyl ether, it was deemed necessary to deprotect ***2.10*** prior to coupling with ***2.13***.

2.2.1 Deprotection and Coupling Step

Deprotection of ***2.10*** was carried out using tetrabutylammonium fluoride (TBAF) at 0 °C. Although TBAF is widely used in silyl deprotection chemistry, it nevertheless remains quite an aggressive reagent and prolonged exposure to a delicate substrate, such as the one generated here, did lead to excessive product deterioration. Hence, this reaction was monitored fastidiously, and upon completion was rapidly concentrated and loaded straight on to silica for purification, without the conventional work-up.



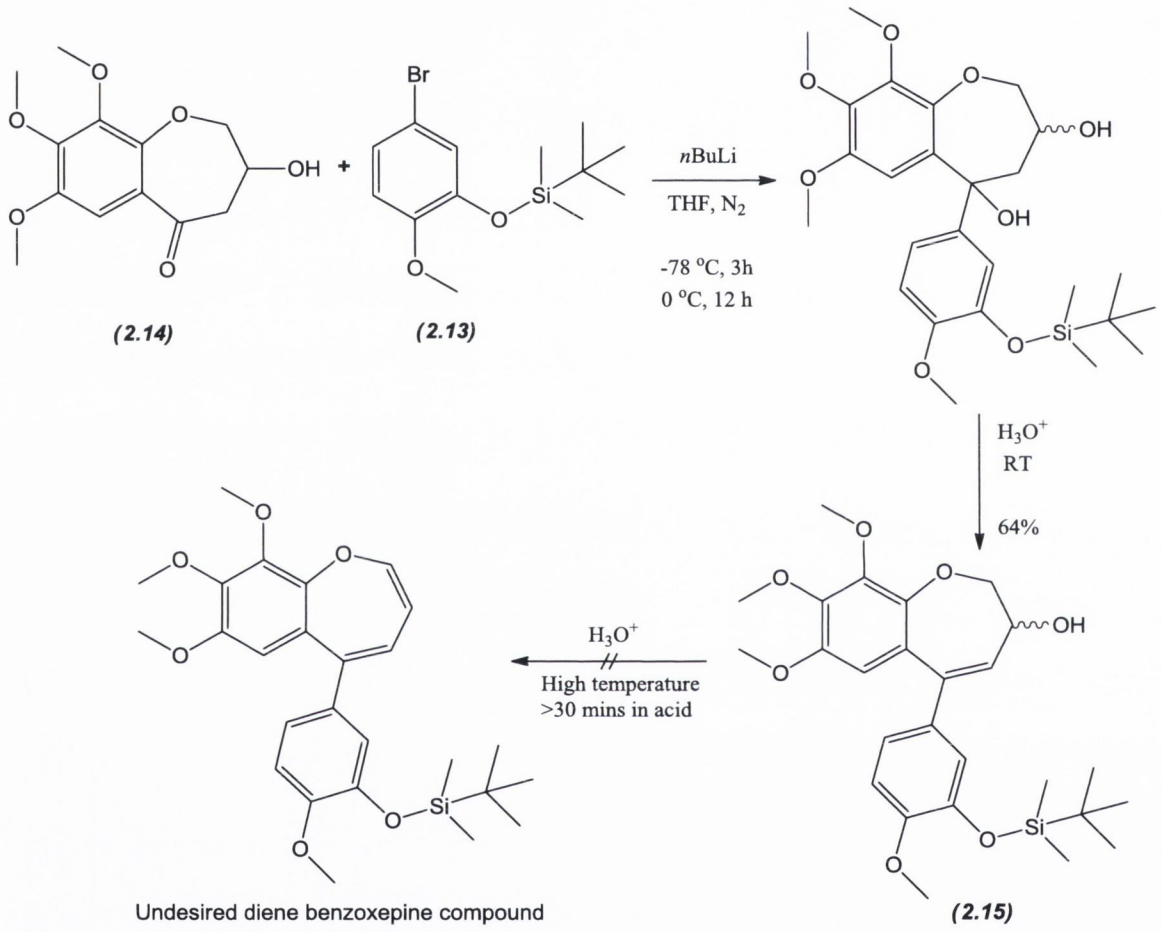
(2.10) ***(2.14)***

Scheme 2.12. TBAF deprotection of the *tert*-butyldiphenyl silyl ether 2.10 to give secondary alcohol 2.14

One of the major degradation by-products for this reaction is the alkene; arising from elimination of the alcohol moiety. This was a reoccurring problem throughout the syntheses of all benzoxepinone compounds as the intermediates possessing the secondary alcohol at this position were predisposed to spontaneous elimination.

The coupling step itself was another very sensitive transformation, particularly with regard to its exposure to water; this reaction could be severely compromised even by atmospheric moisture. Substrates were therefore thoroughly dried under vacuum for several days before use, and reaction temperatures, times and conditions monitored carefully. The initial product of this reaction is actually a diol compound, which upon acidic work-up furnishes the desired enol (Scheme 2.13). Care was required with this reaction owing to the innate tendency of the secondary alcohol moiety to eliminate even under mild provocation by the incentive to form a

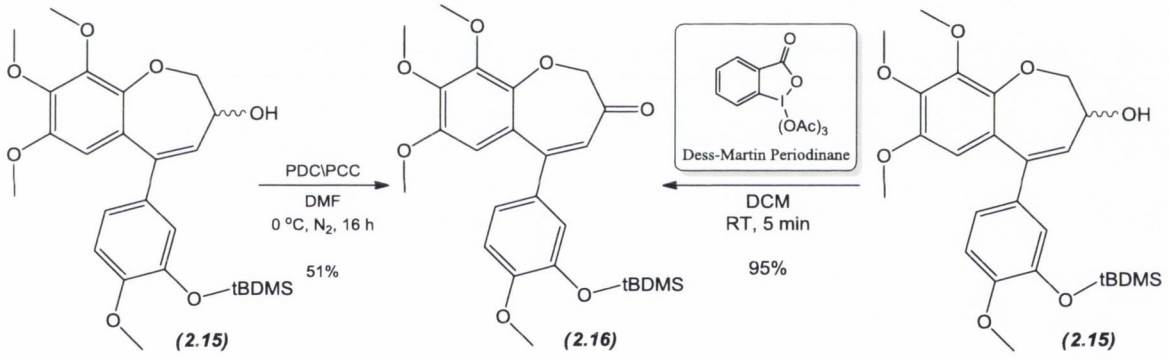
highly conjugated diene derivative. It was observed that without the acidic work-up the diol persisted indefinitely, while a lingering work up resulted in heavy forfeiture of product to the diene. Dilute acid, quick extraction and evaporation at low temperature were among the strategies employed to optmise the transformation. It was also noticed that the diol which survived the gentle acid wash gradually converted to ***2.15*** when left over time.



Scheme 2.13. Organolithium coupling with acidic work up to give 2.15. Prolonged exposure to aqueous HCl solution causes elimination to undesired diene (bottom left)

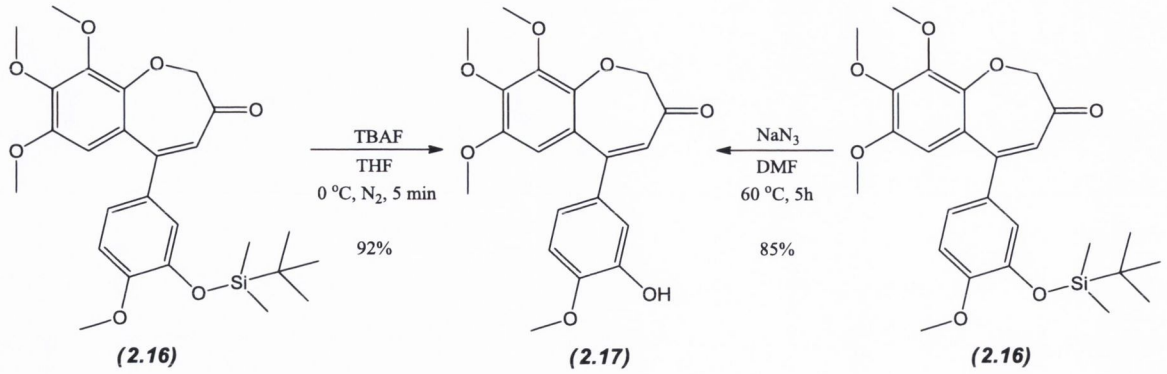
Having successfully obtained the alcohol ***2.15***, we worked quickly to convert it to the more stable ketone. Originally, we used pyridinium dichromate (PDC), although yields associated with this reagent were average at best (around 50%). After the two inefficient steps previous, and a lengthy synthesis overall, it was important to optimise the final steps to ensure an adequate quantity of final product. Moreover, the PDC reaction required the use of dry DMF, a solvent

which can be difficult to fully remove due to its high boiling point after the reaction has gone to completion. Pyridinium chlorochromate (PCC) was also tried, but to no appreciable benefit. A viable alternative was to use Dess-Martin periodinane, an iodine-based oxidising agent[222], known to oxidise even sensitive enol alcohols like ***2.15***. Nucleophilic attack of the alcohol on iodine (oxidation state V) displaces a labile basic acetate ion which abstracts a proton from the alcohol carbon to form acetic acid as a by-product. In deprotonating the alcohol carbon, the carbonyl is simultaneously formed and the new ketone is released from the periodinane complex. The application of this reagent in place of the chromium based reagents improved every aspect of the reaction; complete conversion of the alcohol to the ketone took place using only one equivalent of this reagent in DCM at room temperature, and anhydrous conditions were not only unnecessary but in fact discouraged[223]. Work-up of the reaction consisted of a simple base wash and few, if any, by-products accompanied the desired compound ***2.16*** (Scheme 2.14).



Scheme 2.14. Oxidation of alcohol 2.15 to ketone 2.16

In the final step, deprotection of the phenolic silyl ether ***2.16*** was typically carried out with TBAF. In this instance, *tert*-butyldimethylsilyl ethers can be cleaved much more rapidly than corresponding *tert*-butyldiphenylsilyl ethers, and this reaction was complete within minutes (Scheme 2.15). An alternative method for deprotection of a silyl group established by White[207] utilised sodium azide, which over a course of 5 hours, under mild conditions (heating to 50-60 °C) gave the phenol ***2.17*** (formerly ***RS5.04***), in a clean and gentle manner. While the use of the difficult-to-remove DMF as a solvent in this method undermines its applicability somewhat, there is nonetheless an inherent value in having a mild alternative to TBAF deprotection available for a more appropriate situation.



Scheme 2.15. Deprotection methods for dimethyl silyl ethers.

2.2.2 Structural Elucidation of 2.17

The identity of benzoxepinone compound ***2.17*** was confirmed by NMR and mass spectroscopy. Although not the most challenging structure, understanding this molecule unambiguously in terms of its characteristic spectroscopic behaviour is advantageous not only for compound ***2.17***, but serve as a predictive blueprint for analogues and hybrid compounds in particular whose synthesis is described in Chapter 4.

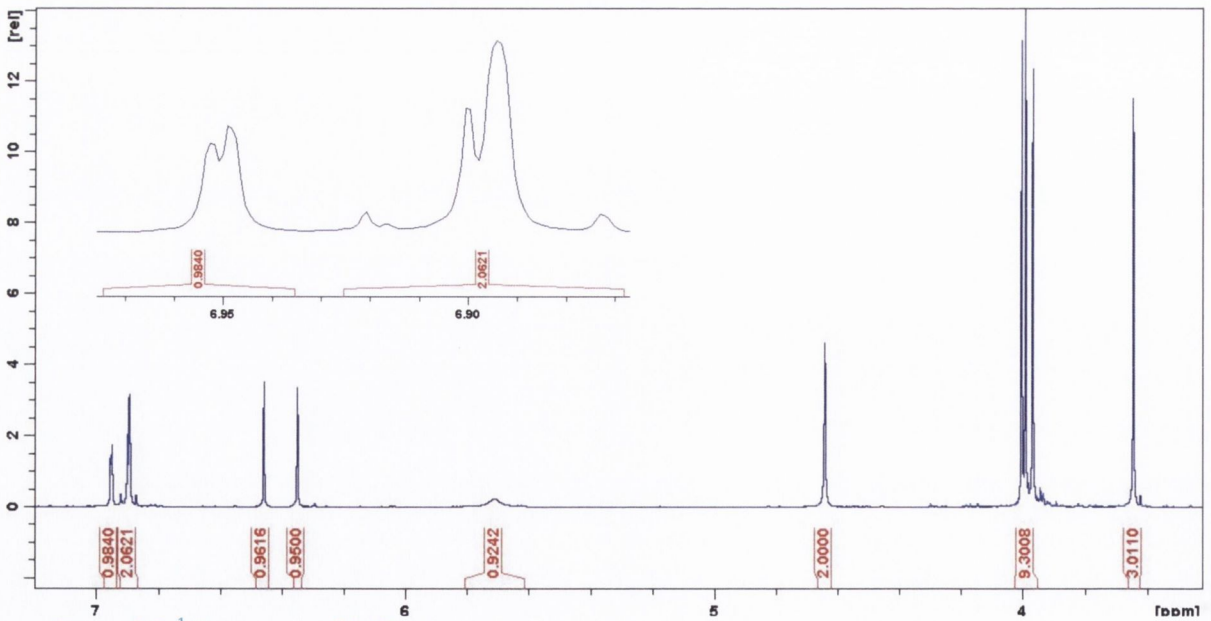


Figure 2.2. ^{1}H spectrum of 2.17

With seven oxygen atoms in the molecule, it was no surprise to find a lack of upfield hydrogens on the ^{1}H NMR spectrum (Figure 2.2). The lowest recorded peaks are those of the methoxy protons, observed between 3-4.0 ppm as four singlets integrating to three hydrogens each. With three of these grouped closely together around 4.0 ppm, and with another somewhat isolated around 3.6 ppm, putative assumptions could be made that these are the three A-ring and single C-ring methoxy groups respectively, however, a closer look at the HMBC spectrum dismisses the notion; the most upfield methoxy peak (3.6 ppm) couples to the same carbon (110.4 ppm) the A-ring hydrogen is attached to, thus must be associated with the A ring itself.

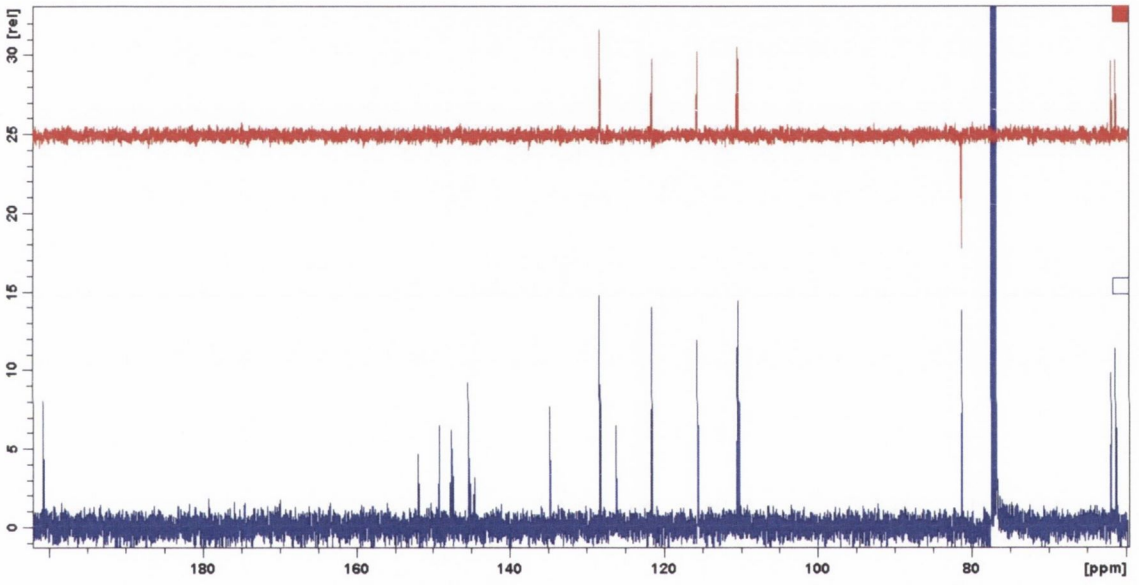


Figure 2.3 Full ^{13}C spectrum (bottom) and DEPT 135° (top) of phenol 2.17

Both hydrogen and carbon signals of the sole methylene group are easily identifiable; the hydrogen signal is found quite downfield for a CH_2 at 4.7 ppm, while the DEPT 135° spectrum (Figure 2.3) easily distinguishes the corresponding carbon at 81 ppm. The next downfield hydrogen signal is that of the phenol; a broad singlet at 5.7 ppm as the HSQC spectrum confirms that it is not attached to a carbon. (Figure 2.4)

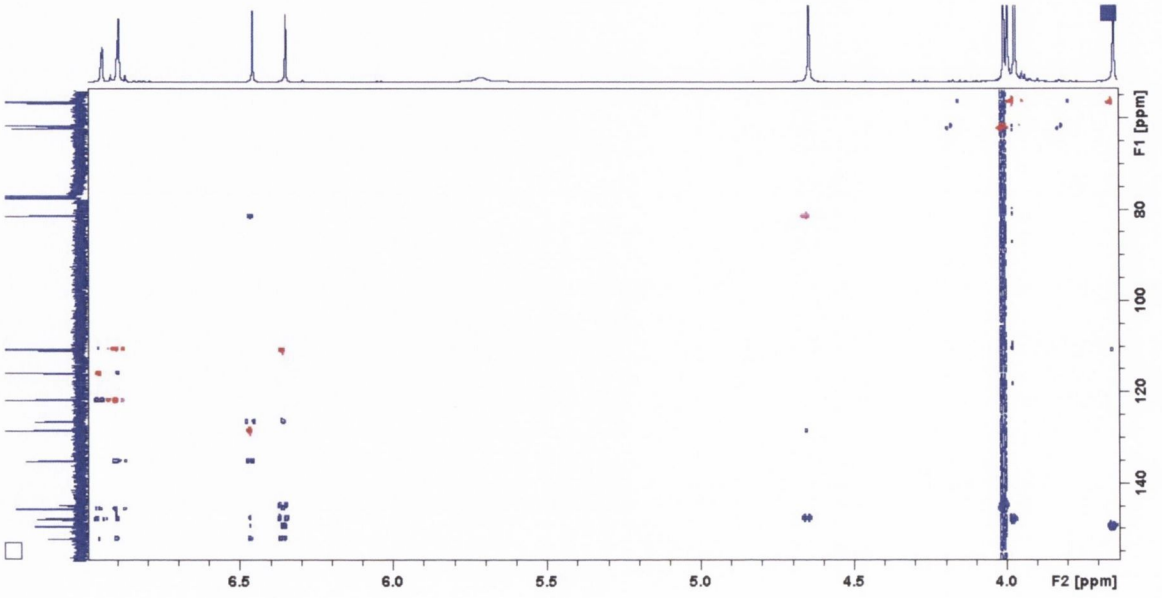


Figure 2.4. HSQC (red\pink) and HMBC (blue\green) correlation spectra of 2.17 (ketone omitted)

Downfield, toward the aromatic region of the ^{1}H spectra, the remaining five hydrogens on ***2.17*** are accounted for. We can split this cluster of signals into two approximately 0.5 ppm apart; two singlets further upfield (6.3 – 6.5 ppm) and a group of overlapping signals nearer 7.0 ppm. The former group are obviously the A-ring hydrogen and the double bond hydrogen; both are isolated hydrogen atoms that could only ever give rise to singlets. Again, one could assume that the more upfield peak is that of the double bond hydrogen, given that alkene hydrogens are typically found more upfield than aromatics, but closer inspection of HSQC and HMBC spectra proves that this is not the situation; instead associating this peak with aromatic and methoxy peaks indicative of the A-ring hydrogen, while correlating the downfield peak at 6.5 ppm with the methylene carbon at 81 ppm. The strongly electron withdrawing ketone group has a powerful enough deshielding effect to push the alkene signal downfield further than the A-ring aromatic peak, itself coerced upfield by three electron donating methoxy groups on the phenyl ring. The final group of downfield hydrogens (6.85 – 7.0 ppm) are those on the aromatic C-ring. Clear and patent signalling patterns were not observed in this case, a result of signal overlap. Together, the group integrate for three hydrogens, in the form of a multiplet (6.93 – 6.86 ppm, 2 H) and an asymmetrical doublet (1 H).

With the ^{1}H spectrum defined, ^{13}C spectra, DEPT and two dimensional spectroscopic techniques are applied to complete the elucidation. Carbon signals can be grouped for convenience; four

methoxy groups are found to resonate between 55 – 62 ppm, sole double bond signal at 81 ppm (DEPT 135° confirmed), aromatic and double bond carbon signals are seen to resonate between 110 – 155 ppm with the carbonyl carbon at 200 ppm.

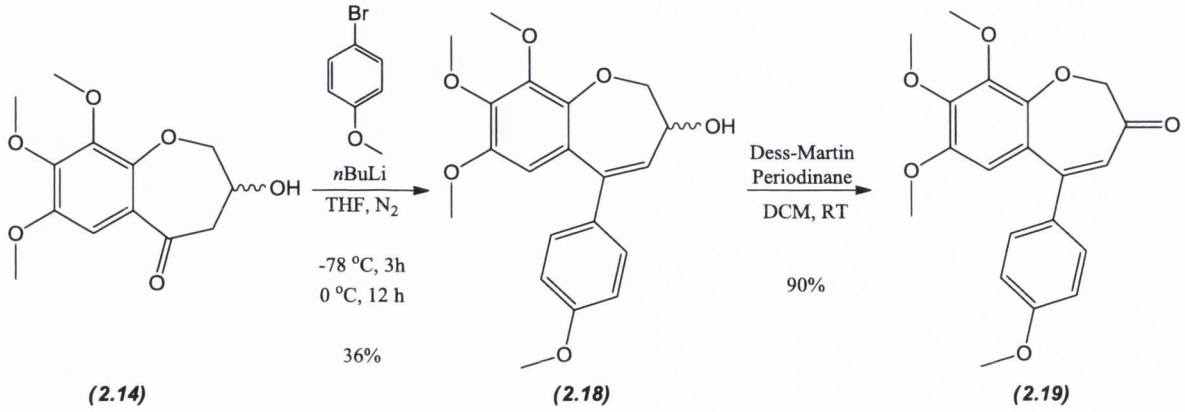
HRMS analysis further confirmed the identity of ***2.17***, with a detected ion mass of 373.1209 m/z corresponding to a singularly protonated ***2.17*** ion. The IR absorption spectrum corroborated with the other analytical techniques; showing broad phenolic O-H stretching at 3298 cm^{-1} and ketone C=O absorption at 1643 cm^{-1}; the expected range for an enone carbonyl group[224].

2.3 Analogues of 2.17 – Synthetic strategy 3

With primary target ***2.17*** obtained, and with reserves of ketone precursor ***2.14*** in our possession, the focus turned to derivatives of ***2.17***. One such example was the simple para-methoxy benzoxepinone ***2.19***; essentially the ***2.17*** skeleton without the hydroxyl substituent on the C-ring. In addition to investigating its biological activity, we were interested in this compound from the perspective of the novel ring contraction and rearrangement reactions discussed in Chapter 3. On the way to this compound, the alcohol intermediate ***2.18*** was also of interest; it was rationalised that this compound may be more stable to elimination than the corresponding alcohol derivative of ***2.17*** thus with this compound in hand would enable us to better evaluate and compare the alcohol against the analogous ketone ***2.19***, to consolidate our understanding of the importance of these differing functional groups in this particular position.

2.3.1 Para-methoxy C ring analogues

Commercially available 4-bromoanisole was acquired and coupled to the hydroxyketone precursor ***2.14*** using the organolithium method (Scheme 2.16). The resultant alcohol ***2.18*** was oxidised using Dess-Martin periodinane as before to furnish ketone ***2.19***. Both compounds were completely characterised by NMR, IR and HRMS analysis. A characteristic feature of both compounds was the symmetrical aromatic region with regard the C-ring hydrogens in their NMR spectra, consisting of two well defined doublets, which further simplified their elucidation.



Scheme 2.16. Synthesis of alcohol 2.18 and ketone 2.19

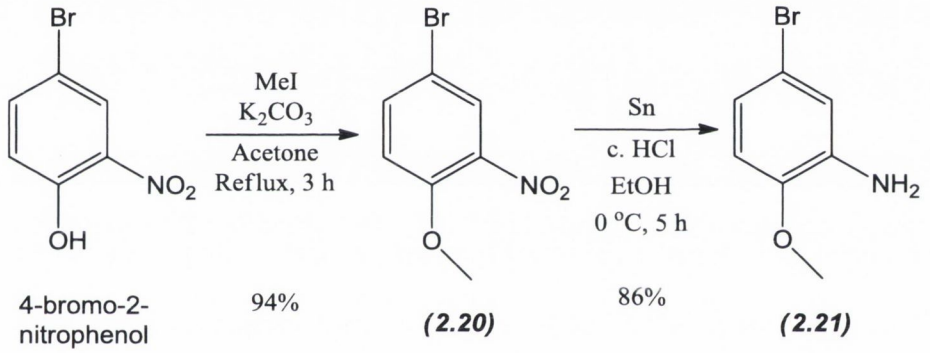
2.3.2 Aniline C ring analogue

The aniline version of ***2.17*** presented the isosteric possibility of improved activity over that which the phenol ***2.17*** could offer itself; could an aniline functional group form improved hydrogen bonding with the carbonyl oxygen of the threonine α177 of tubulin? Furthermore, in terms of hybrid drugs, this simple switch in functional group affords a marked improvement in terms of stability of the amide bond binding both pharmacophores together, over the phenolic ester. In turn this presents an opportunity for the creation of both neutral and acidic amino acid prodrug derivatives of the aniline, which should be amenable to enzymatic activation either by APN, for neutral amino acids, and the sister enzyme APA, for acidic amino acid derivatives.

Synthesis of the aniline benzoxepinone did necessitate a deviation in synthetic strategy; organolithium coupling is not possible with the protected aniline functional groups. Instead, the plan was to employ palladium-based Suzuki coupling[225]; a reaction that has proven reliable for our group over many years. To apply this approach we also had to make minor modifications to the earlier steps of this synthesis. Unlike organolithium coupling, Suzuki coupling requires aryl or vinyl substrates, so with regard to the AB-ring, the B-ring double bond needed to be introduced in advance. Furthermore, simply presenting the B-ring as an enol is not appropriate either; the C-O^- bond would be too strong for rearrangement around palladium. Instead, we would implement a more labile ligand, an enol triflate, in place of the enol. Triflates have long been used as starting materials in palladium cross coupling reactions, with a history of positive performance throughout this field[226].

2.3.2.1 Synthesis of a new C-ring precursor for aniline based TBAs

The synthesis of the C-ring commenced from the commercially available starting material, 4-bromo-2-nitrophenol, which was alkylated with iodomethane under basic conditions to give ***2.20*** (Scheme 2.17). Clean conversion of the nitrophenol to the anisole meant flash column chromatography could fortunately be avoided. Reduction of the nitro group to the aniline ***2.21*** was achieved with tin powder and concentrated hydrochloric acid. Caution was needed upon neutralising the reaction with sodium hydroxide; thus the reaction was brought to 0 °C to temper the strong exothermic response.



4-bromo-2-nitrophenol

94%

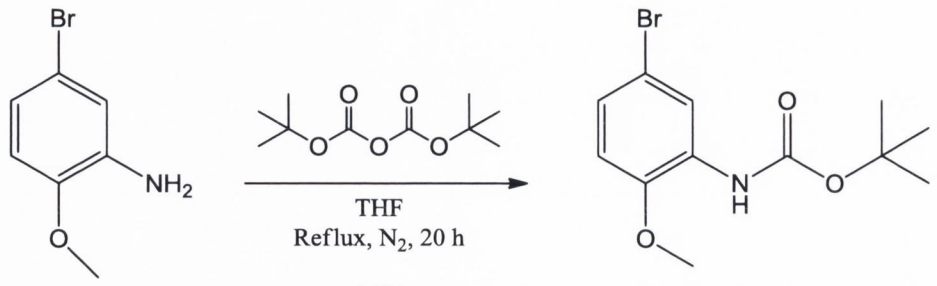
(2.20)

86%

(2.21)

Scheme 2.17. Aniline Synthesis 2.21

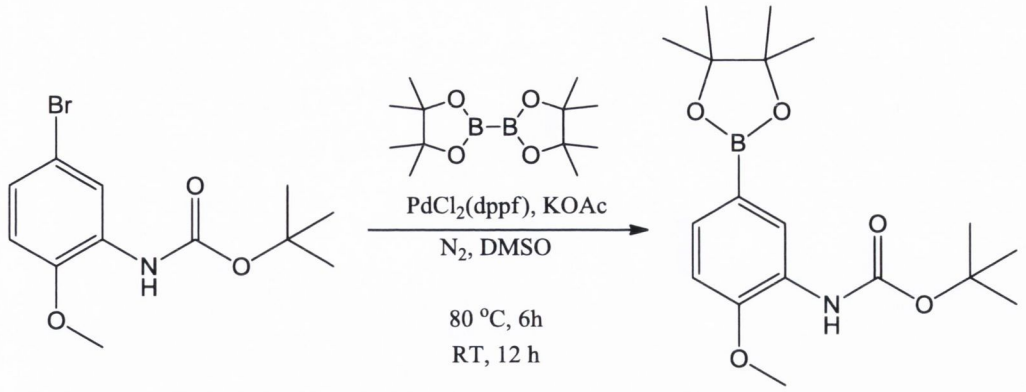
The aniline group was then *N*-protected with a Boc group using the carbonic anhydride, di-*tert*-butyl dicarbonate. This reaction was very slow and required heat to activate, although upon eventual completion, yields of ***2.22*** were actually quite high (Scheme 2.18).



(2.21) ***(2.22)***

Scheme 2.18. Boc protection of aniline 2.21

Now protected, the bromine on the aniline ring ***2.22*** was converted to the suitable boronic ester ***2.23*** necessary for Suzuki coupling (Scheme 2.19). Usually, boronic acids are usually preferred to boronic esters for Suzuki coupling, but attempts to convert the bromine to the boronic acid had previously proved unsuccessful. The aryl boron pinacol ester was prepared via the Miyaura borylation reaction[227], whereby oxidative addition of an aryl halide onto the catalytic palladium(0) species is followed by transmetallation of the boron species, which has been activated to do so by the base (potassium acetate in this case) either by coordinating to the boron to enhance its nucleophilicity, or by displacing the halogen coordinated to the palladium(II) to form a highly reactive Pd-O bond. Reductive elimination from the palladium releases boronic ester ***2.23***, with the formation of a new carbon-boron bond. Heat is required for the initial cross coupling of ***2.22***, but the subsequent displacements can occur at room temperature. In accordance with reports from the literature, we found electron donating groups like the methoxy group to slow the reaction down somewhat, however upon completion ***2.23*** was obtained in a relatively high yield (76%).



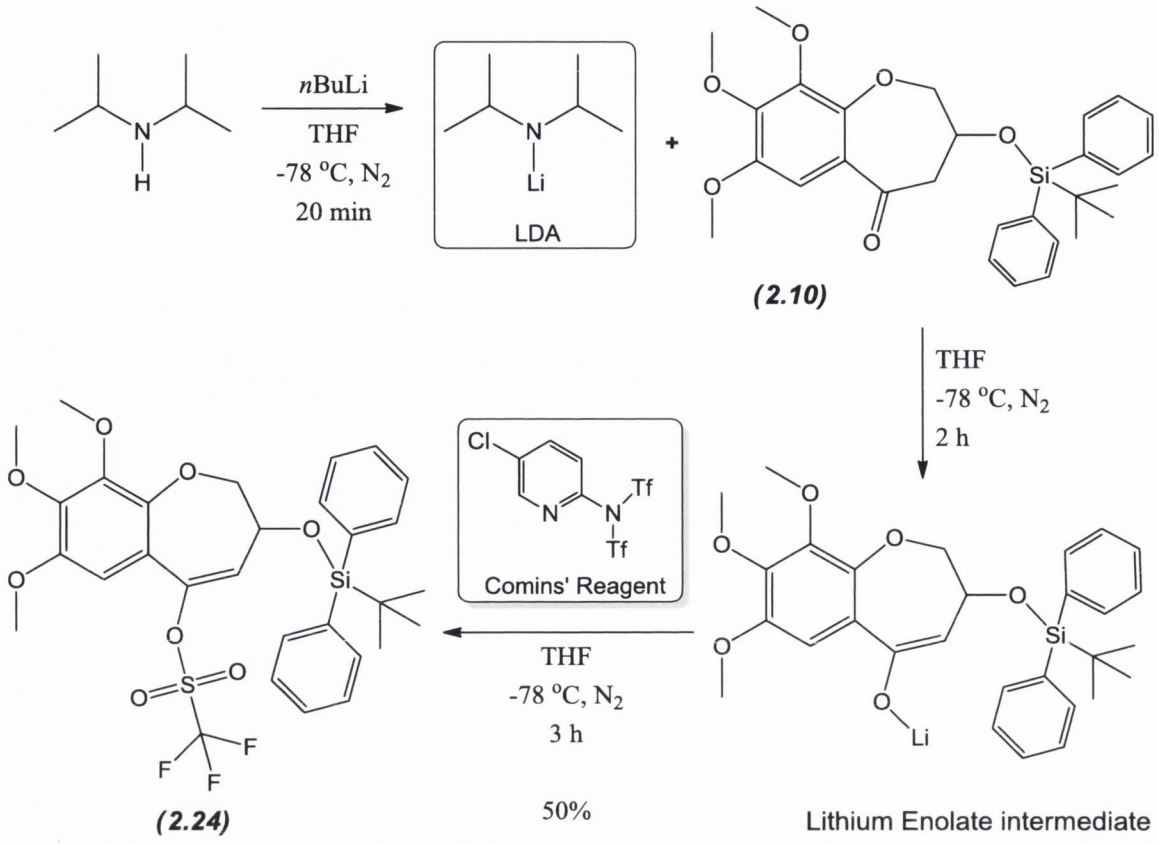
(2.22) 76% *(2.23)*

Scheme 2.19. Miyaura borylation of bromine to the boronic ester 2.23

2.3.3 Aniline C ring analogue – alteration of AB ring

With the C-ring now prepared for the next palladium based coupling reaction, attention turned back to the AB-ring. Cognisant that the AB-rings ***2.10*** or ***2.14*** would require modification before attempting the Suzuki coupling step, we set about the adaptation of the ketone group into an aforementioned enol triflate. With the ketone not nucleophilic enough to cause displacement of a halotriflate or triflic anhydride, and not wishing to synthesise and isolate an enol separately, we actuated a triflation reaction built around the use of Comins' reagent[228]. In this reaction, we would create the enol *in situ* using the powerful, non-nucleophilic base lithium diisopropylamide (LDA), similarly generated *in situ*. Nucleophilic attack from the enol to the electrophilic sulfur on Comins' reagent would displace the triflate group from the amino chloropyridine moiety from which it originated.

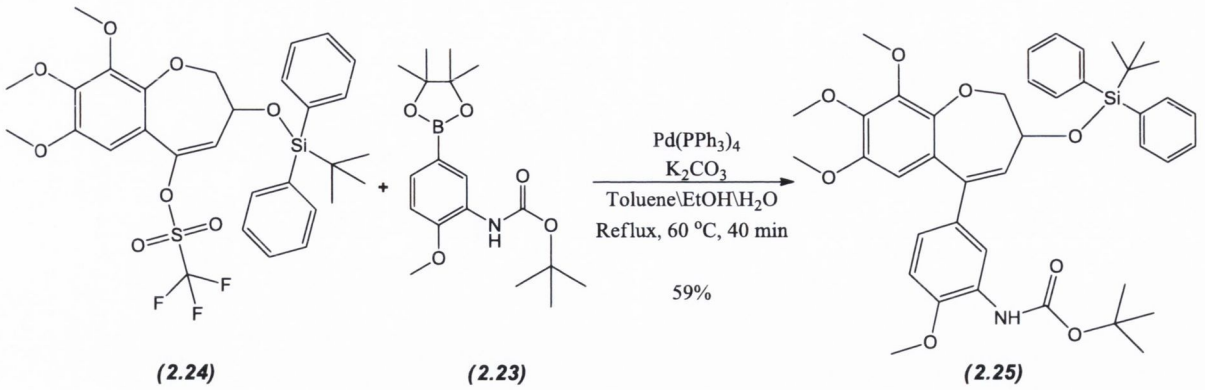
The triflation of ***2.10*** (Scheme 2.20) was initially problematic, with several failed attempts. The sensitivity of the highly reactive intermediates in the one pot synthesis of LDA, enol and triflate product meant there was little margin for error and meticulous synthetic and anhydrous technique was demanded. It became apparent over time that keeping all intermediates generously solvated with THF at all times was of upmost importance, and notable improvements in yield were recorded, although only ever to a very moderate degree.



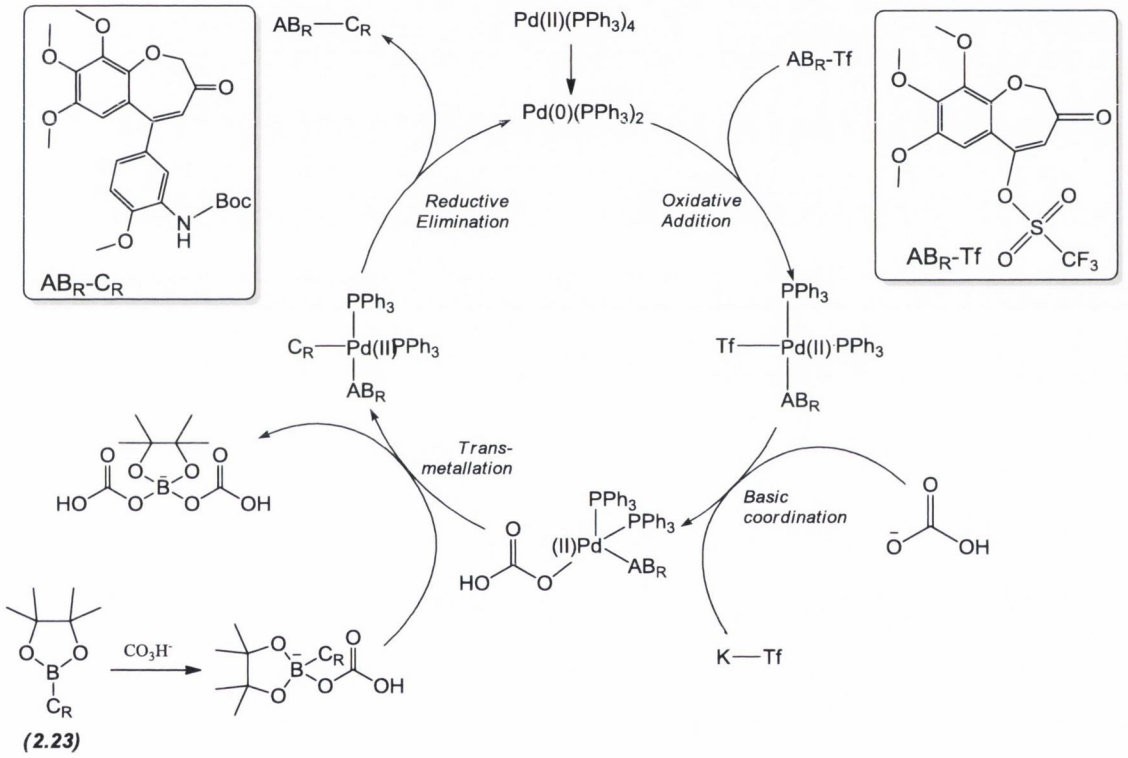
Scheme 2.20. One pot synthesis of triflate 2.24 from ketone 2.10

2.3.4 Aniline C ring analogue – Coupling

Suzuki coupling of enol triflate ***2.24*** with aryl boronic ester ***2.23*** took place under reflux using tetra*kis*(triphenylphosphine) palladium(0) as the catalyst, using potassium carbonate as base (Scheme 2.21). The operative mode of the Suzuki cross coupling was similar to that of the Miyaura borylation; oxidative addition, this time with the vinyl triflate onto the palladium(0) occurs first, basic coordination of the carbonate to the palladium(II) displaces the triflate moiety and transmetalation of the base-activated boronic ester follows. With both AB-ring and C-ring now coordinated on palladium(II), reductive elimination ultimately results in coupling of the two groups together as one, silyl ether ***2.25***, while simultaneously regenerating the palladium(0) species (Scheme 2.22).



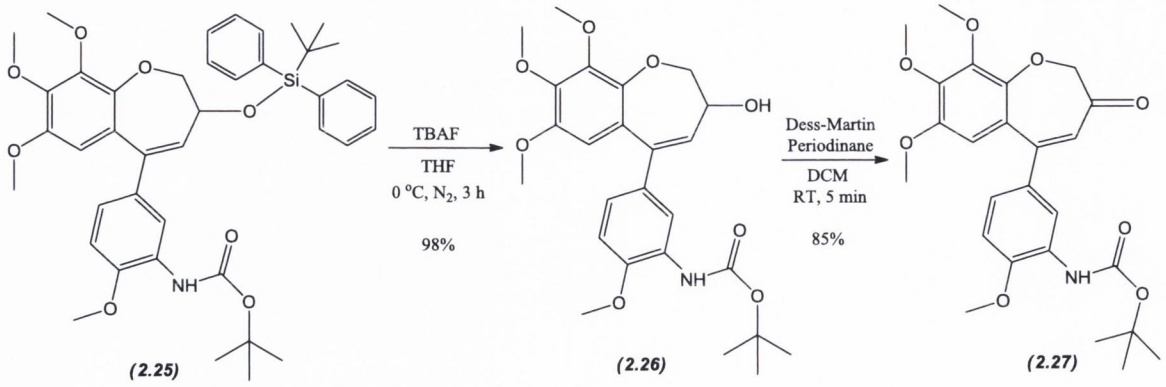
Scheme 2.21. Suzuki coupling of triflate 2.34 and boronic ester 2.23



Scheme 2.22 Catalytic cycle for Suzuki coupling of triflate 2.34 (AB_R-Tf) to boronic ester 2.23 (C_R) through triphenylphosphine palladium(0) and K_2CO_3 as a base to furnish product 2.25 (AB_R-C_R)

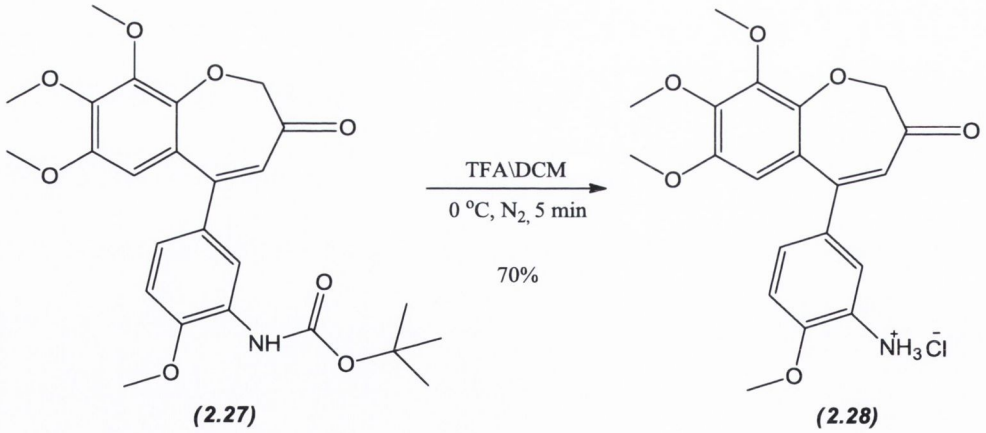
2.3.5 Aniline C ring analogue – Final Steps

Deprotection of the silyl ether ***2.25*** took place with TBAF as before, with diligence paid with regard to the time spent in contact with the aggressive TBAF. Again elimination was a prominent cause for concern. Oxidation of resultant alcohol ***2.26*** to ketone ***2.27*** was then carried out using Dess-Martin periodinane as the oxidising agent (Scheme 2.23).



Scheme 2.23. Deprotection and oxidation steps for ketone 2.27

Once the ketone ***2.27*** was formed, the *N*-Boc group was removed with 50% trifluoroacetic acid (TFA) in DCM under anhydrous conditions (Scheme 2.23). Removal of the volatile solvent left the TFA salt, which upon basification with 5% $NaHCO_3$ gave the free aniline, which was subsequently converted to its corresponding salt by passage of gaseous HCl over an ether solution of the aniline.



Scheme 2.24. Deprotection of aniline 2.27 to give aniline salt 2.28

2.3.6 Aniline C ring analogue – Structural Elucidation

The identity of the aniline ***2.28*** was confirmed through a range of spectroscopic techniques in the free base form, due to its superior solubility in deuterated chloroform, thus resulting in

better resolved spectra than the salt derivative. Obviously, with major similarities in common with phenol compound ***2.17***, it was intuitive that first one would concentrates on those parallels as a starting point. The four methoxy groups are easily identified in the ^{1}H NMR spectrum (Figure 2.5), in the same range and pattern as ***2.17***. So too, their corresponding carbon signals. Likewise, the methylene group also mirrors that of the phenol ***2.17***, with equivalent hydrogens signalling as one peak at 4.6 ppm, with the corresponding carbon found resonating at 81 ppm, confirmed by DEPT 135°. Unlike the hydroxyl group of the phenol compound, a signal for the aniline NH_2 hydrogens were difficult to detect and often absent on the ^{1}H spectrum, resonating as a very broad singlet, at approximately 3.1 ppm.

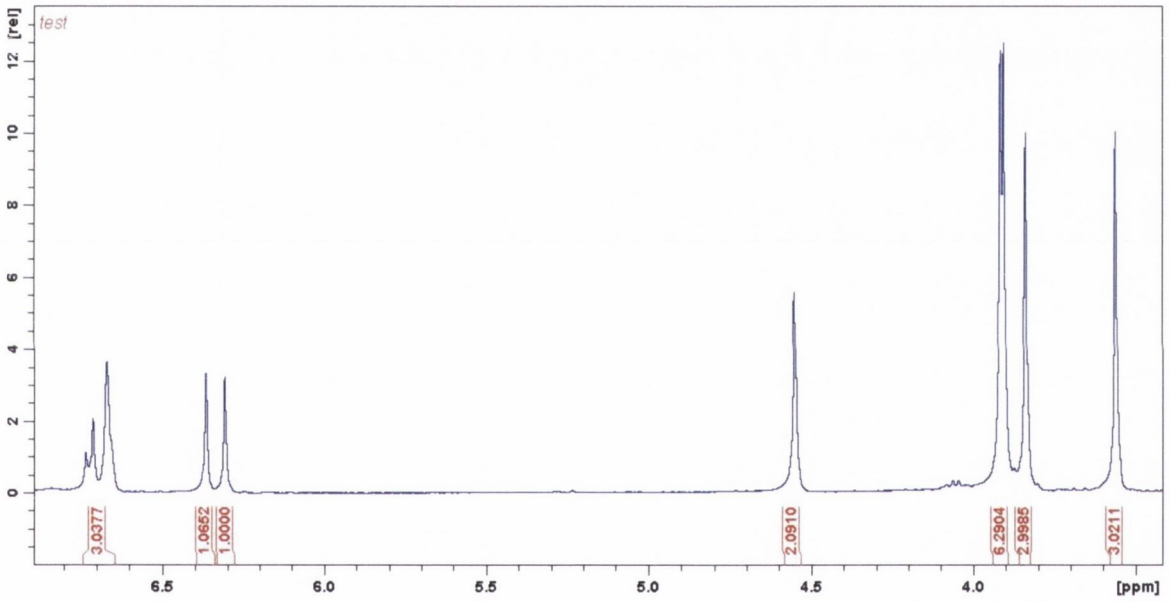


Figure 2.5. ^{1}H spectrum of aniline 2.28

Aromatic protons and the double bond hydrogen were easier to determine, the latter resonated at 6.5 ppm, slightly further downfield from the A-ring hydrogen at 6.4 ppm. Next, two C-ring hydrogens were found resonating together as a broadish asymmetrical peak at 6.75 ppm, followed closely by a signal that integrated for one hydrogen at 6.8 ppm. The coarse signals in this region was reminiscent of the proton signal overlap seen with ***2.17***. Altogether, these C-ring signals were found slightly upfield relative to ***2.17***; 6.7 – 6.82 ppm in the aniline vs. 6.87 – 6.96 ppm in the phenol, indicating a slightly stronger electron-donating\shielding effect from the lone pair on the aniline. This notion is somewhat rationalised in terms of anilines' generally weak

basic activity compared against aliphatic amines; electrons are drawn into the ring making them relatively less inclined to participate in basic or nucleophilic behaviour.

The ^{13}C NMR spectra (Figure 2.6) followed similar patterns to ***2.17***. Of the remaining signals, the ketone was found resonating at 200 ppm, the DEPT 90° spectrum distinguished aromatic and double bond CHs from remaining aromatic and quaternary carbon signals.

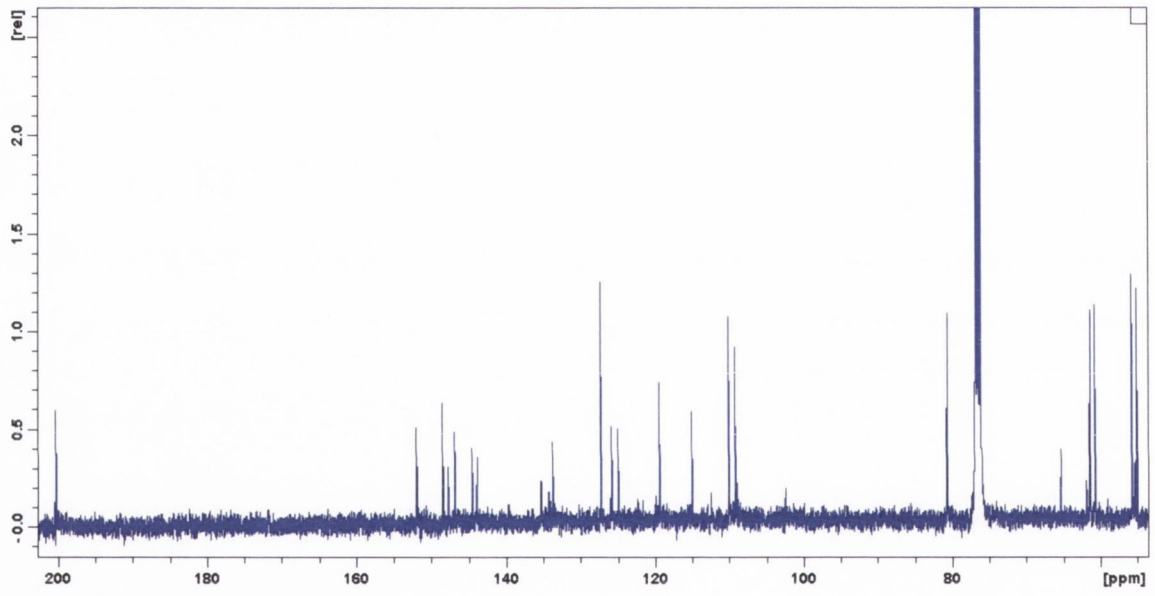
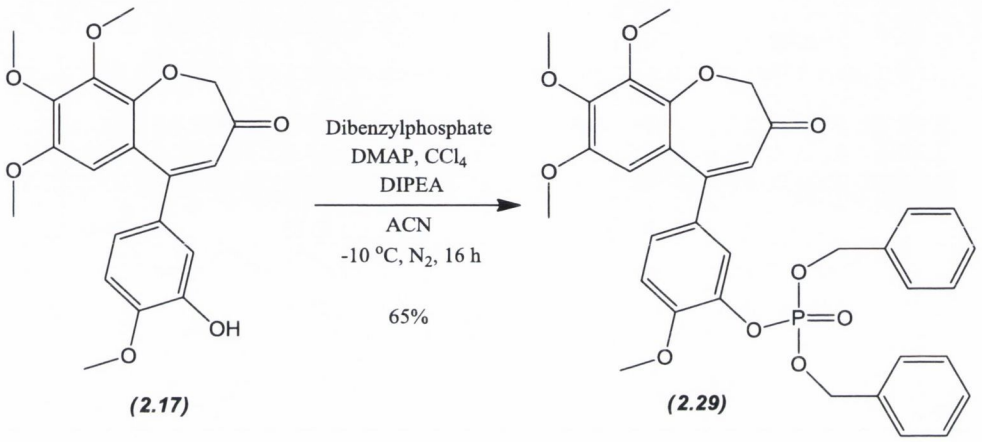


Figure 2.6. ^{13}C spectrum for 2.28

HRMS found the relevant protonated molecular ion of mass 372.9862. IR absorption found N-H band at 3374.4 cm^{-1}, alkane absorptions at 2932.5 and 2852.9 cm^{-1}, and the enone ketone absorption at 1657.4 cm^{-1}.

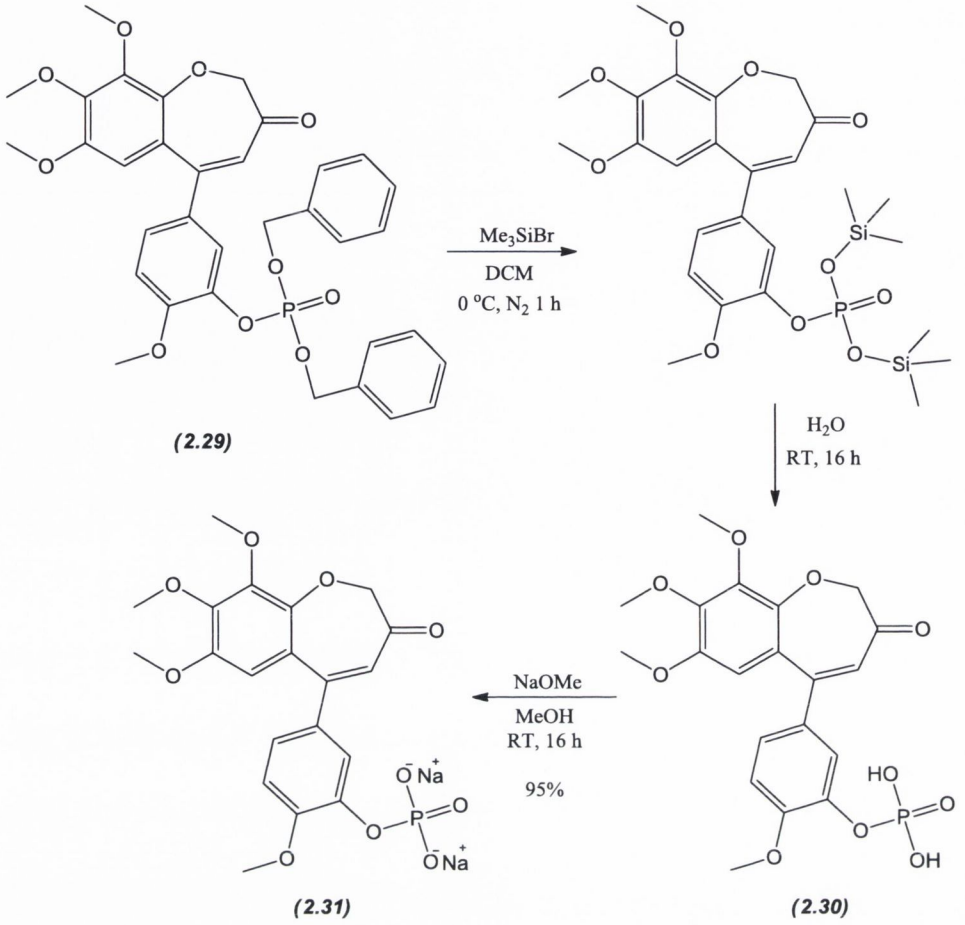
2.4 Phosphate Salt Prodrug

In the introduction, the concept of improved therapeutic effect and enhanced solubility of CA-4 by its presentation as a phosphate prodrug (CA-4-P) was discussed. With this in mind we embarked on the synthesis of the phosphate salt prodrug of the phenol ***2.17***, by essentially following the methodology employed in the preparation of CA-4 phosphate[229].



Scheme 2.25. Formation of a phosphate ester 2.29 with dibenzylphosphate

The first step (Scheme 2.25) involved phosphorylation of the phenol by reacting with dibenzyl phosphate, with DMAP as a catalyst and DIPEA as a tertiary base[230]. The phosphate ester ***2.29*** then underwent dealkylation with bromotrimethylsilane (BTMS)[231] and the subsequent treatment of the trimethylsilyl diester intermediate with water generated the phosphonic acid ***2.30***, a procedure that avoided the use of aggressive acidic or basic conditions. The acid was converted to the disodium salt ***2.31*** with sodium methoxide in methanol (Scheme 2.26).



Scheme 2.26. Formation of the phosphate salt 2.31 from the phosphate ester 2.29

2.5 Biological Evaluation of benzoxepinone compounds

Having secured efficient synthetic methods for the preparation of benzoxepinone phenol ***2.17*** and related compounds; alcohol ***2.18***, ketone ***2.19*** and aniline ***2.28***, extensive biological evaluation was then conducted by E. Prokopiou for her doctoral thesis on these compounds[232]. This section will highlight some of the most relevant assays carried out and the results derived from this series of compounds to date. These include anti-proliferative data and procedures designed to probe their impact on microtubule dynamics, as well as *ex vivo* assays that investigate their anti-angiogenic and anti-vasculature activity.

The anti-proliferative effects of these compounds were first assessed using an MTT assay. In this assay[233], the tetrazolic molecule (3-(4,5-dimethylthiazol-2-yl)-2,5-diphenyltetrazolium bromide (MTT) which is yellow in solution gets reduced by an enzyme, mitochondrial reductase, activated

only in viable cells, not in cells which have undergone apoptosis or indeed necrosis. The product of this biotransformation are crystals of the tetrazole opened formazan, which when solubilised give rise to a characteristic purple coloured solution, the absorbance of which can be measured by the plate reader at 500-600 nm wavelength to quantify the degree of cellular death. IC_{50} values for the lead compounds from this chapter were determined on both endothelial cells (HUVECs) and tumour cells (PC-3), with combretastatin A-4 used as a comparative control (Table 2.1).

Table 2.1. Best fit IC_{50} values ± SEM of benzoxepinone lead compounds from MTT assay (n=3)

	HUVECs (μM)	PC-3 cells (μM)
CA-4	4.03 ± 1.73 (nM)	14.01 ± 0.58 (nM)
2.17	4.91 ± 1.01 (nM)	4.67 ± 1.45 (nM)
2.18	4.02 ± 2.80	0.14 ± 0.04
2.19	1.09 ± 0.41	10.0 ± 4.03 (nM)
2.28	0.23 ± 0.15	0.36 ± 0.21

The MTT assay showed encouraging anti-proliferative activity for phenol ***2.17*** in particular, with IC_{50} values on par with CA-4 for the HUVEC cell line and less than CA-4 in the tumour cell line. Furthermore, the presence of oxygen in the B-ring to potentially improve TBA activity over the aliphatic B-ring was justified, with superior activity noted for ***2.17*** over its analogue, phenol ***RS180*** (IC_{50} = 65.05 nM and 50.65 nM; HUVECs and PC-3 cells respectively), from the doctoral thesis of Shah[204]. Comparison of derivatives ***2.18*** versus ***2.19*** indicated that the ketone group was favoured to increase activity, with ketone ***2.19*** exhibiting lower IC_{50} values in both cell lines. Aniline ***2.28*** performed well in both cell lines, although not enough to eclipse the phenol ***2.17***.

As mentioned briefly during the introduction, TBAs provoke cell death indirectly by causing arrest of the cell cycle at the G_2/M phase. During the G_2 phase, cells repair any damaged DNA and reorganise, before commencing mitosis during the M phase. Inhibition of tubulin polymerisation interferes with these cell cycle dynamics, causing arrest at the G_2/M phase. These cells fail the following cycle check point and are directed towards apoptosis. Cells arrested at the

G_2/M phase by microtubule disruption by TBAs are accompanied by increased levels of intracellular DNA[234], which can be quantified by flow cytometry[235]. Using this rationale, the proportion of a cell population under arrest of lead compound ***2.17***, the most efficacious drug based on the cell MTT assay above, was identified after 24 hour incubation using propidium iodide (PI) stain. At a concentration of 1 μM, phenol ***2.17*** induced G_2/M arrest of 71.20 ± 7.12%, slightly better than CA-4 (69.62 ±8.30%) and considerably higher than the control (31.44 ± 0.82%) (Figure 2.7).

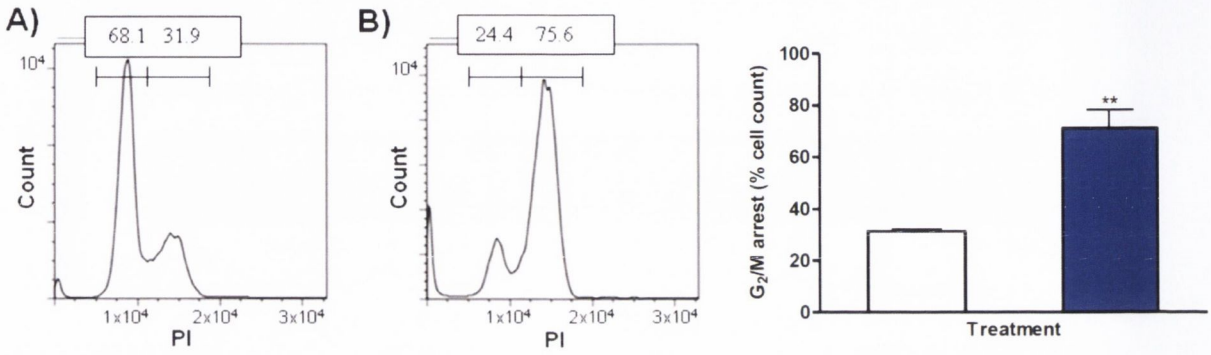


Figure 2.7. Cell cycle histograms of cells arrested in G_2\M phase of control (left, 0.1% DMSO) and those treated with 1 μM 2.17 (middle) after PI staining. Percentage of cells arrested shown (right) for control (white) and for 2.17 (blue)

Confirmation that lead compound ***2.17*** caused disruption of the microtubule cytoskeleton was determined via immunofluorescence staining[234c]. Nuclei were stained blue with 4',6-diamidino-2-phenylindole (DAPI), while α-tubulin subunits were stained green with the antibody Alexa Fluor® 488. Using confocal microscopy, substantial reduction of stained microtubule fibres around the nuclei of HUVECs could be visually observed after 30 minutes treatment with 1 μM of ***2.17*** compared to the control (Figure 2.8).

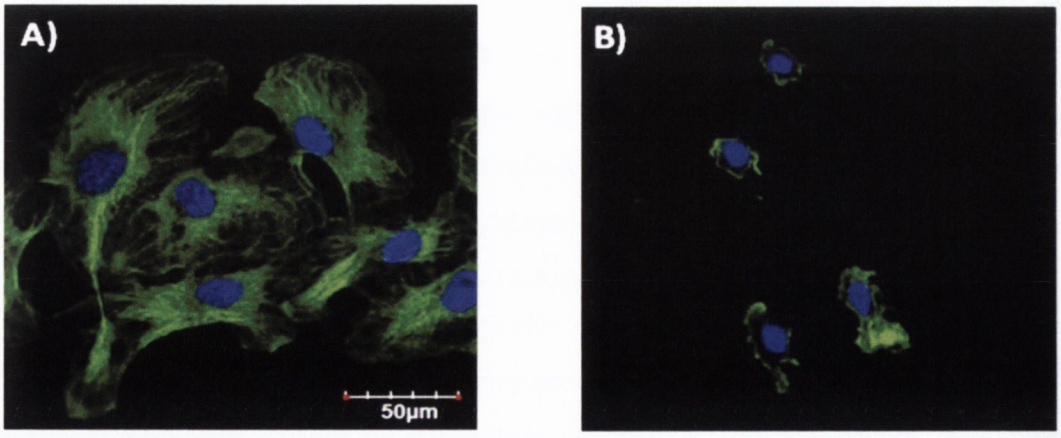


Figure 2.8. Images following immunofluorescent staining, representing the disruption of microtubules in HUVECs of control (left) and after 30 min treatment of 2.17 (right). α-tubulin stained green with DAPI, around the nuclei, which stain blue.

Next, the anti-vascular response of ***2.17*** was gauged in part by the analysis of the *in vitro* change in endothelial cell morphology of HUVECs. Whereas the control cells maintained a well structured, confluent monolayer with little or no abnormalities, within one hour both 0.1 μM and 1 μM ***2.17*** induced rapid, obvious alterations in cell shape; the endothelial contraction and blebbing characteristic of VDAs, while cell contents also darkened and the endothelium was disrupted. Reduced cell area was also evident. Only a minor recovery of endothelial cells was observed three hours following drug washout.

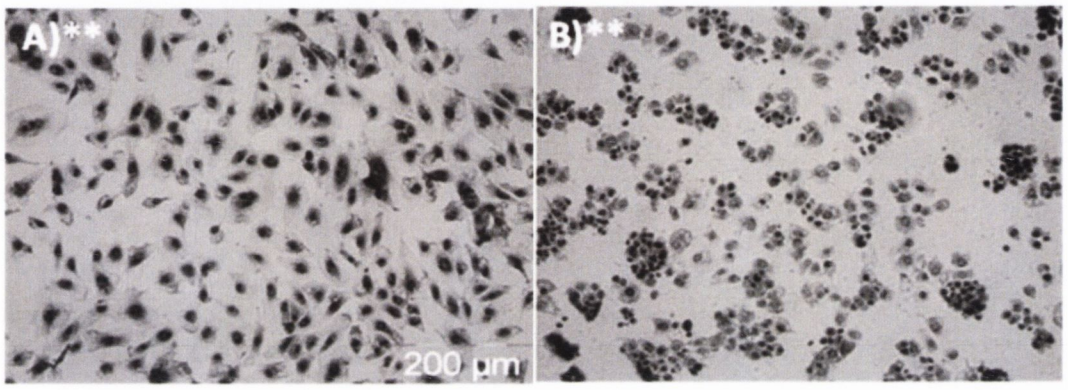


Figure 2.9. Change in endothelial cell morphology observed in (B)** (0.1 μM 2.17) relative to control (A)** (0.1% DMSO), 3 hours after drug washout.

The anti-vascular response was further investigated by a rat aortic ring assay[236]. In this *ex vivo* assessment, an aorta is excised from a male Wistar rat and cultured on matrigel. After several days' incubation, the aorta begins to sprout nascent endothelial vessels lined with pericytes and fibroblasts, replicating those found *in vivo*. Breakdown of the resultant neovasculature established 7-9 days after incubation can be induced by VDA administration, which is examined microscopically at different intervals over 24 hours. In the case of ***2.17***, vessel breakdown was not deemed significant at 10 nM, unlike CA-4. A much improved anti-vasculature effect was instead seen at 50 nM after 4 hours. In comparison, a 100 nM solution of the analogue ***RS180*** was required to elicit a comparable result.

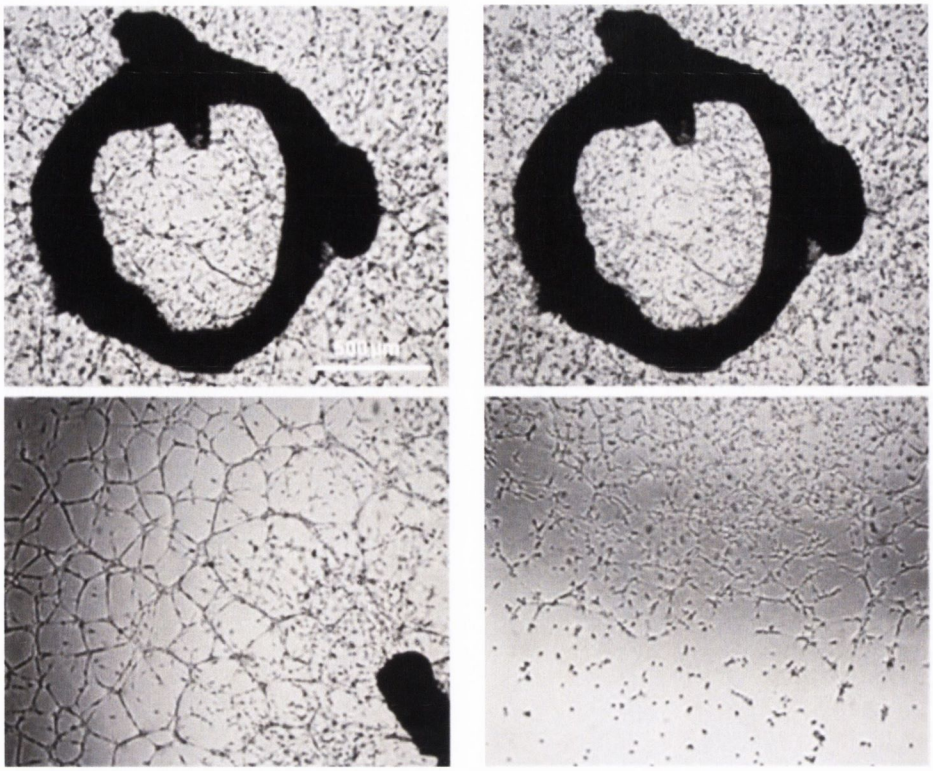


Figure 2.10. Rat aortic ring assay illustrating the anti-vascular activity of 2.17. Observable breakdown in the vascular network of aortic ring treated 4 hours previously with 50 nM 2.17 (right) compared to the control (left).

The rat aortic ring assay can also be further manipulated to inspect the anti-angiogenic properties of ***2.17***. For this assay, the test compound is administered on the first day, prior to the formation of a vascular network. After 8 days, the extent to which neovascularisation occurs was appraised by microscopically comparing the microvessel density to that of the control. Once again, 10 nM ***2.17*** had an insignificant effect, although 50 and 100 nM concentrations did invoke the desired anti-angiogenic response comprehensively.

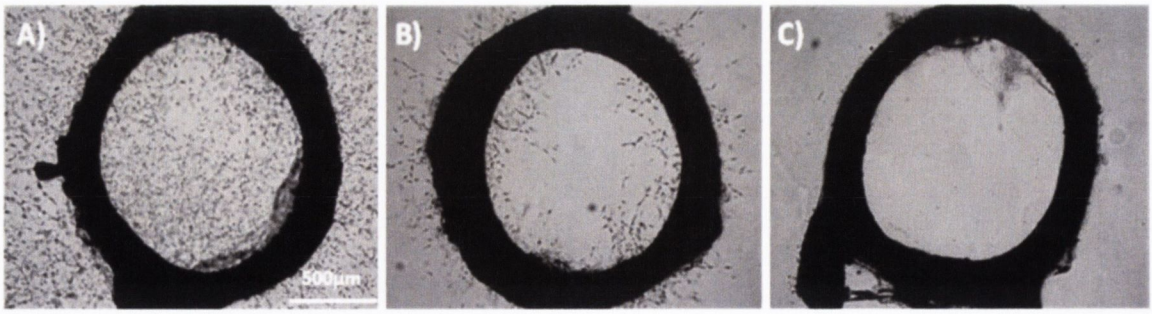


Figure 2.11. Rat aortic rings illustrating the anti-angiogenic effect of 2.17. A) Control (0.1% DMSO, B) 10 nM 2.17 and C) 50 nM 2.17.

2.6 Conclusions from Chapter 2

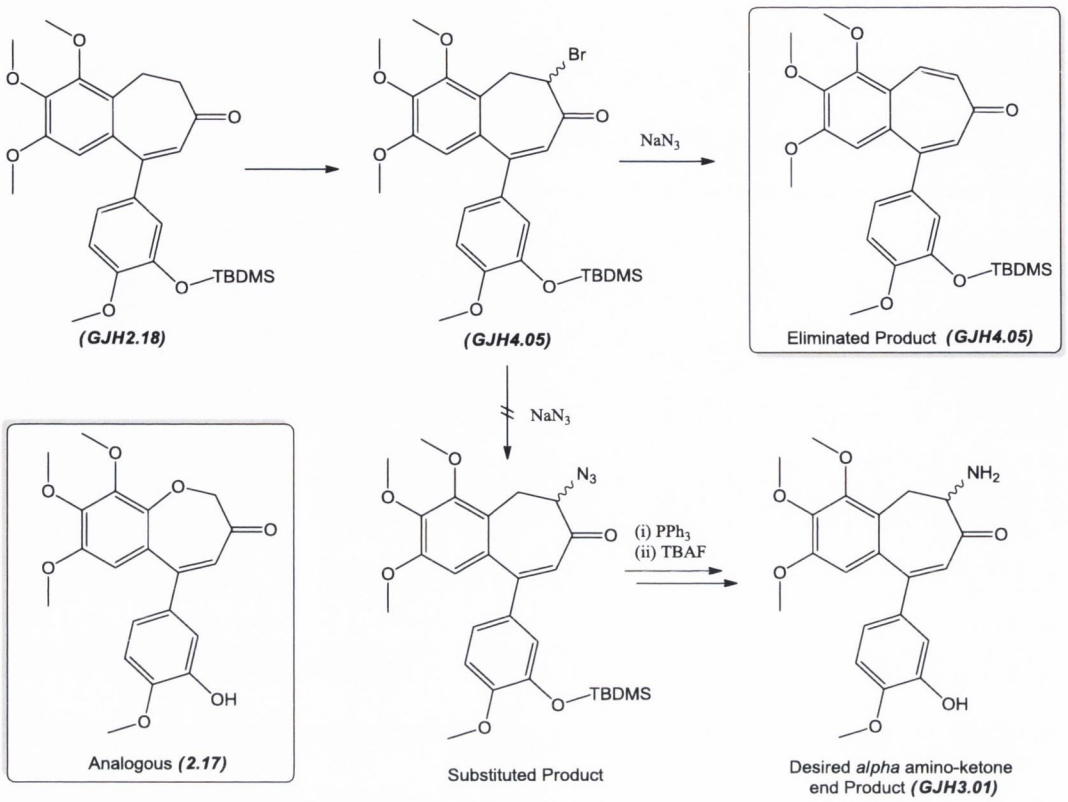
In this chapter, the focus of the work carried out centred on the procurement of the tubulin binding agents with a biaryl benzoxepinone backbone. The first objective was to furnish a useful AB-ring precursor molecule, from which a small series of benzoxepinone compounds could be synthesised. This was achieved on a multigram scale repeatedly, despite a quite long synthetic route (10 steps). From this, the lead compound ***2.17*** was the primary target, having performed well in tubulin inhibition assays carried out by Shah[204]. This was eventually obtained within 16 steps. Additionally, four novel analogues were synthesised; paramethoxy alcohol ***2.18*** and ketone ***2.19***, aniline ***2.28*** and phosphate salt prodrug ***2.31***. In particular, synthesis of the aniline required a considerable deviation for the standard synthetic procedure, with regard to the coupling of the AB-ring to the aniline C-ring.

Apart from the prodrug ***2.31***, the benzoxepinone lead compounds here were submitted for biological evaluation. All of these compounds had anti-proliferative effect on both HUVECs and PC-3 cells. As the most efficacious of these, ***2.17***, it underwent further *in vitro* and *ex vivo* evaluation to assess its anti-mitotic, anti-vascular and anti-angiogenic effects, and performed well in each. The isosteric aniline version, ***2.28***, showed encouraging anti-proliferative activity but to a lesser degree than the phenol. The two compounds without nucleophilic C-ring substituents, ***2.18*** and ***2.19***, also exerted meritorious anti-mitotic effects, indicating that while nucleophilic substituents on the C-ring were favoured, they are not essential. That ketone ***2.19*** exhibited higher efficacy than the alcohol ***2.18*** in direct comparison over two cell lines further signifies the QSAR assumptions that carbonyl groups on the B-rings are most preferential for tubulin binding.

Chapter 3 – Novel Ring Contraction and the Synthesis of 4-aryl coumarin Series of TBAs

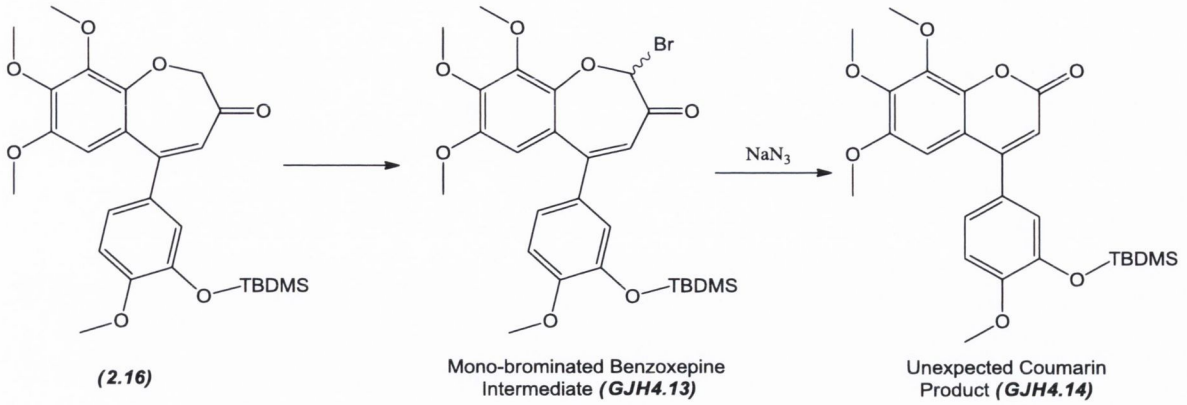
3.0 Background

The second family of tubulin inhibitors focussed on were of serendipitous origin. Hudson[206] was working with a phenol lead compound, analogous to ***2.17*** but for a fully aliphatic B-ring, with the intention of adding an amino group alpha to the carbonyl (Scheme 3.1). The purpose of this work was to ultimately create a designed multiple ligand capable of inhibiting both tubulin polymerisation and Aminopeptidase N (APN). Amino-ketones are well recognised for their zinc chelating properties and compounds of this type are known APN inhibitors[237]. The approach undertaken was to first brominate at this position, then displace this good leaving group with a nitrogen based nucleophile, such as azide, which upon reduction via Staudinger conditions[238] aimed to afford the amino ketone (***GJH3.01***). Hudson reported great difficulty not only with the bromination reaction itself but also apparent elimination of the azide intermediate to furnish the highly conjugated dienone. While this compound itself had inherent tubulin binding activity, insertion of the amino functionality adjacent to the carbonyl group remained an important objective. Thus to circumvent the elimination reaction the protected benzoxepinone ***2.17*** intermediate was used instead, containing the phenolic oxygen atom in place of the benzylic methylene.



Scheme 3.1. Overview of Hudson's synthesis on aliphatic B-ring compounds, analogous to 2.17. Attempted bromide substitution with NaN_3 instead resulted in elimination to the dienone (top right)

However, while elimination was avoided, azide substitution instead provoked an unexpected ring contraction to a 6-membered unsaturated lactone structure, which was confirmed unambiguously by X-ray crystallography to be the corresponding 4-aryl coumarin (***GJH4.14***, Scheme 3.2). To the best of our knowledge, a reaction of this type has never been reported in the literature before. When this compound was deprotected it was found to significantly inhibit tubulin polymerisation, even more so than the parent benzoxepinone compound ***2.17***.

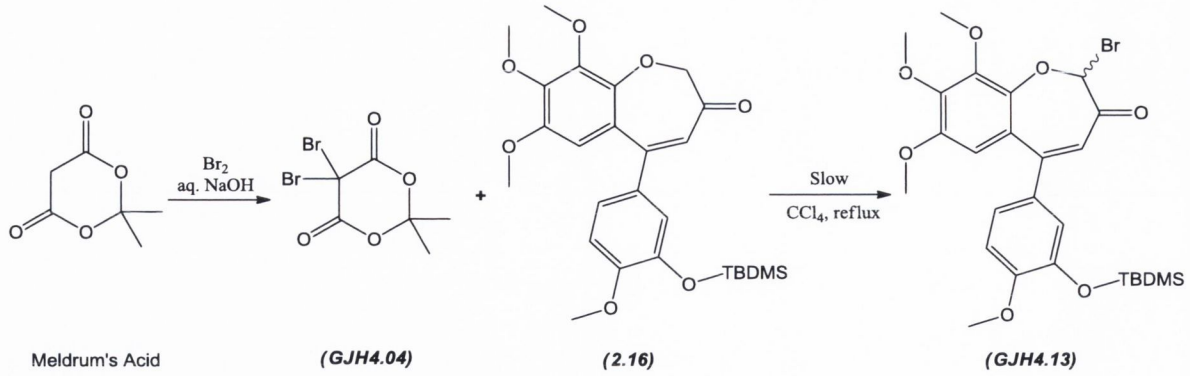


Scheme 3.2. Azide ring contraction on 2.16

In view of the unique reaction that led to the formation of the 4-phenyl-coumarin and its promising biological activity, it was decided to explore in greater detail the scope of this reaction and secondly to generate a series of compounds based on these scaffolds for biological evaluation. The aims of the work described in this chapter were therefore to; (i) optimise the bromination reaction, (ii) explore the azide reaction in greater detail, (iii) investigate the effect of using other nucleophiles to explore the substitution reaction and (iv) to identify a more efficient method to synthesise the class of 4-aryl coumarins.

3.1 Optimisation of the bromination reaction alpha to the carbonyl group of 2.16

Selective bromination of a compound like ***2.16*** can be problematic. In theory, any of the carbon-hydrogen bonds could be susceptible to substitution by bromine with addition across the double bond on the B-ring or on the activated aromatic rings a distinct possibility. Furthermore, bromination reactions have an intrinsic tendency to continue past mono-bromination on methylene carbons[239] and early reaction attempts by Hudson[206] were plagued with unwelcome di-bromination. The initial method used by Hudson to induce selective mono-bromination alpha to the carbonyl first employed the use of the dibrominated derivative of Meldrum's acid as the bromine source[240] (Scheme 3.3). Unfortunately this reagent was found to be largely ineffective in promoting this transformation on the benzoxepinone B-rings discussed here, and thus was not pursued further over the course of the bromide-based studies discussed in this chapter.

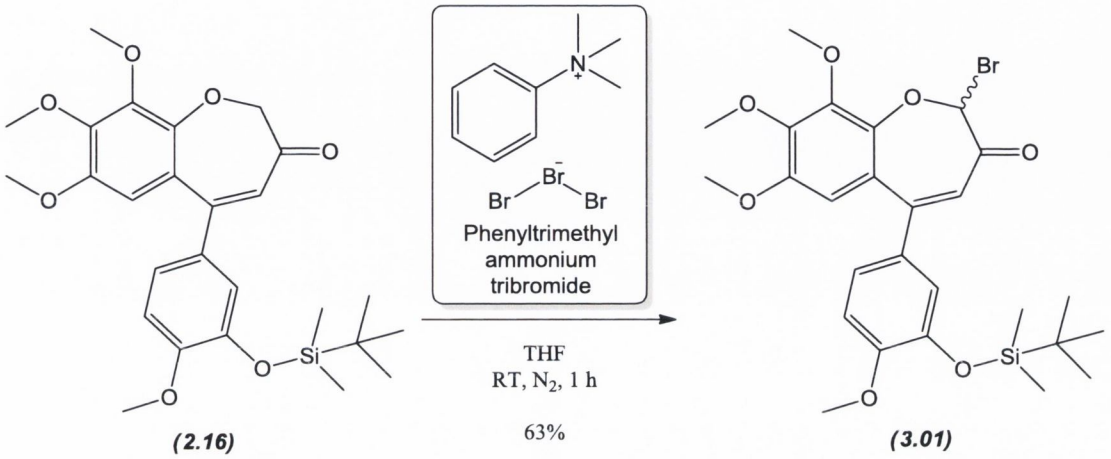


Scheme 3.3. First Hudson method for selective bromination.

The alternative was to use phenyltrimethylammonium tribromide (PTAB)[241]. It has been shown that this reagent is selective for bromination alpha to the carbonyl, even in the presence of an alkene or an activated aromatic ring[242]. This method tends to di-brominate over time, especially with the aliphatic B-rings synthesised by Hudson, but seemingly less so in corresponding benzoxepinones. The original method used PTAB in ethyl acetate with a catalytic amount of sulphuric acid at room temperature. While our initial attempts with this reaction did generate the desired monobromide, significant by-products formed with almost identical R_f values on TLC to that of the desired monobrominated derivative. It was possible to secure the desired monobrominated product, albeit in low yields (~30%) with careful consideration to the gradient system used when purifying by flash column chromatography.

In order to afford appreciable quantities of the desired lead compound, enough for thorough biological evaluation, it was important that we optimise this reaction step. In this context, it has been previously reported that the role of the solvent can be influential in facilitating the bromination reaction under consideration here[243]. In the hope of optimising the PTAB reaction, we replaced ethyl acetate with anhydrous tetrahydrofuran and conducted the reaction under nitrogen without acid catalysis[244] (Scheme 3.4). THF is a good choice of solvent as it is effective at keeping Br_3^- stable as a species, which has very different behaviour and selectivity to that of elemental Br_2. In addition, THF can act as a buffer to liberated HBr, which by its acidic nature can prompt several detrimental side reactions in sensitive molecules. Put into practice, this simple change greatly improved the cleanliness of the reaction, and although conversion was most

often incomplete a significant portion of starting ketone ***2.16*** was able to be recovered each time.



Scheme 3.4. Optimised PTAB bromination of ketone 2.16 in THF

Rapid purification and isolation of the alpha bromoketone ***3.01*** was essential. This compound is highly unstable with an innate predisposition to breakdown. Every precaution was undertaken for even temporary storage; the compound was kept refrigerated where possible, in solution and the occupied glassware wrapped in aluminium foil to protect it from sunlight. Subsequent substitution reactions on ***3.01*** had to be carried out almost immediately upon acquisition of a pure sample. However, we first had to verify the authenticity of the product. This proved no easy feat as prolific decomposition of the compound occurred freely in deuterated chloroform; giving rise to multiple impurities in solution and thus resulted in the generation of complex NMR spectra. The nucleophilic nature of deuterated methanol only exacerbated this behaviour, so too did deuterated dimethyl sulfoxide with its potent oxidative properties. However, the compound showed excellent stability in deuterated dimethylformamide, unconventional as an NMR solvent due to the high cost associated relative to the other available solvents. Once able to isolate and elucidate ***3.01***, and keep it relatively quiescent in an NMR solvent, we decided to further exploit this situation; to probe the ring contraction step by monitoring its progress *in situ*.

3.2 NMR studies of nucleophilic substitution based rearrangements

3.2.1 Substrate Overview

The bromine compound ***3.01*** conserved most of the typical NMR features for benzoxepinone compounds, like those we have previously discussed in Chapter 2. Once again the methoxy groups were seen as a group of four singlets; from 3.7 – 4.0 ppm in the ^{1}H spectrum (Figure 3.1) and from 55 – 62 ppm in the ^{13}C spectrum (Figure 3.2). The silyl ether groups were found to resonate as expected; at 0.2 ppm for the dimethyl groups and at 1.0 ppm for the *tert*-butyl CH_3 groups in terms of hydrogen, corresponding to ^{13}C peaks at -4.5 and 25.9 ppm respectively. Aromatic signals for C-ring hydrogens were actually quite well resolved; as two doublets and a singlet in the hydrogen spectrum. The A-ring CH signal was predictably upfield, at 6.44 ppm and 111 ppm for ^{1}H and ^{13}C respectively. The double bond hydrogen resonated at 6.53 ppm and 125 ppm. The hydrogen of the CHBr signal was found downfield at 6.95 ppm, with its corresponding carbon at 87 ppm.

The carbon-bromine bond was signified with a peak on the IR spectrum at 838.9 cm^{-1}. The absorption of the C=O stretch of the ketone was also found at 1726.0 cm^{-1}. Using mass spectroscopy, the correct ion for the sodium adduct of ***3.01*** could eventually be found at 587.1044 m/z, although typically these bromides proved short-lived under the high temperature associated with mass spectroscopy conditions.

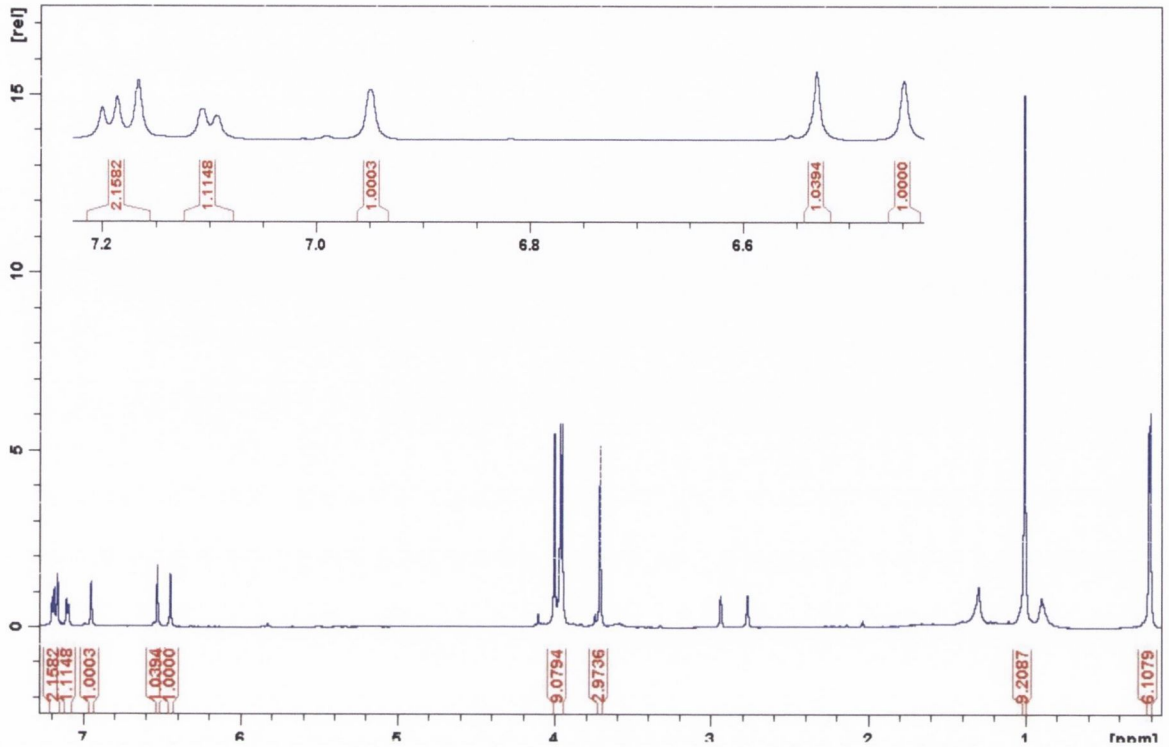


Figure 3.1 ^{1}H NMR spectrum of bromide 3.01 in DMF-d_7.

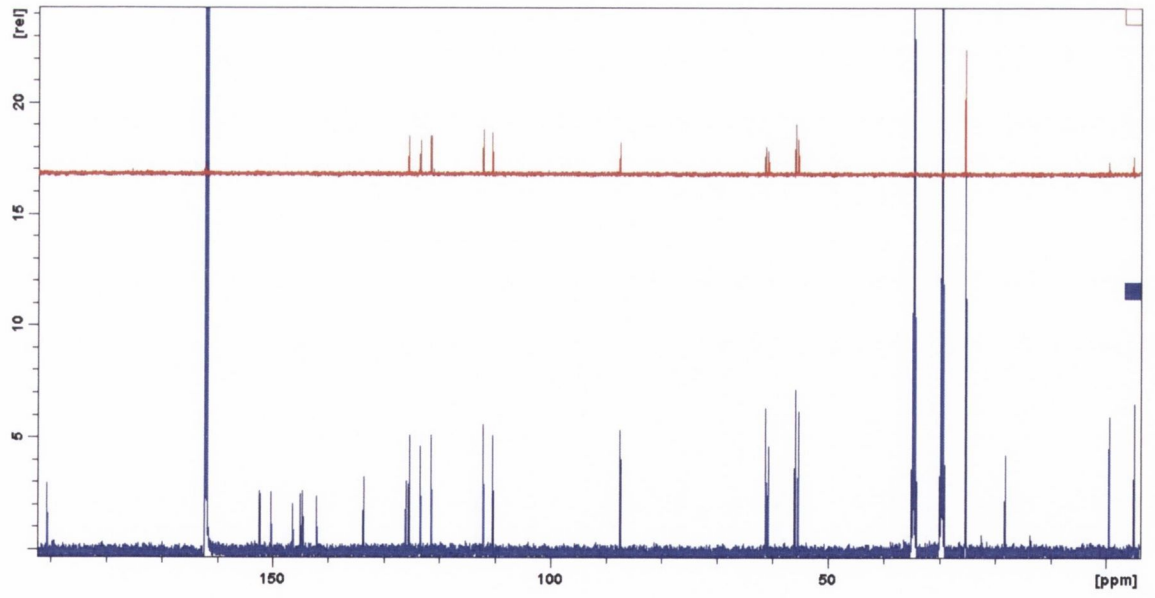


Figure 3.2. ^{13}C NMR spectrum of 3.01 in DMF-d_7

3.2.2 Azide Substitution and ring contraction of 3.01

In the earlier work by Hudson, DMF was employed as the solvent for the azide substitution reactions. With ***3.01*** particularly stable in this solvent, we could replicate the method used in laboratory in the NMR tube itself and monitor the progress of this novel transformation by NMR. Once dissolved in DMF-d_7, the ^{1}H and ^{13}C spectra were recorded as a starting point, before ten equivalents of sodium azide was added to the solution. Back inside the spectrometer, at 25 °C, both the ^{1}H and ^{13}C spectra were recorded at various time intervals (Scheme 3.3 and 3.4).

The ^{1}H NMR spectrum indicated that at the 11 minute time-point that approximately half of the bromide starting material had been consumed; all hydrogen peaks had doubled-up, and each of these peaks were of similar intensity to one another. Also present at this time-point in the ^{1}H NMR spectrum was a new peak at 5.9 ppm corresponding to what was considered to be the proton resonance of the CHN_3, shifted slightly upfield from that of the parent CHBr resonance. At the 60 minute time-point, the spectrum began to simplify again as most of the azide was consumed, albeit with rather broad peaks and trace amounts of the azide-intermediate. Also noticeable was the evolution of considerable amounts of gaseous substances as by-products of the reaction. A very clean spectrum was observed at the 90 minute time-point with superior resolution and well defined ^{1}H resonances. Overall the spectrum recorded at this time-point was similar in every respect to that of the spectrum of the 4-phenyl-coumarin ***3.02***, obtained by Hudson. Strong evidence from this ^{1}H NMR data suggests that transient azide substitution of the bromide does indeed take place but that this intermediate is unstable and readily rearranges, through transient intermediates undetectable given the relatively long timeframe involved in capturing ^{13}C spectra, through loss of gaseous molecules of nitrogen and hydrogen cyanide, to give the 4-aryl coumarin ***3.02***.

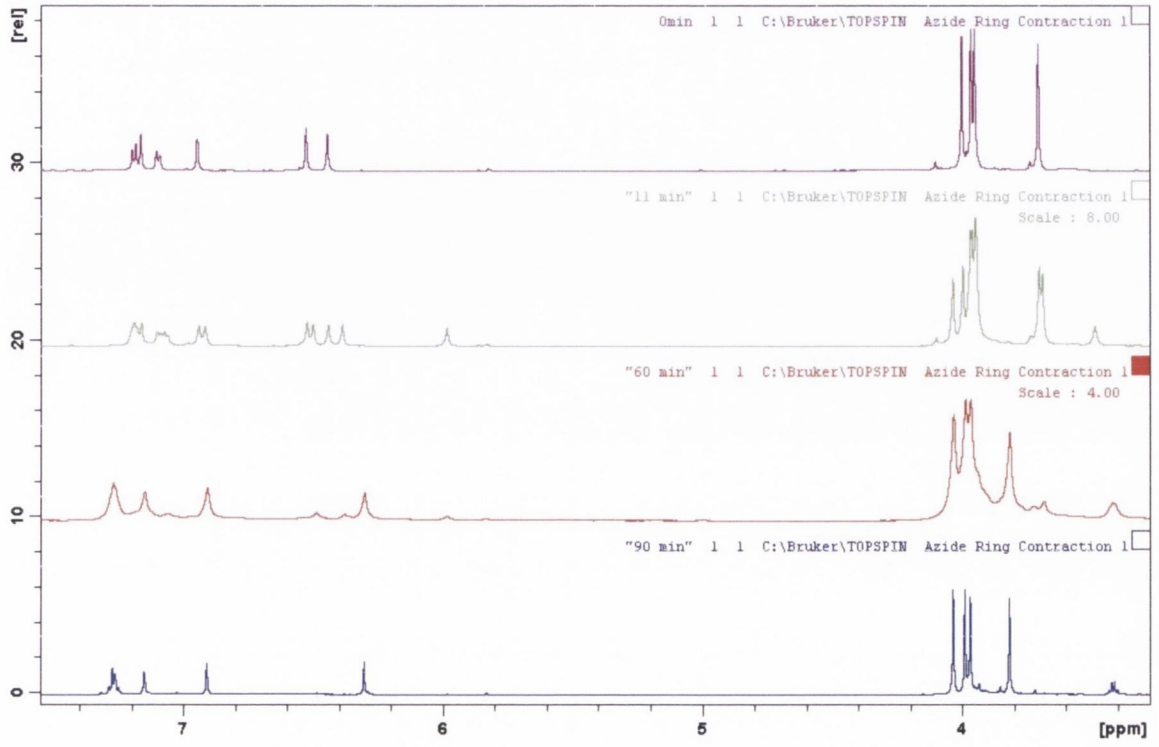


Figure 3.3. Superimposed ^{1}H spectra recorded during the ring contraction of 3.01 to 3.02 (peaks below 3 ppm not included)

The ^{13}C spectrum was even more interesting, particularly in the carbonyl region of the spectrum (Figures 3.4 and 3.5). We were able to capture a ^{13}C NMR spectrum two minutes after the introduction of sodium azide, in which we could survey a host of new carbon signals, many of similar intensity to the bromide; illustrating the immediacy of the halide displacement. Between this point and that of the next spectrum at 11 minutes we could clearly see the formation of a new carbonyl carbon signal at 191.8 ppm, with concurrent reduction of the initial carbonyl signal at 190.7 ppm. By 40 minutes, the latter peak had disappeared completely and the former was also showing signs of intensity reduction itself. The spectrum at 60 minutes was bereft of either keto signals. Instead it appeared as though another new carbonyl was established, culminating between 40 – 60 minutes. At 159 ppm, it was significantly further upfield, the signal was much more like that of an ester, or in this case lactone carbonyl carbon signal.

Further upfield, we could also monitor the reduction of the carbon-bromine signal (Scheme 3.6). Paralleling the rise and ultimate decline of the intermediate carbonyl peak, from 2 minutes we could witness the generation of a carbon-azide signal at ~94.0 ppm that would eventually diminish fully by 60 minutes. A DEPT 90° spectrum, taken after 11 minutes, provided confirmation that this carbon signal bore a single hydrogen. Furthermore, a comparison of the various NMR spectra generated confirmed the change from a starting material with 15 hydrogen-associated carbons to a compound with just 14.

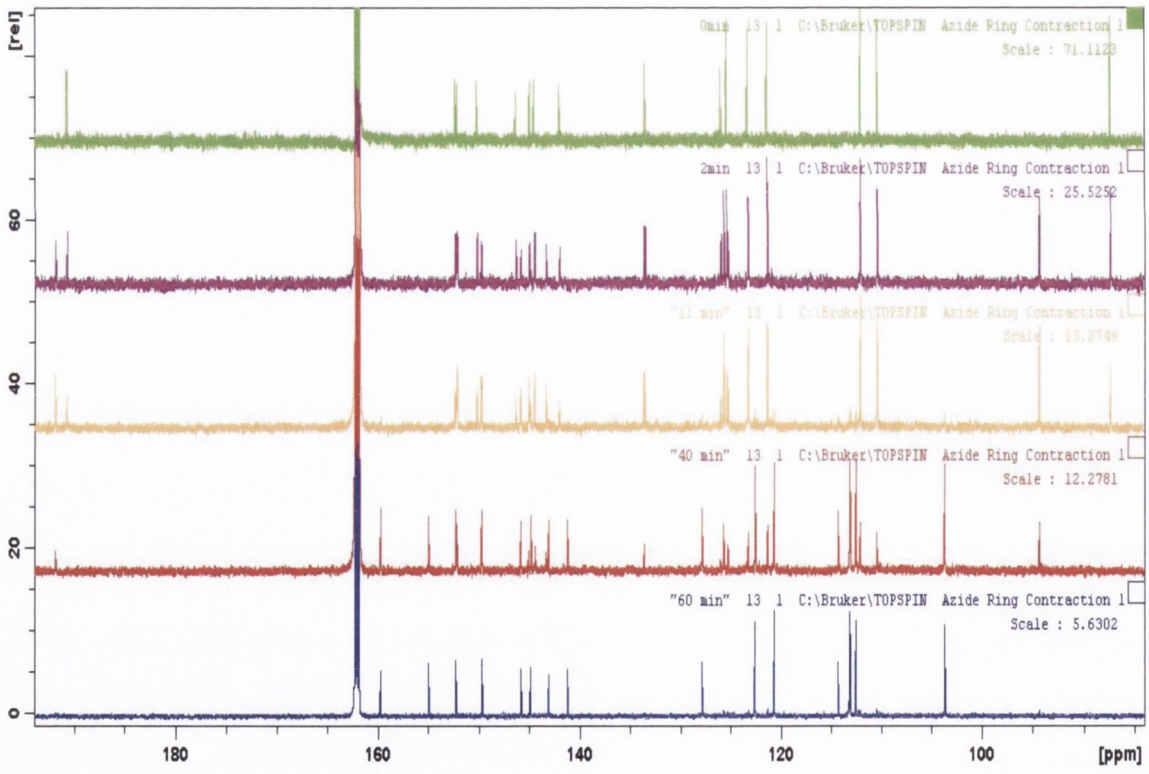


Figure 3.4 ^{13}C spectrum of ring contraction reaction over various time-points

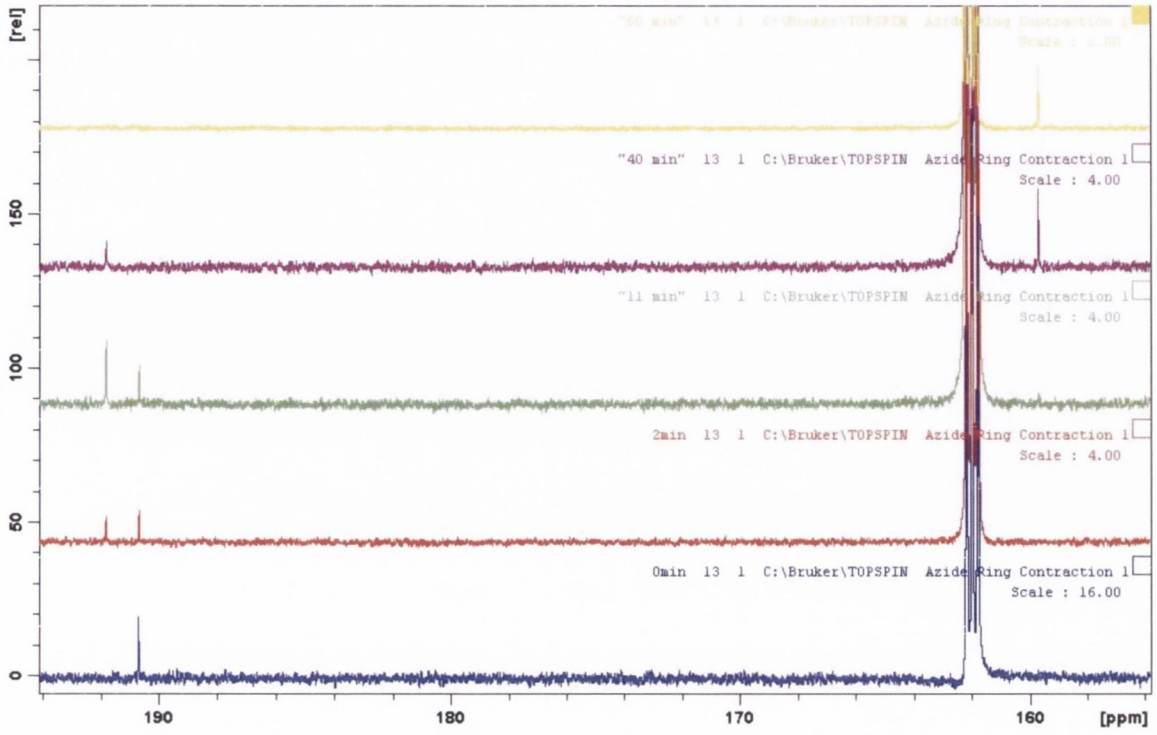


Figure 3.5. Closer look at the change (bottom to top) of keto carbonyl signal, first from 190 to 191 ppm, then from 191 to that associated with a lactone at 159 ppm.

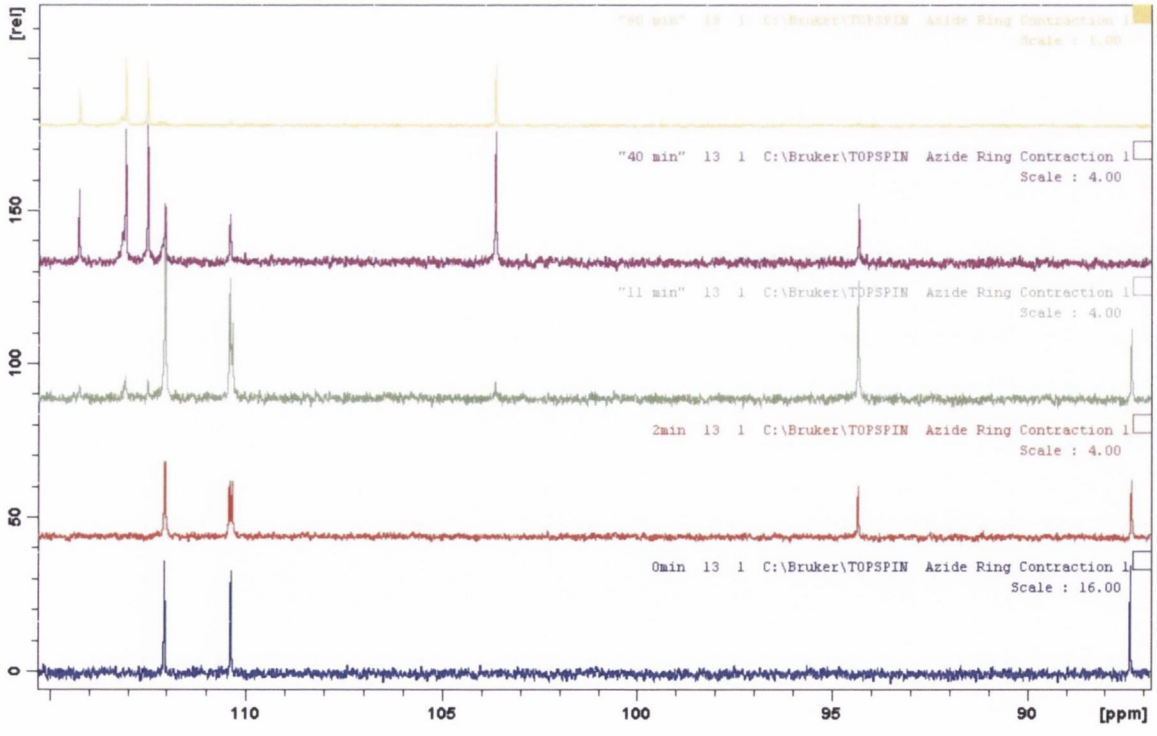
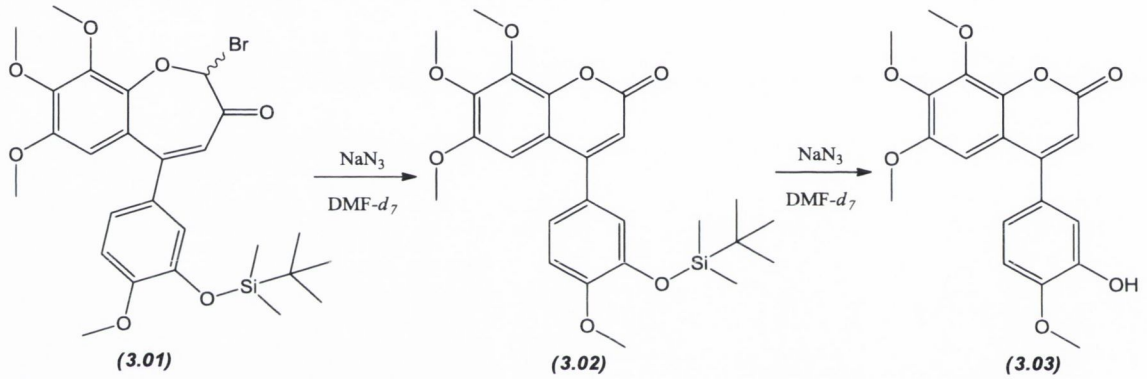


Figure 3.6. Loss of C-Br signal (87 ppm), formation of a transient CH signal (94 ppm) from intermediate.

Close to this region, both the carbons and hydrogens of aromatic or alkene nature were also changing positions. What complicated the situation was that the signals would retain a similar pattern throughout the chemical transformations, yet the nature of the signals themselves would often have changed. For example, as the CHBr signal at 6.9 ppm diminishes, the new aromatic peak for the A-ring hydrogen of the product arises simultaneously in an almost identical position, almost 0.5 ppm from its original position. As the aromatic signal shifted downfield, the alkene hydrogen began to resonate slightly further upfield in concert, in a similar position to where the A-ring hydrogen was found originally. Likewise, the corresponding alkene carbon jumps around 12 ppm upfield.

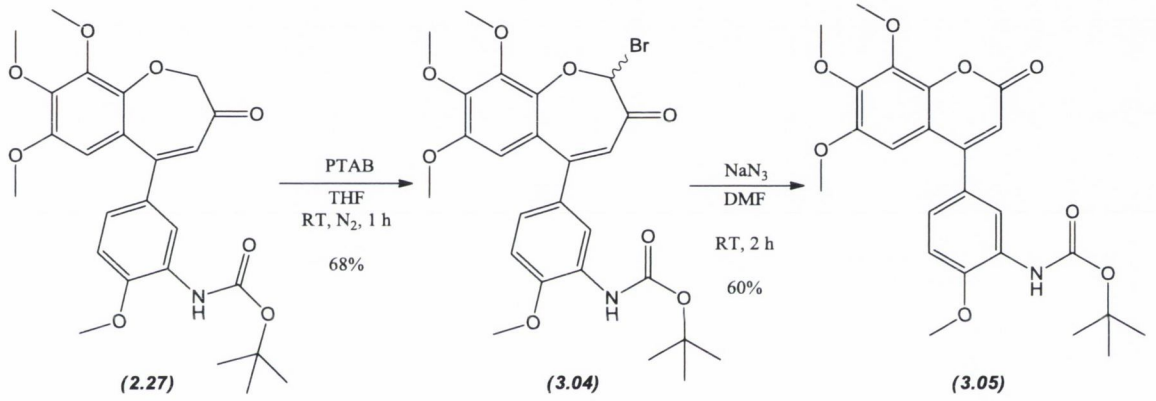


Scheme 3.5. Sodium azide induced ring contraction, and later deprotection of the silyl ether

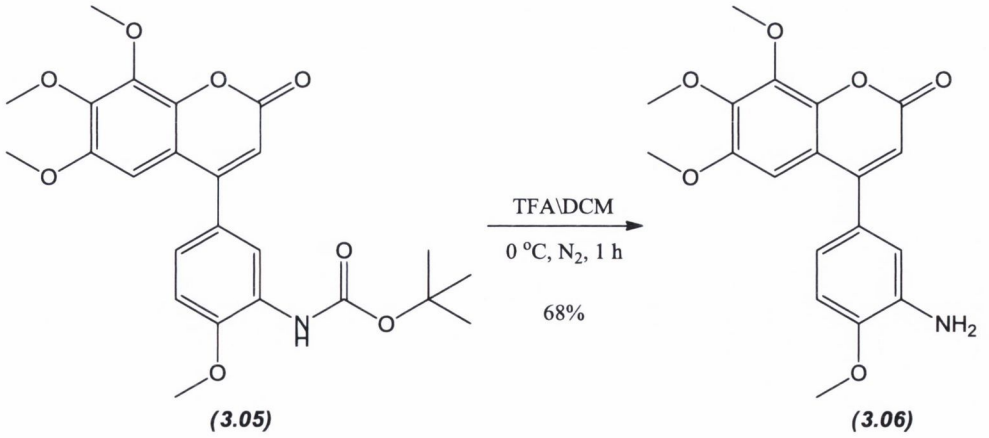
In Chapter 2, azide deprotection of *tert*-butyl-dimethyl silyl protecting groups was discussed. The reaction required elevated temperatures before significant deprotection was observed. We exploited this observation here as we were able to proceed with the ring contraction at room temperature without any discernible deprotection over the timeframe of the experiment. Nevertheless, over an extended time period of 4-weeks, complete deprotection of the silyl group was observed at room temperature (Scheme 3.5). Clearly, as described in Chapter 2, the rate of the deprotection step could have been substantially increased by heating the sample to 60 °C for approximately 5 hours where complete deprotection would be observed over this time interval.

3.2.3 Ring contraction of aniline and paramethoxy benzoxepinones

After the successful ring contraction above, we decided to broaden the scope of the reaction to include some of the other 7-membered ring systems synthesised in Chapter 2. Of these, we were particularly interested in the aniline benzoxepinone ***2.28***, as it was anticipated that ring contraction be met with a correlating increase in potency, akin to that of observed in the case of the phenol[206]. Bromination of the Boc-protected aniline ***2.27*** was carried out under the same (Scheme 3.6) conditions as before to give the halide ***3.04***, which upon exposure to sodium azide ring contracted to the 4-aryl coumarin ***3.05*** which following *N*-Boc deprotection in 50% TFA in DCM afforded the aniline **3.06** (Scheme 3.7).

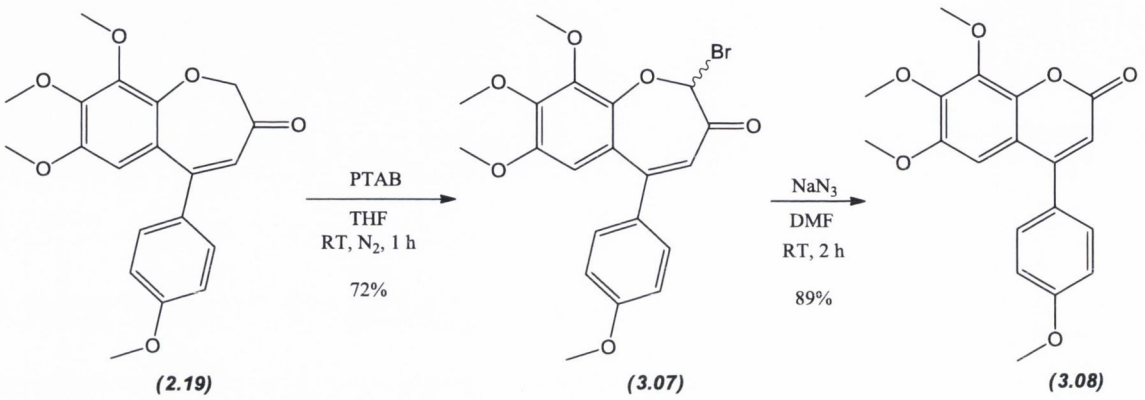


Scheme 3.6. Bromination and ring contraction of aniline precursor 2.27.



Scheme 3.7. Deprotection of Boc group to generate final aniline compound 3.06

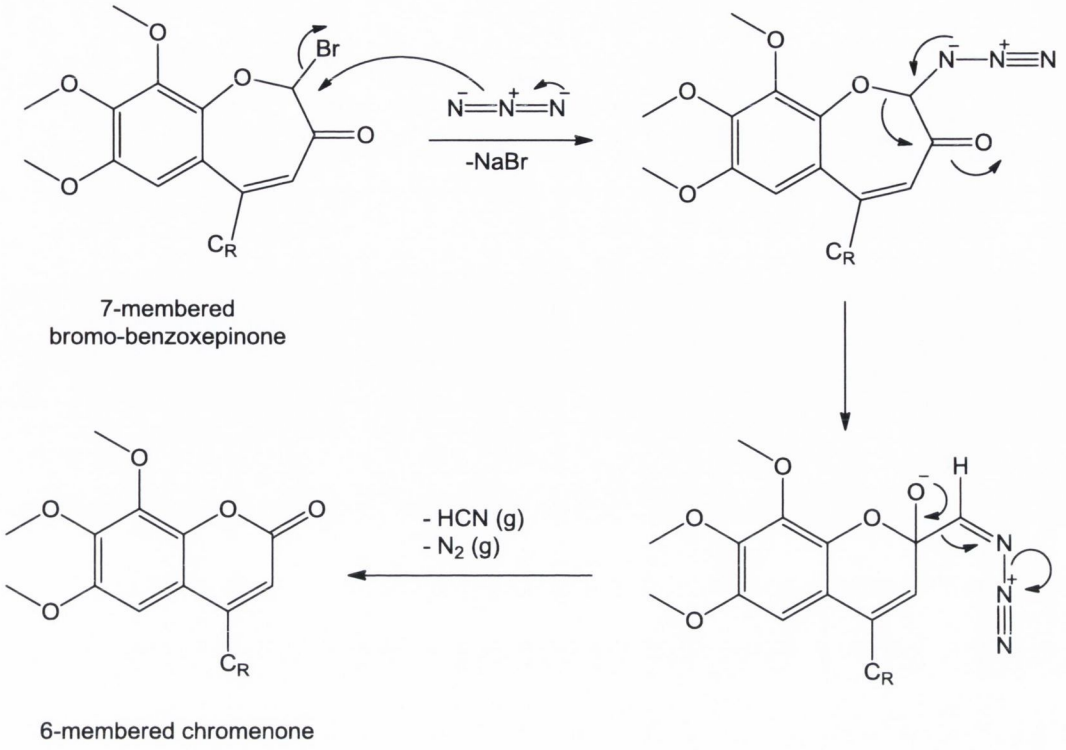
Using an identical procedure to that employed for the previous bromination reaction the bromo derivative of paramethoxy benzoxepinone ***2.19*** was also furnished which upon azide substitution afforded the 4-aryl-coumarin analogue ***3.08*** (Scheme 3.8).



Scheme 3.8. Bromination and ring contraction of paramethoxy analogue 2.19

3.2.4 Proposed mechanism for novel ring contraction

From the NMR study outlined earlier, a direct substitution intermediate was identified, believed to the organic azide. Little was detected between this and the final chromenone product, suggesting rapid transformation upon activation of this azide intermediate. Below we have postulated the mechanism for this novel reaction based on our current understanding (Scheme 3.9).



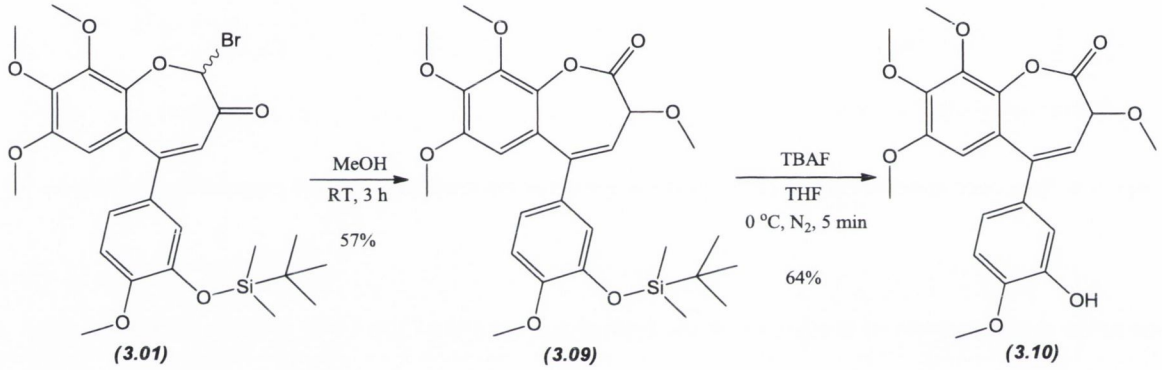
Scheme 3.9. Proposed mechanism of azide mediated ring contraction, where C_R is any of the 3 C-rings.

Upon azide displacement of the bromine via typical S_N2 means at the CHBr carbon, electrons are pushed from the negative charge residing on nitrogen to form a double bond with its attached carbon. In doing so, to keep valency of this carbon at 4, the weakest bond is broken, the C-O, with rapid migration of the phenolic oxygen on to the electron deficient carbonyl carbon. Naturally this involves delocalisation of electrons from the carbonyl to the electronegative oxygen. Restoration of the carbonyl, to form the confirmed new lactone group, ultimately releases the nitrogen containing moiety, by pushing electrons toward the double bond to form hydrogen cyanide, which simultaneously pushes electrons to the positively charged nitrogen to release neutral nitrogen gas.

The observation of the gaseous by-products as the reaction progresses substantiates the above claim. Also, the formation of the stable lactone structure provides the driving force for such a reaction, in addition to the entropic motive of the release of aforementioned gaseous products.

3.2.5 Effect of different nucleophiles on bromoketone functionality

After repeating the ring contraction step with three different substrates, we had garnered a great deal of confidence in the reproducibility and practicality of this new reaction. Turning our attention back to the bromides, we wished to investigate the outcome of using different nucleophiles in the substitution reaction and their overall stability considering how quickly the azide product rearranges to the ring contracted derivative. A range of nucleophiles were investigated; those based on oxygen included H_2O and MeOH, while NH_3 was also investigated in the nitrogen series. Ethanethiolate and thiocyanate anions served as simple sulphur based nucleophile to investigate the rate of substitution.



Scheme 3.9. Methanol induced rearrangement of 3.01.

Water was ineffectual when used as the nucleophile. However, it was noted that an almost instantaneous reaction started to occur when the bromide was dissolved in methanol. Upon isolating a fresh, clean sample of bromoketone ***3.01***, methanol induced conversion at room temperature to a predominant compound was monitored by TLC, which was then isolated by flash column chromatography and subjected to analysis by NMR (Scheme 3.9). The resultant spectral data generated was interesting from a number of perspectives. First of all, as expected, there was no evidence of ring contraction; mass spectrometry reported an ion too heavy to account for the lighter coumarin ***3.02***, and while the ^{1}H and ^{13}C signals (Figures 3.7 and 3.9) for the CHBr group had indeed disappeared, there were new peaks to take their place. Although an extra CH_3 peak was observed the product obtained was certainly more complex than that representing S_N2 substitution of the bromine by a methoxy group. Interestingly, the downfield ketone carbonyl signal in ^{13}C spectrum had disappeared, and on the ^{1}H spectrum the normal

singlets for the CH groups on the B-ring were split into doublets, suggesting, based on coupling constants of ~8 Hz, that they now resided adjacent to each other (Figure 3.8). Collectively, these observations were pointing towards the possibility of a rearranged product to form a new 7-membered lactone product ***3.09***. This hypothesis was supported by the discovery of a new carbonyl peak at 170 ppm, indicative of an ester or lactone functionality.

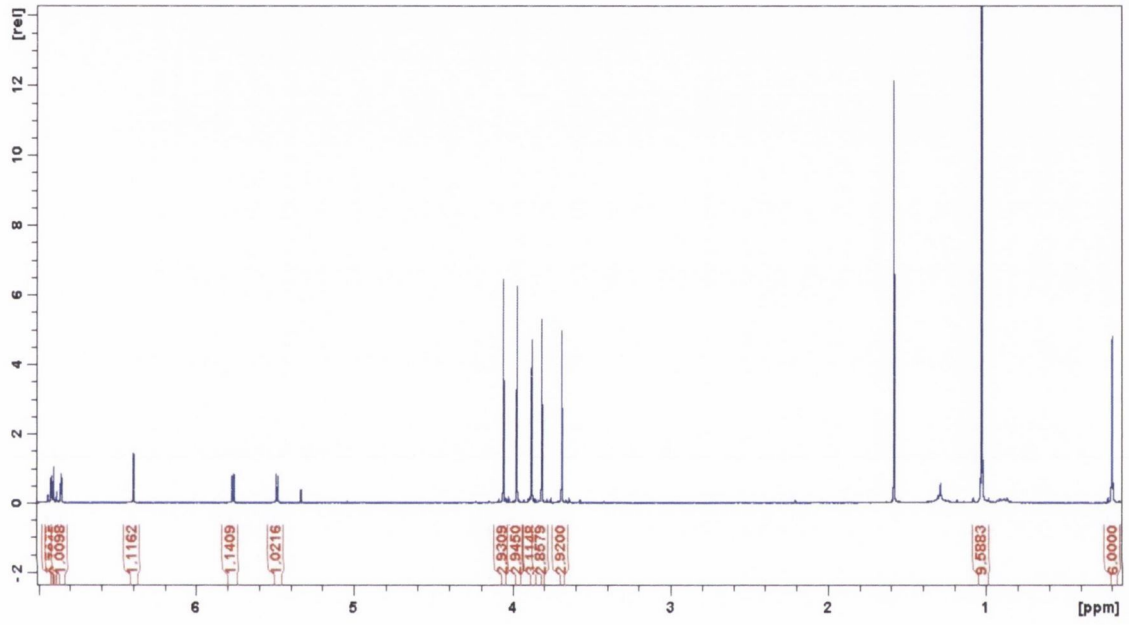


Figure 3.7. ^{1}H spectrum of 3.09

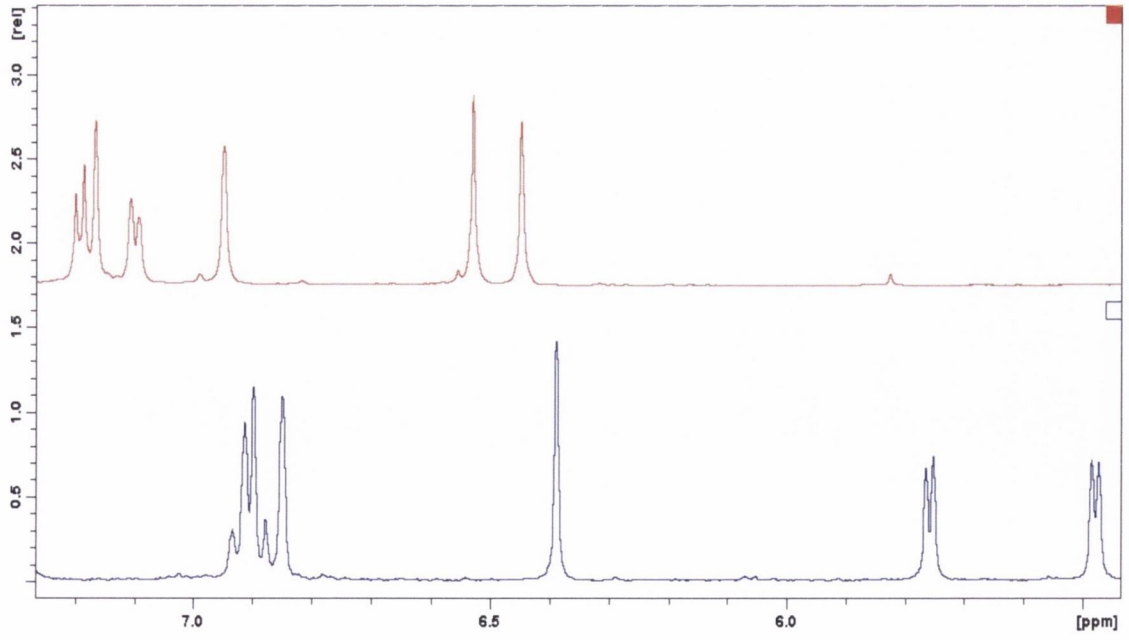


Figure 3.8. Comparison of the downfield regions in ^{1}H NMR of bromide 3.01 and rearranged 3.09

Also remarkable was the incidental deprotection of the silyl group over time. Methanol is not deemed to be sufficiently reactive enough under normal conditions to induce deprotection of even the most labile silyl ethers. However, *tert*-butyldimethyl silyl ethers are acid sensitive[245] and it is probable the residual HBr generated as a by-product slowly deprotects the ether to give phenol ***3.10***.

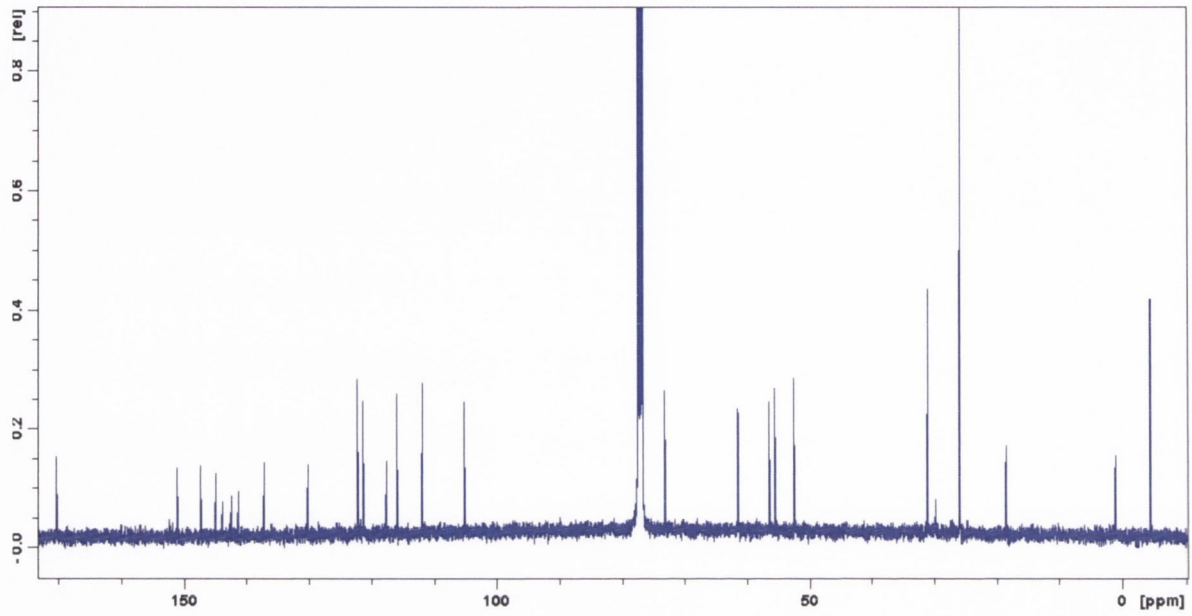


Figure 3.9. Complete ^{13}C spectrum for 3.09

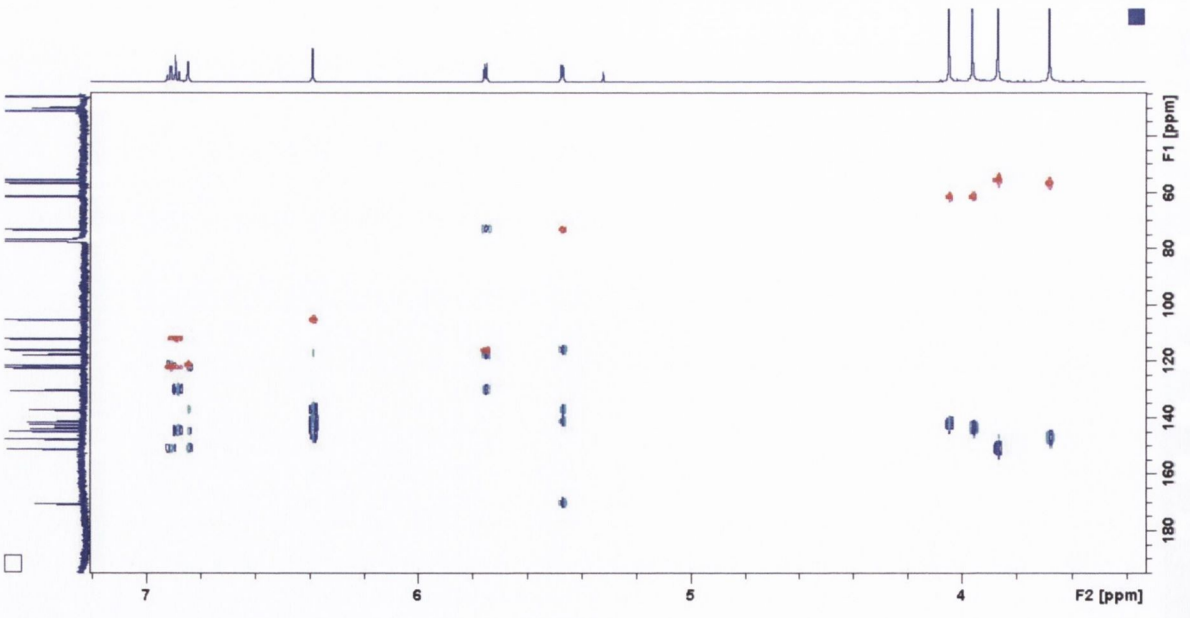
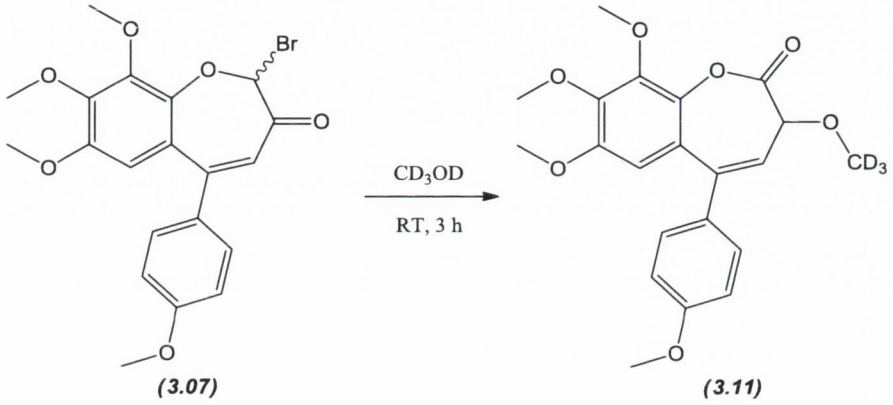


Figure 3.10. HSQC (red) and HMBC (blue) spectra of rearranged product 3.09.

The methanol rearrangement of ***3.01*** was also carried out in deuterated methanol in an NMR tube, mirroring the technique used for azide ring contraction discussed previously, in the hope we could espy some valuable mechanistic clues as the reaction progressed. Unfortunately, this proved rather more difficult given the tendency of the bromoketone to spontaneously form multiple products in solution, one of which was deemed to be silyl deprotection to ***3.10***. To minimize the impact of unwanted deprotection, we repeated the procedure on the bromide of the paramethoxy benzoxepinone ***3.07*** which reacted in the same way to give the rearranged lactone product ***3.11*** (Scheme 3.10). This reaction was considerably less complicated than for ***3.01***, but even so the simultaneous formation of a significant by-product made for an opaque field of view when it came to scrutinising potential transient intermediates amidst the multiple NMR spectra.

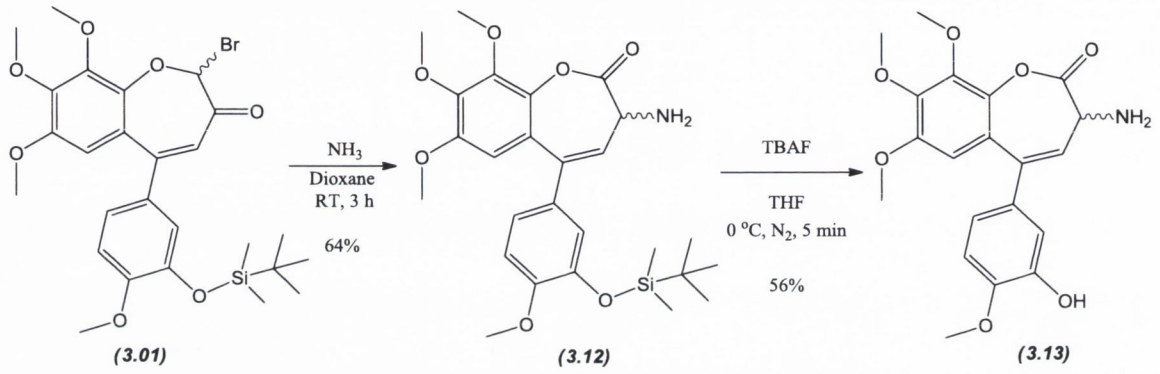


(3.07) ***(3.11)***

Scheme 3.10. Methanol rearrangement also took place with 3.07 to give lactone 3.11

The next nucleophile we investigated was ammonia. To reiterate, Hudson had originally brominated ketone ***2.16*** with the intention of later introducing an amine group alpha to the carbonyl. While azide obviously did not fulfil that purpose, we decided to test out whether ammonia could do so instead. Once again; would the nucleophilic ammonia simply displace the bromine, rearrange as methanol had done or even cause ring contraction as witnessed with the azide ion? We added 0.5 M ammonia solution (in dioxane) to a fresh sample of bromoketone ***3.01*** and stirred the reaction at room temperature. Despite the reputation of ammonia as a good nucleophile, the reaction was quite slow, and did not reach completion. By TLC, we could see a single new product had formed, which we promptly separated and purified. Reviewing the spectroscopic results, it appeared the ketone functionality once again was lost by conversion to an ester moiety, yet ^{13}C NMR and mass spectroscopy results discounted ring contraction. N-H

COSY spectra determined the retention of ammonia on the molecule with NH signals on the ^1H spectrum as broad singlets at 5.60 and 6.78 ppm. From the prior experience of the methanol induced rearrangement, alongside the usual NMR techniques, we were able to recognise the equivalent rearrangement of the ammonia group and the carbonyl to form the amino lactone ***3.12*** (Scheme 3.11). Again, the double bond and CHN signals splitting into doublets suggested adjacency to each other, while conversion of the ketone carbonyl carbon at 190 ppm to a peak at 172 ppm reinforced the view that rearrangement had taken place. Once isolated, the silyl ether was deprotected with TBAF and the free phenol of the aminobenzoxepinone ***3.13*** was submitted for evaluation.



Scheme 3.11. Ammonia rearrangement reaction on 3.01 and subsequent deprotection of 3.12 with TBAF to give phenol 3.13

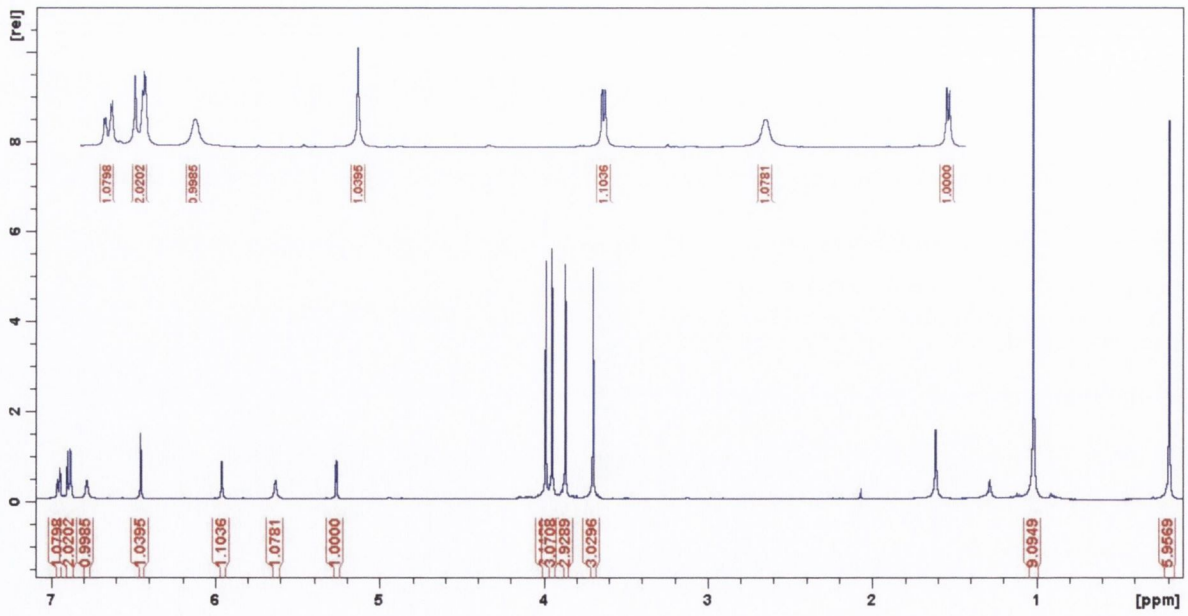


Figure 3.11. ^1H spectrum of ammonia rearranged product 3.12, showing splitting of the alkene and $CHNH_2$ signals into doublets in the downfield region (insert)

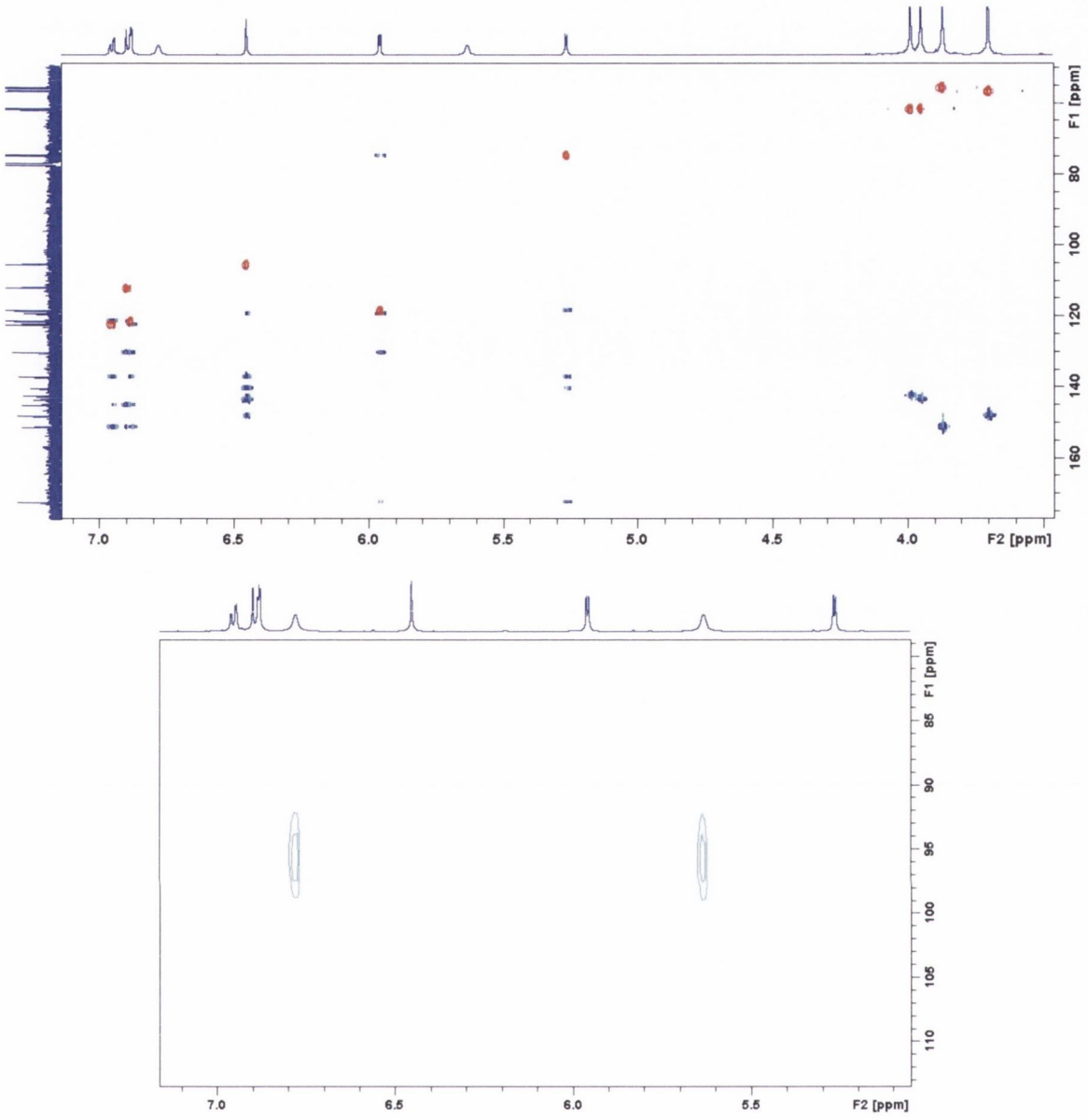
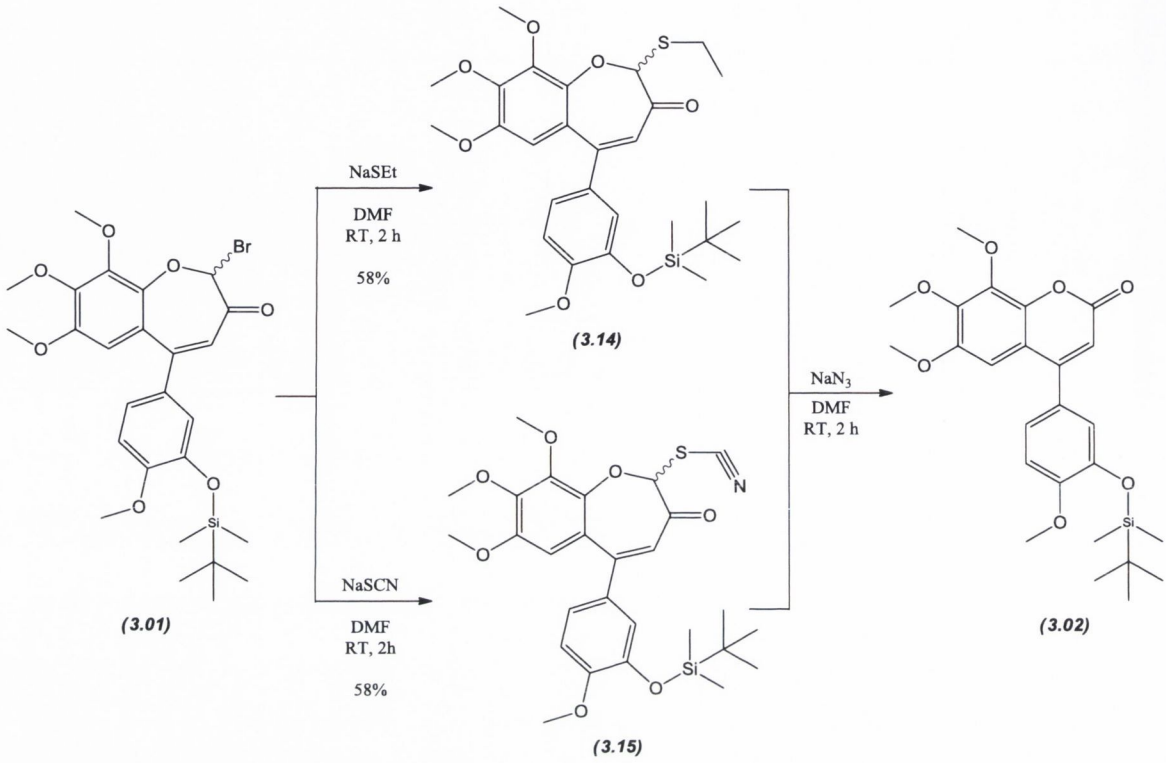


Figure 3.12. Top: HSQC (red) and HMBC (blue\green) spectra of 3.12. HMBC shows the correlation of the doublets CHN (5.27 ppm) and alkene CH (5.96 ppm) to the newly established carbonyl carbon at 172 ppm. Bottom: N-H COSY of 3.12 confirms correlation of broad singlets to hydrogens on anime group.

Sulfur based nucleophiles were next to be tested on the bromoketone. Sodium ethanethiolate and sodium thiocyanate were chosen due to their simplicity and ease of access. Separately, both compounds substituted for bromine in ***3.01***, with no observable rearrangement or ring contraction; the ketone carbonyl peak remained in its usual resonance position in both cases. However, complications did arise when trying to remove the TBDMS group of both of these compounds. Use of the usual TBAF method resulted in breakdown of the compounds. Interestingly, when the deprotection reactions were repeated using the sodium azide method, we noticed that both compounds ring contracted into the 4-aryl coumarin ***3.02***, suggesting that

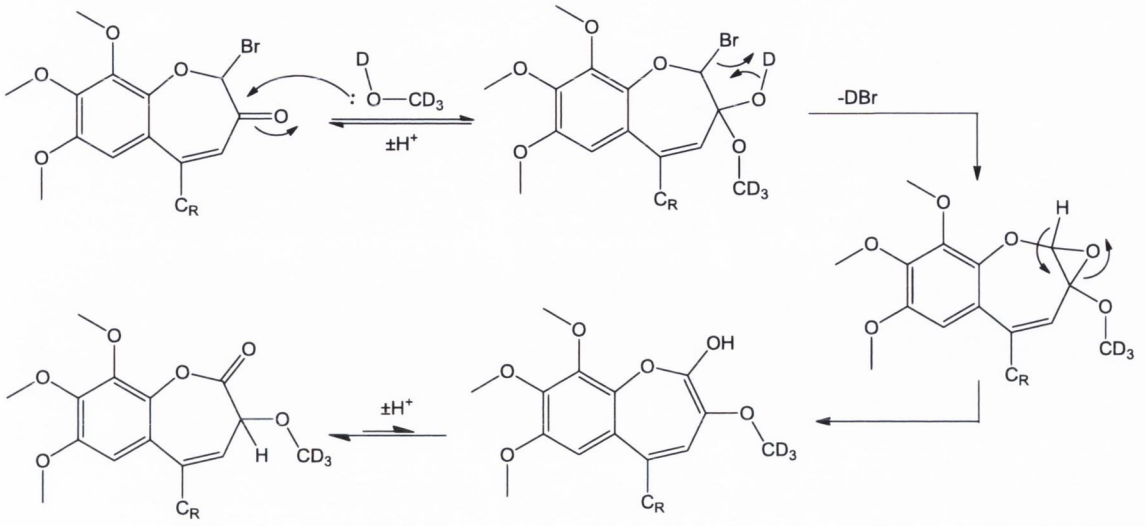
both thio products essentially served the same function as the bromine group in the azide reactions above.



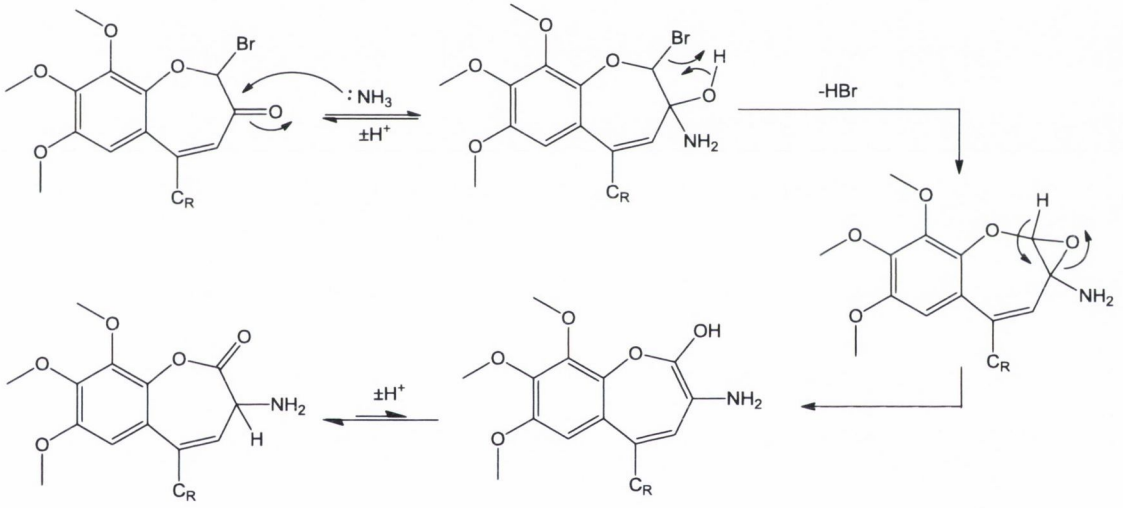
Scheme 3.12. Sulfur based nucleophiles first caused straight substitution of the bromine, but deprotection afterwards with sodium azide invoked ring contraction.

3.2.6 Proposed mechanisms for methanol and ammonia induced rearrangements

Unlike in the case of the azide mediated ring contraction, when the reaction of deuterated methanol and the bromide reactant was monitored in an NMR tube, there was little to suggest straight nucleophilic displacement of the bromine. Once activated, the time between the formation of the rearranged product was short, with no stable intermediate identified. We believe that the nucleophilic behaviour of the methanol, and similarly for the ammonia, reacts at the carbonyl rather than at the bromine. As this occurs, an alcohol is formed which itself reacts intramolecularly to displace the bromine, through the formation of an epoxide ring. When this strained ring is opened, the net result is relocation of the oxygen to the adjacent carbon as an enol which tautomerises to the keto-form (Schemes 3.13 and 3.14). Ammonia based rearrangements on similar alpha-bromo ketones through epoxyamines have been proposed before[246].

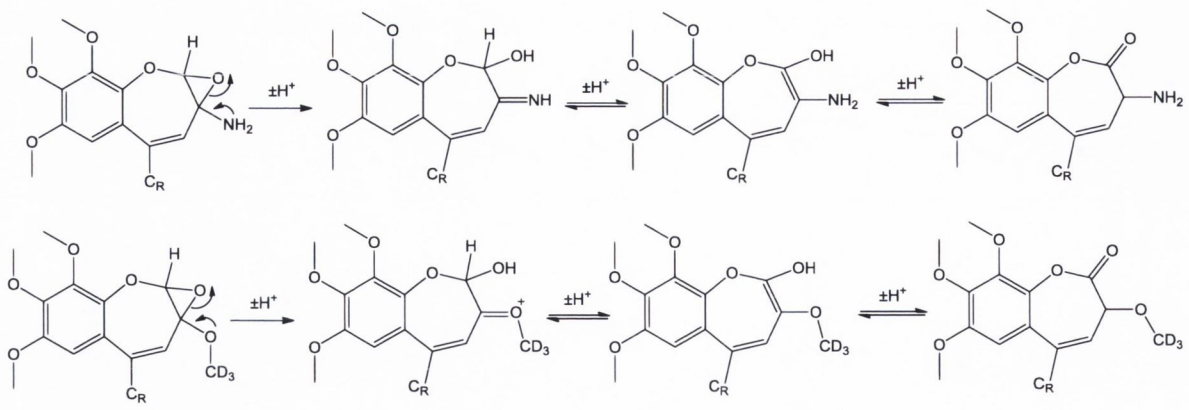


Scheme 3.13. One proposed mechanism for methanol induced rearrangement to 7-membered lactones



Scheme 3.14. One proposed mechanism for ammonia induced rearrangement to 7-membered lactones

We remain unsure about the exact means of epoxide ring opening. Elimination of the hydrogen presents a realistic scenario, although elsewhere transient α-hydroxyimine formation has been suggested[246] (Scheme 3.15). Unfortunately, it is difficult to declare with certainty which one of these the most likely mechanistic pathway, although the net result is essentially the same.

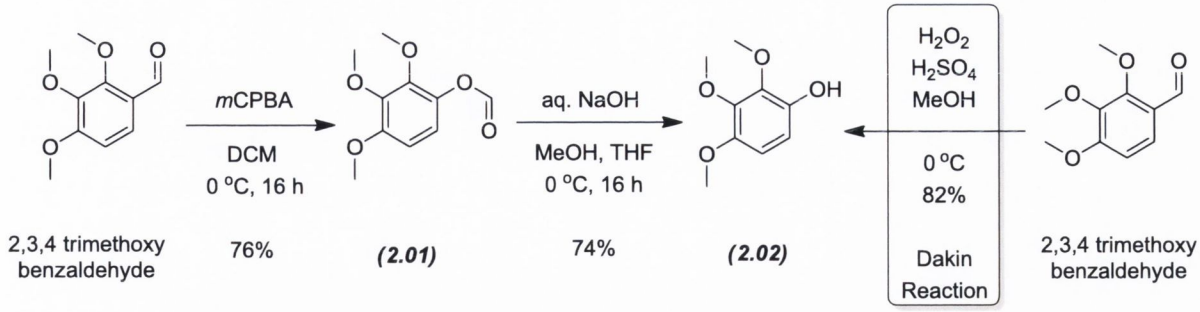


Scheme 3.15. Alternate proposals for epoxide ring opening

3.3.1 Shorter synthetic route to 4-aryl coumarin compounds; synthesis of a versatile precursor

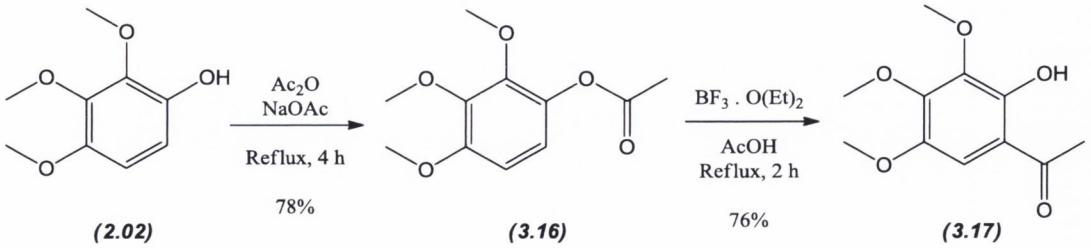
Due to the excellent performance of the 4-aryl coumarins in preliminary assays, a more efficient method was devised for the large-scale synthesis of these promising compounds. While the existing synthetic route to this point was satisfactory, including the azide-mediated ring contraction step, it was necessary to couple each C-ring moiety to the AB-ring before bromination could be attempted. In doing so, we had to commit to a single final compound at the coupling stage, one at a time, and repeat the proceding steps separately for each derivative. We felt it would be advantageous, if instead, we could synthesise a common coumarin based AB-ring scaffold first, to which we could introduce diversity at a later stage.

There are several methods available in the literature for the synthesis of 4-aryl coumarin compounds[247]. The new method we devised takes reaction steps from some of these and improvements to others that we optimised during their synthesis. As in the synthesis of benzoxepinone series, the starting point was again 2,3,4 trimethoxybenzaldehyde. Initially, synthesis began with Baeyer-Villiger oxidation of the 2,3,4 trimethoxybenzaldehyde introducing an oxygen atom on to the phenyl ring (formate ester ***2.01***) and hydrolysis under basic conditions would liberate the necessary phenol ***2.02***. Later, this means was replaced with the more proficient Dakin oxidation reaction to save time and product (Scheme 3.16).



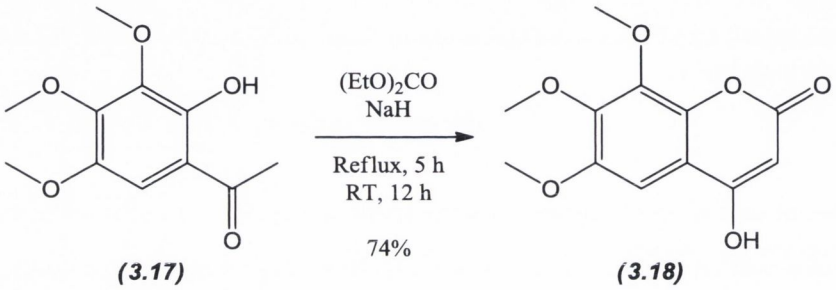
Scheme 3.16. Synthesis of 2.02 by Baeyer-Villiger oxidation and subsequent hydrolysis (left) or new Dakin oxidation approach (right)

The resultant phenol was then *O*-acetylated with acetic anhydride and sodium acetate. A four hour reflux afforded methyl ester ***3.16*** (Scheme 3.17). Next the acetyl group migrated on to the adjacent aromatic carbon with the use of the Lewis acid boron trifluoride, to give keto-phenol ***3.17***. This reaction, known as the Fries rearrangement, sees a lone pair on the carbonyl of the phenyl ester attack electron deficient boron, to form a polarised complex (B^- -- O^+) that stimulates rearrangement of the boron group onto the phenolic oxygen. Doing so prompts the dissociation of the acyl group from the phenolic oxygen to form a free, and highly reactive, acylium ion. Electrophilic aromatic substitution then takes place, which is *ortho/para* selective. The regiochemistry may be manipulated by controlling the temperature; low temperature favours the *para* position while high temperature favours the *ortho* position. In this case, with only the *ortho* and *meta* positions available, exclusive ortho acetylation occurs anyway. Basic work up with sodium hydroxide both hydrolyses the boron complex and neutralises any resultant HF.



Scheme 3.17. Acetylation of phenol 2.02 and subsequent Fries rearrangement to keto-phenol 3.17

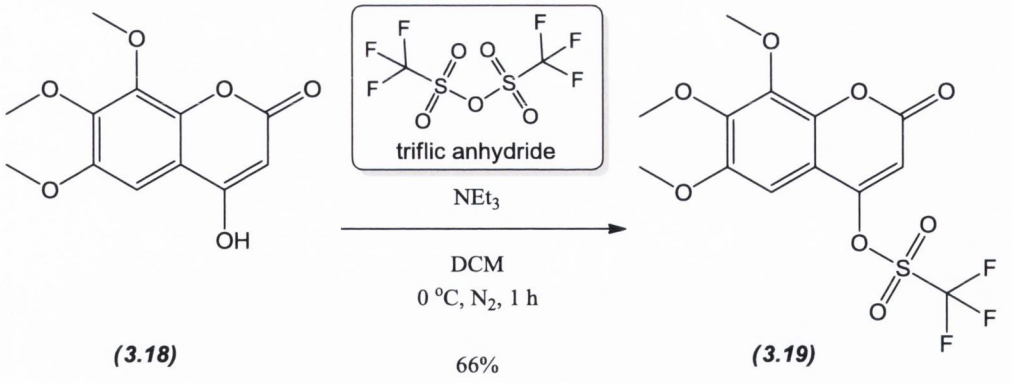
Next the keto-phenol ***3.17*** underwent crossed Claisen condensation with diethyl carbonate to give the desired coumarin backbone (Scheme 3.18). Sodium hydride was used as the base, and the product formed was the conjugated enolate ***3.18*** as expected. This compound was very insoluble in almost all solvents which made its purification difficult. Isolation and characterisation was therefore deferred to the following step.



(3.17) ***(3.18)***

Scheme 3.18. 4-Hydroxycoumarin 3.18 formation with diethyl carbonate, sodium hydride and 3.17

In order to couple on our C-rings, we had to convert the hydroxycoumarin ***3.18*** to an appropriate substrate for Suzuki coupling. Due to our success with triflates in the coupling reactions in Chapter 2, and their use in the synthesis of 4-aryl coumarins in the literature, we decided to form the triflate derivative of ***3.18***. With ***3.18*** in enolate form, we could avoid using the Comins' reagent[228] necessary for the ketone compound ***2.24*** and the corresponding exacting conditions its usage imposed. Instead we went with triflic anhydride, based on its regular use on very similar reactions found in the literature[248]. Triflation was much easier with the anhydride reagent; the reaction was carried out at 0 °C and in DCM for one hour to afford triflate ***3.19*** (Scheme 3.19). Prolonged exposure to the triflic anhydride was nevertheless avoided, for fear the triflic acid by-product could hydrolyse the product.

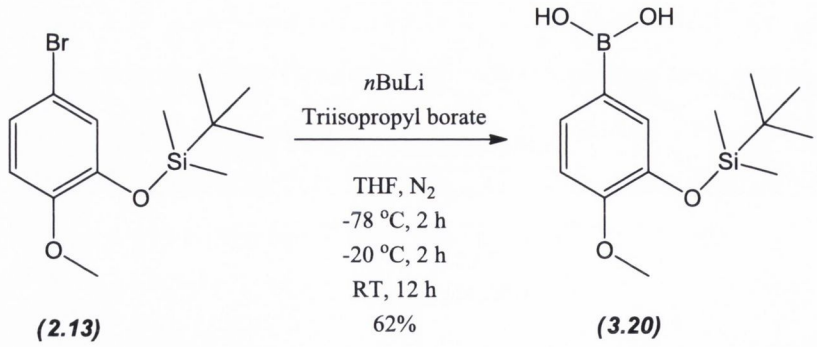


Scheme 3.19. Triflation of 4-hydroxycoumarin 3.18 with triflic anhydride.

3.3.2 Coupling of chromenone precursor *3.19* to various C-rings to synthesise an array of 4-aryl coumarin compounds

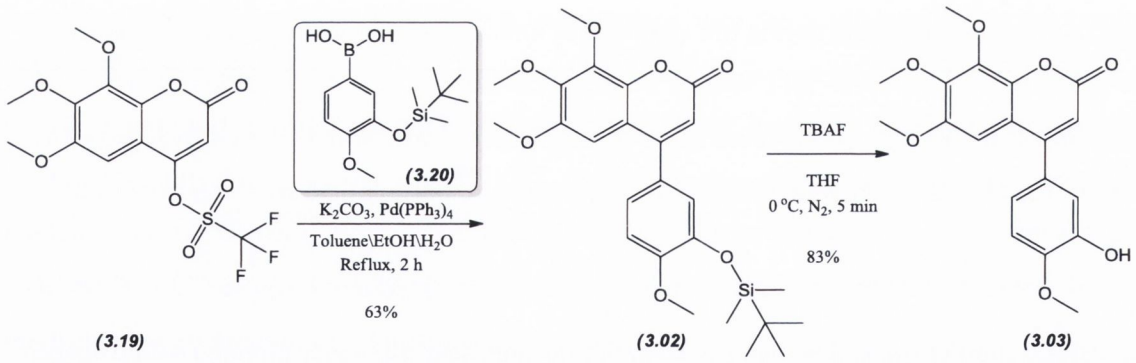
Triflate ***3.19*** would serve as a useful precursor for a series of 4-aryl coumarin compounds. Its synthesis was amenable to scale up and the triflate itself proved stable, even over long periods. Its solubility was much less an issue than the antecedent enolate ***(3.18)*** and its relatively high R_f value on TLC meant it was also a great deal easier to identify and purify by flash column chromatography. However, in order to eventually synthesise lead compound ***3.03*** we had to adjust the bromine C-ring ***2.13*** to a group more acquiescent to Suzuki coupling. Based on the success of aryl boron coupling during the synthesis of aniline ***2.28***, we decided to continue using boron-based substrates. Given that boronic acids are considered preferable to boronic esters in the arylation of triflates[225b], we targeted those for the C-ring of ***3.03*** and its derivatives, except in the case of the aniline which demonstrated incompatibility to boronic acid synthesis previously.

The transformation of the aryl bromide ***2.13*** to the boronic acid was easily effected over a single step (Scheme 3.20) by the use of butyl lithium and triisopropyl borate at -78 °C[249]. This was a different approach to the palladium based Miyaura borylation, but effectively generated ***3.20***.



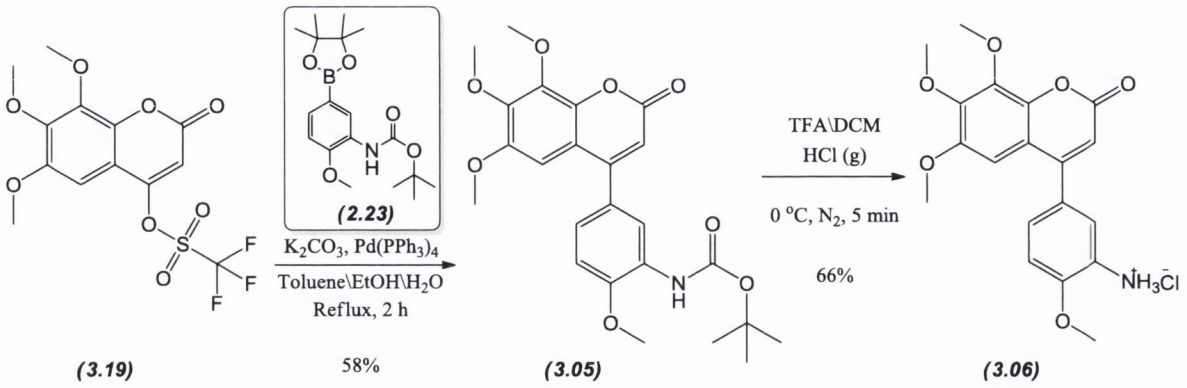
Scheme 3.20. Conversion of the aryl bromide 2.13 to the boronic acid 3.20

Aryl boronic acid ***3.20*** was coupled with triflate ***3.19*** under the same conditions employed for Suzuki coupling reactions described in Chapter 2, to give tricyclic ***3.02***. TBAF deprotection of the *tert*-butyldimethylsilyl ether protecting group afforded final compound ***3.03*** (Scheme 3.21). The original synthesis developed by Hudson, involving the bromination and ring contraction reactions, prepared this lead compound via a linear route consisting of 16 consecutive steps (excluding C-ring synthesis). We had now constructed the same molecule in just 7, and in a fashion much more agreeable for replication on a large scale.



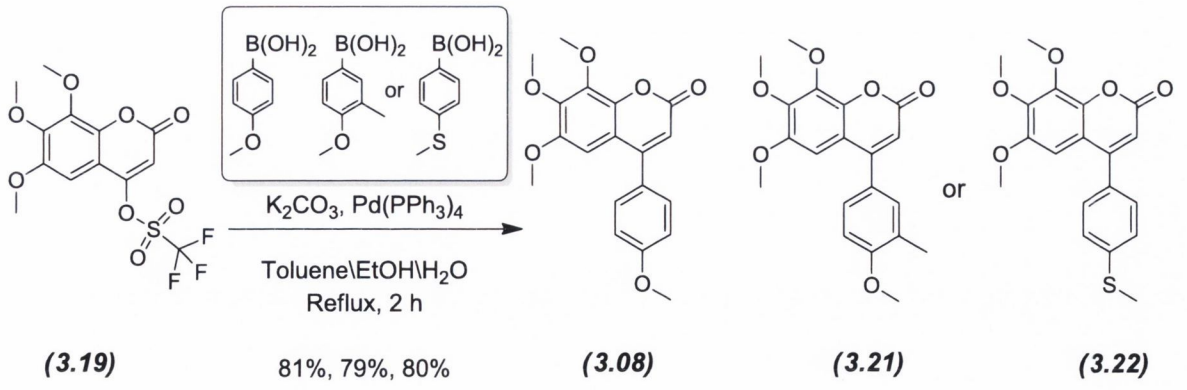
Scheme 3.21. Suzuki coupling of triflate 3.19 with boronic acid 3.20 to give 4-aryl coumarin intermediate 3.02. TBAF deprotection of 3.02 gives final lead compound, phenol 3.03

Utilising the previously prepared *N*-Boc protected aniline aryl boronic ester ***2.23***, triflate ***3.19*** was Suzuki coupled to synthesise aniline ***3.05***. Again, treatment with TFA thereafter removed the Boc group as before, and treatment of an ether solution with gaseous HCl yielded anilinium salt ***3.06*** (Scheme 3.22).



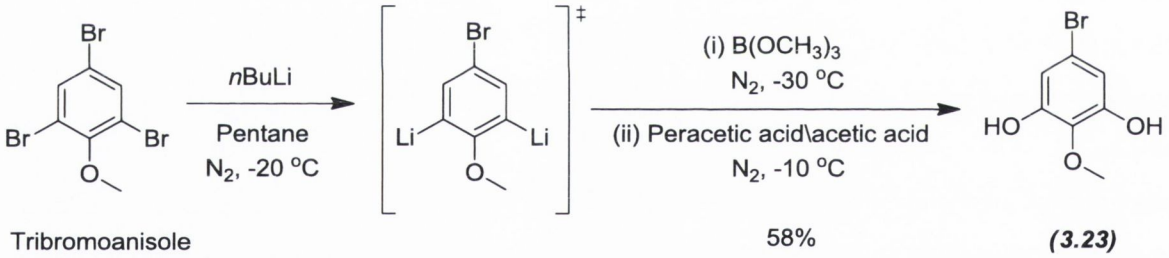
Scheme 3.22. Suzuki coupling between aryl boronic ester 2.23 with triflate 3.19 to give 4-aryl coumarin 3.05, which was deprotected to aniline salt 3.06.

Having established an optimised method for synthesis of 4-aryl coumarins in general, we decided to expand the series by varying the substituents on the C-ring. With a variety of aryl boronic acids accessible from earlier work, we coupled three of these; a simple 4-methoxyboronic acid, a 3-methyl-4-methoxyboronic acid and a 4-thioanisole boronic acid, seperately to triflate ***3.19***. As a result, each in a single step, we generated three extra 4-aryl coumarins, two of which were novel, ***3.21*** and thioanisole ***3.22***, in addition to the paramethoxy chromenone ***3.08*** synthesised previously via azide ring contraction (Scheme 3.23). While these compounds were not expected to be intensely efficacious, we hoped their evaluation would at least grant us a better understanding as to the degree of change permitted on the C-ring that would still preserve activity.



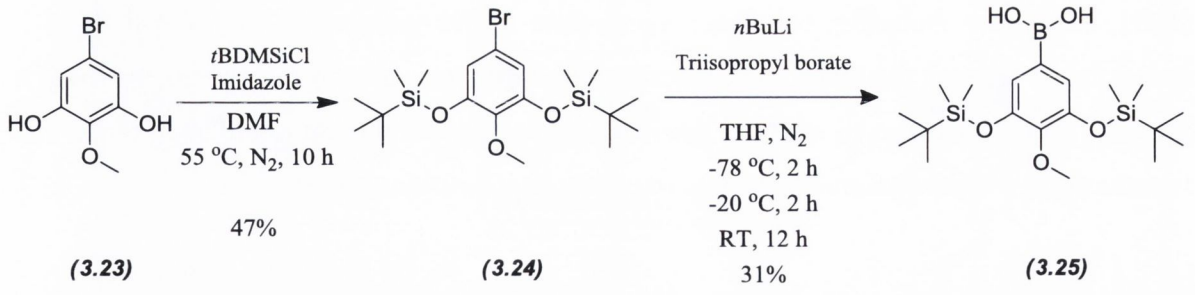
Scheme 3.23. Suzuki coupling with commercially available aryl boronic acids granted three more 4-aryl coumarin final compounds.

In the procurement of paramethoxy chromene derivative ***3.08***, we would be able to contrast its activity alongside phenol ***3.03***, and judge the extent to which the phenolic hydroxyl group is of benefit. Conversely, we were intrigued as to the possible repercussions an extra *meta* hydroxyl group on the C-ring would have on activity. Would an extra hydrophilic, nucleophilic moiety enhance binding to tubulin or result in exclusion from the active site? Unfortunately, the synthesis of a diol C-ring was complicated by the lack of a commercially available starting material analogous to that used during the synthesis of boronic acid ***3.20***. As an alternative, tribromoanisole was used as a starter molecule, and using butyl lithium in a pentane suspension at -20 °C, we were able to displace only the two bromines *ortho* to the methoxy group[250]. Using trimethyl borate we could in situ promote borylation of the dianion intermediate, and subsequent introduction of peracetic acid oxidised the borane groups to afford the methoxyresorcinol intermediate ***3.23*** in one pot (Scheme 3.24). This reaction was somewhat temperamental, with an intricate series of crucial temperature changes throughout, and a fresh solution of peracetic acid proved to be critical to its success.



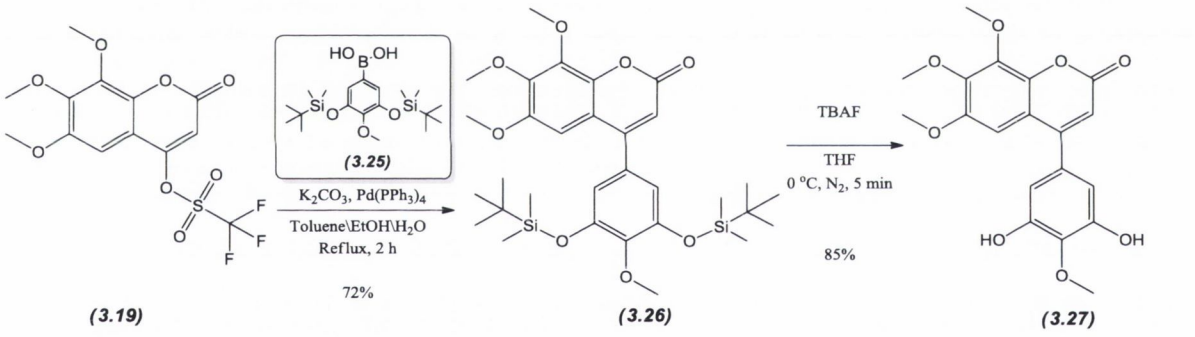
Scheme 3.24. One pot, boron based hydration of tribromoanisole, through a dianionic intermediate to give diol 3.23.

Once formed, the diol ***3.23*** was protected as the silyl ether ***3.24***. Unlike the silyl protection of ***3.20***, this transformation was carried out at the higher temperature of 55 °C in order to optimise the transformation, pre-empting any mono-silyl protection likely to occur under ambient conditions. Once acquired, this bromide intermediate ***3.24*** was converted to the boronic acid ***3.25*** using the same approach for the mono-hydroxylated product ***3.20*** (Scheme 3.25).



Scheme 3.25. Diol protection and conversion to an appropriate boronic acid 3.25

Boronic acid ***3.25*** was coupled to triflate precursor ***3.19*** as per the Suzuki method used for the synthesis of ***3.02***, resulting in 4-aryl coumarin ***3.26***. TBAF deprotection gave the expected diol compound ***3.27*** (Scheme 3.26).



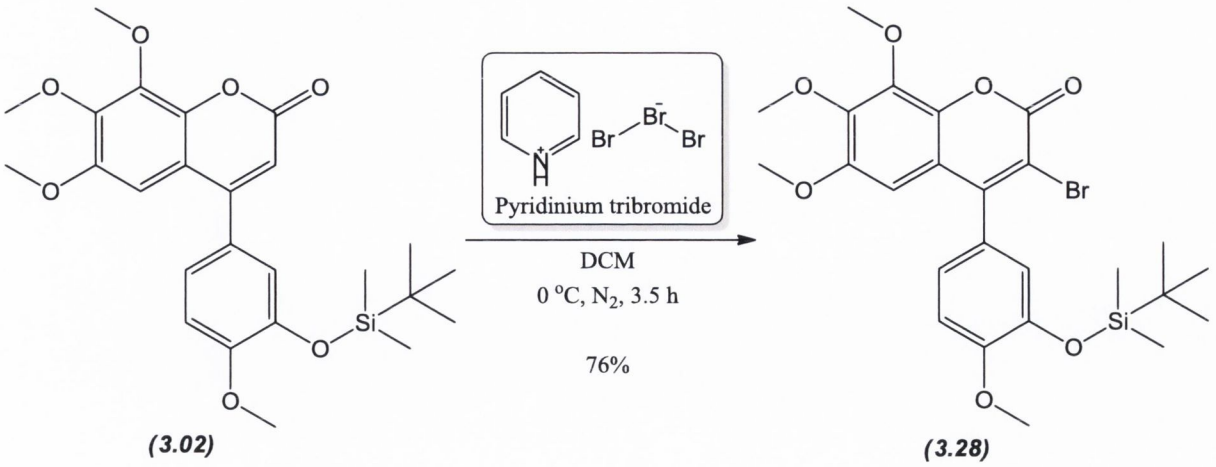
Scheme 3.26. Suzuki coupling of 3.25 to 3.19, with subsequent deprotection, resulting in diol 3.27

3.4 Functionalisation of the alkene and creation of a bi-faceted tubulin binding ligand

One downside to the 4-aryl coumarin series of compounds is that there are fewer feasible sites aside from the C-ring on to which we could couple on potential congruent partners to build a bivalent hybrid molecule. On the other hand, the benzoxepinone series offers not only option to brominate the B-ring (***3.01***, ***3.04***, ***3.07*** etc), which could be quite easily displaced to affix a linker at that position, but there is also the additional possibility of reducing the ketone to a nucleophilic alcohol, on to which we could couple a linker or a second pharmacophore directly. In relation to the latter, it has been shown elsewhere in our laboratory that enantiomerically pure stereoisomers of analogous benzocycloheptan-ol compounds can be prepared (by G.

Stack), and hybrid molecules have been synthesised at this position via the alcohol (by E. Breen[211]) . To broaden the scope and applicability of the 4-aryl coumarin compounds, we made tentative investigations as to what the alkene group on the B-ring could afford us in terms of introducing new functional groups that would permit later functionalization.

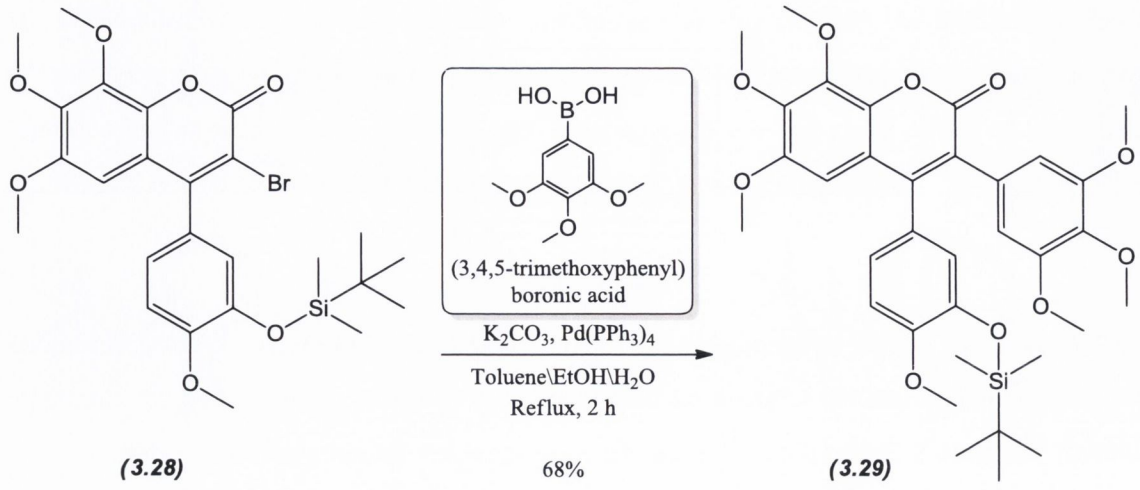
Enones systems are typically functionalised alpha to the carbonyl by way of the Baylis-Hillman reaction[251] to give alcohols, which in our case would be a useful handle for conjugation of a linker moiety. A tertiary amine nucleophile, such as 1,4-diazabicyclo[2.2.2]octane (DABCO) undergoes Michael addition to form a zwitterionic enolate which over time promotes aldol style C-C bond formation with an aldehyde. Elimination releases the amine preferentially, meaning the resultant alcohol is preserved. DABCO has a reputation of inefficiency with cyclic enones, and variations involving DMAP[252] and imidazole[253] in place of DABCO have shown marked improvement on such molecules. However, all three reagents failed to illicit any reaction with ***3.03*** and formaldehyde. The reactions are known to be slow at ambient condition, with a timescale of days/weeks, so the reactions were retried in a microwave, again without any noticeable alteration except traces of silyl deprotection. We decided to switch the plan to instead introduce bromine to the double bond, to form a vinyl bromide which we were confident we could couple using the palladium based methods that were effectual previously. As PTT was shown already not to brominate on the alkene system in ***2.16***, we used a different reagent, pyridinium tribromide[254], advocated by White on similar aryl alkene systems[207]. Bromine was successfully introduced onto the double bond of ***3.03*** in this fashion to yield bromide ***3.28*** without any evidence of addition across the double bond (Scheme 3.27).



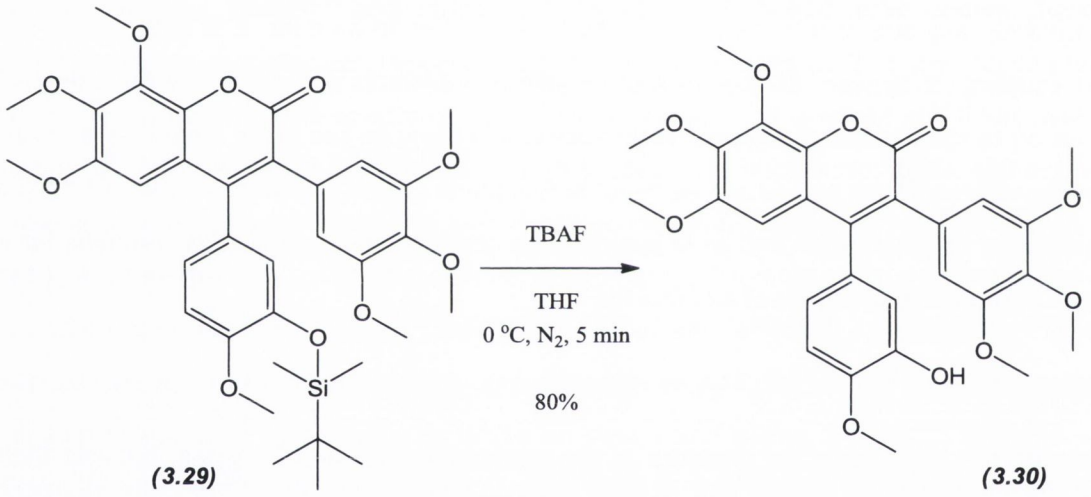
Scheme 3.27. Bromination of the alkene 3.02 to give vinyl bromine 3.28

Unfortunately, any attempts to couple aliphatic boronic acids to bromine ***3.28*** didn't work. For Suzuki coupling, it appears as though aryl or alkene substrates are necessary for oxidative addition on to the palladium complex. Aromatics would likely be too bulky for use as a linker, while alkene linkers with two Suzuki susceptible functional groups on either end would have a propensity for polymerisation and were avoided. We could however, exploit the bromine for a separate purpose; the synthesis of a bi-faceted TBA.

The importance of not only the presence of the methoxy groups on the A-ring, but also their spatial arrangement, for tubulin binding has been a well established concept in combretastatin based TBA research[209]. By coupling on an additional trimethoxyphenyl ring on to vinyl bromide ***3.28***, on the opposite face of the stilbenoid skeleton, we could create a TBA that could hypothetically bind to the colchicine binding site on tubulin from either face of the molecule. Using the commercially available aryl boronic acid 3,4,5 trimethoxyphenyl boronic acid, and under Suzuki conditions, we synthesised the triaryl compound ***3.29*** (Scheme 3.28). TBAF or sodium azide deprotection of ***3.29*** afforded the free phenol ***3.30*** (Scheme 3.29).



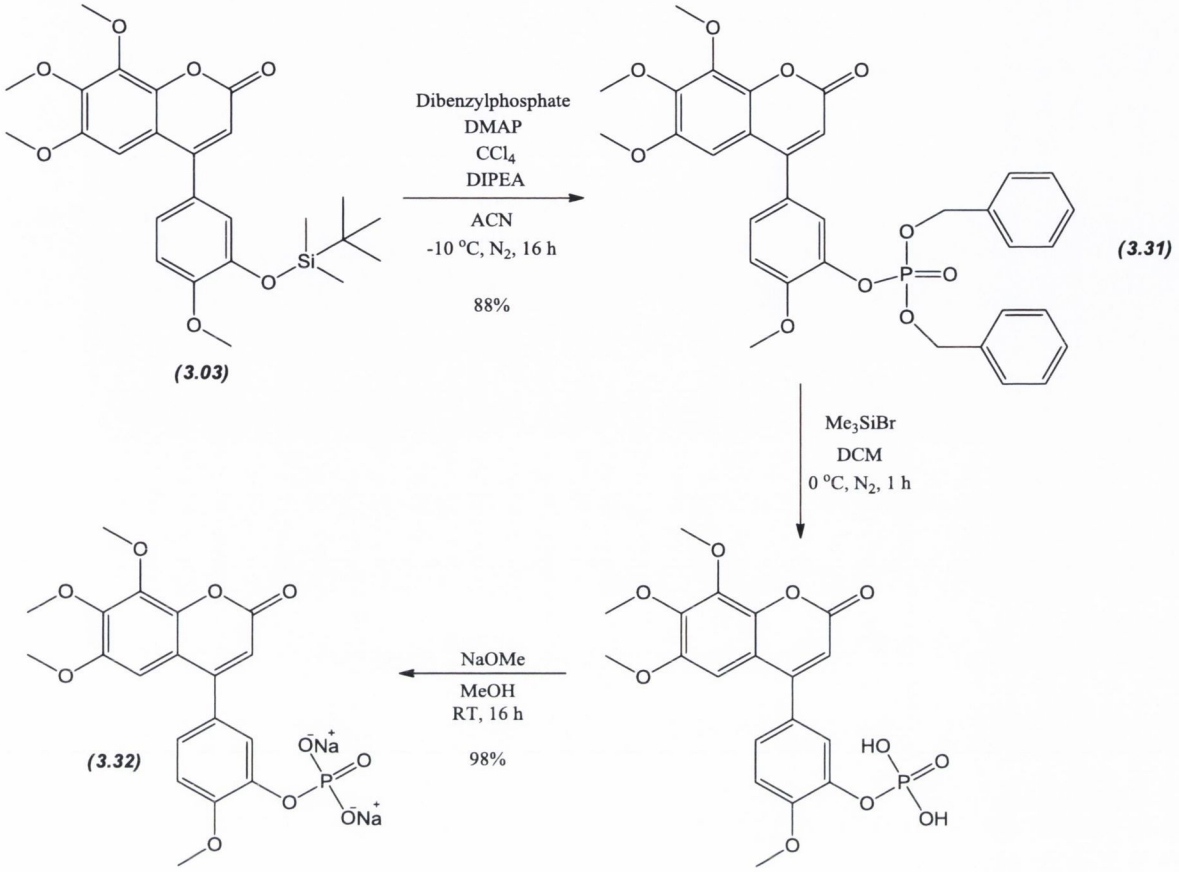
Scheme 3.28. Suzuki coupling of bromide 3.28 with trimethoxyphenyl boronic acid



Scheme 3.29. Deprotection of silyl ether 3.29 to give free phenol 3.30

3.5 Phosphate salt prodrug of phenol 3.03

As was the case in Chapter 2, the phenol lead compound was converted to a phosphate salt. As before, the rationale was that it would serve as a prodrug, increasing the solubility and releasing phenol ***3.03*** *in vivo*, as CA-4-P successfully does with CA-4. The route to the phosphate from the phenol was the same as with the synthesis of ***2.31***. The 4-aryl coumarin ***3.03*** was first converted to a phosphate ester ***3.31*** with dibenzyl phosphite, the alkyl groups were then removed by BTMS to give the phosphonic acid intermediate, which was converted to the desired phosphate salt ***3.32*** with sodium methoxide in methanol[229, 231a] (Scheme 3.30).



Scheme 3.30. Synthesis of the phosphate salt prodrug 3.32 of phenol 3.03

3.6 Biological evaluation of the 4-aryl coumarin series of TBAs

Here the results of the lead compounds synthesised in this chapter are succinctly reported. Again, the biological testing of these molecules was conducted by E. Prokopiou for her doctoral thesis[232].

First, the cell proliferation assay was carried out using MTT on endothelial and tumour cells as before, to determine the most efficacious compounds. For the most part, the 4-aryl coumarins demonstrated enhanced inhibitory activity, relative to the benzoxepinones from Chapter 2. Among these, phenol ***3.03*** and aniline ***3.06*** were the most efficacious, both better than CA-4 against tumour cells, and the most active our lab has produced to date. Chromenones ***3.08***, ***3.21*** and ***3.22*** also demonstrated reasonably good activity, but were not pursued any further, partly

as their design made incorporation into a hybrid molecule difficult. The presence of an additional phenol group on to the 4-aryl coumarin skeleton drastically reduced the biological activity, as seen with diol ***3.27***, particularly when juxtaposed with the potent ***3.03***; a 1000 fold difference in inhibition. Compound ***3.30***, was likewise disappointing, although it could be rationalised that the additional, bulky trimethoxyphenyl ring causes considerable steric hindrance when binding to tubulin, and also renders the phenol group inaccessible to its preferred domain at the binding site.

Table 3.1. Best fit IC_{50} values ± SEM of 4-aryl coumarin lead compounds from MTT assay (n=3)

	HUVECs (nM)	PC-3 cells (nM)
CA-4	4.03 ± 1.73	14.01 ± 0.58
2.17	4.91 ± 1.01	4.67 ± 1.45
3.03	5.56 ± 1.36	4.70 ± 1.19
3.06	1.45 ± 1.15	3.82 ± 1.15
3.08	12.03 ± 0.58	8.50 ± 0.40
3.13	1.94 ± 1.73 (μM)	-
3.21	7.04 ± 12.12	11.03 ± 1.15
3.22	3.01 ± 1.15	8.50 ± 3.46
3.27	3.51 ± 2.05 (μM)	6.10 ± 3.50 (μM)
3.30	14.56 ± 1.54 (μM)	4.75 ± 1.13 (μM)

In the cell cycle arrest assay, a significant percentage of ***3.03*** and ***3.06*** treated cells were rendered incapacitated in the G_2/M phase at 0.5 μM (81.22 ± 1.43% and 77.91 ± 3.72% for ***3.03*** and ***3.06*** respectively) and 1 μM (81.42 ± 4.20% and 69.63 ± 3.11% for ***3.03*** and ***3.06*** respectively) compared to the control (31.44 ± 0.82%). In terms of the microtubule organisation, both lead compounds demonstrated emphatic reduction of stained α-tubulin and long microtubule filaments at 1 μM upon immunofluorescent staining.

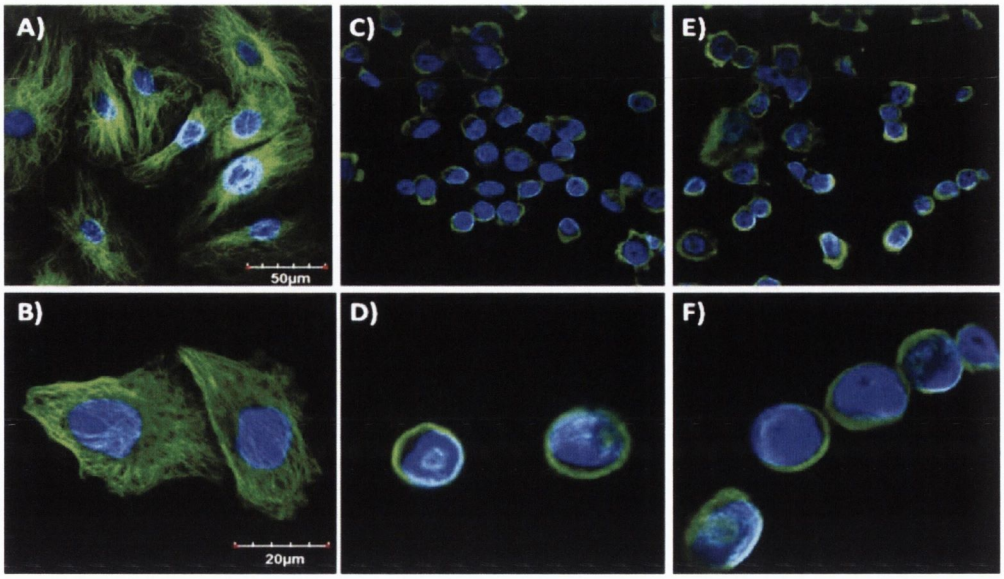


Figure 3.13 Disruption of microtubule cytoskeleton; marked absence of microtubule fibres (green) surrounding the nuclei (blue) following treatment with lead compounds 3.03 and 3.06. A-B) Control (0.1% DMSO), C-D) Phenol chromenone 3.03 (1 µM), E-F) Aniline chromenone 3.06 (1 µM)

Both ***3.03*** and ***3.06*** induced changes in the endothelial monolayer and caused significant blebbing, indicative of cytoskeletal alteration and which clearly illustrates their exciting anti-vascular properties. This effect was possible at 0.1 µM for both test compounds, although in each of the two cases the effects did begin to reverse after 3 hours. However, this transitory phenomenon could be manipulated for therapeutic benefit; acute, potent injury of the endothelium would be much more detrimental for the more vulnerable tumour blood vessel, whereas the normal blood vessels would most likely withstand such an assault given adequate time to heal. Unfortunately this assay and the rat aortic ring assays do not accurately reflect the unique composition of the tumour microvasculature, or account for any difference there may be between it and normal vasculature.

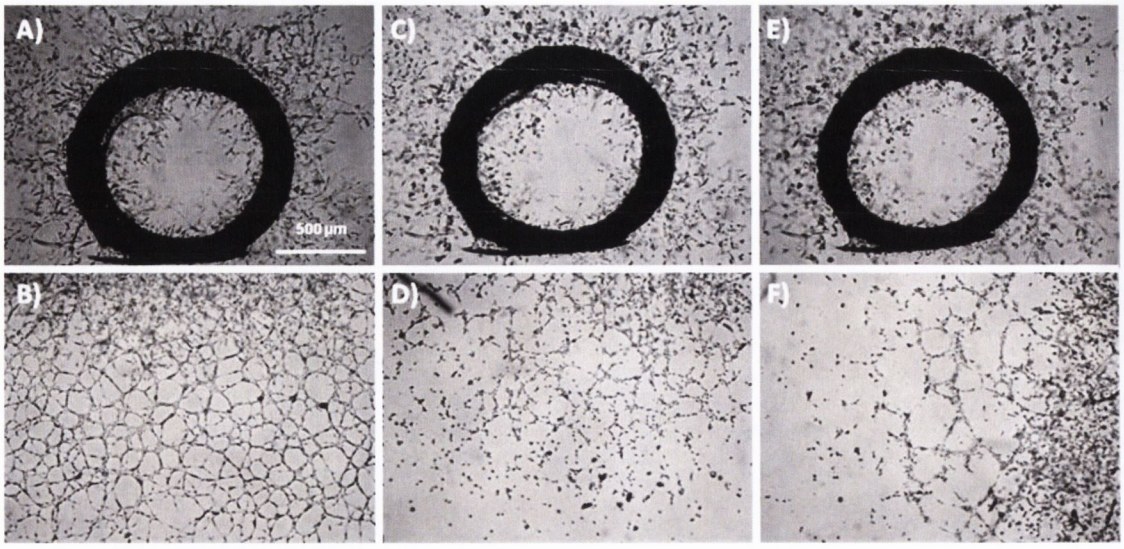


Figure 3.14. Example of the anti-vascular effect of the 4-aryl coumarins. Images A-B) represent the aortic ring before the administration of phenol 3.03. Images C-D) show ablation of the vascular network, 4 hours after treatment with 3.03 (10 nM). Images E-F) 24 hours after treatment with 3.03 (10 nM).

In the rat aortic ring assays, marked improvement in activity was witnessed for both ***3.03*** and ***3.06*** over lead benzoxepinone compound ***2.17***. In the anti-vascular assay, the 4-aryl coumarins demonstrated potent activity at 10 nM, with patent breakdown of the established microvessels, for 4 hours after treatment, compared to 50 nM of ***2.17***. These results are in line with those of CA-4. When retried with the anti-angiogenic version of the assay, even more encouraging activity was observed with ***3.03*** and ***3.06***, at 5 nM concentrations, although ultimately this was not deemed statistically significant. At 10 nM, statistically significant inhibition of angiogenesis was almost absolute, compared with 50 nM ***2.17***, even surpassing the effect observed with CA-4.

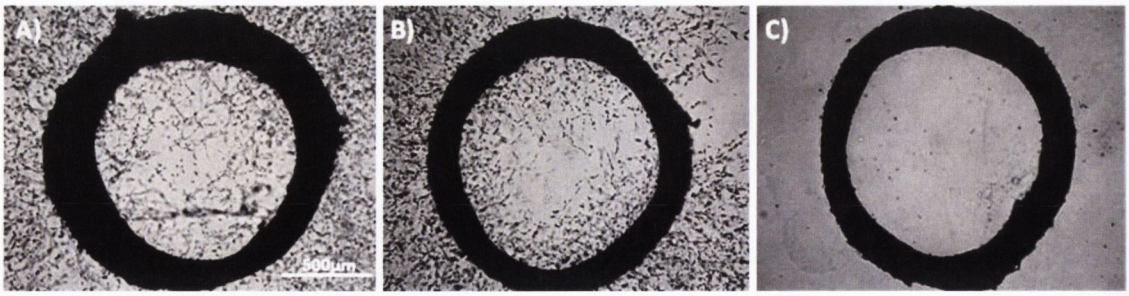


Figure 3.15. Example of the anti-angiogenic effect of the 4-aryl coumarins. Compared to the control A) (0.1% DMSO), aniline 3.06 shows both insignificant and significant impediment of neovascularisation at B) 5 nM and C) 10 nM concentrations respectively.

3.7 Conclusions

The work in this chapter focussed on a series of 6-membered 4-aryl coumarin tubulin binding agents. As observed by Hudson, bromination alpha to the carbonyl on benzoxepinone compound ***2.16*** forms a product sensitive to ring contraction treatment with an azide nucleophile. Here, we first optimised the temperamental bromination step, to one highly reliable and practical, and then monitored the novel ring contraction transformation as it happened through shifts in the NMR spectrum. In doing so, we can also confirm the displacement of the bromine with the azide just before the intermediate collapses to form the chromenone B-ring. Furthermore, we extended the bromination and ring contraction to analogous substrates to show reproducibility, and also demonstrated the outcome of treating the bromides with different nucleophiles. In this latter case, methanol and ammonia both prompted nucleophilic rearrangement of the bromo-benzoxepinone backbone to form 7-membered lactone compounds, while sulphur based nucleophiles instead displaced the bromine in a straightforward way, but later ring contracted themselves under azide treatment.

The 4-aryl coumarins from the ring contraction of benzoxepinones are encouraging tubulin binding agents. To assess their therapeutic value, a new synthetic route was implemented, considerably hastening their synthesis. A range of 4-aryl coumarins were prepared by this method, including phenol ***3.03***, aniline ***3.06***, paramethoxyphenyl coumarin ***3.08*** , methyl-paramethoxyphenyl coumarin ***3.21***, parathioanisole coumarin ***3.22***, diphenol ***3.27***, while a new type of compound ***3.30*** was afforded by functionalization of protected phenol ***3.02*** and palladium coupling of an additional trimethoxyphenyl ring. Phosphate prodrug ***3.22*** was prepared by the same method for phosphate salt as in Chapter 2. Phenol ***3.03*** and aniline ***3.06*** performed excellently in their subsequent biological evaluation, the most potent of this lab group to date, demonstrating excellent anti-mitotic, anti-vascular and anti-angiogenic activity through a range of different *in vitro* and *ex vivo* assays.

Chapter 4 – Synthesis of a series of Novel Hybrid Molecules and Designed Multiple Ligands

4.0 Background

Having secured efficient methods for the syntheses of lead compounds ***2.17***, ***2.28***, ***3.03*** and ***3.06***, our attention turned to the idea of creating multivalent hybrid and designed multiple ligand based compounds, which would incorporate these potent vasculature disrupting agents into their overall design. At the outset, the implementation of a number of key physiochemical features was desirable, namely the idea of inserting groups that *in vivo*, would either introduce slow or controlled, targeted release properties into the molecular composition. In doing so, these elements of variable release could ultimately allow for the compounds' presentation for high dose chemotherapeutic regimens, yet the design is such that their impact would mimic that of a low dose, metronomic dosing type schedule, strategies which have already proven successful in both anti-vascular and anti-angiogenic therapies[255].

The delivery of anti-vascular agents with these potential therapeutic benefits is only possible if there are substantial distinctions between normal physiology and the pathology of the tumour and its surrounding environment. In this context, the biomarker APN is expressed exclusively on tumour vasculature undergoing angiogenesis but not on normal, quiescent vasculature[175]. It is also expressed on a variety of tumour cells themselves, including those found in the breast, colon and prostate[176-177]. Thus, the compounds under discussion in this chapter are designed in such a way as to have a component, which targets APN; in this way acting as a molecular chaperone towards tissue where this enzyme is expressed in high concentration. Thus, the hypothesis is that when hybrid or designed multiple ligand based drugs with an APN binding component are administered intravenously, they should be sequestered in APN-rich tumour regions. The torpid, often stagnant blood flow throughout the tumour vasculature is conducive to further localise the drug in this area, while the porous nature of the vessels themselves could allow the drug to leak from the circulation to the tumour mass itself. Beyond the enhanced delivery of a TBA component, with an APN inhibitor like bestatin included, our bivalent agents should also invoke supplemental anti-angiogenic and anti-metastatic responses of its own[159, 174].

Bestatin serves as an ideal candidate for integration on to a prototypical hybrid due to the low toxicity it elicits to normal cells; allowing us to accurately judge the benefit of conjugation over the TBA-effect alone, without the concern of dose-dependent adverse effects which could

otherwise obscure their evaluation. The solid track record of bestatin as an agent in combination therapy[256] reinforced its intuitive role as the second pharmacophore alongside our TBAs. In addition, the TBAs synthesised in Chapters 2 and 3 are also lipophilic and quite insoluble in aqueous media, and it is hoped that with a polar di- or tri- peptide attached the overall molecule would have enhanced solubility over the lone TBA.

The designed multiple ligand molecule that is also the subject of the work described in this chapter takes advantage of the promising data obtained by fellow PhD student, B. Moran. He demonstrated that insertion of a hydroxamic acid group into our TBAs delivers compounds with dual activity against APN and tubulin polymerisation.

Thus, the aims of the work described in this chapter are to;

(i) Present the TBA in prodrug form by attaching inhibitory peptides for APN on to the C-rings of our most active TBAs.

(ii) Link the peptides both via labile ester and rigid, slower releasing amide groups.

(iii) Create designed multiple ligands with hydroxamic acid based functionality grafted on.

(iv) Synthesise a 'controlled release' designed multiple ligand by attaching a substrate for APN onto the C-ring substituents of the DML, which is usually sensitive to such functionalization in terms of its activity.

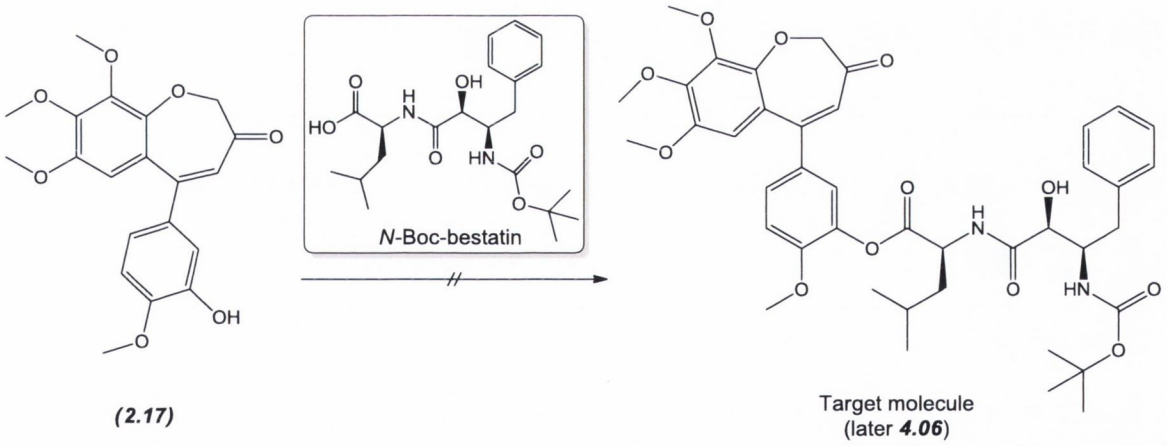
4.1 Peptide based hybrid drugs

The syntheses of TBAs outlined in Chapters 2 and 3 resulted in the identification of three closely related compounds of considerable promise; phenolic benzoxepinone ***2.17***, phenolic chromenone ***3.03*** and aniline chromenone ***3.06***. Though their biological activities are comparable, in terms of hybrid drugs we should be able to influence the differing release of these drugs depending on the C-ring functional group, be it phenol or aniline, based on the stability of the conjugate bond holding both groups together. Hybrids consisting of a phenolic ester would most likely dissociate relatively quickly, either by ubiquitous esterase enzymes

found in the blood[257] or via hydrolysis at physiological pH. Anilide based hybrids, consisting of a much more stable amide bond would probably be more resistant to hydrolysis under physiological conditions, therefore more dependent on the role of xenobiotic amidase or peptidase enzymes (of which APN could be one of many) to release the aniline TBA component, ultimately at a much slower rate than the corresponding phenol version *in vivo*.

4.1.1 Phenolic ester hybrid based on benzoxepinone 2.17

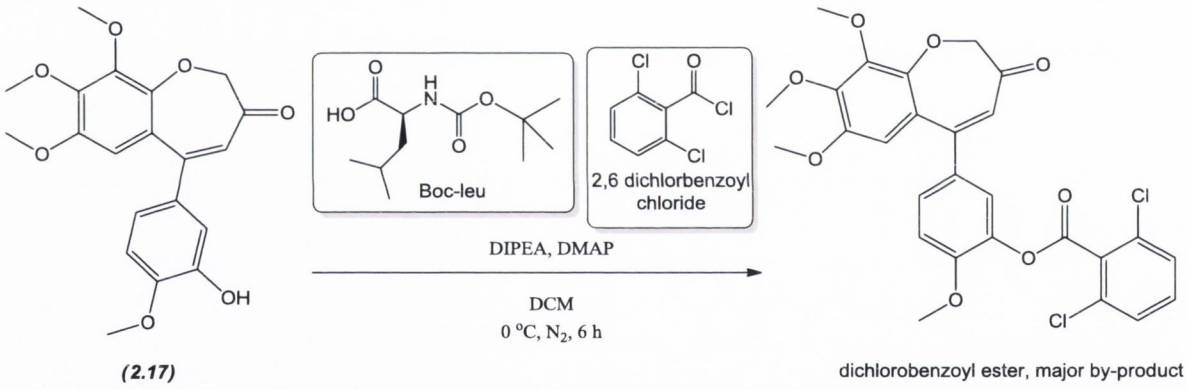
Synthesis of a hybrid molecule involving both phenol lead compounds, ***2.17*** and ***3.03,*** would naturally entail the formation of an ester bond. Unfortunately, none of our many attempts to couple *N*-Boc-bestatin directly to either ***2.17*** or ***3.03*** were successful, using standard coupling conditions (Scheme 4.1). The likely explanation is that the carboxylic acid couples preferentially with its own free secondary alcohol on the AHPA moiety, either intramolecularly to form a 6-membered lactone, or with a separate molecule to form a dimer molecule or an even longer polymeric chain.



Scheme 4.1. Direct coupling of phenol 2.17 and bestatin was not possible.

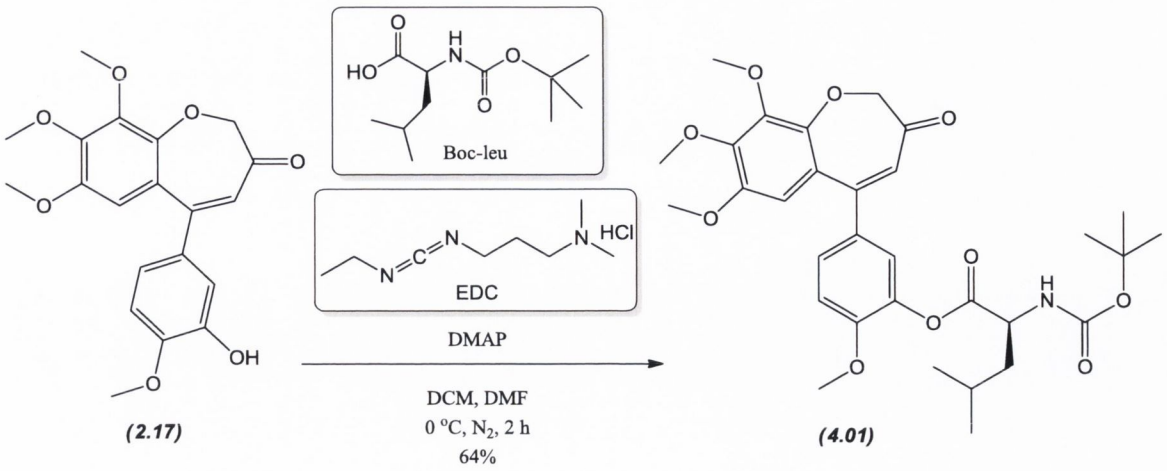
We were therefore obligated into making a tactical switch; to instead employ a longer, linear stepwise approach. Coupling of *N*-Boc-leucine to ***2.17*** using 2,6-dichlorobenzoyl chloride as coupling reagent in DIPEA, DMAP and anhydrous DCM[258], afforded phenolic ester ***4.01*** in moderate yield (30-40%). As substantial quantities of the 2,6 dichlorobenzoyl ester of ***2.17*** also

formed (Scheme 4.2), an alternative coupling reagent was investigated. The water-soluble version of dicyclohexylcarbodiimide, ethyl dimethylaminopropyl carbodiimide (EDC, Scheme 4.3) proved to be a very effective alternative for two reasons. First and foremost, a higher yield was obtained (64%), and secondly the resulting urea by-product is both water-soluble and more polar than the corresponding dicyclohexylurea (DCU) by-product of DCC making purification by flash column chromatography straightforward. We advocated use of the Boc protection strategy over that of an Fmoc strategy, based on the fact that Fmoc deprotection would involve the use of basic conditions that would put our newly formed ester bond at high risk of hydrolysis. Phenolic esters are even more susceptible to basic hydrolysis than aliphatic esters, and it was proved elsewhere in our lab by Breen[211] that an analogous phenol ester bond was not stable in the presence of either piperidine or TBAF. Meanwhile, we felt confident that using an organic acid like TFA under anhydrous conditions would likely selectively deprotect the *N*-Boc group.

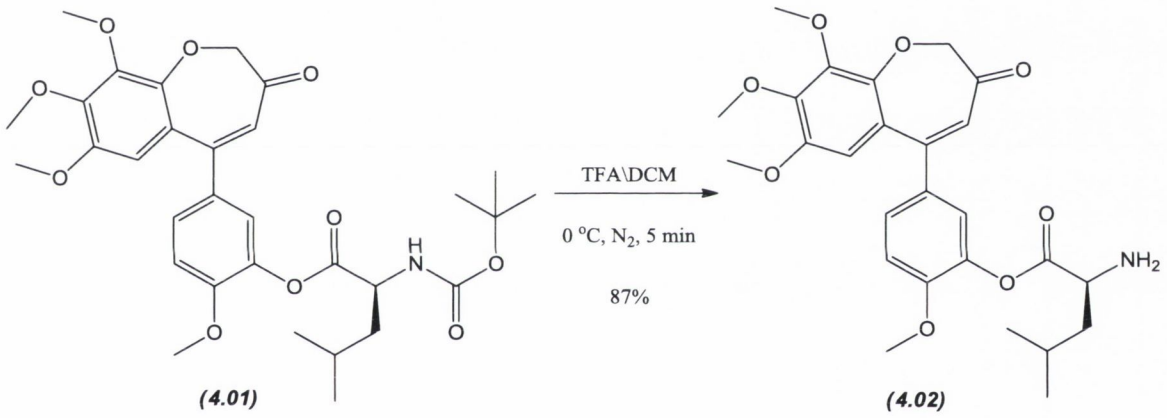


Scheme 4.2. Using the coupling reagent 2,6 dichlorobenzoyl chloride unfortunately generated the dichlorobenzoyl ester as the predominant product

Having secured the leucine ester ***4.01***, the *N*-Boc group, as hoped was removed by using anhydrous 50% trifluoroacetic acid in DCM, akin to the method used in standard peptide coupling methodology (Scheme 4.4). Avoiding water was essential in this step as it prevented unwanted hydrolysis of the labile ester group under these conditions. Liberation of the free amine was accomplished by washing the salt, dissolved in DCM, under mild conditions with 5% aq. $NaHCO_3$ solution.



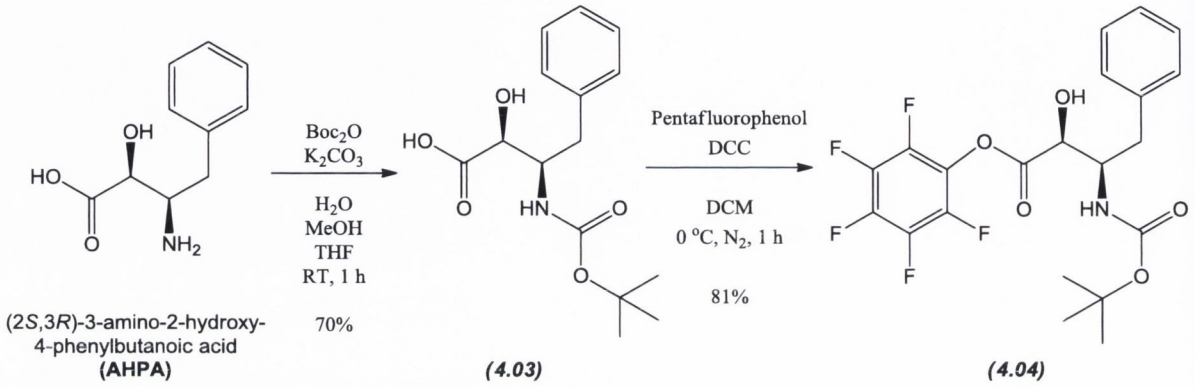
Scheme 4.3. EDC coupling of *N*-Boc protected leucine on to phenol 2.17



Scheme 4.4. TFA deprotection of the carbamate 4.01

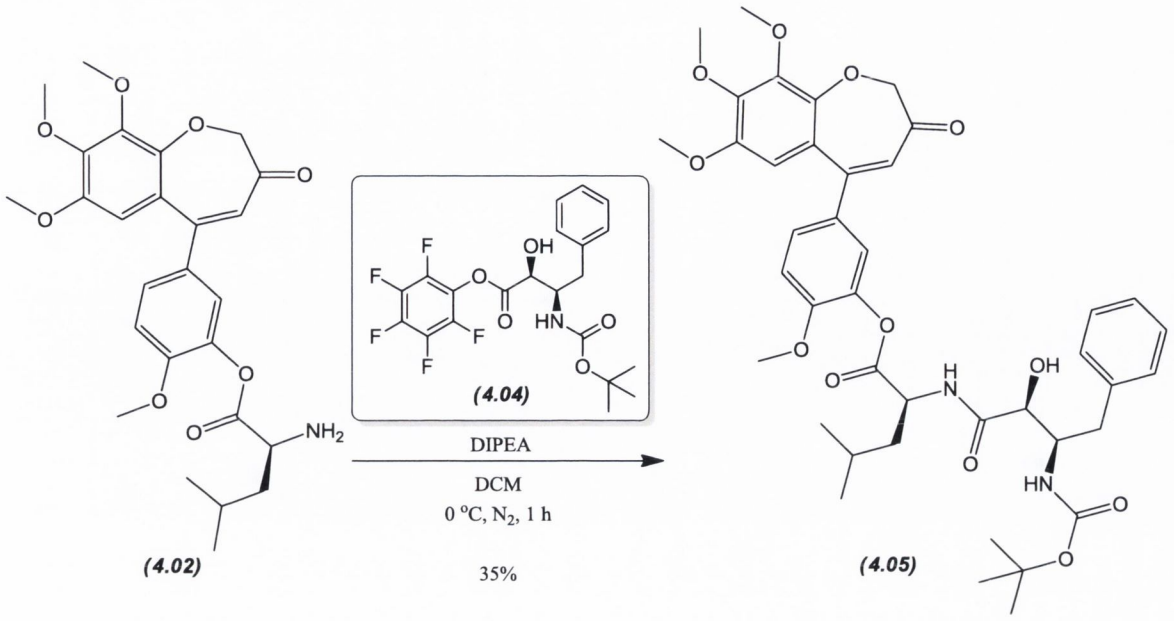
Coupling of the free amine ***4.02*** to 2-amino-3-hydroxy phenyl butanoic acid (AHPA) moiety necessitated protection of its amino group. AHPA was therefore dissolved in a solution consisting of THF:methanol:water and with treated potassium carbonate and di-*tert*-butyldicarbonate for 1 hour at room temperature. After acidic work-up, the *N*-Boc derivative ***4.03*** was obtained. Next, the carboxylic acid moiety was activated prior to coupling as a pentafluorophenyl (PFP) ester ***4.04***, generally accomplished with pentafluorophenol and DCC in anhydrous DCM over the course of 1 hour (Scheme 4.5). Problematic issues with this step included the removal of unreacted pentafluorophenol, and the DCC urea by-product DCU. Purification of the activated ester was facilitated by cooling the reaction down before the

filtration step to aid precipitation of the insoluble DCU by-product and purification by flash column chromatography. Interestingly, changing the coupling reagent to EDC did little to effect the rate of the reaction or the overall yield of the activated ester.



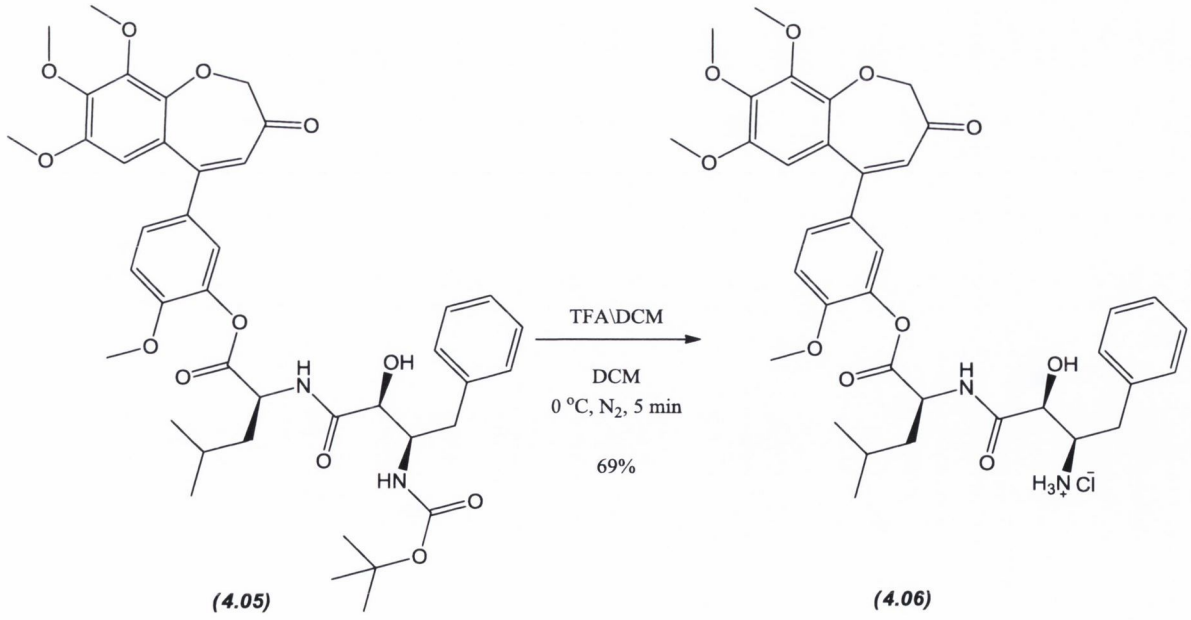
Scheme 4.5. Boc protection of AHPA and subsequent formation of the PFP ester 4.03

The PFP ester functional group is a labile one, and thus it was recommended to react ***4.04*** at the earliest possible convenience. With the free amine ***4.02*** already in our possession, we then coupled the two substrates together, using diisopropylamine as a tertiary base, in anhydrous DCM at 0 °C (Scheme 4.6). At the endpoint of the reaction, the solvent was reduced in volume and product isolated following purification by flash column chromatography.



Scheme 4.6. Coupling of PFP ester 4.04 on to free amine 4.02, to form amide 4.05

Deprotection of the *N*-Boc group of ***4.05*** was again achieved by treating ***4.05*** with a 50% solution of TFA in DCM under anhydrous conditions at 0 °C. The resultant TFA salt was treated with 5% aq. $NaHCO_3$ to liberate the free amine ***4.06*** which was then directly converted to its hydrochloride salt form (Scheme 4.7).



Scheme 4.7. Final deprotection of Boc group to furnish our first hybrid molecule 4.06

4.1.2 Structural Elucidation of hybrid 4.06

Coupling of the highly functionalised bestatin dipeptide motif on to phenol ***2.17*** meant almost doubling the mass of the molecule, and of course was met with a corresponding sharp increase in the level of complexity with regard to its structural elucidation. To resolve this, it was logical to first identify some of the prominent features of ***4.06*** common to phenol ***2.17***, and analyse the remaining spectral data. For example, the four methoxy groups could be easily recognised both in ^{1}H (four singlets 3.86 – 3.46 ppm) and ^{13}C NMR (four signals 61.5 – 55.5 ppm) (Figures 4.1 and 4.2). The CH_2 from the B-ring was found at 4.66 ppm on the ^{1}H NMR, as a singlet, which helped to distinguish it from the CH_2 on the AHPA or leucine moieties, while the carbon signal was predictably found at 81 ppm. The A-ring hydrogen and double bond hydrogen were found close to each other as two singlets at 6.22 and 6.29 ppm respectively. Unfortunately, there was overlap between two of the C-ring aromatic hydrogen signals and the five aromatic signals of the AHPA phenyl ring, which obscured the region between 7.35 – 7.15 ppm, although through ^{1}H integration values and HSQC we could justify that these signals were accounted for. A weakly split doublet was found relatively isolated in the aromatic region at 6.98 ppm. Using a combination of HSQC and HMBC spectra we attributed this to the C-ring hydrogen *ortho* to the ester bond, with the *J* value of just 2.1 Hz indicative of only *meta* coupling supporting this belief. Using HSQC and HMBC correlations on the identified aromatic and alkene peaks we could verify all of the associated quaternary aromatic carbons.

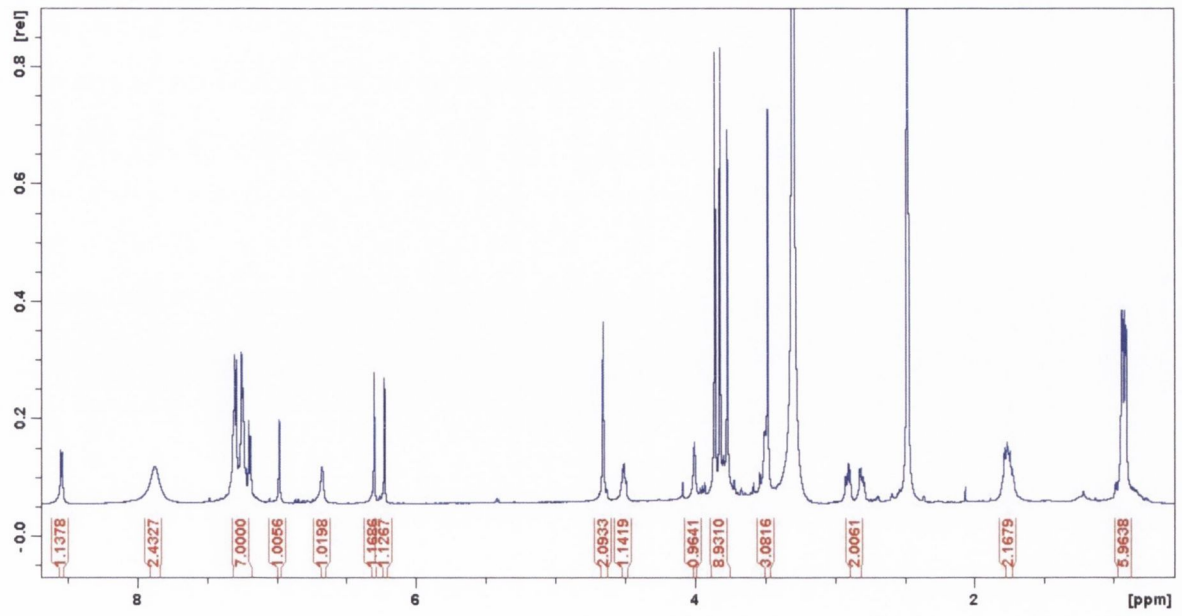


Figure 4.1. Complete ^{1}H spectrum of 4.06 in DMSO-d_6

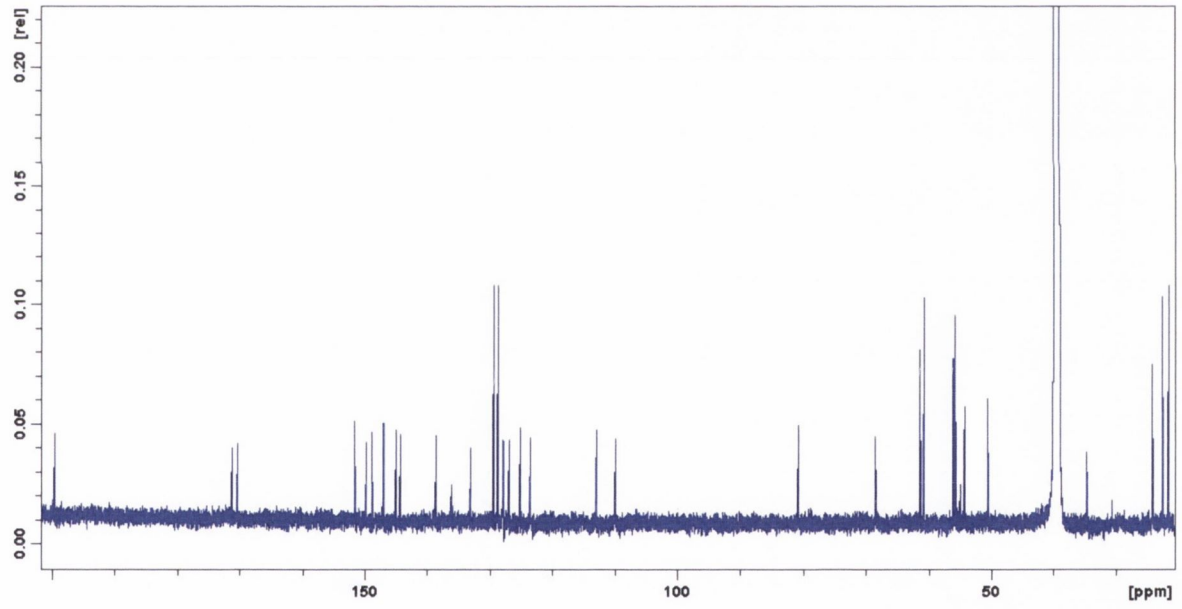


Figure 4.2. Complete ^{13}C spectrum of 4.06 in DMSO-d_6

With most of the benzoxepinone based hydrogen and carbonyl signals identified, attention was focussed on those of the bestatin motif. We were able to obtain an N-H HSQC spectrum (Figure 4.3) that allowed us to confirm the hydrogen signals associated with both the amines at 7.88 and 8.54 ppm. A C-H HSQC could in turn attest the association of the furthest downfield signal (8.54 ppm) with one of the carbonyls at 171 ppm. This confirmed the nature of both the hydrogen and

the 171 ppm carbon signal as those of the amide. Furthermore, the other upfield carbonyl signal at 170 ppm could then be read as the ester carbonyl, and the remaining broad nitrogen signal at 7.88 ppm could be addressed as that of the free amine. With regard to the former, the HMBC spectrum showed its association with a ^{1}H multiplet at 4.51 ppm; the adjacent leucyl CH. HSQC of that peak found its carbon at 50.6 ppm. At the other end of the leucyl aliphatic chain, both methyl groups were quite easily identifiable on the ^{1}H spectrum as a pair of doublets between 0.96 – 0.88 ppm. Using this as a landmark, we could find, first their corresponding carbons by HSQC (21.6, 22.6 ppm), and second their neighbouring CH (24.2 ppm) and CH_2 (39.9 ppm, CH_2 character verified by DEPT 135°) by HMBC and selective TOCSY (Figure 4.4). HSQC correlations on these newly defined carbon peaks gave their related ^{1}H signals.

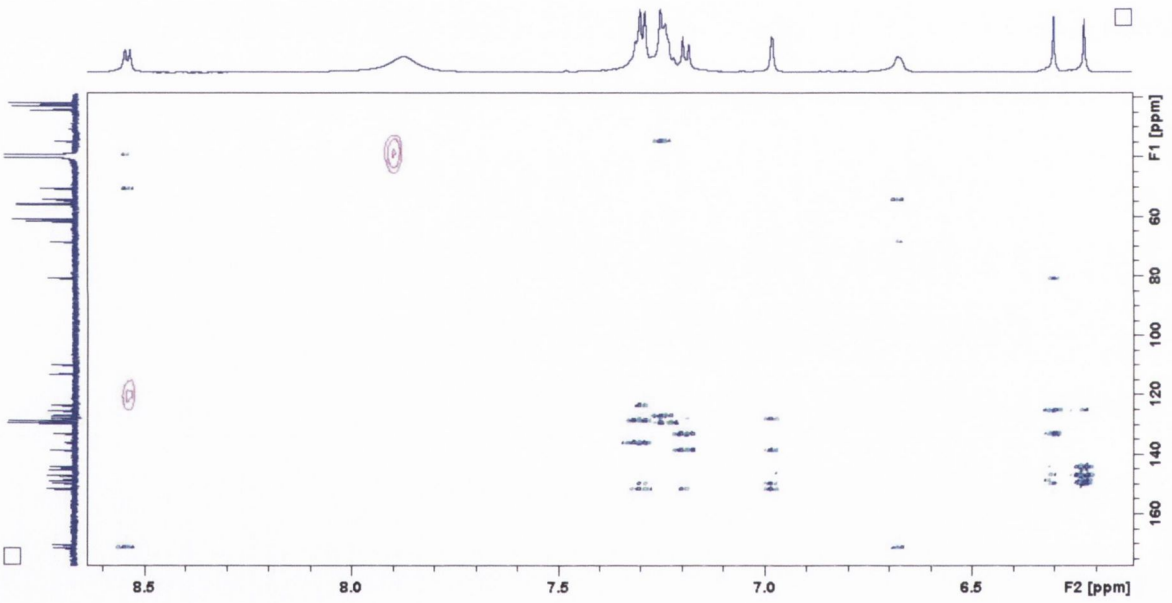


Figure 4.3. N-H COSY spectrum (purple) used to distinguish the downfield 1H signals as NHs. Overlapping HMBC spectrum (blue\green) shows the correlation of the furthest downfield NH and the carbonyl at 171 ppm, marking it as an amide.

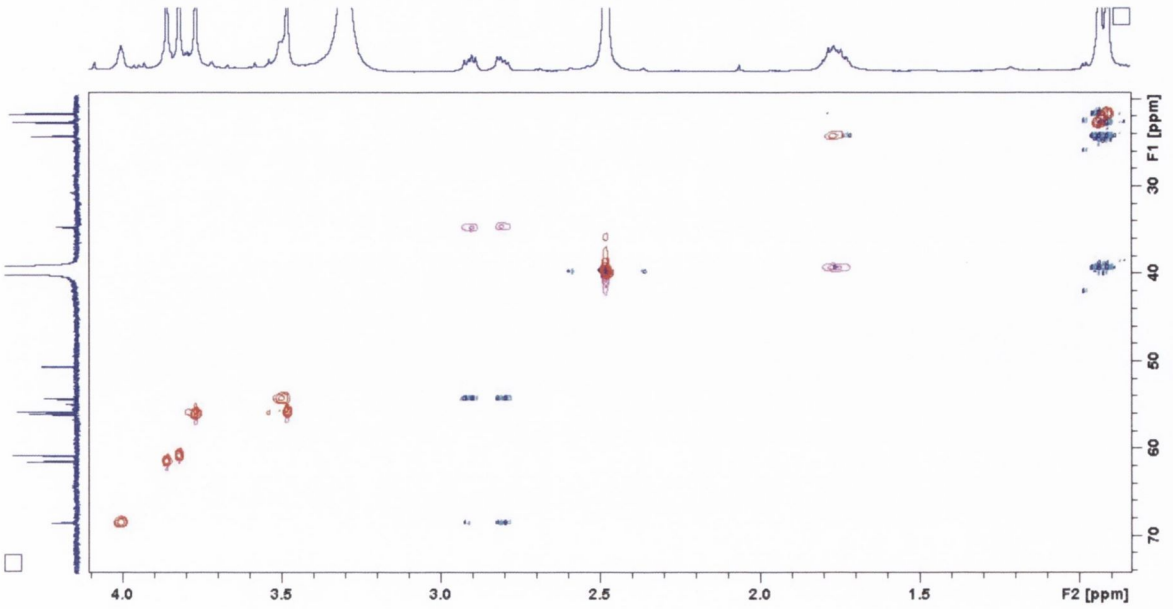


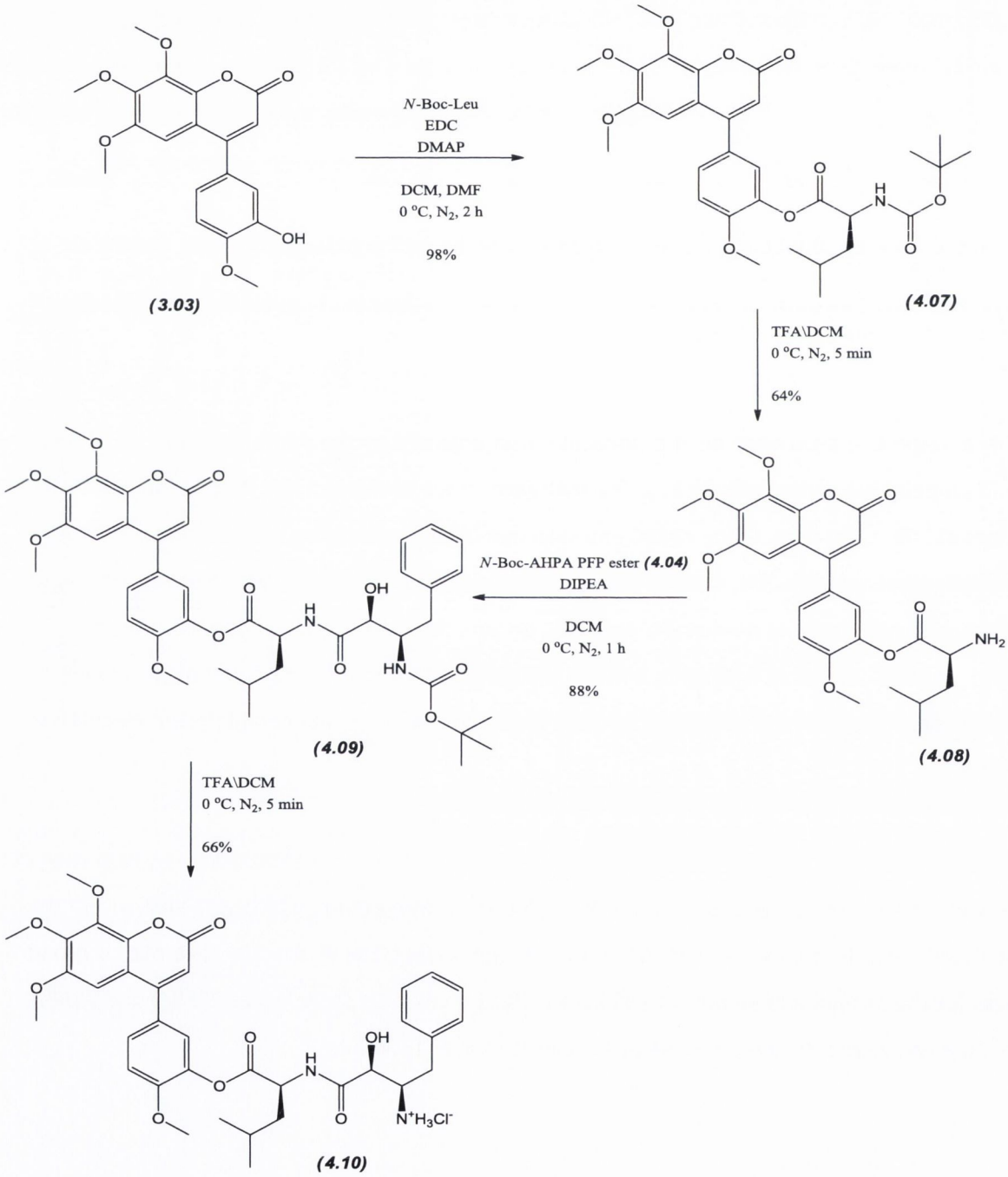
Figure 4.4. From the HMBCs (blue\green) associated with the methyl groups at 0.9 ppm, and the CH_2 of the AHPA at 2.8-2.9 ppm, we could detect nearby leucyl and AHPA aliphatic ^{13}C signals respectively. Moreover, HSQC (red\pink), overlapped here, were used in conjunction to prove the corresponding ^{1}H signals of the newly distinguished groups.

With a single CH_2 group left on the molecule, that adjacent to the AHPA aryl ring, DEPT 135° could pinpoint the carbon effortlessly. The hydrogens were confirmed as a double multiplet with ranges at 2.78 - 2.93 ppm. Using HMBC and selective TOCSY spectra, we were able to see evident correlation between the CH_2 carbon and hydrogen signals respectively, which we could use to attribute its neighbouring quaternary aromatic carbon, the CHN group and the even the further CHOH. A broad singlet at 6.68 ppm, with no correlated carbon on HSQC, could be concluded as the hydrogen signal of the secondary alcohol, and with that we could complete the elucidation of ***4.06***.

Mass spec found an ion at 663.2912 for the protonated free amine, which was well within the calculated value by elemental composition (3.28 ppm away). The IR spectra gave rise to broad peaks for the alcohol and amides at 3394.2 and 3211.6 cm^{-1}; CH stretches at 2955.9 and 2868.6 cm^{-1}; the enone and the amide peaks as a broad stretch at 1674.0 cm^{-1}.

4.1.3 Phenolic ester hybrid based on 4-aryl coumarin 3.03

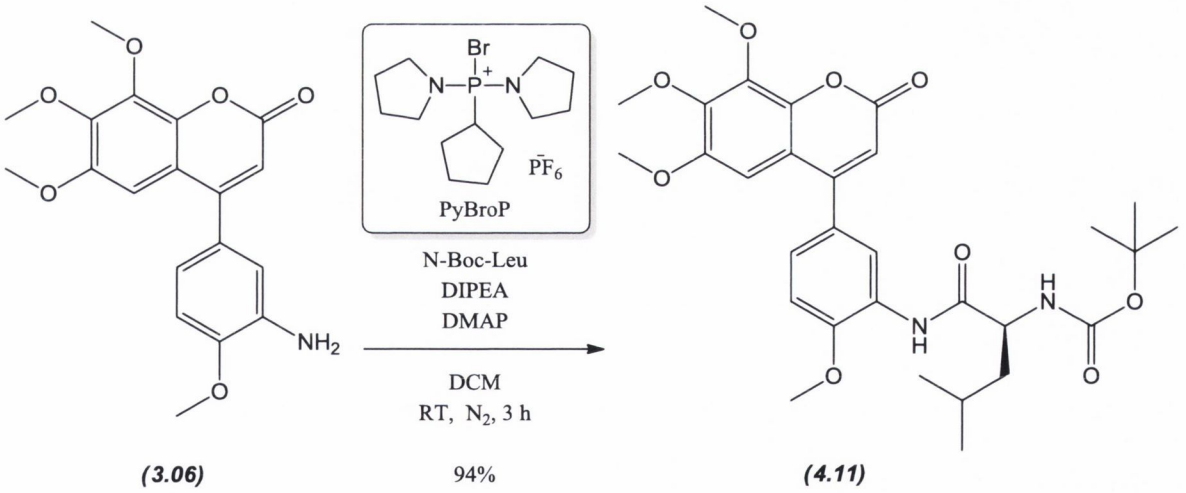
The synthesis of hybrids based on the 4-aryl coumarin ***3.03*** followed an identical synthetic route. Phenol ***3.03*** was coupled to *N*-Boc protected leucine via EDC ***(4.07)***, and then deprotected with TFA to give the free amine ***4.08***. The amine was coupled with the pentafluorophenyl ester of *N*-Boc AHPA ***4.04*** to give phenolic ester ***4.09***. The Boc group was then removed with TFA to give the final hybrid molecule; amine salt ***4.10*** (Scheme 4.8).



Scheme 4.8. Synthesis of 4-aryl coumarin derivative 4.10 of hybrid 4.06

4.2.1 Anilide hybrid based on 4-aryl coumarin 3.06

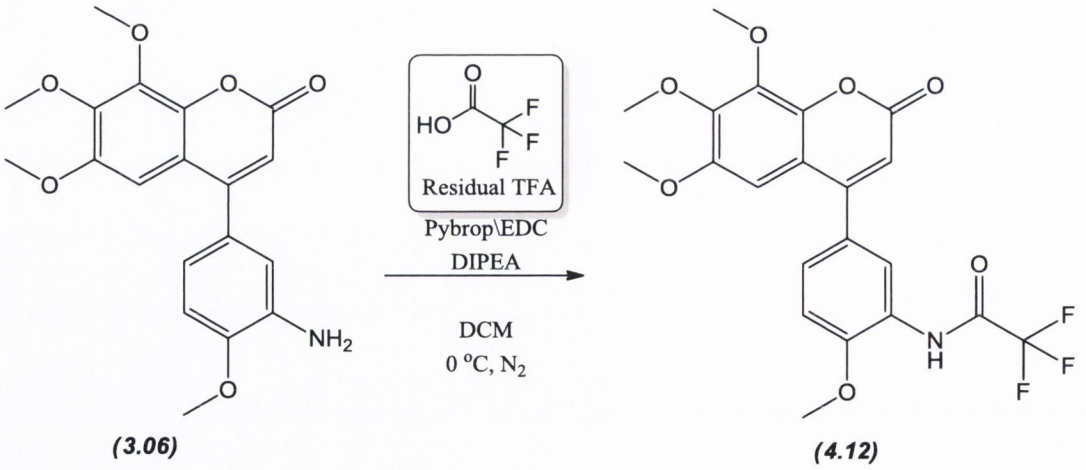
After the successful acquisition of the phenolic ester hybrids ***4.06*** and ***4.10***, we aimed to expand the hybrid series with the synthesis of the aniline analogue of ***4.10***; attaching the bestatin motif on to aniline ***3.06***, which demonstrated potent anti-vascular and anti-angiogenic activity *in vitro* and *ex vivo* (see Chapter 3). The aniline group was coupled to leucine using bromo-*tris*-pyrrolidino phosphonium hexafluorophosphate (PyBroP), a coupling reagent that was designed for use on amine compounds with low nucleophilicity like anilines and *N*-alkylated amines and *N*-methylated amino acids[259]. PyBroP first forms an acyloxyphosphonium salt with the carboxylic acid on leucine. It is believed that the bromine anion can act as a nucleophile on the carbonyl carbon of this new ester to form a new acyl bromide, displacing the phosphine oxide. Either way, aminolysis of either labile acyl species occurs with our aniline ***3.06*** to give amide ***4.11*** without discernible racemisation (Scheme 4.9). An advantage of this method over the EDC method is that its better solubility in DCM means that use of DMF is avoided entirely, as DMF tends to linger through work up if the organic layers are not excessively washed with water or 5% aqueous LiCl solution.



Scheme 4.9. PyBroP method for coupling of aniline 3.06 to N-Boc leucine, to give amide 4.11

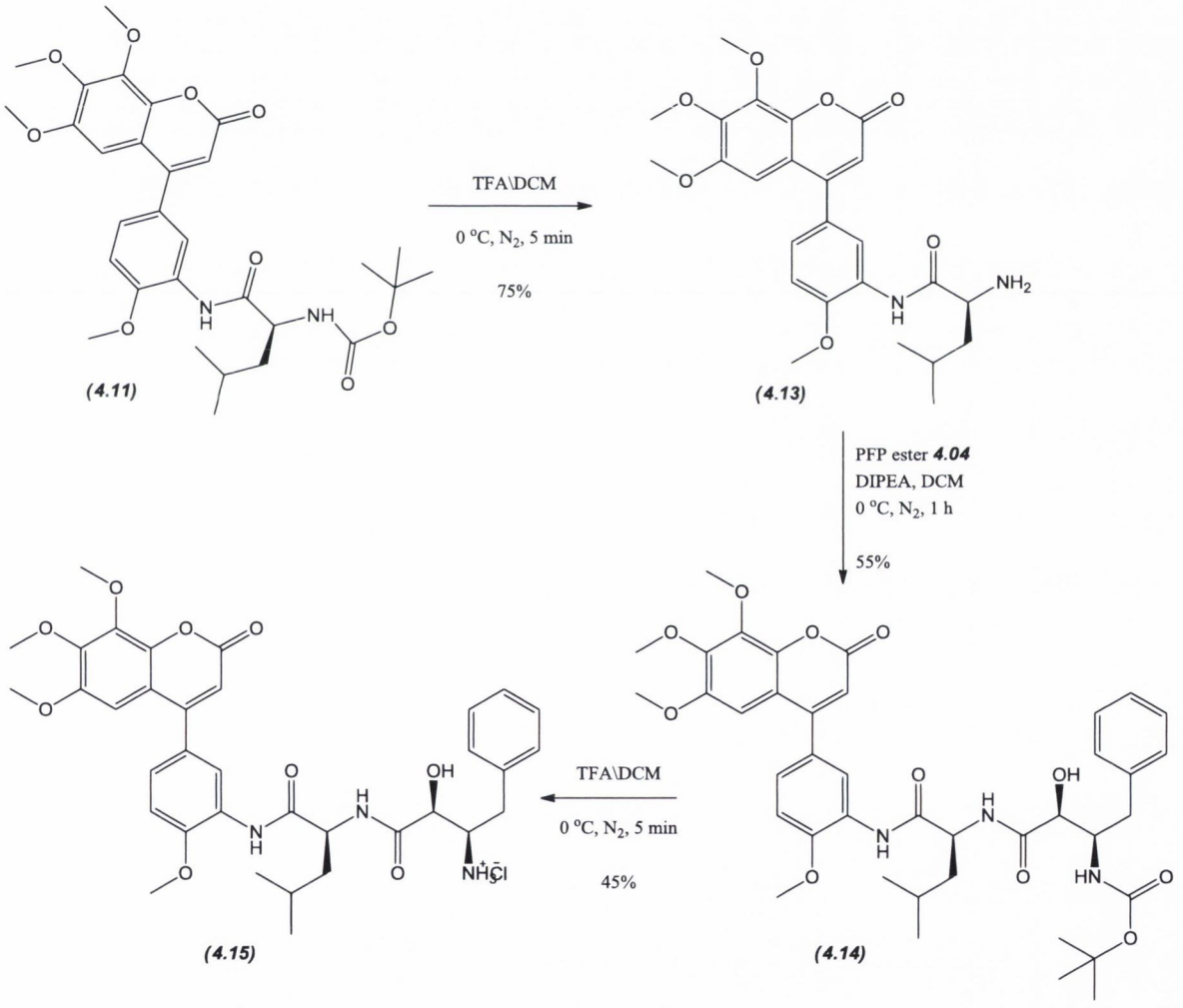
Although anilide ***4.11*** was successfully formed, the initial turnover was modest, with yields commonly found less than 30%. We found it difficult to optimise the yield of the reaction, even when excess PyBroP, DMAP and DIPEA were used. By TLC, we were confused as the starting

aniline ***3.06*** and the product ***4.11*** were the only apparent detectable substances by UV. With limited amounts of anilines ***2.28*** and ***3.06*** available, and after the lengthy synthesis to make them, the situation was not sustainable. It was usual in situations such as this, to reclaim the unreacted starting material and recommence the reaction again. While initially the isolated starting material resembled that of the aniline ***3.06*** as it gave a positive test with ninhydrin stain, a mass spec ion of identical mass, had an identical R_f on TLC and the ^1H NMR appeared very similar to that of the aniline ***3.06***, although increased difficulty in resolubilising the compound in a range of the solvents did cast a degree of doubt. It was not until a ^{19}F NMR spectrum was attained and we found evidence of fluorine (found at -76.2 ppm) that could rationalise the situation. Residual TFA from the deprotection of the Boc-aniline ***3.05*** was being carried through to the coupling steps, most probably as a TFA salt of the aniline from some of the larger-scale reactions. Under the coupling conditions, the TFA moiety was being coupled on to the anilines to form the trifluoroacetamide ***4.12*** leading to the disappointing yields of the expected coupled product ***4.11***. Both the aniline and the trifluoroacetamide had identical R_f values on TLC and perhaps not unexpected, the mass spectrum of the acetamide gave rise to a deceptive fragment ion of identical mass to the parent aniline. In further couplings, we made sure to use saturated $NaHCO_3$ (rather than the 5% solution as used previously) during the work ups of ***2.28*** and ***3.06*** to quench any lingering TFA able to survive the more dilute base wash. This small tactical change was eventually able to afford us much approved yields of up to 94% of ***4.11*** (Scheme 4.9).



Scheme 4.10. Undesirable trifluoroacetamide 4.12 formed during coupling reactions of anilines 3.06

The anilide ***4.11*** was deprotected under the usual conditions, 50% TFA in DCM, again followed by work-up with saturated $NaHCO_3$. Boc protected AHPA was then coupled to the free amine ***4.13*** via the *N*-Boc AHPA PFP ester. The resultant Boc-bestatin hybrid ***4.14*** was deprotected once more to give the final anilide hybrid compound ***4.15*** (Scheme 4.11). The product was confirmed by the presence of similar NMR features to that of the phenolic ester hybrids above; on ^{13}C spectrum the lactone carbonyl was again found at 161 ppm, the anilide carbonyl at 170 ppm, but with a marked shift in the aromatic hydrogen peak ortho to the anilide group downfield at 8.37 ppm relative to the phenolic ester compounds.



Scheme 4.11. Synthesis of aniline hybrid 4.15

4.3.1 Tripeptide based hybrids

Binding between the APN and its substrates involves a tight fit at the active site, with several separate dipole moments and non-covalent interactions between enzyme and the ligand to stabilise the docking process[183, 260]. As outlined in the introduction, the hydroxyl and carbonyl groups of bestatin form the most important bidentate coordination with the positively charged zinc ion, and the positively charged free amine group is coordinated to 2-3 electronegative glutamate residues. The amide N-H forms hydrogen bonding with an adjacent leucine carbonyl, while an oxygen on the carboxylate group does likewise but in reverse with a corresponding glycine amide N-H. Further stabilisation comes from weak van der Waals forces between the phenylalanine side chain lined by glycine, alanine, threonine and two methionines which make up a major hydrophobic cleft (the S_1 site). Similarly, the leucine group is found snugly bound in another hydrophobic pocket consisting of isoleucine, asparagine and alanine (S_1') (Figure 4.5).

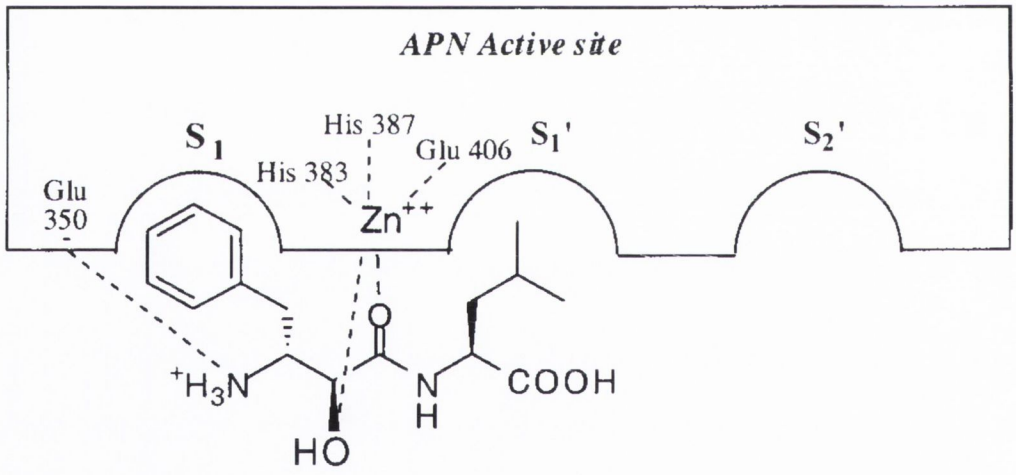


Figure 4.5 Oversimplified schematic[155] of APN binding site and the interactions involved and its hydrophobic pockets S_1, S_1' and S_2'

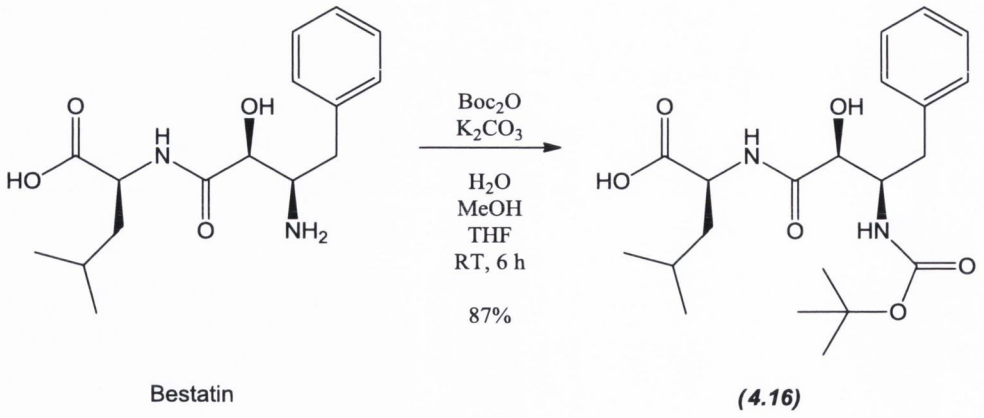
However, there are other hydrophobic clefts on APN not occupied by bestatin (such as S_2') and longer peptide chains are able to fill several simultaneously. Phebestin (AHPA-val-phe tripeptide, IC_{50} (APN) = 0.015 μM) and probestin[180] (AHPA-val-pro-pro, tetrapeptide, IC_{50} (APN) = 0.05 μM) are both longer peptide chains that have higher affinity for APN binding than bestatin (IC_{50} (APN) = 16.9 μM)[261]. The improved affinity for APN is no doubt related to the maximised interactions

between drug and enzyme. The doctoral thesis of E. McCormack[205] from this laboratory investigated the effect of coupling small peptide APN substrates on to the colchicine derivative *N*-deacetylcolchicine, and found inhibitory APN activity that surpassed that of bestatin, whilst he was also able to preserve the tubulin binding activity of colchicine. He was able to conclude that the maximum size of the peptide chain should be no longer than 3 amino acids in length, and that the AHPA moiety was again key for APN activity.

With this in mind we decided to elongate the peptide chain on the 4-aryl coumarin hybrids. It was hypothesised that increasing the chain with a small, neutral hydrophobic amino acid such as another leucine would potentiate the APN binding and inhibitory activity, while also serving to confine the hybrid drug for a longer duration in the dense APN region of the tumour microenvironment. Accordingly, we decided to synthesise tri-peptide conjugates containing an additional leucine or alanine residue. Here, we were also investigating the heightened lipophilic character of the leucine residue over alanine on APN activity.

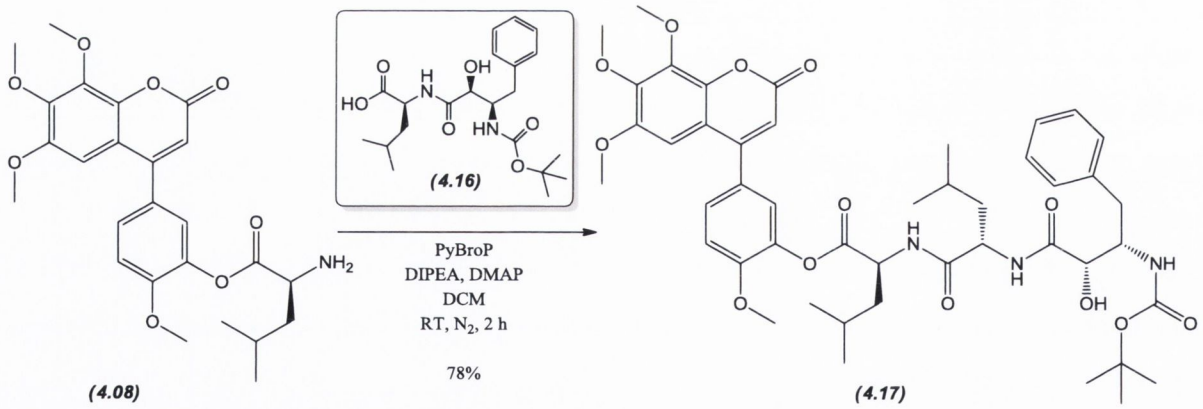
4.3.1 Synthesis of the tripeptide based hybrid molecules of 4-aryl coumarins 3.03 and 3.06

With the same leucine-chromenone compound garnered in the synthesis of dipeptide hybrid ***4.10***, we aimed to couple bestatin on directly, avoiding the less efficient stepwise approach. This was not possible for the dipeptide hybrids themselves due to the poor nucleophilicity of the phenol or aniline functional groups, such that the alcohol group on bestatin successfully competes to cyclise or dimerize. However, with a free amine; a much more powerful nucleophile, this was no longer an issue and direct peptide coupling was feasible. We protected bestatin as an *N*-Boc carbamate in the same fashion as we did with leucine, using the Boc-anhydride under basic conditions (Scheme 4.12).



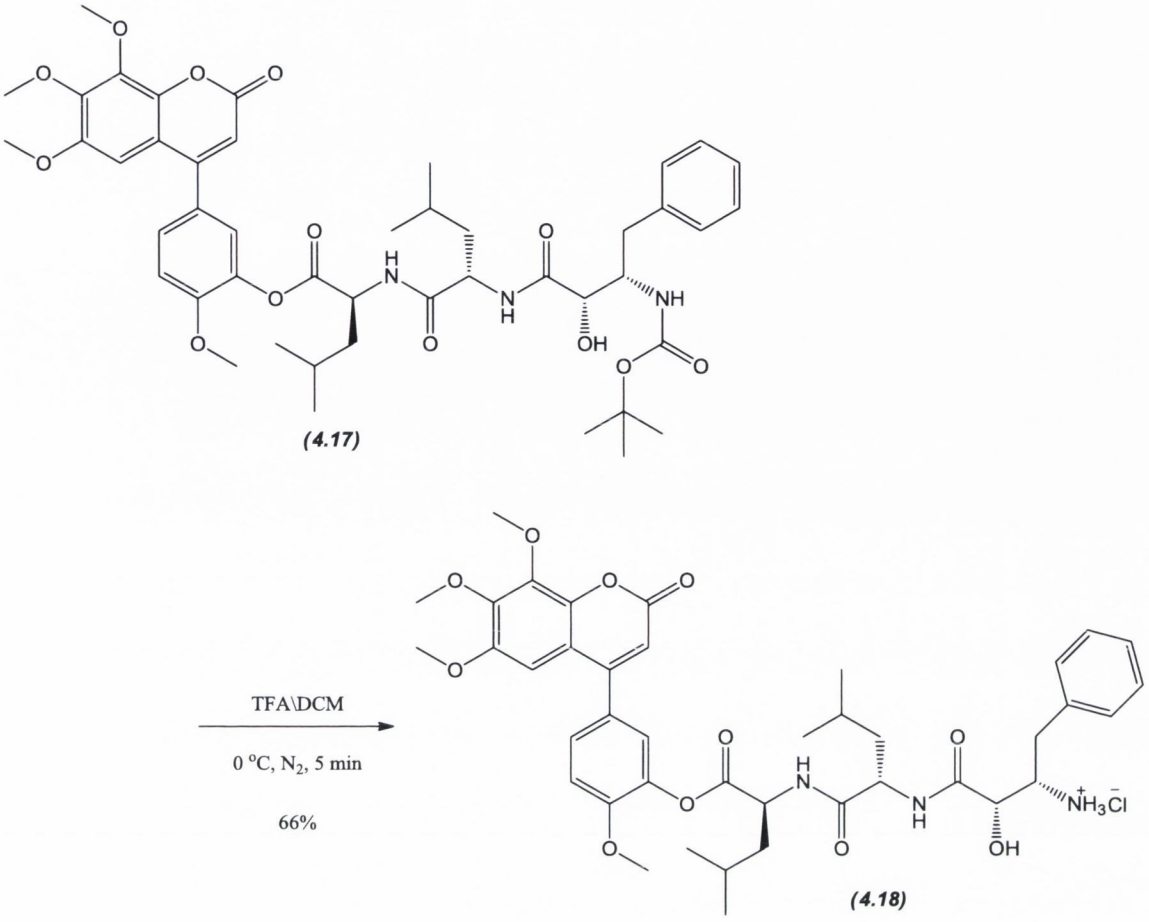
Scheme 4.12. Boc Protection of bestatin under basic conditions

N-Boc bestatin ***(4.16)*** was then coupled directly on to the free amine ***4.08*** either with PyBroP or using the PFP ester approach (Scheme 4.13). PyBroP was the more preferred coupling reagent used to synthesise the tripeptide ***4.17***, as it was less time consuming, and in particular avoided both the use of bothersome DCC reagent entirely and the formation of an extra, unstable PFP ester intermediate.



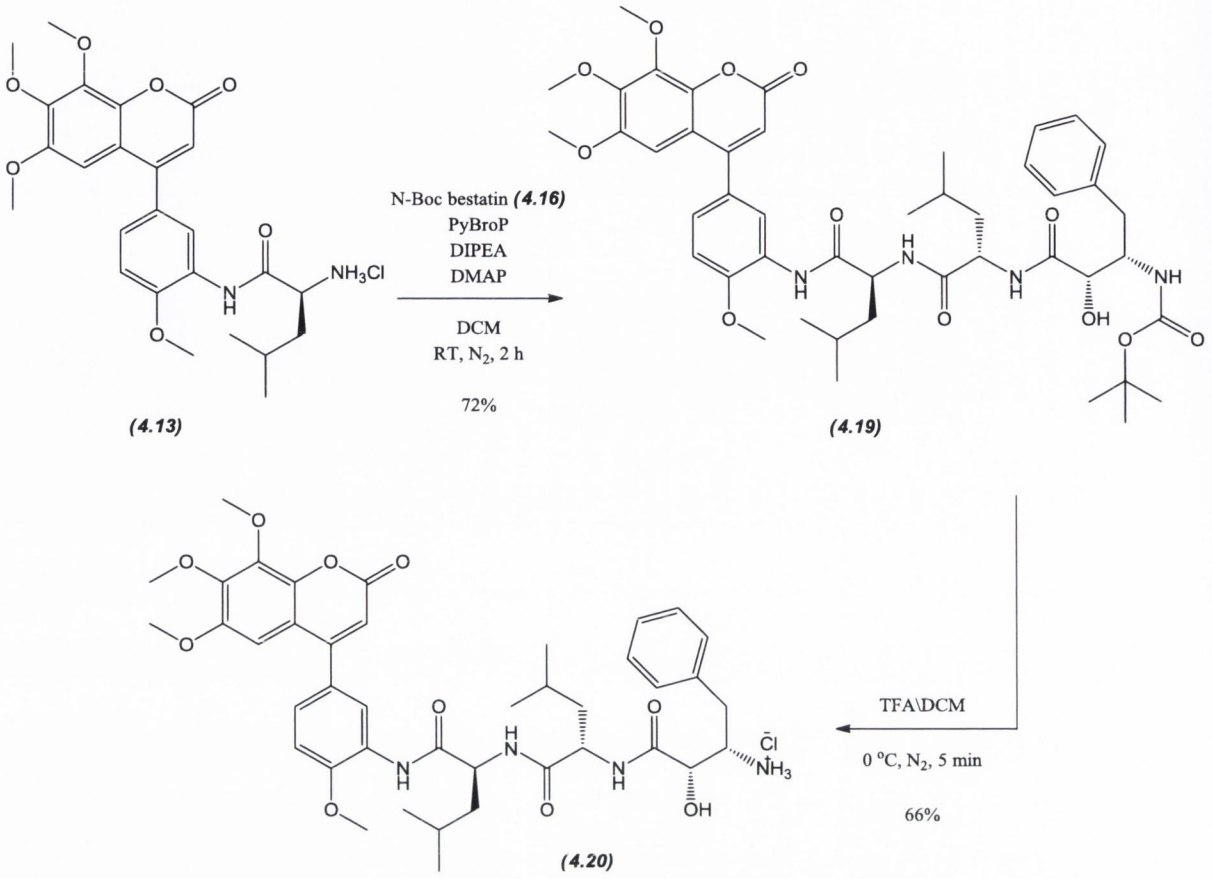
Scheme 4.13. Coupling of *N*-Boc bestatin to amine 4.08

Selective removal of the N-Boc group was achieved by carrying out this step under anhydrous conditions using 50% TFA in DCM to afford the corresponding TFA salt of ***4.17*** (Scheme 4.14).



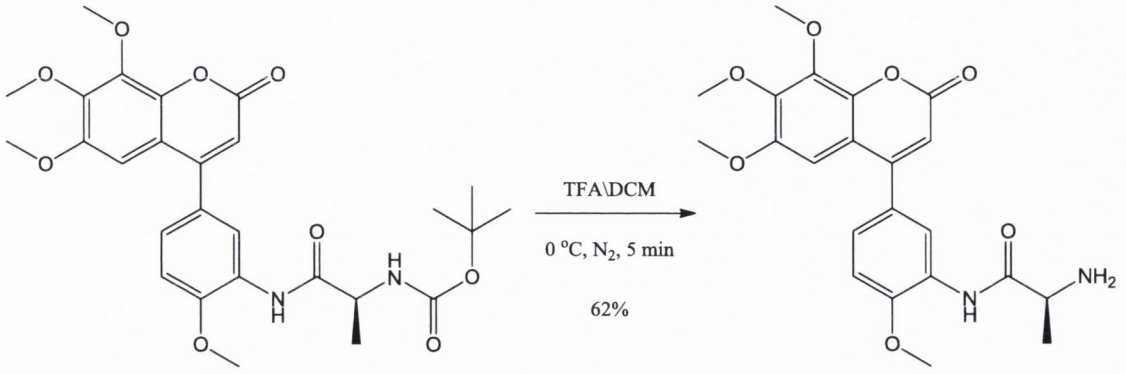
Scheme 4.14. Deprotection to give tripeptide 4.18

The synthesis of the phenolic tripeptide hybrid molecule ***4.18*** was mirrored for the analogous aniline version. Amine ***4.13*** was coupled to N-Boc bestatin ***4.16***, again with PyBroP as the coupling reagent to give carbamate ***4.19***. Subsequent deprotection under the usual 50% TFA in DCM gave the anilide tripeptide ***4.20*** as an amine salt (Scheme 4.15).



Scheme 4.15. Synthesis of anilide tripeptide hybrid molecule

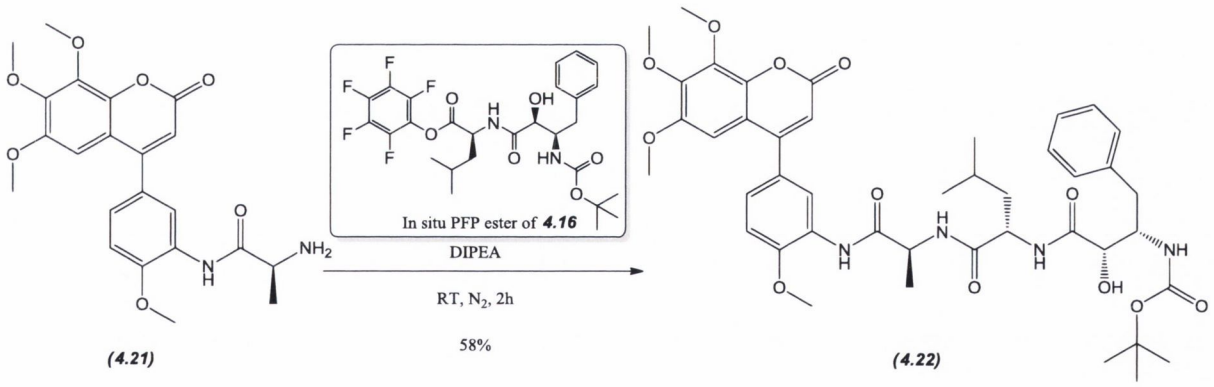
As we had perfected a very efficient method for the synthesis of aniline ***3.06***, a substantial quantity was donated to E. C. Breen for use in prodrug studies. Breen had coupled a variety of different amino acids directly on to the aniline to investigate the activity of these prodrug derivatives in comparison to some of her own, as a substrate for both APN and a related enzyme Aminopeptidase A (APA, also known as glutamyl aminopeptidase). APA is also overexpressed on the vasculature of human tumours in an active state[262]. Inhibitors of APA have demonstrated anti-angiogenic activity, and hence APA has potential as a therapeutic target. In the case of Breen's prodrug studies, taking advantage of the high expression levels of APA and APN on tumour vasculature, she coupled a series of amino acids including glutamic acid and alanine onto ***3.06***. In return, she kindly donated the latter, intermediate ***3.06-Ala***, which was used as the starting point for the synthesis of anilide tripeptide hybrid ***4.23***. Alanine, with its small, neutral lipophilic side chain, better fit the criteria for a tripeptide hybrid substrate for APN than the larger, polar side chains on amino acids like glutamic acid for example.



N-Boc-***(3.06)***-Ala ***(4.21)***

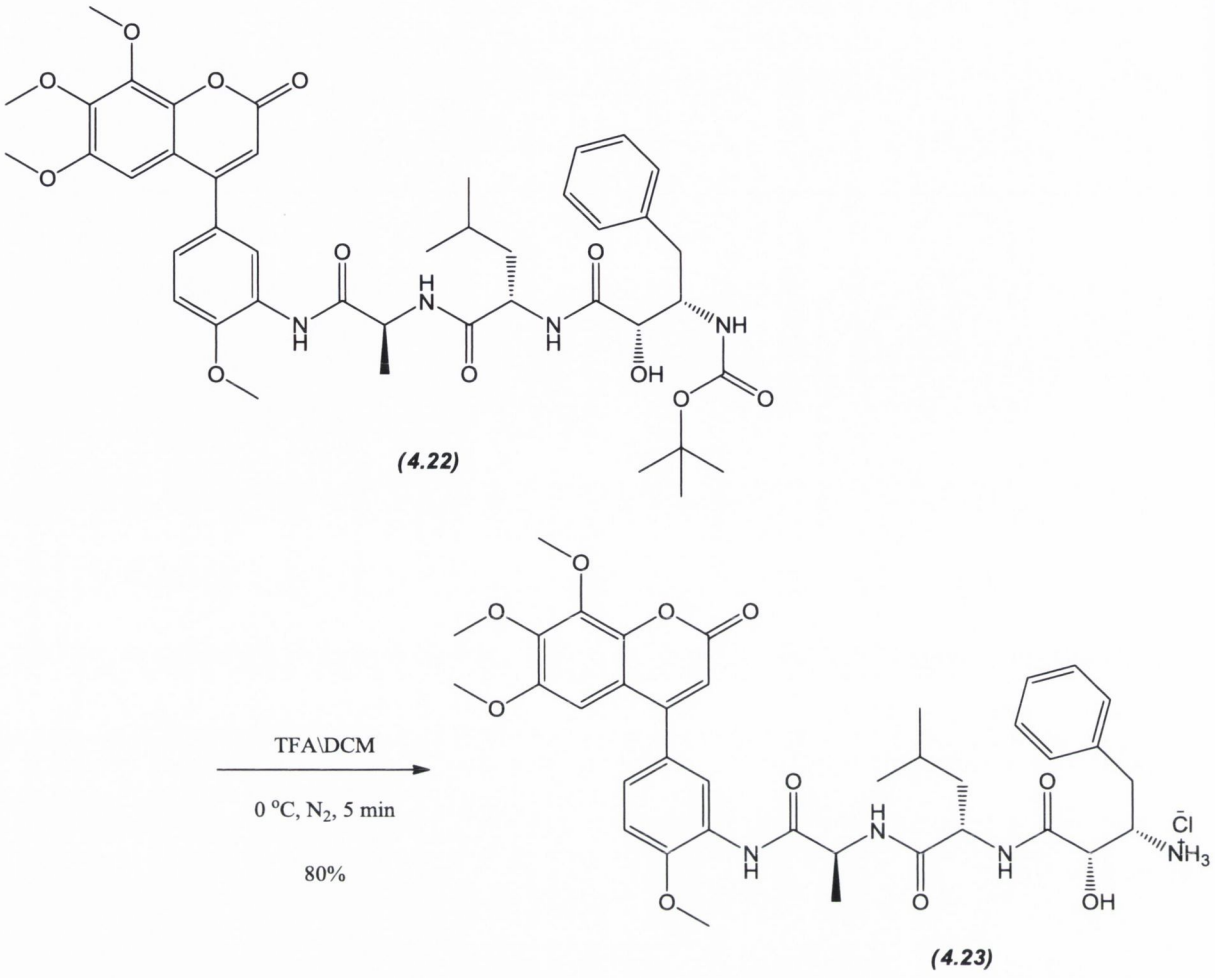
Scheme 4.16. Deprotection of the Boc protected alanine prodrug from Breen with TFA in anhydrous DCM

The alanine intermediate was first *N*-Boc deprotected to the free amine ***4.21*** with 50% TFA in anhydrous DCM, treated with saturated $NaHCO_3$ (Scheme 4.16). Coupling to bestatin was straightforward with either PyBroP or by adding the amine to the PFP ester of bestatin, generated in situ, to produce the tripeptide hybrid ***4.22*** (Scheme 4.17). Deprotection of the Boc group gave the amine salt ***4.23*** (Scheme 4.18).



(4.21) ***(4.22)***

Scheme 4.17. Coupling of the alanine prodrug 4.21 to N-Boc bestatin 4.16



(4.22)

(4.23)

Scheme 4.18. Final step for alanine anilide tripeptide hybrid molecule 4.23

4.4.1 The Designed Multiple Ligand approach

Another concept we developed was the construction of a Designed Multiple Ligand (DML), a drug that exhibits activity at more than one biological target[263]. Traditionally, development of medicinal compounds has long focussed on a 'one drug, one target, one disease' theme; the magic bullet. There is logic in this approach from the perspective that selectivity for a particular enzyme or receptor would theoretically avoid the adverse effects that most often undermine the therapeutic effect of a new lead compound. It also affords a degree of patency with regard to the response being reflected by the actions of a single biochemical pathway. That said, diseases like cancer are unfortunately not so simplistic; cancer by its nature is far reaching with a heavy corruptive influence on a plethora of biological signalling processes and cascades, hence the reliance on combination chemotherapy treatments to tackle several of these processes at once.

In recent years, research has begun to embrace the idea of the DML, now regarding the ability of a drug to modulate different targets to be a valuable asset.

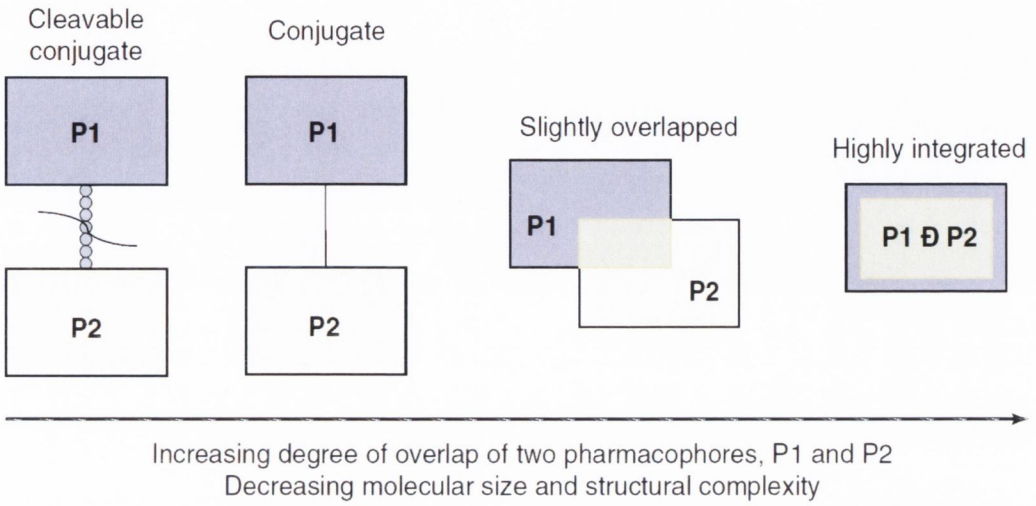
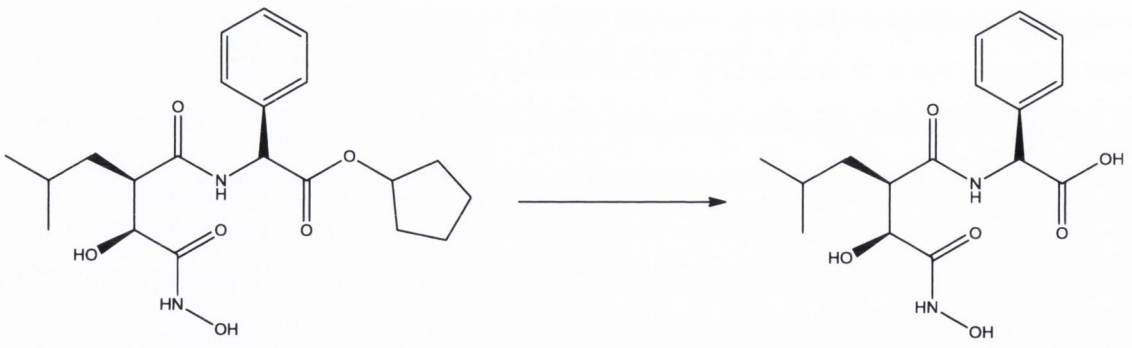


Figure 4.6. Schematic representation of pharmacophore position on a cleavable hybrid molecule (left), a covalent conjugate molecule (non cleavable, 2nd from left), and two DMLs (right) with differing degrees of structural overlap[264]

The DML idea is distinct from that of the hybrid molecule. Hybrid molecules are essentially two separate agents conjugated together, whereas the DML incorporates two pharmacophores on to a single molecule, but with considerable overlap between the two structurally. A DML cannot be lysed into separate active agents as is possible with a hybrid, but its design has other pertinent advantages. DMLs are more condensed structurally, which helps keep the molecular weight low, while hybrid molecules inevitably create bulk. Furthermore, the smaller size and multi-target functional groups mean that DML compounds are more likely to comply with the Lipinski rule of five criteria[265].

Our DML would focus on the same targets as the hybrid molecules; tubulin and APN, but with different presentation. While it was feasible to retain the ABC ring structure prominent in our TBA components, complete with the C-ring functionality imperative to realise the utmost of its potential, incorporating bestatin or an analogous peptide ligand for APN activity was not practical. We instead took a different approach. As mentioned previously, APN is a matrix metalloproteinase (MMP), with a critical dependency on zinc for activity. Inhibitors of MMPs are

thus often based around interference with the zinc moiety in some way. Of the many of zinc targeted MMP inhibitors synthesised, over 90% of them involve the same functional group; the hydroxamic acid[266]. Hydroxamic acids chelate to zinc in bidentate fashion, along with three protein ligands, to form part of a 5 membered system around the metal ion in a thermodynamically ideal trigonal bipyramidal complex[267]; the most favoured for zinc by ligand field theory[268]. This manner of binding to zinc is much stronger than that exhibited by the corresponding carboxylic acid, or even by the hydroxy-amido groups on bestatin. We reasoned we could realistically introduce a hydroxamic group on to the B-ring ketone of the benzoxepine series of compounds, and in doing so create a DML that possessed both an APN binding component (hydroxamic acid) and tubulin binding component (methoxylated diaryl alkene), without the bulk of a hybrid molecule. Hydroxamic acids have been successful as APN inhibitors before[269]. Tosedostat (CHR2797) is a hydroxamic acid containing ester prodrug of CHR79888, which upon ester hydrolysis to give the free carboxylic acid (Figure 4.7) has proven to be over 300 times more potent than bestatin at suppressing tumour cell proliferation *in vitro*, by way of a poorly understood mechanism of amino acid depravation by preventing protein recycling[270]. Orally bioavailable, tosedostat has reached Phase II clinical trials for acute myeloid leukaemia in combination with paclitaxel and has been very well tolerated thus far[271].



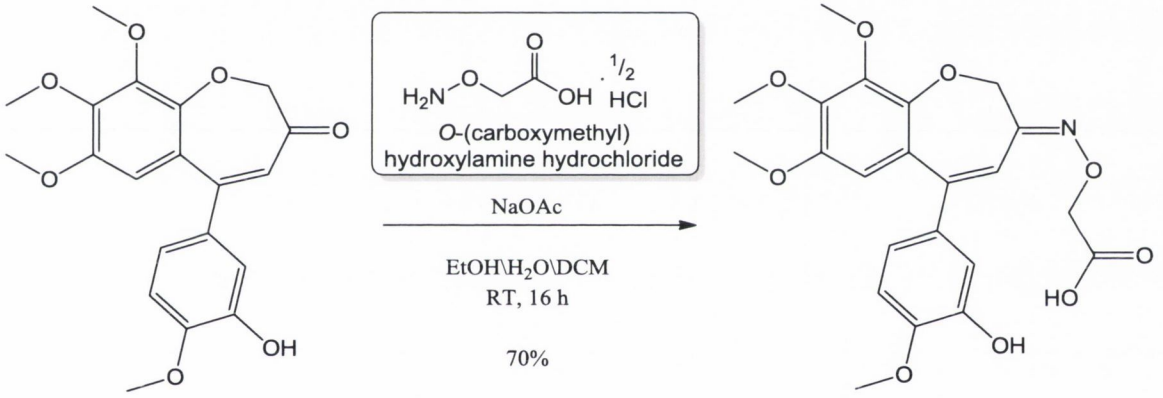
Tosedostat (CHR2797) (CHR79888)

Figure 4.7. Hydroxamic acid based APN inhibitor tosedostat and the release of its pharmacologically active metabolite CHR79888, which retains the hydroxamic acid group essential for its activity.

4.4.2 Synthesis of hydroxamic acid DMLs

We began the synthesis of a series of hydroxamic acid based DML compounds on the archetypical phenol benzoxepinone lead compound ***2.17***. We were able to successfully introduce

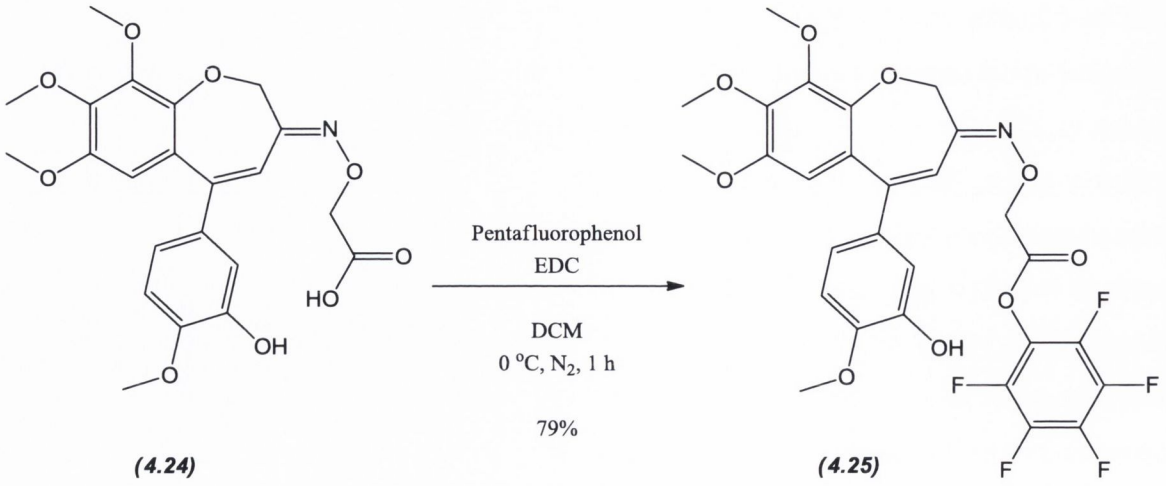
oxime functionality onto the B-ring ketone position, without the need to first reduce the ketone to the alcohol in a separate reaction to facilitate its removal; a scenario that would have brought with it a considerable risk of elimination of a significant portion of a valuable compound to the ineffectual diene. This transformation to the oxime ***4.24*** was achieved using the reagent *O*-(carboxymethyl)hydroxylamine hemihydrochloride as a nucleophile, with sodium acetate as a base in a water\ethanol solution (Scheme 4.19). The reaction was a little slow, usually left overnight, but reliable and quite high yielding, even at room temperature. Importantly, the oxime formation was possible with the phenol left unprotected. One drawback was that, although expected, the oxime product came in the form of a mix of *syn* and *anti* isomers, which added considerable complexity to the assignment of the hydrogen and carbon resonances, complicating their structural elucidation.



(2.17) ***(4.24)***

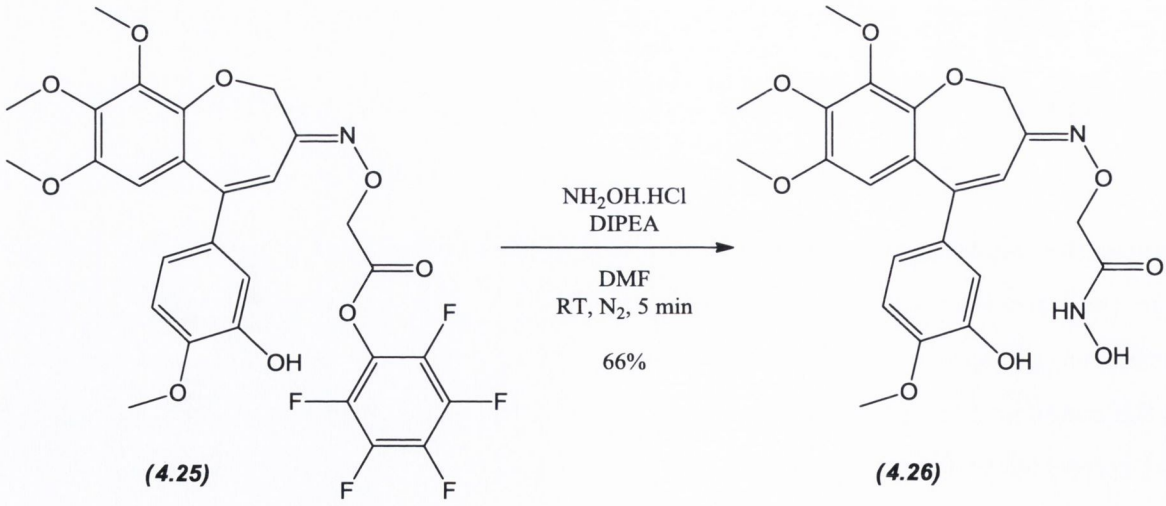
Scheme 4.19. Oxime formation of ketone 2.17 to give oxime carboxylic acid 4.24

To pave the way for hydroxamic acid functionality, we had to form a more labile leaving group than the carboxylic acid OH. The previous reliability of the PFP ester formation and its subsequent displacement to make way for another nucleophile from our hybrid syntheses gave us the confidence to use this method again to form the hydroxamic acid. PFP ester formation was accomplished for ***4.25*** with pentafluorophenol, and this time we used EDC as a coupling reagent (Scheme 4.20). This reaction was again very reproducible, and we saw no incidence of nucleophilic attack or displacement from the free C-ring phenol to form dimers or intramolecular cyclised products.



Scheme 4.20. PFP ester formation 4.25 from carboxylic acid 4.26

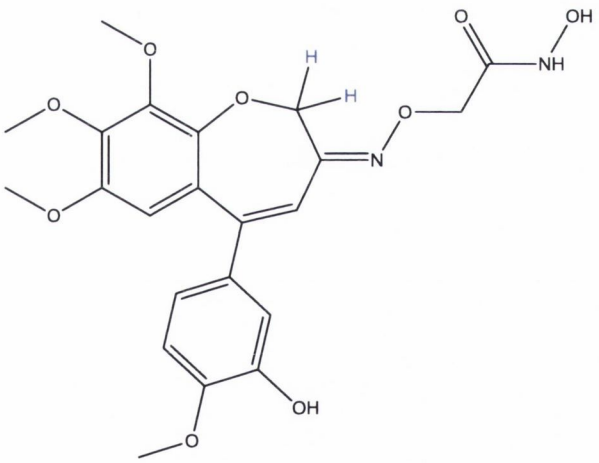
With the PFP ester in place, we had a good leaving group present, and nucleophilic acyl substitution was then possible. Using hydroxylamine, and with DIPEA as a base to augment its nucleophilicity, we were able to generate the hydroxamic acid ***4.26*** in minutes at room temperature (Scheme 4.21). The only issue with this reaction was the use of DMF, which was difficult to remove at this late stage of the synthesis. Nevertheless, this was manageable with 5% aq. LiCl solution and multiple water washings of the organic layers during work up.



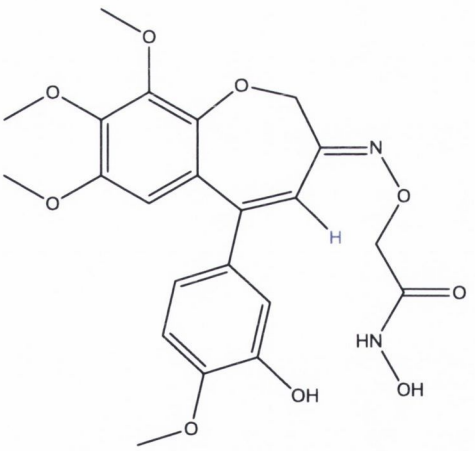
Scheme 4.21. Formation of the phenolic version of the hydroxamic acid DML 4.26

4.4.3 Structural Elucidation of hydroxamic acid 4.26

As alluded to previously, the presence of *syn* and *anti* geometric stereoisomers around the oxime double bond made elucidation of the NMR spectra more difficult. According to the Cahn–Ingold–Prelog rules, the side of our oxime that possesses the phenolic oxygen bonded to the A-ring is given priority over the alkene side, as oxygen has higher atomic number than carbon[272]. Therefore the nomenclature of the isomers is designated based on the orientation of the oxime N-O bond to the highest priority side; the isomer with both the oxime N-O and the phenolic A-ring oxygen together is the *syn* (*cis*, or *Z*), and that with the highest priority group and the N-O bond on opposite faces of the molecule is denoted the *anti* (*trans*, or *E*) isomer. Here we had a situation whereby some of the hydrogen signals on our ^{1}H NMR had split or doubled, but some had remained the same or overlapped. This was to be expected; obviously in the case of the *anti* stereoisomer, the proximity through space of the hydroxamic group to the C-ring and alkene group would cause chemical inequivalence relative to the *syn* isomer, where these groups were distant from each other.



syn - (*Z*) - stereoisomer of ***4.26***



anti - (*E*) - stereoisomer of ***4.26***

Figure 4.8. Syn and anti stereoisomers around the oxime double bond

A noticeable difference in the signal intensities of both the ^{1}H and ^{13}C peaks allowed us to distinguish between the two compounds present collectively in each spectrum (Figures 4.9 and

4.10). For example, the sole aromatic hydrogen on the A-ring was present as two peaks at around 6.3 ppm. Integration of the smaller of these two peaks, that of the minor isomer, demonstrated a 1 : 1.4 ratio of the minor to major ratio. This ratio is subjective based on what pair combination is chosen, but the general consensus is roughly that of a 1 : 1.35 – 1.7 ratio of minor to major. Comparison of ^{13}C signals showed an even more stark contrast in peak intensity although this was considered a less reliable judge of isomer ratio.

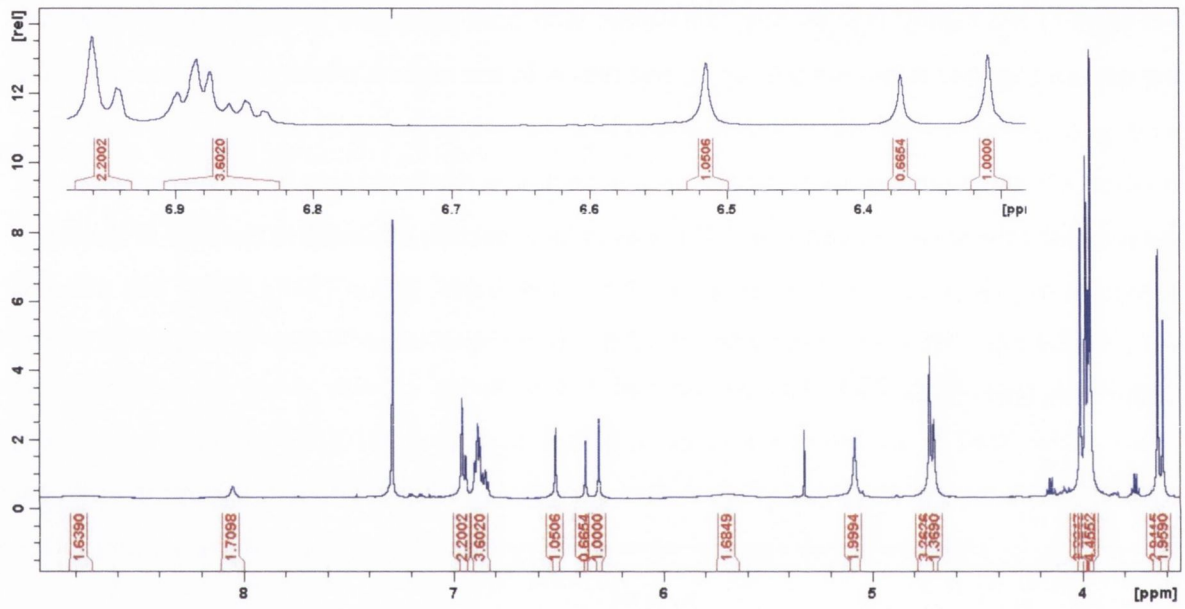


Figure 4.9. ^{1}H spectrum of 4.26, containing both major and minor isomers, which can be differentiated by the intensity of their peaks.

The methoxy groups resonate similar to those seen before; a major-minor pair was found 3.6 ppm, with three more methoxy signals clustered closely together around 3.9-4.0 ppm, although some peak overlap was observed here. On the ^{13}C spectrum the methoxy peaks are simply seen doubled up, with relatively little shift change between the isomers. More difficult were the two methylene moieties on the molecule; both of these had an ether oxygen and a carbonyl carbon on either side making distinction between the two ambiguous. However, with the aid of the HSQC spectrum, both methylene pairs can still be accounted for; a minor peak at 4.71 ppm, an overlapping major and minor peak at 4.73 ppm and a quite broad major peak at 5.1 ppm. These proton signals correlate to four ^{13}C peaks between 71-74 ppm.

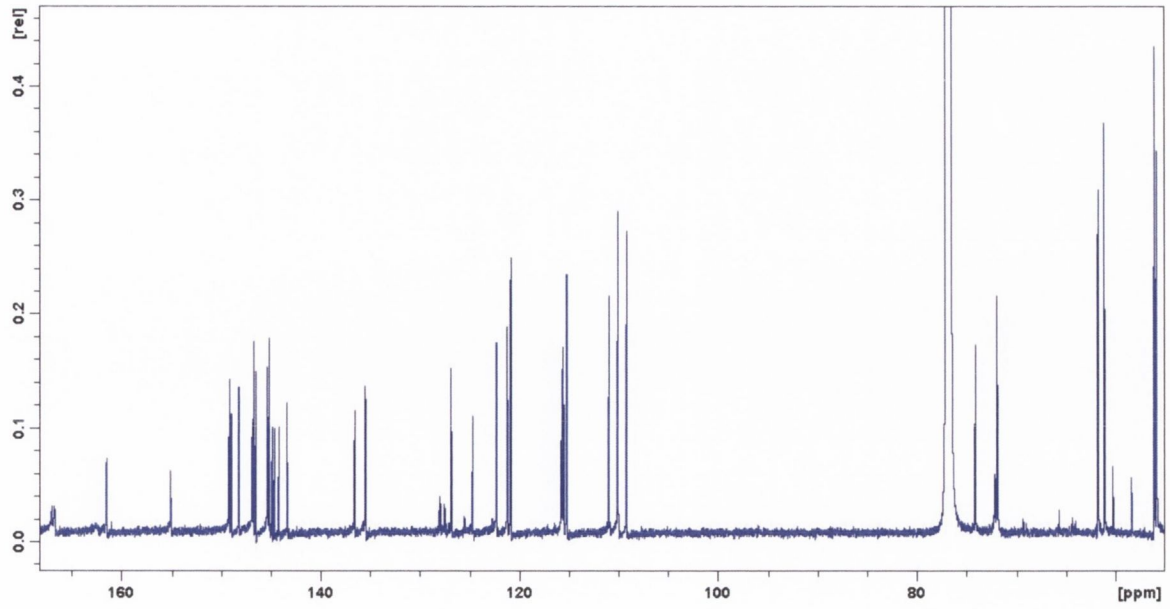


Figure 4.10. ^{13}C spectrum of hydroxamic acid 4.26. Many of the carbon signals are doubled up throughout the spectrum

Besides the A-ring hydrogen signals discussed already, the remaining aromatic region appeared complex. To start with, the major alkene hydrogen signal at 6.5 ppm (122 ppm in ^{13}C) was not accompanied by a nearby minor peak; this minor peak had shifted downfield, into the multiplets between 6.6-7.0 ppm. Integration of this region in the ^{1}H spectrum totalled 5.8 relative to 1.0 the A-ring signal was assigned. This accounted for the remaining 7 aromatic and alkene peaks (3 major, 4 minor), bearing in mind the value of the minor peaks was approximated at 0.67 ($(3 \times 1.0) + (4 \times 0.67) = 5.68$). From the obvious size difference of signals in the ^{13}C spectrum, the HSQC spectrum (Figure 4.11) was able to assign each of individual remaining major and minor aromatic peaks in this region, with the minor alkene signal found to resonate at 6.96 ppm and 116 ppm for ^{1}H and ^{13}C respectively. The carbon signals for the aromatics, both with hydrogens and without hydrogens were as expected; chiefly between 109-135 ppm for ArCHs, and 124-150 ppm for ArCs. The remaining alkene carbon overlapped for both isomers at 155 ppm, as did the oxime carbon at 162 ppm. The hydroxamic acid carbonyl was found doubled up at 167 ppm on the ^{13}C spectrum, with the broad NH and OH signals at 8.1 and 8.8 ppm respectively on the 1H spectrum. The phenolic hydrogen was observed as a broad singlet further upfield near its usual position at 5.7 ppm.

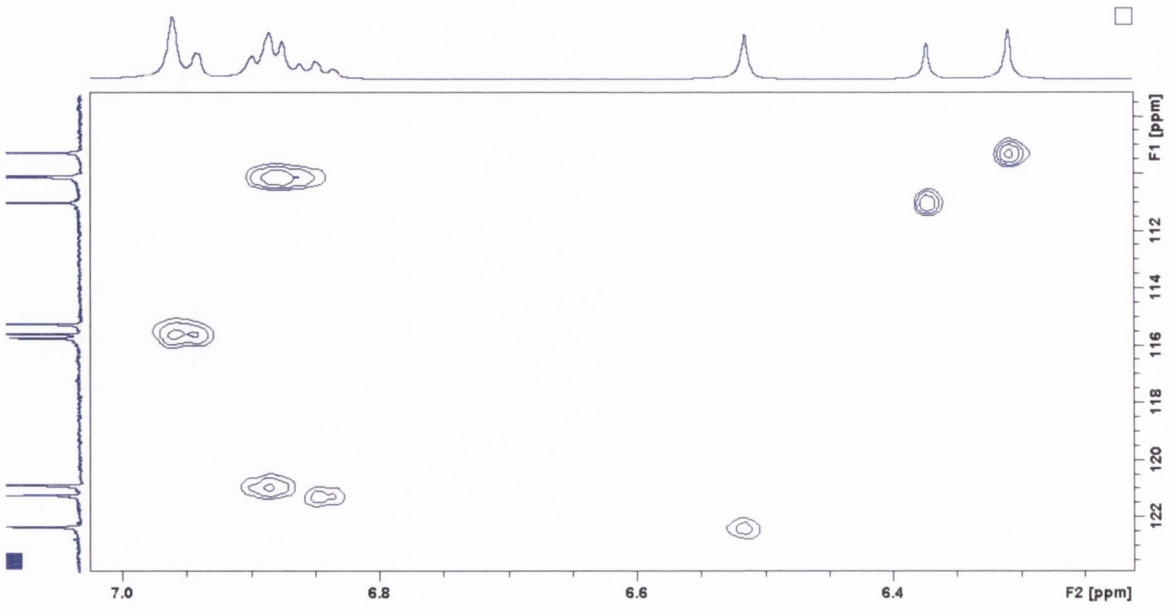
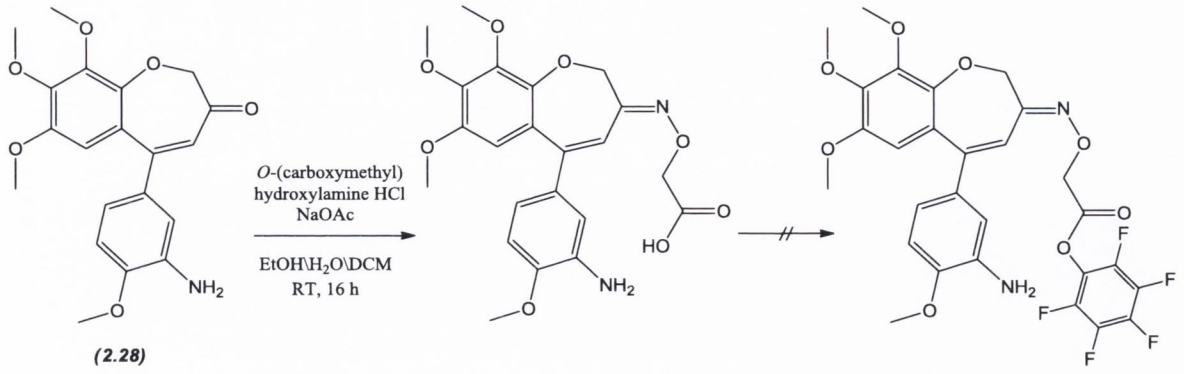


Figure 4.11. HSQC of hydroxamic acid 4.26

From the information derived above, it can be postulated that the major isomer is the *syn* isomer. The most convincing rationale being that in the case of the minor isomer, suspected *anti* isomer, the lone pair electrons on the ether oxygen is proximate to the alkene hydrogen, creating a weak dipole that deshields its nuclei through space relative to the *syn* isomer. Conversely, for the *syn* isomer, it can be assumed that the major methylene signal at 5.1 is that on the B-ring; their nuclei deshielded in a similar way.

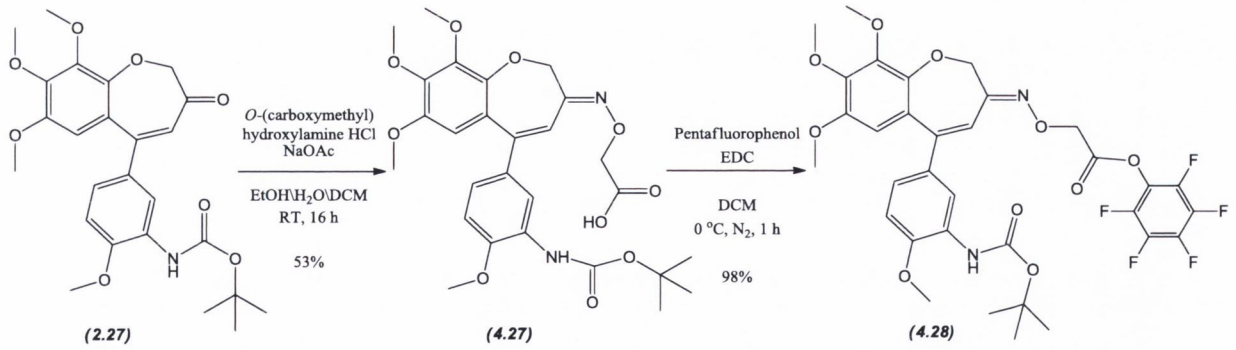
4.4.4 Aniline derivative of 4.26

The next aim of the work described in this chapter was to procure the aniline hydroxamic acid derivative ***4.26***. As we did with the synthesis of the intermediate ***4.24***, we started with the C-ring unprotected, using aniline lead compound ***2.28***. Although we were able to introduce the oxime to this ketone species without any problems, the subsequent PFP esterification step was not so straightforward, and several unidentified by-products predominated over the desired PFP ester (Scheme 4.22) as indicated following TLC analysis of the reaction mixture most likely because of interference of the weakly nucleophilic aniline with the PFP ester. This eventuality rendered ***2.28*** unsuitable as a starting point in this synthetic course, so instead it was necessary to use the precursor, Boc carbamate ***2.27***.

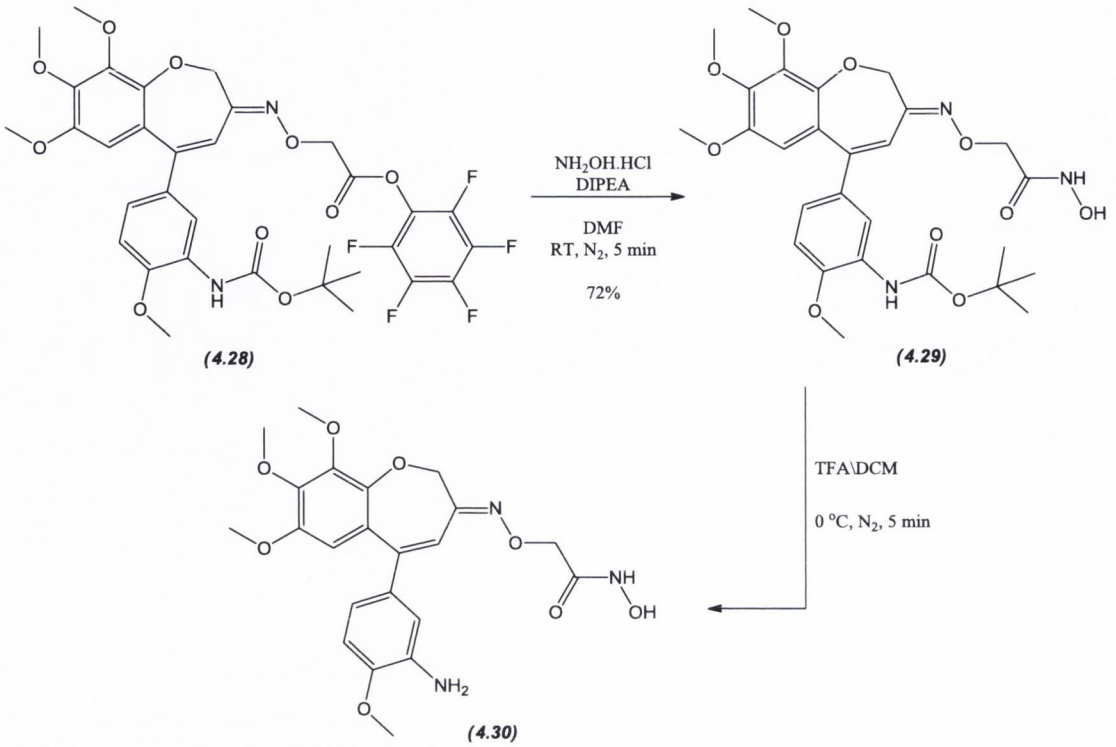


Scheme 4.22. Ultimately unsuccessful attempted synthesis of PFP ester, using unprotected aniline starting material

The oxime was introduced to the ketone of ***2.27*** in the same manner as per oxime ***4.24***. This time conversion of the carboxylic acid ***4.27*** to the PFP ester ***4.28*** was not problematic (Scheme 4.23). The PFP ester was quickly converted to hydroxamic acid ***4.29*** using the method described for the synthesis of 4.26. Finally, *N*-Boc deprotection with 50% TFA in DCM afforded the aniline ***4.30*** (Scheme 4.24).



Scheme 4.23 Oxime and later PFP ester synthesis on ketone 2.27



Scheme 4.24. Final steps in the synthesis of aniline hydroxamic acid 4.30

4.5.1 Controlled release of DML 4.30

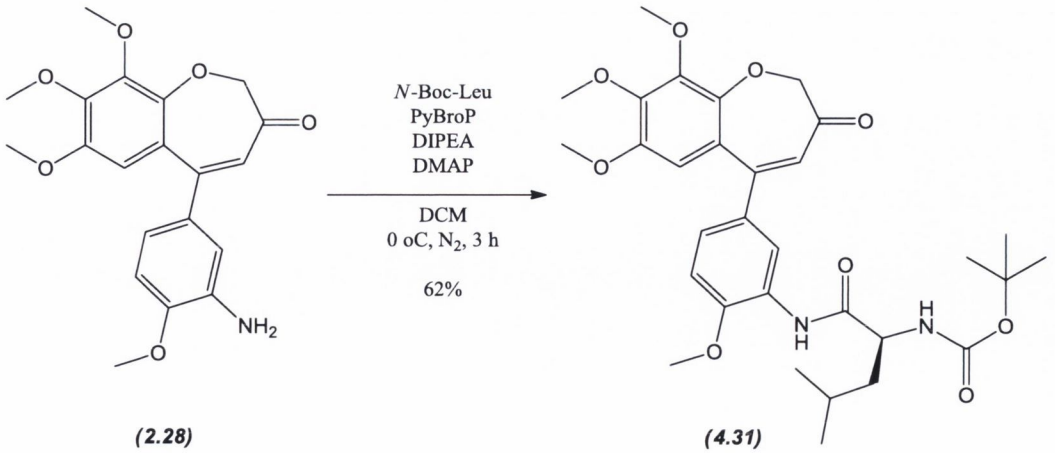
Given the promise of the DML design, we considered the option of their controlled release *in vivo*. Bearing in mind the overexpression of APN, APA and other such peptidase enzymes in the tumour microenvironment, we hypothesised that by having an amino acid substrate coupled on to the C-ring, we could effectively present a DML whereby the tubulin binding component is presented in prodrug form. The hypothesis underlying this concept is based on the upregulated expression of APN on tumour vasculature undergoing angiogenesis and on certain tumour cell types relative to the blood circulation[168a]. While it is appreciated that there is a certain level of APN activity in circulation, it is reasonable to assume that in tumour environment that the level of this enzyme will be at significantly higher concentration. Thus, with the hydroxamic acid based APN inhibitor attached to the B-ring of our design, and the neutral amino acid leucine appended onto the C-ring, it is anticipated that the rate of hydrolysis of the leucine residue on the C-ring to activate the tubulin binding component will be negligible in circulation, but once it has docked onto the tumour tissue environment that the rate of hydrolysis of the leucine prodrug residue will be substantially increased. The net impact of all this imitates the controlled release, low metronomic dose of the tubulin based VDA in the tumour microenvironment. Metronomic

chemotherapy has already produced encouraging results in tubulin binding[273], anti-vascular[255a] and anti-angiogenic[255b, 274] approaches, with milder toxicities also allowing for extended duration dosage schedules and prolonged survival times in preclinical models[275]. In an adjunct role, there is also evidence to suggest that continuous, low dose exposure to anti-tumour agents can avert the mobilisation of circulating endothelial cell progenitors that otherwise reinforce the tumour vascular bed and aid revascularisation[276].

For this approach to work, we selected the aniline based DML ***4.30***, reasoning that the anilide bond would confer much more the requisite stability than the phenol analogue ***4.26***. The tendency for the phenolic ester to hydrolyse more rapidly, even under physiological pH rather than just enzymes specific for that purpose, undermined its credence as a controlled release prodrug candidate. Breen had previously shown in her prodrug studies that the leucine residue is rapidly removed, by both APN and APA expressing PC-3 cells, from prodrug forms of ***3.06*** and related compounds which do not possess hydroxamic acid functionality.

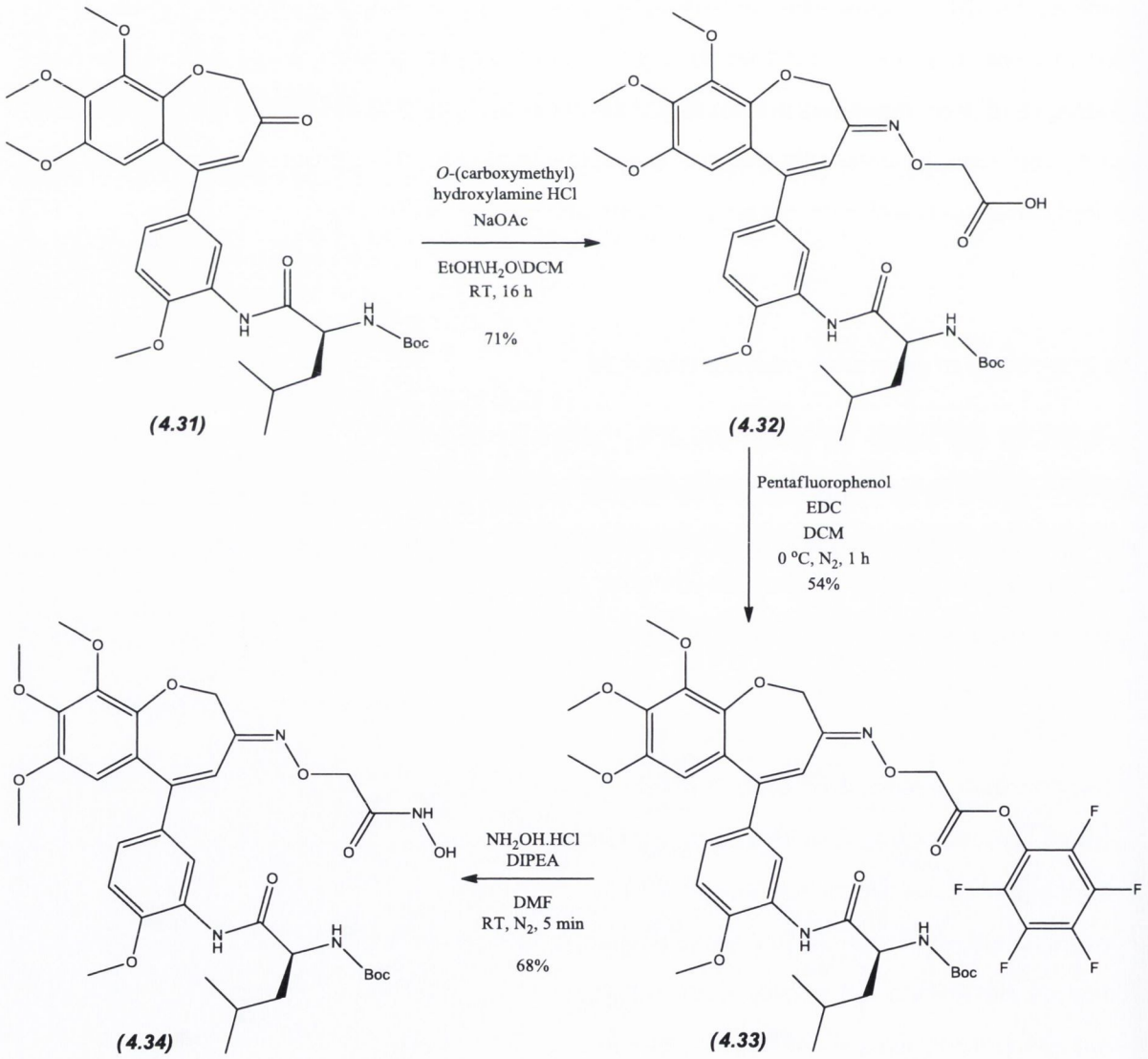
4.5.2 Synthesis of controlled released DML 4.35

Synthesis of the anilide candidate began by coupling N-Boc leucine on to aniline ***2.28*** via the PyBroP method to give N-Boc protected anilide ***4.31*** (Scheme 4.25). We were not prepared to risk coupling on the amino acid until after the synthesis of hydroxamic acid, hence the coupling step came first.

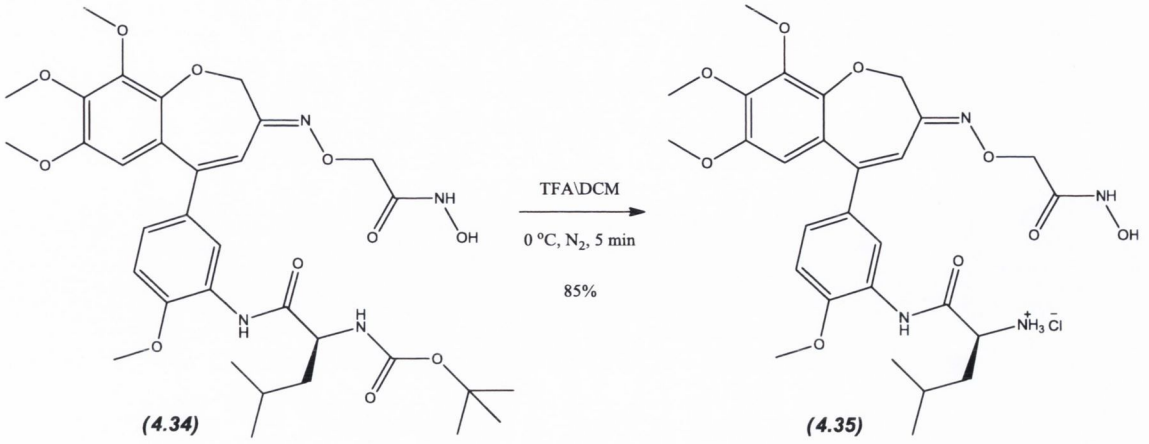


Scheme 4.25. *N*-Boc leucine coupling on to 2.28

Next, we introduced the oxime carboxylic acid moiety, again using *O*-carboxymethyl hydroxylamine and sodium acetate in ethanol\water. Once isolated, carboxylic acid ***4.32*** was then converted to its corresponding PFP ester ***4.33*** using the standard procedure of treating it with DCC and pentafluorophenol. Treatment of ***4.33*** with hydroxylamine hydrochloride afforded the hydroxamic acid 4.34 (Scheme 4.26). Finally, removal Boc carbamate on hydroxamic acid ***4.34*** with 50% TFA in DCM gave us the desired controlled release DML ***4.35*** as a free amine salt (Scheme 4.27).



Scheme 4.26. Hydroxamic acid 4.34 synthesis on *N*-boc leucine anilide TBA

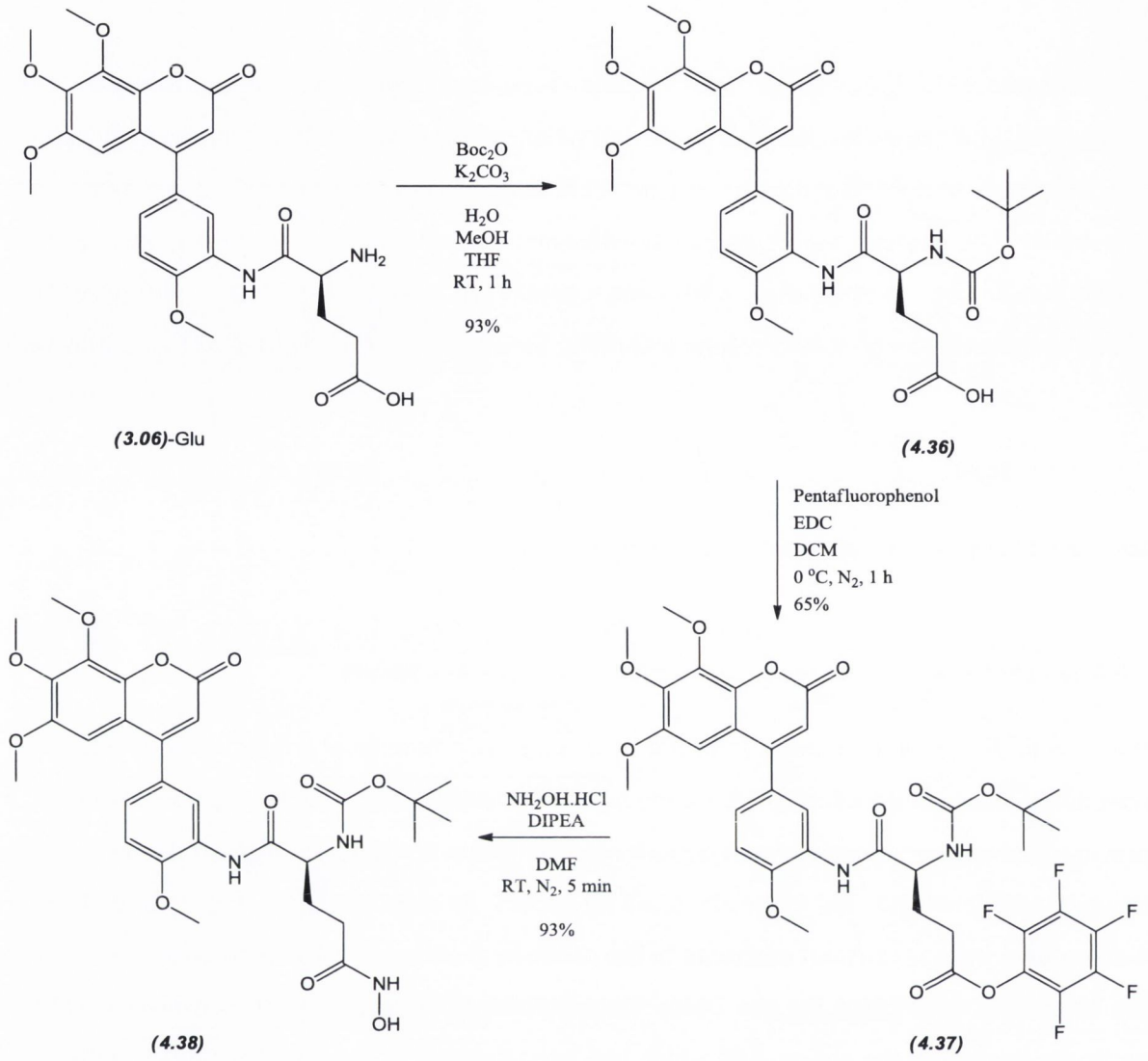


Scheme 4.27. Deprotection give controlled release DML 4.35

4.6 Attempts to incorporate hydroxamic acids on to 4-aryl coumarins

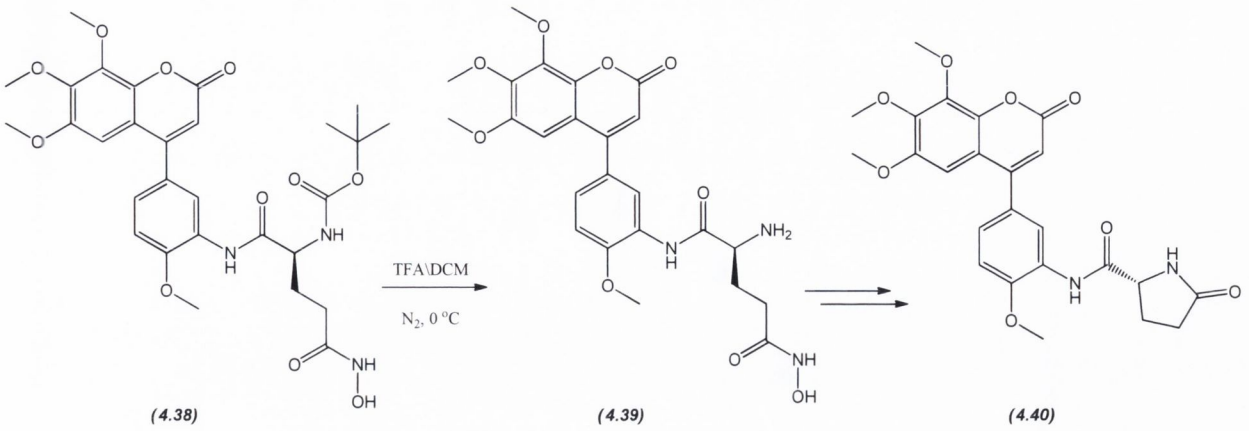
With a reliable synthetic route to form the hydroxamic acid functional group now in place, we considered means of introducing this moiety on to the 4-aryl coumarin compounds. As discussed previously, the chromenone skeleton is much more limited in terms of feasible introductory sites to which additional chemical fragments could be grafted. As expected, the B-ring lactone of the 4-aryl coumarins was resistant to change to the oxime by *O*-carboxymethyl hydroxylamine under the conditions established for the DMLs. Unperturbed, other angles were considered; with particular interest in the aniline ***3.06*** which had been donated to the aforementioned prodrug study by Breen with glutamic acid conjugated ***(3.06-Glu)***. Recognising the opportunity to transform the carboxylic acid side chain to the hydroxamic acid, we reasoned this synthesis was a realisable way of combining the APN binding hydroxamic acid with a chromenone VDA. Admittedly, this new target molecule deviates from the DML model that our hydroxamic acids have been used for so far; the requisition for hydrolysis of the anilide bond in APN-rich regions to release the functional tubulin binding component renders it more like the hybrids molecules designed earlier.

The amine ***3.06-Glu*** was first *N*-Boc protected with the anhydride. Conversion of the carboxylic acid ***4.36*** to the PFP ester ***4.37*** and then the hydroxamic acid ***4.38*** proceeded by the same methods as outlined for the synthesis of ***4.26*** (Scheme 4.28).



Scheme 4.28. Transformation of a glutamic acid carboxylic acid (3.06)-Glu to a hydroxamic acid 4.38 via the PFP ester 4.37

Next, the carbamate was cleaved with 50% TFA in DCM to reveal the free amine (Scheme 4.29). However, it became increasingly clear that there was something amiss with the final product, after a number of subtle hints were considered together. Firstly, the ^{1}H NMR spectra showed no sign of either hydroxamic acid hydrogen signals, the NH or the OH. While this would not always be cause for concern, bearing in mind the unreliability of these functional groups to appear in proton spectra and the possibility of deuterium exchange, our suspicions were compounded by the presence of the carbonyl signal at 179 ppm on the ^{13}C spectrum; further downfield than it had been in the antecedent Boc-protected hydroxamic acid compound ***4.38*** (171 ppm).



Scheme 4.29. Formation of lactam 4.40, from intramolecular cyclisation between the hydroxamic acid the newly liberated amine.

Bearing in mind the driving force for 5 membered ring formations, it was proposed that the hydroxamic acid had cyclised with the free amine to form a lactam. Neither NMR nor IR could confirm this hypothesis. Mass spectroscopy found ions both for the hydroxamic acid ***4.39*** (502.3455 m\z) and ***4.40*** (469.2614). In order to quantify the relative abundances of each of these compounds LC-MS of the product mixture was undertaken. Using a gradient system of water and methanol, and using optimised selective ion monitoring to identify each compound by the mass of its molecular ion, both compounds were clearly separated and identified. Using the area of the resultant peaks it can be determined that the lactam was indeed the primary product, suggesting almost a 30 fold excess over the remaining hydroxamic acid (20,809,952 vs 718,938). It remains unclear whether the 5 membered ring has an innate predisposition to cyclise or if the acidic environment employed in *N*-Boc deprotection prompts activation of the hydroxamic acid group to nucleophilic attack of the amine.

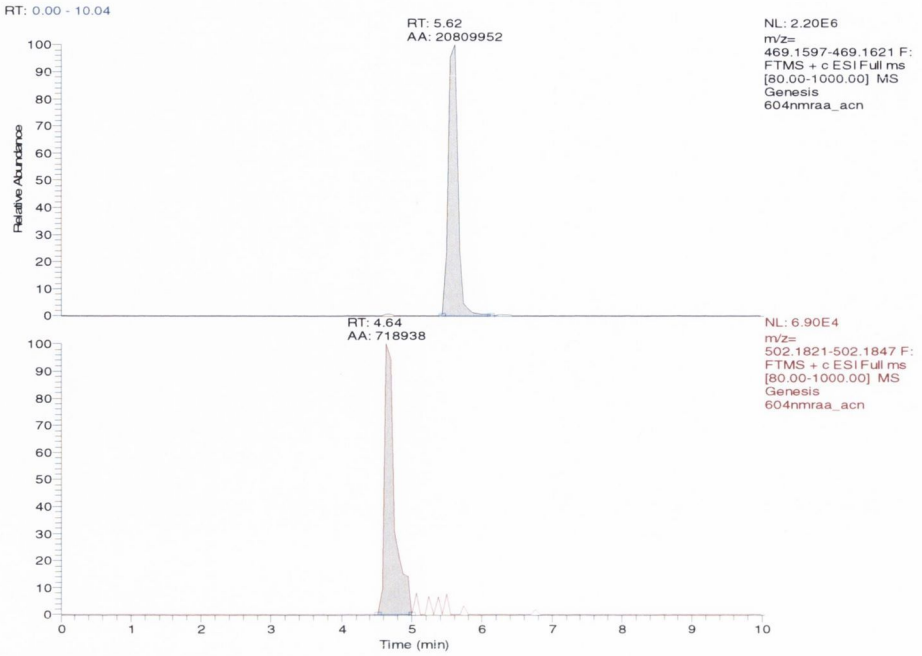


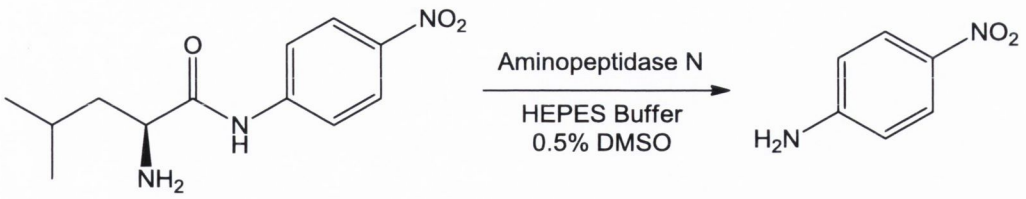
Figure 4.12. Chromatogram of the LC-MS separation of lactam 4.40 (top) and hydroxamic acid 4.39. Gradient system of H_2O:MeOH (95:5 – 20:80) (0.1% acetic acid) employed. Selective ion monitoring used to record compounds, using molecular ion values (within 5 ppm)

4.7 APN inhibition assay

Each of the compounds discussed in this chapter have been designed to bind to APN. While the primary reason for the inclusion of an APN-binding component to a hybrid molecule or designed multiple ligand was to facilitate localisation of the anti-mitotic and anti-vascular compounds described in Chapters 2 and 3, it was nevertheless pertinent to evaluate their activity as antagonists of APN. An APN inhibition assay was therefore carried out with these molecules, measuring their ability to inhibit its enzymatic cleavage of L-leucine-*p*-nitroanilide[277]. This colorimetric assay quantifies the extent to which the substrate, L-leucine-p-nitroanilide (colourless in solution) is converted to the metabolite *p*-nitroaniline (bright yellow in solution) in the presence of an APN inhibitor (Scheme 4.30), relative to when an inhibitor is absent. After 2 hours incubation at 37 °C, spectrophotometric measurement of a range of inhibitor concentrations at 405 nm in HEPES buffer and 0.5% DMSO allowed a dose-response curve to percentage inhibition to be plotted using the formula :

$$\%\ APN\ Inhibition = 100 - \left[\frac{mean\ absorbance\ of\ test\ compound}{mean\ absorbance\ of\ negative\ control} \times 100\right]$$

where an equivalent sample containing no inhibitor was used as the negative control.



L-Leucine *p*-nitroanilide (colourless)

p-Nitroaniline (yellow)

Scheme 4.30. APN cleavage of L-leucine *p*-nitroanilide to the coloured *p*-nitroaniline

The plot of percentage inhibition against the log concentration of the inhibitor gave the desired IC_{50} values (Table 4.1).

Table 4.1. IC_{50} values for APN enzymatic inhibition assay

Compound	IC_{50} (μM) ± SEM
Benzoxepinone phenolic ester Hybrid 4.06	46.75 ±1.44
4-aryl coumarin phenolic ester hybrid 4.10	42.98 ± 1.23
4-aryl coumarin anilide hybrid 4.15	11.77 ± 1.37
Phenolic tripeptide hybrid 4.18	11.67 ± 1.21
Anilide tripeptide hybrid 4.20	29.94 ± 1.20
Anilide tripeptide hybrid 4.23	20.31 ± 1.28
Phenolic DML 4.26	4.476 ± 1.31
Aniline DML 4.30	33.56 ± 1.22
Controlled release Leu-DML 4.35	143.4 ± 3.70
Bestatin	32.55 ± 1.40

The results from the assay were interesting, although no obvious trend among the compounds was evident. Of the bestatin based hybrids, aniline dipeptide hybrid ***4.15*** (IC_{50} = 11.77 ± 1.37 μM) and phenolic ester tripeptide hybrid ***4.18*** (IC_{50} = 11.67 ± 1.21 μM) were particularly active; each three times more potent than bestatin (IC_{50} = 32.55 ± 1.40 μM). Aniline based tripeptides ***4.20*** and ***4.23*** were marginally better APN inhibitors than bestatin, while phenolic ester dipeptide hybrids ***4.06*** and ***4.10*** proved less effective. The most powerful inhibitor was one of the DMLs, phenolic hydroxamic acid ***4.26*** (IC_{50} = 4.476 ± 1.31 μM), over 7-fold greater than both bestatin and its aniline analogue ***4.30***. However, the controlled release DML ***4.35*** (IC_{50} = 143.4 ± 3.70 μM), was much less active than any of the compounds tested, perhaps due to steric hindrance of this considerably more bulky DML at the binding site.

4.8 Biological evaluation of hybrid compound *4.06*

To date, only the benzoxepinone-based phenolic ester hybrid ***4.06*** has undergone biological evaluation (E. Prokopiou[232]). That said, the testing for this hybrid archetype was extensive, with the promising activity of ***4.06*** warranting investigation *in vivo*. Here, the most pertinent of these results are reported.

Cell proliferation was assessed by the MTT assay as in Chapters 2 and 3. The hybrid ***4.06*** proved to be the potent hybrid molecule tested by Prokopiou, but its activity was no better than the benzoxepinone TBA ***2.17*** which upon which it was built; IC_{50} values for ***4.06*** were 10.31 ± 1.22 nM (HUVECs) and 5.41 ± 1.37 nM (PC-3 cells) compared to 4.91 ± 1.01 nM (HUVECs) and 4.67 ± 1.45 nM (PC-3 cells) for ***2.17***. The activity of ***4.06*** was noticeably similar to a 1:1 combination of ***2.17*** and bestatin; 14.80 ± 1.13 nM (HUVECs) and 5.43 ± 1.07 nM (PC-3 cells), suggesting dissociation of ***4.06*** under assay conditions. For the G_2\M cell cycle arrest study, moderate activity was exhibited on HUVECs (35.72 ± 1.61% arrested at 1 μM), but the anti-mitotic effect was more pronounced on PC-3 cells (79.02 ± 0.72 % at 1 μM). Immunofluorescent staining again demonstrated the disruption of the microtubule organisation, to a comparable degree to ***2.17*** alone at the same concentration (1 μM).

Powerful anti-vascular activity was observed for ***4.06*** upon analysis of the changes of the endothelial cell morphology. Rounding up, blebbing and a severe interruption in confluency were noticeable upon examination of HUVECs treated with just 0.1 μM ***4.06***, with no regression to their normal state visible 3 hours following drug washout. In the rat aortic ring assay, the efficacy of ***4.06*** mirrored that of the tubulin binding moiety ***2.17***; little or insignificant activity at 10 μM concentrations for both the anti-vascular and anti-angiogenic model, but potent activity at 50 μM. As the anti-vascular effect of ***4.06*** is solely reliant on tubulin binding component ***2.17***, not bestatin, it can be concluded that full release of the TBA from the hybrid is achieved. Regarding the anti-angiogenic effect, the similarity of the effect of ***4.06*** to ***2.17*** implies there is little synergism between the TBA and the bestatin moieties at this concentration. The concentration of bestatin in this case is too low to have an appreciable benefit, with bestatin induced suppression of angiogenesis previously described at higher concentrations (80-300 μM)[188, 278].

In vivo, hybrid ***4.06*** was evaluated against a s.c. PC-3 tumour xenograft model. Administration of the hybrid was at a dose of 50 mg\kg given by i.p. on alternate days over the course of 24 days. Two dimensional tumour measurements taken every two days were used to calculate tumour volume. Over the duration of the study, ***4.06*** promoted a significant decrease in tumour growth rate versus the control (10% DMSO in wfi), derived from the Mann-Whitney *U*-test. In total, the growth delay calculated using relative tumour volumes was estimated at 4.42 days. To gauge the systemic toxicity of ***4.06***, body weight measurements were taken every two days. Body weight measurements of the ***4.06*** treated group were slightly below those of the control, but within the limits and following the maximum weight loss (day 14, 1.77%) recovery was observed.

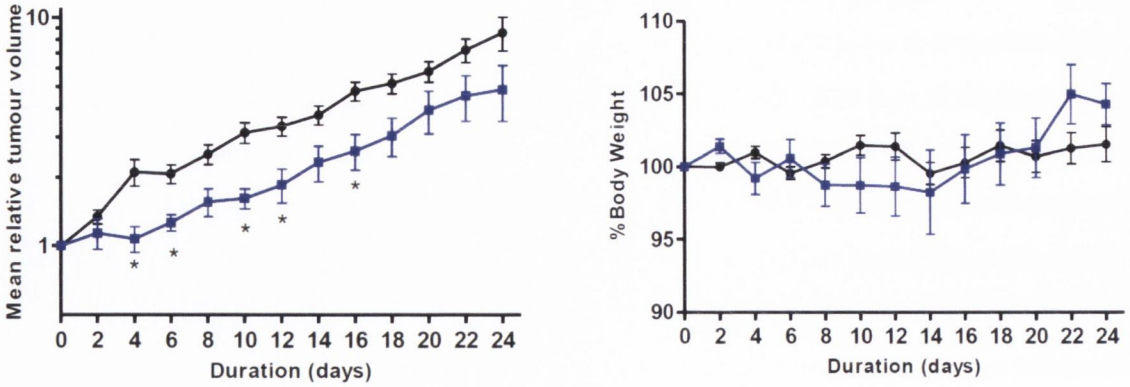


Figure 4.13. Left : Difference in tumour growth in terms of tumour volume of control treated PC-3 tumours (black) versus those treated with hybrid 4.06 (blue). Asterisks denote days with statistically significant reduced volume. Right : Body weight measurements of control animals (black) versus those treated with 4.06 (blue).

Upon histological analysis of three ***4.06*** treated tumours themselves, using haematoxylin and eosin (H&E) staining techniques, two medium sized tumours showed signs of emphatic necrosis at the tumour core, complete with a characteristic viable rim of resistant tissue at the periphery. However, one other smaller tumour didn't show any sign of necrotic tissue at all. Due to the limitation of sample tumours, and the variations in size it is inconclusive as to whether necrosis is directly as a result of ***4.06*** treatment alone, or proportional to the levels of hypoxia related to tumour size.

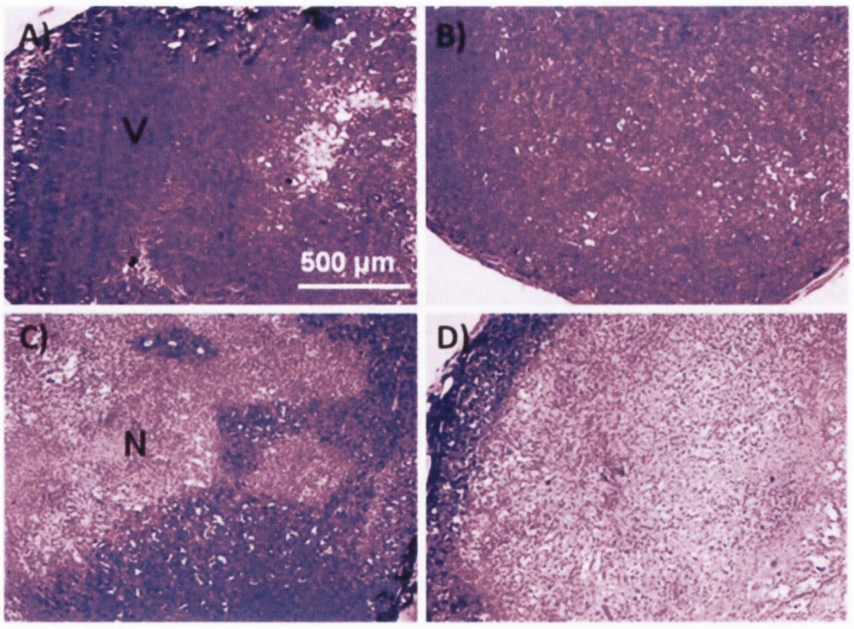


Figure 4.14. H&E stained tumours. Control tumours (A-B, 10% DMSO) show viable tissue (V, deep purple colour) in comparison to 4.06 treated tumours (C-D, 50 mg\kg), in which extensive necrotic tissue (N, light pink) is found at the core. On 4.06 treated tumours, a peripheral ring of viable tissue is found on each.

Three other tumours were also excised, processed stained with a CD31 antibody to determine functional endothelial cells. Relative to the controls, it was found that the tumours treated with ***4.06*** not only possessed substantially lower levels of tumour vasculature, but that these vessels also appeared more narrow than those seen in the controls. These results exemplify the anti-vascular and anti-angiogenic effects of ***4.06***.

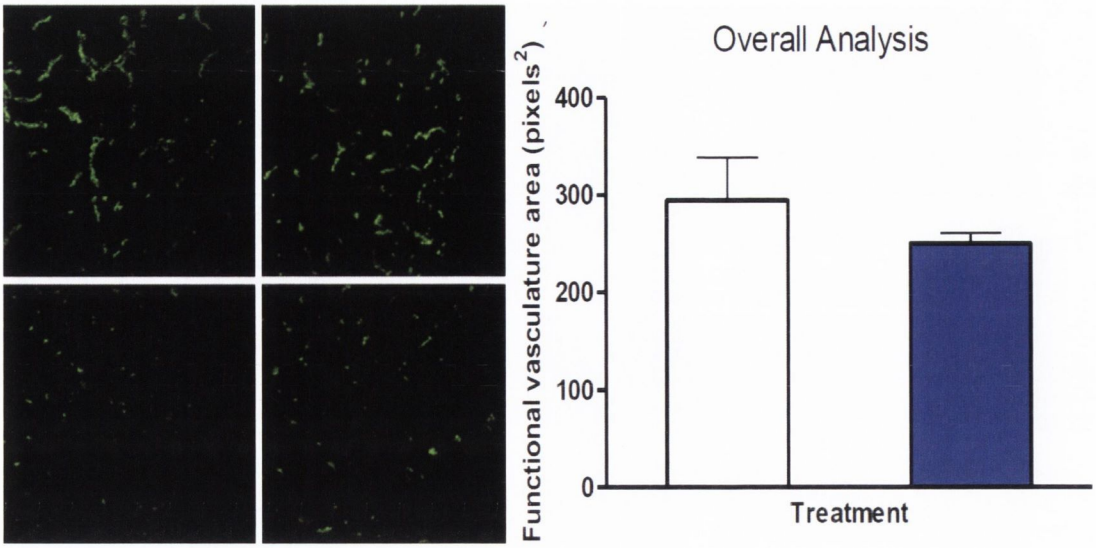


Figure 4.15. Left : Comparison of the functional vasculature of control tumours (top two images, 10% DMSO) against those treated with 4.06 (bottom two images, 50 mg\kg), using CD31 antibody (green) to stain endothelial cells. Right : Quantified, a collective reduction in vasculature area is recorded for 4.06 treated tumours (blue) over control (white)

4.9 Conclusions

At the beginning of this chapter, novel bestatin-based hybrids were synthesised, containing the three most promising tubulin binding VDAs from Chapters 2 and 3; benzoxepinone phenol ***2.17***, phenolic 4-aryl coumarin ***3.03*** and aniline 4-aryl coumarin ***3.06***, to form dipeptide hybrids ***4.06***, ***4.10*** and ***4.15*** respectively. Furthermore, leucine-bestatin tripeptide hybrids of phenol ***3.03*** and aniline ***3.06*** were also synthesised, ***4.18*** and ***4.20*** respectively, as well as ***4.23***, the alanine-bestatin hybrid of aniline ***3.06***. Each of these was tested for APN inhibition, with ***4.15*** and ***4.18*** particularly active against the enzyme, with IC_{50} values lower than established APN inhibitor bestatin.

Also synthesised was a series of designed multiple ligands (DMLs); molecules which integrate both an APN binding component and an overlapping pharmacophore for tubulin inhibition on to a single structure. Consisting of a hydroxamic acid for zinc chelation on APN, and the methoxylated diaryl tubulin scaffold for tubulin binding, phenol ***4.26*** and aniline ***4.30*** were synthesised. Another hydroxamic acid, ***4.35***, was synthesised, essentially ***4.30*** with the leucine coupled to the aniline, with the aim being gradual, controlled release of DML ***4.30*** by the peptidase enzymes such as APN, which densely populate the unique vasculature that surround a

growing tumour mass. On the APN assay, phenol DML ***4.26*** demonstrated powerful APN inhibition, much lower than bestatin.

Of all the compounds synthesised in this chapter phenol benzoxepinone hybrid ***4.06*** has been the most thoroughly assessed for biological activity. At the end of this chapter, the extent of its biological evaluation is reviewed, including that *in vivo*, where ***4.06*** caused a growth delay of 4.42 days in the tumour of a PC-3 xenograft model.

Chapter 5 – Experimental

5.0 Experimental Section

5.1 General Methods

Starting materials were procured primarily from Sigma Aldrich® Ireland at an appropriately high grade and were not characterised before use. N-Butyllithium and deuterated chloroform were procured from Acros Organics®. (2S,3R)-3-Amino-2-hydroxyl-4-phenyl-butyric acid was procured from Bosche Scientific, NJ. 2-[N,N-Bis(trifluoromethylsulfonyl)amino]-5-chloropyridine was procured from Apollo Scientific®.

Nuclear Magnetic Resonance (NMR) spectroscopy was performed primarily using a Bruker DPX-400 MHz FT NMR spectrometer at 25 °C at either 400.13 MHz for 1 H NMR spectra or 100.61 MHz for 13C NMR spectra. Resonance positions were assigned relative to the singlet $CHCl_3$ peak at 7.28 ppm for ^{1}H NMR and at the middle peak of the $CHCl_3$ peak at 77.0 ppm for ^{13}C NMR. For samples in deuterated chloroform, positions were assigned relative to the middle peak of the multiplet at 3.30 ppm and 49.0 ppm for ^{1}H and ^{13}C respectively. All coupling constants (*J*) were recorded in Hz. Spectra were processed and analysed on Bruker Topspin-NMR® software version 2.1.

Legend for NMR assignments : s=singlet, d=doublet, t=triplet, q=quartet, dd=double doublet, ddd=double double doublet, dt=double triplet, m=multiplet, br=broad peak. ArH=aromatic hydrogen on ^{1}H spectrum, ArF=aromatic fluorine, ArC=aromatic quaternary carbon, ArCH=aromatic carbon bearing a hydrogen, ArCF=aromatic carbon bearing a fluorine

Infrared spectrum was recorded using either a Perkin Elmer® FT-IR spectrophotometer Spectrum 100 with an attenuated total reflection (ATR) accessory featuring a Zinc selenide (ZnSe) crystal, on which the sample in any state could be applied, or on a Perkin Elmer® FT-IR spectrophotometer Paragon 100, where the samples were analysed as films on NaCl discs.

The LTQ-XL ion trap mass spectrometer was coupled to the Accela LC system via an electrospray ionization (ESI) probe. The capillary temperature was maintained at 350 °C, sheath gas flow rate 50 arbitrary units, auxiliary gas flow rate 5 arbitrary units, sweep gas flow rate 0 arbitrary units, source voltage 3.20 kV, source current 100 μA, capillary voltage 43.00 V and tube lens 100 V. Compounds were detected in positive ion mode using selected ion monitoring (SIM).

All high resolution mass spectra (HRMS) were detected by a Thermo Scientific® LTQ-Orbitrap Discovery mass spectrometer and analysis of the spectra was carried out using the Xcalibur program.

Melting points (MP) were recorded on an Electrotherm® melting point apparatus.

Compounds were named using ChemAxon® Marvin Beans software or ChemBioOffice Chemdraw version 12.0.

Thin Layer Chromatography (TLC) was carried out on Merck Silica gel F254 on pre-coated aluminium plates. Column chromatography was carried out with silica gel 60 (230-400 mesh). Both of these silicon materials were procured from Merck Laboratories®. Compounds were visualised under UV light at 254 and 365 nm wavelength, using the stains potassium permanganate, vanillin, ninhydrin and anisaldehyde where appropriate.

Anhydrous DCM was distilled over powdered calcium hydride. Anhydrous THF was prepared by reflux over powdered lithium aluminium hydride for at least 4 h, after which the distillate was collected and added to fresh sodium pieces with benzophenone for 2 h or until the colour changes from a navy blue to a homogenous dark purple colour is maintained throughout; at which point the colourless distillate could be collected for immediate practical use.

5.2 Experimental for Chapter 2

Synthesis of intermediate 2,3,4-trimethoxyphenyl formate *(2.01)*

To a solution of 2,3,4 trimethoxybenzaldehyde (15.00 g, 0.07645 moles) in DCM (75 mL) was added *m*CPBA (20.59 g, 77% purity, 0.0917 moles) in DCM (120 mL) and the reagents stirred at 0 °C overnight. The reaction was then filtered through paper with DCM to remove *m*CPBA precipitate before the filtrate was concentrated *in vacuo*. The resultant fraction was then washed with aq. $NaHCO_3$ solution (3 × 250 mL, 5%), water (250 mL) and saturated aq. NaCl solution (250 mL) sequentially. The organic layer was then dried with $MgSO_4$ and concentrated under vacuum to afford formate ester ***(2.01)*** as a brown oil (12.34 g, 0.0582 moles, 76%).

^{1}H NMR (400 MHz, CHLOROFORM-*d*) δ_H ppm : 3.87 (3 H, s, OCH_3), 3.90 (3 H, s, OCH_3), 3.91 (3 H, s, OCH_3), 6.65 (1 H, d, ArH, *J*=9 Hz), 6.82 (1 H, d, ArH, *J*= 9 Hz), 8.29 (1 H, s, CHO)

^{13}C NMR (101 MHz, CHLOROFORM-*d*) δ_C ppm : 56.2 (OCH_3), 61.1 (OCH_3), 61.2 (OCH_3), 106.5 (ArCH), 116.4 (ArCH), 136.8 (ArC), 143.1 (ArC), 145.6 (ArC), 152.2 (ArC), 159.6 (C=O)

ν_{max} cm^{-1} : 3075.6, 2817.7, 1685.8, 1416.3, 1299.8, 1261.1, 746.7

Synthesis of intermediate 2,3,4-trimethoxyphenol *(2.02)*

Formate ester ***(2.01)*** was then re-dissolved in MeOH (50 mL) and THF (30 mL) and cooled to 0 °C before aq. NaOH solution (40 mL, 2.5 M) was added. After 1 h the reaction was allowed reach room temperature and left stirring overnight. The organic solvents were then removed *in vacuo* and the reaction acidified with aq. HCl solution (50 mL, 2 M). The reaction was then extracted with diethyl ether (3 × 100 mL), dried with $MgSO_4$ and concentrated *in vacuo* to afford phenol ***(2.02)*** (7.88 g, 0.04278 moles, 74%) as a brown oil.

^{1}H NMR (400 MHz, CHLOROFORM-*d*) δ_H ppm : 3.83 (3 H, s, OCH_3), 3.91 (3 H, s, OCH_3), 3.397 (3 H, s, OCH_3), 5.48 (1 H, br. s., OH) 6.59 (1 H, d, ArH, *J*= 8.6 Hz), 6.64 (1 H, d, ArH, *J*= 8.6 Hz)

^{13}C NMR (101 MHz, CHLOROFORM-*d*) δ_C ppm : 56.6 (OCH_3), 60.9 (OCH_3), 61.3 (OCH_3), 107.6 (ArCH), 108.5 (ArCH), 140.7 (ArC), 142.3 (ArC), 143.3 (ArC), 146.9 (ArC)

ν_{max} cm^{-1} : 3422.6, 2940.4, 2834.8, 1600.5, 1491.4, 1480.0, 1091.1

HRMS : calculated 184.0736, found 183.0675 ($H - H^+$)

Synthesis of intermediate 2,3,4-trimethoxyphenol *(2.02)* via acid catalysed Dakin Oxidation

2,3,4 trimethoxybenzaldehyde (50.35 g, 0.26 moles), hydrogen peroxide (37.82 g, 0.334 moles, 30% solution) and conc. sulphuric acid (5 mL) were stirred together at 0 °C. Methanol (250 mL) was carefully added portionwise and the reaction kept at 0 °C for 1 h. The reaction was then quenched with aq. NaOH (200 mL, 2 M) and methanol removed *in vacuo*. The remaining aqueous mixture was extracted with diethyl ether (3 × 200 mL). The aqueous layer was then acidified with aq. HCl (250 mL, 2 M) and extracted with diethyl ether (3 × 250 mL) to afford phenol (2.02) (39.28, 0.213 moles, 82%) as a brown oil.

1H NMR ($CDCl_3$, 400 MHz) δ_H : 3.83 (3H, s, OCH_3), 3.91 (3H, s, OCH_3), 3.397 (3H, s, OCH_3), 5.48 (1H, br s, OH) 6.59 (1H, d, Ar-H, J = 8.6 Hz), 6.64 (1H, d, Ar-H, J = 8.6 Hz)

13C NMR ($CDCl_3$, 400 MHz) δ_C : 56.6 (OCH_3), 60.9 (OCH_3), 61.3 (OCH_3), 107.6 (ArCH), 108.5 (ArCH), 140.7 (ArC), 142.3 (ArC), 143.3 (ArC), 146.9 (ArC)

ν_{max} cm^{-1} : 3422.6, 2940.4, 2834.8, 1600.5, 1491.4, 1480.0, 1091.1

HRMS : calculated 184.0736, found 183.0675 ($H - H^+$)

Synthesis of intermediate ethyl 2-(2,3,4-trimethoxyphenoxy)acetate *(2.03)*

Phenol ***(2.02)*** (0.98 g, 0.00532 moles) was dissolved in acetone (30 mL) and potassium carbonate (3.265 g, 0.0236 moles) added, followed by ethyl bromoacetate (1.24 mL, 0.01172 moles) and the reaction refluxed for 6 h. The reaction mixture was then filtered through paper to remove solid K_2CO_3 and washed with ethyl acetate. The filtrate was then dried with magnesium sulphate, concentrated *in vacuo* and purified by column chromatography (5-3:1, hexane : ethyl acetate) to afford ethyl ester ***(2.03)***, as a yellow oil (1.37 g, 0.00507 moles, 95%).

^{1}H NMR (400 MHz, CHLOROFORM-*d*) δ_H ppm : 1.30 (3 H, dt, $CH_2\underline{CH_3}$, *J*=7.15, 4.77 Hz), 3.82 (3 H, s, OCH_3), 3.90 (3 H, s, OCH_3), 3.95 (3 H, s, OCH_3), 4.22 - 4.29 (2 H, m, $CO\underline{CH_2}CH_3$), 4.63 (2 H, s, OCH_2CO), 6.54 (2 H, d, ArH, *J*=9.05 Hz), 6.60 (2 H, d, *J*=9.05 Hz)

^{13}C NMR (101 MHz, CHLOROFORM-*d*) δ_C ppm 13.5 ($CH_2\underline{C}H_3$), 55.6 (OCH_3), 59.7 (OCH_3), 60.5 ($CO\underline{C}H_2CH_3$), 61.6 (OCH_3), 66.6 ($O\underline{C}H_2CO$), 105.7 (ArCH), 109.3 (ArCH), 142.8 (ArC), 143.7 (ArC), 145.4 (ArC), 148.3 (ArC), 168.5 (C=O)

ν_{max} cm^{-1} : 2984.0, 2939.2, 1748.5, 1591.4, 1120.2.

HRMS : calculated 270.1103, found 271.1212 ($M + H^+$), 293.1017 ($M + Na^+$)

Synthesis of intermediate 2-(2,3,4-trimethoxyphenoxy)acetic acid *(2.04)*

Ethyl ester ***(2.03)*** (1.37 g, 0.00507 moles) was dissolved in MeOH (8.5 mL) and THF (5 mL) and cooled to 0 °C. Aq. NaOH (7 mL, 2.5 M) was then added and the reaction stirred for 1 h, after which it was allowed reach room temperature and left stirring overnight. The organic solvents were subsequently removed by vacuum and aq. HCl (10 mL, 2 M) added. The mixture was extracted with ether (4 × 50 mL), dried with $MgSO_4$ and condensed *in vacuo*. NaOH (25 mL, 2.5 M) was then added and the reaction extracted with ether (3 × 50 mL). Aq. HCl solution (40 mL, 2 M) was added to the resulting aqueous phase, and then extracted with ether (3 × 100 mL). After drying with $MgSO_4$, solvents were removed *in vacuo* to afford acid ***(2.04)*** (1.10 g, 0.00454 moles, 90%) as a yellow solid.

^{1}H NMR (400 MHz, CHLOROFORM-*d*) δ_H ppm : 3.85 (3 H, s, OCH_3), 3.92 (3 H, s, OCH_3), 3.98 (3 H, s, OCH_3), 4.67 (2 H, s, OCH_2CO), 6.6 (1 H, d, ArH, *J*= 8.92 Hz), 6.68 (1 H, d, ArH, *J*=8.96 Hz)

^{13}C NMR (101 MHz, CHLOROFORM-*d*) δ_C ppm : 55.8 (OCH_3), 60.8 (OCH_3), 61.2 (OCH_3), 67.8 (OCH_2COOH), 106.2 (ArCH), 110.6 (ArCH), 142.6 (ArC), 143.9 (ArC), 145.1 (ArC), 149.1 (ArC), 176.6 (COOH)

ν_{max} cm^{-1} : 3004.3, 2834.9, 1713.8, 1599.5

HRMS : calculated 242.0790, found 243.0863 ($M + H^+$), 265.0678 ($M + Na^+$)

Mp: 53-55 °C

Synthesis of intermediate 2,2-dimethyl-5-[3-(2,3,4-trimethoxyphenyl)propanoyl]-1,3-dioxane-4,6-dione *(2.05)*

Acid ***(2.04)*** (0.93 g, 0.00384 moles) was dissolved in dry dichloromethane (5 mL) at 0 °C under an atmosphere of nitrogen and neat oxalyl chloride(0.72 mL, 0.00826 moles) carefully introduced via syringe. One drop of dimethylformamide was also added and the reaction allowed stir for 1 h. Solvents were then completely evaporated off under vacuum to leave a goopy brown liquid. In the same reaction vessel was added a mixture of Meldrum's acid (0.56 g, 0.00384 moles) and DMAP (0.94 g, 0.00768 moles) in dry dichloromethane (12 mL). The reaction was stirred at 0 °C for 1 h and solvents removed *in vacuo* before aq. HCl solution (20 mL, 2 M) was added to quench the DMAP. The mixture was extracted with dichloromethane (3 × 50 mL), the organic layers were dried with magnesium sulphate and solvents removed *in vacuo* to afford Meldrum's product ***(2.05)*** (1.29 g, 0.0035 moles, 91%).

^{1}H NMR (400 MHz, CHLOROFORM-*d*) δ_H ppm : 1.78 (6 H, s, 2 × CH_3), 3.83 (3 H, s, OCH_3), 3.92 (3 H, s, OCH_3), 3.96 (3 H, s, OCH_3), 5.47 (2 H, s, CH_2), 6.56 (1 H, d, ArH, *J*=8.9 Hz), 6.65 (1 H, d, ArH, *J*=8.9 Hz)

^{13}C NMR (101 MHz, CHLOROFORM-*d*) δ_C ppm : 26.5 (2 × CH_3), 55.8 (OCH_3), 60.8 (OCH_3), 60.9 (OCH_3), 68.9 (CH_2), 89.8 (CH), 105.6 ($\underline{C}(O)_2(CH_3)_2$), 105.8 (ArCH), 109.2 (ArCH), 143.0 (ArC), 143.8 (ArC), 145.4 (ArC), 148.6 (ArC), 170.9 (2 × OC=O), 192.2 ($H_2C\underline{C}$=O)

ν_{max} cm^{-1} : 2942.0, 1737.2, 1570.8, 1421.8, 1395.9, 1279.2, 1262.4, 1231.9, 1173,7, 1037.1

HRMS : calculated 368.1107, found 366.9961 ($H - H^+$)

Synthesis of intermediate methyl 4-(2,3,4-trimethoxyphenoxy)-3-oxobutanoate *(2.06)*

Meldrum's product ***(2.05)*** was then dissolved in toluene (105 mL) and MeOH (30 mL) and refluxed together for 12 h. The solvents were then removed *in vacuo* and ester product ***(2.06)*** purified by column chromatography (3:1 hexane : ethyl acetate) to give a orange oil (0.76 g, 0.00255 moles, 73%).

^{1}H NMR (400 MHz, CHLOROFORM-*d*) δ_H ppm : 3.72 (2 H, s, $COCH_2CO$), 3.77 (3 H, s, OCH_3), 3.84 (3 H, s, OCH_3), 3.92 (3 H, s, OCH_3), 3.93 (3 H, s, OCH_3), 4.64 (2 H, s, OCH_2CO), 6.57 (2 H, s, 2 × ArH)

^{13}C NMR (101 MHz, CHLOROFORM-*d*) δ_H ppm : 31.0 ($CH_2\underline{C}H_3$), 45.2 (C=O$\underline{C}H_2$C=O), 52.0 ($\underline{C}H_2CH_3$), 55.8 (OCH_3), 60.8 (OCH_3), 61.9 (OCH_3), 74.3 (Ar$O\underline{C}H_2$C=O), 105.9 (ArCH), 109.1 (ArCH), 137.5 (2 × ArC), 145.2 (ArC), 148.7 (ArC), 167.0 ($\underline{C}$=OCH_2CH_3), 200.1 ($\underline{C}$=OCH_2C=O)

ν_{max} cm^{-1} : 2931.6, 2826.9, 1753.7, 1738.0, 1491.9, 1115.0

HRMS : calculated 298.1053, found 297.2210 ($M - H^+$),

Sodium borohydride reduction of *(2.06)* to in methyl 3-hydroxy-4-(2,3,4-trimethoxyphenoxy)-butanoate *(2.07)*

To a stirred solution of keto-ester ***(2.06)*** (1.74 g, 0.0058 moles) in MeOH (30 mL) at 0 °C was added sodium borohydride (0.221 g, 0.0058 moles) portion-wise. After 3 h, a further dose of sodium borohydride (0.23 g, 0.0058 moles) was introduced and reaction stirred for a further 1-2 h. The reaction was quenched with water (50 mL) and acidified with aq. HCl solution (2 M) to pH

5. MeOH was then removed under reduced pressure and the product then isolated by extraction with diethyl ether (4 × 100 mL) before being dried with magnesium sulphate and dried *in vacuo*. After column chromatography (2:1, hexane : ethyl acetate), alcohol ***(2.07)*** (0.77 g, 0.00256 moles, 44%) was obtained as a white-yellow oil.

^{1}H NMR (400 MHz, CHLOROFORM-*d*) δ_H ppm : 2.68 (2 H, m, $CH_2C{=}O$), 3.35 (1 H, br. s., OH), 3.75 (3 H, s, OCH_3), 3.84 (3 H, s, OCH_3), 3.912 (3 H, s, OCH_3), 3.916 (3 H, s, OCH_3), 4.00 (2 H, m, O $C\underline{H}_2COH$), 4.42 (1 H, m, $C\underline{H}OH$), 6.58 (1 H, d, ArH, *J*=8.87 Hz), 6.66 (1 H, d, ArH, *J*=8.87 Hz)

^{13}C NMR (101 MHz, CHLOROFORM-*d*) δ_C ppm : 37.36 ($\underline{C}H_2C{=}O$), 51.5 (OCH_3), 55.8 (OCH_3), 60.8 (OCH_3), 60.9 (OCH_3), 66.3 (CHOH), 73.3 ($O\underline{C}H_2CHOH$), 106.2 (ArCH), 109.7 (ArCH), 142.9 (ArC), 143.9 (ArC), 146.0 (ArC), 148.3 (ArC), 171.9 (C=O)

ν_{max} cm^{-1} : 3475.1, 2934.2, 2830.2, 1733.8, 1489.4

HRMS : calculated 300.1209, found 323.1095 ($M + Na^+$)

Cerium chloride catalysed sodium borohydride reduction of *(2.06)* to in methyl 3-hydroxy-4-(2,3,4-trimethoxyphenoxy)butanoate *(2.07)*

Cerium (III) chloride heptahydrate (1.26 g, 0.00339 moles) was added to a stirred solution of MeOH (12.5 mL) and keto-ester ***(2.06)*** (1.01 g, 0.00339 moles). The reaction was cooled to 0 °C before sodium borohydride (0.2 g, 0.00508 moles) was added in one portion. After 15 min, the reaction was quenched with water (50 mL) and acidified with aq. HCl solution (2 M) to pH 7. MeOH was then removed under reduced pressure and the product then isolated by extraction with diethyl ether (4 × 100 mL) before being dried with magnesium sulphate and dried *in vacuo*. After column chromatography (2:1, hexane : ethyl acetate), alcohol ***(2.07)*** (0.48 g, 0.00162 moles, 55%) was obtained as a white-yellow oil.

^{1}H NMR (400 MHz, CHLOROFORM-*d*) δ_H ppm : 2.68 (2 H, m, $CH_2C{=}O$), 3.35 (1 H, br. s., OH), 3.75 (3 H, s, OCH_3), 3.84 (3 H, s, OCH_3), 3.912 (3 H, s, OCH_3), 3.916 (3 H, s, OCH_3), 4.00 (2 H, m, O $C\underline{H}_2COH$), 4.42 (1 H, m, $C\underline{H}OH$), 6.58 (1 H, d, ArH, *J*=8.87 Hz), 6.66 (1 H, d, ArH, *J*=8.87 Hz)

^{13}C NMR (CDCl3, 400 MHz) δC : 37.36 ($\underline{C}H_2C{=}O$), 51.5 (OCH_3), 55.8 (OCH_3), 60.8 (OCH_3), 60.9 (OCH_3), 66.3 (CHOH), 73.3 ($O\underline{C}H_2CHOH$), 106.2 (ArCH), 109.7 (ArCH), 142.9 (ArC), 143.9 (ArC), 146.0 (ArC), 148.3 (ArC), 171.9 (C=O)

ν_{max} cm^{-1} : 3475.1, 2934.2, 2830.2, 1733.8, 1489.4

HRMS : calculated 300.1209, found 323.1095 ($M + Na^+$)

Yeast catalysed reduction of *(2.06)* to methyl 3-hydroxy-4-(2,3,4-trimethoxyphenoxy)butanoate *(2.07)*

Keto-ester ***(2.06)*** (3.00 g, 0.01006 moles), Baker's yeast (30 g), petroleum ether (150 mL) and water (20 mL) were shaken together for 24 h at RT. After this the yeast was filtered and rinsed with large volumes of ethyl acetate (approx 1-2 L). All organic filtrate was dried with magnesium sulphate and condensed under reduced pressure. After purification by column chromatography (2:1, hexane : ethyl acetate), alcohol ***(2.07)*** (2.0 g, 0.00666 moles, 66%) was obtained as a white-yellow oil.

^{1}H NMR (CDCl3, 400 MHz) δH : 2.68 (2 H, m, $CH_2C=O$), 3.35 (1 H, br. d., OH), 3.75 (3 H, s, OCH_3), 3.84 (3 H, s, OCH_3), 3.912 (3 H, s, OCH_3), 3.916 (3 H, s, OCH_3), 4.00 (2 H, m, O $C\underline{H}_2COH$), 4.42 (1 H, m, $C\underline{H}OH$), 6.58 (1 H, d, ArH, *J*=8.87 Hz), 6.66 (1 H, d, ArH, *J*=8.87 Hz)

^{13}C NMR (CDCl3, 400 MHz) δC : 37.36 ($CH_2C=O$), 51.47 (OCH_3), 55.84 (OCH_3), 60.77 (OCH_3), 60.96 (OCH_3), 66.34 (CHOH), 73.29 ($O\underline{C}H_2CHOH$), 106.16 (ArCH), 109.70 (ArCH), 142.86 (ArC), 143.95 (ArC), 146.04 (ArC), 148.27 (ArC), 171.9 (C=O)

ν_{max} cm^{-1} : 3475.1, 2934.2, 2830.2, 1733.8, 1489.4

HRMS : calculated 300.1209, found 323.1095 ($M + Na^+$)

Synthesis of intermediate methyl 3-[(*tert*-butyldiphenylsilyl)oxy]-4-(2,3,4-trimethoxyphenoxy)butanoate *(2.08)*

Alcohol ***(2.07)*** (2.73 g, 0.0091 moles) was then stirred in dry DMF (25 mL), imidazole (0.99 g, 0.0146 moles) and *tert*-butyl diphenylchloro silane (3.55 mL, 3.75 g, 0.0137 moles) under an atmosphere of nitrogen overnight. The reaction was quenched with brine (50 mL), extracted with ether (3 × 100 mL) and dried with magnesium sulphate before evaporation of organic solvents *in vacuo*. After purification via column chromatography (6:1, hexane : ethyl acetate), silyl ether ***(2.08)*** (4.57 g, 0.00848 moles, 93%) was obtained as a clear viscous oil.

^{1}H NMR (400 MHz, CHLOROFORM-*d*) δ_H ppm : 1.06 (9 H, s, $C(CH_3)_3$), 2.75 (2 H, ddd, $C\underline{H}_2COOCH_3$, *J*=1.00 Hz), 3.61 (3 H, s, OCH_3), 3.81 (3 H, s, OCH_3), 3.82 (3 H, s, OCH_3), 3.89 (3 H, s, OCH_3), 4.15 (2 H, q, OCH_2, *J*=7.03 Hz), 4.53 (1 H, d, CHSi, *J*=6.02 Hz), 6.28 (1 H, d, ArH, *J*=9.29 Hz), 6.46 (1 H, d, ArH, *J*=9.29 Hz), 7.35 - 7.47 (6 H, m, 6 × ArH), 7.70 - 7.75 (4 H, m, 4 × ArH)

^{13}C NMR (101 MHz, CHLOROFORM-*d*) δ_C ppm : 18.8 ($C(\underline{C}H_3)_3$), 26.4 ($\underline{C}(CH_3)_3$), 39.5 ($\underline{C}H_2$), 51.4 (OCH_3), 56.4 (OCH_3), 61.0 (OCH_3), 61.1 (OCH_3), 68.9 ($\underline{C}HOSi$), 72.0 ($O\underline{C}H_2CHOSi$), 106.2 (ArCH), 108.3 (ArCH), 127.2 (2 × ArCH), 127.2 (2 × ArCH), 129.3 (ArCH), 129.4 (ArCH), 132.9 (ArC), 133.22 (ArC), 135.40 (2 × ArCH), 135.4 (2 × ArCH), 143.0 (q$\underline{C}$), 143.6 (ArC), 146.3 (ArC), 147.7 (ArC), 171.1 (C=O).

ν_{max} cm^{-1} : 2931.6, 2850.3, 1738.0, 1491.9

HRMS : calculated 538.2387, found 539.4054 ($M + Na^+$)

Synthesis of 3-[(*tert*-butyldiphenylsilyl)oxy]-4-(2,3,4-trimethoxyphenoxy)butanoic acid *(2.09)*

Protected ester ***(2.08)*** (3.61 g, 0.0067 moles) was hydrolysed with aq. NaOH solution (20 mL, 2 M) in MeOH\THF (25 mL : 15 mL) at RT for 2 h. The organic solvents were subsequently removed by vacuum and aq. HCl solution (10 mL, 2 M) added. The mixture was extracted with ether (4 × 50 mL), dried with magnesium sulphate and condensed *in vacuo*. Aq. NaOH solution (25 mL, 2.5 M) was then added and the reaction extracted with ether (3 × 50 mL). Aq. HCl solution (40 mL, 2 M) was added to the *resulting aqueous phase*, and then extracted with ether (3 × 100 mL). After drying with magnesium sulphate and concentrating *in vacuo*, acid product ***(2.09)*** (2.96 g, 0.00564 moles, 84%) was obtained without the need for column chromatography.

^{1}H NMR (400 MHz, CHLOROFORM-*d*) δ_H ppm : 1.08 (9 H, s, $C(CH_3)_3$), 2.8 (2 H, ddd, $\underline{C}H_2COOH$, *J*=25.5, 15.75, 5.75 Hz), 3.83 (6 H, s, 2 x OCH_3), 3.9 (5 H, m, 1 x OCH_3, 1 x $OC\underline{H}_2CH$-O), 4.51 (1 H, m, CHOSi), 6.31 (1 H, d, ArH, *J*=9 Hz), 6.48 (1 H, d, ArH, *J*=9 Hz), 7.37-7.75 (10 H, m, 10 × ArH)

^{13}C NMR (101 MHz, CHLOROFORM-*d*) δ_C ppm : 19.3 ($\underline{C}(CH_3)_3$), 26.9 ($C(\underline{C}H_3)_3$), 39.4 ($\underline{C}H_2COOH$), 56.4 (OCH_3), 61.2 (OCH_3), 61.2 (OCH_3), 68.6 (CHO-Si), 72.2 ($O\underline{C}H_2CH$-O), 106.5 (ArCH), 108.7 (ArCH), 127.6 (ArCH), 127.73 (ArCH), 129.81 (ArCH), 129.9 (ArCH), 133.08 (ArC), 133.56 (ArC), 135.84 (ArCH), 135.92 (ArCH), 143.37 (ArC), 144.0 (ArC), 146.59 (ArC), 148.18 (ArC), 176.99 (COOH)

ν_{max} cm^{-1} : 2925.3, 2848.3, 1710.6

HRMS : calculated 524.2230, found 523.1917 ($M - H^+$), 547.2124 ($M + Na^+$)

Synthesis of 3-[(*tert*-butyldiphenylsilyl)oxy]-7,8,9-trimethoxy-2,3,4,5-tetrahydro-1-benzoxepin-5-one *(2.10)*

To acid ***(2.09)*** (0.50 g, 0.953 mmoles) in dry DCM (4 mL) and dry DMF (2-3 drops) under nitrogen was added oxalyl chloride (2.5 mL, 2 M in DCM) dropwise at 0 °C. After a period of 2 h, solvents were evaporated over 2-3 h. The resulting acyl chloride intermediate was then redissolved in dry DCM (10 mL) and cooled to -10 °C under a nitrogen atmosphere. Tin (IV) chloride solution (0.92 mL, 1M in DCM) was then added and the mixture was allowed to react for 30 min. The reaction was quenched with brine and then extracted with ether (3 x 50 mL). After drying with magnesium sulphate and subsequent evaporation the mixture was then purified by column chromatography (5:1 hexane : ethyl acetate) to yield cyclised ketone ***(2.10)*** (0.37 g, 0.00073, 77%) as a yellow-brown oil.

^{1}H NMR (400 MHz, CHLOROFORM-*d*) δ_H ppm : 1.06 (9 H, s, $C(CH_3)_3$), 3.08 (2 H, m, $CH_2C=O$), 3.88 (3 H, s, OCH_3), 3.92 (3 H, s, OCH_3), 3.99 (3 H, s, OCH_3), 4.05-4.19 (2 H, m, C-O$\underline{CH_2}$CHO), 4.48 (1 H, m, CHO-Si), 7.14 (1 H, s, ArH), 7.38-7.75 (10 H, m, 10 × ArH)

^{13}C NMR (101 MHz, CHLOROFORM-*d*) δ_C ppm : 18.7 ($\underline{C}(CH_3)_3$), 26.3 ($C(\underline{C}H_3)_3$), 49.3 ($\underline{C}H_2C=O$), 55.7 (OCH_3), 60.8 (OCH_3), 61.4 (OCH_3), 70.5 (CHO-Si), 78.3 ($O\underline{C}H_2CH$-O), 104.8 (ArCH), 123.6 (ArC), 127.3 (ArCH), 127.4 (ArCH), 129.5 (ArCH), 129.6 (ArCH), 132.6 (ArC), 132.9 (ArC), 135.2 (ArCH), 135.4 (ArCH), 144.2 (ArC), 146.8 (ArC), 148.2 (ArC), 151.8 (ArC), 195.1 (C=O)

ν_{max} cm^{-1} : 2931.6, 2858.3, 1675.2, 1591.4, 1109.7

HRMS : calculated 506.2125, found 507.2172 ($M + H^+$), 529.1692 ($M + Na^+$)

Synthesis of intermediate 5-bromo-2-methoxyphenyl formate *(2.11)*

To a solution of 5-bromo-2-methoxy anisaldehyde (10.00 g, 0.0465 moles) in DCM (40 mL) was added *m*CPBA (12.50 g, 77 % purity, 0.0558 moles) in DCM (80 mL) and the reagents stirred at 0 °C overnight. The reaction was then filtered through paper with DCM to remove *m*CPBA

precipitate before the filtrate was concentrated *in vacuo*. The resultant fraction was then washed with aq. $NaHCO_3$ solution (3 x 250 mL, 5%), water (250 mL) and saturated NaCl solution (250 mL) sequentially. The organic layer was then dried with $MgSO_4$ and concentrated to afford a brown oil (2.11) (10.05 g, 0.041 moles, 88%).

^{1}H NMR (400 MHz, CHLOROFORM-*d*) δ_H ppm : 3.95 (3 H, s, OCH_3), 6.92 (1 H, d, ArH, *J*=8.78 Hz), 7.65 (1 H, dd, ArH, *J*=8.91, 2.64 Hz), 7.93 (1 H, d, ArH, *J*=2.51 Hz), 10.40 (1 H, s, CHO)

^{13}C NMR (400 MHz, CHLOROFORM-*d*) δ_C ppm : 56.0 (OCH_3), 113.5 (ArCBr), 113.8 (ArCH), 126.1 (ArC), 131.0 (ArCH), 138.3 (ArCH), 160.8 (ArC), 188.4 (C=O)

ν_{max} cm^{-1} : 2971.1, 2832.6, 2549.4, 1677.0, 1415.9, 1276.8, 898.8

Synthesis of intermediate 5-bromo-2-methoxyphenol *(2.12)*

Formate ester ***(2.11)*** (10.05 g, 0.041 moles) was dissolved in MeOH (50 mL) and THF (30 mL) at 0 °C. Aq. NaOH solution (50 mL, 2.5 M) was then added and allowed to stir overnight. The organic solvents were then removed *in vacuo* and the reaction acidified with aq. HCl solution (50 mL, 2 M). The reaction was then extracted with diethyl ether (3 × 100 mL), dried with $MgSO_4$ and concentrated *in vacuo* to afford phenol ***(2.12)*** as a yellow solid (6.61 g, 0.0326 moles, 80%).

^{1}H NMR (400 MHz, CHLOROFORM-*d*) δ_H ppm : 3.78 (3 H, s, OCH_3), 6.61 (1 H, d, ArH, *J*= 8 Hz), 6.91 (1 H, d, ArH, *J*= 8 Hz), 7.03 (1 H, s, ArH).

^{13}C NMR (101 MHz, CHLOROFORM-*d*) δ_C ppm : 55.8 (OCH_3), 111.3 (ArCH), 112.8 (ArCH), 117.1 (ArCH), 112.1 (ArCH), 145.5 (ArC), 146.3 (ArC)

ν_{max} cm^{-1} : 3285.4, 1629.1, 1248.9, 685.9

HRMS: calculated 201.9629, found 224.9666 ($M + Na^+$)

Mp : 60-62 °C

Synthesis of intermediate 5-bromo-2-methoxyphenoxy(*tert*-butyl)dimethylsilane *(2.13)*

Phenol ***(2.12)*** (6.61 g, 0.0326 moles) stirred in dry DMF (50 mL), imidazole (3.54 g, 0.052 moles) and *tert*-butyl dimethylchloro silane (7.35 g, 0.0488 moles) under an atmosphere of nitrogen

overnight. The reaction was quenched with brine (50 mL), extracted with ether (3 × 100 mL) and dried with magnesium sulphate. After purification via column chromatography (6:1, hexane : ethyl acetate), silyl ether ***(2.15)*** (8.816 g, 0.0278 moles, 86%) was obtained as a colourless viscous oil.

^{1}H NMR (400 MHz, CHLOROFORM-*d*) δ_H ppm : 0.18 (6 H, s, 2 x $SiCH_3$), 1.102 (9 H, s, 3 x $C(CH_3)_3$), 3.803 (3 H, s, OCH_3), 6.73 (1 H, d, ArH, *J*=9 Hz), 7.0 (1 H, d, ArH, *J*=2.5 Hz), 7.04 (1 H, dd, ArH, *J*=9, 2.5 Hz).

^{13}C NMR (101 MHz, CHLOROFORM-*d*) δ_C ppm : -5.14 (2 × $Si(CH_3)$), 17.97 ($\underline{C}(CH_3)_3$), 25.2 ($C(\underline{C}H_3)_3$), 55.13 (OCH_3), 111.87 (ArCBr), 112.71 (ArCH), 123.61 (ArCH), 123.95 (ArCH), 145.49 (ArC) 149.97 (ArC)

ν_{max} cm^{-1} 3031.7, 1625.5, 1260.6, 689.8

HRMS : calculated 316.0494, found 339.0422 ($M + Na^+$)

Synthesis of intermediate 3-hydroxy-7,8,9-trimethoxy-3,4-dihydro-2H-1-benzoxepin-5-one *(2.14)*

Silyl ether ***(2.10)*** (1.21 g, 0.00239 moles) was dissolved in anhydrous THF (20 mL) at 0 °C under an atmosphere of nitrogen. To this, tetrabutylammonium fluoride (2.63 mL, 1 M solution in THF, 0.00263 moles) was added dropwise and the reaction monitored by TLC (approx 3 h). Upon completion dry silica was added to the reaction mixture, solvents evaporated at low temperature and the resulting powder loaded and run through a pre-packed silica column (1:1, hexane : ethyl acetate) to afford keto-alcohol ***(2.14)*** (0.26 g, 0.97 mmoles, 41%) as a dark mahogany-brown oil.

^{1}H NMR (400 MHz, CHLOROFORM-*d*) δ_H ppm : 3.19 (2 H, ddd, $CH_2C=O$, *J*=55.5, 12, 5.5 Hz), 3.88 (3 H, s, OCH_3), 3.96 (3 H, s, OCH_3), 4.00 (3 H, s, OCH_3), 4.22 (2 H, ddd, OCH_2, *J*=65, 14.5, 7.15 Hz), 4.49 - 4.57 (1 H, m, $C\underline{H}OH$), 7.12 (1 H, s, ArH)

^{13}C NMR (101 MHz, CHLOROFORM-*d*) δ_C ppm : 50.4 ($\underline{C}H_2C=O$), 56.2 (OCH_3), 61.3 (OCH_3), 61.8 (OCH_3), 70.1 (COH), 80.1 (OCH_2), 105.3 (ArCH), 123.3 (ArH), 144.5 (ArC), 147.5 (ArC), 148.7 (ArC), 152.5 (ArC), 195.2 (C=O)

ν_{max} cm^{-1} : 3367.8, 2939.4, 1657.7, 1592.9

HRMS : calculated 268.0947, 269.1013 ($M + H^+$), 291.0842 ($M + Na^+$)

Synthesis of intermediate 5-{3-[(*tert*-butyldimethylsilyl)oxy]-4-methoxyphenyl}-7,8,9-trimethoxy-2,3-dihydro-1-benzoxepin-3-ol *(2.15)*

To a stirred solution of C-ring ***(2.13)*** (0.85 g, 0.0027 moles) in dry THF (5 mL) was added dropwise *n*-butyllithium (1.1 mL, 0.0027 moles, 2.5 M solution in hexanes) at -78 °C under an atmosphere of nitrogen. After 40 min, hydroxy-ketone ***(2.14)*** (0.24 g, 0.885 mmoles) in THF (5 mL) was introduced to the reaction dropwise at -78 °C, and the reaction allowed proceed for 3 h. The reaction was then allowed to reach 0 °C and left at this temperature overnight, after which the reaction was quenched with aq. HCl solution (50 mL, 1 M) and quickly extracted with diethyl ether (3 × 50 mL). Monitored by TLC, when adequate conversion to the desired alcoholic compound was complete the organic phase was dried with $MgSO_4$, filtered and condensed on a rotary evaporator at low temperature (max 30 °C). The crude sample was then purified via flash column chromatography (3:1, hexane : ethyl acetate) to isolate enol ***(2.15)*** (0.28 g, 0.573 mmoles, 64%) as an orange oil.

^{1}H NMR (400 MHz, CHLOROFORM-*d*) δ_H ppm : 0.18 (6 H, s, 2 × $SiCH_3$), 1.01 (9 H, s, $C(CH_3)_3$), 3.59 (3 H, s, OCH_3), 3.86 (3 H, s, OCH_3), 3.95 (3 H, s, OCH_3), 4.00 (3 H, s, OCH_3), 4.06 - 4.58 (2 H, ddd, CH_2, *J*=194, 12, 2.85 Hz), 4.45 - 4.53 (1 H, m, C<u>H</u>OH), , 6.13 (1 H, dd, *J*=4.75, 1.15 Hz), 6.27 (1 H, s, ArH), 6.81 (1 H, m, ArH), 6.82 - 6.85 (2 H, m, ArH)

^{13}C NMR (101 MHz, CHLOROFORM-*d*) δ_C ppm : -4.6 (2 × $SiCH_3$), 18.5 (<u>C</u>$(CH_3)_3$), 25.7 ($C(\underline{C}H_3)_3$), 55.5 (OCH_3), 56.0 (OCH_3), 61.3 (OCH_3), 61.9 (OCH_3), 70.5 (CHOH), 78.9 (CH_2), 109.7 (ArCH), 111.4 (ArCH), 121.9 (ArCH), 122.5 (ArCH), 125.7 (ArC), 130.6 (C=<u>C</u>H), 136.2 (ArC), 139.0 (ArC), 142.6 (ArC), 144.5 (ArC), 145.2 (<u>C</u>=CH), 148.1 (ArC), 148.2 (ArC), 150.5 (ArC)

ν_{max} cm^{-1} : 3490.4, 2892.5, 1623.8, 1253.8

HRMS : calculated 488.2230, found 489.2291 ($M + H^+$)

Synthesis of intermediate 5-{3-[(*tert*-butyldimethylsilyl)oxy]-4-methoxyphenyl}-7,8,9-trimethoxy-2H-1-benzoxepin-3-one *(2.16)* with PDC

To a stirred solution of ***(2.15)*** (0.86 g, 0.0018 moles) in anhydrous DMF (10 mL) was added pyridinium dichromate (1.3 g, 0.00352 moles) portion-wise at 0 °C under an atmosphere of nitrogen. After 16 h the reaction was quenched by the addition of water (50 mL) and the product was extracted with diethyl ether (3 × 100 mL). The ether extracts were combined, dried over $MgSO_4$, filtered and concentrated *in vacuo*. The residue was purified by flash column chromatography (1:1 hexane : ethyl acetate) and all homogenous fractions were collected and the solvent was evaporated off to afford ***(2.16)*** as a white solid (0.44 g, 0.91 mmoles, 51%).

^{1}H NMR (400 MHz, CHLOROFORM-*d*) δ_H ppm : 0.18 (6 H, s, 2 × CH_3), 1.01 (9 H, s, $C(CH_3)_3$), 3.63 (3 H, s, OCH_3), 3.88 (3 H, s, OCH_3), 4.00 (3 H, s, OCH_3), 4.02 (3 H, s, OCH_3), 4.65 (2 H, s, CH_2), 6.33 (1 H, s, ArH), 6.44 (1 H, s, C=CH), 6.87 (1 H, d, ArH, *J*=2.10 Hz), 6.89 (1 H, s, ArH), 6.95 (1 H, dd, *J*=8.25, 2.10 Hz)

^{13}C NMR (101 MHz, CHLOROFORM-*d*) δ_C ppm : -5.0 (2 × $SiCH_3$), 18.0 ($\underline{C}(CH_3)_3$), 25.2 ($C(\underline{C}H_3)_3$), 55.0 (OCH_3), 55.7 (OCH_3), 60.9 (OCH_3), 61.5 (OCH_3), 80.7 (CH_2), 109.9 (ArCH), 110.9 (C=$\underline{C}$H), 121.3 (ArCH), 122.6 (ArCH), 125.8 (ArC), 127.5 (ArCH), 133.7 (ArC), 144.2 (ArC), 144.7 (ArC), 144.8 (ArC), 145.0 (ArC), 146.9 (ArC), 148.7 (ArC), 151.5 ($\underline{C}$=CH), 151.6 (ArC), 200.2 (C=O)

ν_{max} cm^{-1} : 2932.8, 1689.8, 1594.2

HRMS : calculated 486.2073, found 509.1949 ($M + Na^+$)

Synthesis of intermediate 5-{3-[(*tert*-butyldimethylsilyl)oxy]-4-methoxyphenyl}-7,8,9-trimethoxy-2H-1-benzoxepin-3-one *(2.16)* with Dess-Martin Periodinane

Enone ***(2.15)*** (1.3 g, 0.00266 moles) was dissolved in DCM (25 mL) at RT. To this Dess-Martin periodinane (1.24 g, 0.00293 moles) was added in one portion and the reaction stirred for 5 min. Upon completion, the reaction was quenched with aq. sodium bicarbonate solution (50 mL, 5%) and extracted with diethyl ether (4 × 50 mL). The organic layer was then dried with $MgSO_4$, filtered and condensed *in vacuo* to give product ***(2.16)*** (1.23 g, 0.00253 moles, 95%) following purification by column chromatography (4:1, hexane : ethyl acetate).

^{1}H NMR (400 MHz, CHLOROFORM-*d*) δ_H ppm : 0.18 (6 H, s, 2 × CH_3), 1.01 (9 H, s, $C(CH_3)_3$), 3.63 (3 H, s, OCH_3), 3.88 (3 H, s, OCH_3), 4.00 (3 H, s, OCH_3), 4.02 (3 H, s, OCH_3), 4.65 (2 H, s, CH_2), 6.33 (1 H, s, ArH), 6.44 (1 H, s, C=CH), 6.87 (1 H, d, ArH, *J*=2.10 Hz), 6.89 (1 H, s, ArH), 6.95 (1 H, dd, *J*=8.25, 2.10 Hz)

^{13}C NMR (101 MHz, CHLOROFORM-*d*) δ_C ppm : -5.0 (2 × $SiCH_3$), 18.0 ($\underline{C}(CH_3)_3$), 25.2 ($C(\underline{C}H_3)_3$), 55.0 (OCH_3), 55.7 (OCH_3), 60.9 (OCH_3), 61.5 (OCH_3), 80.7 (CH_2), 109.9 (ArCH), 110.9 (C=$\underline{C}$H), 121.3 (ArCH), 122.6 (ArCH), 125.8 (ArC), 127.5 (ArCH), 133.7 (ArC), 144.2 (ArC), 144.7 (ArC), 144.8 (ArC), 145.0 (ArC), 146.9 (ArC), 148.7 (ArC), 151.5 ($\underline{C}$=CH), 151.6 (ArC), 200.2 (C=O)

ν_{max} cm^{-1} : 2932.8, 1689.8, 1594.2

HRMS : calculated 486.2073, found 509.1949 ($M + Na^+$)

Synthesis of 5-(3-hydroxy-4-methoxyphenyl)-7,8,9-trimethoxy-2H-1-benzoxepin-3-one *(2.17)* using sodium azide

Silyl ether ***(2.16)*** (0.355 g, 0.73 mmoles) was dissolved in DMF (2 mL) with stirring. To this, sodium azide (0.473 g, 1.73 mmoles) was added and the reaction heated to 60 °C for 5 h. The reaction was then quenched with aq. LiCl solution (50 mL, 5%) and extracted with diethyl ether (3 × 50 mL). The organic layer was then washed with water (3 × 100 mL). The remaining organic layer was then dried with $MgSO_4$, filtered and concentrated *in vacuo*. Purification by flash column chromatography afforded phenol ***(2.17)*** (0.23 g, 0.6205 mmoles, 85%) as a yellow solid.

^{1}H NMR (400 MHz, CHLOROFORM-*d*) δ_H ppm : 3.66 (3 H, s, OCH_3), 3.98 (3 H, s, OCH_3), 4.00 (3 H, s, OCH_3), 4.02 (3 H, s, OCH_3), 4.65 (2 H, s, CH_2), 5.68 (1 H, s, OH), 6.36 (1 H, s, ArH), 6.47 (1 H, s, C=CH), 6.91 (2 H, m, 2 × ArH), 6.96 (1 H, d, ArH, *J*=1.76 Hz)

^{13}C NMR (101 MHz, CHLOROFORM-*d*) δ_C ppm : 56.0 (OCH_3), 56.3 (OCH_3), 61.4 (OCH_3), 61.9 (OCH_3), 81.2 (CH_2), 110.2 (ArCH), 110.4 (ArCH), 115.5 (ArCH), 121.4 (ArCH), 126.1 (ArC), 128.2 (C=$\underline{C}$H), 134.8 (ArC), 144.5 (ArC), 145.2 (ArC), 145.3 (ArC), 147.4 (ArC), 147.5 (ArC), 149.2 (ArC), 151.9 ($\underline{C}$=CH), 200.7 (C=O)

ν_{max} cm^{-1} : 3262.9, 2936.9, 2834.5, 1728.0, 1642.4, 1491.9, 1452.7, 1265.9, 1082.1, 955.9

HRMS : calculated 372.1209, found 373.1282 ($M + H^+$)

MP : 151 – 153 °C

Synthesis of 5-(3-hydroxy-4-methoxyphenyl)-7,8,9-trimethoxy-2H-1-benzoxepin-3-one *(2.17)* using TBAF

Silyl ether ***(2.16)*** (0.51 g, 0.00105 moles) was dissolved in anhydrous THF (10 mL) under an atmosphere of nitrogen at 0 °C. Tetrabutylammonium fluoride (1.15 mL, 0.00115 moles, 1 M in THF) was then added dropwise and the reaction stirred for 5 min. Upon completion dry silica was added to the reaction mixture, solvents evaporated at low temperature and the resulting powder loaded and run through a pre-packed silica column (1:1, hexane : ethyl acetate) to afford phenol ***(2.17)*** (0.36 g, 0.966 mmoles, 92%) as a canary yellow solid.

^{1}H NMR (400 MHz, CHLOROFORM-*d*) δ_H ppm : 3.66 (3 H, s, OCH_3), 3.98 (3 H, s, OCH_3), 4.00 (3 H, s, OCH_3), 4.02 (3 H, s, OCH_3), 4.65 (2 H, s, CH_2), 5.68 (1 H, s, OH), 6.36 (1 H, s, ArH), 6.47 (1 H, s, C=CH), 6.91 (2 H, m, 2 × ArH), 6.96 (1 H, d, ArH, *J*=1.76 Hz)

^{13}C NMR (101 MHz, CHLOROFORM-*d*) δ_H ppm : 56.0 (OCH_3), 56.3 (OCH_3), 61.4 (OCH_3), 61.9 (OCH_3), 81.2 (CH_2), 110.2 (ArCH), 110.4 (ArCH), 115.5 (ArCH), 121.4 (ArCH), 126.1 (ArC), 128.2 (C=<u>C</u>H), 134.8 (ArC), 144.5 (ArC), 145.2 (ArC), 145.3 (ArC), 147.4 (ArC), 147.5 (ArC), 149.2 (ArC), 151.9 (<u>C</u>=CH), 200.7 (C=O)

ν_{max} cm^{-1} : 3298.1, 2936.7, 2834.5, 1643.8, 1452.7, 1265.9, 1122.6

HRMS : calculated 372.1209, found 373.1282 ($M + H^+$)

MP : 151 – 153 °C

Synthesis of 7,8,9-trimethoxy-5-(4-methoxyphenyl)-2,3-dihydro-1-benzoxepin-3-ol *(2.18)*

Bromoanisole (2.54 g, 0.0136 moles) was dissolved in dry THF (15 mL) in a 3-necked round bottom flask at -78 °C under an atmosphere of nitrogen. Butyllithium (5.44 mL, 0.0136 moles, 2.5 M in hexanes) was added dropwise and the reaction allowed to stir at -78 °C for 40 min. Separately, 3-hydroxy-7,8,9-trimethoxy-3,4-dihydro-2H-1-benzoxepin-5-one (0.73 g, 2.72 mmoles) was dissolved in dry THF (10 mL) and then added to the reaction mixture in the 3-necked round bottom flask. After 4 h at -78 °C, the reaction was allowed to reach 0 °C and left stirring at this temperature overnight. The reaction was then washed with aq. HCl solution (50 mL, 1 M) and quickly extracted with diethyl ether (4 × 50 mL). After drying with $MgSO_4$, the reaction was concentrated under reduced pressure and purified by column chromatography (2:1, hexane : ethyl acetate) to afford alcohol ***(2.18)*** (0.35 g, 0.98 mmoles, 36%) as a yellow solid.

^{1}H NMR (400 MHz, CHLOROFORM-*d*) δ_H ppm : 3.59 (3 H, s, OCH_3), 3.86 (3 H, s, OCH_3), 3.95 (3 H, s, OCH_3), 3.99 (3 H, s, OCH_3), 4.11 – 4.56 (2 H, ddd, CH_2, *J*=180, 11.7, 2.9 Hz), 4.32 - 4.46 (1 H, m, C<u>H</u>OH), 4.49 (1 H, br. s., OH), 6.15 (1 H, d, CH=C, *J*=5.1 Hz), 6.26 (1 H, s, ArH), 6.90 (2 H, d, ArH, *J*=8.8 Hz), 7.22 (2 H, d, ArH, *J*=8.8 Hz)

^{13}C NMR (101 MHz, CHLOROFORM-*d*) δ_C ppm : 55.3 (OCH_3), 56.0 (OCH_3), 61.2 (OCH_3), 61.8 (OCH_3), 70.4 (COH), 79.2 (CH_2), 109.6 (ArCH), 113.4 (2 × ArCH), 125.7 (ArC), 130.2 (2 × ArCH), 130.8 (<u>C</u>H=C), 135.7 (ArC), 138.8 (ArC), 142.6 (ArC), 145.2 (<u>C</u>=CH), 148.1 (ArC), 148.2 (ArC), 158.9 (ArC)

ν_{max} cm^{-1} : 3484.8, 2935.3, 1572.9, 1509.7, 1248.1, 905.7, 730.3

HRMS : calculated 358.1416, found 381.1333 (M + Na^+)

Mp : 222 °C (decomposition)

Synthesis of 7,8,9-trimethoxy-5-(4-methoxyphenyl)-2H-1-benzoxepin-3-one *(2.19)*

Alcohol ***(2.18)*** (0.23 g, 0.642 mmoles) was dissolved in DCM (10 mL) and Dess-Martin periodinane (0.42 g, 0.99 mmoles) was added. The reaction was stirred at RT for 5 min. The reaction was then quenched with aq. sodium bicarbonate solution (50 mL, 5%) and extracted with diethyl ether (4 × 50 mL). The organic layer was then dried with $MgSO_4$, filtered and condensed to give product ***(2.19)*** (0.21 g, 0.578 mmoles, 90%) which was obtained in pure form, without column chromatography, as a yellow solid.

^{1}H NMR (400 MHz, CHLOROFORM-*d*) δ_H ppm : 3.64 (3 H, s, OCH_3), 3.89 (3 H, s, OCH_3), 4.00 (3 H, s, OCH_3), 4.02 (3 H, s, OCH_3), 4.66 (2 H, s, CH_2), 6.33 (1 H, s, CH=C), 6.48 (1 H, s, ArH), 6.95 (2 H, d, 2 × ArH, *J*=8.5 Hz), 7.33 (2 H, d, 2 × ArH, *J*=8.5 Hz)

^{13}C NMR (101 MHz, CHLOROFORM-*d*) δ_C ppm : 54.9 (OCH_3), 55.7 (OCH_3), 60.9 (OCH_3), 61.5 (OCH_3), 80.8 (CH_2), 109.9 (ArCH), 113.3 (2 × ArCH), 127.6 (<u>C</u>H=C), 128.8 (ArC), 130.2 (2 × ArCH), 133.3 (ArC), 144.1 (ArC), 144.8 (ArC), 147.0 (ArC), 148.7 (<u>C</u>=CH), 151.5 (ArC), 160.1 (ArC), 200.2 (C=O)

ν_{max} cm^{-1} : 2938.0, 1659.7, 1604.9, 1510.1, 1491.5

HRMS : calculated 356.1260, found 357.1328 (M + H^+); 379.1144 (M + Na^+)

Synthesis of intermediate 4-bromo-1-methoxy-2-nitrobenzene *(2.20)*

4-Bromo-2-nitrophenol (25.00 g, 0.115 moles) was dissolved in acetone (300 mL), and iodomethane (71.4 mL, 162.00 g, 1.147 moles) as added, followed by potassium carbonate (47.70 g, 0.345 moles). The reaction mixture was stirred and refluxed for 3 h. Solvent volume was reduced *in vacuo* and quenched with aq. HCl (200 mL). Additional water (100 mL) was added to ensure full solvation of K_2CO_3. After extraction with diethyl ether (3 × 250 mL), the combined organic layers were dried with $MgSO_4$, filtered and concentrated *in vacuo*. Following purification by column chromatography (9:1, hexane : ethyl acetate), anisole compound ***(2.20)*** (25.15 g, 0.108 moles, 94%) was isolated as a white solid.

^{1}H NMR (400 MHz, CHLOROFORM-*d*) δ_H ppm : 3.98 (3 H, s, OCH_3), 7.01 (1 H, d, ArH, *J*=10 Hz), 7.68 (1 H, d, *J*=2.5 Hz), 8.02 (1 H, s, ArH)

^{13}C NMR (101 MHz, CHLOROFORM-*d*) δ_C ppm : 56.7 (OCH_3), 112.2 (ArC), 115.6 (ArCH), 129.0 (ArCH), 130.5 (ArC), 136.8 (ArCH), 152.0 (ArC)

ν_{max}: 1604.2, 1516.7,1343.7, 1148.5

HRMS : calculated 230.9531, found 253.9424 ($M + Na^+$)

Mp : 90-91 °C

Synthesis of intermediate 5-bromo-2-methoxyaniline *(2.21)*

Nitrobenzene compound ***(2.20)*** (15.00 g, 0.065 moles) was dissolved in EtOH (450 mL) at RT before conc. HCl (225 mL) was carefully added, followed by tin powder (15 g). After 5 h, solvent volume was reduced *in vacuo*, and the resulting oil stirred and cooled to 0 °C using an ice bath. To the reaction mixture NaOH (350 mL, 2.5 M) was slowly introduced. The reaction was then extracted with DCM (3 × 300 mL), dried with $MgSO_4$, filtered and condensed under reduced pressure. The crude extract was then purified by column chromatography (6:1, hexane : ethyl acetate) to afford aniline ***(2.21)*** (11.26 g, 0.0557 moles, 86%) as a white solid.

^{1}H NMR (400 MHz, CHLOROFORM-*d*) δ_H ppm : 3.85 (3 H, s, OCH_3), 6.66 (1 H, d, ArH, *J*=7.5 Hz), 6.84 (1 H, d, ArH, *J*=2.5), 6.88 (1 H, s, ArH), 7.84 (2 H, br. S, NH_2)

^{13}C NMR (101 MHz, CHLOROFORM-*d*) δ_C ppm : 55.0 (OCH_3), 111.3 (ArCH), 112.9 (ArC), 117.3 (ArCH), 120.4 (ArCH), 137.4 (ArC), 146.2 (ArC)

ν_{max}: 3472.25, 3380.57, 3003.91, 2959.8, 2906.88, 2837.18, 1611.33, 1502.16, 1221.28

HRMS : calculated 200.9789, found 201.9863 ($M + H^+$)

Mp : 88-90 °C

Synthesis of intermediate *tert*-butyl N-(5-bromo-2-methoxyphenyl)carbamate *(2.22)*

Aniline compound ***(2.21)*** (11.26 g, 0.0557 moles), di-*tert*-butyl dicarbonate (24.33 g, 0.1114 moles) and anhydrous THF (150 mL) were stirred together under an atmosphere of nitrogen. The reaction mixture was refluxed gently over the course of 2 working days. Upon completion, validated by TLC, the reaction was quenched with brine (100 mL) and the organic solvent volume reduced *in vacuo*. The mixture was then extracted with diethyl ether (3 × 100 mL) before drying with $MgSO_4$, filtration and evaporation under reduced pressure. After purification by flash column chromatography (10:1, hexane : ethyl acetate), Boc-protected aniline ***(2.22)*** (15.98 g, 0.0053 moles, 95%) was isolated as a white solid.

^{1}H NMR (400 MHz, CHLOROFORM-*d*) δ_H ppm : 1.55 (9 H, s, $C(CH_3)_3$), 3.86 (3 H, s, OCH_3), 6.70 (1 H, s, ArH), 6.72 (1 H, s, ArH), 7.08 (1 H, dd, ArH, *J*=8.78, 2.26 Hz), 8.31 (1 H, br. s., NH_2)

^{13}C NMR (101 MHz, CHLOROFORM-*d*) δ_C ppm : 27.0 ($C(\underline{C}H_3)_3$), 56.1 (OCH_3), 79.9 ($\underline{C}(CH_3)_3$), 111.1 (ArCH), 114.2 (ArC), 120.8 (ArCH), 124.6 (ArCH), 129.0 (ArC), 146.3 (ArC), 152.3 (C=O)

ν_{max}: 3079.2, 1632.32, 1501.7, 1409.0

HRMS : calculated 301.0314, 302.0698 ($M + H^+$)

Mp : 75-78 °C

Synthesis of *tert*-butyl N-[2-methoxy-5-(tetramethyl-1,3,2-dioxaborolan-2-yl)phenyl]carbamate, *(2.23)*

In a three necked round bottom flask was stirred potassium acetate (1.55 g, 0.0158 moles), [1,1'-Bis(diphenylphosphino)ferrocene] dichloropalladium(II) (1.47 g, 0.000159 moles) and

bis(pinacolate)diboron (1.47 g, 0.00579 moles) under an atmosphere of nitrogen. To this *tert*-butyl N-(5-bromo-2-methoxyphenyl)carbamate ***(2.22)*** (1.59 g, 0.0053 moles) in DMSO (30 mL) was added and the reaction heated to 80 °C for 6 h, then left stirring at RT overnight. The reaction was extracted between diethyl ether (100 mL) and water (100 mL). The palladium species were then filtered through paper and the remaining organic layer dried with magnesium sulphate before being condensed *in vacuo*. Purification by column chromatography (12:1, hexane : ethyl acetate) afforded boronic ester ***(2.23)*** (0.45 g, 0.0012 moles, 76%) as a white-pink solid.

^{1}H NMR (400 MHz, CHLOROFORM-*d*) δ_H ppm : 1.28 (12 H, s, 4 × CH_3), 1.49 (9 H, s, 3 × $C(CH_3)_3$), 3.85 (3 H, s, OCH_3), 6.81 (1 H, d, ArH, *J*= 8 Hz), 7.0 (1 H, s, ArH), 7.42 (1 H, dd, ArH, *J*= 4.9, 1.3 Hz), 8.42 (1 H, br. s., NH)

^{13}C NMR (400 MHz, CHLOROFORM-*d*) δ_C ppm : 24.8 (4 × CH_3), 28.3 ($C(\underline{C}H_3)_3$), 55.5 (OCH_3), 74.9 ($\underline{C}(CH_3)_3$), 80.0 (2 × $\underline{C}(CH_3)_2COB$), 109.2 (ArCH), 124.0 (ArC), 127.5 (ArC), 129.8 (2 × ArCH), 150.0 ($Ar\underline{C}$-OCH_3), 152.6 (C=O)

ν_{max}: 3052.2, 1628.3, 1432.0, 1178.5, 1118.4

HRMS : calculated 349.2061, found 348.1989 ($M - H^+$)

Mp : 105 °C

Synthesis of 7,8,9-trimethoxy-3-[(2,3,3-trimethylbutan-2-yl)oxy]-2,3-dihydro-1-benzoxepin-5-yl trifluoromethanesulfonate *(2.24)*

Diisopropylamine (0.307 g, 0.43 mL, 0.0035 moles) was dissolved in anhydrous THF (5 mL) in a clean, dry 3-necked round bottomed flask, and cooled to -78 °C under an atmosphere of nitrogen. *n*-Butyllithium (1.22 mL, 0.00305 moles, 2.5 M in hexanes) was then added dropwise and left to react for 20 min, maintaining a clear, homogenous solution with additional anhydrous THF if necessary. Ketone ***(2.10)*** (1.03 g, 0.00203 moles) was dissolved separately in anhydrous THF (10 mL) before this mixture was transferred to the reaction mixture in the 3 necked round bottomed flask. This reaction was left stirring at -78 °C for 2 h. 2-[*N,N*-Bis(trifluoromethylsulfonyl)amino]-5-chloropyridine (1.60 g, 0.0041 moles) was dissolved separately in anhydrous THF (10 mL) and added to the reaction mixture. After 3 h, the reaction was quenched with water (50 mL) and extracted with diethyl ether (3 × 50 mL). The combined

organic layers were then dried with $MgSO_4$, filtered and condensed *in vacuo*. Purification by column chromatography (8:1, hexane : ethyl acetate) left triflate ***(2.24)*** (0.65 g, 0.00102 moles, 50%) as a viscous oil.

^{1}H NMR (400 MHz, CHLOROFORM-*d*) δ_H ppm : 1.11 (9 H, s, $C(CH_3)_3$), 3.85 (3 H, s, OCH_3), 3.90 (3 H, s, OCH_3), 3.95 (3 H, s, OCH_3), 4.11 (2 H, ddd, CH_2, *J*=51, 12, 4.5 Hz), 4.68 (1 H, m, CHOSi), 5.97 (1 H, d, C=CH, *J*=4 Hz), 6.82 (1 H, s, ArH), 7.37 - 7.53 (6 H, m, 6 × ArH), 7.69 - 7.76 (4 H, m, 4 × ArH)

^{13}C NMR (101 MHz, CHLOROFORM-*d*) δ_C ppm : 18.8 ($\underline{C}(CH_3)_3$), 26.4 ($C(\underline{C}H_3)_3$), 55.6 (OCH_3), 60.9 (OCH_3), 61.4 (OCH_3), 67.3 (CHOSi), 74.2 (CH_2), 103.8 (C=$\underline{C}$H), 117.0 (ArCH), 124.4 (ArCH), 127.3 (ArCH), 127.5 (4 × ArCH), 129.3 (ArCH), 129.7 (ArCH), 132.3 (ArCH), 134.3 (2 × ArCH), 135.3 (2 × ArC), 135.3 (ArC), 143.0 (ArC), 144.0 (ArC), 146.6 (ArC), 148.3 (ArC)

^{19}F NMR (376 MHz, CHLOROFORM-*d*) δ_F ppm : -74.58 (CF_3)

ν_{max} cm^{-1} : 3512.1, 2946.9, 2830.9, 1723.6, 1557.4, 1253.7, 1034.2

HRMS: calculated 638.1617, found 661.1519 ($M + Na^+$)

Synthesis of intermediate *tert*-butyl N-(5-{3-[(*tert*-butyldiphenylsilyl)oxy]-7,8,9-trimethoxy-2,3-dihydro-1-benzoxepin-5-yl}-2-methoxyphenyl)carbamate *(2.25)*

Triflate ***(2.24)*** (0.65 g, 1.02 mmoles), boronic ester ***(2.23)*** (0.43 g, 1.22 mmoles) and potassium carbonate (0.42 g, 3.05 mmoles) were dissolved in a toluene : ethanol : water mixture (3:1:1, 30 mL). To this biphasic system tetrakis(triphenylphosphine)palladium(0) (59 mg, 50.9 µmoles) was added and the reaction stirred at 60 °C for 40 min. The reaction was then quenched with brine (50 mL) and extracted with ethyl acetate (3 × 50 mL) before being dried with $MgSO_4$ and concentrated *in vacuo*. After column chromatography (3:1, hexane : ethyl acetate), carbamate ***(2.25)*** (0.42 g, 0.597 mmoles, 59%) was obtained as a brown oil.

^{1}H NMR (400 MHz, CHLOROFORM-*d*) δ_H ppm : 1.08 (9 H, s, $(CH_3)_3$), 3.62 (3 H, s, OCH_3), 3.86 (3 H, s, OCH_3), 3.90 (3 H, s, OCH_3), 3.91 (3 H, s, OCH_3), 4.34 (2 H, d, CH_2, *J*=6.5 Hz), 4.48 - 4.56 (1 H, m, CHOSi), 6.21 - 6.27 (2 H, m, 1 × CH=C, 1 × ArH), 6.72 - 6.82 (2 H, m, ArH), 7.07 (1 H, s, ArH), 7.35 - 7.46 (6 H, m, ArH), 7.64 - 7.76 (4 H, m, ArH), 8.05 (1 H, br. s., NH)

^{13}C NMR (101 MHz, CHLOROFORM-*d*) δ_C ppm : 18.7 ($\underline{C}(CH_3)_3$), 26.4 ($C(\underline{C}H_3)_3$), 27.9 ($C(\underline{C}H_3)_3$), 55.3 (OCH_3), 55.7 (OCH_3), 59.9 ($\underline{C}(CH_3)_3$), 60.7 (OCH_3), 61.4 (OCH_3), 69.7 (CHOSi), 81.0 (CH_2), 107.4

(ArC), 108.4 (ArCH), 108.9 (CH=C), 110.5 (ArCH), 118.2 (ArCH), 122.4 (ArCH), 127.2 (2 × ArCH), 127.3 (2 × ArCH), 129.3 (ArCH), 129.3 (ArCH), 131.4 (CNH), 133.1 (ArC), 133.2 (ArC), 135.3 (2 × ArCH), 135.4 (2 ×ArCH), 137.1 (ArC), 141.7 (C=C), 145.3 (ArC), 145.4 (ArC), 146.6 (ArC), 147.9 (ArC), 149.5 (ArC), 152.2 (C=O)

ν_{max} cm^{-1} : 3435.4, 2930.3, 2856.9, 2250.9, 1730.5, 1589.9, 1527.9

HRMS : calculated 711.3227, found 712.3320 ($M + H^+$)

Synthesis of intermediate *tert*-butyl N-[5-(3-hydroxy-7,8,9-trimethoxy-2,3-dihydro-1-benzoxepin-5-yl)-2-methoxyphenyl]carbamate *(2.26)*

Silyl ether *tert*-butyl *N*-(5-{3-[(*tert*-butyldiphenylsilyl)oxy]-7,8,9-trimethoxy-2,3-dihydro-1-benzoxepin-5-yl}-2-methoxyphenyl)carbamate ***(2.25)*** (0.63 g, 0.885 mmoles) was dissolved in anhydrous THF (10 mL) under an atmosphere of nitrogen. To this tetrabutylammonium fluoride (1.10 mL, 1.06 mmoles, 1 M) was added dropwise and the reaction cooled to 0 °C. The reaction was monitored by TLC and after 2 h the reaction was loaded directly onto silica and purified by column chromatography (1:1, hexane : ethyl acetate) to afford alcohol ***(2.26)*** (0.41 g, 0.87 mmoles, 98%) as a clear oil.

^{1}H NMR (400 MHz, CHLOROFORM-*d*) δ_H ppm : 1.53 (9 H, s, $(CH_3)_3$), 3.59 (3 H, s, OCH_3), 3.92 (3 H, s, OCH_3), 3.95 (3 H, s, OCH_3), 3.98 (3 H, s, OCH_3), 4.06 – 4.56 (2 H, ddd, CH_2, *J*=196, 12.0, 2.5 Hz), 4.43 - 4.50 (1 H, m, CHOH), 6.17 (1 H, d, CH=C, *J*=4.5 Hz), 6.30 (1 H, s, ArH), 6.83 (2 H, s, ArH), 7.13 (1 H, s, ArH), 8.10 (1 H, br. s., NH).

^{13}C NMR (101 MHz, CHLOROFORM-*d*) δ_C : 27.9 ($C(CH_3)_3$), 55.3 (OCH_3), 55.8 (OCH_3), 60.8 (OCH_3), 61.4 (OCH_3), 70.0 (CHOH), 78.4 (CH_2), 79.9 ($C(CH_3)_3$), 108.8 (ArCH), 109.6 (ArCH), 118.3 (C=CH), 122.7 (ArCH), 125.2 (ArC), 127.3 (ArC), 130.7 (ArCH), 135.9 (ArC), 138.6 (ArC), 142.1 (ArC), 144.6 (ArC), 146.4 (C=CH), 147.7 (ArC), 147.7 (ArC), 152.2 (C=O)

ν_{max} cm^{-1} : 3435.1, 2932.7,2250.1, 1727.34, 1590.3, 1527.5

HRMS : calculated 473.2050, found 496.1962 ($M + Na^+$)

Synthesis of *tert*-butyl N-[2-methoxy-5-(7,8,9-trimethoxy-3-oxo-2H-1-benzoxepin-5-yl)phenyl]carbamate *(2.27)*

Alcohol ***(2.26)*** (0.41 g, 0.87 mmoles) was dissolved in DCM (20 mL) and Dess-Martin periodinane (1.1 g, 2.6 mmoles) was added. The reaction was stirred at RT for 5 min. The reaction was then quenched with aq. sodium hydrogencarbonate solution (50 mL, 5%) and extracted with diethyl ether (4 × 50 mL), dried with $MgSO_4$, filtered and condensed *in vacuo*. Ketone product ***(2.27)*** (0.35 g, 0.742 mmoles, 85%) was eventually obtained following column chromatography (3:1, hexane : ethyl actetate) as a sticky yellow oil.

^{1}H NMR (400 MHz, CHLOROFORM-*d*) δ_H ppm : 1.53 (9 H, s, C($\underline{C}H_3)_3$), 3.65 (3 H, s, OCH_3), 3.95 (3 H, s, OCH_3), 4.00 (3 H, s, OCH_3), 4.01 (3 H, s, OCH_3), 4.64 (2 H, s, CH_2), 6.38 (1 H, s, C=$\underline{C}$H), 6.50 (1 H, s, ArH), 6.88 (1 H, d, ArH, *J*=8.5 Hz), 6.98 (1 H, d, ArH, *J*=7.5 Hz), 7.12 (1 H, s, ArH), 8.16 (1 H, br. s., NH)

^{13}C NMR (101 MHz, CHLOROFORM-*d*) δ_C ppm : 27.9 (C($\underline{C}H_3)_3$), 55.4 (OCH_3), 55.8 (OCH_3), 60.9 (OCH_3), 61.5 (OCH_3), 80.2 ($\underline{C}(CH_3)_3$), 80.5 (CH_2), 109.0 (ArCH), 110.3 (C=$\underline{C}$H), 118.5 (ArCH), 123.2 (ArCH), 125.7 (ArC), 127.6 (ArC), 127.9 (ArCH), 133.9 (ArC), 144.1 (ArC), 144.6 (ArC), 147.1 (ArC), 147.9 (ArC), 148.6 (ArC), 151.7 ($\underline{C}$=CH), 152.1 (Boc-$\underline{C}$=O), 199.9 ($CH_2\underline{C}$=O)

ν_{max} cm^{-1} : 3434.8, 3352.7, 2961.4, 2927.5, 2845.4, 1727.4, 1663.67, 1583.6, 1525.11

HRMS : calculated 471.1893, found 472.1968 ($M + H^+$)

Synthesis of 2-methoxy-5-(7,8,9-trimethoxy-3-oxo-2H-1-benzoxepin-5-yl)anilinium chloride *(2.28)*

To carbamate ***(2.27)*** (15.00 mg, 0.032 mmoles) in a round bottomed flask flushed with nitrogen, was added trifluoroacetic acid in DCM (1:1, 1 mL) and the reaction cooled to 0 °C. After 5 min the reaction was dried, concentrated *in vacuo*. The reaction was then redissolved in diethyl ether (10 mL) and washed with sodium hydrogencarbonate (1 mL). The organic layer was concentrated *in vacuo* and HCl gas blown through, to afford anilinium salt ***(2.28)*** (9.10 mg, 0.022 mmoles, 70%) as a yellow solid.

^{1}H NMR (400 MHz, CHLOROFORM-*d*) δ_H ppm : 3.09 (2 H, s, NH_2), 3.65 (3 H, s, OCH_3), 3.93 (3 H, s, OCH_3), 3.99 (3 H, s, OCH_3), 4.01 (3 H, s, OCH_3), 4.64 (2 H, s, CH_2), 6.40 (1 H, s, ArH), 6.46 (1 H, s, C=CH), 6.72 - 6.84 (3 H, m, 3 × ArH)

^{13}C NMR (101 MHz, CHLOROFORM-*d*) δ_C ppm : 55.1 (OCH_3), 55.8 (OCH_3), 60.9 (OCH_3), 61.5 (OCH_3), 80.7 (CH_2), 109.3 (ArCH), 110.1 (ArCH), 115.1 (C=<u>C</u>H), 119.5 (ArCH), 125.1 (ArC), 125.9 (ArC), 127.4 (ArCH), 133.8 (ArC), 143.9 (ArC), 144.7 (ArC), 146.9 (ArC), 147.8 (ArC), 148.6 (ArC), 152.0 (<u>C</u>=CH), 200.3 (C=O)

ν_{max} cm^{-1} : 3374.4, 2932.5, 2852.9, 1657.4, 1616.6, 1491.5, 1238.1, 1129.5, 1092.8

HRMS : calculated 371.1369, found 372.9862 ($M + H^+$)

MP : 160 °C (decomposition)

Synthesis of intermediate dibenzyl 2-methoxy-5-(7,8,9-trimethoxy-3-oxo-2H-1-benzoxepin-5-yl)phenyl phosphate *(2.29)*

Phenol 5-(3-hydroxy-4-methoxyphenyl)-7,8,9-trimethoxy-2H-1-benzoxepin-3-one ***(2.17)*** (66.00 mg, 0.177 mmoles) and 4-dimethylaminopyridine (1.10 mg, 9 µmoles) were stirred in acetonitrile (3 mL) under an atmosphere of nitrogen and the reaction cooled to -10 °C. Carbon tetrachloride (0.083 mL, 0.0855 mmoles) was then added to the mixture, followed by diisopropylethylamine (0.065 mL, 0.37 mmoles). After 30 min, dibenzylphosphate (0.06 mL, 0.26 mmoles) was subsequently added and the reaction left stirring overnight. The reaction was then worked up with monobasic potassium phosphate (50 mL, 0.5 M) and extracted with diethylether (4 × 50 mL). After concentration under reduced pressure and drying with $MgSO_4$, the reaction was purified by column chromatography (2:1 hexane:ethyl acetate) to afford phosphate ester ***(2.29)*** (72.00 mg, 0.114 mmoles, 65%) as a clear oil.

^{1}H NMR (400 MHz, CHLOROFORM-*d*) δ_H ppm : 3.63 (3 H, s, OCH_3), 3.87 (3 H, s, OCH_3), 3.99 (3 H, s, OCH_3), 4.02 (3 H, s, OCH_3), 4.65 (2 H, s, OCH_2C=O), 5.18 (2 H, s, $POCH_2$), 5.19 (2 H, s, $POCH_2$), 6.30 (1 H, s, C=CH), 6.41 (1 H, s, ArH), 6.97 (1 H, d, ArH, *J*=8.53 Hz), 7.09 (1 H, t, ArH, *J*=3.25 Hz), 7.22 (1 H, d, ArH, *J*=7.53 Hz), 7.34 (10 H, s, 10 × ArH)

^{13}C NMR (101 MHz, CHLOROFORM-*d*) δ_C : 55.5 (OCH_3), 55.8 (OCH_3), 60.9 (OCH_3), 61.5 (OCH_3), 69.5 ($POCH_2$), 69.6 ($POCH_2$), 80.7 (<u>C</u>H_2C=O), 109.6 (C=<u>C</u>H), 111.8 (ArCH), 122.3 (ArCH), 125.2

(ArCH), 126.5 (ArCH), 127.5 (4 × ArCH), 128.0 (ArC), 128.1 (4 × ArCH), 128.2 (2 × ArCH), 133.5 (ArC), 135.0 (ArC), 134.9 (ArC), 138.8 (ArC), 144.2 (ArC), 144.8 (ArC), 146.9 (ArC), 148.8 (ArC), 150.2 (ArC), 151.3 (C=CH), 199.9 (C=O)

^{31}P NMR (162 MHz, CHLOROFORM-*d*) δ_P ppm : -4.70 (P=O)

ν_{max} cm^{-1} : 3478.5, 2926.3, 2854.0, 1660.7, 1513.8, 1455.9, 1270.7, 1014.1, 998.8

HRMS : calculated 632.1811, found 633.1891 ($M + H^+$)

Synthesis of 2-methoxy-5-(7,8,9-trimethoxy-3-oxo-2H-1-benzoxepin-5-yl)phenyl disodium phosphate *(2.31)*

Phosphate ***(2.29)*** (72.00 mg, 0.114 mmoles) was dissolved in anhydrous DCM and cooled to 0 °C. Bromotrimethyl silane (0.031 mL, 0.24 mmoles) was then added dropwise and the reaction was allowed to stir for 1 h. The DCM was then removed *in vacuo*, water (20 mL) added to the flask and the reaction allowed stir overnight. The aqueous layers were then separated with diethyl ether (3 × 30 mL), before the aqueous phase was concentrated *in vacuo*. When dry, the residue was dissolved in MeOH (20 mL) and sodium methoxide (11.00 mg, 0.22 mmoles) added. The resulting mixture was allowed stir overnight. The solvent was then removed *in vacuo* and the resulting residue quickly rinsed with deionised water (3 × 5 mL) to remove the sodium methoxide. Diethyl ether was added (20 mL) and then quickly removed *in vacuo* to encourage crashing out of the salt ***(2.31)*** (54.00 mg, 0.108 moles, 95%) as a pale brown solid.

^{1}H NMR (400 MHz, DMSO-d_6) δ_H ppm : 3.57 (3 H, s, OCH_3), 3.81 (3 H, s, OCH_3), 3.84 (3 H, s, OCH_3), 3.88 (3 H, s, OCH_3), 4.66 (2 H, s, CH_2), 6.32 (1 H, s, ArH), 6.35 (1 H, s, C=CH), 6.93 - 7.13 (3 H, m, 3 × ArH)

^{13}C NMR (101 MHz, DMSO-d_6) δ_C ppm : 55.6 (OCH_3), 55.9 (OCH_3), 60.8 (OCH_3), 61.4 (OCH_3), 80.7 (CH_2), 110.2 (ArCH), 112.2 (ArCH), 120.7 (ArCH), 124.1 (ArCH), 125.3 (ArC), 127.5 (C=CH), 132.5 (ArC), 144.1 (ArC), 144.9 (ArC), 146.9 (ArC), 148.8 (ArC), 150.8 (C=CH), 151.21 (ArC), 151.28 (ArC), 199.8 (C=O)

^{31}P NMR (162 MHz, DMSO-d_6) δ_P ppm : 0.59 (P=O)

ν_{max} cm^{-1} : 3385.9, 2484.0, 2082.4, 1737.4, 1599.4

MP : 208-211 °C, decomposition.

5.3 Experimental for Chapter 3

Synthesis of 2-bromo-5-{3-[(*tert*-butyldimethylsilyl)oxy]-4-methoxyphenyl}-7,8,9-trimethoxy-2H-1-benzoxepin-3-one *(3.01)* with PTAB in ethyl acetate.

To a solution of 5-{3-[(*tert*-butyldimethylsilyl)oxy]-4-methoxyphenyl}-7,8,9-trimethoxy-2H-1-benzoxepin-3-one ***(2.16)*** (50.00 mg, 0.103 mmoles) in ethyl acetate (2 mL) was added H_2SO_4 (2 µL) in ethyl acetate (20 µL). Phenyltrimethylammonium tribromide (39.00 mg, 0.103 mmol) was then added to the stirred solution. After 90 min, the reaction was quenched by the addition of aq. $NaHCO_3$ solution (50 mL, 5% solution) and the product was extracted with ethyl acetate (3 × 50 mL). The combined organic extracts were washed with aq. NaCl solution (50 mL, saturated solution). The organic fraction was dried over $MgSO_4$, filtered and concentrated *in vacuo*. The resulting residue was purified by flash column chromatography (3:1, hexane : ethyl acetate). All homogenous fractions were collected and the solvent was evaporated to afford bromide ***(3.01)*** as a yellow oil (20.00 mg, 0.0355 mmoles, 36%).

^{1}H NMR (400 MHz, DMF-d_7) δ_H ppm: 0.20 (3 H, s, $SiCH_3$), 0.21 (3 H, s, $SiCH_3$), 1.00 (9 H, s, $C(C\underline{H}_3)_3$), 3.71 (3 H, s, OCH_3), 3.95 (3 H, s, OCH_3), 3.97 (3 H, s, OCH_3), 4.00 (3 H, s, OCH_3), 6.44 (1 H, s, ArH), 6.53 (1 H, s, C=CH), 6.95 (1 H, s, CHBr), 7.10 (1 H, d, ArH, *J*=8.5 Hz), 7.17 (1 H, s, ArH), 7.19 (1H, d, *J*=9 Hz, ArH)

^{13}C NMR (101 MHz, DMF-d_7) δ_c ppm: -5.2 (2 × $Si\underline{C}H_3$), 18.1 ($\underline{C}(CH_3)_3$), 25.2 ($C(\underline{C}H_3)_3$), 55.2 (OCH_3), 55.7 (OCH_3), 60.6 (OCH_3), 61.2 (OCH_3), 87.3 ($\underline{C}HBr$), 110.4 (ArCH), 112.0 (ArCH), 121.4 (ArCH), 123.3 (ArCH), 125.4 (C=$\underline{C}$H), 125.9 (ArC), 133.5 (ArC), 141.9 (ArC), 144.5 (ArC), 144.9 (ArC), 150.2 (ArC) 152.2 ($\underline{C}$=CH), 152.3 (ArC), 190.7 (C=O)

ν_{max} cm^{-1} : 2933.9, 1726.0, 1512.3, 1130.7, 838.9

HRMS : calculated 564.1179, found at 587.1044 ($M + Na^+$)

Synthesis of 2-bromo-5-{3-[(*tert*-butyldimethylsilyl)oxy]-4-methoxyphenyl}-7,8,9-trimethoxy-2H-1-benzoxepin-3-one *(3.01)* using PTAB in THF

To a solution of 5-{3-[(*tert*-butyldimethylsilyl)oxy]-4-methoxyphenyl}-7,8,9-trimethoxy-2H-1-benzoxepin-3-one ***(2.16)*** (0.23 g, 0.473 mmoles) in dry THF (3 mL), at room temperature and under an atmosphere of nitrogen, was added dropwise phenyltrimethylammonium tribromide (0.231 g, 0.614 mmoles) in dry THF (3 mL) and the reaction progress monitored by TLC. After approximately 1 h the reaction was quenched with cold water (50 mL) and extracted with diethyl ether (3 × 50 mL) before drying with $MgSO_4$ and concentration under reduced pressure. The reaction mixture was then rapidly purified by column chromatography (3:1 hexane : ethyl acetate) to afford bromide ***(3.01)*** as a viscous yellow oil (0.17 g, 0.301 mmol, 63%).

^{1}H NMR (400 MHz, DMF-d_7) δ_H ppm: 0.20 (3 H, s, $SiCH_3$), 0.21 (3 H, s, $SiCH_3$), 1.00 (9 H, s, $C(C\underline{H}_3)_3$), 3.71 (3 H, s, OCH_3), 3.95 (3 H, s, OCH_3), 3.97 (3 H, s, OCH_3), 4.00 (3 H, s, OCH_3), 6.44 (1 H, s, ArH), 6.53 (1 H, s, C=CH), 6.95 (1 H, s, CHBr), 7.10 (1 H, d, ArH, *J*=8.5 Hz), 7.17 (1 H, s, ArH), 7.19 (1H, d, *J*=9 Hz, ArH)

^{13}C NMR (400 MHz, DMF-d_7) δ_c ppm : -5.2 (2 × $Si\underline{C}H_3$), 18.1 ($\underline{C}(CH_3)_3$), 25.2 ($C(\underline{C}H_3)_3$), 55.2 (OCH_3), 55.7 (OCH_3), 60.6 (OCH_3), 61.2 (OCH_3), 87.3 ($\underline{C}HBr$), 110.4 (ArCH), 112.0 (ArCH), 121.4 (ArCH), 123.3 (ArCH), 125.4 (C=$\underline{C}$H), 125.9 (ArC), 133.5 (ArC), 141.9 (ArC), 144.5 (ArC), 144.9 (ArC), 150.2 (ArC) 152.2 ($\underline{C}$=CH), 152.3 (ArC), 190.7 (C=O)

ν_{max} cm^{-1} : 2933.9, 1726.0, 1512.3, 1130.7, 838.9

HRMS : calculated 564.1179, found at 587.1044 ($M + Na^+$)

Synthesis and NMR study of intermediate 4-{3-[(*tert*-butyldimethylsilyl)oxy]-4-methoxyphenyl}-6,7,8-trimethoxychromen-2-one *(3.02)* and final lead compound 4-(3-hydroxy-4-methoxyphenyl)-6,7,8-trimethoxychromen-2-one *(3.03)* by azide induced ring contraction.

Bromide ***(3.01)*** (24.00 mg, 0.0424 mmoles) was dissolved in deuterated DMF (0.5 mL) and comprehensive control spectra (^{1}H, ^{13}C, DEPT etc) recorded from the NMR spectrometer (600 MHz). Sodium azide (14.00 mg, 0.212 mmoles) was then introduced, the tube swiftly replaced in the NMR spectrometer and new set of spectra immediately recorded at 25 °C. Fresh ^{1}H and ^{13}C spectra were further recorded over regular intervals (every 10 – 20 min), until no discernible

changes could be detected over the course of an hour. At this point, compound was in silyl ether ***(3.02)*** form. New spectra were acquired 24 h, 48 h and 4 weeks after the introduction of sodium azide, where full deprotection of the silyl ether to afford phenol ***(3.03)*** was determined.

4-{3-[(*tert*-butyldimethylsilyl)oxy]-4-methoxyphenyl}-6,7,8-trimethoxychromen-2-one *(3.02)* :

^{1}H NMR (600 MHz, DMF-d_7) □ ppm 0.24 (6 H, s, 2 × $SiCH_3$), 1.02 (9 H, s, $(CH_3)_3$), 3.82 (3 H, s, OCH_3), 3.97 (3 H, s, OCH_3), 3.99 (3 H, s, OCH_3), 4.04 (3 H, s, OCH_3), 6.30 (1 H, s, C=CH), 6.91 (1 H, s, ArH), 7.15 (1 H, d, ArH, *J*=1.51 Hz), 7.24 - 7.30 (2 H, m, 2 × ArH)

13C NMR (151 MHz, DMF-d_7) δC : -5.2 (2 × SiCH3) , 18.1 ($\underline{C}(CH_3)_3$), 25.1 ($C(\underline{C}H_3)_3$), 55.23 (OCH_3), 55.7 (OCH_3), 60.7 (OCH_3), 61.3 (OCH_3), 103.6 (ArCH), 112.5 (C=$\underline{C}$H), 113.0 (ArCH), 114.3 (ArC), 120.6 (ArCH), 122.6 (ArCH), 127.8 (ArC), 141.1 (ArC), 143.1 (ArC), 144.8 (ArC), 145.8 (ArC), 149.6 (ArC), 152.2 (ArC), 155.9 (ArC), 159.7 (C=O)

ν_{max} cm^{-1} : 2916.4, 1725.7, 1260.1, 1091.7

HRMS : calculated 472.1917, found 473.1978 ($M + H^+$)

4-(3-hydroxy-4-methoxyphenyl)-6,7,8-trimethoxychromen-2-one *(3.03)* :

^{1}H NMR (600 MHz, DMF-d_7) δ_H ppm : 3.85 (3 H, s, OCH_3), 3.93 (3 H, s, OCH_3), 3.98 (3 H, s, OCH_3), 4.03 (3 H, s, OCH_3), 6.29 (1 H, s, C=CH), 7.02 (1 H, s, ArH), 7.06 (1 H, dd, ArH, *J*=8.28, 2.26 Hz), 7.17 (1 H, d, ArH, *J*=8.28 Hz), 7.29 (1 H, d, ArH, *J*=2.26 Hz)

^{13}C NMR (151 MHz, DMF-d_7) δ_C ppm : 55.4 (OCH_3), 55.8 (OCH_3), 60.7 (OCH_3), 61.2 (OCH_3), 103.7 (ArCH), 112.2 (C=$\underline{C}$H), 112.5 (ArCH), 114.1 (ArC), 115.7 (ArCH), 119.6 (ArCH), 127.7 (ArC), 142.9 (ArC), 145.6 (ArC), 147.5 (ArC), 149.50 (ArC), 149.55 (ArC), 155.4 ($\underline{C}$=CH), 159.8 (C=O)

ν_{max} cm^{-1} : 3373.5, 2924.3, 1721.5, 1389.1

HRMS : Calculated 358.1053, found 381.0944 ($M + Na^+$)

MP : 152 – 157 °C

Synthesis of intermediate *tert*-butyl N-[5-(2-bromo-7,8,9-trimethoxy-3-oxo-2H-1-benzoxepin-5-yl)-2-methoxyphenyl]carbamate *(3.04)*

To a solution of *tert*-butyl N-[2-methoxy-5-(7,8,9-trimethoxy-3-oxo-2H-1-benzoxepin-5-yl)phenyl]carbamate ***(2.27)*** (0.11 g, 0.233 mmoles) in dry THF (3 mL) at RT, and under an atmosphere of nitrogen, was added dropwise phenyltrimethylammonium tribromide (0.11 g, 0.303 mmoles) in dry THF (3 mL) and the reaction progress monitored by TLC. After approximately 1 h the reaction was quenched with cold water (50 mL) and extracted with diethyl ether (3 × 50 mL) before drying with $MgSO_4$ and concentration under reduced pressure. The reaction mixture was then purified by column chromatography (3:1 hexane : ethyl acetate) to afford *tert*-butyl N-[5-(2-bromo-7,8,9-trimethoxy-3-oxo-2H-1-benzoxepin-5-yl)-2-methoxyphenyl]carbamate ***(3.04)*** as a viscous yellow oil (87 mg, 0.16 mmol, 68%).

^{1}H NMR (400 MHz, CHLOROFORM-*d*) δ_H ppm : 1.54 (9 H, s, $(CH_3)_3$), 3.66 (3H, s, OCH_3), 3.96 (3 H, s, OCH_3), 4.02 (3 H, s, OCH_3), 4.02 (3 H, s, OCH_3), 6.44 (1H, s, ArH), 6.49 (1 H, d, CH=C, *J*=1.00 Hz), 6.72 (1 H, d, CHBr *J*=1.00 Hz), 6.89 (1 H, d, ArH, *J*=8.53 Hz), 6.99 (1 H, dd, ArH *J*=8.53, 2.01 Hz), 7.14 (1 H, s, ArH), 8.17 (1H, br. s, NH)

^{13}C NMR (101 MHz, CHLOROFORM-*d*) δ_C ppm : 27.9 ($C(\underline{C}H_3)_3$), 55.4 (OCH_3), 55.7 (OCH_3), 60.8 (OCH_3), 61.3 (OCH_3), 80.3 ($\underline{C}(CH_3)_3$), 85.8 (CBr), 109.0 (ArCH), 110.2 (ArCH), 118.5 (C=$\underline{C}$H), 123.3 (ArCH), 125.6 (ArC), 125.7 (ArCH), 127.6 (ArC), 133.7 (ArC), 141.8 (ArC), 144.6 (ArC), 145.7 (ArC), 148.0 (ArC), 149.4 (ArC), 152.1 ($\underline{C}$=CH), 152.7 (NC=O), 190.2 (C=O)

ν_{max} cm^{-1} : 3430.5, 2977.8, 2938.9, 2843.8, 1724.9, 1650.7, 1528.5

Ring contraction of 7-membered ketone *tert*-butyl N-[5-(2-bromo-7,8,9-trimethoxy-3-oxo-2H-1-benzoxepin-5-yl)-2-methoxyphenyl]carbamate *(3.04)* to give 6-membered lactone *tert*-butyl 2-methoxy-5-(6,7,8-trimethoxy-2-oxo-2H-chromen-4-yl)phenylcarbamate *(3.05)*

Bromide ***(3.04)*** (18.00 mg, 0.033 mmoles) was dissolved in DMF (5 mL) at room temperature. Sodium azide (10.00 mg, 0.165 mmoles) was then added and the reaction allowed stir while being monitored by TLC. Upon completion the reaction was quenched with water (30 mL) and extracted with ditheyl ether (3 × 30 mL) to give chromenone product ***(3.05)*** (9.00 mg, 0.022 mmoles, 60%) as a yellow oil.

^{1}H NMR (400 MHz, CHLOROFORM-*d*) δ_H ppm : 1.50 (9 H, s, $(CH_3)_3$), 3.80 (3 H, s, OCH_3), 3.96 (3 H, s, OCH_3), 4.01 (3 H, s, OCH_3), 4.04 (3 H, s, OCH_3), 6.31 (1 H, s, C=CH), 6.94 (1 H, s, ArH), 6.98 (1 H, d, ArH, *J*=8.53 Hz), 7.10 (1 H, dd, ArH, *J*=8.03, 2.01 Hz), 7.14 (1 H, s, ArH), 8.31 (1 H, br. s., NH)

^{13}C NMR (101 MHz, CHLOROFORM-*d*) δ_C ppm : 27.7 ($C(\underline{C}H_3)_3$), 55.4 (OCH_3), 55.6 (OCH_3), 60.9 (OCH_3), 61.3 (OCH_3), 80.2 ($\underline{C}(CH_3)_3$), 103.1 (ArCH), 109.8 (ArCH), 112.6 (C=$\underline{C}$H), 113.9 (ArC), 118.0 (ArC), 122.1 (ArCH), 127.4 (ArC), 127.7 (ArC), 140.7 (ArC), 142.7 (ArC), 145.2 (ArC), 148.3 (ArC), 149.1 (ArC), 152.2 ($\underline{C}$=CH), 155.0 (NC=O), 160.4 (C=O)

ν_{max} cm^{-1} : 3452.6, 2939.5, 1724.3, 1530.8, 1390.3

HRMS : calculated 457.1737, found 480.1620 ($M + Na^+$)

Synthesis of 4-(3-amino-4-methoxyphenyl)-6,7,8-trimethoxy-2H-chromen-2-one, *(3.06)*

Boc-protected aniline ***(3.05)*** (97.00 mg, 0.21 mmoles) in a round bottomed flask flushed with nitrogen, was added trifluoroacetic acid in DCM (1:1, 1 mL) and the reaction cooled to 0 °C. After 5 min the reaction was dried; concentrated *in vacuo*. The reaction was then redissolved in diethyl ether (10 mL) and washed with sodium hydrogencarbonate (1 mL). The organic layer was concentrated *in vacuo* and gaseous HCl blown through, to afford anilinium salt compound ***(3.06)*** (49.00 mg, 0.138 mmoles, 68%) was obtained as a white solid.

^1H NMR (400 MHz, CHLOROFORM-*d*) δ_H ppm : 3.05 (2 H, br. s., NH_2), 3.75 (3 H, s, OCH_3), 3.94 (3 H, s, OCH_3), 4.00 (3 H, s, OCH_3), 4.04 (3 H, s, OCH_3), 6.25 (1 H, s, C=CH), 6.79 (1 H, s, ArH), 6.81 (2 H, s, 2 × ArH), 6.9 (1 H, d, ArH, *J*= 8.11 Hz)

^{13}C NMR (101 MHz, CHLOROFORM-*d*) δ_C ppm : 55.6 (OCH_3), 56.4 (OCH_3), 61.5 (OCH_3), 61.9 (OCH_3), 103.6 (ArCH), 110.3 (C=$\underline{C}$H), 113.2 (ArCH), 114.7 (2 × ArC) 118.8 (ArCH), 125.5 (ArCH), 128.2 (ArC), 141.3 (ArC), 143.4 (ArC), 145.8 (ArC), 149.5 (2 × ArC), 155.9 ($\underline{C}$=CH), 160.9 (C=O)

ν_{max} cm^{-1} : 3444.4, 2956.5, 2926.5, 2855.7, 1730.0, 1571.0, 1462.1, 1383.9, 1286.9, 1129.4

HRMS : calculated 357.1717, found 358.2184 ($M + H^+$) and 380.1364 ($M + Na^+$)

MP : 223 – 226 °C

Synthesis of intermediate 2-bromo-7,8,9-trimethoxy-5-(4-methoxyphenyl)-2H-1-benzoxepin-3-one *(3.07)*

To a solution 7,8,9-trimethoxy-5-(4-methoxyphenyl)-2H-1-benzoxepin-3-one ***(2.19)*** (0.18 g, 0.51 mmol) in dry THF (3 mL), at room temperature and under an atmosphere of nitrogen, was added dropwise phenyltrimethylammonium tribromide (0.25 g, 0.66 mmol) in dry THF (3 mL) and the reaction progress monitored by TLC. After approximately 1 h the reaction was quenched with cold water (50 mL) and extracted with diethyl ether (3 × 50 mL) before drying with $MgSO_4$ and concentration under reduced pressure. The reaction mixture was then purified by column chromatography (5:1 hexane:ethyl acetate) to afford bromide 2-bromo-7,8,9-trimethoxy-5-(4-methoxyphenyl)-2H-1-benzoxepin-3-one as a viscous yellow oil ***(3.07)*** (0.15 mg, 0.37 mmol, 72%).

^{1}H NMR (600 MHz, CHLOROFORM-*d*) δ_H ppm : 3.65 (3 H, s, OCH_3), 3.89 (3 H, s, OCH_3), 4.01 (3 H, s, OCH_3), 4.03 (3 H, s, OCH_3), 6.38 (1 H, s, ArH), 6.47 (1 H, d, C=CH, *J*=1.51 Hz), 6.74 (1 H, d, CHBr, *J*=1.51 Hz), 6.97 (2 H, d, 2 × ArH, *J*=8.66 Hz), 7.33 (2 H, d, 2 × ArH, *J*=8.66 Hz)

^{13}C NMR (151 MHz, CHLOROFORM-*d*) δ_C ppm : 55.4 (OCH_3), 56.1 (OCH_3), 61.2 (OCH_3), 61.7 (OCH_3), 86.4 (CHBr), 110.3 (ArCH), 113.8 (2 × ArCH), 125.8 (C=CH), 126.1 (ArC), 130.8 (2 × ArCH), 133.6 (ArC), 142.3 (ArC), 145.0 (ArC), 146.3 (ArC), 149.9 (ArC), 152.8 (C=CH), 160.8 (ArC), 190.8 (C=O)

ν_{max} cm^{-1} : 2940.8, 2840.9, 2253.2, 1652.8, 1604.9

Ring contraction from 7-membered benzoxepinone 2-bromo-7,8,9-trimethoxy-5-(4-methoxyphenyl)-2H-1-benzoxepin-3-one *(3.07)* to 6-membered coumarin 6,7,8-trimethoxy-4-(4-methoxyphenyl)-2H-chromen-2-one *(3.08)*

Bromide ***(3.07)*** (10.00 mg, 0.023 mmoles) was dissolved in DMF (5 mL) at room temperature. Sodium azide (7.00 mg, 0.115 mmoles) was then added and the reaction allowed stir while being monitored by TLC. Upon completion the reaction was quenched with water (30 mL) and extracted with diethyl ether (3 × 30 mL) to give chromenone product ***(3.08)*** (7.00 mg, 0.0205 mmoles, 89%) as a yellow powder.

^{1}H NMR (400 MHz, CHLOROFORM-*d*) δ_H ppm : 3.77 (3 H, s, OCH_3), 3.92 (3 H, s, OCH_3), 4.03 (3 H, s, OCH_3), 4.07 (3 H, s, OCH_3), 6.29 (1 H, s, C=CH), 6.75 (1 H, s, ArH), 7.06 (2 H, d, 2 × ArH, *J*= 8.6 Hz), 7.42 (2 H, d, 2 ×ArH, *J*=8.6 Hz)

^{13}C NMR (101 MHz, CHLOROFORM-*d*) δ_C ppm : 54.9 (OCH_3), 55.8 (OCH_3), 61.1 (OCH_3), 61.5 (OCH_3), 102.8 (ArCH), 113.0 (C=CH), 113.9 (2 × ArCH), 114.1 (ArC), 127.3 (ArC), 129.3 (2 × ArCH), 140.9 (ArC), 142.9 (ArC), 145.4 (ArC), 149.1 (ArC), 154.9 (C=CH), 160.31 (1 × ArC, 1 × C=O)

ν_{max} cm^{-1} : 2938.1, 1659.7, 1604.9, 1510.1, 1491.5

HRMS : calculated 342.1103, found 365.1034 ($M + Na^+$)

MP : 141 - 143 °C

Synthesis of 5-{3-[(*tert*-butyldimethylsilyl)oxy]-4-methoxyphenyl}-3,7,8,9-tetramethoxy-2,3-dihydro-1-benzoxepin-2-one *(3.09)* and 5-(3-hydroxy-4-methoxyphenyl)-3,7,8,9-tetramethoxy-2,3-dihydro-1-benzoxepin-2-one *(3.10)*

2-bromo-5-{3-[(*tert*-butyldimethylsilyl)oxy]-4-methoxyphenyl}-7,8,9-trimethoxy-2,3-dihydro-1-benzoxepin-3-one ***(3.01)*** (0.21 g, 0.371 mmol) was stirred in MeOH (5 mL) at RT and the reaction monitored by thin layer chromatography. After a period of approximately 3 h, the reaction mixture was extracted with diethyl ether (5 × 50 mL) over water (100 mL). The combined organic layers were dried with magnesium sulphate and concentrated under reduced pressure. After purification by column chromatography (2:1 ethyl acetate : hexane) to afford 5-{3-[(*tert*-butyldimethylsilyl)oxy]-4-methoxyphenyl}-3,7,8,9-tetramethoxy-2,3-dihydro-1-benzoxepin-2-one ***(3.09)*** (0.11g, 0.213 mmol, 57%) and 5-(3-hydroxy-4-methoxyphenyl)-3,7,8,9-tetramethoxy-2,3-dihydro-1-benzoxepin-2-one ***(3.10)*** as a viscous clear oils.

5-{3-[(*tert*-butyldimethylsilyl)oxy]-4-methoxyphenyl}-3,7,8,9-tetramethoxy-2,3-dihydro-1-benzoxepin-2-one *(3.09)* :

^1H NMR (400 MHz, CHLOROFORM-*d*) δ_H ppm : 0.19 (6 H, d, 2 × $SiCH_3$), 1.02 (9 H, s, $C(CH_3)_3$), 3.68 (3 H, s, OCH_3), 3.81 (3 H, s, OCH_3), 3.86 (3H, s, OCH_3), 3.97 (3 H, s, OCH_3), 4.05 (3H, s, OCH_3), 5.48 (1 H, d, $CH(OCH_3)$, *J*=5.1 Hz), 5.76 (1 H, d, C=CH, *J*=5.1 Hz), 6.39 (1 H, s, ArH), 6.85 (1 H, d, ArH, *J*=2 Hz), 6.90 (1 H, s, ArH), 6.92 (1 H, d, ArH)

^{13}C NMR (101 MHz, CHLOROFORM-*d*) δ_C ppm : -4.5 (2 × $SiCH_3$), 18.4 ($C(CH_3)_3$), 25.7 ($C(CH_3)_3$), 52.4 ($CH(OCH_3)$), 55.5 (OCH_3), 56.4 (OCH_3), 61.3 (OCH_3), 61.4 (OCH_3), 73.1 ($CH(OCH_3)$), 105.1 (ArCH), 111.8 (ArCH), 115.9 (C=CH), 117.5 (ArC), 121.2 (ArCH), 122.1 (ArCH), 130.1 (ArC), 137.1 (ArC), 141.3 (ArC), 142.3 (ArC), 143.7 (ArC), 144.8 (ArC), 147.3 (C=CH), 151.0 (ArC), 170.3 (C=O)

ν_{max} cm^{-1} : 2932.4, 2856.9, 1756.6, 1509.4

HRMS : calculated 516.2179, found 539.2076 ($M + Na^+$)

5-(3-hydroxy-4-methoxyphenyl)-3,7,8,9-tetramethoxy-2,3-dihydro-1-benzoxepin-2-one *(3.10)* :

^1H NMR (400 MHz, CHLOROFORM-*d*) δ_H ppm : 3.69 (3 H, s, OCH_3), 3.80 (3 H, s, OCH_3), 3.96 (6 H, s, 2 × OCH_3), 4.05 (3 H, s, OCH_3), 5.47 (1 H, d, C<u>H</u>(OCH_3), *J*=5 Hz), 5.67 (1 H, br. s., OH), 5.78 (1 H, s, C=CH, *J*=5 Hz), 6.42 (1 H, s, ArH), 6.88 (2 H, m, 2 × ArH), 6.96 (1 H, d, ArH, *J*=1.5 Hz)

^{13}C NMR (101 MHz, CHLOROFORM-*d*) δ_C ppm : 52.4 (OCH_3), 55.9 (OCH_3), 56.5 (OCH_3), 61.3 (OCH_3), 61.4 (OCH_3), 72.9 (<u>C</u>H(OCH_3)), 105.3 (ArCH), 110.4 (ArCH), 114.9 (ArCH), 115.9 (C=<u>C</u>H), 117.3 (ArC), 120.4 (ArCH), 130.7 (ArC), 137.1 (<u>C</u>=CH), 141.3 (ArC), 142.3 (ArC), 143.8 (ArC), 145.5 (ArC), 146.6 (ArC), 147.2 (ArC), 170.2 (C=O)

ν_{max} cm^{-1} : 3428.9, 2929.4, 1750.4, 1510.7, 1460.4

HRMS : calculated 402.1315, found 425.1352 ($M + Na^+$), 441.1160 ($M + K^+$)

Synthesis of 5-(3-hydroxy-4-methoxyphenyl)-3,7,8,9-tetramethoxy-2,3-dihydro-1-benzoxepin-2-one *(3.10)*

Silyl ether ***(3.09)*** (0.11 g, 0.213 mmoles) was dissolved in anhydrous THF (10 mL) under an atmosphere of nitrogen at 0 °C. Tetrabutylammonium fluoride (0.24 mL, 1 M in THF, 0.234 mmoles) was then added dropwise and the reaction stirred for 5 min. Upon completion dry silica was added to the reaction mixture, solvents evaporated at low temperature and the resulting powder loaded and run through a pre-packed silica column (1:1, hexane : ethyl acetate) to afford phenol ***(3.10)*** (0.06 g, 0.149 mmoles, 64%) as clear oil.

^1H NMR (400 MHz, CHLOROFORM-*d*) δ_H ppm : 3.69 (3 H, s, OCH_3), 3.80 (3 H, s, OCH_3), 3.96 (6 H, s, 2 × OCH_3), 4.05 (3 H, s, OCH_3), 5.47 (1 H, d, C<u>H</u>(OCH_3), *J*=5 Hz), 5.67 (1 H, br. s., OH), 5.78 (1 H, s, C=CH, *J*=5 Hz), 6.42 (1 H, s, ArH), 6.88 (2 H, m, 2 × ArH), 6.96 (1 H, d, ArH, *J*=1.5 Hz)

^{13}C NMR (101 MHz, CHLOROFORM-*d*) δ_C ppm : 52.4 (OCH_3), 55.9 (OCH_3), 56.5 (OCH_3), 61.3 (OCH_3), 61.4 (OCH_3), 72.9 (<u>C</u>H(OCH_3)), 105.3 (ArCH), 110.4 (ArCH), 114.9 (ArCH), 115.9 (C=<u>C</u>H), 117.3 (ArC), 120.4 (ArCH), 130.7 (ArC), 137.1 (<u>C</u>=CH), 141.3 (ArC), 142.3 (ArC), 143.8 (ArC), 145.5 (ArC), 146.6 (ArC), 147.2 (ArC), 170.2 (C=O)

ν_{max} cm^{-1} : 3428.9, 2929.4, 1750.4, 1510.7, 1460.4

HRMS : calculated 402.1315, found 425.1352 ($M + Na^+$), 441.1160 ($M + K^+$)

Synthesis of 3,7,8,9-tetramethoxy-5-(4-methoxyphenyl)-3H-1-benzoxepin-2-one *(3.11)*

Bromide (3.07) (30 mg, 0.08 mmoles) was dissolved in deuterated methanol (0.5 mL) in an NMR tube. ^1H and ^{13}C NMR spectra were run immediately upon insertion into the spectrometer, and repeated over regular intervals (20 min) over 3 h; until no further spectral changes were observed between scans.

^1H NMR (600 MHz, METHANOL-d_4) δ_H ppm : 3.71 (3 H, s, OCH_3), 3.82 (3 H, s, OCH_3), 3.89 (3 H, s, OCH_3), 3.95 (3 H, s, OCH_3), 3.98 (3 H, s, OCH_3), 4.48 (1 H, s, C<u>H</u>OCH_3), 5.79 (1 H, s, C=CH), 6.53 (1 H, s, ArH), 6.99 (2 H, d, 2 × ArH, *J*=8.66 Hz), 7.39 (1 H, d, 2 × ArH, *J*=8.66 Hz)

^{13}C NMR (151 MHz, METHANOL-d_4) δ_C ppm : 53.1 (OCH_3) 54.8 (OCH_3), 55.9 (OCH_3), 60.7 (OCH_3), 60.8 (OCH_3), 72.8 (<u>C</u>HOCH_3), 105.4 (ArCH), 114.0 (2 × ArH), 116.0 (ArC), 116.3 (C=<u>C</u>H), 118.0 (ArC), 129.7 (2 × ArC), 134.1 (ArC), 137.1 (ArC), 141.7 (ArC), 142.3 (ArC), 143.8 (ArC), 147.5 (ArC), 160.2 (<u>C</u>=CH), 170.6 (C=O)

ν_{max} cm^{-1} : 2931.3, 2842.0, 1750.0, 1608.9, 1511.4, 1458.6

HRMS : calculated 386.1366, found 387.1204 ($M + H^+$)

Synthesis of 3-amino-5-{3-[(*tert*-butyldimethylsilyl)oxy]-4-methoxyphenyl}-7,8,9-trimethoxy-2,3-dihydro-1-benzoxepin-2-one *(3.12)*

2-bromo-5-{3-[(*tert*-butyldimethylsilyl)oxy]-4-methoxyphenyl}-7,8,9-trimethoxy-2,3-dihydro-1-benzoxepin-3-one ***(3.01)*** (0.21 g, 0.371 mmol) was stirred with ammonia (0.5 M in dioxane, 3.5 mL, 1.75 mmol) at room temperature for 3 h, after which solvents were removed under reduced pressure. The remaining crude mixture was then loaded onto silica gel and purified via column chromatography (2:1, hexane : ethyl acetate) to afford target compound 2-amino-5-{3-[(*tert*-butyldimethylsilyl)oxy]-4-methoxyphenyl}-7,8,9-trimethoxy-2,3-dihydro-1-benzoxepin-3-one ***(3.12)*** (0.12 g, 0.239 mmol, 64%) as a viscous brown oil.

^1H NMR (400 MHz, CHLOROFORM-*d*) δ_H ppm : 0.19 (6 H, s, 2 × $SiCH_3$), 1.02 (9 H, s, $C(CH_3)_3$), 3.70

(3 H, s, OCH_3), 3.87 (3 H, s, OCH_3), 3.95 (3 H, s, OCH_3), 3.99 (3 H, s, OCH_3), 5.27 (1 H, d, C<u>H</u>NH_2, *J*= 3.5 Hz), 5.60 (1 H, br. s., NH), 5.96 (1 H, d, C=CH, *J*=3.5 Hz), 6.45 (1 H, s, ArH), 6.78 (1 H, br. s., NH), 6.89 (2 H, m, 2 × ArH), 6.95 (1 H, dd, ArH, *J*= 8.2 Hz, 2.2 Hz)

^{13}C NMR (101 MHz, CHLOROFORM-*d*) δ_C ppm : -4.6 (2 × $SiCH_3$), 18.4 (<u>C</u>$(CH_3)_3$), 25.7 ($C(\underline{C}H_3)_3$), 55.4 (OCH_3), 56.4 (OCH_3), 61.3 (OCH_3), 61.6 (OCH_3), 74.5 (CNH_2), 105.2 (ArCH), 111.8 (ArCH), 118.1 (ArC), 119.0 (C=<u>C</u>H), 121.1 (ArCH), 122.1 (ArCH), 129.9 (ArC), 136.8 (ArC), 140.1 (ArC), 142.2 (ArC), 143.3 (ArC), 144.8 (ArC), 147.8 (<u>C</u>=CH), 151.0 (ArC), 172.2 (C=O)

ν_{max} cm^{-1} : 2931.44, 1694.26, 1510.13, 1460.43, 1419.02

HRMS : calculated 501.2183, found 500.2109 ($M - H^+$), 524.2087 ($M + Na^+$), 540.2076 ($M + K^+$)

Synthesis of 3-amino-5-(3-hydroxy-4-methoxyphenyl)-7,8,9-trimethoxy-2,3-dihydro-1-benzoxepin-2-one *(3.13)*

2-amino-5-{3-[(*tert*-butyldimethylsilyl)oxy]-4-methoxyphenyl}-7,8,9-trimethoxy-2,3-dihydro-1-benzoxepin-3-one ***(3.12)*** (0.12 g, 0.239 mmol) was dissolved in dry THF (2 mL) under an atmosphere of nitrogen at 0 °C and tetrabutylammonium fluoride (0.26 mL, 1 M solution, 0.263 mmol) added dropwise. After 5 min the reaction was loaded onto silica and purified by column chromatography (1:1 hexane : ethyl acetate) to afford target molecule 3-amino-5-(3-hydroxy-4-methoxyphenyl)-7,8,9-trimethoxy-2,3-dihydro-1-benzoxepin-2-one ***(3.13)*** (0.051 g, 0.131 mmol, 56%) as a yellow solid.

^{1}H NMR (400 MHz, CHLOROFORM-*d*) δ_H ppm : 3.72 (3 H, s, OCH_3), 3.95 (3 H, s, OCH_3), 3.96 (3 H, s, OCH_3), 3.99 (3 H, s, OCH_3), 5.26 (1 H, s, C<u>H</u>NH_2), 5.76 (1 H, br. s., OH), 5.81 (1 H, br. s., NH), 5.98 (1 H, s, C=CH), 6.48 (1 H, s, ArH), 6.79 (1 H, br. s., NH), 6.97 (3 H, m, 3 × ArH)

^{13}C NMR (101 MHz, CHLOROFORM-*d*) δ_C ppm : 55.9 (OCH_3), 56.5 (OCH_3), 61.3 (OCH_3), 61.6 (OCH_3), 74.4 (CNH_2), 105.3 (ArCH), 110.6 (ArCH), 114.9 (ArCH), 118.3 (C=<u>C</u>H), 120.4 (ArCH), 122.1 (ArCH), 130.6 (ArC), 136.8 (ArC), 140.1 (ArC), 142.1 (ArC), 143.3 (ArC), 145.5 (ArC), 146.6 (<u>C</u>=CH), 147.8 (ArC), 172.3 (C=O)

ν_{max} cm^{-1} : 3335.9, 2925.5, 1689.7, 1581.7, 1510.3, 1459.97

HRMS : calculated 387.1318, found 386.1248 ($M - H^+$), 410.1222 ($M + Na^+$)

Synthesis of intermediate 5-{3-[(*tert*-butyldimethylsilyl)oxy]-4-methoxyphenyl}-2-(ethylsulfanyl)-7,8,9-trimethoxy-2H-1-benzoxepin-3-one *(3.14)*

Bromine ***(3.01)*** (80 mg, 0.141 mmoles) was dissolved in DMF (1 mL) and stirred at RT. Sodium ethanethiol (18 mg, 0.212 mmoles) was subsequently added and the reaction monitored by TLC. Upon completion the reaction was quenched with water (20 mL) and extracted with diethyl ether (3 × 50 mL). The organic layers were then washed with LiCl solution (50 mL, 5%), dried with $MgSO_4$, filtered and concentrated *in vacuo*. After purification with column chromatography (4:1, hexane : ethyl acetate) sulfonyl compound ***(3.14)*** (45 mg, 0.082 mmoles, 58%) as a clear oil.

^{1}H NMR (600 MHz, CHLOROFORM-*d*) δ_H ppm : 0.19 (6 H, d, 2 × $SiCH_3$), 1.02 (9 H, s, $(CH_3)_3$), 1.53 (3 H, t, $SCH_2C\underline{H}_3$, *J*=7.53 Hz), 3.37 - 3.61 (2 H, dm, $SC\underline{H}_2CH_3$), 3.66 (3 H, s, OCH_3), 3.89 (3 H, s, OCH_3), 4.01 (3 H, s, OCH_3), 4.07 (3 H, s, OCH_3), 5.20 (1 H, s, SCH), 6.36 (1 H, s, ArH), 6.52 (1 H, s, C=CH), 6.86 (1 H, d, ArH, *J*=2.26 Hz), 6.90 (1 H, d, ArH, *J*=8.28 Hz), 6.97 (1 H, dd, ArH, *J*=8.47, 2.07 Hz)

^{13}C NMR (151 MHz, CHLOROFORM-*d*) δ_C ppm : -4.4 (2 × $SiCH_3$), 6.4 ($SCH_2\underline{C}H_3$), 18.6 ($\underline{C}(CH_3)_3$), 25.8 ($C(\underline{C}H_3)_3$), 46.7 ($S\underline{C}H_2$), 55.6 (OCH_3), 56.3 (OCH_3), 61.5 (OCH_3), 62.3 (OCH_3), 96.8 ($S\underline{C}H$), 110.3 (ArCH), 111.6 (ArCH), 121.9 (ArCH), 123.3 (ArCH), 126.1 (ArC), 127.7 ($C=\underline{C}H$), 133.1 (ArC), 143.9 (ArC), 145.0 (ArC), 145.1 (ArC), 150.5 (ArC), 152.0 (ArC), 152.6 ($\underline{C}=CH$), 192.4 (C=O)

ν_{max} cm^{-1} : 2932.9, 2342.9, 1509.8, 1140.8, 735.2

Synthesis of intermediate [(5-{3-[(*tert*-butyldimethylsilyl)oxy]-4-methoxyphenyl}-7,8,9-trimethoxy-3-oxo-2H-1-benzoxepin-2-yl)sulfanyl]formonitrile *(3.15)*

Bromine ***(3.01)*** (90 mg, 0.16 mmoles) was dissolved in DMF (1 mL) and stirred at RT. Sodium thiocyanate (19 mg, 0.24 mmoles) was subsequently added and the reaction monitored by TLC. Upon completion the reaction was quenched with water (20 mL) and extracted with diethyl ether (3 × 50 mL). The organic layers were then washed with LiCl solution (50 mL, 5%), dried with $MgSO_4$, filtered and concentrated *in vacuo*. After purification with column chromatography (4:1, hexane : ethyl acetate) sulfonyl compound ***(3.15)*** (50 mg, 0.092 mmoles, 58%) as a clear oil.

^{1}H NMR (600 MHz, CHLOROFORM-*d*) δ_C ppm : 0.19 (6 H, s, 2 × $SiCH_3$), 1.02 (9 H, s, $C(CH_3)_3$), 3.66 (3 H, s, OCH_3), 3.90 (3 H, s, OCH_3), 4.03 (3 H, s, OCH_3), 4.10 (3 H, s, OCH_3), 6.15 (1 H, s, SCH), 6.38

(1 H, s, ArH), 6.48 (1 H, s, C=CH), 6.86 (1 H, d, ArH, *J*=1.88 Hz), 6.90 (1 H, d, *J*=8.28 Hz), 6.96 (1 H, dd, *J*=8.28, 1.88 Hz)

^{13}C NMR (151 MHz, CHLOROFORM-*d*) δ_C ppm : -4.6 (2 × $SiCH_3$), 18.4 ($\underline{C}(CH_3)_3$), 25.6 ($C(\underline{C}H_3)_3$), 55.4 (OCH_3), 56.2 (OCH_3), 61.4 (OCH_3), 62.0 (OCH_3), 93.0 (S$\underline{C}$H), 109.2 (S$\underline{C}$N), 110.5 (ArCH), 111.4 (ArCH), 121.8 (ArCH), 123.3 (ArCH), 125.48 (C=$\underline{C}$H), 125.52 (ArC), 133.4 (ArC), 143.1 (ArC), 144.8 (ArC), 145.3 (ArC), 146.1 (ArC), 150.4 (ArC), 152.5 (ArC), 154.2 ($\underline{C}$=CH), 191.4 (C=O)

ν_{max} cm^{-1} : 2930.7, 2856.8, 2162.9, 1721.4, 1653.0, 1509.6, 1087.8, 841.3

Synthesis of intermediate 2,3,4-trimethoxyphenyl acetate *(3.16)*

Phenol ***(2.02)*** (4.28 g, 0.023 moles) and sodium acetate (4.19 g, 0.0511 moles) were refluxed together in acetic anhydride (22 mL) for 4 h. Afterwards, solvents were then removed under strong vacuum before the remainder was dissolved in water (50 mL) and extracted with DCM (3 × 50 mL). After evaporation, reaction was redissolved in diethyl ether (50 mL) and washed with water (3 × 50 mL). After the organic layer was dried with magnesium sulphate and concentrated under reduced pressure, ***(3.16)*** (4.08 g, 0.018 moles, 78%) was obtained as a light brown clear oil.

^{1}H NMR (400 MHz, CHLOROFORM-*d*) δ_H ppm : 2.34 (3 H, s, CH_3), 3.87 (3 H, s, OCH_3), 3.91 (6 H, s, 2 × OCH_3), 6.64 (1 H, d, ArH, *J*= 9 Hz), 6.76 (1 H, d, ArH, *J*= 9 Hz).

^{13}C NMR (101 MHz, CHLOROFORM-*d*) δ_C ppm : 20.8 (CH_3), 55.7 (OCH_3), 60.5 (OCH_3), 60.6 (OCH_3), 105.9 (ArCH), 116.2 (ArCH), 137.3 (ArC), 142.6 (ArC), 145.3 (ArC), 151.3 (ArC), 169.1 (C=O)

ν_{max} cm^{-1} : 3508.6, 2995.15, 2941.9, 2836.8, 1768.3, 1634.6, 1600.1, 1489.7, 1241.1, 1206.9, 1094.8, 1051.3

HRMS: calculated 226.0841, found 249.0729 ($M + Na^+$), 227.2266 ($M + H^+$)

Synthesis of 1-(2-hydroxy-3,4,5-trimethoxyphenyl)ethan-1-one *(3.17)*

Ester ***(3.16)*** (4.08 g, 0.018 moles) was stirred in glacial acetic acid (5 mL) and boron trifluoride diethyl etherate (7.76 mL, 0.063 moles) added dropwise via syringe. Reaction was then refluxed for 2 h and then poured into aq. NaOH solution (100 mL, 2.5 M) and extracted with diethyl ether

(3 × 100 mL). After drying with magnesium sulphate and being condensed *in vacuo*, product ***(3.17)*** (3.11 g, 0.0.137 moles, 76%) was obtained as a brown solid.

^{1}H NMR (400 MHz, CHLOROFORM-*d*) δ_H ppm : 2.31 (3 H, s, CH_3), 3.64 (3 H, s, OCH_3), 3.69 (3 H, s, OCH_3), 3.81 (3 H, s, OCH_3), 6.70 (1 H, s, ArH)

^{13}C NMR (101 MHz, CHLOROFORM-*d*) δ_C ppm : 25.9 (CH_3), 55.8 (OCH_3), 60.2 (OCH_3), 60.5 (OCH_3), 106.7 (ArCH), 113.5 (ArC), 140.5 (ArC), 144.4 (ArC), 148.9 (ArC), 152.2 (ArC), 202.7 (C=O)

ν_{max} cm^{-1} : 3007.4, 2976.5, 2937.9, 2834.4, 1625.2, 1489.1, 1268.6, 1069.7, 961.1, 812.1, 726.2

HRMS : calculated 226.0841, found 227.0905 ($M + H^+$)

MP :

Synthesis of intermediate 4-hydroxy-6,7,8-trimethoxychromen-2-one *(3.18)*

Keto-phenol ***(3.17)*** (2.13 g, 0.00942 moles) was dissolved in diethyl carbonate (27 mL) and stirred while sodium hydride (3.77 g, 0.0943 moles, 60% in dispersion oil) was very slowly added. When this was complete, the resultant green solution was refluxed for 5 h and then left stirring overnight at RT. The minimum amount of MeOH was added to quench the reaction. The reaction was then poured into diethyl ether (100 mL) and washed with water (5 × 50 mL). The combined aqueous layers were then acidified with dilute aq. HCl (50 mL). The aqueous phase was then extracted with DCM (4 × 50 mL), dried with magnesium sulphate and condensed under reduced pressure. The residue was then washed with diethyl ether and dried under high vacuum. This cyclised alcohol intermediate ***(3.18)*** (1.77 g, 0.007 moles, 74%) was obtained as a white solid.

Synthesis of intermediate 6,7,8-trimethoxy-2-oxochromen-4-yl trifluoromethanesulfonate *(3.19)*

This cyclised alcohol intermediate ***(3.18)*** (1.77 g, 0.007 moles) was then stirred with triethylamine (1.3 mL, 0.0091 moles) in anhydrous DCM (45 mL) at 0 °C under an atmosphere of nitrogen. To this trifluoromethanesulphonic anhydride (2.57 g, 1.51 mL, 0.0091 moles) was added slowly via syringe. Reaction was allowed to stir for 1 h before being diluted with an hexane : ethyl acetate mixture (1:1, 100 mL) and passed through a plug of silica. Solvents were

then removed *in vacuo* at a low temperature before being purified by column chromatography (9:1 hexane : ethyl acetate) to afford triflate ***(3.19)*** (1.77 g, 0.00462 moles, 66%) as a reddish-white solid.

^{1}H NMR (400 MHz, CHLOROFORM-*d*) δ_H ppm : 3.94 (3 H, s, OCH_3), 4.05 (6 H, s, 2 × OCH_3), 6.43 (1 H, s, C=CH), 6.84 (1 H, s, ArH)

^{13}C NMR (101 MHz, CHLOROFORM-*d*) δ_C ppm : 55.9 (OCH_3), 61.2 (OCH_3), 61.6 (OCH_3), 97.3 (C=<u>C</u>H), 104.1 (ArCH), 108.1 (ArC), 116.4 (CF_3) , 140.9 (ArC), 142.6 (ArC), 147.4 (ArC), 150.3 (ArC), 156.7 (<u>C</u>=CH), 159.1 (C=O)

^{19}F NMR (376 MHz, CHLOROFORM-*d*) δ_F ppm : 73.3 (CF_3)

ν_{max} cm^{-1} : 2946.9, 1737.15, 1570.8, 1421.8, 1395.9, 1281.6, 1262.4, 1173.7, 1037.1

HRMS: calculated 384.0127, found 385.0198 ($M + H^+$)

MP : 151-153 °C

Synthesis of {3-[(*tert*-butyldimethylsilyl)oxy]-4-methoxyphenyl} boronic acid *(3.20)*

To a stirred solution of aryl bromide ***(2.13)*** (1.00 g, 0.00316 moles) in dry THF (1.6 mL) at -78 °C under an atmosphere of nitrogen, was added butyllithium (2 mL, 0.00504 moles, 2.5M solution in hexanes) dropwise over 10 min. After this, triisopropyl borate (3.8 mL, 0.0164 moles) was added dropwise and reaction allowed stir at this temperature for 2 h before a further 2 h stirring at -20 °C and finally overnight at RT. The reaction was then quenched with water (10 mL) and extracted with diethyl ether (3 × 20 mL). After drying with magnesium sulphate the product was purified via column chromatography (4:1 hexane : ethyl acetate) to afford ***(3.20)*** (0.55 g, 0.00195 moles, 62%) as a white solid.

^{1}H NMR (400 MHz, CHLOROFORM-*d*) δ_H ppm : 0.25 (6 H, s, 2 × CH_3), 1.08 (9 H, s, 3 × CH_3), 3.92 (3 H, s, OCH_3), 7.00 (1 H, d, ArH, *J*=8.35 Hz), 7.68 (1 H, d, ArH, *J*=1.5 Hz), 7.83 (1 H, dd, ArH, *J*=8.35, 1.55 Hz)

^{13}C NMR (101 MHz, CHLOROFORM-*d*) δ_C ppm : -4.9 (2 × $SiCH_3$), 18.08 (<u>C</u>(CH_3)$_3$), 25.3 (C(<u>C</u>H_3)$_3$), 54.9 (OCH_3), 110.8 (ArCH), 126.9 (ArCH), 129.8 (ArCH), 144.1 (ArC), 154.3 (ArC)

ν_{max} cm^{-1} : 3435.4, 2977.9, 2935.0, 1729.5, 1520.3, 1367.8, 1234.7, 1153.9

HRMS : calculated 282.1489, found 281.1370 ($M - H^+$)

Synthesis of intermediate 4-{3-[(*tert*-butyldimethylsilyl)oxy]-4-methoxyphenyl}-6,7,8-trimethoxychromen-2-one, *(3.02)*, via Suzuki coupling

Triflate ***(3.19)*** (0.20 g, 0.00052 moles), boronic acid ***(3.20)*** (0.18 g, 0.000635 moles) and potassium carbonate (0.22 g, 0.00156 moles) were dissolved and stirred in a biphasic toluene:ethanol:water mixture (3:1:1, 10 mL). To this tetra*kis*(triphenylphosphine)palladium(0) (0.03 g, 0.000026 moles) was added and the reaction refluxed for 2 h. Reaction then diluted with ethyl acetate (3 × 50 mL), dried with magnesium sulphate and concentrated *in vacuo*. After column chromatography (3:1 hexane : ethyl acetate) silyl ether product ***(3.02)*** (0.15 g, 0.000318 moles, 63%) was obtained.

^{1}H NMR (400 MHz, CHLOROFORM-*d*) δ_H ppm : 0.21 (6 H, s, 2 × CH_3), 1.02 (9 H, s, 3 × CH_3), 3.77 (3 H, s, OCH_3), 3.91 (3 H, s, OCH_3), 4.03 (3 H, s, OCH_3), 4.07 (3 H, s, OCH_3), 6.28 (1 H, s, C=CH), 6.77 (1 H, s, ArH), 7.00 (3 H, m, 3 × ArH).

^{13}C NMR (101 MHz, CHLOROFORM-*d*) δ_C ppm : -4.9 (2 × $SiCH_3$) , 17.9 ($\underline{C}(CH_3)_3$), 25.2 ($C(\underline{C}H_3)_3$), 55.0 (OCH_3), 55.8 (OCH_3), 61.1 (OCH_3), 61.5 (OCH_3), 102.8 (ArCH), 111.6 (C=$\underline{C}$H), 113.0 (ArC), 114.1 (ArCH), 120.5 (ArCH), 121.6 (ArCH), 127.6 (ArC), 140.9 (ArC), 142.9 (ArC), 144.7 (ArC), 145.4 (ArC), 149.1 (ArC), 151.8 (ArC), 154.8 ($\underline{C}$=CH), 160.4 (C=O)

ν_{max} cm^{-1} : 2916.4, 1725.7, 1260.1, 1091.7

HRMS : calculated 472.1917, found 473.1978 ($M + H^+$)

Synthesis of 4-(3-hydroxy-4-methoxyphenyl)-6,7,8-trimethoxy-2H-chromen-2-one, *(3.03)*, with TBAF

Silyl ether ***(3.02)*** (0.15 g, 0.318 mmoles) in THF (10 mL) was cooled to 0 °C and stirred. To this, tetrabutylammonium fluoride (0.32 mL, 0.32 mmoles) was added and reaction progress monitored by TLC. After approximately 5 min the reaction was quenched with brine (100 mL) and extracted with diethyl ether (3 × 75 mL). After drying with magnesium sulphate, the reaction was filtered and concentrated *in vacuo* at a low temperature, before being immediately purified

by column chromatography (1:1 hexane : ethyl acetate). Phenol ***(3.03)*** (94 mg, 0.262 mmoles, 83%) was obtained as a light yellow solid.

^{1}H NMR (400 MHz, CHLOROFORM-*d*) δ_H ppm : 3.79 (3 H, s, OCH_3), 4.01 (3 H, s, OCH_3), 4.03 (3 H, s, OCH_3), 4.08 (3 H, s, OCH_3), 5.80 (1 H, br. s., OH), 6.29 (1 H, s, C=CH), 6.79 (1 H, s, ArH), 7.00 (2 H, m, 2 × ArH), 7.07 (1 H, d, ArH, *J*=2.03 Hz)

^{13}C NMR (101 MHz, CHLOROFORM-*d*) δ_C ppm : 55.6 (OCH_3), 55.9 (OCH_3), 61.1 (OCH_3), 61.5 (OCH_3), 103.4 (ArCH), 110.8 (C=<u>C</u>H), 113.6 (ArCH), 114.5 (ArC), 114.6 (ArCH), 120.5 (ArCH), 128.3 (ArC), 140.9 (ArC), 142.9 (ArC), 145.4 (2 × ArC), 147.7 (ArC), 149.6 (ArC), 155.4 (<u>C</u>=CH), 160.7 (C=O)

ν_{max} cm^{-1} : 3373.5, 2924.3, 1721.5, 1389.1

HRMS : calculated 358.1053, 381.0944 ($M + Na^+$)

MP : 152 – 157 °C

Synthesis of intermediate *tert*-butyl 2-methoxy-5-(6,7,8-trimethoxy-2-oxo-2H-chromen-4-yl)phenylcarbamate *(3.05)*, via Suzuki coupling

Triflate ***(3.19)*** (0.115 g, 0.3 mmoles), aryl boronic ester ***(2.23)*** (0.125 g, 0.36 mmoles) and potassium carbonate (0.125 g, 0.9 mmoles) were dissolved and stirred in a biphasic toluene:ethanol:water mixture (3:1:1, 10 mL). To this tetra*kis*(triphenylphosphine)palladium(0) (17 mg, 0.015 mmoles) was added and the reaction refluxed for 2 h. Reaction then diluted with ethyl acetate (3 × 50 mL), dried with magnesium sulphate and concentrated *in vacuo.* After purification with flash column chromatography (3:1, hexane : ethyl acetate), *N*-Boc-protected aniline ***(3.05)*** (97 mg, 0.21 mmoles, 58%) was obtained as a yellow oil.

^{1}H NMR (400 MHz, CHLOROFORM-*d*) δ_H ppm : 1.50 (9 H, s, $(CH_3)_3$), 3.80 (3 H, s, OCH_3), 3.96 (3 H, s, OCH_3), 4.01 (3 H, s, OCH_3), 4.04 (3 H, s, OCH_3), 6.31 (1 H, s, C=CH), 6.94 (1 H, s, ArH), 6.98 (1 H, d, ArH, *J*=8.53 Hz), 7.10 (1 H, dd, ArH, *J*=8.03, 2.01 Hz), 7.14 (1 H, s, ArH), 8.31 (1 H, br. s., NH)

^{13}C NMR (101 MHz, CHLOROFORM-*d*) δ_C ppm : 27.7 (C(<u>C</u>$H_3)_3$), 55.4 (OCH_3), 55.6 (OCH_3), 60.9 (OCH_3), 61.3 (OCH_3), 80.2 (<u>C</u>$(CH_3)_3$), 103.1 (ArCH), 109.8 (ArCH), 112.6 (C=<u>C</u>H), 113.9 (ArC), 118.0 (ArC), 122.1 (ArCH), 127.4 (ArC), 127.7 (ArC), 140.7 (ArC), 142.7 (ArC), 145.2 (ArC), 148.3 (ArC), 149.1 (ArC), 152.2 (<u>C</u>=CH), 155.0 (NC=O), 160.4 (C=O)

v_{max} cm^{-1} : 3452.6, 2939.5, 1724.3, 1530.8, 1390.3

HRMS : calculated 457.1737, found 480.1620 ($M + Na^+$)

Synthesis of 4-(3-amino-4-methoxyphenyl)-6,7,8-trimethoxy-2H-chromen-2-one *(3.06)*

N-Boc protected aniline ***(3.05)*** (97 mg, 0.21 mmoles) was reacted with an anhydrous DCM : triflouroacetic acid (0.5 mL : 0.5 mL) mixture in a roundbottom flask flushed with nitrogen. After 10 min stirring at 0 °C, the DCM\triflouroacetic acid mixture was removed *in vacuo*. The remainder was then basified with sodium hydrogencarbonate solution (50 mL, 5%) and extracted with diethyl ether (3 × 50 mL). After concentrating the volume of solvent, a salt of the compound was then made by bubbling gaseous HCl through the ether solution. Impurities were removed by rinsing the insoluble salt with diethyl ether. Aniline compound ***(2.34)*** (49 mg, 0.138 mmoles, 66%) was obtained as a brown solid.

^{1}H NMR (400 MHz, CHLOROFORM-*d*) δ_H ppm : 3.05 (2 H, br. s., NH_2), 3.75 (3 H, s, OCH_3), 3.94 (3 H, s, OCH_3), 4.00 (3 H, s, OCH_3), 4.04 (3 H, s, OCH_3), 6.25 (1 H, s, C=CH), 6.79 (1 H, s, ArH), 6.81 (2 H, s, 2 × ArH), 6.9 (1 H, d, ArH, *J*= 8.11 Hz)

^{13}C NMR (101 MHz, CHLOROFORM-*d*) δ_C ppm : 55.6 (OCH_3), 56.4 (OCH_3), 61.5 (OCH_3), 61.9 (OCH_3), 103.6 (ArCH), 110.3 (C=<u>C</u>H), 113.2 (ArCH), 114.7 (2 × ArC) 118.8 (ArCH), 125.5 (ArCH), 128.2 (ArC), 141.3 (ArC), 143.4 (ArC), 145.8 (ArC), 149.5 (2 × ArC), 155.9 (<u>C</u>=CH), 160.9 (C=O)

v_{max} cm^{-1} : 3420.3, 2951.7, 2926.5, 2855.7, 1730.0, 1571.0, 1462.1, 1383.9, 1286.9, 1129.4

HRMS : calculated 357.1717, found 358.2184 ($M + H^+$), 380.1364 ($M + Na^+$)

Synthesis of 6,7,8-trimethoxy-4-(4-methoxyphenyl)-2H-chromen-2-one *(3.08)*

Triflate ***(3.19)*** (0.46 g, 0.00119 moles), 4-methoxyphenylboronic acid (0.22 g, 0.001447 moles) and potassium carbonate (0.49 g, 0.00356 moles) were dissolved and stirred in a biphasic toluene:ethanol:water mixture (3:1:1, 10 mL). To this tetra*kis*(triphenylphosphine)palladium(0) (80 mg, 0.026 mmoles) was added and the reaction refluxed for 2 h. Reaction then diluted with ethyl acetate (3 × 50 mL), dried with magnesium sulphate and concentrated *in vacuo*. After

purification by flash column chromatography (3:1 hexane : ethyl acetate), ***(3.08)*** (0.33g, 0.971 mmoles, 81%) was obtained as a yellow powder.

^{1}H NMR (400 MHz, CHLOROFORM-*d*) δ_H ppm : 3.77 (3 H, s, OCH_3), 3.92 (3 H, s, OCH_3), 4.03 (3 H, s, OCH_3), 4.07 (3 H, s, OCH_3), 6.29 (1 H, s, C=CH), 6.75 (1 H, s, ArH), 7.06 (2 H, d, 2 × ArH, *J*= 8.6 Hz), 7.42 (2 H, d, 2 × ArH, *J*= 8.6 Hz)

^{13}C NMR (101 MHz, CHLOROFORM-*d*) δ_C ppm : 54.9 (OCH_3), 55.8 (OCH_3), 61.1 (OCH_3), 61.5 (OCH_3), 102.8 (ArCH), 113.0 (C=CH), 113.9 (2 × ArCH), 114.1 (ArC), 127.3 (ArC), 129.3 (2 × ArCH), 140.9 (ArC), 142.9 (ArC), 145.4 (ArC), 149.1 (ArC), 154.9 (C=CH), 160.31 (1 × C=O, 1 × ArC)

ν_{max} cm^{-1} : 2938.1, 1659.7, 1604.9, 1510.1, 1491.5

HRMS : calculated 342.1103, found 365.1034 (M + Na^+)

Mp : 141-143 °C

Synthesis of 6,7,8-trimethoxy-4-(4-methoxy-3-methylphenyl)-2H-chromen-2-one *(3.21)*

Triflate ***(3.19)*** (0.40 g, 0.00104 moles), 4-methoxy-3-methylphenylboronic acid (0.21 g, 0.00127 moles) and potassium carbonate (0.43 g, 0.00312 moles) were dissolved and stirred in a biphasic toluene:ethanol:water mixture (3:1:1, 10 mL). To this tetra*kis*(triphenylphosphine)palladium(0) (0.06 g, 0.052 mmoles) was added and the reaction refluxed for 2 h. Reaction then diluted with ethyl acetate (3 × 50 mL), dried with magnesium sulphate and concentrated *in vacuo*. After purification by flash column chromatography (2:1 hexane : ethyl acetate), 4-aryl coumarin ***(3.21)*** (0.29 g, 0.822 mmoles, 79%) was obtained as a yellow powder.

^{1}H NMR (400 MHz, CHLOROFORM-*d*) δ_H ppm : 2.31 (3 H, s, CH_3), 3.77 (3 H, s, OCH_3), 3.94 (3 H, s, OCH_3), 4.03 (3 H, s, OCH_3), 4.07 (3 H, s, OCH_3), 6.28 (1 H, s, C=CH), 6.79 (1 H, s, ArH), 6.97 (1 H, d, ArH, *J*= 8.6 Hz), 7.42 (2 H, dd, 2 × ArH, *J*= 8.6, 6.5 Hz)

^{13}C NMR (101 MHz, CHLOROFORM-*d*) δ_C ppm : 15.9 (CH_3) 55.0 (OCH_3), 55.8 (OCH_3), 61.1 (OCH_3), 61.5 (OCH_3), 102.9 (ArCH), 109.5 (ArCH), 112.9 (C=CH), 114.2 (ArC), 126.7 (ArCH), 126.9 (ArC), 126.9 (ArC), 130.2 (ArCH), 140.9 (ArC), 142.9 (ArC), 145.3 (ArC), 149.0 (ArC), 154.9 (C=CH), 158.5 (ArC), 160.4 (C=O)

ν_{max} cm^{-1} : 2995.2, 2942.9, 2837.3, 1717.9, 1606.8, 1556.6, 1503.76, 1388.7, 1259.0

HRMS : calculated 356.1260, found 379.1180 ($M + Na^+$)

Mp : 151-152°C

Sythesis of 6,7,8-trimethoxy-4-[4-(methylsulfanyl)phenyl]-2H-chromen-2-one, *(3.22)*

Triflate ***(3.19)*** (0.40g, 0.00104 moles), 4-methylthiophenylboronic acid (0.21g, 0.00127 moles) and potassium carbonate (0.43 g, 0.00312 moles) were dissolved and stirred in a biphasic toluene:ethanol:water mixture (3:1:1, 10 mL). To this tetra*kis*(triphenylphosphine)palladium(0) (0.06 g, 0.052 mmoles) was added and the reaction refluxed for 2 h. Reaction then diluted with ethyl acetate (3 × 50 mL), dried with magnesium sulphate and concentrated *in vacuo.* After purification by flash column chromatography (2:1 hexane : ethyl acetate), thioanisole chromenone ***(3.22)*** (0.30 g, 0.832 mmoles, 80%) was obtained as a yellow powder.

^{1}H NMR (400 MHz, CHLOROFORM-*d*) δ_H ppm : 2.59 (3 H, s, SCH_3), 3.77 (3 H, s, OCH_3), 4.03 (3 H, s, OCH_3), 4.08 (3 H, s, OCH_3), 6.3 (1 H, s, C=CH), 6.71 (1 H, s, ArH), 7.40 (4 H, s, 4 × ArH)

^{13}C NMR (101 MHz, CHLOROFORM-*d*) δ_C ppm : 14.9 (SCH_3), 55.8 (OCH_3), 61.1 (OCH_3), 61.5 (OCH_3), 102.8 (ArCH), 113.0 (C=<u>C</u>H), 114.1 (ArC), 125.9 (2 × ArCH), 127.3 (ArC), 131.5 (2 × ArCH), 140.9 (ArC), 143.1 (ArC), 145.5 (ArC), 149.1 (ArC), 154.9 (<u>C</u>=CH), 160.5 (C=O)

ν_{max} cm^{-1} : 2918.6, 2850.2, 1718.9, 1561.4, 1404.0, 1282.5, 1086.3

HRMS : calculated 358.0875, found 381.8757 ($M + Na^+$)

MP : 156 – 159 °C

Synthesis of intermediate 5-bromo-2-methoxybenzene-1,3-diol *(3.23)*

To a 3 necked round bottom flask flushed with nitrogen, containing tribromoanisole (2.00 g, 0.0058 moles), was added anhydrous pentane (40 mL) and the reaction mixture cooled to -20 °C. To this suspension, butyllithium (11.6 mL, 0.029 moles, 2.5 M in hexanes) was added dropwise over 10 min, and the reaction allowed to reach -10 °C for 15 min. The reaction vessel was then cooled to -30 °C and trimethylborate (3.23 mL, 0.029 moles) added in one portion, after which the temperature allowed rise to 0 °C for 30 min. The reaction was then cooled again to -10 °C and fresh peracetic acid (7.5 mL, 40% in acetic acid) added dropwise over 30 min. After all the

reagent has been administered, the reaction was warmed to 0 °C over 30 min, then once more cooled to -10 °C and slowly quenched with $NaHSO_3$ solution (10 mL, saturated) over 30 minutes. Water (75 mL) was then added and the product extracted with diethyl ether (3 × 100 mL), dried with magnesium sulphate, filtered and concentrated under reduced pressure. Purification by column chromatography (2:1 hexane : ethyl acetate) afforded diol ***(3.23)*** (0.74 g, 0.003384 moles, 58%) as a brown-red solid.

^{1}H NMR (400 MHz, CHLOROFORM-*d*) δ_H ppm : 0.88 (3 H, s, OCH_3), 5.39 (2 H, br. s., 2 × OH), 6.70 (2 H, s, 2 × ArH)

^{13}C NMR (101 MHz, CHLOROFORM-*d*) δ_C ppm : 60.7 (OCH_3), 111.3 (2 × ArCH), 116.4 (ArCBr), 133.5 (ArC), 149.2 (2 × ArC-OH)

ν_{max} cm^{-1} : 3074.4, 2922.8, 2659.9, 2549.6, 1693.3, 1574.9, 1416.8, 1304.2, 747.8

HRMS : calculated 217.9579, found 219.9560 ($M + H^+$)

MP : 124-127 °C

Synthesis of intermediate 5-bromo-3-[(tert-butyldimethylsilyl)oxy]-2-methoxyphenoxy(tert-butyl)dimethylsilane *(3.24)*

Diol ***(3.23)*** (1.32 g, 0.00603 moles), *tert*-butyldimethylchloro silane (2.27 g, 0.015 moles) and imidazole (2.28 g, 0.0332 moles) were stirred together in anhydrous DMF (3.6 mL) under an atmosphere of nitrogen, and heated to 55 °C for 10 h. Reaction was quenched with aq. NaCl solution (35 mL, saturated) and extracted with diethyl ether (3 × 50 mL), dried with magnesium sulphate, filtered and solvents removed *in vacuo*. Bromo silyl diether ***(3.24)*** (1.26 g, 0.0028 moles, 47%) was obtained as a clear, brown oil.

^{1}H NMR (400 MHz, CHLOROFORM-*d*) δ_H ppm : 0.12 (6 H, s, 2 × $SiCH_3$), 0.23 (6 H, s, 2 × $SiCH_3$), 0.93 (9 H, s, $C(CH_3)_3$), 1.02 (9 H, s, $C(CH_3)_3$), 3.84 (3 H, s, OCH_3), 6.56 (1 H, d, ArH, *J*=2 Hz), 6.77 (1 H, d, ArH, *J*=2 Hz)

^{13}C NMR (101 MHz, CHLOROFORM-*d*) δ_C ppm : -5.12 (2 × $SiCH_3$), 17.9 (2 × $\underline{C}(CH_3)_3$), 25.2 (2 × $C(\underline{C}H_3)_3$), 59.5 (OCH_3), 114.6 (ArC), 117.6 (2 × ArCH), 142.04 (ArC), 150.14 (2 × ArC)

ν_{max} cm^{-1} : 2930.5, 1574.3, 1482.6, 1085.2, 1011.0

HRMS : calculated 446.1308, found 447.1331 ($H + H^+$)

Synthesis of intermediate {3,5-bis[(*tert*-butyldimethylsilyl)oxy]-4-methoxyphenyl}boronic acid *(3.25)*

To a stirred solution of bromo silyl diether ***(3.24)*** (1.26 g, 0.0028 moles) in dry THF (2 mL) at -78 °C under an atmosphere of nitrogen, was added *n*-butyllithium (1.8 mL, 0.0045 moles, 2.5 M solution in hexanes) dropwise over 10 min. After this, triisopropyl borate (3.38 mL, 0.0147 moles) was added dropwise and reaction allowed stir at this temperature for 2 h before a further 2 h stirring at -20 °C, and finally overnight at RT. The reaction was then quenched with water (10 mL) and extracted with diethyl ether (3 × 20 mL). After drying with magnesium sulphate the boronic acid product ***(3.25)*** was purified via column chromatography (6:1, hexane : ethyl acetate) to give a white solid (0.35 g, 0.85 mmoles, 31%).

^{1}H NMR (400 MHz, CHLOROFORM-*d*) δ_H ppm : 0.26 (12 H, s, 4 × $SiCH_3$), 1.08 (18 H, s, 2 × $C(CH_3)_3$), 3.84 (OCH_3), 7.35 (2 H, s, 2 × ArH)

^{1}H NMR (400 MHz, CHLOROFORM-*d*) δ_H ppm : -4.5 (2 × $SiCH_3$), 18.4 ($\underline{C}(CH_3)_3$), 25.8 ($C(\underline{C}H_3)_3$), 59.9 (OCH_3), 119.7 (2 × ArCH), 121.6 (ArC), 147.1 (2 × ArC), 149.6 (ArC)

ν_{max} cm^{-1} : 3440.4, 2986.2, 2935.0, 2840.6, 1730.1, 1598.9, 1540.3, 1238.1, 1153.1

HRMS : calculated 412.2276, found 411.2196 ($H - H^+$)

Synthesis of intermediate 4-(3,5-dihydroxy-4-methoxyphenyl)-6,7,8-trimethoxychromen-2-one *(3.27)*

Triflate ***(3.19)*** (0.27 g, 0.695 mmoles), boronic acid ***(3.25)*** (0.35 g, 0.849 mmoles) and potassium carbonate (0.29 g, 0.0021 moles) were dissolved and stirred in a biphasic toluene:ethanol:water mixture (3:1:1, 10 mL). To this tetra*kis*(triphenylphosphine)palladium(0) (41 mg, 0.035 mmoles) was added and the reaction refluxed for 2 h. Reaction then diluted with ethyl acetate (3 × 50 mL), dried with magnesium sulphate and concentrated *in vacuo*. After purification by flash column chromatography (2:1 hexane : ethyl acetate), coupled product ***(3.26)*** (0.30 g, 0.5 mmoles, 72%) was obtained as a yellow liquid. *tert*-Butyldiphenyl silyl protecting groups were then cleaved using tetrabutylammonium fluoride (1 mL, 0.001 moles) in THF (20 mL) at 0 °C, under an atmosphere of nitrogen. After 20 min, the solvent was concentrated *in vacuo* at a low

temperature and loaded directly on to silica gel. Following purification via column chromatography (100% ethyl acetate), diol chromenone ***(3.27)*** (0.16 g, 0.43 mmoles, 85%) was obtained as a yellow solid.

^{1}H NMR (400 MHz, CHLOROFORM-*d*) δ_H ppm : 3.80 (3 H, s, OCH_3), 3.90 (3 H, s, OCH_3), 3.98 (3 H, s, OCH_3), 4.02 (3 H, s, OCH_3), 6.27 (1 H, s, C=CH), 6.53 (2 H, s, 2 × ArH), 6.97 (1 H, s, ArH)

^{13}C NMR (101 MHz, CHLOROFORM-*d*) δ_C ppm : 55.5 (OCH_3), 60.2 (OCH_3), 61.3 (OCH_3), 104.3 (ArCH), 105.8 (2 × ArCH), 112.8 (C=CH), 114.6 (ArC), 135.1 (ArC), 113.9 (ArC), 138.9 (ArC), 140.8 (ArC), 147.0 (2 × ArC), 147.5 (ArC), 147.9 (ArC), 157.7 (C=CH), 160.6 (C=O)

ν_{max} cm^{-1} : 3415.7, 1672.0, 1555.2, 1445.4, 1357.4, 1091.6, 1059.4, 836.2, 825.5

HRMS : calculated 374.1002, found 375.1070 ($M + H^+$), 397.0890 ($M + Na^+$)

MP : 230 °C

Synthesis of intermediate 3-bromo-4-{3-[(*tert*-butyldimethylsilyl)oxy]-4-methoxyphenyl}-6,7,8-trimethoxychromen-2-one *(3.28)*

Silyl ether ***(3.02)*** (98 mg, 0.21 mmoles) and pyridinium tribromide (67 mg, 0.21 mmoles) were stirred together in anhydrous DCM (1.5 mL) at 0 °C under an atmosphere of nitrogen. After 2 h, an additional equivalent of pyridinium tribromide (67 mg, 0.21 mmoles) was added and the reaction allowed to reach RT. After a further 90 min, the reaction was quenched with $NaHCO_3$ (20 mL, 5%) and extracted with DCM (3 × 30 mL). The combined organic layers were dried with $MgSO_4$, filtered and concentrated *in vacuo*. After purification with flash column chromatography (5 : 1, hexane : ethyl acetate), vinyl bromide ***(3.28)*** (88 mg, 0.16 mmoles, 76%) was obtained as a colourless oil.

^{1}H NMR (400 MHz, CHLOROFORM-*d*) δ_H ppm : 0.21 (6 H, d, 2 × $SiCH_3$, *J*=4.02 Hz), 1.02 (9 H, s, $C(CH_3)_3$), 3.67 (3 H, s, OCH_3), 3.93 (3 H, s, OCH_3), 4.01 (3 H, s, OCH_3), 4.07 (3 H, s, OCH_3), 6.33 (1 H, s, ArH), 6.81 (1 H, d, ArH, *J*=2.01 Hz), 6.86 (1 H, dd, ArH, *J*=8.28, 2.26 Hz), 7.03 (1 H, d, ArH, *J*=8.03 Hz)

^{13}C NMR (101 MHz, CHLOROFORM-*d*) δ_C ppm : -5.0 (2 × $SiCH_3$), 18.0 ($\underline{C}(CH_3)_3$), 25.3 ($C(\underline{C}H_3)_3$), 55.0 (OCH_3), 55.7 (OCH_3), 61.0 (OCH_3), 61.6 (OCH_3), 97.7 (C=CBr), 103.1 (ArCH), 111.6 (ArCH), 114.1

(ArC), 120.4 (ArCH), 121.2 (ArCH), 127.6 (ArC), 142.9 (ArC), 144.7 (ArC), 145.4 (ArC), 149.1 (ArC), 151.8 (ArC), 152.3 (ArC), 154.8 (C=CBr), 160.3 (C=O)

ν_{max} cm^{-1} : 2938.8, 2859.7, 2335.1, 2253.1, 2028.2, 1722.0, 1508.8, 908.4, 731.2

HRMS : calculated 550.1022, found 551.1083 ($M + H^+$), 573.0901 ($M + Na^+$)

Synthesis of intermediate 4-{3-[(tert-butyldimethylsilyl)oxy]-4-methoxyphenyl}-6,7,8-trimethoxy-3-(3,4,5-trimethoxyphenyl)chromen-2-one ***(3.29)***

Vinyl bromide ***(3.28)*** (38.4 mg, 0.07 mmoles), boronic acid 3,4,5 trimethoxyphenylboronic acid (22.2 mg, 0.105 mmoles) and potassium carbonate (29 mg, 0.21 mmoles) were dissolved and stirred in a toluene:ethanol:water mixture (3:1:1, 5 mL). To this tetra*kis*(triphenylphosphine)palladium(0) (4 mg, 3.5 μmoles) was added and the reaction refluxed for 2 h. The reaction was then quenched with brine (50 mL) and extracted with ethyl acetate (3 × 50 mL) before being dried with $MgSO_4$ and concentrated in vacuo. After column chromatography (3:1, hexane:ethyl acetate) chromenone product ***(3.29)*** was obtained (30.4 mg, 0.0467 mmoles, 68%) as a brown oil.

^{1}H NMR (600 MHz, CHLOROFORM-*d*) δ_H ppm : -0.05 (3 H, s, $SiCH_3$), 0.04 (3 H, s, $SiCH_3$), 0.92 (9 H, s, $(CH_3)_3$), 3.67 (9 H, s, 3 × OCH_3), 3.80 (3 H, s, OCH_3), 3.83 (3 H, s, OCH_3), 4.02 (3 H, s, OCH_3), 4.09 (3 H, s, OCH_3), 6.38 (2 H, s, 2 × ArH), 6.50 (1 H, s, ArH), 6.57 (1 H, d, ArH, *J*=1.9 Hz), 6.80 (1 H, dd, ArH, *J*=8.3, 1.9 Hz), 6.86 (1 H, d, ArH, *J*=8.3 Hz)

^{13}C NMR (151 MHz, CHLOROFORM-*d*) δ_C ppm : -5.3 ($SiCH_3$), -5.2 ($SiCH_3$), 18.1 ($\underline{C}(CH_3)$), 25.4 ($C(\underline{C}H_3)_3$), 55.3 (OCH_3), 55.7 (2 × OCH_3), 56.0 (OCH_3), 60.5 (OCH_3), 61.3 (OCH_3), 61.7 (OCH_3), 103.9 (ArCH), 107.9 (2 × ArCH), 111.3 (ArCH), 115.9 (C=C), 121.8 (ArCH), 122.6 (ArCH), 125.1 (ArC), 127.3 (ArC), 129.4 (ArC), 137.1 (ArC), 140.8 (ArC), 142.1 (ArC), 144.9 (ArC), 145.4 (ArC), 149.4 (C=C), 151.1 (2 × ArC) 152.4 (2 × ArC), 160.8 (C=O)

ν_{max} cm^{-1} : 2931.3, 2856.1, 1715.2, 1582.6, 1507.0, 1461.9, 1417.1, 1124.90

HRMS : calculated 638.2547, found 639.2620 ($M + H^+$)

Synthesis of 4-(3-hydroxy-4-methoxyphenyl)-6,7,8-trimethoxy-3-(3,4,5-trimethoxyphenyl) chromen-2-one *(3.30)*

Silyl ether ***(3.29)*** 4-{3-[(*tert*-butyldimethylsilyl)oxy]-4-methoxyphenyl}-6,7,8-trimethoxy-3-(3,4,5-trimethoxyphenyl)chromen-2-one (70.0 mg, 0.11 mmoles), was dissolved in anhydrous DCM (5 mL) at 0 °C, under an atmosphere of nitrogen. To this tetrabutylammonium fluoride (0.12 mL, 0.12 mmol) was added dropwise and the reaction allowed stir for 5 min. The reaction mixture was then transferred directly onto silica and the reaction purified by column chromatography (1:1, hexane:ethyl acetate) to afford phenol ***(3.30)*** (47 mg, 0.088 mmoles, 80%) as an orange solid.

^{1}H NMR (600 MHz, CHLOROFORM-*d*) δ_H : 3.69 (6 H, s, 2 × OCH_3), 3.72 (3 H, s, OCH_3), 3.82 (3 H, s, OCH_3), 3.90 - 3.92 (3 H, s, OCH_3), 4.03 (3 H, s, OCH_3), 4.11 (3 H, s, OCH_3), 5.74 (1 H, s, OH), 6.39 (2 H, s, 2 × ArH), 6.51 (1 H, s, ArH), 6.58 (1 H, dd, ArH, *J*=8.3, 2.3 Hz), 6.78 (1 H, s, ArH), 6.79 (1 H, d, ArH, *J*=5.3 Hz)

^{13}C NMR (151 MHz, CHLOROFORM-*d*) δ_C : 55.7 (OCH_3), 55.8 (2 × OCH_3), 56.2 (OCH_3), 60.6 (OCH_3), 61.3 (OCH_3), 61.8 (OCH_3), 104.0 (ArCH), 108.0 (2 × ArCH), 110.3 (ArCH), 115.3 (ArCH), 115.9 (C=C), 121.0 (ArCH), 125.3 (ArC), 127.8 (ArC), 129.3 (ArC), 137.1 (ArC), 140.8 (ArC), 142.1 (ArC), 145.4 (ArC), 145.5 (ArC), 146.3 (ArC), 149.4 (ArC), 151.2 (C=C), 152.3 (2 × ArC), 160.8 (C=O)

ν_{max} cm^{-1} : 3416.5, 2929.5, 2854.2, 1714.6, 1620.7, 1462.5, 1125.1

HRMS : calculated 524.1680, found 525.1766 ($M + H^+$), 547.1586 ($M + Na^+$)

MP : 233-237 °C

Synthesis of intermediate 2-methoxy-5-(6,7,8-trimethoxy-2-oxochromen-4-yl)phenyl bis[(benzyloxy)methyl]phosphinate *(3.31)*

Phenol 4-(3-hydroxy-4-methoxyphenyl)-6,7,8-trimethoxychromen-2-one ***(3.03)*** (0.28 g, 0.787 mmoles) and 4-dimethylaminopyridine (5 mg, 44 µmoles) were stirred in acetonitrile (10 mL) under an atmosphere of nitrogen and the reaction cooled to -10 °C. Carbon tetrachloride (0.38 mL, 3.93 mmoles) was then added to the mixture, followed by diisopropylethylamine (0.29 mL, 1.65 mmoles). After 30 min, dibenzylphosphate (0.26 mL, 1.18 mmoles) was subsequently added and the reaction left stirring overnight. The reaction was then worked up with monobasic

potassium phosphate (50 mL, 0.5 M solution) and extracted with diethylether (4 × 50 mL). After concentration under reduced pressure and drying with $MgSO_4$, the reaction was purified by column chromatography (2:1, hexane:ethyl acetate) to afford phosphate ester ***(3.31)*** (0.41 g, 0.69 mmoles, 88%) as a clear oil.

^{1}H NMR (600 MHz, CHLOROFORM-*d*) δ_H ppm : 3.73 (3 H, s, OCH_3), 3.88 (3 H, s, OCH_3), 4.01 (3 H, s, OCH_3), 4.06 (3 H, s, OCH_3), 5.17 - 5.22 (4 H, m, 2 × CH_2), 6.20 (1 H, s, C=CH), 6.71 (1 H, s, ArH), 7.06 (1 H, d, ArH, *J*=9.08 Hz), 7.23 - 7.25 (2 H, m, 2 × ArH), 7.27 - 7.36 (10 H, m, 10 × ArH)

^{13}C NMR (151 MHz, CHLOROFORM-*d*) δ_C ppm : 55.9 (OCH_3), 56.1 (OCH_3), 61.3 (OCH_3), 61.8 (OCH_3), 69.9 (CH_2), 69.94 (CH_2), 102.9 (ArCH), 112.8 (C=<u>C</u>H), 113.5 (ArCH), 121.7 (ArCH), 125.8 (ArCH), 127.8 (4 × ArCH), 127.9 (ArCH), 128.4 (4 × ArCH), 128.5 (ArCH), 135.2 (ArC), 135.3 (ArC), 139.5 (ArC), 139.6 (ArC), 141.2 (ArC), 143.2 (ArC), 145.8 (ArC), 149.6 (ArC), 151.7 (ArC), 151.8 (ArC), 153.9 (<u>C</u>=CH), 160.4 (C=O)

^{31}P NMR (162 MHz, CHLOROFORM-*d*) δ_P ppm : -4.69 (P=O)

ν_{max} cm^{-1} : 2941.5, 2252.4, 1715.8, 1610.9, 1515.3, 1389.3, 1277.9, 1130.5, 1009.3, 904.4, 723.3, 696.6

HRMS : calculated 618.1655, found 641.1539 ($M + Na^+$)

Synthesis of disodium 2-methoxy-5-(6,7,8-trimethoxy-2-oxochromen-4-yl)phenyl phosphate *(3.32)*

The phosphate ester 2-methoxy-5-(6,7,8-trimethoxy-2-oxochromen-4-yl) phenyl bis[(benzyloxy)methyl]phosphinate ***(3.31)*** (0.41 g, 0.69 mmoles) was dissolved in anhydrous DCM under N_2 gas and cooled to 0 °C. Bromotrimethyl silane (0.19 mL, 1.45 mmoles) was then added dropwise and the reaction was allowed to stir for 1 h. The DCM was then removed *in vacuo*, water (50 mL) added to the flask and the reaction allowed stir overnight. The aqueous layers were then separated with diethyl ether (3 × 50 mL), before the aqueous phase was concentrated *in vacuo*. When dry, the residue (0.30 g, 0.68 mmoles) was dissolved in MeOH (20 mL) and sodium methoxide (0.07 g, 1.37 mmoles) added. The resulting mixture was allowed stir overnight. The solvent was then removed *in vacuo* and the resulting residue quickly rinsed with deionised water (3 × 5 mL) to remove the sodium methoxide. Diethyl ether was added (20 mL)

and then quickly removed *in vacuo* to encourage crashing out of the pure salt ***(3.32)*** (0.33 g, 0.682 moles, 98%) as a white solid.

^{1}H NMR (400 MHz, DMSO-d_6) δ_H ppm : 3.76 (3 H, s, OCH_3), 3.81 (3 H, s, OCH_3), 3.87 (3 H, s, OCH_3), 3.91 (3 H, s, OCH_3), 6.27 (1 H, s, C=CH), 6.99 (1 H, s, ArH), 7.11 (1 H, dd, ArH, *J*=13.25, 8.00 Hz), 7.80 (1 H, s, ArH), 8.19 (1 H, s, ArH)

^{13}C NMR (151 MHz, DMSO-d_6) δ_C ppm : 55.8 (OCH_3), 56.3 (OCH_3), 61.3 (OCH_3), 61.8 (OCH_3), 103.8 (ArCH), 112.5 (C=<u>C</u>H), 112.8 (ArCH), 114.1 (ArC), 120.5 (ArCH), 121.8 (ArCH), 126.8 (ArC), 141.0 (ArC), 142.8 (ArC), 144.1 (ArC), 145.4 (ArC), 149.6 (ArC), 151.6 (ArC), 155.3 (<u>C</u>=CH), 160.0 (ArC)

^{31}P NMR (162 MHz, DMSO-d_6) δ_P ppm : -4.93 (P=O)

ν_{max} cm^{-1} : 3390.5, 2477.1, 2071.4, 1730.2, 1605.3, 1120.7, 972.0

HRMS : calculated 482.0355, found 483.0465 ($M + Na^+$)

MP : 200-202 °C, decomposition.

5.4 Experimental - Chapter 4

Synthesis of intermediate 2-methoxy-5-(7,8,9-trimethoxy-3-oxo-2H-1-benzoxepin-5-yl)phenyl 2-{[(*tert*-butoxy)carbonyl]amino}-4-methylpentanoate *(4.01)*

Phenol 5-(3-hydroxy-4-methoxyphenyl)-7,8,9-trimethoxy-2H-1-benzoxepin-3-one ***(2.17)*** (0.22 g, 0.6 mmoles) was dissolved in anhydrous DCM (5 mL) and cooled to 0 °C under an atmosphere of nitrogen. To this was added sequentially N-Boc-Leucine (0.27 g, 0.12 mmoles) in anhydrous DCM (5 mL), N-(3-dimethylaminopropyl)-N′-ethylcarbodiimide (0.23 g, 0.12 mmoles) in anhydrous DCM (5 mL, with few drops of dry DMF) and dimethylaminopyridine (4.3 mg, 0.35 mmoles). The reaction was then monitored by TLC and, when complete, quenched with water (20 mL), before extraction with diethyl ether (3 × 50 mL), being dried over $MgSO_4$, filtered and concentrated *in vacuo*. The resulting crude product was then purified by column chromatography (6:1, hexane : ethyl acetate) to give carbamate product ***(4.01)*** (0.224 g, 0.384 mmoles, 64 %) as a brown oil.

^{1}H NMR (400 MHz, CHLOROFORM-*d*) δ_H ppm : 1.03 (6 H, d, 2 × CH_3, *J*=6.02 Hz), 1.46 (9 H, s, $C(CH_3)_3$), 1.67 (1 H, m, C<u>H</u>$(CH_3)_2$), 1.87 (2 H, m, Leu-CH_2), 3.65 (3 H, s, OCH_3), 3.89 (3 H, s, OCH_3),

3.99 (6 H, s, 2 × OCH_3), 4.53 - 4.60 (1 H, m, C<u>H</u>NH), 4.64 (2 H, s, CH_2CO), 4.97 (1 H, d, NH, *J*=8.53 Hz), 6.34 (1 H, s, C=CH), 6.47 (1 H, s, ArH), 7.01 (1 H, d, ArH, *J*=8.53 Hz), 7.06 (1 H, s, ArH), 7.31 (1 H, d, ArH, *J*=8.53 Hz)

^{13}C NMR (101 MHz, CHLOROFORM-*d*) δ_C ppm : 22.9 ($CH(\underline{C}H_3)_2$), 24.8 ($\underline{C}H(CH_3)_2$), 28.3 (3 × $C(\underline{C}H_3)_3$), 41.6 (Leu-CH_2), 52.2 (CHNH), 55.9 (OCH_3), 56.1 (OCH_3), 61.3 (OCH_3), 61.9 (OCH_3), 79.9 ($\underline{C}(CH_3)_3$), 81.2 ($\underline{C}H_2CO$), 110.0 (ArH), 112.1 (C=<u>C</u>H), 124.2 (ArCH), 125.7 (ArC), 127.9 (ArCH), 128.4 (ArCH), 133.9 (ArC), 139.1 (ArC), 144.6 (ArC), 145.2 (ArC), 147.4 (ArC), 149.3 (ArC), 150.7 (ArC), 152.0 (<u>C</u>=CH), 155.4 (Boc-O<u>C</u>=O), 171.6 (Ar-O<u>C</u>=O), 200.48 ($OCH_2\underline{C}$=O)

ν_{max} cm^{-1} : 2944.5, 1749.7, 1648.0, 1513.2, 1376.8, 1115.6

HRMS: calculated 585.2574, found 608.2556 ($M + H^+$)

Synthesis of intermediate 2-methoxy-5-(7,8,9-trimethoxy-3-oxo-2H-1-benzoxepin-5-yl)phenyl 2-amino-4-methylpentanoate *(4.02)*

To carbamate 2-methoxy-5-(7,8,9-trimethoxy-3-oxo-2H-1-benzoxepin-5-yl) phenyl 2-{[(*tert*-butoxy)carbonyl]amino}-4-methylpentanoate ***(4.01)*** (0.19 g, 0.39 mmoles) under an atmosphere of nitrogen was added trifluoroacetic acid:DCM (1:1, 1 mL) at 0 °C. After 5 min, the reaction was left in concentrated *in vacuo*. The residue left was redissolved in ether (10 mL) and stirred, to which sodium hydrogencarbonate (1 mL, 5%) was added for 5 min. The organic layer was then separated and dried with $MgSO_4$, filtered, before being condensed under reduced pressure to afford free amine ***(4.02)*** (0.165 g, 0.304 mmoles, 87%) as a brown solid.

^{1}H NMR (400 MHz, CHLOROFORM-*d*) δ_H ppm : 1.01 (6 H, t, 2 × CH_3, *J*=7.03 Hz), 1.55 - 1.65 (1 H, m, $C\underline{H}(CH_3)_2$), 1.76 - 1.99 (2 H, m, Leu-CH_2), 2.21 (2 H, br. s., NH_2), 3.66 (3 H, s, OCH_3), 3.75 - 3.81 (1 H, m, C<u>H</u>NH_2), 3.89 (3 H, s, OCH_3), 3.99 (6 H, s, 2 × OCH_3), 4.65 (2 H, s, CH_2C=O), 6.35 (1 H, s, C=CH), 6.48 (1 H, s, ArH), 6.99 - 7.05 (2 H, m, 2 × ArH), 7.28 - 7.32 (1 H, m, ArH)

^{13}C NMR (101 MHz, CHLOROFORM-*d*) δ_C ppm : 21.4 (1 × $CH(\underline{C}H_3)_2$), 22.6 (1 × $CH(\underline{C}H_3)_2$), 24.3 ($\underline{C}H(CH_3)_2$), 43.3 (Leu-CH_2), 52.4 ($CHNH_2$), 55.5 (OCH_3), 55.7 (OCH_3), 60.9 (OCH_3), 61.5 (OCH_3), 80.7 ($\underline{C}H_2CO$), 109.5 (ArCH), 111.6 (C=<u>C</u>H), 123.6 (ArCH), 125.3 (ArC), 127.4 (ArCH), 127.9 (ArCH), 133.5 (ArC), 138.8 (ArC), 144.1 (ArC), 144.8 (ArC), 146.9 (ArC), 148.8 (ArC), 150.3 (ArC), 151.6 (<u>C</u>=CH), 174.0 (Ar-O<u>C</u>=O), 200.11 ($OCH_2\underline{C}$=O)

ν_{max} cm^{-1} : 3400.2, 2899.9, 1745.2, 1675.4, 1598.3, 1509.3, 1367.6

HRMS : calculated 485.205, found 508.1924 ($M + Na^+$)

MP : 140-142 °C

Synthesis of intermediate 3-{[(*tert*-butoxy)carbonyl]amino}-2-hydroxy-4-phenylbutanoic acid *(4.03)*

Potassium carbonate (0.142 g, 0.00102 moles) was dissolved and stirred in distilled water (2 mL), before (2*S*,3*R*)-3-amino-2-hydroxy-4-phenylbutric acid (0.20 g, 0.00102 moles) was added. MeOH (1 mL) was added to aid solvation. To this solution, di-*tert*-butyl dicarbonate (0.22 g, 0.00102 moles) in THF (2 mL, HPLC grade) was added and the reaction stirred at RT for 1 h. Organic solvents were then removed *in vacuo*, and the resulting aqueous solution acidified with aq. HCl solution (30 mL, 1 M) and then extracted with diethyl ether (3 × 30 mL). The organic layer was then dried with magnesium sulphate, filtered and condensed under reduced pressure to afford carbamate ***(4.03)*** (0.21 g, 0.711 mmoles, 70%) without the need for flash column chromatography as a white solid.

^{1}H NMR (400 MHz, METHANOL-d_4) δ_H ppm : 1.35 (9 H, s, $C(CH_3)_3$), 2.87 – 2.96 (2 H, dd, CH_2, *J*=5, 3 Hz), 4.12 (1 H, d, C<u>H</u>OH, *J*=3 Hz), 4.29 (1 H, q, C<u>H</u>NH_2, *J*= 5 Hz), 7.22-7.34 (5 H, m, 5 × ArH)

^{13}C NMR (101 MHz, METHANOL-d_4) δ_C ppm : 27.7 ($C(\underline{C}H_3)_3$), 38.1 (CH_2), 54.8 (CHNH), 70.4 (CHOH), 79.5 ($\underline{C}(CH_3)_3$), 126.3 (ArCH), 128.3 (2 × ArCH), 129.6 (2 × ArCH), 137.9 (ArC), 156.2 (NHC=O), 175.2 (COOH)

ν_{max} cm^{-1} : 3397.3, 2974.3, 1697.5, 1507.3, 1165.7, 1087.5, 698.7

HRMS : calculated 295.1419, found 318.1328 ($M + Na^+$)

MP : 100-101 °C

Synthesis of intermediate pentafluorophenyl 3-{[(*tert*-butoxy)carbonyl]amino}-2-hydroxy-4-phenylbutanoate *(4.04)*

To a solution of anhydrous DCM (3 mL) containing Boc-protected AHPA ***(4.03)*** (0.191 g, 0.65 mmoles), at 0 °C and under N_2 atmosphere, was added first pentafluorophenol (0.12 g, 0.65 mmoles) in anhydrous DCM (1 mL), and then N,N'-dicyclohexylcarbodiimide (0.133 g, 0.65 mmoles). Over 1 h, the reaction was gradually allowed to reach RT. The reaction was again cooled to 0 °C just before the mixture was filtered several times with paper, washed with minimum diethyl ether and concentrated under vacuum. The resulting crude mixture rapidly purified by flash column chromatography (10 : 1, hexane : ethyl acetate) before PFP ester ***(4.04)*** (0.24 g, 0.52 mmoles, 81%) was obtained as an orange oil.

^{1}H NMR (400 MHz, CHLOROFORM-*d*) δ_H ppm : 1.44 (9 H, s, $C(CH_3)_3$), 3.08 (2 H, dd, CH_2, *J*=4.2, 3 Hz), 4.47 (1 H, d, CHOH, *J*= 9 Hz), 4.58 (1 H, q, CHNH, 4.5 Hz), 7.33 (5 H, m, 5 × ArH)

^{13}C NMR (101 MHz, CHLOROFORM-*d*) δ_C ppm : 27.6 ($C(CH_3)_3$), 37.5 (CH_2), 54.7 (CHNH), 70.7 (CHOH), 80.1 ($C(CH_3)_3$), 126.3 (ArCH), 128.2 (2 × ArCH), 128.9 (2 × ArCH), 131.7 (ArC), 136.2 (ArC), 138.0 (ArC), 138.7 (ArC), 139.4 (ArC), 140.6 (ArC), 141.8 (ArC), 155.7 (NHC=O), 169.4 (C=O)

^{19}F NMR (376 MHz, CHLOROFORM-*d*) δ_F ppm : -171.1, -165.5, -162.9, -158.2, -152.8

ν_{max} cm^{-1} : 3329.6, 2930.5, 2850.2, 1749.3, 1625.7, 1517.4, 1164.7, 700.8

HRMS : calculated 461.1262, found 484.1153 ($M + Na^+$)

Synthesis of intermediate 2-methoxy-5-(7,8,9-trimethoxy-3-oxo-2H-1-benzoxepin-5-yl)phenyl 2-(3-{[(*tert*-butoxy)carbonyl]amino}-2-hydroxy-4-phenylbutanamido)-4-methylpentanoate (4.05)

Amine ***(4.02)*** (0.165 g, 0.34 mmoles), was dissolved in anhydrous DCM (5 mL) under an atmosphere of nitrogen, and cooled to 0 °C. To this was added, in anhydrous DCM and under nitrogen, pentafluorophenyl ester pentafluorophenyl 3-{[(*tert*-butoxy) carbonyl]amino}-2-hydroxy-4-phenylbutanoate ***(4.04)*** (0.14 g, 0.296 mmoles), followed by diisopropylethylamine (62 µl, 0.355 mmoles). The reaction was then monitored by TLC until such time as no further progress was observed. Solvent was then removed by blowing off with nitrogen gas and the remaining residue purified via column chromatography (1:1, hexane : ethyl acetate) to afford Boc-bestatin compound ***(4.05)*** (90 mg, 0.11 mmoles, 35%) as a brown residue.

^{1}H NMR (400 MHz, CHLOROFORM-*d*) δ_H ppm : 1.02 (6 H, dd, $CH(CH_3)_2$), *J*=8.03, 6.53 Hz), 1.41 (9 H, s, $C(CH_3)_3$), 1.72 - 1.96 (3 H, m, 1 × $C\underline{H}(CH_3)_2$, 1 × Leu-CH_2), 3.04 - 3.31 (2 H, m, Ar-CH_2), 3.65 (3 H, s, OCH_3), 3.89 (3 H, s, OCH_3), 3.98 (1 H, s, $C\underline{H}NH$), 4.01 (6 H, s, 2 × OCH_3), 4.21 (1 H, d, $C\underline{H}OH$, *J*=2.76 Hz), 4.65 (2 H, s, OCH_2), 4.86 - 4.94 (1 H, m, Leu-$C\underline{H}NH$), 5.01 (1 H, d, NH, *J*=7.03 Hz), 5.74 - 5.92 (1 H, br. s, OH), 6.33 (1 H, s, ArH), 6.47 (1 H, s, CH=C), 7.01 (1 H, d, ArH, *J*=8.53 Hz), 7.06 (1 H, d, ArH, *J*=2.01 Hz), 7.22 - 7.28 (3 H, m, 3 × ArH), 7.30 - 7.36 (3 H, m, 3 × ArH), 7.38 (1 H, br. s., NH)

^{13}C NMR (101 MHz, CHLOROFORM-*d*) δ_C ppm : 21.6 (1 × $CH(\underline{C}H_3)_2$), 23.1 (1 × $CH(\underline{C}H_3)_2$), 24.8 ($\underline{C}H(CH_3)_2$), 28.2 ($C(\underline{C}H_3)_3$), 31.9 (ArC-$\underline{C}H_2$), 41.4 (Leu-CH_2), 50.4 (Leu-$\underline{C}HNH$), 56.0 (OCH_3), 56.2 (OCH_3), 61.3 (OCH_3), 61.9 (OCH_3), 74.8 (COH), 77.2 ($\underline{C}HN$-Boc) 80.7 ($\underline{C}(CH_3)_3$), 81.1 (OCH_2), 110.1 (ArCH), 112.1 (ArCH), 124.1 (ArCH), 125.7 (ArC), 126.7 (C=$\underline{C}H$), 128.0 (ArCH), 128.4 (ArCH), 128.6 (2 × ArCH), 129.3 (2 × ArCH), 134.0 (ArC), 138.0 (ArC), 139.1 (ArC), 144.7 (ArC), 145.3 (ArC), 147.5 (ArC), 149.3 (ArC), 150.8 (ArC), 152.0 ($\underline{C}$=CH), 156.1 (Boc-C=O) 170.5 (Ar-OC=O), 172.7 (Leu-NC=O), 200.5 (CH_2C=O)

ν_{max} cm^{-1} : 3306.7, 2949.8, 1788.4, 1675.7, 1513.8, 1259.5, 1123.6, 1034.3, 710.8

HRMS : calculated 762.3364, found 785.3245 (M + Na^+)

Synthesis of 2-methoxy-5-(7,8,9-trimethoxy-3-oxo-2H-1-benzoxepin-5-yl)phenyl 2-(3-amino-2-hydroxy-4-phenylbutanamido)-4-methylpentanoate *(4.06)*

To carbamate compound ***(4.05)*** (0.9 g, 0.11 mmoles), under an atmosphere of nitrogen, was added trifluoroacetic acid in anhydrous DCM (1:1, 1 mL). The reaction was stirred at 0 °C for 5 min, after which the solvent was concentrated *in vacuo*. The crude residue was then redissolved in diethyl ether (10 mL), with the minimum amount of DCM (few drops until fully solubilised), and aq. sodium hydrogencarbonate (0.5 mL, 5% solution) added. This biphasic mixture was then allowed to stir for 5 min before the aqueous layer was removed. The remaining organic layer was then dried with $MgSO_4$, and gaseous HCl (from conc. HCl\H_2SO_4) was then blown through, prompting a yellow salt to crash out. This salt was then washed with diethyl ether (3 × 5 mL) which was decanted off, to leave amine salt ***(4.06)*** (50 mg, 0.076 mmoles, 69%) as a yellow solid.

^{1}H NMR (600 MHz, DMSO-d_6) δ_H ppm : 0.92 (6 H, dd, 2 × CH_3, *J*=14.68, 5.65 Hz), 1.69 - 1.82 (3 H, m, 1 × $CH(CH_3)_2$, 1 × Leu-CH_2), 2.78 - 2.93 (2 H, m, ArC-CH_2), 3.48 (3 H, s, OCH_3), 3.49 - 3.52 (1 H, m, $C\underline{H}NH_3$), 3.77 (3 H, s, OCH_3), 3.82 (3 H, s, OCH_3), 3.86 (3 H, s, OCH_3), 3.99 - 4.02 (1 H, m,

C<u>H</u>OH), 4.48 - 4.54 (1 H, m, Leu-C<u>H</u>NH), 4.65 (2 H, s, OCH_2), 6.22 (1 H, s, ArH), 6.29 (1 H, s, C=CH), 6.67 (1 H, br. s., OH), 6.98 (1 H, d, ArH, *J*=2.11 Hz), 7.18 (1 H, s, ArH), 7.19 (1 H, s, ArH), 7.21 - 7.26 (3 H, m, 3 × ArH), 7.29 - 7.33 (2 H, m, 2 × ArH), 7.87 (2 H, br. s., NH_2), 8.53 (1 H, d, NH)

^{13}C NMR (151 MHz, DMSO-d_6) δ_C ppm : 21.6 (1 × CH(<u>C</u>H_3)$_2$), 22.6 (1 × CH(<u>C</u>H_3)$_2$), 24.2 (<u>C</u>H(CH_3)$_2$), 34.6 (ArC-<u>C</u>H_2), 39.3 (Leu-CH_2), 50.6 (CHNH), 54.3 (<u>C</u>HNH_2), 55.8 (OCH_3), 56.0 (OCH_3), 60.8 (OCH_3), 61.4 (OCH_3), 68.5 (CHOH), 80.8 (OCH_2), 109.9 (ArCH), 112.9 (ArCH), 123.5 (ArCH), 125.2 (ArC), 126.9 (ArCH), 127.9 (1 × ArCH, 1 × C=CH), 128.6 (2 × ArCH), 129.3 (2 × ArCH), 133.1 (ArC), 136.1 (ArC), 138.5 (ArC), 144.2 (ArC), 145.0 (ArC), 147.0 (ArC), 148.8 (ArC), 149.7 (<u>C</u>=CH), 151.6 (ArC), 170.3 (OC=O), 171.3 (NHC=O), 199.6 (CH_2<u>C</u>=O)

ν_{max} cm^{-1} : 3394.2, 3211.6, 2955.9, 2868.6, 1764.6, 1674.0, 1510.3, 1456.8, 1375.4, 1272.4, 1131.1, 1022.3, 734.1

HRMS : calculated 662.2839 (free amine), found 663.2912 ($M + H^+$)

MP : 130 °C

Synthesis of intermediate 2-methoxy-5-(6,7,8-trimethoxy-2-oxochromen-4-yl)phenyl 2-{[(*tert*-butoxy)carbonyl]amino}-4-methylpentanoate *(4.07)*

Phenol ***(3.03)*** (0.12 g, 0.335 mmoles) was dissolved in anhydrous DCM (4 mL) and cooled to 0 °C under an atmosphere of nitrogen. To this was added sequentially *N*-Boc-Leucine (0.39 g, 1.68 mmoles) in anhydrous DCM (3 mL), N-(3-dimethylaminopropyl)-N′-ethylcarbodiimide (0.21 g, 1.68 mmoles) in anhydrous DCM (3 mL) and dimethylaminopyridine (3.2 mg, 0.17 mmoles). DMF (2-3 drops) was used to encourage the EDC into solution. The reaction was then monitored by TLC and, when complete quenched with water (20 mL), before extraction with diethyl ether (3 × 50 mL), being dried over $MgSO_4$, filtered and concentrated *in vacuo*. The resulting crude product was then purified by column chromatography (6:1, hexane : ethyl acetate) to give carbamate product ***(4.07)*** (0.19 g, 0.332 mmoles, 98 %) as a milky white oil.

^{1}H NMR (400 MHz, CHLOROFORM-*d*) δ_H ppm : 0.95 (3 H, d, Leu-CH_3, *J*=6.02 Hz), 1.02 (3 H, d, Leu-CH_3, *J*=6.02 Hz), 1.45 (9 H, s, C(CH_3)$_3$), 1.50 - 1.58 (1 H, m, C<u>H</u>(CH_3)$_2$), 1.61 - 1.92 (2 H, m, CH_2), 3.77 (3 H, s, OCH_3), 3.91 (3 H, s, OCH_3), 4.00 (3 H, s, OCH_3), 4.05 (3 H, s, OCH_3), 4.57 (1 H, m, C<u>H</u>NH), 4.95 - 5.07 (1 H, m, NH), 6.30 (1 H, s, C=CH), 6.77 (1 H, s, ArH), 7.12 (1 H, d, ArH, *J*=8.03 Hz), 7.23 (1 H, s, ArH), 7.34 (1 H, d, ArH, *J*=7.53 Hz)

^{13}C NMR (101 MHz, CHLOROFORM-*d*) δ_C ppm : 21.4 (Leu-CH_3), 22.4 (Leu-CH_3), 24.4 ($\underline{C}H(CH_3)_2$), 27.8 ($C(\underline{C}H_3)_3$), 41.0 (CH_2), 51.9 (CHNH), 55.5 (OCH_3), 55.8 (OCH_3), 61.0 (OCH_3), 61.4 (OCH_3), 79.6 ($\underline{C}(CH_3)_3$), 102.5 (ArCH), 112.4 (C=$\underline{C}$H), 113.0 (ArCH), 113.7 (ArC), 122.9 (ArCH), 126.7 (ArCH), 127.3 (ArC), 138.9 (ArC), 140.9 (ArC), 142.8 (ArC), 145.4 (ArC), 149.2 (ArC), 151.8 (ArC), 153.8 (ArC), 160.3 (Lactone-O$\underline{C}$=O), 171.3 (Ar-O$\underline{C}$=O), 176.4 (Boc-O$\underline{C}$=O)

ν_{max} cm^{-1} : 3351.9, 2959.4, 2872.24, 1766.2, 1720.1, 1615.2, 1558.9, 1513.9, 1389.4, 1274.1, 1134.1

HRMS : calculated 571.2417, found 594.2313 ($M + Na^+$)

Synthesis of intermediate 2-methoxy-5-(6,7,8-trimethoxy-2-oxochromen-4-yl)phenyl 2-amino-4-methylpentanoate *(4.08)*

To carbamate 2-methoxy-5-(7,8,9-trimethoxy-3-oxo-2H-1-benzoxepin-5-yl) phenyl 2-{[(*tert*-butoxy)carbonyl]amino}-4-methylpentanoate ***(4.07)*** (0.19 g, 0.332 mmoles) under an atmosphere of nitrogen was added trifluoroacetic acid:DCM (1:1, 1 mL) at 0 °C. After 5 min, the reaction was concentrated *in vacuo*. The residue left was redissolved in ether (10 mL) and stirred, to which sodium hydrogencarbonate (1 mL, 5%) was added for 5 min. The organic layer was then separated and dried with $MgSO_4$, filtered, before being condensed under reduced pressure to afford free amine ***(4.08)*** (0.10 g, 0.212 mmoles, 64%) as a brown solid.

^{1}H NMR (400 MHz, CHLOROFORM-*d*) δ_H ppm : 0.92 - 1.00 (6 H, m, 2 × Leu-CH_3), 1.81 - 2.05 (2 H, m, CH_2), 1.95 - 2.02 (1 H, m, $C\underline{H}(CH_3)_2$), 3.75 (3 H, s, OCH_3), 3.87 (3 H, s, OCH_3), 3.99 (3 H, s, OCH_3), 4.03 (3 H, s, OCH_3), 4.16 - 4.27 (1 H, m, $C\underline{H}NH_2$), 6.22 (1 H, s, C=CH), 6.72 (1 H, s, ArH), 7.09 (1 H, d, ArH, *J*=8.53 Hz), 7.20 (1 H, s, ArH), 7.33 (1 H, d, ArH, *J*=8.28 Hz), 7.82 (2 H, br. S, NH_2)

^{13}C NMR (101 MHz, CHLOROFORM-*d*) δ_C ppm : 21.9 (2 × Leu-CH_3), 24.3 ($\underline{C}H(CH_3)_2$), 39.7 (CH_2), 51.7 (CHNH), 56.0 (OCH_3), 56.2 (OCH_3), 61.5 (OCH_3), 61.9 (OCH_3), 103.0 (ArCH), 112.7 (C=$\underline{C}$H), 113.5 (ArCH), 114.1 (ArC), 122.9 (ArCH), 127.8 (ArCH), 127.8 (ArC), 138.9 (ArC), 141.3 (ArC), 143.2 (ArC), 145.9 (ArC), 149.8 (ArC), 151.8 (ArC), 154.1 ($\underline{C}$=CH), 160.7 (Lactone-O$\underline{C}$=O), 168.3 (Ar-O$\underline{C}$=O)

ν_{max} cm^{-1} : 3434.8, 2961.4, 2252.4, 1767.2, 1692.8, 1615.9, 1556.5, 1514.4, 1389.9, 1201.1, 1133.9, 733.4

HRMS : calculated 471.1893, found 472.1806 ($M + H^+$)

Synthesis of 2-methoxy-5-(6,7,8-trimethoxy-2-oxochromen-4-yl)phenyl 2-(3-amino-2-hydroxy-4-phenylbutanamido)-4-methylpentanoate *(4.10)*

Amine ***(4.08)*** (10 mg, 0.021 mmoles), was dissolved in anhydrous DCM (2 mL) under an atmosphere of nitrogen, and cooled to 0 °C. To this was added, in anhydrous DCM and under nitrogen, pentafluorophenyl ester pentafluorophenyl 3-{[(*tert*-butoxy) carbonyl]amino}-2-hydroxy-4-phenylbutanoate ***(4.04)*** (0.14 g, 0.296 mmoles), followed by diisopropylethylamine (62 µl, 0.355 mmoles). The reaction was then monitored by TLC until such time as no further progress was observed. Solvent was then removed by blowing off with nitrogen gas and the remaining residue purified via column chromatography (1:1, hexane : ethyl acetate) to afford Boc-bestatin compound ***(4.09)*** (14 mg, 0.0187 mmoles, 88%) as a brown residue. This compound was then treated with TFA in dry DCM (1:1, 1 mL) under nitrogen at 0 °C for 5 minutes, after which the solvents were removed by concentrated *in vacuo*. The resultant residue was reconstituted in diethyl ether (5 mL) and DCM (4-5 drops), before aq. $NaHCO_3$ solution (1 mL, saturated) was added and stirred for 5 min. The aqueous layer was removed by Pasteur pipette, and the organic layer was dried with $MgSO_4$, filtered and concentrated to around 2 mL *in vacuo*. Gaseous HCl (from conc. $HCl\backslash H_2SO_4$) was then blown through, prompting a yellow salt to crash out. This salt was then washed with diethyl ether (3 × 5 mL) which was decanted off, to leave amine salt ***(4.10)*** (8 mg, 0.0123 mmoles, 66%) as a yellow solid.

^{1}H NMR (400 MHz, CHLOROFORM-*d*) δ_H ppm : 1.02 (6 H, dd, 2 × $SiCH_3$, *J*=8.78, 6.27 Hz), 1.63 - 1.99 (2 H, m, Leu-CH_2), 1.76 - 1.82 (1 H, m, C<u>H</u>$(CH_3)_2$), 3.00 - 3.26 (2 H, m, Ar-CH_2), 3.77 (3 H, s, OCH_3), 3.79 (1 H, m, C<u>H</u>NH_2), 3.90 (3 H, s, OCH_3), 4.02 (3 H, s, OCH_3), 4.04 - 4.08 (3 H, s, OCH_3), 4.21 (1 H, br. s., C<u>H</u>OH), 4.90 (1 H, br. s., C<u>H</u>NH), 5.03 (1 H, d, *J*=9.54 Hz), 5.08 (1 H, d, 1 × NH, *J*=7.53 Hz), 5.91 (1 H, br. s., OH), 6.29 (1 H, s, C=CH), 6.75 (1 H, s, ArH), 6.95 - 7.14 (3 H, m, ArH), 7.19 - 7.37 (5 H, m, ArH), 7.43 (1 H, br. s., NH)

^{13}C NMR (101 MHz, CHLOROFORM-*d*) δ_C ppm : 21.2 (Leu-CH_3), 22.6 (Leu-CH_3), 24.3 ($CH(CH_3)_2$), 35.5 (Ar-CH_2), 40.7 (Leu-CH_2), 50.1 (CHNH), 54.1 (CHNH), 55.6 (OCH_3), 55.8 (OCH_3), 61.1 (OCH_3), 61.5 (OCH_3), 74.1 (CHOH), 102.5 (ArCH), 112.3 (ArCH), 113.0 (C=<u>C</u>H), 113.8 (ArC), 120.0 (ArCH), 122.9 (ArCH), 126.2 (ArCH), 128.1 (2 × ArCH), 128.8 (2 × ArCH), 129.0 (ArC), 137.5 (ArC), 138.8

(ArC), 140.9 (ArC), 145.5 (ArC), 149.3 (ArC), 151.7 (ArC), 153.9 (ArC), 155.0 (C=CH), 160.3 (Lactone-OC=O), 170.9 (Ar-OC=O), 172.5 (HN-C=O)

ν_{max} cm^{-1} : 3227.8, 2928.1, 2868.4, 2583.3, 1764.8, 1718.3, 1512.1, 1386.3, 1271.3, 1129.8

HRMS : calculated 648.2683, found 649.2740 ($M + H^+$), 671.2573 ($M + Na^+$)

Synthesis of intermediate *tert*-butyl N-(1-{[2-methoxy-5-(6,7,8-trimethoxy-2-oxochromen-4-yl)phenyl]carbamoyl}-3-methylbutyl)carbamate *(4.11)*

Amine salt ***(3.06)*** (0.15 g, 0.42 mmoles) was dissolved in anhydrous DCM (3 mL) under an atmosphere of nitrogen at 0 °C. To this was added sequentially in dry DCM; *N*-Boc leucine (0.29 g, 0.00126 moles), PyBroP (0.59 g, 0.00126 moles) and diisopropylamine (0.22 mL, 0.00126 mmoles). The reaction was gradually allowed to reach RT and the reaction was monitored via TLC. The reaction was then quenched with aq. HCl (20 mL, 1 M) and extracted with diethyl ether (3 × 30 mL). The organic layer was then dried with $MgSO_4$, filtered and concentrated *in vacuo* before the residue was then purifed by column chromatography (3:1, hexane : ethyl acetate) to give carbamate product ***(4.11)*** as a clear yellowish oil (0.17 g, 0.396 mmoles, 94%)

^{1}H NMR (400 MHz, CHLOROFORM-*d*) δ_H ppm : 0.95 (3 H, d, Leu-CH_3, *J*=6 Hz), 1.00 (3 H, d, Leu-CH_3, *J*=6 Hz), 1.45 (9 H, s, $C(CH_3)_3$), 1.75 - 1.78 (1 H, m, $CH(CH_3)_2$), 1.68 - 1.92 (2 H, m, CH_2), 3.75 (3 H, s, OCH_3), 3.89 (3 H, s, OCH_3), 3.95 (3 H, s, OCH_3), 4.00 (3 H, s, OCH_3), 4.45 (1 H, m, CHNH), 6.28 (1 H, s, C=CH), 6.81 (1 H, s, ArH), 7.05 (1 H, d, ArH, *J*=8.03 Hz), 7.18 (1 H, s, ArH), 7.43 (1 H, d, ArH, *J*=7.53 Hz), 8.51 (2 H, d, 2 × NHCO, *J*=2.26 Hz)

^{13}C NMR (101 MHz, CHLOROFORM-*d*) δ_C ppm : 21.2 (Leu-CH_3), 22.2 (Leu-CH_3), 24.1 ($CH(CH3)_2$), 28.2 ($C(CH_3)_3$), 39.7 (CH_2), 52.4 (CHNH), 55.5 (OCH_3), 55.8 (OCH_3), 61.0 (OCH_3), 61.4 (OCH_3), 79.5 ($C(CH_3)_3$), 102.6 (ArCH), 112.2 (C=CH), 113.4 (ArCH), 113.9 (ArC), 122.7 (ArCH), 127.1 (ArCH), 127.5 (ArC), 137.9 (ArC), 141.1 (ArC), 142.8 (ArC), 144.7 (ArC), 149.4 (ArC), 152.2 (ArC), 154.9 (ArC), 160.1 (Lactone-OC=O), 171.4 (Ar-OC=O), 175.9 (Boc-OC=O)

ν_{max} cm^{-1} : 3347.6, 2963.4, 2888.24, 1753.2, 1715.2, 1615.2, 1589.9, 1515.0, 1389.4

HRMS : calculated 570.2577, found 569.3926 ($M - H^+$)

Synthesis of intermediate 2-amino-N-[2-methoxy-5-(6,7,8-trimethoxy-2-oxochromen-4-yl)phenyl]-4-methylpentanamide *(4.13)*

To carbamate compound ***(4.11)*** (0.16 g, 0.396 mmoles), under an atmosphere of nitrogen, was added trifluoroacetic acid in anhydrous DCM (1:1, 1 mL). The reaction was stirred at 0 °C for 5 min, after which the solvent was concentrated *in vacuo*. The crude residue was then redissolved in diethyl ether (10 mL), with the minimum amount of DCM (few drops until fully solubilised), and aq. sodium hydrogencarbonate (0.5 mL, 5% solution) added. This biphasic mixture was then allowed to stir for 5 min before the aqueous layer was removed. The remaining organic layer was then dried with $MgSO_4$, and gaseous HCl (from conc. $HCl\backslash H_2SO_4$) was then blown through, prompting a yellow salt to crash out. This salt was then washed with diethyl ether (3 × 5 mL) which was decanted off, to leave amine salt ***(4.13)*** (0.14 g, 0.297 mmoles, 75%) as a yellow solid.

^{1}H NMR (600 MHz, DMSO-d_6) δ_H ppm : 0.97 (3 H, d, Leu-CH_3, *J*=5.9 Hz), 0.99 (3 H, d, Leu-CH_3, *J*=5.9 Hz), 1.73 - 1.87 (2 H, dm, Leu-CH_2), 1.78 - 1.80 (1 H, m, $CH(CH_3)_2$), 3.71 (3 H, s, OCH_3), 3.85 (1 H, m, $CHNH_2$, *J*=6.80 Hz), 3.90 (3 H, s, OCH_3), 3.93 (3 H, s, OCH_3), 3.94 (3 H, s, OCH_3), 4.40 (2 H, br. s., NH_2), 6.20 (1 H, s, C=CH), 6.88 (1 H, s, ArH), 7.02 (1 H, d, ArH, *J*=8.28 Hz), 7.12 (1 H, dd, ArH, *J*=8.47, 2.07 Hz), 7.59 (1 H, s, ArH), 8.51 (1 H, d, N<u>H</u>CO, *J*=2.26 Hz)

^{13}C NMR (151 MHz, DMSO-d_6) δ_C ppm : 21.2 (Leu-CH_3), 21.5 (Leu-CH_3), 23.9 (<u>C</u>H$(CH_3)_2$), 39.8 (Leu-CH_2), 51.3 (CHNH), 55.9 (OCH_3), 56.0 (OCH_3), 61.2 (OCH_3), 61.6 (OCH_3), 103.5 (ArCH), 110.5 (ArCH), 112.8 (C=<u>C</u>H), 114.2 (ArC), 119.5 (ArCH), 123.7 (ArCH), 127.4 (ArC), 127.6 (ArC), 140.9 (ArC), 142.9 (ArC), 145.5 (ArC), 149.4 (ArC), 149.7 (ArC), 155.4 (<u>C</u>=CH), 160.5 (Lactone-OC=O), 174.4 (Ar-NC=O)

ν_{max} cm^{-1} : 3381.6, 2946.9, 2874.3, 1770.8, 1705.9, 1513.5, 1289.4, 733.4

HRMS : calculated 470.2053, found 471.2133 ($M + H^+$), 493.1944 ($M + Na^+$)

Synthesis of intermediate *tert*-butyl N-{1-hydroxy-1-[(1-{[2-methoxy-5-(6,7,8-trimethoxy-2-oxochromen-4-yl)phenyl]carbamoyl}-3-methylbutyl)carbamoyl]-3-phenylpropan-2-yl}carbamate *(4.14)*

Amine ***(4.13)*** (0.14 g, 0.3 mmoles) was dissolved in anhydrous DCM (5 mL) under an atmosphere of nitrogen and cooled to 0 °C. To this was added, in anhydrous DCM and under nitrogen, pentafluorophenyl ester ***(4.04)*** (0.22 g, 0.75 mmoles), followed by diisopropylethylamine (0.16

mL, 0.9 mmoles). The reaction was then monitored by TLC until such time as no further progress was observed. Solvent was then removed by blowing off with nitrogen gas and the remaining residue purified via column chromatography (1:1, hexane : ethyl acetate) to afford Boc-bestatin compound ***(4.14)*** (0.1 mg, 0.13 mmoles, 55%) as a brown residue.

^{1}H NMR (600 MHz, CHLOROFORM-*d*) δ_H ppm : 0.95 (3 H, d, Leu-CH_3, *J*=5.87 Hz), 0.99 (3 H, d, Leu-CH_3, *J*=5.87 Hz), 1.40 (9 H, s, $C(CH_3)_3$), 1.63 - 1.85 (2 H, dm, Leu-CH_2), 1.68 - 1.73 (1 H, m, $CH(CH_3)_2$), 3.04 - 3.30 (2 H, m, Ar-CH_2), 3.80 (3 H, s, OCH_3), 3.96 (3 H, s, OCH_3), 4.03 (3 H, s, OCH_3), 4.07 (3 H, s, OCH_3), 4.22 (1 H, m, C<u>H</u>OH, *J*=2.20 Hz), 4.59 - 4.66 (1 H, m, Leu-C<u>H</u>NH), 5.01 (1 H, d, NH, *J*=7.34 Hz), 6.30 (1 H, s, C=CH), 6.90 (1 H, s, ArH), 7.02 (1 H, d, ArH, *J*=8.07 Hz), 7.19 (2 H, d, 2 × ArH, *J*=8.80 Hz), 7.25 (2 H, m, 2 × ArH, *J*=8.10 Hz), 7.32 (2 H, t, 2 × ArH, *J*=7.44 Hz), 7.39 (1 H, br. s., NH), 8.51 (3 H, s, 2 × NH, 1 × ArH)

^{13}C NMR (151 MHz, CHLOROFORM-*d*) δ_C ppm : 21.5 (Leu-CH_3), 22.9 (Leu-CH_3), 24.6 (<u>C</u>H$(CH_3)_2$), 28.0 (C(<u>C</u>$H_3)_3$), 38.9 (Ar-CH_2) 40.1 (Leu-CH_2), 52.2 (CHNH), 55.8 (<u>C</u>HNH-Boc), 55.9 (OCH_3), 56.1 (OCH_3), 61.3 (OCH_3), 61.7 (OCH_3), 74.7 (CHOH), 80.8 (<u>C</u>$(CH_3)_3$), 103.2 (ArCH), 110.4 (ArCH), 113.3 (C=<u>C</u>H), 114.2 (ArC), 120.4 (ArCH), 124.1 (ArCH), 126.6 (ArCH), 127.2 (ArC), 127.9 (ArC), 128.5 (2 × ArCH), 129.1 (2 × ArCH), 137.8 (ArC), 141.2 (ArC), 143.2 (ArC), 145.6 (ArC), 149.2 (ArC), 149.5 (<u>C</u>=CH), 155.0 (Boc-OC=O), 160.6 (Lactone-C=O), 169.6 (2 × NHC=O)

ν_{max} cm^{-1} : 3301.1, 2957.6, 2870.8, 1705.9, 1656.9, 1537.5, 1389.6, 1169.8, 739.8

HRMS : calculated 747.3367, found 746.3337 ($M - H^+$), 770.3231 ($M + Na^+$)

Synthesis of 2-(3-amino-2-hydroxy-4-phenylbutanamido)-N-[2-methoxy-5-(6,7,8-trimethoxy-2-oxochromen-4-yl)phenyl]-4-methylpentanamide *(4.15)*

To a stirred solution of carbamate ***(4.14)*** (55 mg, 0.0736 mmoles) was added trifluoroacetic acid:DCM (1:1, 1 mL) at 0 °C under an atmosphere of nitrogen. After 5 min, the reaction was in concentrated *in vacuo*. The residue left was redissolved in ether (10 mL) and stirred, to which sodium hydrogencarbonate (1 mL, saturated solution) was added and stirred for 5 min. The organic layer was then separated and dried with $MgSO_4$, filtered, before being condensed under reduced pressure to afford free amine ***(4.15)*** (21 mg, 0.0324 mmoles, 45%) as a yellow solid.

^{1}H NMR (600 MHz, CHLOROFORM-*d*) δ_H ppm : 0.93 (3 H, d, Leu-CH_3, *J*=5.65 Hz), 0.96 (3 H, d, Leu-CH_3, *J*=5.65 Hz), 1.52 - 1.85 (2 H, m, Leu-CH_2), 1.65 - 1.71 (1 H, m, $CH(CH_3)_2$), 2.80 - 3.16 (2 H, dm,

Ar-CH_2), 3.71 (3 H, s, OCH_3), 3.74 (1 H, s, C<u>H</u>NH_2), 3.90 (3 H, s, OCH_3), 3.95 (3 H, s, OCH_3), 3.99 (3 H, s, OCH_3), 4.28 (1 H, s, C<u>H</u>OH), 4.39 (1 H, m, OH) 4.51 (1 H, d, C<u>H</u>NH, *J*=6.78 Hz), 6.23 (1 H, s, C=CH), 6.84 (1 H, s, ArH), 7.01 (2 H, d, ArH, *J*=8.28 Hz), 7.17 (2 H, m, 2 × ArH, *J*=8.28 Hz), 7.20 - 7.25 (2 H, m, 2 × ArH), 7.26 - 7.31 (2 H, m, ArH), 7.35 (2 H, s, NH_2), 8.32 (2 H, br. s., 2 × NHCO), 8.37 (1 H, m, ArH)

^{13}C NMR (151 MHz, CHLOROFORM-*d*) δ_C ppm : 21.0 (Leu-CH_3), 21.6 (Leu-CH_3), 24.1 (<u>C</u>H$(CH_3)_3$), 34.0 (Ar-<u>C</u>H_2), 39.6 (Leu-CH_2), 52.2 (CHNH), 54.4 (C<u>H</u>NH_2), 55.2 (OCH_3), 55.3 (OCH_3), 60.6 (OCH_3), 61.0 (OCH_3), 67.9 (CHOH), 102.7 (ArCH), 110.0 (ArCH), 112.2 (C=<u>C</u>H), 113.6 (ArC), 120.3 (ArCH), 124.0 (ArCH), 126.3 (ArC), 126.7 (ArC), 126.8 (ArCH), 128.2 (2 × ArCH), 128.5 (2 × ArCH), 134.3 (ArC), 140.4 (ArC), 142.4 (ArC), 145.1 (ArC), 149.0 (ArC), 149.3 (ArC), 155.1 (<u>C</u>=CH), 160.8 (Lactone-O<u>C</u>=O), 169.8 (Ar-NH<u>C</u>=O), 171.3 (NHC=O)

ν_{max} cm^{-1} : 3299.1, 2954.3, 2922.9, 2853.0, 2476.5, 1723.4, 1654.0, 1451.1, 1385.9, 1092.8, 1049.6, 700.0

HRMS : calculated 647.2843, found 648.2888 ($M + H^+$)

Synthesis of N-Boc Bestatin *(4.16)*

Bestatin (0.675 g, 0.0022 moles) and potassium carbonate (0.36 g, 0.0026 moles) were dissolved in THF (10 mL) and water (10 mL) at 0 °C. To this di-*tert*-butyl dicarbonate (0.57 g, 0.0026 moles) in THF (5 mL) was added and the reaction allowed warm to RT. After stirring for 6 h, the reaction was quenched with aq. NaOH solution (50 mL, 2.5 M). The reaction mixture was then quenched with diethyl ether (3 × 50 mL). The organic layers were dried with $MgSO_4$, filtered and concentrated *in vacuo* to afford carbamate ***(4.16)*** (0.78 g, 0.00191 moles, 87%) as a white crystalline solid.

^{1}H NMR (600 MHz, CHLOROFORM-*d*) δ_H ppm : 0.90 (3 H, d, Leu-CH_3, *J*=6 Hz), 0.92 (3 H, d, Leu-CH_3, *J*=6 Hz), 1.28 (9 H, s, $C(CH_3)_3$), 1.6 – 1.69 (2 H, m, Leu-CH_2), 1.65-1.67 (1 H, m, C<u>H</u>$(CH_3)_2$), 2.84 (1 H, d, Ar-CH_2, *J*=5.1 Hz), 4.05 (1 H, m , C<u>H</u>NH-Boc), 4.18 (1 H, m, C<u>H</u>OH), 4.61 (1 H, t, CHNH, *J*=6.7 Hz), 5.17 (1 H, d, NH, 78 Hz), 6.35 (1 H, br. s., OH), 7.18-7.25 (5 H, m, 5 × ArH), 7.42 (1 H, m, NH)

^{13}C NMR (151 MHz, CHLOROFORM-*d*) δ_C ppm : 21.4 (Leu-CH_3), 23.1 (Leu-CH_3), 24.8 (<u>C</u>H$(CH_3)_2$), 28.2 ($C(\underline{C}H_3)_3$), 36.6 (Ar-CH_2), 40.7 (Leu-CH_2), 50.5 (CHNH-Boc), 55.3 (CHNH), 73.6 (CHOH), 80.4

(C(CH$_3$)$_3$), 126.5 (ArCH), 128.5 (2 × ArCH), 129.3 (ArCH), 129.6 (ArCH), 138.1 (ArC), 157.4 (Boc-NHC=O), 173.6 (COOH), 175.6 (HOCH-C=O)

ν_{max} cm^{-1} : 3439.9, 2961.4, 1750.2, 1689.2, 1527.5, 1508.1, 1455.7

HRMS : calculated 408.2260, found 431.2149 (M + Na$^+$)

MP : 99-100 °C

Synthesis of intermediate 2-methoxy-5-(6,7,8-trimethoxy-2-oxochromen-4-yl)phenyl 2-[2-(3-{[(*tert*-butoxy)carbonyl]amino}-2-hydroxy-4-phenylbutanamido)-4-methylpentanamido]-4-methylpentanoate *(4.17)*

Amine salt ***(4.08)*** (26 mg, 0.056 mmoles) was dissolved in anhydrous DCM (3 mL) under an atmosphere of nitrogen at 0 °C. To this was added sequentially in dry DCM; *N*-Boc bestatin ***(4.16)*** (23 mg, 0.056 moles), PyBroP (26 mg, 0.056 moles) and diisopropylamine (29 µL, 0.168 mmoles). The reaction was gradually allowed to reach RT and the reaction was monitored via TLC. After approximately 2 h, the reaction was quenched with aq. HCl solution (20 mL, 1 M) and extracted with diethyl ether (3 × 30 mL). The organic layer was then dried with $MgSO_4$, filtered and concentrated *in vacuo* before the residue was then purifed by column chromatography (3:1, hexane : ethyl acetate) to give carbamate product ***(4.17)*** as a clear yellowish oil (37 mg, 0.0437 mmoles, 78%).

^{1}H NMR (600 MHz, CHLOROFORM-*d*) δ_H ppm : 0.90 - 0.91 (3 H, d, Leu-CH$_3$, *J*=6.02), 0.95 (3 H, d, Leu-CH$_3$, *J*=6.02 Hz), 1.01 (3 H, d, Leu-CH$_3$, *J*=6.40 Hz), 1.02 (3 H, d, Leu-CH$_3$, *J*=6.40 Hz), 1.41 (9 H, s, C(CH$_3$)$_3$), 1.59 - 1.77 (2 H, m, Leu-CH$_2$), 1.62 - 1.68 (1 H, m, CH(CH$_3$)$_2$), 1.78 - 1.95 (2 H, m, Leu-CH$_2$), 1.79 - 1.86 (1 H, m, CH(CH$_3$)$_2$), 3.02 - 3.28 (2 H, m, Ar-CH$_2$), 3.79 (3 H, s, OCH$_3$), 3.91 (3 H, s, OCH$_3$), 4.03 (3 H, s, OCH$_3$), 4.07 (3 H, s, OCH$_3$), 4.15 - 4.18 (1 H, m, CHOH), 4.49 - 4.54 (1 H, m, CHNH-Boc), 4.83 (2 H, dd, 2 × CHNH, *J*=13.74, 8.09 Hz), 4.99 (1 H, d, NH, *J*=7.53 Hz), 6.31 (1 H, s, C=CH), 6.69 (1 H, br. s., OH), 6.77 (1 H, s, ArH), 7.07 (1 H, d, NH, *J*=8.36 Hz), 7.12 (1 H, d, ArH, *J*=8.66 Hz), 7.18 - 7.28 (5 H, m, 4 × ArH, 1 × NH), 7.31 (2 H, m, 2 × ArH, *J*=7.50 Hz), 7.34 - 7.37 (1 H, dd, ArH, *J*=4.40, 2.23 Hz)

^{13}C NMR (151 MHz, CHLOROFORM-*d*) δ_C ppm : 21.5 (Leu-CH$_3$), 21.8 (Leu-CH$_3$), 22.7 (Leu-CH$_3$), 22.9 (Leu-CH$_3$), 24.4 (CH(CH$_3$)$_2$), 24.8 (CH(CH$_3$)$_2$), 28.0 (C(CH$_3$)$_3$), 29.5 (Ar-CH$_2$), 40.2 (Leu-CH$_2$) 41.0 (Leu-CH$_2$), 48.0 (CHNH), 51.0 (CHNH), 51.0 (CHNH-Boc), 55.9 (OCH$_3$), 56.1 (OCH$_3$), 61.3 (OCH$_3$),

61.8 (OCH_3), 74.5 (CHOH), 81.2 ($\underline{C}(CH_3)_3$), 102.9 (ArCH), 112.6 (ArCH), 113.5 (C=$\underline{C}$H), 114.1 (ArC), 123.2 (ArCH), 126.6 (ArCH), 127.0 (ArCH), 127.7 (ArC), 128.4 (ArC), 128.5 (2 × ArCH), 129.1 (2 × ArCH), 137.8 (ArC), 139.2 (ArC), 141.3 (ArC), 143.2 (ArC), 145.8 (ArC), 149.6 (ArC), 152.0 ($\underline{C}$=CH), 154.0 (Boc-NH$\underline{C}$=O), 160.3 (Lactone-OC=O), 170.6 (Ar-O$\underline{C}$=O), 171.4 (CHNH$\underline{C}$=O), 172.9 (HOCH-$\underline{C}$=O)

ν_{max} cm^{-1} : 3357.5, 3294.4, 2957.7, 1770.9, 1721.6, 1643.2, 1551.6, 1514.4, 1389.5, 1275.1, 1170.2, 1132.2, 747.7

HRMS : calculated 861.4048, found 884.3894 ($M + Na^+$)

Synthesis of 2-methoxy-5-(6,7,8-trimethoxy-2-oxochromen-4-yl)phenyl 2-[2-(3-amino-2-hydroxy-4-phenylbutanamido)-4-methylpentanamido]-4-methylpentanoate *(4.18)*

To carbamate compound ***(4.17)*** (12 mg, 0.014 mmoles), under an atmosphere of nitrogen, was added trifluoroacetic acid in anhydrous DCM (1:1, 1 mL). The reaction was stirred at 0 °C for 5 min, after which the solvent was concentrated *in vacuo*. The crude residue was then redissolved in diethyl ether (10 mL), with the minimum amount of DCM (few drops until fully solubilised), and aq. sodium hydrogencarbonate solution (0.5 mL, saturated solution) added. This biphasic mixture was then allowed to stir for 5 min before the aqueous layer was removed. The remaining organic layer was then dried with $MgSO_4$, and gaseous HCl (from conc. HCl\H_2SO_4) was then blown through, prompting a yellow salt to crash out. This salt was then washed with diethyl ether (3 × 5 mL) which was decanted off, to leave amine salt ***(4.18)*** (7 mg, 0.09 mmoles, 66%) as a white solid.

^{1}H NMR (600 MHz, DMSO-d_6) δ_H ppm : 0.86 (3 H, d, Leu-CH_3, *J*=6.40 Hz), 0.87 - 0.88 (3 H, d, Leu-CH_3, *J*=5.94 Hz), 0.87 - 0.89 (3 H, d, Leu-CH_3, *J*=5.94 Hz), 0.95 (3 H, d, Leu-CH_3, *J*=6.40 Hz), 1.48 - 1.79 (4 H, m, 2 × Leu-CH_2), 1.73 - 1.76 (2 H, m, 2 × $C\underline{H}(CH_3)_2$), 2.76 - 2.99 (2 H, m, Ar-CH_2), 3.52 (1 H, br. s., $C\underline{H}NH_2$), 3.71 (3 H, s, OCH_3), 3.86 (3 H, s, OCH_3), 3.90 (3 H, s, OCH_3), 3.94 (3 H, s, OCH_3), 3.97 - 4.03 (1 H, m, CHOH), 4.38 - 4.43 (1 H, m, $C\underline{H}NH_2$), 4.49 - 4.59 (1 H, m, $C\underline{H}$NH), 6.35 (1 H, s, C=CH), 6.60 (1 H, d, OH, *J*=6.9 Hz), 6.76 (1 H, s, ArH), 7.26 - 7.30 (4 H, m, 4 × ArH), 7.34 (3 H, m, 3 × ArH), 7.49 - 7.54 (1 H, m, ArH), 7.90 (2 H, br. s., NH_2), 8.06 - 8.12 (1 H, d, NH, *J*=7.83 Hz), 8.62 - 8.66 (1 H, d, *J*=7.49 Hz)

^{13}C NMR (151 MHz, DMSO-d_6) δ_C ppm : 21.7 (Leu-CH_3), 22.2 (Leu-CH_3), 23.0 (Leu-CH_3), 23.2 (Leu-CH_3), 24.4 ($\underline{C}H(CH_3)_2$), 24.5 ($\underline{C}H(CH_3)_2$), 35.0 (Ar-CH_2), 40.4 (Leu-CH_2), 41.2 (Leu-CH_2), 50.8 (CHNH), 51.1 (CHNH), 54.7 ($CHNH_2$), 56.1 (OCH_3), 56.4 (OCH_3), 61.4 (OCH_3), 61.8 (OCH_3), 68.8 (CHOH), 103.3 (ArCH), 113.5 (ArCH), 113.8 (C=$\underline{C}$H), 114.0 (ArC), 123.5 (ArCH), 127.2 (ArCH) 127.3 (ArCH), 127.9 (ArC), 129.0 (2 × ArCH), 129.7 (2 × ArCH), 136.5 (ArC), 139.1 (ArC), 141.1 (ArC), 142.9 (ArC), 145.6 (ArC), 149.6 (ArC), 152.3 (ArC), 153.8 ($\underline{C}$=CH), 159.8 (Lactone-O$\underline{C}$=O), 170.8 (Ar-O$\underline{C}$=O), 171.0 (HNC=O), 172.4 (HNC=O)

ν_{max} cm^{-1} : 3316.3, 3209.7, 2953.8, 2924.6, 2869.7, 2580.1, 1768.7, 1721.1, 1663.4, 1634.3, 1512.7, 1386.5, 1269.3, 1131.4, 733.4, 699.4

HRMS : calculated 761.3524, found 762.3601 ($M + H^+$), 796.3229 ($M + Cl^-$)

Synthesis of intermediate *tert*-butyl N-[1-hydroxy-1-({1-[(1-{[2-methoxy-5-(6,7,8-trimethoxy-2-oxochromen-4-yl)phenyl]carbamoyl}-3-methylbutyl)carbamoyl]-3-methylbutyl}carbamoyl)-3-phenylpropan-2-yl]carbamate *(4.19)*

To a stirred solution of free amine ***(4.13)*** (25 mg, 0.053 mmoles) in anhydrous DCM (1 mL) at 0 °C, was added Boc-bestatin ***(4.16)*** (25 mg, 0.053 mmoles), PyBroP (25 mg, 0.053 mmoles) and diisopropylethylamine (21 mg, 0.16 mmoles), in that order under an atmosphere of nitrogen. The reaction was allowed to reach RT and stirred for 2 h before quenching with aq. HCl solution (20 mL, 1 M). The reaction was extracted with diethyl ether (3 ×30 mL), dried with magnesium sulfate, filtered and concentrated *in vacuo*. The resultant residue was then purified by column chromatography (3:1, hexane : ethyl acetate) to give carbamate product ***(4.19)*** as a brown oil (31 mg, 0.038 mmoles, 72%).

^{1}H NMR (600 MHz, CHLOROFORM-*d*) δ_H ppm : 0.8 - 1.0 (12 H, m, 4 × Leu-CH_3), 1.28 (9 H, s, $C(CH_3)_3$), 1.357 - 1.477 (2 H, m, Leu-CH_2), 1.438 - 1.467 (1 H, m, $\underline{C}H(CH_3)_2$), 1.594 - 1.792 (2 H, m, Leu-CH_2), 1.662 - 1.729 (1 H, m, $\underline{C}H(CH_3)_2$), 2.885 - 3.169 (2 H, m, Ar-CH_2), 3.89 (3 H, s, OCH_3), 3.91 (3 H, s, OCH_3), 4.01 (3 H, s, OCH_3), 4.04 (3 H, s, OCH_3), 4.06 - 4.09 (1 H, m, CHOH), 4.17 - 4.20 (1 H, m, C$\underline{H}$NH), 4.47 (1 H, m, C$\underline{H}$NH-Boc), 4.99 (1 H, m, C$\underline{H}$NH), 5.32 (2 H, br. s., 2 × NH), 5.64 (1 H, br. s. OH), 6.37 (1 H, s, C=CH), 6.69 (1 H, s, ArH), 7.02 (1 H, s, ArH), 7.12 (1 H, d, ArH, *J*=8.66 Hz), 7.19 (2 H, d, 2 × ArH, *J*=7.22 Hz), 7.22 – 7.36 (4 H, m, 3 × ArH, 1 × NH), 7.63 (1 H, d, ArH, *J*=9.85 Hz), 7.99 (1 H, br. s., NH)

^{13}C NMR (151 MHz, CHLOROFORM-*d*) δ_C ppm : 22.3 (Leu-CH_3), 22.6 (Leu-CH_3), 23.2 (Leu-CH_3), 24.6 (Leu-CH_3), 25.2 ($\underline{C}H(CH_3)_2$), 25.4 ($\underline{C}H(CH_3)_2$), 28.1 ($C(\underline{C}H_3)_3$), 29.7 (Ar-CH_2), 40.2 (Leu-CH_2) 41.4 (Leu-CH_2), 49.3 (CHNH), 51.0 (CHNH), 51.5 (CHNH), 55.9 (OCH_3), 56.2 (OCH_3), 61.1 (OCH_3), 61.7 (OCH_3), 70.5 (CHOH), 81.2 ($\underline{C}(CH_3)_3$), 103.1 (ArCH), 112.6 (ArCH), 113.2 (C=$\underline{C}$H), 114.0 (ArC), 123.2 (ArCH), 126.4 (ArCH), 126.8 (ArCH), 127.7 (ArC), 128.4 (ArC), 128.9 (2 × ArCH), 129.4 (2 × ArCH), 134.8 (ArC), 138.7 (ArC), 141.9 (ArC), 143.6 (ArC), 145.8 (ArC), 149.8 (ArC), 152.0 ($\underline{C}$=CH), 155.50 (Boc-NH$\underline{C}$=O), 160.3 (Lactone-OC=O), 171.5 (CHNH$\underline{C}$=O), 172.0 (Ar-O$\underline{C}$=O), 172.9 (HOCH-$\underline{C}$=O)

ν_{max} cm^{-1} : 3337.5, 3281.4, 2946.7, 1788.0, 1721.6, 1653.4, 1551.0, 1389.5, 1275.1, 1132.2, 743.3

HRMS : calculated 860.4208, found 861.4680 ($M + H^+$), 883.4070 ($M + Na^+$), 895.3793 ($M + Cl^-$)

Synthesis of (2S)-2-[(2S)-2-[(2S,3S)-3-amino-2-hydroxy-4-phenylbutanamido]-4-methylpentanamido]-N-[2-methoxy-5-(6,7,8-trimethoxy-2-oxochromen-4-yl)phenyl]-4-methylpentanamide *(4.20)*

To carbamate compound ***(4.19)*** (31 mg, 0.038 mmoles), under an atmosphere of nitrogen, was added trifluoroacetic acid in anhydrous DCM (1:1, 1 mL). The reaction was stirred at 0 °C for 5 min, after which the solvent was concentrated *in vacuo*. The crude residue was then redissolved in diethyl ether (10 mL), with the minimum amount of DCM (few drops until fully solubilised), and aq. sodium hydrogencarbonate (0.5 mL, saturated solution) added. This biphasic mixture was then allowed to stir for 5 min before the aqueous layer was removed. The remaining organic layer was then dried with $MgSO_4$, and gaseous HCl (from conc. HCl\H_2SO_4) was then blown through, prompting a yellow salt to crash out. This salt was then washed with diethyl ether (3 × 5 mL) which was decanted off, to leave amine salt ***(4.23)*** (19 mg, 0.0025 mmoles, 66%) as a yellow residue.

^1H NMR (600 MHz, METHANOL-d_4) δ_H ppm : 0.89 - 1.02 (12 H, m, 4 × Leu-CH_3), 1.56 - 1.86 (4 H, m, 2 × Leu-CH_2), 1.69 - 1.76 (2 H, m, $C\underline{H}(CH_3)_2$), 2.84 - 3.18 (2 H, m, Ar-CH_2), 3.81 (3 H, s, OCH_3), 3.83 (1 H, d, $CHNH_2$, *J*=3.08 Hz), 3.99 (3 H, s, OCH_3), 4.00 (3 H, s, OCH_3), 4.04 (3 H, s, OCH_3), 4.15 - 4.18 (1 H, d, C$\underline{H}$OH, *J*=3.08 Hz), 4.47 - 4.51 (1 H, t, C$\underline{H}$NH, *J*=7.02 Hz), 4.60 - 4.66 (1 H, t, C$\underline{H}$NH, *J*=7.5 Hz), 6.31 - 6.34 (1 H, s, C=CH), 6.71 (1 H, d, ArH, *J*=8.75 Hz), 6.86 - 6.90 (1 H, d, ArH, *J*=8.75 Hz), 7.01 (1 H, s, ArH), 7.24 (1 H, d, ArH, 8.75 Hz), 7.27 – 7.34 (3 H, m, 2 × ArH, 1 × NH), 7.35 - 7.40 (2 H, m, 2 × ArH), 7.61 - 7.67 (1 H, m, NH), 7.72 - 7.76 (1 H, m, NH), 8.26 (1 H, s, ArH)

^{13}C NMR (151 MHz, METHANOL-d_4) δ_C ppm : 23.5 (Leu-CH_3), 23.8 (Leu-CH_3), 24.9 (Leu-CH_3), 25.03 (Leu-CH_3), 27.5 ($\underline{C}H(CH_3)_2$), 27.6 ($\underline{C}H(CH_3)_2$),34.7 (Ar-CH_2), 43.1 (Leu-CH_3), 43.5 (Leu-CH_3), 55.0 (CHNH), 55.6 (CHNH), 57.9 (OCH_3), 58.3 (OCH_3), 63.4 (OCH_3), 63.9 (OCH_3), 71.5 (CHOH), 106.5 (ArCH), 114.4 (ArCH), 115.3 (C=$\underline{C}$H), 117.2 (ArC), 125.0 (ArCH), 128.2 (ArCH), 130.4 (ArCH), 131.7 (2 × ArCH), 132.1 (2 × ArCH), 138.2 (ArC), 144.2 (ArC), 146.0 (ArC), 149.0 (ArC), 152.9 (ArC), 159.0 ($\underline{C}$=CH), 164.6 (Lactone-OC=O), 174.6 (Ar-OC=O), 175.1 (HOHC-$\underline{C}$=O), 176.6 (HN-C=O)

ν_{max} cm^{-1} : 3360.5, 2924.3, 2853.4, 1721.8, 1658.2, 1455.7, 1261.3, 795.2, 737.1

HRMS : calculated 760.3683, found 759.3641 ($M - H^+$), 761.3724 ($M + H^+$), 783.3538 ($M + Na^+$), 795.3408 ($M + Cl^-$)

Synthesis of intermediate 2-amino-N-[2-methoxy-5-(6,7,8-trimethoxy-2-oxochromen-4-yl)phenyl]propanamide *(4.21)*

To *tert*-butyl N-(1-{[2-methoxy-5-(6,7,8-trimethoxy-2-oxochromen-4-yl)phenyl]carbamoyl}ethyl) carbamate ***(3.06-Ala)*** (20 mg, 0.038 mmoles), was added trifluoroacetic acid in anhydrous DCM (1:1, 1 mL) under an atmosphere of nitrogen,. The reaction was stirred at 0 °C for 5 min, after which the solvent was concentrated *in vacuo*. The crude residue was then redissolved in diethyl ether (10 mL), with the minimum amount of DCM (few drops until fully solubilised), and aq. sodium hydrogencarbonate (0.5 mL, saturated solution) added. This biphasic mixture was then allowed to stir for 5 min before the aqueous layer was removed. The remaining organic layer was then dried with $MgSO_4$, and gaseous HCl (from conc. HCl\H_2SO_4) was then blown through, prompting a yellow salt to crash out. This salt was then washed with diethyl ether (3 × 5 mL) which was decanted off, to leave pure amine salt ***(4.21)*** (10 mg, 0.024, 62%) as a yellow solid.

^{1}H NMR (600 MHz, DMSO-d_6) δ_H ppm : 1.32 (3 H, d, CH_3, *J*=6.78 Hz), 3.55 (1 H, q, C$\underline{H}NH_2$, *J*=6.80 Hz), 3.71 (3 H, s, OCH_3), 3.90 (3 H, s, OCH_3), 3.93 (3 H, s, OCH_3), 3.94 (3 H, s, OCH_3), 6.18 (1 H, s, C=CH), 6.87 (1 H, s, ArH), 7.02 (1 H, d, ArH, *J*=8.28 Hz), 7.12 (1 H, dd, ArH, *J*=8.47, 2.07 Hz), 8.51 (1 H, d, ArH, *J*=2.26 Hz), 10.00 (2 H, br. s., NH_2)

^{13}C NMR (151 MHz, DMSO-d_6) δ_C ppm : 21.4 (Ala-CH_3), 51.3 ($CHNH_2$), 55.9 (OCH_3), 56.0 (OCH_3), 61.2 (OCH_3), 61.6 (OCH_3), 103.5 (ArCH), 110.5 (ArCH), 112.8 (C=$\underline{C}$H), 114.2 (ArC), 119.5 (ArCH), 123.7 (ArCH), 127.4 (ArC), 127.6 (ArC), 140.9 (ArC), 142.9 (ArC), 145.5 (ArC), 149.4 (ArC), 149.7 (ArC), 155.4 ($\underline{C}$=CH), 160.5 (Lactone-OC=O), 174.4 (Ar-OC=O)

ν_{max} cm^{-1} : 3344.7, 2968.4, 2912.42, 1670.9, 1615.2, 1551.2, 1512.2

HRMS : calculated 428.1584, found 429.1646 ($M + H^+$)

MP : 171-174 °C

Synthesis of intermediate *tert*-butyl N-[1-hydroxy-1-({1-[(1-{[2-methoxy-5-(6,7,8-trimethoxy-2-oxochromen-4-yl)phenyl]carbamoyl}ethyl)carbamoyl]-3-methylbutyl}carbamoyl)-3-phenylpropan-2-yl]carbamate *(4.22)*

Free amine ***(4.21)*** (10 mg, 0.0233 mmoles) was dissolved and stirred in anhydrous DCM (1 mL) at 0 °C under an atmosphere of nitrogen. This was added to the Boc-protected pentafluorophenol ester of bestatin (21 mg, 0.035 mmoles) in anhydrous DCM (2 mL) formed previously, followed by diisoprorylethyl amine (10 mg, 0.0122 mL, 0.07 mmoles). After around 2 h, the reaction was reduced by concentrated *in vacuo*, filtered through paper to remove traces of DCU from the PFP ester formation and promptly purified by flash column chromatography (1:1, hexane: ethyl acetate). Carbamate ***(4.22)*** (11 mg, 0.0134 mmoles, 58%) was obtained as a brown oil.

^{1}H NMR (600 MHz, CHLOROFORM-*d*) δ_H ppm : 0.92 (3 H, d, Leu-CH_3, *J*=6.40 Hz), 0.96 (3 H, d, Leu-CH_3, *J*=6.40 Hz), 1.40 (9 H, s, $C(CH_3)_3$), 1.48 (3 H, d, Ala-CH_3, *J*=6.78 Hz), 1.59 - 1.76 (2 H, m, CH_2), 1.70 - 1.73 (1 H, m, $C\underline{H}(CH_3)_2$), 3.02 - 3.26 (2 H, m, Ar-CH_2), 3.80 (3 H, s, OCH_3), 3.98 (3 H, s, OCH_3), 4.03 (3 H, s, OCH_3), 4.07 (3 H, s, OCH_3), 4.19 (2 H, br. s., 1 × NH, 1 × $C\underline{H}OH$), 4.50 - 4.56 (1 H, m, $C\underline{H}NH$), 4.61 (1 H, dt, Boc-NHC$\underline{H}$, *J*=14, 7.1 Hz), 5.02 (1 H, d, NH, *J*=8.28 Hz), 5.81 (1 H, s, OH), 6.31 (1 H, s, C=CH), 6.91 (1 H, s, ArH), 6.97 (1 H, d, NH, *J*=7.53 Hz), 7.03 (1 H, d, ArH, *J*=8.66 Hz), 7.20 (1 H, dd, ArH, *J*=8.28, 2.26 Hz), 7.22 - 7.27 (4 H, m, 3 × ArH, 1 × NH), 7.29 - 7.33 (3 H, m, 3 × ArH), 8.45 (1 H, s, NH), 8.51 (1 H, d, ArH, *J*=2.25).

^{13}C NMR (151 MHz, CHLOROFORM-*d*) δ_C ppm : 17.5 (Ala-CH_3), 21.3 (Leu-CH_3), 23.0 (Leu-CH_3), 24.4 ($\underline{C}H(CH_3)_2$), 28.0 ($C(\underline{C}H_3)_3$), 29.5 (Ar-CH_2), 40.3 (Leu-CH_2), 49.9 (CHNH), 51.2 (CHNH), 55.8 (CHNH), 55.9 (OCH_3), 56.2 (OCH_3), 61.3 (OCH_3), 61.7 (OCH_3), 74.1 (CHOH), 80.6 ($\underline{C}(CH_3)_3$), 103.3 (ArCH), 110.3 (ArCH), 113.3 (C=$\underline{C}$H), 114.2 (ArC), 120.4 (ArCH), 124.1 (ArCH), 126.6 (ArCH), 127.1 (ArC), 127.9 (ArC), 128.5 (2 × ArCH), 129.2 (2 × ArCH), 137.7 (ArC), 141.2 (ArC), 142.8 (ArC), 145.7 (ArC), 149.2 (ArC), 149.5 (ArC), 157.9 ($\underline{C}$=CH), 154.9 (Boc-$\underline{C}$=O), 160.7 (Lactone-O$\underline{C}$=O), 170.0 (HNC=O), 171.9 (HNC=O), 173.1 (HOCH-$\underline{C}$=O)

ν_{max} cm^{-1} : 3299.9, 2926.6, 2855.1, 2246.4, 1713.1, 1701.1, 1532.3, 1493.8, 1453.1, 1389.8, 1259.3, 1093.8, 735.0

HRMS : calculated 818.3738, found 841.3425 ($M + Na^+$)

Synthesis of 2-(3-amino-2-hydroxy-4-phenylbutanamido)-N-(1-{[2-methoxy-5-(6,7,8-trimethoxy-2-oxochromen-4-yl)phenyl]carbamoyl}ethyl)-4-methylpentanamide *(4.23)*

To carbamate compound ***(4.22)*** (10 mg, 0.0122 mmoles), under an atmosphere of nitrogen, was added trifluoroacetic acid in anhydrous DCM (1:1, 1 mL). The reaction was stirred at 0 °C for 5 min, after which the solvent was condensed *in vacuo*. The crude residue was then redissolved in diethyl ether (10 mL), with the minimum amount of DCM (few drops until fully solubilised), and aq. sodium hydrogencarbonate solution (0.5 mL, saturated solution) added. This biphasic mixture was then allowed to stir for 5 min before the aqueous layer was removed. The remaining organic layer was then dried with $MgSO_4$, and gaseous HCl (from conc. $HCl\backslash H_2SO_4$) was then blown through, prompting a yellow salt to crash out. This salt was then washed with diethyl ether (3 × 5 mL) which was decanted off, to leave amine salt ***(4.23)*** (8 mg, 0.00978 mmoles, 80%) as a yellow residue.

^1H NMR (600 MHz, METHANOL-d_4) δ_H ppm : 0.98 (3 H, d, Leu-CH_3, J=6 Hz), 1.02 (3 H, d, Leu-CH_3, J=6 Hz), 1.47 (3 H, d, Ala-CH_3, J=7 Hz), 1.61 - 1.80 (2 H, m, Leu-CH_2), 1.68 - 1.74 (1 H, m, C<u>H</u>$(CH_3)_2$), 2.88 - 3.18 (2 H, m, Ar-CH_2), 3.81 (3 H, s, OCH_3), 3.99 (3 H, s, OCH_3), 4.00 (3 H, s, OCH_3), 4.04 (3 H, s, OCH_3), 4.15 - 4.17 (1 H, m, C<u>H</u>OH), 4.45 - 4.51 (1 H, m, C<u>H</u>NH), 4.55 - 4.63 (2 H, m, 2 × C<u>H</u>NH), 6.33 (1 H, s, C=CH), 7.02 (1 H, s, ArH), 7.24 (1 H, d, J=8 Hz), 7.26 - 7.39 (7 H, m, 6 × ArH, 1 × NH), 8.12 (1 H, d, NH, J=13 Hz), 8.29 - 8.31 (1 H, d, ArH, J=2.2 Hz) 8.33 (1 H, m, NH)

^{13}C NMR (151 MHz, METHANOL-d_4) δ_C ppm : 16.8 (Ala-CH_3), 21.1 (Leu-CH_3), 22.4 (Leu-CH_3), 24.9 (<u>C</u>H$(CH_3)_2$), 35.5 (Ar-CH_2), 40.9 (Leu-CH_2), 50.2 (CHNH), 52.4 (CHNH), 55.3 ($CHNH_2$), 55.7 (OCH_3), 55.8 (OCH_3), 60.9 (OCH_3), 61.3 (OCH_3), 68.8 (CHOH), 103.8 (ArCH), 111.4 (ArCH), 112.7 (C=<u>C</u>H), 114.6 (ArC), 122.1 (ArCH), 125.5 (ArCH), 127.3 (ArC), 127.6 (ArCH), 127.7 (ArC), 129.1 (2 × ArCH), 129.5 (2 × ArCH), 135.7 (ArC), 137.4 (ArC), 141.6 (ArC), 143.4 (ArC), 146.4 (ArC), 150.4 (ArC), 156.4 (<u>C</u>=CH), 161.9 (Lactone-O<u>C</u>=O), 171.6 (HNC=O), 172.2 (HNC=O), 172.4 (HOC-<u>C</u>=O)

ν_{max} cm^{-1} : 2920.6, 1715.6, 1668.5, 1512.5, 1448.9, 1386.9, 1251.8, 1131.5, 1092.9, 1049.9

HRMS : calculated 718.3214, found 717.3173 ($M - H^+$), 719.3267 ($M + H^+$), 741.3078 ($M + Na^+$)

Synthesis of intermediate ({[(3E)-5-(3-hydroxy-4-methoxyphenyl)-7,8,9-trimethoxy-2H-1-benzoxepin-3-ylidene]amino}oxy)acetic acid *(4.24)*

Phenol ***(2.17)*** (36 mg, 0.097 mmoles), sodium acetate (13 mg, 0.15 mmoles), and *O*-carboxymethyl hydroxylamine hemihydrochloride (12 mg, 0.11 mmoles) were stirred for 16 h in EtOH:Water:DCM (8:2:1, 5.5 mL) at RT. The reaction was then quenched with aq. HCl solution (20 mL, 1 M) and extracted with diethyl ether (3 × 30 mL) to give carboxylic acid ***(4.24)*** (30 mg, 0.067 mmoles, 70%) as a clear residue.

^{1}H NMR (600 MHz, CHLOROFORM-*d*) δ_H : 3.61 (3 H, s, OCH_3, minor isomer), 3.64 (3 H, s, OCH_3, major isomer), 3.95 (3 H, s, OCH_3, major isomer), 3.96 (3 H, s, OCH_3, major isomer), 3.96 (3 H, s, OCH_3, minor isomer), 3.98 (3 H, s, OCH_3, minor isomer), 3.99 (3 H, s, OCH_3, minor isomer), 4.01 (3 H, s, OCH_3, major isomer), 4.72 (4 H, s, CH_2, 1 × CH_2 major isomer, 1 × CH_2 minor isomer), 4.73 (2 H, s, CH_2, minor isomer), 5.14 (2 H, s, CH_2, major isomer), 6.30 (1 H, s, ArH, major isomer), 6.37 (1 H, s, ArH, minor isomer), 6.55 (1 H, s, C=CH, major isomer), 6.84 - 6.91 (4 H, m, 2 × major isomer ArH, 2 × minor isomer ArH), 6.96 (1 H, s, ArH, minor isomer), 6.97 (1 H, s, ArH, major isomer), 7.06 (1 H, s, C=CH, minor isomer).

^{13}C NMR (151 MHz, CHLOROFORM-*d*) δ_C : 51.5 (OCH_3, major isomer), 51.6 (OCH_3, minor isomer), 55.7 (OCH_3, minor isomer), 55.8 (OCH_3, major isomer), 60.8 (OCH_3, major isomer), 60.9 (OCH_3, minor isomer), 61.4 (OCH_3, minor isomer), 61.5 (OCH_3, major isomer), 69.8 (CH_2, minor isomer), 70.1 (CH_2, major isomer), 72.0 (CH_2, major isomer), 74.1 (CH_2, minor isomer), 108.8 (ArCH, major isomer), 109.6 (ArCH, minor isomer), 109.7 (ArCH, major isomer), 110.5 (ArCH, minor isomer), 114.9 (ArCH, major isomer), 115.3 (ArCH, minor isomer), 116.2 (C=<u>C</u>H, minor isomer), 120.6 (ArCH, major isomer), 121.0 (ArCH, minor isomer), 122.5 (C=<u>C</u>H, major isomer), 124.7 (ArCH, minor isomer), 126.8 (ArCH, major isomer), 135.4 (ArC, major isomer), 136.4 (ArC, minor isomer), 142.8 (ArC, major isomer), 143.4 (ArC, minor isomer), 143.8 (ArC, major isomer), 144.2 (ArC, minor isomer), 144.66 (ArC, minor isomer), 144.74 (ArC, major isomer), 145.0 (ArC, major isomer), 145.5 (ArC, minor isomer), 146.2 (ArC, major isomer), 147.8 (ArC, minor isomer), 148.6 (ArC, minor isomer), 148.7 (ArC, major isomer), 154.1 (2 × <u>C</u>=CH, both isomers), 160.4 (2 × C=N, both isomers), 174.0 (C=O, major isomer), 174.1 (C=O, minor isomer)

ν_{max} cm^{-1} : 3425.1, 2937.1, 2840.6, 1738.3, 1579.4, 1508.8, 1491.9, 1458.4, 1409.9, 1277.9, 1128.9, 1088.8, 961.5

HRMS : calculated 445.1373, found 446.1436 ($M + H^+$)

Synthesis of intermediate pentafluorophenyl 2-({[(3E)-5-(3-hydroxy-4-methoxyphenyl)-7,8,9-trimethoxy-2H-1-benzoxepin-3-ylidene]amino}oxy)acetate *(4.25)*

Carboxylic acid ***(4.24)*** (24 mg, 0.054 mmoles) was dissolved in anhydrous DCM (2 mL) under nitrogen gas and cooled to 0 °C. To this was added sequentially; pentafluorophenol (9 mg, 0.056 mmoles) in dry DCM (1 mL) and N-(3-dimethylaminopropyl)-N′-ethylcarbodiimide (9.3 mg, 0.056 mmoles) in anhydrous DCM:DMF (1:0.5 mL). The reaction was allowed stir for 1 h when the reaction was quenched with water (20 mL) and extracted with diethyl ether (3 × 30 mL). The resultant crude compound was purified via column chromatography (3:1, hexane:ethyl acetate) to give pentafluorophenyl ester ***(4.25)*** (26 mg, 0.043 mmoles, 79%) as a clear oil.

^{1}H NMR (600 MHz, CHLOROFORM-*d*) δ_H ppm : 3.61 (3 H, s, OCH_3, minor isomer), 3.64 (3 H, s, OCH_3, major isomer), 3.95 (3 H, s, OCH_3, major isomer), 3.962 (3 H, s, OCH_3, major isomer), 3.966 (3 H, s, OCH_3, minor), 3.98 (3 H, s, OCH_3, minor isomer), 3.99 (3 H, s, OCH_3, minor isomer), 4.01 (3 H, s, OCH_3, major isomer), 4.76 (2 H, s, CH_2, minor isomer), 5.01 (4 H, s, 1 × CH_2 major isomer, 1 × CH_2 minor isomer), 5.16 (2 H, s, CH_2, major isomer), 5.64 (1 H, s, OH, major isomer), 5.67 (1 H, s, OH, minor isomer), 6.30 (1 H, s, ArH, major isomer), 6.37 (1 H, s, ArH, minor isomer), 6.55 (1 H, s, C=CH, major isomer), 6.84 - 6.91 (4 H, m, 2 × major isomer ArH, 2 × minor isomer ArH), 6.96 (1 H, d, ArH, *J*=1.88 Hz, minor isomer), 6.97 (1 H, d, ArH *J*=2.26 Hz, major isomer), 7.08 (1 H, s, C=CH, minor isomer)

^{13}C NMR (151 MHz, CHLOROFORM-*d*) δ_C ppm : 55.83 (OCH_3, major isomer), 55.86 (OCH_3, minor isomer), 56.06 (OCH_3, minor isomer), 56.09 (OCH_3, major isomer), 61.12 (OCH_3, major isomer), 61.15 (OCH_3, minor isomer), 61.70 (OCH_3, major isomer), 61.73 (OCH_3, minor isomer), 69.8 (CH_2, minor isomer), 70.1 (CH_2, major isomer), 72.2 (CH_2, major isomer), 74.4 (CH_2, minor isomer), 109.2 (ArCH, major isomer), 109.9 (ArCH, minor isomer), 110.0 (ArCH, major isomer), 110.9 (ArCH, minor isomer), 115.2 (ArCH, major isomer), 115.6 (ArCH, minor isomer), 116.4 (ArCH, minor isomer), 120.9 (ArCH, major isomer), 121.3 (ArCH, minor isomer), 122.7 (ArCH, major isomer), 125.01 (ArC, minor isomer), 127.04 (ArC, major isomer), 135.7 (ArC, major isomer), 136.8 (ArC, minor isomer), 137.0 (4 × ArCF, both isomers), 138.6 (4 × ArCF, both isomers), 140.3 (2 × ArCF, both isomers), 143.2 (ArC, major isomer), 143.9 (ArC, minor isomer), 144.3 (ArC, major isomer), 144.6 (ArC, minor isomer), 145.0 (ArC, minor isomer), 145.1 (ArC, major isomer), 145.4

(ArC, major isomer), 145.9 (ArC, minor isomer), 146.55 (ArC, major isomer), 146.6 (ArC, major isomer), 148.2 (ArC, minor isomer), 148.9 (ArC, minor isomer), 149.1 (ArC, major isomer), 154.8 (C=CH, major isomer), 154.8 (C=CH, minor isomer), 161.1 (2 × C=N, both isomers), 165.5 (C=O, major isomer), 165.8 (C=O, minor isomer)

^{19}F NMR (376 MHz, CHLOROFORM-*d*) δ_F ppm : -169 (1 F, m, minor isomer), -164 (2 F, m, minor isomer), -164 (2 F, m, minor isomer), -162 (2 F, m, major isomer), -158 (1 F, m, major isomer), -153 (2 F, d, *J*=18.35 Hz, major isomer)

ν_{max} cm^{-1} : 3440.3, 2936.6, 2847.5, 1811.9, 1581.7, 1515.5, 1492.6, 1459.2, 1410.3, 1278.5, 1086.9, 997.6

HRMS : calculated 611.1215, found 612.1307 ($M + H^+$), 634.1125 ($M + Na^+$)

Synthesis of N-hydroxy-2-({[(3E)-5-(3-hydroxy-4-methoxyphenyl)-7,8,9-trimethoxy-2H-1-benzoxepin-3-ylidene]amino}oxy)acetamide *(4.26)*

To a stirred solution of pentafluorophenyl ester ***(4.25)*** (20 mg, 0.033 mmoles) in dry DMF (1 mL), under an atmosphere of nitrogen was added hydroxylamine hydrochloride (2.5 mg, 0.036 mmoles) in dry DMF (0.5 mL) and neat diisopropylethylamine (4.6 mg, 0.036 mmoles). The reaction was stirred for 5 min before the reaction was quenched with water (20 mL) and extracted with diethyl ether (3 × 30 mL). The combined organic layers were further washed once with aq. LiCl solution (50 mL, 5%) and then water (5 × 30 mL), before being dried with $MgSO_4$, filtered and concentrated *in vacuo* to afford hydroxamic acid ***(4.26)*** (10 mg, 0.022 mmoles, 66%) as a yellow oil.

^{1}H NMR (600 MHz, CHLOROFORM-*d*) δ_H ppm : 3.62 (3 H, s, OCH_3, minor isomer), 3.64 (3 H, s, OCH_3, major isomer), 3.96 (6 H, s, 2 × OCH_3, 2 × major isomer), 3.97 (3 H, s, OCH_3, minor isomer), 3.99 (6 H, s, 2 × OCH_3, 2 × minor isomer), 4.01 (3 H, s, OCH_3, major isomer), 4.71 (2 H, s, CH_2, minor isomer), 4.73 (4 H, s, 2 × CH_2, 1 × major isomer, 1 × minor isomer), 5.09 (2 H, s, CH_2, major isomer), 5.69 (1 H, br. s.,), 6.31 (1 H, s, ArH, major isomer), 6.37 (1 H, s, ArH, minor isomer), 6.52 (1 H, s, C=CH, major isomer), 6.83 - 6.91 (4 H, m, 4 × ArH, 2 × major isomer, 2 × minor isomer), 6.94 (1 H, s, ArH, minor isomer), 6.96 (2 H, s, 1 × ArH, major isomer, 1 × C=CH, minor isomer), 8.05 (1 H, br. s., NH), 8.78 (1 H, br. s., OH)

^{13}C NMR (151 MHz, CHLOROFORM-*d*) δ_C ppm : 55.8 (OCH_3, major isomer), 55.9 (OCH_3, minor isomer), 56.1 (OCH_3, minor isomer, 56.1 (OCH_3, major isomer), 61.1 (OCH_3, major isomer), 61.2 (OCH_3, minor isomer), 61.7 (OCH_3, major isomer), 61.8 (OCH_3, minor isomer), 71.9 (CH_2, minor isomer), 72.0 (CH_2, major isomer), 72.2 (CH_2, minor isomer), 74.1 (CH_2, major isomer), 109.2 (ArCH, major isomer), 110.0 (ArCH, minor isomer), 110.1 (ArCH, major isomer), 111.0 (ArCH, minor isomer), 115.2 (ArCH, major isomer), 115.6 (ArCH, minor isomer), 115.7 (C=CH, minor isomer), 120.9 (ArCH, major isomer), 121.2 (ArCH, minor isomer), 122.3 (C=CH, major isomer), 124.7 (ArC, minor isomer), 126.9 (ArC, major isomer), 135.5 (ArCH, major isomer), 136.6 (ArCH, minor isomer), 143.3 (ArC, major isomer), 144.1 (ArC, minor isomer), 144.6 (ArC, minor isomer), 144.9 (ArC, minor isomer), 145.1 (ArC, minor isomer), 145.2 (ArC, major isomer), 146.5 (ArC, major isomer), 146.7 (ArC, major isomer), 146.9 (ArC, minor isomer), 148.2 (ArC, major isomer), 149.0 (ArC, minor isomer), 149.2 (ArC, major isomer), 155.1 (2 × C=CH, both isomers), 161.5 (2 × C=N, both isomers), 166.7 (C=O, major isomer) 167.0 (C=O, minor isomer)

ν_{max} cm^{-1} : 3295.2, 2931.6, 1667.6, 1579.9, 1508.9, 1492.0, 1458.1, 1409.8, 1374.3, 1277.9, 1248.9, 1128.9, 1088.8, 961.8, 912.1, 733.2

HRMS : calculated 460.1482, found 461.1544 ($M + H^+$)

Synthesis of intermediate *tert*-butyl N-{5-[(3E)-3-{[(hydroxycarbamoyl)methoxy]imino}-7,8,9-trimethoxy-2H-1-benzoxepin-5-yl]-2-methoxyphenyl}carbamate *(4.29)*

Ketone ***(2.27)*** (93 mg, 0.195 mmoles), sodium acetate (26 mg, 0.31 mmoles), and *O*-carboxymethyl hydroxylamine hemihydrochloride (24 mg, 0.215 mmoles) were stirred for 16 h in EtOH:Water:DCM (8:2:1, 5.5 mL) mixture at RT. The reaction was then quenched with aq. HCl solution (20 mL, 1 M) and extracted with diethyl ether (3 × 30 mL) to give carboxylic acid ***(4.27)*** (55 mg, 0.101 mmoles, 53%) as a clear residue. This product was reconstituted in DCM (5 mL) under nitrogen gas and cooled to 0 °C. To this was added sequentially; pentafluorophenol (21 mg, 0.11 mmoles) in dry DCM (1 mL) and N-(3-dimethylaminopropyl)-N′-ethylcarbodiimide (23 mg, 0.11 mmoles) in dry DCM:DMF (1:0.5 mL). The reaction was allowed stir for 1 h when the reaction was quenched with water (20 mL) and extracted with diethyl ether (3 × 30 mL). The resultant crude compound was purified via column chromatography (3:1, hexane:ethyl acetate) to give pentafluorophenyl ester ***(4.25)*** (70 mg, 0.0985 mmoles, 98%) as a clear oil. Once isolated and pure, this PFP ester was instantly dissolved in anhydrous DMF (3 mL) with hydroxylamine

hydrochloride (75 mg, 0.11 mmoles) under an atmosphere of nitrogen. Neat diisopropylethylamine (14 mg, 0.11 mmoles) was then added to the reaction mixture. After 5 min, water (20 mL) was added and the mixture extracted with diethyl ether (3 × 30 mL). The combined organic layers were further washed once with aq. LiCl solution (50 mL, 5%) and then water (5 × 30 mL), before being dried with $MgSO_4$, filtered and concentrated *in vacuo* to afford hydroxamic acid ***(4.29)*** (40 mg, 0.071 mmoles, 72%) as a yellow oil.

^{1}H NMR (600 MHz, CHLOROFORM-*d*) δ_H ppm : 1.53 (18 H, s, 2 × $(CH_3)_3$, both isomers), 3.61 (3 H, s, OCH_3, minor isomer), 3.64 (3 H, s, OCH_3, major isomer), 3.93 (3 H, s, OCH_3, major isomer), 3.95 (3 H, s, OCH_3, minor isomer), 3.96 (3 H, s, OCH_3, major isomer), 3.977 (3 H, s, OCH_3, minor isomer), 3.984 (3 H, s, OCH_3, minor isomer), 4.01 (3 H, s, OCH_3, major isomer), 4.69 (4 H, br. s., 2 × 2 × N=C-C$\underline{H}_2$, both isomers), 5.07 (4 H, br. s., 2 × N-O-C$\underline{H}_2$, both isomers), 6.32 (1 H, s, ArH, major isomer), 6.39 (1 H, s, ArH, minor isomer), 6.52 (1 H, s, C=CH, major isomer), 6.815 - 6.984 (7 H, m, 2 × ArH, major isomer, 2 × ArH, minor isomer, 2 × NH, both isomers, 1 × C=CH, minor isomer), 7.122 (1 H, br. s., NH, major isomer), 7.150 (1 H, br. s., NH, minor isomer), 8.120 (2 H, br. s., ArH, both isomers), 8.96 (2 H, br. s., OH, both isomers)

^{13}C NMR (151 MHz, CHLOROFORM-*d*) δ_C ppm : 28.5 (C($\underline{C}H_3)_3$, both isomers), 55.7 (OCH_3, major isomer), 55.8 (OCH_3, minor isomer), 56.3 (OCH_3, both isomers), 61.3 (OCH_3, both isomers), 61.8 (OCH_3, major isomer), 61.9 (OCH_3, minor isomer), 71.8 (CH_2, both isomers), 73.9 (CH_2, both isomers), 80.6 ($\underline{C}(CH_3)_3$, both isomers), 109.39 (ArCH, minor isomer), 109.44 (ArCH, major isomer), 109.6 (ArCH, major isomer), 111.4 (ArCH, minor isomer), 116.2 (C=$\underline{C}$H, minor isomer), 118.7 (ArCH, major isomer), 119.1 (ArCH, minor isomer), 122.7 (C=$\underline{C}$H, major isomer), 123.4 (ArCH, major isomer), 123.5 (ArCH, minor isomer), 124.7 (ArC, minor isomer), 127.1 (ArC, major isomer), 127.9 (ArC, major isomer), 135.2 (ArC, major isomer), 136.2 (ArC, minor isomer), 143.5 (ArC, major isomer), 144.3 (ArC, minor isomer), 144.7 (ArC, minor isomer), 145.1 (ArC, minor isomer), 145.5 (ArC, major isomer), 146.7 (ArC, major isomer), 147.7 (ArC, both isomers), 148.2 (ArC, minor isomer), 149.16 (ArC, minor isomer), 149.20 (ArC, major isomer), 152.7 (Boc-OC=O, both isomers), 154.65 ($\underline{C}$=CH, both isomers), 161.53 (C=N, major isomer), 161.61 (C=N, minor isomer), 171.1 (HOHN-C=O, major isomer), 172.8 (HOHN-C=O, minor isomer)

ν_{max} cm^{-1} : 3429.9, 3301.26, 2933.3, 2855.0, 2246.4, 1727.7, 1681.8, 1589.3, 1527.5, 1491.7, 1457.2, 1369.4, 1246.6, 1155.9, 1090.9, 966.8, 914.8, 733.2

HRMS : calculated 559.2166, found 558.2112 ($M - H^+$), 560.2243 ($M + H^+$), 582.2061 ($M + Na^+$), 594.1881 ($M + Cl^-$)

Synthesis of 2-({[(3E)-5-(3-amino-4-methoxyphenyl)-7,8,9-trimethoxy-2H-1-benzoxepin-3-ylidene]amino}oxy)-N-hydroxyacetamide *(4.30)*

To carbamate compound ***(4.29)*** (40 mg, 0.071 mmoles), under an atmosphere of nitrogen, was added trifluoroacetic acid in anhydrous DCM (1:1, 1 mL). The reaction was stirred at 0 °C for 5 min, after which the solvent was concentrated *in vacuo*. The crude residue was then redissolved in diethyl ether (10 mL), with the minimum amount of DCM (few drops until fully solubilised), and aq. sodium hydrogencarbonate (0.5 mL, saturated solution) added. This biphasic mixture was then allowed to stir for 5 min before the aqueous layer was removed. The remaining organic layer was then dried with $MgSO_4$, and gaseous HCl (from conc. $HCl\backslash H_2SO_4$) was then blown through, prompting a yellow salt to crash out. This salt was then washed with diethyl ether (3 × 5 mL) which was decanted off, to leave amine salt ***(4.30)*** (19 mg, 0.0042 mmoles, 58%) as an orange/brown residue.

^{1}H NMR (600 MHz, METHANOL-d_4) δ_H ppm : 3.62 (3 H, s, OCH_3, minor isomer), 3.64 (3 H, s, OCH_3, major isomer), 3.86 (3 H, s, OCH_3, major isomer), 3.87 (3 H, s, OCH_3, major isomer), 3.88 (3 H, s, OCH_3, minor isomer), 3.90 (3 H, s, OCH_3, minor isomer), 3.93 (3 H, s, OCH_3, minor isomer), 3.94 (3 H, s, OCH_3, major isomer), 4.64 (4 H, m, 2 × CH_2, both isomers), 5.02 (4 H, m, 2 × CH_2, both isomers), 6.24 (1 H, s, ArH, major isomer), 6.35 (1 H, s, minor isomers), 6.39 (1 H, s, C=CH), 6.86 (1 H, d, ArH, *J*=8.80 Hz, major isomer), 7.00 (2 H, m, 1 × ArH, minor isomer, 1 × C=CH, minor isomer), 7.07 (2 H, m, 2 × ArH, 1 × major isomer, 1 × minor isomer), 8.02 (1 H, m, ArH, major isomer), 8.09 (1 H, s, ArH, minor isomer).

^{13}C NMR (151 MHz, METHANOL-d_4) δ_C ppm : 55.62 (OCH_3, major isomer), 55.66 (OCH_3, minor isomer), 55.9 (2 × OCH_3, 1 × major isomer, 1 × minor isomer), 60.7 (OCH_3, major isomer), 60.9 (OCH_3, minor isomer), 61.4 (OCH_3, major isomer), 61.5 (OCH_3, minor isomer), 72.1 (CH_2, both isomers), 75.3 (CH_2, both isomers), 109.2 (ArCH, major isomer), 109.9 (ArCH, minor isomer), 110.5 (ArCH, minor isomer), 116.2 (C=<u>C</u>H, minor isomer), 122.1 (ArCH, major isomer), 123.0 (C=<u>C</u>H, major isomer), 123.3 (ArCH, major isomer), 124.7 (ArC, minor isomer), 125.3 (ArC, major isomer), 125.6 (ArC, major isomer), 126.3 (ArCH, major isomer), 126.9 (ArCH, minor isomer), 134.4 (ArC, major isomer), 135.1 (ArC, minor isomer), 142.6 (ArC, major isomer), 143.1 (ArC, minor isomer), 143.5 (ArC, major isomer), 144.4 (ArC, minor isomer), 145.1 (ArC, minor isomer), 146.1 (ArC, major isomer), 146.7 (ArC, major isomer), 147.1 (ArC, minor isomer), 148.2 (ArC minor isomer), 148.6 (ArC, major isomer), 148.9 (ArC, minor isomer), 154.4 (<u>C</u>=CH, minor

isomer), 154.8 (C=CH, major isomer), 160.3 (C=N, minor isomer), 160.6 (C=N, major isomer), 171.6 (H_2C-C=O, major isomer), 172.1 (H_2C-C=O, minor isomer)

ν_{max} cm^{-1} : 3372.6, 2919.5, 2850.9, 1735.6, 16.73.6, 1602.3, 1494.5, 1465.7, 1096.3, 1018.5, 901.2, 799.2, 735.4

HRMS : calculated 459.1642, found 458.1603 ($M - H^+$), 482.1511 ($M + Na^+$)

Synthesis of *tert*-butyl N-(1-{[2-methoxy-5-(7,8,9-trimethoxy-3-oxo-2H-1-benzoxepin-5-yl)phenyl]carbamoyl}-3-methylbutyl)carbamate *(4.31)*

Amine salt ***(2.28)*** (51 mg, 0.071 mmoles) was dissolved in anhydrous DCM (3 mL) under an atmosphere of nitrogen at 0 °C. To this was added sequentially in dry DCM; N-Boc leucine (0.16 g, 0.685 mmoles), PyBroP (0.32 g, 0.685 mmoles) and diisopropylamine (0.125 mL, 0.0.685 mmoles). The reaction was gradually allowed to reach RT and the reaction was monitored via TLC. The reaction was then quenched with aq. HCl solution (20 mL, 1 M) and extracted with diethyl ether (3 × 30 mL). The organic layer was then dried with $MgSO_4$, filtered and concentrated *in vacuo* before the residue was then purifed by column chromatography (3:1, hexane : ethyl acetate) to give carbamate product ***(4.11)*** as a light brown oil (50 mg, 0.086 mmoles, 62%).

^{1}H NMR (600 MHz, CHLOROFORM-*d*) δ_H ppm : 0.99 (6 H, t, 2 × Leu-CH_3, *J*=6.40 Hz), 1.49 (9 H, s, $(CH_3)_3$), 1.53 - 1.82 (2 H, m, Leu-CH_2), 1.69 - 1.78 (1 H, m, C<u>H</u>$(CH_3)_2$), 3.64 (3 H, s, OCH_3), 3.95 (3 H, s, OCH_3), 3.99 (3 H, s, OCH_3), 4.00 (3 H, s, OCH_3), 4.63 (2 H, s, OCH_2C=O), 4.68 (1 H, ddd, COC<u>H</u>NH, *J*=3.40 Hz), 4.97 (1 H, br. s., ArNH), 5.29 (1 H, d, CHN<u>H</u>, *J*=8.66 Hz), 6.37 (1 H, s, ArH), 6.47 (1 H, s, C=CH), 6.91 (1 H, d, ArH, *J*=8.66 Hz), 7.07 (1 H, d, ArH, *J*=7.53 Hz), 8.42 (1 H, s, ArH)

^{13}C NMR (151 MHz, CHLOROFORM-*d*) δ_C ppm : 23.3 (CH(<u>C</u>$H_3)_2$), 24.5 (<u>C</u>H$(CH_3)_2$), 28.2 (C(<u>C</u>$H_3)_3$), 40.9 (Leu-CH_2), 48.5 (CHNH), 55.8 (OCH_3), 56.2 (OCH_3), 61.1 (OCH_3), 61.7 (OCH_3), 79.2 (<u>C</u>$(CH_3)_3$), 80.8 (OCH_2), 109.5 (ArCH), 110.6 (ArCH), 120.7 (ArCH), 124.9 (ArCH), 125.9 (ArC), 128.4 (C=<u>C</u>H), 134.2 (ArC), 144.5 (ArC), 145.0 (ArC), 147.4 (ArC), 148.9 (ArC), 149.0 (2 × ArC), 151.7 (<u>C</u>=CH), 155.7 (Boc-C=O), 170.6 (ArNC=O), 200.1 (CH_2<u>C</u>=O)

ν_{max} cm^{-1} : 3317.3, 2957.7, 2928.7, 2871.1, 1697.4, 1649.7, 1582.4, 1531.5, 1491.4, 1457.5, 1365.6, 1258.15, 1170.1

HRMS : calculated 584.2734, found 583.2708 ($M - H^+$)

Synthesis of intermediate ({[(3E)-5-[3-(2-{[(*tert*-butoxy)carbonyl]amino}-4-methylpentanamido)-4-methoxyphenyl]-7,8,9-trimethoxy-2H-1-benzoxepin-3-ylidene]amino}oxy)acetic acid (4.32)

Ketone **(4.31)** (50 mg, 0.086 mmoles), sodium acetate (11 mg, 0.137 mmoles), and *O*-carboxymethyl hydroxylamine hemihydrochloride (10 mg, 0.094 mmoles) were stirred for 16 h in EtOH:Water:DCM (8:2:1, 5.5 mL) mixture at RT. The reaction was then quenched with aq. HCl solution (20 mL, 1 M) and extracted with diethyl ether (3 × 30 mL) to give carboxylic acid ***(4.32)*** (40 mg, 0.061 mmoles, 71%) as a clear residue.

^{1}H NMR (600 MHz, CHLOROFORM-*d*) δ_H ppm : 0.95 - 1.02 (12 H, t, 2 × Leu-CH_3, both isomers), 1.46 (9 H, s, $C(CH_3)_3$, minor isomer), 1.48 (9 H, s, $C(CH_3)_3$, major isomer), 1.53 - 1.84 (4 H, m, 2 × Leu-CH_2, both isomers), 1.74 - 1.82 (2 H, m, 2 × $C\underline{H}(CH_3)_2$, both isomers), 3.59 (3 H, s, OCH_3, minor isomer), 3.62 (3 H, s, OCH_3, major isomer), 3.93 (3 H, s, OCH_3, major isomer), 3.94 (3 H, s, OCH_3, minor isomer), 3.96 (3 H, s, OCH_3, major isomer), 3.97 (3 H, s, OCH_3, minor isomer), 3.98 (3 H, s, OCH_3, minor isomer), 4.00 (3 H, s, OCH_3, major isomer), 4.28 - 4.37 (2 H, m, $C\underline{H}NH$, both isomers), 4.62 (2 H, s, CH_2, minor isomer), 4.70 (2 H, s, CH_2, major isomer), 4.71 - 4.74 (2 H, s, CH_2, minor isomer), 5.08 (2 H, br. s., 2 × NH, both isomers), 5.13 (2 H, s, CH_2, major isomer 6.29 (1 H, s, ArH, major isomer), 6.36 (1 H, s, ArH, minor isomer), 6.54 (1 H, s, C=CH, major isomer), 6.85 - 6.90 (2 H, m, 1 × ArH, major isomer, 1 × ArH, minor isomer), 6.99 - 7.07 (3 H, m, 2 × ArH, minor isomer, 1 × C=CH, major isomer), 8.36 (1 H, s, ArH, minor isomer), 8.40 (1 H, s, ArH, major isomer), 8.45 (1 H, br. s., COOH, major isomer), 8.48 (1 H, br. s., COOH minor isomer)

^{13}C NMR (151 MHz, CHLOROFORM-*d*) δC : 21.7 (Leu-CH_3, minor isomer), 22.8 (Leu-CH_3, minor isomer), 22.9 (2 × Leu-CH_3, major isomer), 24.8 (2 × $C\underline{H}(CH_3)_2$, both isomers), 28.3 ($C(\underline{C}H_3)_3$, major isomer), 30.3 ($C(\underline{C}H_3)_3$, minor isomer), 41.1 (Leu-CH_2, minor isomer), 41.2 (Leu-CH_3, major isomer), 54.0 (2 × CHNH, both isomers), 55.84 (OCH_3, major isomer), 55.90 (OCH_3, minor isomer), 56.3 (OCH_3, both isomers), 61.2 (OCH_3, both isomers), 61.78 (OCH_3, major isomer), 61.84 (OCH_3, minor isomer), 69.5 (CH_2, minor isomer), 70.9 (CH_2, major isomer), 72.4 (CH_2, major isomer), 74.4 (CH_2, minor isomer), 80.2 ($\underline{C}(CH_3)_3$, minor isomer), 80.3 ($\underline{C}(CH_3)_3$, major isomer) 109.49 (ArCH, major isomer), 109.58 (ArCH, major isomer), 111.3 (ArCH, minor isomer), 116.9 (C=$\underline{C}$H, minor isomer), 120.7 (ArCH, major isomer), 121.1 (ArCH, minor isomer), 123.4 (C=$\underline{C}$H, major isomer),

125.0 (ArCH, major isomer), 125.3 (ArCH, minor isomer), 125.5 (ArCH, minor isomer), 127.0 (ArC, minor isomer), 127.2 (ArC, major isomer), 128.2 (ArC, minor isomer), 135.3 (ArC, major isomer), 135.7 (ArC, minor isomer), 136.4 (ArC, minor isomer), 143.3 (ArC, major isomer), 143.9 (ArC, major isomer), 144.0 (ArC, minor isomer), 144.6 (ArC, minor isomer), 145.5 (ArC, major isomer), 146.7 (major isomer), 148.1 (ArC, minor isomer), 148.2 (ArC, minor isomer), 148.3 (ArC, major isomer), 149.1 (ArC, major isomer), 151.5 (ArC, minor isomer), 154.4 (C=CH, major isomer), 155.8 (2 × N-Boc-C=O, both isomers), 157.9 (C=CH, minor isomer), 160.7 (2 × C=N, both isomers), 170.7 (Ar-NHC=O, major isomer), 170.8 (Ar-NHC=O, minor isomer), 173.3 (COOH, major isomer), 173.9 (COOH, minor isomer).

ν_{max} cm^{-1} : 3319.1, 2956.5, 2934.4, 2869.6, 2251.2, 1696.2, 1586.1, 1532.6, 1492.4, 1410.0, 1258.0, 1167.2, 1131.7, 1088.8, 1025.6, 963.8, 915.8, 875.9, 733.8

HRMS : calculated 657.2898, found 680.2814 ($M + Na^+$)

Synthesis of intermediate pentafluorophenyl 2-({[(3E)-5-[3-(2-{[(*tert*-butoxy)carbonyl]amino}-4-methylpentanamido)-4-methoxyphenyl]-7,8,9-trimethoxy-2H-1-benzoxepin-3-ylidene]amino}oxy)acetate *(4.33)*

Carboxylic acid ***(4.32)*** (30 mg, 0.046 mmoles) was dissolved in DCM (4 mL) under nitrogen gas and cooled to 0 °C. To this was added sequentially; pentafluorophenol (10 mg, 0.051 mmoles) in dry DCM (1 mL) and N-(3-dimethylaminopropyl)-N′-ethylcarbodiimide (10 mg, 0.051 mmoles) in dry DCM:DMF (1:0.5 mL). The reaction was allowed stir for 1 h when the reaction was quenched with water (20 mL) and extracted with diethyl ether (3 × 30 mL). The resultant crude compound was purified via column chromatography (3:1, hexane:ethyl acetate) to give pentafluorophenyl ester ***(4.33)*** (20 mg, 0.0243 mmoles, 54%) as a clear oil.

^{1}H NMR (600 MHz, CHLOROFORM-*d*) δ_H ppm : 0.96 (3 H, d, Leu-CH_3, major isomer, *J*=6.78 Hz), 0.98 - 1.04 (9 H, m, 3 × Leu-CH_3, 2 × minor isomer, 1 × major isomer), 1.46 (9 H, s, $C(CH_3)_3$, minor isomer), 1.50 (9 H, s, $C(CH_3)_3$, major isomer), 1.68 - 1.84 (4 H, m, 2 × Leu-CH_2, both isomers), 1.75 - 1.80 (2 H, m, 2 × C<u>H</u>$(CH_3)_2$, both isomers), 3.60 (3 H, s, OCH_3, minor isomer), 3.63 (3 H, s, OCH_3, major isomer), 3.94 (3 H, s, OCH_3, major isomer), 3.95 (3 H, s, OCH_3, minor isomer), 3.96 (3 H, s, OCH_3, major isomer), 3.98 (6 H, s, 2 × OCH_3, minor isomers), 4.01 (3 H, s, OCH_3, major isomer), 4.29 (1 H, m, C<u>H</u>NH, major isomer), 4.69 (1 H, m, C<u>H</u>NH, minor isomer), 4.74 (2 H, s, CH_2, minor isomer), 4.95 (1 H, br. s., NH, minor isomer), 5.00 (2 H, s, CH_2, minor isomer), 5.01 (2 H, s, CH_2,

major isomer), 5.15 (2 H, s, CH_2, major isomer), 5.28 (1 H, br. s., NH, major isomer), 6.30 (1 H, s, ArH, major isomer), 6.36 (1 H, s, ArH, minor isomer), 6.56 (1 H, s, C=CH, major isomer), 6.86 - 6.91 (2 H, m, 2 × ArH, 1 × major isomer, 1 × minor isomer), 7.01 - 7.08 (3 H, m, 1 × C=CH, minor isomer, 2 × ArH, 1 × major isomer, 1 × minor isomer), 8.04 (1 H, s, NH, minor isomer), 8.38 (1 H, s, 1 × ArH, minor isomer), 8.44 (1 H, d, 1 × ArH, major isomer, J=6.06 Hz), 8.47 (1 H, s, NH, major isomer)

^{13}C NMR (151 MHz, CHLOROFORM-*d*) δ_C ppm : 21.7 (Leu-CH_3, minor isomer), 21.8 (Leu-CH_3, minor isomer), 22.8 (Leu-CH_3, major isomer), 23.3 (Leu-CH_3), 24.5 ($\underline{C}H(CH_3)_2$, minor isomer), 24.7 ($\underline{C}H(CH_3)_2$), 28.15 ($C(\underline{C}H_3)_3$, minor isomer), 28.20 ($C(\underline{C}H_3)_3$, major isomer), 41.1 (Leu-CH_2, major isomer), 42.5 (Leu-CH_3, minor isomer), 48.2 (CHNH, minor isomer), 53.8 (CHNH, major isomer), 55.8 (2 × OCH_3, 1 × major isomer, 1 × minor isomer), 56.2 (2 × OCH_3, 1 × major isomer, 1 × minor isomer), 61.09 (OCH_3, major isomer), 61.11 (OCH_3, minor isomer), 61.66 (OCH_3, major isomer), 61.70 (OCH_3, minor isomer), 69.7 (CH_2, minor isomer), 70.1 (CH_2, major isomer), 72.1 (CH_2, major isomer), 74.0 (CH_2, minor isomer), 79.4 ($\underline{C}(CH_3)_3$, major isomer), 80.2 ($\underline{C}(CH_3)_3$, minor isomer), 109.32 (ArCH, major isomer), 109.38 (ArCH, major isomer), 111.1 (ArCH, minor isomer), 116.7 (C=$\underline{C}$H, minor isomer), 120.49 (ArCH, major isomer), 120.92 (ArCH, minor isomer), 123.1 (C=$\underline{C}$H, major isomer), 124.7 (2 × ArCH, 1 ×major isomer, 1 × minor ArCH), 125.0 (ArCH, minor isomer), 126.97 (ArC, minor isomer), 127.01 (ArC, major isomer), 131.2 (ArCF, both isomers), 135.2 (ArC, major isomer), 136.3 (ArC, minor isomer), 136.9 (ArCF, both isomers), 138.6 (ArCF, both isomers), 140.0 (ArCF, both isomers), 141.8 (ArCF, both isomers), 143.2 (ArC, major isomer), 143.9 (ArC, minor isomer), 144.2 (ArC, major isomer), 144.5 (ArC, minor isomer), 145.4 (ArC, major isomer), 146.0 (ArC, minor isomer), 146.6 (ArC, major isomer), 146.7 (ArC, minor isomer), 147.3 (ArC, major isomer), 148.01 (ArC, minor isomer), 148.07 (ArC, minor isomer), 148.09 (ArC, major isomer), 149.01 (ArC, minor isomer), 149.03 (ArC, major isomer), 154.6 ($\underline{C}$=CH, both isomers), 155.7 (N-Boc-$\underline{C}$=O, both isomers), 161.0 (C=N, both isomers), 165.5 (COOAr, major isomer), 165.8 (COOAr, minor isomer), 170.5 (Ar-NHC=O, major isomer), 172.9 (Ar-NHC=O, minor isomer)

^{19}F NMR (376 MHz, CHLOROFORM-*d*) δ_F ppm : -169.4 (1 F, m, ArF, minor isomer), -164.5 (1 F, t, ArF, major isomer), -163.3 (2 F, d, 2 × ArF, minor isomer), -162.6 (2 F, m, 2 × ArF, major isomer), -157.9 (2 F, d, 2 × ArF, minor isomer), -152.3 (2 F, d, 2 × ArF, major isomer),

ν_{max} cm^{-1} : 3391.3, 3309.2, 2956.5, 2929.8, 2864.7, 2855.1, 1814.4, 1792.7, 1700.2, 1645.6, 1517.9, 1492.2, 1367.6, 1257.2, 1169.9, 1131.8, 1087.7, 1002.6

HRMS : calculated 823.2740, found 846.2675 ($M + Na^+$)

Synthesis of intermediate *tert*-butyl N-[1-({5-[(3E)-3-{[(hydroxycarbamoyl)methoxy]imino}-7,8,9-trimethoxy-2H-1-benzoxepin-5-yl]-2-methoxyphenyl}carbamoyl)-3-ethylbutyl]carbamate *(4.34)*

PFP ester ***(4.33)*** (20 mg, 0.0243 mmoles) was in dry DMF (1 mL), under an atmosphere of nitrogen was added hydroxylamine hydrochloride (1.9 mg, 0.027 mmoles) in dry DMF (0.5 mL) and neat diisopropylethylamine (3.5 mg, 0.027 mmoles, 4.7 µL). The reaction was stirred for 5 min before the reaction was quenched with water (20 mL) and extracted with diethyl ether (3 × 30 mL). The combined organic layers were further washed once with aq. LiCl solution (50 mL, 5%) and then water (5 × 30 mL), before being dried with $MgSO_4$, filtered and concentrated *in vacuo* to afford hydroxamic acid ***(4.34)*** (11 mg, 0.0164 mmoles, 68%) as an orange oil.

^{1}H NMR (600 MHz, CHLOROFORM-*d*) δ_H ppm : 0.96 (3 H, d, Leu-CH_3, *J*=6.78 Hz, major isomer), 0.98 - 1.03 (9 H, m, 3 × Leu-CH_3, 1 × major isomer, 2 × minor isomer), 1.45 (9 H, s, $C(CH_3)_3$, minor isomer), 1.46 (9 H, s, $C(CH_3)_3$, major isomer), 1.61 - 1.84 (4 H, m, 2 × Leu-CH_2, both isomers), 1.71-1.79 (2 H, m, C<u>H</u>$(CH_3)_2$, both isomers), 3.63 (3 H, s, OCH_3, minor isomer), 3.64 (3 H, s, OCH_3, major isomer), 3.95 (3 H, s, major isomer), 3.96 (3 H, s, OCH_3, minor isomer), 3.97 (3 H, s, OCH_3, major isomer), 3.988 (3 H, s, OCH_3, minor isomer), 3.992 (3 H, s, OCH_3, minor isomer), 4.01 (1 H, s, OCH_3, major isomer), 4.31 (1 H, m, C<u>H</u>NH, major isomer), 4.70 (1 H, m, C<u>H</u>NH, minor isomer), 4.73 - 4.87 (4 H, m, 2 × CH_2, 1 × major isomer, 1 × minor isomer), 5.04 (2 H, br. s., CH_2, minor isomer), 5.08 (2 H, br. s., CH_2, major isomer), 5.12 - 5.15 (1 H, m), 6.31 (1 H, s, ArH, major isomer), 6.41 (1 H, ArH, minor isomer), 6.53 (1 H, s, C=CH, major isomer), 6.88 (2 H, m, 2 × ArH, 1 × major, 1 × minor isomer), 7.01 – 7.06 (3 H, m, 1 × C=CH, minor isomer, 2 × ArH, 1 × major isomer, 1 × minor isomer), 8.04 (1 H, br. s., NH, minor isomer), 8.44 (1 H, s, ArH, major isomer), 8.46 (1 H, s, ArH, minor isomer), 8.49 (1 H, br. s., NH, major isomer)

^{13}C NMR (151 MHz, CHLOROFORM-*d*) δ_C ppm : 21.9 (Leu-CH_3, minor isomer), 22.65 (Leu-CH_3, minor isomer), 22.7 (Leu-CH_3, major isomer), 23.4 (Leu-CH_3, major isomer), 24.79 (<u>C</u>H$(CH_3)_2$, minor isomer), 24.85 (<u>C</u>H$(CH_3)_2$, major isomer), 28.0 (C(<u>C</u>$H_3)_3$, minor isomer), 30.5 (C(<u>C</u>$H_3)_3$, major isomer), 41.0 (Leu-CH_2, major isomer), 42.7 (Leu-CH_2, minor isomer), 48.4 (CHNH, minor isomer), 54.0 (CHNH, major isomer), 55.87 (OCH_3, major isomer), 55.92 (OCH_3, minor isomer), 56.3 (OCH_3, both isomers), 61.2 (OCH_3, major isomer), 61.3 (OCH_3, minor isomer), 61.8 (OCH_3, major isomer),

61.9 (OCH_3, minor isomer), 64.5 (CH_2, minor isomer), 71.9 (CH_2, major isomer), 72.3 (CH_2, minor isomer), 74.5 (CH_2, major isomer), 79.5 ($\underline{C}(CH_3)_3$, major isomer), 82.1 ($\underline{C}(CH_3)_3$, minor isomer), 109.5 (ArCH, major isomer), 109.6 (ArCH, major isomer), 111.1 (ArCH, minor isomer), 116.7 (C=$\underline{C}$H, minor isomer), 120.5 (ArCH, major isomer), 121.2 (ArCH, minor isomer), 122.7 (C=$\underline{C}$H, major isomer), 124.9 (ArCH, minor isomer), 125.3 (ArC, minor isomer), 125.5 (2 × ArCH, 1 × major isomer, 1 × minor isomer), 127.0 (ArC, major isomer), 134.8 (ArC, minor isomer), 135.2 (ArC, minor isomer), 135.0 (ArC, major isomer), 135.8 (ArC, major isomer), 143.5 (ArC, major isomer), 144.2 (ArC, minor isomer), 145.5 (ArC, major isomer), 146.3 (ArC, minor isomer), 146.7 (ArC, major isomer), 148.23 (ArC, minor isomer), 148.3 (ArC, major isomer), 148.4 (ArC, minor isomer), 149.0 (ArC, minor isomer), 149.3 (ArC, major isomer), 154.5 ($\underline{C}$=CH, minor isomer), 155.4 ($\underline{C}$=CH, major isomer), 155.7 (Boc-O$\underline{C}$=O, major isomer), 155.75 (Boc-O$\underline{C}$=O, minor isomer), 163.3 (C=N, major isomer), 164.3 (C=N, minor isomer), 166.0 (H_2C-C=O, minor isomer), 169.3 (H_2C-C=O, major isomer), 170.8 (Ar-NH-C=O, major isomer), 179.1 (Ar-NH-C=O, minor isomer)

ν_{max} cm^{-1} : 3299.5, 2951.7, 2917.9, 2854.0, 1711.6, 1532.3, 1460.9, 1367.5, 1259.4, 1091.6, 1013.4

HRMS : calculated 672.3007, found 695.2567 ($M + Na^+$)

Synthesis of 2-amino-N-{5-[(3E)-3-{[(hydroxycarbamoyl)methoxy]imino}-7,8,9-trimethoxy-2H-1-benzoxepin-5-yl]-2-methoxyphenyl}-4-methylpentanamide (4.35)

To carbamate compound ***(4.34)*** (11 mg, 0.0164 mmoles), under an atmosphere of nitrogen, was added trifluoroacetic acid in anhydrous DCM (1:1, 1 mL). The reaction was stirred at 0 °C for 5 min, after which the solvent was concentrated *in vacuo*. The crude residue was then redissolved in diethyl ether (10 mL), with the minimum amount of DCM (few drops until fully solubilised), and aq. sodium hydrogencarbonate (0.5 mL, saturated solution) added. This biphasic mixture was then allowed to stir for 5 min before the aqueous layer was removed. The remaining organic layer was then dried with $MgSO_4$, and gaseous HCl (from conc. HCl\H_2SO_4) was then blown through, prompting a yellow salt to crash out. This salt was then washed with diethyl ether (3 × 5 mL) which was decanted off, to leave amine salt ***(4.23)*** (8 mg, 0.0014 mmoles, 85%) as a brown residue.

^{1}H NMR (600 MHz, METHANOL-d_4) δ_H ppm : 0.93 (6 H, m, 2 × Leu-CH_3, major isomer), 0.97 (6 H, m, 2 × Leu-CH_3, minor isomer), 1.48 - 1.78 (4 H, m, 2 × Leu-CH_2, both isomers), 1.59 - 1.66 (2 H,

m, C<u>H</u>$(CH_3)_2$), 3.53 (3 H, s, OCH_3, minor isomer), 3.54 (3 H, s, OCH_3, major isomer), 3.86 (3 H, s, OCH_3, major isomer), 3.87 (3 H, s, OCH_3, major isomer), 3.88 (3 H, s, OCH_3, minor isomer), 3.89 (3 H, s, OCH_3, minor isomer), 3.91 (3 H, s, OCH_3, minor isomer), 3.92 (3 H, s, OCH_3, major isomer), 4.14 (1 H, m, C<u>H</u>NH, major isomer), 4.21 (1 H, m, C<u>H</u>NH, minor isomer), 4.64 (4 H, m, 2 × CH_2, both isomers), 5.02 (4 H, m, 2 × CH_2, both isomers), 6.22 (1 H, s, ArH, major isomer), 6.33 (1 H, s, minor isomers), 6.42 (1 H, s, C=CH), 6.86 (1 H, d, ArH, *J*=8.80 Hz, major isomer), 6.99 (2 H, m, 1 × ArH, minor isomer, 1 × C=CH, minor isomer), 7.04 (2 H, m, 2 × ArH, 1 × major isomer, 1 × minor isomer), 8.03 (1 H, m, ArH, major isomer), 8.10 (1 H, s, ArH, minor isomer)

^{13}C NMR (151 MHz, METHANOL-d_4) δ_C ppm : 21.7 (Leu-CH_3, minor isomer), 22.1 (Leu-CH_3, major isomer), 24.0 (<u>C</u>H$(CH_3)_2$, both isomers), 40.3 (Leu-CH_2, major isomer), 40.4 (Leu-CH_2, minor isomer), 52.3 (CHNH, major isomer), 55.62 (OCH_3, major isomer), 55.66 (OCH_3, minor isomer), 55.9 (2 × OCH_3, 1 × major isomer, 1 × minor isomer), 60.96 (OCH_3, major isomer), 60.99 (OCH_3, minor isomer), 61.08 (CHNH, minor isomer), 61.56 (OCH_3, major isomer), 61.59 (OCH_3, minor isomer), 71.8 (CH_2, both isomers), 74.4 (CH_2, both isomers), 109.2 (ArCH, major isomer), 110.0 (ArCH, minor isomer), 110.7 (ArCH, minor isomer), 116.7 (C=<u>C</u>H, minor isomer), 122.3 (ArCH, major isomer), 123.0 (C=<u>C</u>H, major isomer), 123.3 (ArCH, major isomer), 124.3 (ArC, minor isomer), 125.1 (ArC, major isomer), 125.6 (ArC, major isomer), 126.3 (ArCH, major isomer), 126.8 (ArCH, minor isomer), 134.4 (ArC, major isomer), 135.1 (ArC, minor isomer), 142.6 (ArC, major isomer), 143.4 (ArC, minor isomer), 143.84 (ArC, major isomer), 144.7 (ArC, minor isomer), 145.1 (ArC, minor isomer), 146.0 (ArC, major isomer), 146.7 (ArC, major isomer), 147.1 (ArC, minor isomer), 148.1 (ArC minor isomer), 148.6 (ArC, major isomer), 149.3 (ArC, minor isomer), 155.4 (<u>C</u>=CH, minor isomer), 155.9 (<u>C</u>=CH, major isomer), 160.3 (C=N, minor isomer), 160.6 (C=N, major isomer), 167.1 (Ar-NH-C=O, minor isomer), 167.4 (Ar-NH-C=O, major isomer), 172.6 (H_2C-C=O, major isomer), 176.6 (H_2C-C=O, minor isomer)

ν_{max} cm^{-1} : 3279.7, 2924.6, 2853.7, 1673.4, 1633.6, 1539.2, 1492.7, 1458.5, 1260.8, 1200.9, 1131.9, 1091.1, 721.2

HRMS : calculated 572.2482, found 573.2621 ($M + H^+$)

Synthesis of intermediate 4-{[(*tert*-butoxy)carbonyl]amino}-4-{[2-methoxy-5-(6,7,8-trimethoxy-2-oxochromen-4-yl)phenyl]carbamoyl}butanoic acid (4.36)

Potassium carbonate (14.2 mg, 0.102 mmoles) was dissolved and stirred in distilled water (2 mL), before 4-amino-4-{[2-methoxy-5-(6,7,8-trimethoxy-2-oxochromen-4-yl)phenyl]carbamoyl} butanoic acid (**(3.06)**-Glu) (50 mg, 0.103 mmoles) was added. MeOH (1 mL) was added to aid solvation. To this solution, di-*tert*-butyl dicarbonate (22 mg, 0.102 mmoles) in THF (2 mL, HPLC grade) was added and the reaction stirred at RT for 1 h. Organic solvents were then removed *in vacuo*, and the resulting aqueous solution acidified with aq. HCl solution (30 mL, 1 M) and then extracted with diethyl ether (3 × 30 mL). The organic layer was then dried with magnesium sulphate, filtered and condensed under reduced pressure to afford carbamate ***(4.36)*** (56 mg, 0.096 mmoles, 93%) without the need for flash column chromatography as a white residue.

^{1}H NMR (600 MHz, CHLOROFORM-*d*) δ_H ppm : 1.47 (9 H, s, $C(CH_3)_3$), 1.97 - 2.29 (2 H, m, $C\underline{H}_2CHN$), 2.46 - 2.65 (2 H, m, $CH_2C{=}O$), 3.80 (3 H, s, OCH_3), 3.93 (3 H, br. s., OCH_3), 4.02 (3 H, s, OCH_3), 4.05 (3 H, s, OCH_3), 4.44 - 4.54 (1 H, m, $C\underline{H}NH$), 5.50 (1 H, br. s., NH), 6.30 (1 H, s, C=CH), 6.91 (1 H, s, ArH), 6.97 - 7.04 (1 H, m, ArH), 7.19 (1 H, d, ArH, *J*=6.97 Hz), 8.50 (1 H, s, ArH), 8.73 (1 H, br. s., NH)

^{13}C NMR (151 MHz, CHLOROFORM-*d*) δ_C ppm : 28.1 ($C(\underline{C}H_3)_3$), 29.5 ($\underline{C}H_2CHN$), 30.0 ($\underline{C}H_2C{=}O$), 54.3 (CHNH), 55.8 (OCH_3), 56.2 (OCH_3), 61.3 (OCH_3), 61.7 (OCH_3), 80.6 ($\underline{C}(CH_3)_3$), 103.3 (ArCH), 110.4 (ArCH), 113.2 (C=$\underline{C}$H), 114.2 (ArC), 120.4 (ArCH), 124.3 (ArCH), 127.8 (ArC), 141.1 (ArC), 143.2 (ArC), 145.7 (ArC), 146.6 (ArC), 149.4 (ArC), 149.5 (ArC), 155.0 ($\underline{C}$=CH), 155.9 (Boc-$\underline{C}$=O), 160.8 (Lactone-O$\underline{C}$=O), 170.0 (Ar-N-C=O), 176.6 (COOH)

ν_{max} cm^{-1} : 3346.8, 2979.7, 2938.1, 2852.5, 2251.9, 1807.7, 1710.7, 1681.6, 1607.2, 1522.2, 1495.1, 1391.8, 1260.1, 1167.6, 733.5

HRMS : calculated 586.2163, found 587.2217 ($M + H^+$), 609.2032 ($M + Na^+$)

Synthesis of intermediate *tert*-butyl N-[3-(hydroxycarbamoyl)-1-{[2-methoxy-5-(6,7,8-trimethoxy-2-oxochromen-4-yl)phenyl]carbamoyl}propyl]carbamate *(4.38)*

Carboxylic acid ***(4.36)*** (56 mg, 0.0956 mmoles) was dissolved in anhydrous DCM (1 mL) under an atmosphere of nitrogen at 0 °C, before pentafluorophenol (18 mg, 0.0956 mmoles), and N,N'-dicyclohexylcarbodiimide (20 mg, 0.0956 mmoles) were added sequentially in anhydrous DCM (1.5 mL each). Over 1 h, the reaction was gradually allowed to reach RT. The reaction was again cooled to 0 °C just before the mixture was filtered several times with paper, washed with

minimum diethyl ether and concentrated under vacuum. The resulting crude mixture rapidly purified by flash column chromatography (2:1, hexane : ethyl acetate) before PFP ester ***(4.37)*** (47 mg, 0.0624 mmoles, 65%) was obtained. The resultant oil was dissolved in anhydrous DMF (2 mL) under an atmosphere of nitrogen at room temperature. Hydroxylamine hydrochloride (48 mg, 0.0687 mmoles) in anhydrous DMF (1 mL) and diisopropylethylamine (8.9 mg, 0.0687 mmoles) were subsequently added, and the reaction stirred for 5 min. Water (20 mL) was added and the mixture extracted with diethyl ether (3 × 30 mL). The combined organic layers were further washed once with aq. LiCl solution (50 mL, 5%) and then water (5 × 30 mL), before being dried with $MgSO_4$, filtered and concentrated *in vacuo* to afford hydroxamic acid ***(4.38)*** (35 mg, 0.058 mmoles, 93%) as a yellow oil.

^{1}H NMR (400 MHz, CHLOROFORM-*d*) δ_H ppm : 1.43 (9 H, s, $C(CH_3)_3$), 1.93 - 2.11 (2 H, m, $C\underline{H}_2CHN$), 2.28 - 2.57 (2 H, m, $CH_2C=O$), 3.79 (3 H, br. s., OCH_3), 3.96 (3 H, br. s., OCH_3), 4.00 (3 H, s, OCH_3), 4.04 (3 H, s, OCH_3), 4.50 - 4.61 (1 H, m, $C\underline{H}NH$), 5.79 (1 H, br. s., NH), 6.28 (1 H, br. s., C=CH), 6.88 (1 H, s, ArH), 7.01 (1 H, d, ArH, *J*=8.28 Hz), 7.19 (1 H, d, ArH, *J*=8.03 Hz), 8.38 (1 H, br. s., ArH), 9.22 (1 H, br. s., NH), 10.22 (1 H, br. s., OH)

^{13}C NMR (101 MHz, CHLOROFORM-*d*) δ_C ppm : 28.3 ($C(\underline{C}H_3)_3$), 29.7 (CH_2CHN), 30.2 ($CH_2C=O$), 53.8 (CHNH), 56.1 (OCH_3), 56.3 (OCH_3), 61.5 (OCH_3), 61.9 (OCH_3), 80.9 ($\underline{C}(CH_3)_3$), 103.3 (ArCH), 110.7 (ArCH), 113.4 (C=$\underline{C}$H), 114.3 (ArC), 121.3 (ArCH), 124.8 (ArCH), 126.9 (ArC), 127.8 (ArC), 141.3 (ArC), 143.3 (ArC), 145.8 (ArC), 149.7 (ArC), 150.1 (ArC), 155.1 ($\underline{C}$=CH), 156.2 (Boc-$\underline{C}$=O), 160.9 (Lactone-O$\underline{C}$=O), 169.5 (Ar-NH-$\underline{C}$=O), 171.1 (H_2C-$\underline{C}$=O)

ν_{max} cm^{-1} : 3310.8, 2975.8, 2935.6, 2850.2, 1704.5, 1534.9, 1390.8, 1259.1, 1093.5, 732.7

HRMS : calculated 601.2272, found 624.2078 ($M + Na^+$)

Synthesis of N-[2-methoxy-5-(6,7,8-trimethoxy-2-oxochromen-4-yl)phenyl]-5-oxopyrrolidine-2-carboxamide *(4.40)*

To carbamate compound ***(4.38)*** (10 mg, 0.0122 mmoles), under an atmosphere of nitrogen, was added trifluoroacetic acid in anhydrous DCM (1:1, 1 mL). The reaction was stirred at 0 °C for 5 min, after which the solvent was concentrated *in vacuo*. The crude residue was then redissolved in diethyl ether (10 mL), with the minimum amount of DCM (few drops until fully solubilised), and aq. sodium hydrogencarbonate (0.5 mL, saturated solution) added. This biphasic mixture

was then allowed to stir for 5 min before the aqueous layer was removed. The remaining organic layer was then dried with $MgSO_4$, and gaseous HCl (from conc. $HCl\backslash H_2SO_4$) was then blown through, prompting a white salt to crash out. This salt was then washed with diethyl ether (3 × 5 mL) which was decanted off, to leave amine salt ***(4.39)*** (8 mg, 0.00978 mmoles, 80%) as a yellow residue.

^{1}H NMR (400 MHz, CHLOROFORM-*d*) δ_H ppm : 2.24 - 2.75 (2 H, m, C$\underline{H}_2$CHNH), 2.35 - 2.60 (2 H, m, CH_2C=O), 3.82 (3 H, s, OCH_3), 4.01 (3 H, s, OCH_3), 4.04 (3 H, s, OCH_3), 4.08 (3 H, s, OCH_3), 4.36 (1 H, br. s., C$\underline{H}$NH), 6.32 (1 H, s, C=CH), 6.36 (1 H, br. s., NH), 6.90 (1 H, s, ArH), 7.07 (1 H, d, ArH, *J*=7.78 Hz), 7.26 (1 H, d, ArH, *J*=8.28 Hz), 8.37 (1 H, br. s., NH), 8.52 (1 H, s, ArH)

^{13}C NMR (101 MHz, CHLOROFORM-*d*) δ_C ppm : 26.3 ($\underline{C}H_2$CHNH), 29.2 (CH_2C=O), 56.2 (OCH_3), 56.4 (OCH_3), 57.5 (CHNH), 61.6 (OCH_3), 61.9 (OCH_3), 103.4 (ArCH), 110.7 (ArCH), 113.7 (C=$\underline{C}$H), 114.3 (ArC), 120.6 (ArCH), 125.0 (ArCH), 126.5 (ArC), 128.2 (ArC), 141.4 (ArC), 143.4 (ArC), 145.9 (ArC), 149.4 (ArC), 149.7 (ArC), 154.9 ($\underline{C}$=CH), 160.8 (Lactone-O$\underline{C}$=O), 170.0 (Ar-NH$\underline{C}$=O), 179.3 (NHC=O)

ν_{max} cm^{-1} : 3321.4, 2921.2, 2852.1, 1692.5, 1535.9, 1459.2, 1387.9, 1260.4, 803.5

HRMS : For hydroxamic acid : calculated 501.1747, found 502.3455 ($M + H^+$). For cyclic amide : calculated 468.1533, found 469.2614

5.5 APN enzyme assay

All reagents were procured from Sigma-Aldrich®. Greiner 96-well cell culture microplates with solid U-bottom were purchased from Cruinn, Ireland. Absorbance was measures using a FLUOstar Optima 96 well plate reader equipped with thermostat function. The HEPES buffer used was prepared by the dissolution of 50 mM HEPES dry powder and 154 nM NaCl in deionised water, then adjusted to pH 7.4 with aq. NaOH solution and stored at 4 °C.

L-Leucine-p-nitroanilide solution (50 µL, 8 mM in HEPES buffer) and HEPES buffer (40 µL) were pipetted into the wells of a 96-well plate. The test solution (100 µL, 0.5% DMSO in HEPES buffer, concentration varied), the control (0.5% DMSO in HEPES buffer), or bestatin (50 µL in HEPES buffer, 200 µM) was then added to appropriate wells. The reaction was initiated by the addition of 95 mU enzyme solution (10 µL, in HEPES buffer) to each well. Each test well of the 96 well

plate contained a final volume of 200 µL. Each plate was then incubated at 37 °C for 2 h, after which the absorbance was promptly determined via microplate reader. The solutions containing DMSO (0.5%) in HEPES were taken as the positive control, while the negative control was 200 µM bestatin solution in HEPES. A blank containing enzyme, HEPES buffer (150 µL) and substrate (50 µL) solutions also acted as a negative control. Each concentration was run in triplicate on three separate occasions.

Chapter 6 - References

1. UK, C. R., Cancer Incidence Worldwide. Feb-2011 ed.; 2011.
2. Hinnen, P.; Eskens, F. A. L. M., Vascular disrupting agents in clinical development. *Br J Cancer* **2007,** *96* (8), 1159-1165.
3. Baluk, P.; Hashizume, H.; McDonald, D. M., Cellular abnormalities of blood vessels as targets in cancer. *Current Opinion in Genetics & Development* **2005,** *15* (1), 102-111.
4. Hashizume, H.; Baluk, P.; Morikawa, S.; McLean, J. W.; Thurston, G.; Roberge, S.; Jain, R. K.; McDonald, D. M., Openings between defective endothelial cells explain tumor vessel leakiness. *Am J Pathol* **2000,** *156* (Copyright (C) 2010 U.S. National Library of Medicine.), 1363-80.
5. McDonald, D. M.; Choyke, P. L., Imaging of angiogenesis: from microscope to clinic. *Nat Med* **2003,** *9* (6), 713-725.
6. W.G., R.; J., D.; M., N.; Huang, S.; Cavenee, W. K.; Palade, G. E., Host microvasculature influence on tumor vascular morphology and endothelial gene expression. *American Journal of Pathology*

1998, *153* (4), 1239-1248.
7. (a) Ferlay J, S. H., Bray F, Forman D, Mathers C and Parkin DM, Cancer Incidence and Mortality Worldwide. *IARC CancerBase No. 10 [Internet].* **2010**; (b) Bray, F.; Ren, J.-S.; Masuyer, E.; Ferlay, J., Global estimates of cancer prevalence for 27 sites in the adult population in 2008. *International Journal of Cancer* **2012**, n/a-n/a.
8. Cancer Research UK http://info.cancerresearchuk.org/cancerstats/world/index.htm (accessed August 2010).
9. Central Statistics Office Ireland http://www.cso.ie/statistics/principalcausesofdeath.htm.
10. UK, C. R. Cancer is biggest fear but 34 per cent put it down to fate. http://www.cancerresearchuk.org/cancer-info/news/archive/pressrelease/2010-12-08-cancer-is-biggest-fear-but-some-think-it-is-fate.
11. HSE http://www.hse.ie/eng/services/Find_a_Service/National_Cancer_Control_Programme/About_NCCP/ (accessed August).
12. VHI http://www.vhi.ie/personalise/controller/PrItemDisplay?PRYear=2009&prId=5.
13. American Cancer Society. Cancer Facts and Figures 2010. http://www.cancer.org/Research/CancerFactsFigures/CancerFactsFigures/cancer-facts-and-figures-2010.
14. Cancer.gov http://www.cancer.gov/cancertopics/factsheet/NCI/research-funding (accessed August 2010).
15. Irish Cancer Society http://www.cancer.ie/cancerInfo/whatis.php.
16. Cancer Research UK http://info.cancerresearchuk.org/prod_consump/groups/cr_common/@nre/@sta/documents/generalcontent/018070.pdf.
17. Cancer Research UK, Survival Rates.
18. Cancer multidrug resistance. *Nat Biotech*.
19. Marmé, D.; Fusenig, N., *Tumor Angiogenesis: Basic Mechanisms and Cancer Therapy*. Springer: 2007.
20. Algire, G. H.; Chalkley, H. W.; Legallais, F. Y.; Park, H. D., Vasculae Reactions of Normal and Malignant Tissues in Vivo. I. Vascular Reactions of Mice to Wounds and to Normal and Neoplastic Transplants. *Journal of the National Cancer Institute* **1945,** *6* (1), 73-85.

21. Folkman, J., Tumor angiogenesis: therapeutic implications. *N Engl J Med* **1971,** *285* (21), 1182-6.
22. F. Dayan, N. M. M., M. C. Brahami-Horn, J. Pouyssegur, A dialogue between the hypoxia inducible factor and the tumour microenvironment. *Cancer Microenviron.* **2008,** *1*, 53-68.
23. Dvorak, H. F., Rous-Whipple Award Lecture : How tumours make bad blood vessels and stroma. *Am J Pathol* **2003,** *162*, 1747-1757.
24. Ellis, L. M.; Liu, W.; Fan, F.; Jung, Y. D.; Reinmuth, N.; Stoeltzing, O.; Takeda, A.; Akagi, M.; Parikh, A. A.; Ahmad, S., Synopsis of angiogenesis inhibitors in oncology. *Oncology (Williston Park, N.Y.)* **2002,** *16* (5 Suppl 4), 14-22.
25. Herbert, S. P.; Stainier, D. Y. R., Molecular control of endothelial cell behaviour during blood vessel morphogenesis. *Nat Rev Mol Cell Biol* **2011,** *12* (9), 551-564.
26. Wang, Y.; Kaiser, M. S.; Larson, J. D.; Nasevicius, A.; Clark, K. J.; Wadman, S. A.; Roberg-Perez, S. E.; Ekker, S. C.; Hackett, P. B.; McGrail, M.; Essner, J. J., Moesin1 and Ve-cadherin are required in endothelial cells during in vivo tubulogenesis. In *Development*, England, 2010; Vol. 137, pp 3119-28.
27. Adams, R. H.; Alitalo, K., Molecular regulation of angiogenesis and lymphangiogenesis. In *Nat Rev Mol Cell Biol*, England, 2007; Vol. 8, pp 464-78.
28. Bicknell, R.; Lewis, C. E., *Tumour Angiogenesis*. Oxford University Press: 1997.
29. Shima, D. T.; Ruhrberg, C., Angiogenesis. In *The Molecular Biology of Cancer*

Pelengaris, S.; Kahn, M., Eds. Oxford : Blackwell: 2006; pp 411-425.
30. Nagy, J. A.; Dvorak, A. M.; Dvorak, H. F., VEGF-A and the induction of pathological angiogenesis. *Annu. Rev. Pathol.: Mech. Dis.* **2007,** *2* (Copyright (C) 2010 American Chemical Society (ACS). All Rights Reserved.), 251-275.
31. Nagy, J. A.; Chang, S. H.; Dvorak, A. M.; Dvorak, H. F., Why are tumour blood vessels abnormal and why is it important to know? *Br. J. Cancer* **2009,** *100* (Copyright (C) 2010 American Chemical Society (ACS). All Rights Reserved.), 865-869.
32. Less, J. R.; Skalak, T. C.; Sevick, E. M.; Jain, R. K., Microvascular Architecture in a Mammary Carcinoma: Branching Patterns and Vessel Dimensions. *Cancer Research* **1991,** *51* (1), 265-273.
33. Chaplin, D. J.; Olive, P. L.; Durand, R. E., Intermittent blood flow in a murine tumor: radiobiological effects. *Cancer Res* **1987,** *47* (Copyright (C) 2010 U.S. National Library of Medicine.), 597-601.
34. Ellis, L. M.; Hicklin, D. J., VEGF-targeted therapy: mechanisms of anti-tumour activity. *Nat Rev Cancer* **2008,** *8* (8), 579-591.
35. Weidner, N., Intratumor microvessel density as a prognostic factor in cancer. (0002-9440 (Print)).
36. Hollingsworth Hc Fau - Kohn, E. C.; Kohn Ec Fau - Steinberg, S. M.; Steinberg Sm Fau - Rothenberg, M. L.; Rothenberg Ml Fau - Merino, M. J.; Merino, M. J., Tumor angiogenesis in advanced stage ovarian carcinoma. (0002-9440 (Print)).
37. Benjamin, L. E.; Golijanin, D.; Itin, A.; Pode, D.; Keshet, E., Selective ablation of immature blood vessels in established human tumors follows vascular endothelial growth factor withdrawal. *J Clin Invest* **1999,** *103*, 159-165.
38. Millauer B Fau - Wizigmann-Voos, S.; Wizigmann-Voos S Fau - Schnurch, H.; Schnurch H Fau - Martinez, R.; Martinez R Fau - Moller, N. P.; Moller Np Fau - Risau, W.; Risau W Fau - Ullrich, A.; Ullrich, A., High affinity VEGF binding and developmental expression suggest Flk-1 as a major regulator of vasculogenesis and angiogenesis. (0092-8674 (Print)).
39. Patan, S.; Munn, L. L.; Jain, R. K., Intussusceptive Microvascular Growth in a Human Colon Adenocarcinoma Xenograft: A Novel Mechanism of Tumor Angiogenesis. *Microvascular Research* **1996,** *51* (2), 260-272.

40. Carver, L. A.; Schnitzer, J. E., Caveolae: mining little caves for new cancer targets. *Nat Rev Cancer* **2003,** *3* (8), 571-581.
41. W.G., R.; Palade, G. E., Neovasculature induced by vascular endothelial growth factor is fenestrated. *Cancer Research* **1997,** *57*, 765-772.
42. Reinmuth, N.; Liu, W.; Jung, Y. D.; Ahmad, S. A.; Shaheen, R. M.; Fan, F. A. N.; Bucana, C. D.; McMahon, G.; Gallick, G. E.; Ellis, L. M., Induction of VEGF in perivascular cells defines a potential paracrine mechanism for endothelial cell survival. *The FASEB Journal* **2001,** *15* (7), 1239-1241.
43. (a) Orlidge A Fau - D'Amore, P. A.; D'Amore, P. A., Inhibition of capillary endothelial cell growth by pericytes and smooth muscle cells. (0021-9525 (Print)); (b) Hirschi Kk Fau - Rohovsky, S. A.; Rohovsky Sa Fau - Beck, L. H.; Beck Lh Fau - Smith, S. R.; Smith Sr Fau - D'Amore, P. A.; D'Amore, P. A., Endothelial cells modulate the proliferation of mural cell precursors via platelet-derived growth factor-BB and heterotypic cell contact. (0009-7330 (Print)).
44. Allt G Fau - Lawrenson, J. G.; Lawrenson, J. G., Pericytes: cell biology and pathology. (1422-6405 (Print)).
45. Abramsson A Fau - Lindblom, P.; Lindblom P Fau - Betsholtz, C.; Betsholtz, C., Endothelial and nonendothelial sources of PDGF-B regulate pericyte recruitment and influence vascular pattern formation in tumors. (0021-9738 (Print)).
46. Abramsson, A.; Berlin, Ö.; Papayan, H.; Paulin, D.; Shani, M.; Betsholtz, C., Analysis of Mural Cell Recruitment to Tumor Vessels. *Circulation* **2002,** *105* (1), 112-117.
47. Eberhard, A.; Kahlert, S.; Goede, V.; Hemmerlein, B.; Plate, K. H.; Augustin, H. G., Heterogeneity of Angiogenesis and Blood Vessel Maturation in Human Tumors: Implications for Antiangiogenic Tumor Therapies. *Cancer Research* **2000,** *60* (5), 1388-1393.
48. (a) Morikawa, S.; Baluk, P.; Kaidoh, T.; Haskell, A.; Jain, R. K.; McDonald, D. M., Abnormalities in pericytes on blood vessels and endothelial sprouts in tumors. In *Am J Pathol*, United States, 2002; Vol. 160, pp 985-1000; (b) Schlingemann Ro Fau - Rietveld, F. J.; Rietveld Fj Fau - de Waal, R. M.; de Waal Rm Fau - Ferrone, S.; Ferrone S Fau - Ruiter, D. J.; Ruiter, D. J., Expression of the high molecular weight melanoma-associated antigen by pericytes during angiogenesis in tumors and in healing wounds. (0002-9440 (Print)); (c) Wesseling P Fau - Schlingemann, R. O.; Schlingemann Ro Fau - Rietveld, F. J.; Rietveld Fj Fau - Link, M.; Link M Fau - Burger, P. C.; Burger Pc Fau - Ruiter, D. J.; Ruiter, D. J., Early and extensive contribution of pericytes/vascular smooth muscle cells to microvascular proliferation in glioblastoma multiforme: an immuno-light and immuno-electron microscopic study. (0022-3069 (Print)).
49. Enge M Fau - Bjarnegard, M.; Bjarnegard M Fau - Gerhardt, H.; Gerhardt H Fau - Gustafsson, E.; Gustafsson E Fau - Kalen, M.; Kalen M Fau - Asker, N.; Asker N Fau - Hammes, H.-P.; Hammes Hp Fau - Shani, M.; Shani M Fau - Fassler, R.; Fassler R Fau - Betsholtz, C.; Betsholtz, C., Endothelium-specific platelet-derived growth factor-B ablation mimics diabetic retinopathy. (0261-4189 (Print)).
50. Hellstrom, M.; Gerhardt, H.; Kalen, M.; Li, X.; Eriksson, U.; Wolburg, H.; Betsholtz, C., Lack of pericytes leads to endothelial hyperplasia and abnormal vascular morphogenesis. *J Cell Biol* **2001,** *153* (3), 543-53.
51. Vracko, R., Basal lamina scaffold-anatomy and significance for maintenance of orderly tissue structure. (0002-9440 (Print)).
52. Hudson Bg Fau - Kalluri, R.; Kalluri R Fau - Gunwar, S.; Gunwar S Fau - Weber, M.; Weber M Fau - Ballester, F.; Ballester F Fau - Hudson, J. K.; Hudson Jk Fau - Noelken, M. E.; Noelken Me Fau - Sarras, M.; Sarras M Fau - Richardson, W. R.; Richardson Wr Fau - Saus, J.; Saus, J.; et al., The pathogenesis of Alport syndrome involves type IV collagen molecules containing the alpha 3(IV) chain: evidence from anti-GBM nephritis after renal transplantation. (0085-2538 (Print)).
53. (a) Suzuki, O. T.; Sertie, A. L.; Der Kaloustian, V. M.; Kok, F.; Carpenter, M.; Murray, J.; Czeizel, A. E.; Kliemann, S. E.; Rosemberg, S.; Monteiro, M.; Olsen, B. R.; Passos-Bueno, M. R.,

Molecular analysis of collagen XVIII reveals novel mutations, presence of a third isoform, and possible genetic heterogeneity in Knobloch syndrome. *American journal of human genetics* **2002,** *71* (6), 1320-9; (b) Kalluri R Fau - Shield, C. F.; Shield Cf Fau - Todd, P.; Todd P Fau - Hudson, B. G.; Hudson Bg Fau - Neilson, E. G.; Neilson, E. G., Isoform switching of type IV collagen is developmentally arrested in X-linked Alport syndrome leading to increased susceptibility of renal basement membranes to endoproteolysis. (0021-9738 (Print)).

54. Hudson Bg Fau - Reeders, S. T.; Reeders St Fau - Tryggvason, K.; Tryggvason, K., Type IV collagen: structure, gene organization, and role in human diseases. Molecular basis of Goodpasture and Alport syndromes and diffuse leiomyomatosis. (0021-9258 (Print)).

55. Kalluri, R., Basement membranes: structure, assembly and role in tumour angiogenesis. *Nat Rev Cancer* **2003,** *3* (6), 422-433.

56. (a) Steinberg, F.; Konerding, M. A.; Streffer, C., The vascular architecture of human xenotransplanted tumors: histological, morphometrical, and ultrastructural studies. *J Cancer Res Clin Oncol* **1990,** *116* (5), 517-524; (b) Paku, S.; Paweletz, N., First steps of tumor-related angiogenesis. *Lab Invest* **1991,** *65* (3), 334-46.

57. (a) Baluk, P.; Morikawa, S.; Haskell, A.; Mancuso, M.; McDonald, D. M., Abnormalities of basement membrane on blood vessels and endothelial sprouts in tumors. *Am J Pathol* **2003,** *163* (5), 1801-15; (b) Farnoud Mr Fau - Lissak, B.; Lissak B Fau - Kujas, M.; Kujas M Fau - Peillon, F.; Peillon F Fau - Racadot, J.; Racadot J Fau - Li, J. Y.; Li, J. Y., Specific alterations of the basement membrane and stroma antigens in human pituitary tumours in comparison with the normal anterior pituitary. An immunocytochemical study. (0174-7398 (Print)).

58. Inai, T.; Mancuso, M.; Hashizume, H.; Baffert, F.; Haskell, A.; Baluk, P.; Hu-Lowe, D. D.; Shalinsky, D. R.; Thurston, G.; Yancopoulos, G. D.; McDonald, D. M., Inhibition of Vascular Endothelial Growth Factor (VEGF) Signaling in Cancer Causes Loss of Endothelial Fenestrations, Regression of Tumor Vessels, and Appearance of Basement Membrane Ghosts. *The American Journal of Pathology* **2004,** *165* (1), 35-52.

59. Sitohy, B.; Nagy, J. A.; Dvorak, H. F., Anti-VEGF/VEGFR Therapy for Cancer: Reassessing the Target. *Cancer Research* **2012,** *72* (8), 1909-1914.

60. Pettersson, A.; Nagy, J. A.; Brown, L. F.; Sundberg, C.; Morgan, E.; Jungles, S.; Carter, R.; Krieger, J. E.; Manseau, E. J.; Harvey, V. S.; Eckelhoefer, I. A.; Feng, D.; Dvorak, A. M.; Mulligan, R. C.; Dvorak, H. F., Heterogeneity of the angiogenic response induced in different normal adult tissues by vascular permeability factor/vascular endothelial growth factor. *Lab Invest* **2000,** *80* (1), 99-115.

61. Swayne, G. T.; Smaje, L. H.; Bergel, D. H., Distensibility of single capillaries and venules in the rat and frog mesentery. *International journal of microcirculation, clinical and experimental / sponsored by the European Society for Microcirculation* **1989,** *8* (1), 25-42.

62. Nagy, J. A.; Chang, S.-H.; Shih, S.-C.; Dvorak, A. M.; Dvorak, H. F., Heterogeneity of the Tumor Vasculature. *Semin Thromb Hemost* **2010,** *36* (03), 321-331.

63. Cohen, M., *Coronary collaterals: Clinical and experimental observations*. 1985.

64. Nagy, J. A.; Morgan, E. S.; Herzberg, K. T.; Manseau, E. J.; Dvorak, A. M.; Dvorak, H. F., Pathogenesis of ascites tumor growth: angiogenesis, vascular remodeling, and stroma formation in the peritoneal lining. *Cancer Res* **1995,** *55* (2), 376-85.

65. Ren, G.; Michael, L. H.; Entman, M. L.; Frangogiannis, N. G., Morphological characteristics of the microvasculature in healing myocardial infarcts. *The journal of histochemistry and cytochemistry : official journal of the Histochemistry Society* **2002,** *50* (1), 71-9.

66. Egginton, S.; Zhou, A. L.; Brown, M. D.; Hudlicka, O., Unorthodox angiogenesis in skeletal muscle. *Cardiovascular research* **2001,** *49* (3), 634-46.

67. Kerbel, R. S., Inhibition of tumor angiogenesis as a strategy to circumvent acquired resistance to anti-cancer therapeutic agents. *Bioessays* **1991,** *13* (1), 31-6.

68. Thomlinson, R. H.; Gray, L. H., The histological structure of some human lung cancers and the possible implications for radiotherapy. *Br J Cancer* **1955,** *9* (4), 539-49.
69. Bloemendal, H. J.; Logtenberg, T.; Voest, E. E., New strategies in anti-vascular cancer therapy. *Eur J Clin Invest* **1999,** *29* (9), 802-9.
70. Ferrara, N.; Henzel, W. J., Pituitary follicular cells secrete a novel heparin-binding growth factor specific for vascular endothelial cells. *Biochem Biophys Res Commun* **1989,** *161* (2), 851-8.
71. Ferrara, N., VEGF-A: a critical regulator of blood vessel growth. *European cytokine network* **2009,** *20* (4), 158-63.
72. Shiojima, I.; Sato, K.; Izumiya, Y.; Schiekofer, S.; Ito, M.; Liao, R.; Colucci, W. S.; Walsh, K., Disruption of coordinated cardiac hypertrophy and angiogenesis contributes to the transition to heart failure. *J Clin Invest* **2005,** *115* (8), 2108-18.
73. Compernolle, V.; Brusselmans, K.; Acker, T.; Hoet, P.; Tjwa, M.; Beck, H.; Plaisance, S.; Dor, Y.; Keshet, E.; Lupu, F.; Nemery, B.; Dewerchin, M.; Van Veldhoven, P.; Plate, K.; Moons, L.; Collen, D.; Carmeliet, P., Loss of HIF-2alpha and inhibition of VEGF impair fetal lung maturation, whereas treatment with VEGF prevents fatal respiratory distress in premature mice. *Nat Med* **2002,** *8* (7), 702-10.
74. Storkebaum, E.; Lambrechts, D.; Carmeliet, P., VEGF: once regarded as a specific angiogenic factor, now implicated in neuroprotection. *Bioessays* **2004,** *26* (9), 943-54.
75. Soker, S.; Miao, H. Q.; Nomi, M.; Takashima, S.; Klagsbrun, M., VEGF165 mediates formation of complexes containing VEGFR-2 and neuropilin-1 that enhance VEGF165-receptor binding. *Journal of cellular biochemistry* **2002,** *85* (2), 357-68.
76. Ichihara, E.; Kiura, K.; Tanimoto, M., Targeting angiogenesis in cancer therapy. *Acta medica Okayama* **2011,** *65* (6), 353-62.
77. (a) Casanovas, O.; Hicklin, D. J.; Bergers, G.; Hanahan, D., Drug resistance by evasion of antiangiogenic targeting of VEGF signaling in late-stage pancreatic islet tumors. *Cancer Cell* **2005,** *8* (4), 299-309; (b) Waltenberger, J.; Claesson-Welsh, L.; Siegbahn, A.; Shibuya, M.; Heldin, C. H., Different signal transduction properties of KDR and Flt1, two receptors for vascular endothelial growth factor. *J Biol Chem* **1994,** *269* (43), 26988-95.
78. Alvarez, R. H.; Guarneri, V.; Icli, F.; Johnston, S.; Khayat, D.; Loibl, S.; Martin, M.; Zielinski, C.; Conte, P.; Hortobagyi, G. N., Bevacizumab Treatment for Advanced Breast Cancer. *The Oncologist* **2011,** *16* (12), 1684-1697.
79. Wu, J. M.; Staton, C. A., Anti-angiogenic drug discovery: lessons from the past and thoughts for the future. *Expert Opinion on Drug Discovery* **2012,** *7* (8), 723-743.
80. Lohmann, A.; Chia, S., Patients With Metastatic Breast Cancer Using Bevacizumab as a Treatment: Is There Still a Role for it? *Curr. Treat. Options in Oncol.* **2012,** *13* (2), 249-262.
81. Montero, A. J.; Avancha, K.; Gluck, S.; Lopes, G., A cost-benefit analysis of bevacizumab in combination with paclitaxel in the first-line treatment of patients with metastatic breast cancer. *Breast cancer research and treatment* **2012,** *132* (2), 747-51.
82. Mitchell, E. P., Targeted Therapy for Metastatic Colorectal Cancer: Role of Aflibercept. *Clinical colorectal cancer* **2012**.
83. Papadopoulos, N.; Martin, J.; Ruan, Q.; Rafique, A.; Rosconi, M. P.; Shi, E.; Pyles, E. A.; Yancopoulos, G. D.; Stahl, N.; Wiegand, S. J., Binding and neutralization of vascular endothelial growth factor (VEGF) and related ligands by VEGF Trap, ranibizumab and bevacizumab. *Angiogenesis* **2012,** *15* (2), 171-85.
84. Ellis, P. M.; Al-Saleh, K., Multitargeted anti-angiogenic agents and NSCLC: clinical update and future directions. *Critical reviews in oncology/hematology* **2012,** *84* (1), 47-58.
85. Llovet, J. M.; Ricci, S.; Mazzaferro, V.; Hilgard, P.; Gane, E.; Blanc, J.-F.; de Oliveira, A. C.; Santoro, A.; Raoul, J.-L.; Forner, A.; Schwartz, M.; Porta, C.; Zeuzem, S.; Bolondi, L.; Greten, T. F.; Galle, P. R.; Seitz, J.-F.; Borbath, I.; Häussinger, D.; Giannaris, T.; Shan, M.; Moscovici, M.; Voliotis,

D.; Bruix, J., Sorafenib in Advanced Hepatocellular Carcinoma. *New England Journal of Medicine* **2008,** *359* (4), 378-390.
86. Sternberg, C. N.; Davis, I. D.; Mardiak, J.; Szczylik, C.; Lee, E.; Wagstaff, J.; Barrios, C. H.; Salman, P.; Gladkov, O. A.; Kavina, A.; Zarba, J. J.; Chen, M.; McCann, L.; Pandite, L.; Roychowdhury, D. F.; Hawkins, R. E., Pazopanib in locally advanced or metastatic renal cell carcinoma: results of a randomized phase III trial. *Journal of clinical oncology : official journal of the American Society of Clinical Oncology* **2010,** *28* (6), 1061-8.
87. Choueiri, T. K., Axitinib, a novel anti-angiogenic drug with promising activity in various solid tumors. *Current opinion in investigational drugs (London, England : 2000)* **2008,** *9* (6), 658-71.
88. Larkin, J.; Fishman, M.; Wood, L.; Negrier, S.; Olivier, K.; Pyle, L.; Gorbunova, V.; Jonasch, E.; Andrews, L.; Staehler, M., Axitinib for the Treatment of Metastatic Renal Cell Carcinoma: Recommendations for Therapy Management to Optimize Outcomes. *American journal of clinical oncology* **2013**.
89. Polverino, A.; Coxon, A.; Starnes, C.; Diaz, Z.; DeMelfi, T.; Wang, L.; Bready, J.; Estrada, J.; Cattley, R.; Kaufman, S.; Chen, D.; Gan, Y.; Kumar, G.; Meyer, J.; Neervannan, S.; Alva, G.; Talvenheimo, J.; Montestruque, S.; Tasker, A.; Patel, V.; Radinsky, R.; Kendall, R., AMG 706, an oral, multikinase inhibitor that selectively targets vascular endothelial growth factor, platelet-derived growth factor, and kit receptors, potently inhibits angiogenesis and induces regression in tumor xenografts. *Cancer Res* **2006,** *66* (17), 8715-21.
90. Albert, D. H.; Tapang, P.; Magoc, T. J.; Pease, L. J.; Reuter, D. R.; Wei, R. Q.; Li, J.; Guo, J.; Bousquet, P. F.; Ghoreishi-Haack, N. S.; Wang, B.; Bukofzer, G. T.; Wang, Y. C.; Stavropoulos, J. A.; Hartandi, K.; Niquette, A. L.; Soni, N.; Johnson, E. F.; McCall, J. O.; Bouska, J. J.; Luo, Y.; Donawho, C. K.; Dai, Y.; Marcotte, P. A.; Glaser, K. B.; Michaelides, M. R.; Davidsen, S. K., Preclinical activity of ABT-869, a multitargeted receptor tyrosine kinase inhibitor. *Molecular cancer therapeutics* **2006,** *5* (4), 995-1006.
91. Scagliotti, G.; Govindan, R., Targeting Angiogenesis with Multitargeted Tyrosine Kinase Inhibitors in the Treatment of Non-Small Cell Lung Cancer. *The Oncologist* **2010,** *15* (5), 436-446.
92. Cai, Z. W.; Zhang, Y.; Borzilleri, R. M.; Qian, L.; Barbosa, S.; Wei, D.; Zheng, X.; Wu, L.; Fan, J.; Shi, Z.; Wautlet, B. S.; Mortillo, S.; Jeyaseelan, R., Sr.; Kukral, D. W.; Kamath, A.; Marathe, P.; D'Arienzo, C.; Derbin, G.; Barrish, J. C.; Robl, J. A.; Hunt, J. T.; Lombardo, L. J.; Fargnoli, J.; Bhide, R. S., Discovery of brivanib alaninate ((S)-((R)-1-(4-(4-fluoro-2-methyl-1H-indol-5-yloxy)-5-methylpyrrolo[2,1-f][1,2,4] triazin-6-yloxy)propan-2-yl)2-aminopropanoate), a novel prodrug of dual vascular endothelial growth factor receptor-2 and fibroblast growth factor receptor-1 kinase inhibitor (BMS-540215). *J Med Chem* **2008,** *51* (6), 1976-80.
93. Pal, S.; Figlin, R., Future directions of mammalian target of rapamycin (mTOR) inhibitor therapy in renal cell carcinoma. *Targ Oncol* **2011,** *6* (1), 5-16.
94. D'Amato, R. J.; Loughnan, M. S.; Flynn, E.; Folkman, J., Thalidomide is an inhibitor of angiogenesis. *Proceedings of the National Academy of Sciences of the United States of America* **1994,** *91* (9), 4082-5.
95. Morrow, P. K.; Murthy, R. K.; Ensor, J. D.; Gordon, G. S.; Margolin, K. A.; Elias, A. D.; Urba, W. J.; Weng, D. E.; Rugo, H. S.; Hortobagyi, G. N., An open-label, phase 2 trial of RPI.4610 (Angiozyme) in the treatment of metastatic breast cancer. *Cancer* **2012,** *118* (17), 4098-104.
96. Rosca, E. V.; Koskimaki, J. E.; Rivera, C. G.; Pandey, N. B.; Tamiz, A. P.; Popel, A. S., Anti-angiogenic peptides for cancer therapeutics. *Current pharmaceutical biotechnology* **2011,** *12* (8), 1101-16.
97. Fischer, C.; Jonckx, B.; Mazzone, M.; Zacchigna, S.; Loges, S.; Pattarini, L.; Chorianopoulos, E.; Liesenborghs, L.; Koch, M.; De Mol, M.; Autiero, M.; Wyns, S.; Plaisance, S.; Moons, L.; van Rooijen, N.; Giacca, M.; Stassen, J. M.; Dewerchin, M.; Collen, D.; Carmeliet, P.,

Anti-PlGF inhibits growth of VEGF(R)-inhibitor-resistant tumors without affecting healthy vessels. *Cell* **2007,** *131* (3), 463-75.
98. (a) Grepin, R.; Pages, G., Molecular Mechanisms of Resistance to Tumour Anti-Angiogenic Strategies. *Journal of Oncology* **2010,** *2010*; (b) Bergers, G.; Hanahan, D., Modes of resistance to anti-angiogenic therapy. *Nat Rev Cancer* **2008,** *8* (8), 592-603.
99. Sessa, C.; Guibal, A.; Del Conte, G.; Ruegg, C., Biomarkers of angiogenesis for the development of antiangiogenic therapies in oncology: tools or decorations? *Nature clinical practice. Oncology* **2008,** *5* (7), 378-91.
100. Jain, R. K., Normalization of Tumor Vasculature: An Emerging Concept in Antiangiogenic Therapy. *Science* **2005,** *307* (5706), 58-62.
101. Jain, R. K.; Tong, R. T.; Munn, L. L., Effect of Vascular Normalization by Antiangiogenic Therapy on Interstitial Hypertension, Peritumor Edema, and Lymphatic Metastasis: Insights from a Mathematical Model. *Cancer Research* **2007,** *67* (6), 2729-2735.
102. (a) Denekamp, The tumour microcirculation as a target in cancer therapy: a clearer perspective. *European Journal of Clinical Investigation* **1999,** *29* (9), 733-736; (b) Crabtree, H. G.; Cramer, W., The Action of Radium on Cancer Cells. II.--Some Factors Determining the Susceptibility of Cancer Cells to Radium. *Proceedings of the Royal Society of London. Series B, Containing Papers of a Biological Character* **1933,** *113* (782), 238-250.
103. (a) Ning, S.; Bednarski, M.; Oronsky, B.; Scicinski, J.; Saul, G.; Knox, S. J., Dinitroazetidines Are a Novel Class of Anticancer Agents and Hypoxia-Activated Radiation Sensitizers Developed from Highly Energetic Materials. *Cancer Research* **2012,** *72* (10), 2600-2608; (b) Oronsky, B. T.; Scicinski, J. J.; Reid, T.; Knox, S., Beyond antiangiogenesis: vascular modulation as an anticancer therapy-a review. *Translational oncology* **2012,** *5* (3), 133-40.
104. Carmeliet, P., Blood vessels and nerves: common signals, pathways and diseases. *Nat Rev Genet* **2003,** *4* (9), 710-20.
105. Siemann, D. W., The unique characteristics of tumor vasculature and preclinical evidence for its selective disruption by Tumor-Vascular Disrupting Agents. *Cancer treatment reviews* **2011,** *37* (1), 63-74.
106. Landuyt, W.; Verdoes, O.; Darius, D. O.; Drijkoningen, M.; Nuyts, S.; Theys, J.; Stockx, L.; Wynendaele, W.; Fowler, J. F.; Maleux, G.; Van den Bogaert, W.; Anne, J.; van Oosterom, A.; Lambin, P., Vascular targeting of solid tumours: a major 'inverse' volume-response relationship following combretastatin A-4 phosphate treatment of rat rhabdomyosarcomas. *European journal of cancer (Oxford, England : 1990)* **2000,** *36* (14), 1833-43.
107. Alberts, B.; Johnston, A.; Lewis, J.; Raff, M.; Roberts, K.; Walter, P., *Molecular Biology of the Cell*. 5th Edition ed.; Garland Science: 2008; p 1268.
108. Lowe, J.; Li, H.; Downing, K. H.; Nogales, E., Refined structure of alpha beta-tubulin at 3.5 A resolution. *J Mol Biol* **2001,** *313* (5), 1045-57.
109. Kavallaris, M., Microtubules and resistance to tubulin-binding agents. *Nat Rev Cancer* **2010,** *10* (3), 194-204.
110. Westermann, S.; Weber, K., Post-translational modifications regulate microtubule function. *Nat Rev Mol Cell Biol* **2003,** *4* (12), 938-47.
111. Berg, J. M.; Tymoczko, J. L.; Stryer, L., *Biochemistry*. 5th Edition ed.; W. H. Freeman and Company: 2002.
112. Rieder, C. L.; Maiato, H., Stuck in division or passing through: what happens when cells cannot satisfy the spindle assembly checkpoint. *Dev Cell* **2004,** *7* (5), 637-51.
113. Jordan, M. A.; Wilson, L., Microtubules as a target for anticancer drugs. *Nat Rev Cancer* **2004,** *4* (4), 253-65.
114. Altmann, K.-H., Microtubule-stabilizing agents: a growing class of important anticancer drugs. *Current Opinion in Chemical Biology* **2001,** *5* (4), 424-431.

115. Yared, J. A.; Tkaczuk, K. H., Update on taxane development: new analogs and new formulations. *Drug design, development and therapy* **2012,** *6*, 371-84.
116. Pettit, G. R.; Cragg, G. M.; Singh, S. B., Antineoplastic agents, 122. Constituents of Combretum caffrum. *Journal of natural products* **1987,** *50* (3), 386-91.
117. Tozer, G. M.; Kanthou, C.; Parkins, C. S.; Hill, S. A., The biology of the combretastatins as tumour vascular targeting agents. *International journal of experimental pathology* **2002,** *83* (1), 21-38.
118. Dorr, R. T.; Dvorakova, K.; Snead, K.; Alberts, D. S.; Salmon, S. E.; Pettit, G. R., Antitumor activity of combretastatin-A4 phosphate, a natural product tubulin inhibitor. *Investigational new drugs* **1996,** *14* (2), 131-7.
119. Lin, C. M.; Ho, H. H.; Pettit, G. R.; Hamel, E., Antimitotic natural products combretastatin A-4 and combretastatin A-2: studies on the mechanism of their inhibition of the binding of colchicine to tubulin. *Biochemistry* **1989,** *28* (17), 6984-91.
120. Tozer, G. M.; Kanthou, C.; Lewis, G.; Prise, V. E.; Vojnovic, B.; Hill, S. A., Tumour vascular disrupting agents: combating treatment resistance. *The British journal of radiology* **2008,** *81 Spec No 1*, S12-20.
121. (a) Tozer, G. M.; Kanthou, C.; Baguley, B. C., Disrupting tumour blood vessels. *Nat Rev Cancer* **2005,** *5* (6), 423-35; (b) Schwartz, E. L., Antivascular Actions of Microtubule-Binding Drugs. *Clinical Cancer Research* **2009,** *15* (8), 2594-2601.
122. Kanthou, C.; Tozer, G. M., The tumor vascular targeting agent combretastatin A-4-phosphate induces reorganization of the actin cytoskeleton and early membrane blebbing in human endothelial cells. *Blood* **2002,** *99* (6), 2060-9.
123. (a) van Horck, F. P.; Ahmadian, M. R.; Haeusler, L. C.; Moolenaar, W. H.; Kranenburg, O., Characterization of p190RhoGEF, a RhoA-specific guanine nucleotide exchange factor that interacts with microtubules. *J Biol Chem* **2001,** *276* (7), 4948-56; (b) Ren, Y.; Li, R.; Zheng, Y.; Busch, H., Cloning and characterization of GEF-H1, a microtubule-associated guanine nucleotide exchange factor for Rac and Rho GTPases. *J Biol Chem* **1998,** *273* (52), 34954-60.
124. Katoh, K.; Kano, Y.; Noda, Y., Rho-associated kinase-dependent contraction of stress fibres and the organization of focal adhesions. *Journal of The Royal Society Interface* **2011,** *8* (56), 305-311.
125. Huot, J.; Houle, F.; Rousseau, S.; Deschesnes, R. G.; Shah, G. M.; Landry, J., SAPK2/p38-dependent F-actin reorganization regulates early membrane blebbing during stress-induced apoptosis. *J Cell Biol* **1998,** *143* (5), 1361-73.
126. van Gorp, R. M.; Broers, J. L.; Reutelingsperger, C. P.; Bronnenberg, N. M.; Hornstra, G.; van Dam-Mieras, M. C.; Heemskerk, J. W., Peroxide-induced membrane blebbing in endothelial cells associated with glutathione oxidation but not apoptosis. *The American journal of physiology* **1999,** *277* (1 Pt 1), C20-8.
127. Vincent, L.; Kermani, P.; Young, L. M.; Cheng, J.; Zhang, F.; Shido, K.; Lam, G.; Bompais-Vincent, H.; Zhu, Z.; Hicklin, D. J.; Bohlen, P.; Chaplin, D. J.; May, C.; Rafii, S., Combretastatin A4 phosphate induces rapid regression of tumor neovessels and growth through interference with vascular endothelial-cadherin signaling. *J Clin Invest* **2005,** *115* (11), 2992-3006.
128. Milosevic, M. F.; Fyles, A. W.; Hill, R. P., The relationship between elevated interstitial fluid pressure and blood flow in tumors: a bioengineering analysis. *International journal of radiation oncology, biology, physics* **1999,** *43* (5), 1111-23.
129. Brown, N. S.; Bicknell, R., Hypoxia and oxidative stress in breast cancer. Oxidative stress: its effects on the growth, metastatic potential and response to therapy of breast cancer. *Breast Cancer Res* **2001,** *3* (5), 323-7.
130. Griggs, J.; Metcalfe, J. C.; Hesketh, R., Targeting tumour vasculature: the development of combretastatin A4. *Lancet Oncol* **2001,** *2* (2), 82-7.

131. Siemann, D. W.; Chaplin, D. J.; Walicke, P. A., A review and update of the current status of the vasculature-disabling agent combretastatin-A4 phosphate (CA4P). *Expert opinion on investigational drugs* **2009,** *18* (2), 189-97.
132. (a) Mahal, K.; Biersack, B.; Schobert, R., New oxazole-bridged combretastatin A-4 analogues as potential vascular-disrupting agents. *International journal of clinical pharmacology and therapeutics* **2013,** *51* (1), 41-3; (b) Schobert, R.; Biersack, B.; Dietrich, A.; Effenberger, K.; Knauer, S.; Mueller, T., 4-(3-Halo/amino-4,5-dimethoxyphenyl)-5-aryloxazoles and -N-methylimidazoles That Are Cytotoxic against Combretastatin A Resistant Tumor Cells and Vascular Disrupting in a Cisplatin Resistant Germ Cell Tumor Model. *Journal of Medicinal Chemistry* **2010,** *53* (18), 6595-6602.
133. Salmon, H. W.; Siemann, D. W., Effect of the second-generation vascular disrupting agent OXi4503 on tumor vascularity. *Clin Cancer Res* **2006,** *12* (13), 4090-4.
134. Kim, T. J.; Ravoori, M.; Landen, C. N.; Kamat, A. A.; Han, L. Y.; Lu, C.; Lin, Y. G.; Merritt, W. M.; Jennings, N.; Spannuth, W. A.; Langley, R.; Gershenson, D. M.; Coleman, R. L.; Kundra, V.; Sood, A. K., Antitumor and antivascular effects of AVE8062 in ovarian carcinoma. *Cancer Res* **2007,** *67* (19), 9337-45.
135. Tozer, G. M.; Prise, V. E.; Wilson, J.; Cemazar, M.; Shan, S.; Dewhirst, M. W.; Barber, P. R.; Vojnovic, B.; Chaplin, D. J., Mechanisms associated with tumor vascular shut-down induced by combretastatin A-4 phosphate: intravital microscopy and measurement of vascular permeability. *Cancer Res* **2001,** *61* (17), 6413-22.
136. Dark, G. G.; Hill, S. A.; Prise, V. E.; Tozer, G. M.; Pettit, G. R.; Chaplin, D. J., Combretastatin A-4, an agent that displays potent and selective toxicity toward tumor vasculature. *Cancer Res* **1997,** *57* (10), 1829-34.
137. Tozer, G. M.; Prise, V. E.; Wilson, J.; Locke, R. J.; Vojnovic, B.; Stratford, M. R.; Dennis, M. F.; Chaplin, D. J., Combretastatin A-4 phosphate as a tumor vascular-targeting agent: early effects in tumors and normal tissues. *Cancer Res* **1999,** *59* (7), 1626-34.
138. Petit, I.; Karajannis, M. A.; Vincent, L.; Young, L.; Butler, J.; Hooper, A. T.; Shido, K.; Steller, H.; Chaplin, D. J.; Feldman, E.; Rafii, S., The microtubule-targeting agent CA4P regresses leukemic xenografts by disrupting interaction with vascular cells and mitochondrial-dependent cell death. *Blood* **2008,** *111* (4), 1951-61.
139. (a) Shaked, Y.; Ciarrocchi, A.; Franco, M.; Lee, C. R.; Man, S.; Cheung, A. M.; Hicklin, D. J.; Chaplin, D.; Foster, F. S.; Benezra, R.; Kerbel, R. S., Therapy-induced acute recruitment of circulating endothelial progenitor cells to tumors. *Science* **2006,** *313* (5794), 1785-7; (b) Farace, F.; Massard, C.; Borghi, E.; Bidart, J. M.; Soria, J. C., Vascular disrupting therapy-induced mobilization of circulating endothelial progenitor cells. *Annals of oncology : official journal of the European Society for Medical Oncology / ESMO* **2007,** *18* (8), 1421-2.
140. Beauregard, D. A.; Thelwall, P. E.; Chaplin, D. J.; Hill, S. A.; Adams, G. E.; Brindle, K. M., Magnetic resonance imaging and spectroscopy of combretastatin A4 prodrug-induced disruption of tumour perfusion and energetic status. *Br J Cancer* **1998,** *77* (11), 1761-7.
141. Boucher, Y.; Baxter, L. T.; Jain, R. K., Interstitial pressure gradients in tissue-isolated and subcutaneous tumors: implications for therapy. *Cancer Res* **1990,** *50* (15), 4478-84.
142. Hollebecque, A.; Massard, C.; Soria, J. C., Vascular disrupting agents: a delicate balance between efficacy and side effects. *Current opinion in oncology* **2012,** *24* (3), 305-15.
143. Otani, M.; Natsume, T.; Watanabe, J. I.; Kobayashi, M.; Murakoshi, M.; Mikami, T.; Nakayama, T., TZT-1027, an antimicrotubule agent, attacks tumor vasculature and induces tumor cell death. *Japanese journal of cancer research : Gann* **2000,** *91* (8), 837-44.
144. Davis, P. D.; Dougherty, G. J.; Blakey, D. C.; Galbraith, S. M.; Tozer, G. M.; Holder, A. L.; Naylor, M. A.; Nolan, J.; Stratford, M. R.; Chaplin, D. J.; Hill, S. A., ZD6126: a novel vascular-targeting agent that causes selective destruction of tumor vasculature. *Cancer Res* **2002,** *62* (24), 7247-53.

145. Lippert Iii, J. W., Vascular disrupting agents. *Bioorganic & Medicinal Chemistry* **2007,** *15* (2), 605-615.
146. Kim, S.; Peshkin, L.; Mitchison, T. J., Vascular disrupting agent drug classes differ in effects on the cytoskeleton. *PloS one* **2012,** *7* (7), e40177.
147. Eichhorn, M. E.; Strieth, S.; Dellian, M., Anti-vascular tumor therapy: recent advances, pitfalls and clinical perspectives. *Drug Resistance Updates* **2004,** *7* (2), 125-138.
148. Ching, L. M.; Cao, Z.; Kieda, C.; Zwain, S.; Jameson, M. B.; Baguley, B. C., Induction of endothelial cell apoptosis by the antivascular agent 5,6-Dimethylxanthenone-4-acetic acid. *Br J Cancer* **2002,** *86* (12), 1937-42.
149. Wang, L. C.; Thomsen, L.; Sutherland, R.; Reddy, C. B.; Tijono, S. M.; Chen, C. J.; Angel, C. E.; Dunbar, P. R.; Ching, L. M., Neutrophil influx and chemokine production during the early phases of the antitumor response to the vascular disrupting agent DMXAA (ASA404). *Neoplasia (New York, N.Y.)* **2009,** *11* (8), 793-803.
150. (a) Nathan, P.; Zweifel, M.; Padhani, A. R.; Koh, D. M.; Ng, M.; Collins, D. J.; Harris, A.; Carden, C.; Smythe, J.; Fisher, N.; Taylor, N. J.; Stirling, J. J.; Lu, S. P.; Leach, M. O.; Rustin, G. J.; Judson, I., Phase I trial of combretastatin A4 phosphate (CA4P) in combination with bevacizumab in patients with advanced cancer. *Clin Cancer Res* **2012,** *18* (12), 3428-39; (b) Siemann, D. W.; Shi, W., Dual targeting of tumor vasculature: combining Avastin and vascular disrupting agents (CA4P or OXi4503). *Anticancer Res* **2008,** *28* (4B), 2027-31.
151. Siemann, D. W.; Shi, W., Efficacy of combined antiangiogenic and vascular disrupting agents in treatment of solid tumors. *International journal of radiation oncology, biology, physics* **2004,** *60* (4), 1233-40.
152. (a) Workman, P.; Stratford, I. J., The experimental development of bioreductive drugs and their role in cancer therapy. *Cancer metastasis reviews* **1993,** *12* (2), 73-82; (b) Lash, C. J.; Li, A. E.; Rutland, M.; Baguley, B. C.; Zwi, L. J.; Wilson, W. R., Enhancement of the anti-tumour effects of the antivascular agent 5,6-dimethylxanthenone-4-acetic acid (DMXAA) by combination with 5-hydroxytryptamine and bioreductive drugs. *Br J Cancer* **1998,** *78* (4), 439-45.
153. (a) Chow, L. M.; Chan, T. H., Novel classes of dimer antitumour drug candidates. *Current pharmaceutical design* **2009,** *15* (6), 659-74; (b) Breen, E. C.; Walsh, J. J., Tubulin-targeting agents in hybrid drugs. *Current medicinal chemistry* **2010,** *17* (7), 609-39.
154. Luciani, N.; Marie-Claire, C.; Ruffet, E.; Beaumont, A.; Roques, B. P.; Fournie-Zaluski, M. C., Characterization of Glu350 as a critical residue involved in the N-terminal amine binding site of aminopeptidase N (EC 3.4.11.2): insights into its mechanism of action. *Biochemistry* **1998,** *37* (2), 686-92.
155. Bauvois, B.; Dauzonne, D., Aminopeptidase-N/CD13 (EC 3.4.11.2) inhibitors: chemistry, biological evaluations, and therapeutic prospects. *Med Res Rev* **2006,** *26* (1), 88-130.
156. (a) Kawai, M.; Otake, Y.; Hara, Y., High-molecular-mass isoform of aminopeptidase N/CD13 in serum from cholestatic patients. *Clinica chimica acta; international journal of clinical chemistry* **2003,** *330* (1-2), 141-9; (b) Favaloro, E. J.; Browning, T.; Facey, D., CD13 (GP150; aminopeptidase-N): predominant functional activity in blood is localized to plasma and is not cell-surface associated. *Experimental hematology* **1993,** *21* (13), 1695-701.
157. (a) Boonacker, E.; Van Noorden, C. J. F., The multifunctional or moonlighting protein CD26/DPPIV. *European Journal of Cell Biology* **2003,** *82* (2), 53-73; (b) Mina-Osorio, P., The moonlighting enzyme CD13: old and new functions to target. *Trends in Molecular Medicine* **2008,** *14* (8), 361-371; (c) Antczak, C.; De Meester, I.; Bauvois, B., Transmembrane proteases as disease markers and targets for therapy. *J Biol Regul Homeost Agents* **2001,** *15* (2), 130-9.
158. Proost, P.; Mortier, A.; Loos, T.; Vandercappellen, J.; Gouwy, M.; Ronsse, I.; Schutyser, E.; Put, W.; Parmentier, M.; Struyf, S.; Van Damme, J., Proteolytic processing of CXCL11 by CD13/aminopeptidase N impairs CXCR3 and CXCR7 binding and signaling and reduces lymphocyte and endothelial cell migration. *Blood* **2007,** *110* (1), 37-44.

159. Bauvois, B., Transmembrane proteases in cell growth and invasion: new contributors to angiogenesis? *Oncogene* **2004,** *23* (2), 317-29.
160. Sekine, K.; Fujii, H.; Abe, F., Induction of apoptosis by bestatin (ubenimex) in human leukemic cell lines. *Leukemia : official journal of the Leukemia Society of America, Leukemia Research Fund, U.K* **1999,** *13* (5), 729-34.
161. Larsen, S. L.; Pedersen, L. O.; Buus, S.; Stryhn, A., T cell responses affected by aminopeptidase N (CD13)-mediated trimming of major histocompatibility complex class II-bound peptides. *The Journal of experimental medicine* **1996,** *184* (1), 183-9.
162. Vijgen, L.; Keyaerts, E.; Zlateva, K.; Van Ranst, M., Identification of six new polymorphisms in the human coronavirus 229E receptor gene (aminopeptidase N/CD13). *International journal of infectious diseases : IJID : official publication of the International Society for Infectious Diseases* **2004,** *8* (4), 217-22.
163. Kontoyiannis, D. P.; Pasqualini, R.; Arap, W., Aminopeptidase N inhibitors and SARS. *Lancet* **2003,** *361* (9368), 1558.
164. Nomura, R.; Kiyota, A.; Suzaki, E.; Kataoka, K.; Ohe, Y.; Miyamoto, K.; Senda, T.; Fujimoto, T., Human coronavirus 229E binds to CD13 in rafts and enters the cell through caveolae. *Journal of virology* **2004,** *78* (16), 8701-8.
165. Knopfel, M.; Davies, J. P.; Duong, P. T.; Kvaerno, L.; Carreira, E. M.; Phillips, M. C.; Ioannou, Y. A.; Hauser, H., Multiple plasma membrane receptors but not NPC1L1 mediate high-affinity, ezetimibe-sensitive cholesterol uptake into the intestinal brush border membrane. *Biochimica et biophysica acta* **2007,** *1771* (9), 1140-7.
166. Mina-Osorio, P.; Ortega, E., Signal regulators in FcR-mediated activation of leukocytes? *Trends in immunology* **2004,** *25* (10), 529-35.
167. Mina-Osorio, P.; Ortega, E., Aminopeptidase N (CD13) functionally interacts with FcgammaRs in human monocytes. *Journal of leukocyte biology* **2005,** *77* (6), 1008-17.
168. (a) Bhagwat, S. V.; Lahdenranta, J.; Giordano, R.; Arap, W.; Pasqualini, R.; Shapiro, L. H., CD13/APN is activated by angiogenic signals and is essential for capillary tube formation. *Blood* **2001,** *97* (3), 652-9; (b) Hashida, H.; Takabayashi, A.; Kanai, M.; Adachi, M.; Kondo, K.; Kohno, N.; Yamaoka, Y.; Miyake, M., Aminopeptidase N is involved in cell motility and angiogenesis: its clinical significance in human colon cancer. *Gastroenterology* **2002,** *122* (2), 376-86.
169. Mina-Osorio, P.; Shapiro, L. H.; Ortega, E., CD13 in cell adhesion: aminopeptidase N (CD13) mediates homotypic aggregation of monocytic cells. *Journal of leukocyte biology* **2006,** *79* (4), 719-30.
170. Bischoff, J., Cell adhesion and angiogenesis. *J Clin Invest* **1997,** *99* (3), 373-6.
171. Glinsky, V. V.; Glinsky, G. V.; Glinskii, O. V.; Huxley, V. H.; Turk, J. R.; Mossine, V. V.; Deutscher, S. L.; Pienta, K. J.; Quinn, T. P., Intravascular metastatic cancer cell homotypic aggregation at the sites of primary attachment to the endothelium. *Cancer Res* **2003,** *63* (13), 3805-11.
172. Xu, Y.; Wellner, D.; Scheinberg, D. A., Cryptic and regulatory epitopes in CD13/aminopeptidase N. *Experimental hematology* **1997,** *25* (6), 521-9.
173. (a) Albiston, A. L.; Ye, S.; Chai, S. Y., Membrane bound members of the M1 family: more than aminopeptidases. *Protein and peptide letters* **2004,** *11* (5), 491-500; (b) Mina-Osorio, P.; Winnicka, B.; O'Conor, C.; Grant, C. L.; Vogel, L. K.; Rodriguez-Pinto, D.; Holmes, K. V.; Ortega, E.; Shapiro, L. H., CD13 is a novel mediator of monocytic/endothelial cell adhesion. *Journal of leukocyte biology* **2008,** *84* (2), 448-59; (c) Santos, A. N.; Langner, J.; Herrmann, M.; Riemann, D., Aminopeptidase N/CD13 is directly linked to signal transduction pathways in monocytes. *Cellular immunology* **2000,** *201* (1), 22-32.
174. Rangel, R.; Sun, Y.; Guzman-Rojas, L.; Ozawa, M. G.; Sun, J.; Giordano, R. J.; Van Pelt, C. S.; Tinkey, P. T.; Behringer, R. R.; Sidman, R. L.; Arap, W.; Pasqualini, R., Impaired angiogenesis in

aminopeptidase N-null mice. *Proceedings of the National Academy of Sciences of the United States of America* **2007,** *104* (11), 4588-93.
175. Pasqualini, R.; Koivunen, E.; Kain, R.; Lahdenranta, J.; Sakamoto, M.; Stryhn, A.; Ashmun, R. A.; Shapiro, L. H.; Arap, W.; Ruoslahti, E., Aminopeptidase N is a receptor for tumor-homing peptides and a target for inhibiting angiogenesis. *Cancer Res* **2000,** *60* (3), 722-7.
176. Ishii, K.; Usui, S.; Sugimura, Y.; Yoshida, S.; Hioki, T.; Tatematsu, M.; Yamamoto, H.; Hirano, K., Aminopeptidase N regulated by zinc in human prostate participates in tumor cell invasion. *International journal of cancer. Journal international du cancer* **2001,** *92* (1), 49-54.
177. Kehlen, A.; Lendeckel, U.; Dralle, H.; Langner, J.; Hoang-Vu, C., Biological significance of aminopeptidase N/CD13 in thyroid carcinomas. *Cancer Res* **2003,** *63* (23), 8500-6.
178. Petrovic, N.; Bhagwat, S. V.; Ratzan, W. J.; Ostrowski, M. C.; Shapiro, L. H., CD13/APN transcription is induced by RAS/MAPK-mediated phosphorylation of Ets-2 in activated endothelial cells. *J Biol Chem* **2003,** *278* (49), 49358-68.
179. Evans, J. F.; Kargman, S., Bestatin inhibits covalent coupling of [3H]LTA4 to human leukocyte LTA4 hydrolase. *FEBS letters* **1992,** *297* (1-2), 139-42.
180. Aoyagi, T.; Yoshida, S.; Nakamura, Y.; Shigihara, Y.; Hamada, M.; Takeuchi, T., Probestin, a new inhibitor of aminopeptidase M, produced by Streptomyces azureus MH663-2F6. I. Taxonomy, production, isolation, physico-chemical properties and biological activities. *J Antibiot (Tokyo)* **1990,** *43* (2), 143-8.
181. Ito, K.; Nakajima, Y.; Onohara, Y.; Takeo, M.; Nakashima, K.; Matsubara, F.; Ito, T.; Yoshimoto, T., Crystal structure of aminopeptidase N (proteobacteria alanyl aminopeptidase) from Escherichia coli and conformational change of methionine 260 involved in substrate recognition. *J Biol Chem* **2006,** *281* (44), 33664-76.
182. Lendeckel, U.; Kahne, T.; Riemann, D.; Neubert, K.; Arndt, M.; Reinhold, D., Review: the role of membrane peptidases in immune functions. *Advances in experimental medicine and biology* **2000,** *477*, 1-24.
183. Harbut, M. B.; Velmourougane, G.; Reiss, G.; Chandramohanadas, R.; Greenbaum, D. C., Development of bestatin-based activity-based probes for metallo-aminopeptidases. *Bioorganic & medicinal chemistry letters* **2008,** *18* (22), 5932-6.
184. Penning, T. D., Inhibitors of leukotriene A4 (LTA4) hydrolase as potential anti-inflammatory agents. *Current pharmaceutical design* **2001,** *7* (3), 163-79.
185. Jia, M. R.; Wei, T.; Xu, W. F., The Analgesic Activity of Bestatin as a Potent APN Inhibitor. *Frontiers in neuroscience* **2010,** *4*, 50.
186. Yoneda, J.; Saiki, I.; Fujii, H.; Abe, F.; Kojima, Y.; Azuma, I., Inhibition of tumor invasion and extracellular matrix degradation by ubenimex (bestatin). *Clinical & experimental metastasis* **1992,** *10* (1), 49-59.
187. Tsukamoto, H.; Shibata, K.; Kajiyama, H.; Terauchi, M.; Nawa, A.; Kikkawa, F., Aminopeptidase N (APN)/CD13 inhibitor, Ubenimex, enhances radiation sensitivity in human cervical cancer. *BMC cancer* **2008,** *8*, 74.
188. Gao, J. J.; Xue, X.; Gao, Z. H.; Cui, S. X.; Cheng, Y. N.; Xu, W. F.; Tang, W.; Qu, X. J., LYP, a bestatin dimethylaminoethyl ester, inhibited cancer angiogenesis both in vitro and in vivo. *Microvasc Res* **2011,** *82* (2), 122-30.
189. Saino, T.; Seya, K.; Nishizawa, R.; Takita, T.; Aoyagi, T.; Umezawa, H., Synthesis of p-hydroxyubenimex. *J Antibiot (Tokyo)* **1987,** *40* (8), 1165-9.
190. Gordon, E. M.; Godfrey, J. D.; Delaney, N. G.; Asaad, M. M.; Von Langen, D.; Cushman, D. W., Design of novel inhibitors of aminopeptidases. Synthesis of peptide-derived diamino thiols and sulfur replacement analogues of bestatin. *J Med Chem* **1988,** *31* (11), 2199-211.
191. Ocain, T. D.; Rich, D. H., Synthesis of sulfur-containing analogues of bestatin. Inhibition of aminopeptidases by alpha-thiolbestatin analogues. *J Med Chem* **1988,** *31* (11), 2193-9.

192. Corti, A.; Curnis, F.; Arap, W.; Pasqualini, R., The neovasculature homing motif NGR: more than meets the eye. *Blood* **2008,** *112* (7), 2628-35.
193. Curnis, F.; Arrigoni, G.; Sacchi, A.; Fischetti, L.; Arap, W.; Pasqualini, R.; Corti, A., Differential binding of drugs containing the NGR motif to CD13 isoforms in tumor vessels, epithelia, and myeloid cells. *Cancer Res* **2002,** *62* (3), 867-74.
194. Arap, W.; Pasqualini, R.; Ruoslahti, E., Cancer treatment by targeted drug delivery to tumor vasculature in a mouse model. *Science* **1998,** *279* (5349), 377-80.
195. Zhang, Z.; Hatta, H.; Tanabe, K.; Nishimoto, S., A new class of 5-fluoro-2'-deoxyuridine prodrugs conjugated with a tumor-homing cyclic peptide CNGRC by ester linkers: synthesis, reactivity, and tumor-cell-selective cytotoxicity. *Pharm Res* **2005,** *22* (3), 381-9.
196. Curnis, F.; Sacchi, A.; Borgna, L.; Magni, F.; Gasparri, A.; Corti, A., Enhancement of tumor necrosis factor alpha antitumor immunotherapeutic properties by targeted delivery to aminopeptidase N (CD13). *Nat Biotechnol* **2000,** *18* (11), 1185-90.
197. Curnis, F.; Sacchi, A.; Corti, A., Improving chemotherapeutic drug penetration in tumors by vascular targeting and barrier alteration. *J Clin Invest* **2002,** *110* (4), 475-82.
198. (a) Corti, A.; Ponzoni, M., Tumor vascular targeting with tumor necrosis factor alpha and chemotherapeutic drugs. *Ann N Y Acad Sci* **2004,** *1028*, 104-12; (b) Sacchi, A.; Gasparri, A.; Gallo-Stampino, C.; Toma, S.; Curnis, F.; Corti, A., Synergistic antitumor activity of cisplatin, paclitaxel, and gemcitabine with tumor vasculature-targeted tumor necrosis factor-alpha. *Clin Cancer Res* **2006,** *12* (1), 175-82; (c) Sacchi, A.; Gasparri, A.; Curnis, F.; Bellone, M.; Corti, A., Crucial role for interferon gamma in the synergism between tumor vasculature-targeted tumor necrosis factor alpha (NGR-TNF) and doxorubicin. *Cancer Res* **2004,** *64* (19), 7150-5.
199. Meng, J.; Ma, N.; Yan, Z.; Han, W.; Zhang, Y., NGR enhanced the anti-angiogenic activity of tum-5. *J Biochem* **2006,** *140* (2), 299-304.
200. Curnis, F.; Gasparri, A.; Sacchi, A.; Cattaneo, A.; Magni, F.; Corti, A., Targeted delivery of IFNgamma to tumor vessels uncouples antitumor from counterregulatory mechanisms. *Cancer Res* **2005,** *65* (7), 2906-13.
201. Colombo, G.; Curnis, F.; De Mori, G. M.; Gasparri, A.; Longoni, C.; Sacchi, A.; Longhi, R.; Corti, A., Structure-activity relationships of linear and cyclic peptides containing the NGR tumor-homing motif. *J Biol Chem* **2002,** *277* (49), 47891-7.
202. Plesniak, L. A.; Salzameda, B.; Hinderberger, H.; Regan, E.; Kahn, J.; Mills, S. A.; Teriete, P.; Yao, Y.; Jennings, P.; Marassi, F.; Adams, J. A., Structure and Activity of CPNGRC: A Modified CD13/APN Peptidic Homing Motif. *Chemical Biology & Drug Design* **2010,** *75* (6), 551-562.
203. Negussie, A. H.; Miller, J. L.; Reddy, G.; Drake, S. K.; Wood, B. J.; Dreher, M. R., Synthesis and in vitro evaluation of cyclic NGR peptide targeted thermally sensitive liposome. *Journal of controlled release : official journal of the Controlled Release Society* **2010,** *143* (2), 265-73.
204. Shah, R. The Design and Synthesis of Novel Inhibitors of Tubulin Polymerisation University of Dublin, Trinity College, Dublin, 2002.
205. McCormack, E. Design, Synthesis and In Vitro Evaluation of Novel Anti-Cancer Compounds. University of Dublin, Trinity College, Dublin, 2002.
206. Hudson, G. Design, Synthesis and Evaluation of Novel Tumour Vasculature-targeting agents. University of Dublin, Trinity College, Dublin, 2007.
207. White, M. Endothelium as a target in the design of novel tumour angiogenesis/vascular targeting agents. University of Dublin, Trinity College, Dublin, 2008.
208. Kumar, N., Taxol-induced polymerization of purified tubulin. Mechanism of action. *J Biol Chem* **1981,** *256* (20), 10435-41.
209. Combes, S.; Barbier, P.; Douillard, S.; McLeer-Florin, A.; Bourgarel-Rey, V.; Pierson, J. T.; Fedorov, A. Y.; Finet, J. P.; Boutonnat, J.; Peyrot, V., Synthesis and biological evaluation of 4-arylcoumarin analogues of combretastatins. Part 2. *J Med Chem* **2011,** *54* (9), 3153-62.
210. Capraro, H. G.; Brossi, A., *The Alkaloids*. Academic Press, New York: 1984.

211. Breen, E. C. The Design, Synthesis and Preliminary Evaluation of Prodrugs and Hybrid Drugs with Tubulin Polymerisation Inhibitory Activity and Anti-Proliferative Activity. University of Dublin, Trinity College, Dulin, 2012.
212. (a) Bai, R.; Covell, D. G.; Pei, X. F.; Ewell, J. B.; Nguyen, N. Y.; Brossi, A.; Hamel, E., Mapping the binding site of colchicinoids on beta -tubulin. 2-Chloroacetyl-2-demethylthiocolchicine covalently reacts predominantly with cysteine 239 and secondarily with cysteine 354. *J Biol Chem* **2000,** *275* (51), 40443-52; (b) Nguyen, T. L.; McGrath, C.; Hermone, A. R.; Burnett, J. C.; Zaharevitz, D. W.; Day, B. W.; Wipf, P.; Hamel, E.; Gussio, R., A common pharmacophore for a diverse set of colchicine site inhibitors using a structure-based approach. *J Med Chem* **2005,** *48* (19), 6107-16.
213. Rappl, C.; Barbier, P.; Bourgarel-Rey, V.; Grégoire, C.; Gilli, R.; Carre, M.; Combes, S.; Finet, J.-P.; Peyrot, V., Interaction of 4-Arylcoumarin Analogues of Combretastatins with Microtubule Network of HBL100 Cells and Binding to Tubulin†. *Biochemistry* **2006,** *45* (30), 9210-9218.
214. (a) Baeyer, A.; Villiger, V., Ueber die Einwirkung des Caro'schen Reagens auf Ketone. *Berichte der deutschen chemischen Gesellschaft* **1900,** *33* (1), 858-864; (b) Baeyer, A.; Villiger, V., Einwirkung des Caro'schen Reagens auf Ketone. *Berichte der deutschen chemischen Gesellschaft* **1899,** *32* (3), 3625-3633; (c) Renz, M.; Meunier, B., 100 Years of Baeyer–Villiger Oxidations. *European Journal of Organic Chemistry* **1999,** *1999* (4), 737-750.
215. Dakin, H. D., Catechol. *Organic Syntheses* **1923,** *3*, 28.
216. Matsumoto, M.; Kobayashi, K.; Hotta, Y., Acid-catalyzed oxidation of benzaldehydes to phenols by hydrogen peroxide. *The Journal of Organic Chemistry* **1984,** *49* (24), 4740-4741.
217. Robertson, A., 181. Experiments on the synthesis of rotenone and its derivatives. Part II. The synthesis of rissic acid and of derric acid, and the constitution of rotenone, deguelin, and tephrosin. *Journal of the Chemical Society (Resumed)* **1932,** *0* (0), 1380-1388.
218. (a) Dumas, A. M.; Fillion, E., Meldrum's Acids and 5-Alkylidene Meldrum's Acids in Catalytic Carbon–Carbon Bond-Forming Processes. *Accounts of Chemical Research* **2009,** *43* (3), 440-454; (b) Lipson, V. V.; Gorobets, N. Y., One hundred years of Meldrum's acid: advances in the synthesis of pyridine and pyrimidine derivatives. *Molecular diversity* **2009,** *13* (4), 399-419.
219. Bose, A. K.; Manhas, M. S.; Gala, K.; Sahu, D. P.; Hegde, V., A convenient route to α-amido-β-lactams. *Journal of Heterocyclic Chemistry* **1980,** *17* (8), 1687-1689.
220. Luche, J.-L.; Rodriguez-Hahn, L.; Crabbe, P., Reduction of natural enones in the presence of cerium trichloride. *Journal of the Chemical Society, Chemical Communications* **1978,** (14), 601-602.
221. (a) North, M., The Baker's Yeast Reduction of Keto-Esters in Organic Solvents: A One Week Research Project for Undergraduate Students. *Journal of Chemical Education* **1998,** *75* (5), 630-null; (b) Medson, C.; Smallridge, A. J.; Trewhella, M. A., The stereoselective preparation of [beta]-hydroxy esters using a yeast reduction in an organic solvent. *Tetrahedron: Asymmetry* **1997,** *8* (7), 1049-1054; (c) Athanasiou, N.; Smallridge, A. J.; Trewhella, M. A., Baker's yeast mediated reduction of [beta]-keto esters and [beta]-keto amides in an organic solvent system. *Journal of Molecular Catalysis B: Enzymatic* **2001,** *11* (4-6), 893-896.
222. (a) Dess, D. B.; Martin, J. C., A useful 12-I-5 triacetoxyperiodinane (the Dess-Martin periodinane) for the selective oxidation of primary or secondary alcohols and a variety of related 12-I-5 species. *Journal of the American Chemical Society* **1991,** *113* (19), 7277-7287; (b) Dess, D. B.; Martin, J. C., Readily accessible 12-I-5 oxidant for the conversion of primary and secondary alcohols to aldehydes and ketones. *The Journal of Organic Chemistry* **1983,** *48* (22), 4155-4156.
223. Meyer, S. D.; Schreiber, S. L., Acceleration of the Dess-Martin Oxidation by Water. *The Journal of Organic Chemistry* **1994,** *59* (24), 7549-7552.
224. Koos, M.; Repas, M.; Ciha, M.; Zvakova, A., Enones derived from 4-dimethylaminobenzaldehyde. *Chem. Zvesti* **1984,** *38* (2), 231-7.

225. (a) Miyaura, N.; Yamada, K.; Suzuki, A., A new stereospecific cross-coupling by the palladium-catalyzed reaction of 1-alkenylboranes with 1-alkenyl or 1-alkynyl halides. *Tetrahedron Letters* **1979,** *20* (36), 3437-3440; (b) Miyaura, N.; Suzuki, A., Palladium-Catalyzed Cross-Coupling Reactions of Organoboron Compounds. *Chemical Reviews* **1995,** *95* (7), 2457-2483.
226. Ritter, K., Synthetic Transformations of Vinyl and Aryl Triflates. *Journal of Synthetic Organic Chemistry* **1993,** *1993* (8).
227. Ishiyama, T.; Murata, M.; Miyaura, N., Palladium(0)-Catalyzed Cross-Coupling Reaction of Alkoxydiboron with Haloarenes: A Direct Procedure for Arylboronic Esters. *The Journal of Organic Chemistry* **1995,** *60* (23), 7508-7510.
228. Comins, D. L.; Dehghani, A., Pyridine-derived triflating reagents: An improved preparation of vinyl triflates from metallo enolates. *Tetrahedron Letters* **1992,** *33* (42), 6299-6302.
229. Pettit, G. R.; Minardi, M. D.; Hogan, F.; Price, P. M., An efficient synthetic strategy for obtaining 4-methoxy carbon isotope labeled combretastatin A-4 phosphate and other Z-combretastatins. *Journal of natural products* **2010,** *73* (3), 399-403.
230. Silverberg, L. J.; Dillon, J. L.; Vemishetti, P., A simple, rapid and efficient protocol for the selective phosphorylation of phenols with dibenzyl phosphite. *Tetrahedron Letters* **1996,** *37* (6), 771-774.
231. (a) McKenna, C. E.; Schmidhuser, J., Functional selectivity in phosphonate ester dealkylation with bromotrimethylsilane. *Journal of the Chemical Society, Chemical Communications* **1979,** *0* (17), 739-739; (b) McKenna, C. E.; Higa, M. T.; Cheung, N. H.; McKenna, M.-C., The facile dealkylation of phosphonic acid dialkyl esters by bromotrimethylsilane. *Tetrahedron Letters* **1977,** *18* (2), 155-158.
232. Prokopiou, E. M. Preclinical Evaluation of Novel Tumour Vasculature Disrupting Agents. University of Dublin, Trinity College, Dublin, 2013.
233. Mosmann, T., Rapid colorimetric assay for cellular growth and survival: application to proliferation and cytotoxicity assays. *Journal of immunological methods* **1983,** *65* (1-2), 55-63.
234. (a) Lin, H. L.; Chiou, S. H.; Wu, C. W.; Lin, W. B.; Chen, L. H.; Yang, Y. P.; Tsai, M. L.; Uen, Y. H.; Liou, J. P.; Chi, C. W., Combretastatin A4-induced differential cytotoxicity and reduced metastatic ability by inhibition of AKT function in human gastric cancer cells. *The Journal of pharmacology and experimental therapeutics* **2007,** *323* (1), 365-73; (b) Jung, H. J.; Shim, J. S.; Lee, H. B.; Kim, C. J.; Kuwano, T.; Ono, M.; Kwon, H. J., Embellistatin, a microtubule polymerization inhibitor, inhibits angiogenesis both in vitro and in vivo. *Biochem Biophys Res Commun* **2007,** *353* (2), 376-80; (c) Arora, S.; Wang, X. I.; Keenan, S. M.; Andaya, C.; Zhang, Q.; Peng, Y.; Welsh, W. J., Novel microtubule polymerization inhibitor with potent antiproliferative and antitumor activity. *Cancer Res* **2009,** *69* (5), 1910-5.
235. Krishan, A., Rapid flow cytofluorometric analysis of mammalian cell cycle by propidium iodide staining. *J Cell Biol* **1975,** *66* (1), 188-93.
236. Nicosia, R. F.; Ottinetti, A., Growth of microvessels in serum-free matrix culture of rat aorta. A quantitative assay of angiogenesis in vitro. *Lab Invest* **1990,** *63* (1), 115-22.
237. Albrecht, S.; Al-Lakkis-Wehbe, M.; Orsini, A.; Defoin, A.; Pale, P.; Salomon, E.; Tarnus, C.; Weibel, J.-M., Amino-benzosuberone: A novel warhead for selective inhibition of human aminopeptidase-N/CD13. *Bioorganic & Medicinal Chemistry* **2011,** *19* (4), 1434-1449.
238. Staudinger, H.; Meyer, J., Über neue organische Phosphorverbindungen III. Phosphinmethylenderivate und Phosphinimine. *Helvetica Chimica Acta* **1919,** *2* (1), 635-646.
239. Smith, M. B., *Organic Synthesis*. McGraw-Hill Book Co: 1994.
240. (a) Snyder, H. R.; Kruse, C. W., A Synthesis of Diisopropylidene Ethylenetetracarboxylate1. *Journal of the American Chemical Society* **1958,** *80* (8), 1942-1944;

(b) Bloch, R., 5,5-Dibromo-2,2-dimethyl-4,6-dioxo-1,3-dioxane; a new brominating agent for saturated and α,β-unsaturated carbonyl compounds. *Synthesis* **1978,** (2), 140-2.
241. Marquet, A.; Jacques, J., Halogenations selectives au moyen des perhalogenures de phenyltrimethylammonium. *Tetrahedron Letters* **1959,** *1* (9), 24-26.
242. Martin, S. F.; Davidsen, S. K.; Puckette, T. A., Total syntheses of the amaryllidaceae alkaloids (.+-.)-hemanthidine and (.+-.)-pretazettine. *The Journal of Organic Chemistry* **1987,** *52* (10), 1962-1972.
243. (a) Heller, J. E.; Dreiding, A. S., Zur Konfiguration der 2,4,6,8-Tetrabrom-cyclooctan-1,5-dione Reduktion des β-Isomers durch Natrium-borhydrid. *Helvetica Chimica Acta* **1973,** *56* (1), 413-439; (b) Heller, J.; Yogev, A.; Dreiding, A. S., Bishomochinon. *Helvetica Chimica Acta* **1972,** *55* (3), 1003-1025.
244. Jacques, J.; Marquet, A., Selective α-bromination of an aralkyl ketone with phenyltrimethylammonium tribromide : 2-bromoacetyl-6-methoxynaphthalene and 2,2 dibromoacetyl-6-methoxynaphthalene. *Organic Syntheses* **1973,** *53*.
245. Greene, T. W.; Wuts, P. G. M., *Protective Groups in Organic Synthesis*. 4th Edition ed.; John Wiley and Sons, New York: 2007.
246. Stevens, C. L.; Blumbergs, P.; Munk, M., The Reactions of α-Bromo Ketones with Primary Amines1. *The Journal of Organic Chemistry* **1963,** *28* (2), 331-336.
247. Combes, S.; Finet, J.-P.; Siri, D., On the optical activity of the 3-aryl-4-hydroxycoumarin isolated from Millettia griffoniana: molecular modelling and total synthesis. *Journal of the Chemical Society, Perkin Transactions 1* **2002,** *0* (1), 38-44.
248. (a) Boland, G. M.; Donnelly, D. M. X.; Finet, J.-P.; Rea, M. D., Synthesis of neoflavones by Suzuki arylation of 4-substituted coumarins. *Journal of the Chemical Society, Perkin Transactions 1* **1996,** *0* (21), 2591-2597; (b) Bailly, C.; Bal, C.; Barbier, P.; Combes, S.; Finet, J. P.; Hildebrand, M. P.; Peyrot, V.; Wattez, N., Synthesis and biological evaluation of 4-arylcoumarin analogues of combretastatins. *J Med Chem* **2003,** *46* (25), 5437-44.
249. (a) Thompson, W. J.; Gaudino, J., A general synthesis of 5-arylnicotinates. *The Journal of Organic Chemistry* **1984,** *49* (26), 5237-5243; (b) Donnelly, D. M. X.; Finet, J.-P.; Guiry, P. J.; Rea, M. D., Synthesis of C-ring hydroxylated neoflavonoids by ligand coupling reactions. *Synthetic Communications* **1999,** *29*, 2719-2730.
250. Green, K., Improved metalation of 2,4,6-tribromoanisole: synthesis of 2-methoxyresorcinol. *The Journal of Organic Chemistry* **1991,** *56* (13), 4325-4326.
251. Basavaiah, D.; Veeraraghavaiah, G., The Baylis-Hillman reaction: a novel concept for creativity in chemistry. *Chemical Society Reviews* **2012,** *41* (1), 68-78.
252. Lee, K.-Y.; Gong, J.-H.; Kim, J.-N., The Most Simple and Convenient Synthesis of the Baylis-Hillman Adducts of Cycloalkenones:Use of DMAP in Aqueous THF. *Bulletin of the Korean Chemical Society* **2002** *23* (5), 659-660.
253. Gatri, R.; El Gaïed, M. M., Imidazole-catalysed Baylis–Hillman reactions: a new route to allylic alcohols from aldehydes and cyclic enones. *Tetrahedron Letters* **2002,** *43* (43), 7835-7836.
254. McCague, R.; Kuroda, R.; Leclercq, G.; Stoessel, S., Synthesis and estrogen receptor binding of 6,7-dihydro-8-phenyl-9-[4-[2-(dimethylamino)ethoxy]phenyl]-5H-benzocycloheptene, a nonisomerizable analog of tamoxifen. X-ray crystallographic studies. *Journal of Medicinal Chemistry* **1986,** *29* (10), 2053-2059.
255. (a) Kamat, A. A.; Kim, T. J.; Landen, C. N., Jr.; Lu, C.; Han, L. Y.; Lin, Y. G.; Merritt, W. M.; Thaker, P. H.; Gershenson, D. M.; Bischoff, F. Z.; Heymach, J. V.; Jaffe, R. B.; Coleman, R. L.; Sood, A. K., Metronomic chemotherapy enhances the efficacy of antivascular therapy in ovarian cancer. *Cancer Res* **2007,** *67* (1), 281-8; (b) Browder, T.; Butterfield, C. E.; Kraling, B. M.; Shi, B.; Marshall, B.; O'Reilly, M. S.; Folkman, J., Antiangiogenic scheduling of chemotherapy improves efficacy against experimental drug-resistant cancer. *Cancer Res* **2000,** *60* (7), 1878-86.

256. Talmadge, J. E.; Ino, K.; Bierman, P. J., Bestatin for Anti-Cancer Treatments. In *Immunopharmaceuticals*, Kimball, E. S., Ed. CRC Press: 1996; pp 135-166.
257. McCracken, N. W.; Blain, P. G.; Williams, F. M., Nature and role of xenobiotic metabolizing esterases in rat liver, lung, skin and blood. *Biochemical Pharmacology* **1993,** *45* (1), 31-36.
258. Walsh, J. J.; Coughlan, D.; Heneghan, N.; Gaynor, C.; Bell, A., A novel artemisinin-quinine hybrid with potent antimalarial activity. *Bioorganic & medicinal chemistry letters* **2007,** *17* (13), 3599-602.
259. (a) Coste, J.; Frerot, E.; Jouin, P., Coupling N-Methylated Amino Acids Using PyBroP and PyCloP Halogenophosphonium Salts: Mechanism and Fields of Application. *The Journal of Organic Chemistry* **1994,** *59* (9), 2437-2446; (b) Montalbetti, C. A. G. N.; Falque, V., Amide bond formation and peptide coupling. *Tetrahedron* **2005,** *61* (46), 10827-10852.
260. Burley, S. K.; David, P. R.; Lipscomb, W. N., Leucine aminopeptidase: bestatin inhibition and a model for enzyme-catalyzed peptide hydrolysis. *Proceedings of the National Academy of Sciences of the United States of America* **1991,** *88* (16), 6916-20.
261. Xu, W.; Li, Q., Progress in the development of aminopeptidase N (APN/CD13) inhibitors. *Current medicinal chemistry. Anti-cancer agents* **2005,** *5* (3), 281-301.
262. (a) Schlingemann, R. O.; Oosterwijk, E.; Wesseling, P.; Rietveld, F. J.; Ruiter, D. J., Aminopeptidase a is a constituent of activated pericytes in angiogenesis. *J Pathol* **1996,** *179* (4), 436-42; (b) Marchio, S.; Lahdenranta, J.; Schlingemann, R. O.; Valdembri, D.; Wesseling, P.; Arap, M. A.; Hajitou, A.; Ozawa, M. G.; Trepel, M.; Giordano, R. J.; Nanus, D. M.; Dijkman, H. B.; Oosterwijk, E.; Sidman, R. L.; Cooper, M. D.; Bussolino, F.; Pasqualini, R.; Arap, W., Aminopeptidase A is a functional target in angiogenic blood vessels. *Cancer Cell* **2004,** *5* (2), 151-62.
263. (a) Morphy, R.; Rankovic, Z., Designed multiple ligands. An emerging drug discovery paradigm. *J Med Chem* **2005,** *48* (21), 6523-43; (b) O'Boyle, N. M.; Meegan, M. J., Designed multiple ligands for cancer therapy. *Current medicinal chemistry* **2011,** *18* (31), 4722-37.
264. Morphy, R.; Kay, C.; Rankovic, Z., From magic bullets to designed multiple ligands. *Drug discovery today* **2004,** *9* (15), 641-51.
265. Leeson, P., Drug discovery: Chemical beauty contest.
266. Puerta, D. T.; Griffin, M. O.; Lewis, J. A.; Romero-Perez, D.; Garcia, R.; Villarreal, F. J.; Cohen, S. M., Heterocyclic zinc-binding groups for use in next-generation matrix metalloproteinase inhibitors: potency, toxicity, and reactivity. *Journal of biological inorganic chemistry : JBIC : a publication of the Society of Biological Inorganic Chemistry* **2006,** *11* (2), 131-8.
267. (a) Holmes, M. A.; Matthews, B. W., Binding of hydroxamic acid inhibitors to crystalline thermolysin suggests a pentacoordinate zinc intermediate in catalysis. *Biochemistry* **1981,** *20* (24), 6912-6920; (b) Tekeste, T.; Vahrenkamp, H., Enzyme inhibitor modeling with TpZn complexes of functional hydroxamates and oximates. *Inorganica Chimica Acta* **2007,** *360* (5), 1523-1528.
268. Drag, M.; Grzywa, R.; Oleksyszyn, J., Novel hydroxamic acid-related phosphinates: inhibition of neutral aminopeptidase N (APN). *Bioorganic & medicinal chemistry letters* **2007,** *17* (6), 1516-9.
269. Mucha, A.; Drag, M.; Dalton, J. P.; Kafarski, P., Metallo-aminopeptidase inhibitors. *Biochimie* **2010,** *92* (11), 1509-29.
270. Krige, D.; Needham, L. A.; Bawden, L. J.; Flores, N.; Farmer, H.; Miles, L. E.; Stone, E.; Callaghan, J.; Chandler, S.; Clark, V. L.; Kirwin-Jones, P.; Legris, V.; Owen, J.; Patel, T.; Wood, S.; Box, G.; Laber, D.; Odedra, R.; Wright, A.; Wood, L. M.; Eccles, S. A.; Bone, E. A.; Ayscough, A.; Drummond, A. H., CHR-2797: an antiproliferative aminopeptidase inhibitor that leads to amino acid deprivation in human leukemic cells. *Cancer Res* **2008,** *68* (16), 6669-79.

271. (a) Cortes, J.; EJ, F.; KE, Y. In *The OPAL study: A phase II study to evaluate the efficacy, safety, and tolerability of tosedostat (CHR-2797) in elderly subjects with treatment refractory or relapsed acute myeloid leukemia*, 2010 ASCO Annual Meeting, Chicago, J. Clin. Oncol. : Chicago, 2010; (b) Reid, A. H.; Protheroe, A.; Attard, G.; Hayward, N.; Vidal, L.; Spicer, J.; Shaw, H. M.; Bone, E. A.; Carter, J.; Hooftman, L.; Harris, A.; De Bono, J. S., A first-in-man phase i and pharmacokinetic study on CHR-2797 (Tosedostat), an inhibitor of M1 aminopeptidases, in patients with advanced solid tumors. *Clin Cancer Res* **2009,** *15* (15), 4978-85; (c) Lowenberg, B.; Morgan, G.; Ossenkoppele, G. J.; Burnett, A. K.; Zachee, P.; Duhrsen, U.; Dierickx, D.; Muller-Tidow, C.; Sonneveld, P.; Krug, U.; Bone, E.; Flores, N.; Richardson, A. F.; Hooftman, L.; Jenkins, C.; Zweegman, S.; Davies, F., Phase I/II clinical study of Tosedostat, an inhibitor of aminopeptidases, in patients with acute myeloid leukemia and myelodysplasia. *Journal of clinical oncology : official journal of the American Society of Clinical Oncology* **2010,** *28* (28), 4333-8.

272. Prelog, V.; Helmchen, G., Basic Principles of the CIP-System and Proposals for a Revision. *Angewandte Chemie International Edition in English* **1982,** *21* (8), 567-583.

273. Klement, G.; Baruchel, S.; Rak, J.; Man, S.; Clark, K.; Hicklin, D. J.; Bohlen, P.; Kerbel, R. S., Continuous low-dose therapy with vinblastine and VEGF receptor-2 antibody induces sustained tumor regression without overt toxicity. *J Clin Invest* **2000,** *105* (8), R15-24.

274. (a) Hanahan, D.; Bergers, G.; Bergsland, E., Less is more, regularly: metronomic dosing of cytotoxic drugs can target tumor angiogenesis in mice. *J Clin Invest* **2000,** *105* (8), 1045-7; (b) Dellapasqua, S.; Bertolini, F.; Bagnardi, V.; Campagnoli, E.; Scarano, E.; Torrisi, R.; Shaked, Y.; Mancuso, P.; Goldhirsch, A.; Rocca, A.; Pietri, E.; Colleoni, M., Metronomic cyclophosphamide and capecitabine combined with bevacizumab in advanced breast cancer. *Journal of clinical oncology : official journal of the American Society of Clinical Oncology* **2008,** *26* (30), 4899-905.

275. Bagri, A.; Berry, L.; Gunter, B.; Singh, M.; Kasman, I.; Damico, L. A.; Xiang, H.; Schmidt, M.; Fuh, G.; Hollister, B.; Rosen, O.; Plowman, G. D., Effects of anti-VEGF treatment duration on tumor growth, tumor regrowth, and treatment efficacy. *Clin Cancer Res* **2010,** *16* (15), 3887-900.

276. Bertolini, F.; Paul, S.; Mancuso, P.; Monestiroli, S.; Gobbi, A.; Shaked, Y.; Kerbel, R. S., Maximum tolerable dose and low-dose metronomic chemotherapy have opposite effects on the mobilization and viability of circulating endothelial progenitor cells. *Cancer Res* **2003,** *63* (15), 4342-6.

277. Melzig, M. F.; Bormann, H., Betulinic acid inhibits aminopeptidase N activity. *Planta medica* **1998,** *64* (7), 655-7.

278. Aozuka, Y.; Koizumi, K.; Saitoh, Y.; Ueda, Y.; Sakurai, H.; Saiki, I., Anti-tumor angiogenesis effect of aminopeptidase inhibitor bestatin against B16-BL6 melanoma cells orthotopically implanted into syngeneic mice. *Cancer Lett* **2004,** *216* (1), 35-42.

Design and synthesis of tubulin binding agents and their incorporation into novel dual acting hybrid molecules targeting tumour vasculature

By

Adrian Coogan (08133531)

Abstract

This thesis involves the design and synthesis of tubulin binding agents, which aside from their anti-proliferative impact, seek to induce anti-vascular and anti-angiogenic responses on the unique vasculature derived by a growing tumour mass. Once synthesised, studies were conducted on the incorporation of the most active tubulin binding agents into a novel series of hybrid drugs or designed multiple ligands, which serve to complement their therapeutic effect.

The thesis is introduced by a comprehensive overview of the process of angiogenesis, the tumour vasculature network, and the myriad of differences between tumour blood vessels and those of normal vascular systems. Also discussed are the two main interrelated strategies for disrupting the microvasculature of tumours; the anti-angiogenic and anti-vascular approaches, with examples provided for each. The benefit of combination and hybrid therapies is outlined, with particular regard to each side of the concepts we intended to implement; dual targeting of both the tubulin subunits which can eventually cause occlusion of a tumour blood vessel, and the multifunctional enzymatic receptor Aminopeptidase N (APN), expressed solely on tumour vasculature undergoing angiogenesis but not on normal, quiescent vasculature. The introductory chapter ends by outlining the aims of the thesis.

Chapter 2 focuses on the procurement of promising tricyclic benzoxepinone compounds, previously shown to be competitive tubulin binding agents. As this synthesis is optimised, novel derivatives are prepared, and comprehensive biological testing carried out on the most promising compound. A phosphate prodrug of the same compound is also prepared.

Chapter 3 starts by discussing the bromination of the main benzoxepinones from Chapter 2, and the novel ring contraction reaction discovered that converts these to an even more active 4-aryl coumarin series. The novel reaction itself is studied and a mechanism proposed, before the effects of various other nucleophiles are investigated on the bromide intermediate. Two of these in particular give rise to quite unexpected rearrangements and again these transformations are discussed. A new, more efficient synthetic methodology for the procurement of 4-aryl coumarins is implemented, and using this, a range of these chromenone structures are prepared and evaluated.

Chapter 4 centres on the integration of the most active tubulin binding, anti-vascular compounds described in Chapters 2 and 3 into multi-valent drug systems. These include a variety of hybrid drugs based on the existing APN inhibitor bestatin, and also designed multiple ligands which possess a hydroxamic acid functionality, known to have excellent affinity for the zinc containing APN binding site. Following their synthesis they were then evaluated for their APN inhibition activity. Furthermore, one hybrid lead compound was evaluated in a rigorous evaluation regimen not only for *ex vivo* anti-vascular and anti-angiogenic activity, but also for *in vivo* activity in a PC-3 tumour xenograft model, where it was successfully shown by another PhD student to inhibit tumour growth.

Chapter 5 outlines the experimental procedures used in the syntheses of agents from Chapters 2, 3 and 4, and recorded their structural data.
